FOSSIL

DOE/MC/26268--3822
(DE94012256)

The Extraction of Bitumen from Western Oil Sands

Final Report
July 1989 - September 1993

Alex G. Oblad
James W. Bunger
Donald A. Dahlstrom
Milind D. Deo
John V. Fletcher
Francis V. Hanson
Jan D. Miller
J. D. Seader

March 1994

Work Performed Under Contract No.: DE-FC21-89MC26268

For
U.S. Department of Energy
Office of Fossil Energy
Morgantown Energy Technology Center
Morgantown, West Virginia

By
University of Utah
Department of Chemical and Fuels Engineering and
Department of Metallurgical Engineering
Salt Lake City, Utah

DISCLAIMER

This report was prepared as an account of work sponsored by an agency of the United States Government. Neither the United States Government nor any agency thereof, nor any of their employees, makes any warranty, express or implied, or assumes any legal liability or responsibility for the accuracy, completeness, or usefulness of any information, apparatus, product, or process disclosed, or represents that its use would not infringe privately owned rights. Reference herein to any specific commercial product, process, or service by trade name, trademark, manufacturer, or otherwise does not necessarily constitute or imply its endorsement, recommendation, or favoring by the United States Government or any agency thereof. The views and opinions of authors expressed herein do not necessarily state or reflect those of the United States Government or any agency thereof.

This report has been reproduced directly from the best available copy.

Available to DOE and DOE contractors from the Office of Scientific and Technical Information, P.O. Box 62, Oak Ridge, TN 37831; prices available from (615) 576-8401.

Available to the public from the U.S. Department of Commerce, Technology Administration, National Technical Information Service, Springfield, VA 22161, (703) 487-4650.

DISCLAIMER

Portions of this document may be illegible in electronic image products. Images are produced from the best available original document.

DOE/MC/26268--3822
(DE94012256)
Distribution Category UC-123

The Extraction of Bitumen from Western Oil Sands

Final Report
July 1989 - September 1993

Alex G. Oblad
James W. Bunger
Donald A. Dahlstrom
Milind D. Deo
John V. Fletcher
Francis V. Hanson
Jan D. Miller
J. D. Seader

Work Performed Under Contract No.: DE-FC21-89MC26268

For
U.S. Department of Energy
Office of Fossil Energy
Morgantown Energy Technology Center
P.O. Box 880
Morgantown, West Virginia 26507-0880

By
University of Utah
Department of Chemical and Fuels Engineering and
Department of Metallurgical Engineering
1471 Federal Way
Salt Lake City, Utah 84102

March 1994

A No5-110

B-F-K1

TABLE OF CONTENTS

TABLE OF CONTENTS i

LIST OF TABLES x

LIST OF FIGURES xiv

EXECUTIVE SUMMARY 1

INFORMATION REQUIRED FOR THE NATIONAL ENVIRONMENTAL POLICY ACT 12

INTRODUCTION 12
NEPA CHECKLIST 13
Date 13
Activity/Project Name 13
Project Manager/Branch/Division 13
Project/Activity Description 13
Brief Description of Affected Environment 14
Environmental Concerns 16
Additional Information 17
categorical exclusion 19
Recommended NEPA Determination 19

CATEGORICAL EXCLUSION (CX-B) DETERMINATION 20

RECOVERY OF BITUMEN FROM WESTERN TAR SANDS 20
Proposed Action 20
Location 20
Proposed by: 20
Description of the proposed action 20
A. Feedstock 21
B. Produced Bitumen 22
C. Off-Gas Wastes 22
D. Water Wastes 22
E. Solid and Liquid Hazardous Wastes 23
F. CX to Be Applied 23

CHARACTERIZATION OF UINTA BASIN OIL SAND DEPOSITS AND ACQUISITION OF MINED ORE SAMPLES 24

INTRODUCTION 24

PR SPRING OIL SAND DEPOSIT 24
Deposit Location 24
Deposit Description 24
Geology 25
Lithology - Character of Reservoir 27
Resource Estimates 33
Characterization and Analysis of the Bitumen 33
Development History 35
Maxwell Quarry: Section 17, T12S, R25E 41

Uintah County Quarry: Section 32, T14S, R23E 42
Wasatch Tar Sands Quarry: Section 32, T14S, R23 42
Enercor Quarry: Section 32, T12S, R25E 42
U-Tar Quarry: Section 5, T16S, R24E 42
Kerr-McGee Quarry: Section 36, T15S, R22E 42
Kamp Kerogen: Section 2, T14S, R22E 43
Ownership 44
Maxwell Quarry 44
Uintah County Quarry 44
Wasatch Tar Sands Quarry 44
Enercor Quarry 44
U-Tar Quarry 44
Additional Information 45

Report on the September 1992, Uinta Basin Field Trip of the Department of Fuels Engineering, University of Utah 45
UTAR Pit. nwsene Sec. 5. T16S. R24E 45
Enercor Pit, cw/2 nwsw Sec. 32. T12S. R25E 45
Stratigraphy 48

SUNNYSIDE OIL SAND DEPOSIT 49
Deposit Location 49
Reconnaissance of the Sunnyside Oil Sand Deposit 49

FUTURE ACTIVITIES 49

CHARACTERIZATION OF CIRCLE CLIFFS TAR SANDS OF UTAH 50

INTRODUCTION 50

EXPERIMENTAL 52

RESULTS AND DISCUSSION 55
Mineralogical Analysis. 55
Viscosity of Bitumen 57
Elemental Analysis of the Bitumen 57
Fractional Analysis of Bitumen 61
Infrared Spcetroscopic Analysis 63
Oil Sand Processing Considerations 72

FUTURE ACTIVITIES 74

AQUEOUS SEPARATION/RECOVERY OF UINTA BASIN BITUMENS 75

SURFACE CHARACTERIZATION OF WHITEROCKS BITUMEN 75

INTRODUCTION 75

EXPERIMENTAL 78
Reagents 78
Surface and Interfacial Tension Measurements 79
Contact Angle Measurements 82

Zeta Potential Measurements 83

RESULTS AND DISCUSSION 84
Surface Tension from Direct Measurements - Wilhelmy Plate Technique 84
Surface Tension from Contact Angle Measurements 88
Interfacial Tension 104
Electrical Properties of Bitumen Emulsions 116

SUMMARY AND CONCLUSIONS 120
FUTURE ACTIVITIES 123

BITUMEN RELEASE FROM OIL SAND DURING STAGNANT DIGESTION 124

INTRODUCTION 124

EXPERIMENTAL TECHNIQUE 125

RESULTS 127

DISCUSSION 130
Mechanism of Separation 132
Oil Sands of Low Natural Porosity 134

CONCLUSIONS 135

FUTURE ACTIVITIES 136

ENHANCED BITUMEN RECOVERY FROM WHITEROCKS OIL SANDS BY CONTROL OF THE BITUMEN/WATER INTERFACIAL TENSION 137

INTRODUCTION 137

EXPERIMENTAL 138
Reagents 138
Microscopic Observations of Bitumen Release from Oil Sand 139
Hot Water Processing 139

RESULTS AND DISCUSSION 140
Bitumen Release from Oil Sand 140
Correlation of Interfacial Tension with Bitumen Recovery 153

SUMMARY AND CONCLUSIONS 157

FUTURE ACTIVITIES 159

BUBBLE SIZE DISTRIBUTIONS GENERATED DURING OPERATION OF AN AIR-SPARGED HYDROCYCLONE 160

INTRODUCTION 160

EXPERIMENTAL 163

RESULTS AND DISCUSSION 164
Frother Concentration 164
ASH Diameter 166
ASH Length 169
Flowrate Ratio 169

FUTURE ACTIVITIES 171

A DIMENSIONAL ANALYSIS OF CLEANUP OF A BITUMEN CONCENTRATE DERIVED FROM UTAH OIL SAND 172

INTRODUCTION 172

EXPERIMENTAL 173

DIMENSIONAL ANALYSIS 176

RESULTS AND DISCUSSION 180

SUMMARY AND CONCLUSIONS 189

FUTURE ACTIVITIES 189

WATER-BASED SEPARATION PROCESS DESIGN AND DEVELOPMENT FOR UTAH OIL SANDS 190

INTRODUCTION 190

PROCESS STEPS AND PROCESSING STRATEGY 191
Comments on Oil Sand Pretreatment with Diluent 195

MASS BALANCE AND ENERGY BALANCE 196

COMMENTS AND CONCLUSIONS 208

FUTURE ACTIVITIES 209

EXTRACTION OF BITUMEN FROM WESTERN OIL SANDS BY AN ENERGY-EFFICIENT THERMAL METHOD 210

INTRODUCTION 210

REACTOR MODIFICATIONS AND TROUBLESHOOTING 213

PYROLYSIS REACTOR MODEL 219

PREVIOUS MODELING WORK 223

HYDRODYNAMICS 225

PYROLYSIS REACTION SHCEME AND KINETICS 229

ENERGY BALANCES 236
Pyrolysis bed 237
Combustion Bed 240
Second-Stage Combustion Bed 241
Heat Pipes 241

METHOD OF SOLUTION 242
Solid-Phase Products 242
Gas-Phase Products 245
Mass Balance 249
Physical Properties 250
Coding 252

RESULTS 252

CONCLUSIONS 277

INTERNAL MODEL CONTROL STRATEGY FOR TEMPERATURE CONTROL 279

EXPERIMENTAL 282
Reactor system 282
Control system 284

MATHEMATICAL MODEL 285

TRANSIENT RESPONSE 291

CONTROL STRATEGY 296
Transfer function 296
Controller design 298

PROCESS TEST 302

CONCLUSIONS 311

HEAT OF PYROLYSIS OF BITUMEN 312

NOMENCLATURE 316

FLUIDIZED BED PYROLYSIS OF OIL SANDS IN A LARGE DIAMETER REACTOR 321

INTRODUCTION 321

EXPERIMENTAL 322

RESULTS AND DISCUSSION 326
Product Distribution and Yields 326
Liquid Products Quality 333

SUMMARY AND CONCLUSIONS 340

FUTURE ACTIVITIES 341

ROTARY KILN PYROLYSIS OF OIL SANDS 343

PERFORMANCE AND CALIBRATION OF DRY MATERIALS FEEDERS WHEN FEEDING OIL SANDS 343

INTRODUCTION 343

EXPERIMENTAL 344
Feed Materials 344
Experimental Apparatus 345
Methodology 347
Preparation of feed mixtures 347
Feeder calibration procedures 347

RESULTS AND DISCUSSION 348
Feeding performance with small augers 348
Feeding performance with large augers 354

SUMMARY AND CONCLUSIONS 361

NOMENCLATURE 363

FUTURE ACTIVITIES 363

COMBUSTION OF CARBONACEOUS RESIDUES ON SPENT OIL SANDS IN ALABORATORY SCALE DENSE PHASE TRANSPORT REACTOR 364

INTRODUCTION 364

EXPERIMENTAL APPARATUS 364

HYDRODYNAMIC STUDIES 366
Fluidization and Defluidization 366
Flow Regime Transition Studies 373
Particle Residence Time Distribution Studies 377

COMBUSTION EXPERIMENT 378

CONCLUSIONS 384

NOMENCLATURE 385

FUTURE ACTIVITIES 385

SUPERCRITICAL FLUID EXTRACTION OF OIL SAND BITUMEN 386

INTRODUCTION 386

EXPERIMENTAL 386
Experimental Apparatus and Procedure 386
Solvent and Feed Stocks 387

RESULTS AND DISCUSSION 390
Extraction of Hexadecane 390
Extraction of PR Spring Bitumen 390
Pressure Effect 394
Temperature Effect 394
Extraction Product Analysis 397
Modeling the Extraction Process 402

SUMMARY AND CONCLUSIONS 406

FUTURE ACTIVITIES 408

UPGRADING UINTA BASIN OIL SANDS CATALYTIC UPGRADING OF A UINTA BASIN BITUMEN OVER A COMMERCIAL HDM CATALYST 409

INTRODUCTION 409
EXPERIMENTAL 410
Feedstock Preparation and Reactor Startup 410
Catalyst Description and Loading 410
Catalyst Sulfiding 412
Initial Catalyst Deactivation 412
Mass Balances 413
Operating Procedures 417

RESULTS AND DISCUSSION 417
Process Variable Studies 417
Effect of Space Velocity 418
Effect of Temperature 421
Effect of Pressure 423
Preliminary Process Kinetic Stud 427
Sulfur and Residuum Conversions 430

SUMMARY AND CONCLUSIONS 433

FUTURE ACTIVITIES 434

UINTA BASIN BITUMEN HYDROTREATING: A COMPARISON OF HDN AND HDM CATALYST PERFORMANCE 435

INTRODUCTION 435

EXPERIMENTAL 436

RESULTS AND DISCUSSION 439
Effect of Catalyst and Feed on Conversion 439
Effect of Catalyst and Feed on Selectivity 448
Pathways for Residuum Conversion 452

SUMMARY AND CONCLUSIONS 454

FUTURE ACTIVITIES 456

EFFECTS OF COKE ON HDM CATALYST DEACTIVATION 457

INTRODUCTION 457

EXPERIMENTAL 459
Catalysts and Chemicals 459
Coking Runs 460
Physical Properties of Catalysts 462
Activity Tests 463

RESULTS 465
Catalyst Properties 465
Catalyst Activities 470
Relative Activities 470
Temperature Effects on Conversions and Products 474
Apparent Activation Energies 474

DISCUSSION 478
Nature of Coke 478
Catalyst Deactivation 482
Temperature Effect on Activities 484

NOMENCLATURE 486

SUMMARY AND CONCLUSIONS 486

FUTURE ACTIVITIES 488

SIMILITUDE STUDIES IN THREE-PHASE EBULLIETED BED REACTORS 489

INTRODUCTION 489
Calculation of Phase Holdups 491
Development of Similarity Criteria 495
Verification of the Similarity Criteria 501
Practical Procedure for Scale-Down 503
Application at High Pressure 506
Effect of High Pressure 506
Methodology for adjusting u_{br} 508
Similarity Criteria at High Pressure 508

SUMMARY AND CONCLUSIONS 509

NOMENCLATURE 510

FUTURE ACTIVITIES 512

DEVELOPMENT STUDIES OF EQUIPMENT FOR THREE-PRODUCT GRAVITY-SEPARATION OF BITUMEN, SAND AND WATER 513

INTRODUCTION 513

RESULTS AND DISCUSSION 513
Three-Product Classifier 513
Separation of Solids by Particle Size 513
Conveying or Pumping of High Solids Concentration Sand-Water Slurries 514

SUMMARY AND CONCLUSIONS 515

FUTURE ACTIVITIES 516

TECHNICAL AND ECONOMIC COMPARISON OF BITUMEN UPGRADING OPTIONS 517

INTRODUCTION 517

RESULTS AND DISCUSSION 517
Hydropyrolysis-Hydrotreating Upgrading Option 517
Recommended Pilot Plant, Alternative 1 525
Recommended Pilot Plant, Alternative 2. 526
Recommended Pilot Plant, Alternative 3 530
Risk Analysis 532

SUMMARY AND CONCLUSIONS 532

FUTURE ACTIVITIES 534

REFERENCES 544

APPENDIX A
WHITEROCKS OIL SAND DEPOSIT BIBLIOGRAPHY 569

APPENDIX B
ASPHALT RIDGE OIL SAND DEPOSIT BIBLIOGRAPHY 573

APPENDIX C
PR SPRING OIL SAND DEPOSIT BIBLIOGRAPHY 578

APPENDIX D
SUNNYSIDE OIL SAND DEPOSIT BIBLIOGRAPHY 583

APPENDIX E
CIRCLE CLIFFS OIL SAND DEPOSIT BIBLIOGRAPHY 587

APPENDIX F
UNIVERSITY OF UTAH OIL SANDS BIBLIOGRAPHY 589
Theses and Dissertations 589
Final Reports 591
Patents 592
Publications 593

List of Tables

Table 1. Analysis of PR Spring Bitumen Samples 34

Table 2. Analysis of PR Spring Bitumen Sample from UTAR Pit Circa 1982 35

Table 3. Analysis of Native Bitumens from the PR Spring (Utah) Oil Sand Deposit 37

Table 4. Analysis of the Liquid Product from the Fluidized-Bed Pyrolysis of the PR Spring Rainbow I Oil Sand 38

Table 5. Analysis of the Liquid Product from the Fluidized-Bed Pyrolysis of the PR Spring Rainbow II Oil Sand 39

Table 6. Analysis of the Liquid Product from the Fluidized-Bed Pyrolysis of the PR Spring South Oil Sand 40

Table 7. Estimated Major Oil Sand Deposits of Utah[13]. 51

Table 8. Mineralogical Composition of the Dry and Bitumen Free Circle Cliffs Oil Sand. 56

Table 9. Comparison of Circle Cliffs Bitumen Viscosity with Those of the Uinta Basin Bitumens. 57

Table 10. A Comparision of Elemental Composities of Circle Cliffs and Uinta Basin Oil Sand Bitumens of Utah. 59

Table 11. Trends in the Sulphur Content Among the Utah Oil Sand Bitumens. 61

Table 12. Quantitative Fractional Composition of the Circle Cliffs Oil Sand Bitumen Based on SARA Type Analysis. 62

Table 13. Elemental Analyses of the Fractions Derived from Circle Cliffs Oil Sand Bitumen. 64

Table 14. Elemental Analyses of the Fractions Derived from Athabasca Oil Sand Bitumen. 65

Table 15. Fractional Compositions of Bitumens[22,32] 79

Table 16. Physical Properties of the Whiterocks Bitumen Samples[22] . . . 79

Table 17. Surface Tensions for Bitumens 87

Table 18. Comparison of Bitumen Surface Tension Calculated from i) Contact Angle Measurements, ii) Wilhelmy Plate Measurements and iii) by Critical Surface Tension Analysis (21°C) 95

Table 19. Recovery of Bitumen from Whiterocks Oil Sands 155

Table 20. Experimental Conditions 174

Table 21. Physical Parameters 181

Table 22. Steady State Mass Balance for 2000 Tons Per Day of Whiterocks Oil Sand Pilot Plant 197

Table 23. Steady State Energy Balance (Heat Units/Hour) for 2000 Tons Per Day Whiterocks Oil Sand Pilot Plant 203

Table 24. Cost of Chemicals for 100 tpd of Oil Sand Pilot Plant 207

Table 25. First-order Kinetic Rate Constants 234

Table 26. Stoichiometric Constants 235

Table 27. Physical Characteristics of Pseudo-Components 236

Table 28. Base-Case Simulation Parameters 254

Table 29. Best Fit for Adjustable Model Parameters-Combustion Bed Only 255

Table 30: Comparison of the Predicted and Calculated Values of the Heat of Combustion. 314

Table 31. Summary of Product Distributions 327

Table 32. Whiterocks Oil Sands Pyrolysis Products Yields at 773 K . . . 329

Table 33. Whiterocks Oil Sands Pyrolysis Gas Product Yields at 773 K . 331

Table 34. Reduced Pressure Pyrolysis Gas Product Yields Using Whiterocks Oil Sands 333

Table 35. Pour Point of Liquid Products 335

Table 36. Asphaltene Content of Liquid Products 335

Table 37. Conradson Carbon Residue of Liquid Products 336

Table 38. Viscosity and API Gravity of Strainer #2 Liquids 336

Table 39. Calculated Specific Gravity of Liquid Products 337

Table 40. Bitumen Saturation and Moisture Content of Oil Sand Samples Used For Feeder Calibration Studies 345

Table 41. Feeder and Auger Designations 347

Table 42. Statistical Analysis of Average Feed Rates 351

Table 43. Statistical Data for Fresh Mixture Sample Feeding at 70% Speed 355

Table 44. Statistical Data for Used Mixture Feeding at 70% Speed . . . 359

Table 45. Statistical Data for 100% Whiterocks Oil Sand Feeding . . . 359

Table 46. Statistical Data for 100% PR Spring Oil Sand Feeding 361

Table 47. Comparison of Elemental Analysis of Coked Sand and Burnt Sand 382

Table 48. Chemical and Physical Properties of the PR Spring Bitumen . . 389

Table 49. Measured Densities of Propane 394

Table 50. Pseudocomponents for PR Spring Bitumen 405

Table 51. Predicted Properties for Pseudocomponents Using Lee-Kesler Correlations 405

Table 52. Properties of Bitumen and Hydrotreated Total Liquid Product 411

Table 53. Experimental Sequence Performed In This Study 414

Table 54. Effect of WHSV on the Properties of the Hydrotreated Total Liquid Products 419

Table 55. Effect of Temperature on the Properties of the Hydrotreated Total Liquid Products 422

Table 56. Effect of Pressure on the Properties of the Hydrotreated Total Liquid Products 425

Table 57. Analysis of the Whiterocks Bitumen and Bitumen-Derived Liquid 437

Table 58. Properties of the HDN and HDM Catalysts 438

Table 59. Base-Case Conditions and Process Variable Ranges 439

Table 60. Effect of Catalyst Selection on the Product Properties of the Hydrotreated Bitumen from the Whiterocks Oil Sand Formation 441

Table 61. Properties of Whiterocks Bitumen 460

Table 62. HDM Catalyst Coking Conditions 461

Table 63. Properties of Aged Catalysts 466

Table 64. Analysis of Pore Volume and Surface Area Data 469

Table 65. Validation of the Generalized Wake Model 496

Table 66. General Similarity: Six Dimensionless Groups Held Constant . 502

Table 67. Practical Similarity: Two Reduced Similarity Criteria Satisfied 507

Table 68. Results of Profitability Analysis for the Hydropyrolysis-Hydrotreating Upgrading Option 519

Table 69. Summary of the Profitability Analysis of Oil Sands Upgrading Process Options 521

Table 70. Case Study of the Split Ratio in S-1 (S036 T = 668 K) 522

Table 71. Results of Availability Analysis 525

Table 72. Results of Case Study in which Temperature of S036 was Varied (Split ratio in S-1 = 0.15) 526

Table 73. Results of Availability Analysis of Alternative 1 528

Table 74. Results of Availability Analysis of Alternative 2 531

Table 75. Results of Availability Analysis of Alternative 3 534

Table 76. Summary of the Results of Profitability Analysis for Alternatives 1 through 3 535

Table 77. The Expectations and Standard Deviations used in Risk Analysis 537

List of Figures

Figure 1. Location Site Map University of Utah 15

Figure 2. General Geology Map of the PR Spring Oil Sand Deposit 26

Figure 3. Oil Impregnated Zone A in the Douglas Creek Member, PR Springs Oil Sand Deposit 28

Figure 4. Oil Impregnated Zone B in the Douglas Creek Member, PR Springs Oil Sand Deposit 29

Figure 5. Oil Impregnated Zone C in the Douglas Creek Member, PR Springs Oil Sand Deposit 30

Figure 6. Oil Impregnated Zone D in the Douglas Creek Member, PR Springs Oil Sand Deposit 31

Figure 7. Oil Impregnated Zone E in the Parachute Creek Member, PR Springs Oil Sand Deposit 32

Figure 8. Sample Locations from the PR Spring Oil Sand Deposit 36

Figure 9. Stratigraphic Section Underlying the Enercor Site on the PR Springs Oil Sand Deposit. 47

Figure 10. Variation of Circle Cliffs Bitumen Viscosity with Temperature. 58

Figure 11. Infrared Spectrum of the Saturates Fraction of the Circle Cliffs Bitumen. 66

Figure 12. Infrared Spectrum of the Aromatics-I Fraction of the Circle Cliffs Bitumen. 68

Figure 13. Infrared Spectrum of the Resin-I Fraction of the Circle Cliffs Bitumen. 69

Figure 14. Infrared Spectrum of the Asphaltene Fraction of the Circle Cliffs Bitumen. 71

Figure 15. Illustration of the Dynamic Surface Tension Measurements. . . . 81

Figure 16. Effect of Temperature on the Surface Tension of Whiterocks Bitumen 85

Figure 17. Contact Angle Data for Water Drops Placed on the Bitumen Film Formed from the Bitumen-in-toluene Mixture (Curve 1: Thickness of Bitumen Film <1 μm), and from the Bitumen Mechanically Spread on Glass Slide (Curve 2: 5 μm, Curve 3: 0.2 mm) 89

Figure 18. Dynamic Surface Tension of Water, Glycerol, Formamide, Ethylene Glycol, and Diiodomethane, in Contact with Bitumen Drop 91

Figure 19. Determination of the Critical Surface Tension of Wetting of the Whiterocks Bitumens Using Methanol-Water Solutions . . . 100

Figure 20. Determination of the Dispersion Component of the Surface Tension of Whiterocks Bitumen 103

Figure 21. Dynamic Interfacial Tension for the Bitumen/Aqueous Phase Systems (Subscripts 'i' and 'f' Correspond to Initial pH Value of Aqueous Phase and that Measured After Experiment, Respectively) 106

Figure 22. Effect of pH on the Interfacial Tension of Whiterocks Bitumen as Determined by the Wilhelmy Plate Technique 109

Figure 23. Effect of $Na_5P_3O_{10}$ and NaCl Concentration on Interfacial Tension for the Bituminous/Aqueous Phase Systems; Presented as a Function of Salt (A) or Sodium Ion (B) Concentration . . . 111

Figure 24. Effect of Temperature on the Interfacial Tension for the Bitumen/Aqueous Phase System, Measured at Various pH Values . 114

Figure 25. Effect of pH on the Temperature Coefficient of the Bitumen/Aqueous Phase Interfacial Tension 115

Figure 26. Zeta Potential of Whiterocks Bitumen Dispersed in Aqueous Solutions of $Na_5P_3O_{10}$ and NaCl ($1 \cdot 10^{-3}$M) with Varying pH . . . 117

Figure 27. Effect of $Na_5P_3O_{10}$ and NaCl Concentration on the Zeta Potential of Bitumen Droplets; Presented as a Function of Salt (A) and Sodium Ion (B) Concentration 119

Figure 28. Experimental Set-up Used for Stagnant Digestion of Oil Sand. 1 - Oil Sand; 2 - Aqueous Phase; 3 - Bitumen; 4 - Air/Gas Phase; 5 - to Vacuum; 6 - Digestion Vessel; 7 - Hot Plate; 8 - Funnel; 9 - Microscope with Photo Camera or Video Camera; 10 - Photo Camera; 11 - Sensors (pH, Temperature, In Situ IR Spectr.); 12 - Cell with Flat Wall; 13 - Calibrated Tube Composed of Segments; 14 - Magnifying Lens; 15 - Transparent Tubing Joining Tube Segments 126

Figure 29. Stagnant Digestion of PR Spring Oil Sand Pretreated with Kerosene. 131

Figure 30. Postulated Mechanism of Oil Sand Digestion for Water-Based Processing of Oil Sand. (A) Oil Sand Prior Digestion; (B) Oil Sand after Treatment with Diluent; (C) Initial Stage of Digestion, Bitumen has Retracted to Pores, Some Gas Bubbles are Released; (D) Later Stage of Digestion, Bitumen is Displaced from Pores of Consolidated Oil Sand; (E) Later Stage of Digestion - Bitumen is Displaced from Pores of Unconsolidated Oil Sand; Oil Sand Aggregate Falls Apart. White - Mineral; Blue - Gas; Green - Aqueous Phase; Black - Bitumen 133

Figure 31. Illustration of Mechanisms of Bitumen Release from Whiterocks Oil Sands as Observed by Stereoscopic Microscopy 142

Figure 32. The Receding Contact Angle Measured for Bitumen (Containing 10 wt% Kerosene) Drops at Particle Surfaces and the Calculated Bitumen-Solid Work of Adhesion for Varying pH Values 144

Figure 33. The receding Contact Angle Measured for Bitumen (10 wt% Kerosene) Drops at Particle Surfaces and the Calculated Bitumen-Solid Work of Adhesion for Varying $Na_5P_3O_{10}$ Concentration 145

Figure 34. The Receding Contact Angle Measured for Bitumen (10 Wt% Kerosene) Drops at Particle Surfaces and the Calculated Bitumen-Solid Work of Adhesion for Varying NaCl Concentration 146

Figure 35. Spreading Coefficient of Bitumen (10 Wt% Kerosene) at the Water Surface 149

Figure 36. Spreading Coefficient of Bitumen (10 Wt% Kerosene) at the Water Surface for Varying $Na_5P_3O_{10}$ Concentration 150

Figure 37. Spreading Coefficient of Bitumen (10 Wt% Kerosene) at the Water Surface for Varying NaCl Concentration 151

Figure 38. Relationship Between Bitumen Recovery from Gravity Separation and the Bitumen (10 Wt% Kerosene)/Process Water Interfacial Tension 156

Figure 39. The Size Distribution for Air Bubbles Leaving the ASH in the Underflow as a Function of MIBC Concentration, Measurements Were Made for 5 cm Diameter, 16 cm Long ASH 165

Figure 40. Average Bubble Size in the Underflow as a Function of MIBC Concentration for 5 cm ASH and 15 cm ASH Units of Different Lengths (l) and Different Dimensionless Flowrate Ratios (Q^*) 167

Figure 41. Average Bubble Size in the Underflow as a Function of the Dimensionless Flowrate Ratio (Q^*) for 5 cm ASH and 15 cm ASH Units of Different Lengths (L) and for Different MIBC Concentrations 170

Figure 42. Influence of the Second pi Group on pi Group 1 182

Figure 43. Influence of the Third pi Group on pi Group 1 183

Figure 44. Influence of the Fifth pi Group on pi Group 1 184

Figure 45. Influence of the Sixth pi Group on pi Group 1 186

Figure 46. Oil Sand Dissolution Map Based upon pi Groups 2 and 5 187

Figure 47. Oil Sand Dissolution Map Based upon pi Groups 3 and 5 188

Figure 48. Pilot Plant Flow Chart for Bitumen Recovery from Utah Oil Sands 192

Figure 49. Block Diagram of Hot Water Separation Process for Bitumen Recovery from Oil Sands 205

Figure 50. Schematic Diagram of Coupled Thermal Fluidized-bed Oil Sands Extraction Process. 211

Figure 51. Run with Clean Sand (Pyrolysis Pressure Drop Oscillates) . . 218

Figure 52. Run with Clean Sand 220

Figure 53. Some Typical Experimental Oil Yields from Fletcher[134] and Smart[127] 222

Figure 54. First-order Rate Constants Used to Model Bitumen Thermal Pyrolysis as a Function of Temperature. 231

Figure 55. Flow Chart of Pyrolysis-bed Model. 253

Figure 56. Predicted Product Yields of Bitumen Pyrolysis as a Function of Pyrolysis Temperature; $\bar{t}_p$= 20 min. 256

Figure 57. Predicted Oil Yields and Condensed Oil Density from Bitumen Pyrolysis as a Function of Pyrolysis Temperature; $\bar{t}_p$ = 20 min. 257

Figure 58. Predicted Oil Yield as a Function of Pyrolysis Temperature and Average Solids Residence Time. 258

Figure 59. Predicted Oil Yield as a Function of Pyrolysis Temperature and Average Solids Residence Time. 259

Figure 60. Predicted Oil Density as a Function of Pyrolysis Temperature and Average Solids Residence Time. 260

Figure 61. Predicted Oil Density as a Function of Pyrolysis Temperature and Average Solids Residence Time. 261

Figure 62. Predicted Light Gas Yield as a Function of Pyrolysis Temperature and Average Solids Residence Time. 262

Figure 63. Predicted Yield of Coke + Unreacted Bitumen as a Function of Pyrolysis Temperature and Average Solids Residence Time. . . 263

Figure 64. Predicted Coke Yield and Bitumen Conversion as a Function of Pyrolysis Temperature and Average Solids Residence Time. . . 266

Figure 65. Predicted Oil Yield and Density as a Function of Pyrolysis Temperature and Fluidizing-Gas Flow Rate; $\bar{t}_p$= 20 min. 267

Figure 66. Predicted Bed Height as a Function of Oil-Sand Feed Rate, Pyrolysis Temperature, and Average Solids Residence Time. . . 268

Figure 67. Predicted Oil Yield as a Function of Oil-Sand Feed Rate, Pyrolysis Temperature, and Average Solids Residence Time. . . 269

Figure 68. Predicted Oil Density as a Function of Oil-Sand Feed Rate, Pyrolysis Temperature, and Average Solids Residence Time. . . 270

Figure 69. Predicted Bitumen Conversion as a Function of Oil-Sand Feed Rate, Pyrolysis Temperature, and Average Solids Residence Time. 271

Figure 70. Predicted Oil Yield as a Function of Bitumen Quality and Pyrolysis Temperature; $\bar{t}_p$= 20 min. 273

Figure 71. Predicted Oil Yield as a Function of Pyrolysis Temperature and Average Solids Residence Time; w_{HBO} = 0.05. 275

Figure 72. Predicted Oil Yield as a Function of Pyrolysis Temperature and Average Solids Residence Time; w_{HBO} = 0.75. 276

Figure 73. Experimental Apparatus and Instrumentation. 283

Figure 74. Temperature Responses for Slowly Heating the Combustion Bed from Ambient Temperature. 287

Figure 75. Schematic Representation of the Reactor System for an Energy Balance. 288

Figure 76. Comparison of Three Models with Experimental Results. 294

Figure 77. Comparison of Model 3 to Experimental Results for Step Increases in Electrical Power. 295

Figure 78. Temperature Responses to the Setpoint Changes of PID Controllers that are Tuned by IMC Strategy with τ_c = 6 min. . 303

Figure 79. Temperature Responses to the Setpoint Changes of PI Controllers that are Tuned by IMC Strategy with τ_c = 6 min. . 305

Figure 80. Temperature Responses to the Setpoint Changes of PI Controllers that are Tuned by IMC Strategy with τ_c = 40 min. 307

Figure 81. Temperature Responses to the Setpoint Changes of PI Controllers that are Tuned by IMC Strategy with τ_c = 0.5 min. 308

Figure 82. Temperature Responses to the Setpoint Changes of PI Controllers that are Tuned by IMC Strategy with τ_c = 6 min.; Sand Holdup in Combustion Bed = 7.2 kg. 310

Figure 83. Process Flow Diagram 324

Figure 84. Pressure Description for Push and Pull Configurations 325

Figure 85. Liquid Product Yield vs Temperature for Recovery Streams . . 334

Figure 86. Simulated Distillation Cuts versus Temperature 339

Figure 87. Acrison Dry Materials Feeder Schematic 346

Figure 88. Cumulative Weight Delivered Vs. Time for BDF-1.0 D Auger Using 100% Whiterocks Oil Sands 349

Figure 89. Average Feed Rate Vs. Time for 105Z-D feeder using 100% Whiterocks Oil Sand 350

Figure 90. Average Feed Rate Vs. Time for 105Z-D Feeder Using Oil Sands and Spent Sands Mixtures at 70% Speed
a--Fresh Sample; b--Reused Sample 352

Figure 91. Moisture Content Effect on Feed Rate from a BDF-1.5 Feeder (H-Auger Using 100% Whiterocks Oil Sands) 356

Figure 92. Average Feed Rate vs. Time for 105Z-G Feeder Using 100% Whiterocks Oil Sands 357

Figure 93. Average Feed Rate vs. Time for 105Z-G Feeder Using 100% PR Spring Oil Sands; a--Refill Point 358

Figure 94. Feed Rate vs. Motor Speed (%) for 105Z-G Feeder Using 100% Oil Sands 360

Figure 95. Schematic of the Dense Phase Transport Reactor Apparatus . . 365

Figure 96. Reactor Schematic 367

Figure 97. Typical Bed Pressure Drop vs. Gas Superficial Velocity . . . 368

Figure 98a. Pressure Drop vs. Air Superficial Velocity 370

Figure 98b. Pressure Drop vs. Air Superficial Velocity 371

Figure 99. Fluidization Pressure Drop vs. Superficial Velocity 372

Figure 100. Pressure Drop vs Operation Time and Air Superficial Velocity 375

Figure 101. Standard Deviation of Pressure vs Air Superficial Velocity . 376

Figure 102. Tracer Concentration vs Residence Time 379

Figure 103. Coked Sand and Tracer Particle Size Distribution Comparison . 380

Figure 104. Tracer Concentration vs Residence Time 381

Figure 105. Temperature Variation vs Time 383

Figure 106. Schematic of Supercritical Fluid Extraction System 388

Figure 107. Carbon Number Distribution for PR Spring Bitumen 391

Figure 108. Reproducibilty of SFE of PR Spring Bitumen by Propane at a P_r of 3.8(P=17.3 MPa) and a T_r of 1.03 (T=380 K) 392

Figure 109. Operating Conditions for SFE of PR Spring Bitumen by Propane 393

Figure 110. Effect of Pressure on SFE of PR Spring Bitumen by Propane at a T_r of 1.03 (T=380 K) 395

Figure 111. Effect of Temperature on SFE of PR Spring Bitumen by Propane at a P_r of 2.3 (P=10.4 MPa) 396

Figure 112. Effect of Solvent Density on Extraction Yield for PR Spring Bitumen by Propane 398

Figure 113. Simulated Distillation Analyses of SFE of PR Spring Bitumen by Propane at a P_r of 2.3(P=10.4 MPa) and a T_r of 0.92 (T=339 K) 399

Figure 114. Effect of Pressure on Asphaltene Content of Residual Fractions from SFE of PR Spring Bitumen by Propane at a T_r of 1.03 (T=380 K) 400

Figure 115. Effect of Temperature on Asphaltene Content of Residual Fractions from SFE of PR Spring Bitumen by Propane at a P_r of 2.3 (P=10.4 MPa) 401

Figure 116. Effect of Pressure on H/C Atomic Ratio of Residual Fractions from SFE of PR Spring Bitumen by Propane at a T_r of 1.03 (T=380 K) 403

Figure 117. Effect of Temperature on H/C Atomic Ratio of Residual Fractions from SFE of PR Spring Bitumen by Propane at a P_r of 2.3 (P=10.4 MPa) 404

Figure 118. Comparison of Experimental and Predicted Bitu-men Extracted Phase Compositions for Extrac-tion of PR Spring Bitumen by Propane at a P_r of 2.3 (P=10.4 MPa) and a T_r of 0.92(T=339 K) 407

Figure 119. Total Liquid Product API Gravities 415

Figure 120. Typical Catalyst Temperature Profile in Upflow Operation . . 416

Figure 121. Effect of WHSV on Product Distribution and Yields at 664 K and 13.7 MPa 420

Figure 122. Effect of Temperature on Product Distribution and Yields at 0.76 H^{-1} WHSV and 13.7 MPa 424

Figure 123. Pressure versus Hydrogen Consumption at 0.76 H^{-1} WHSV and 664 K 426

Figure 124. First Order Kinetic Plot for Nitrogen, Sulfur, and CCR Conversion over an HDM Catalyst 428

Figure 125. Hydrogen Partial Pressure Dependence for Nitrogen, Sulfur and CCR Conversion over an HDM Catalyst 431

Figure 126. Comparison of Sulfur and Residuum Conversions as a Function of Process Variables 432

Figure 127. Residuum Content vs API Gravity for the BDL-HDN, the BIT-HDN and the BIT-HDM Studies. 442

Figure 128. Arrhenius Plot for Whole Residuum Conversion. 443

Figure.129 Nitrogen Content vs API Gravity for the BDL-HDN, the BIT-HDN and the BIT-HDM Studies. 446

Figure 130. Sulfur Content vs API Gravity for the BDL-HDN, the BIT-HDN and the BIT-HDM Studies. 447

Figure 131. Residuum, Nitrogen and Sulfur Remaining in Samples Hydrotreated in the BDL-HDN Study. 449

Figure 132. Residuum, Nitrogen and Sulfur Remaining in Samples Hydrotreated in the BIT-HDN Study. 450

Figure 133. Residuum, Nitrogen and Sulfur Remaining in Samples Hydrotreated in the BDL-HDM Study. 451

Figure 134. Naphthalene and Indole Reaction Networks 464

Figure 135. Pore Size Distributions of the Sulfided and the BIT-4 Coked (11.1 wt% C) Catalysts 468

Figure 136. Relative Hydrogenation Activities versus wt% C for the Anthracene-, Bitumen-, and Bitumen/NiTPP-coked Catalysts (623 K) 471

Figure 137. Relative Carbon-Nitrogen Hydrogenolysis Activity versus wt% C for the Anthracene-, Bitumen-, and Bitumen/NiTpp-coked Catalysts (623 K) 472

Figure 138. Relative Hydrodenitrogenation Activity versus wt% C for the Anthracene-, Bitumen-, and Bitumen/NiTpp-Coked Catalysts (623 K) 473

Figure 139. Conversion versus Temperature for the Sulfided Catalyst Hydrogenation □; Carbon-Nitrogen Hydrogenolysis ○; and Hydrodenitrogenation △. 475

Figure 140. Conversion versus Temperature for the BIT-4 Coked Catalyst Hydrogenation □; Carbon-Nitrogen Hydrogenolysis ○; and Hydrodenitrogenation △. 476

Figure 141. Tetralin Mole Fraction versus Temperature for the Sulfided and BIT-4 Coked Catalysts 477

Figure 142. Apparent Hydrogenation Activation Energy versus wt% C . . . 479

Figure 143. Apparent Carbon-Nitrogen Hydrogenolysis Activation Energy versus wt% C 480

Figure 144. Flow Diagram of Hydropyrolysis-Hydrotreating Upgrading Option 518

Figure 145. Flow Diagram of the Hydropyrolysis-Hydrotreating Upgrading Option 523

Figure 146. Flow Diagram of Hydropyrolysis-Hydrotreating Upgrading Option Alternative 1 527

Figure 147. Flow Diagram of Hydropyrolysis-Hydrotreating Upgrading Option, Alternative 2 529

Figure 148. Flow Diagram of Hydropyrolysis-Hydrotreating Upgrading Option, Alternative 3 533

Figure 149. The Difference in Flowsheets of Alternatives 1, 2, and 3 . . 536

Figure 150. Probability Density Distribution Histogram of Internal Rate of Return (%) (Alternative 1, Internal Rate of Return mode) . . 538

Figure 151. Probability Density Distribution Histogram of Initial Product Price ($/lb) (Alternative 1, Product Price Mode) 539

Figure 152. Probability Density Distribution Histogram of Internal Rate of Return (%) (Alternative 2, Internal Rate of Return mode) . . 540

Figure 153. Probability Density Distribution Histogram of Initial Product Price ($/lb) (Alternative 2, Product Price Mode) 541

Figure 154. Probability Density Distribution Histogram of Internal Rate of Return (%) (Alternative 3, Internal Rate of Return mode) . . 542

Figure 155. Probability Density Distribution Histogram of Internal Rate of Return (%) (Alternative 3, Internal Rate of Return mode) . . 543

EXECUTIVE SUMMARY

Principal Investigator: A.G. Oblad

The Oil Sand Research and Development Group at the University of Utah revised and updated the environmental assessment of the impact of projected program-related activities for the 1992-1993 contract period in accordance with the requirements of the National Environmental Policy Act.

The characterization of the Asphalt Ridge bitumen was continued and that of the PR Spring and Circle Cliffs oil sands were undertaken during the 1992-1993 contract period. Drum quantity samples of mined ore were obtained from the PR Spring oil sand deposit for process studies. The Sunnyside oil sand deposit was reconnoitered for sample acquisition during 1993-1994 contract period. The Circle Cliffs oil sand bitumen and mineral matter have been characterized. The effect of mineral composition on bitumen recovery, and the quality of the bitumen product that can be expected from the modified hot-water process are discussed. The influence of chemical composition on bitumen viscosity is discussed with respect to the previously reported empirical relationship between the carboxylic acid content and the viscosity of the bitumen.

The 1992/93 oil sand research program for water-based separation technology focused on the fundamental aspects of digestion/separation and on process engineering as required for process scale-up and pilot plant installation. The investigations have demonstrated the importance of surface and interfacial tension effects as well as colloid chemistry effects during modified hot-water processing. Based on the results from our process development work and fundamental studies, it is evident that the modified hot-water process is now ready for pilot plant level operation. A complete flow sheet has been prepared with heat and material balances of the principal steps in the process. Major results obtained during the 1992-1993 contract period pertain to oil sand and bitumen characterization and the development of processing steps such as digestion, separation of phases, and bitumen concentrate clean-up.

The surface and interfacial tension data for bitumen recovered from the Whiterocks oil sands are reported. Experimental data from direct measurements of bitumen surface tension using the Wilhelmy plate method are compared with surface tensions calculated from

Neumann's equation-of-state using contact angle measurements and with Zisman's critical surface tension of wetting. Further, interfacial tension data, which were measured at several temperatures and for varying pH and electrolyte concentration (NaCl, $Na_5P_3O_{10}$) are presented. Finally, zeta potentials at the bitumen/water interface are reported for varying pH and electrolyte concentration (NaCl, $Na_5P_3O_{10}$). These experimental data are further used for the explanation and understanding of the bitumen disengagement mechanism.

A new experimental technique for the study of bitumen release from oil sand under stagnant digestion conditions is proposed and the first experimental data are described and discussed. The new stagnant digestion laboratory setup allows simultaneous determination of physical and surface properties of the system, such as the oil sand natural porosity, the wetting ability of the aqueous phase based on the kinetics of air and bitumen displacement from the oil sand, the droplet size of released bitumen, the bitumen-bitumen droplet coalescence time, the extent of bitumen dilution (when diluent was used), the size and electrophoretic mobility of particulates released from the oil sand sample to the aqueous phase, and in-situ IR analysis.

The bitumen release from mineral particle surfaces under stagnant conditions was observed through a microscope for unconsolidated samples of the Whiterocks oil sand and mechanisms of bitumen separation from the mineral surface are discussed with respect to surface/interfacial tension data. The spreading coefficient for bitumen at the water surface was calculated from surface/interfacial tension data to be positive for all pH values of practical significance, and for all $Na_5P_3O_{10}$ and NaCl concentrations considered. The work of adhesion between bitumen droplets and coarse mineral particles of oil sands was calculated and found to depend on the concentration of reagents (Na_2CO_3, $Na_5P_3O_{10}$, NaCl). It is shown that the work of adhesion between bitumen/mineral particle surface and the spreading coefficient for bitumen at the air bubble surface, depend upon the bitumen/water interfacial tension. Thus, in addition to bitumen viscosity considerations, interfacial tension plays an important role in hot-water processing of oil sands. It is demonstrated by the results of hot-water experiments that enhanced separation of bitumen from Whiterocks oil sands may be achieved by control of the bitumen/water interfacial tension which should be less than 2-3 mNm^{-1}. A somewhat reduced but satisfactory separation efficiency was found when the interfacial tension was in the range 4 to 7 mNm^{-1}.

As reported previously, the high specific capacity air-sparged hydrocyclone (ASH), at least 100 times greater than conventional flotation equipment, could offer some advantages for residual bitumen recovery from rougher tailings. A high separation efficiency was achieved with respect to small, free bitumen droplets, while bitumen-sand aggregates reported to the underflow product, (1990/91 Final Report). It was concluded from preliminary experiments that the bubble size may affect the efficiency of bitumen droplet separation from the hot-water process tailings stream. In the current studies, high-speed photography was used to examine the nature of bubble formation in the swirl flow of the ASH and the corresponding bubble size distributions. On this basis, it is expected that these fundamental measurements will help to establish design features and operating conditions for efficient flotation separations of dispersed bitumen from tailings water.

The bitumen concentrate produced in the hot-water process contains a significant amount of water along with residual sand particles. An organic solvent like kerosene needs to be added to the bitumen concentrate in order to reduce the bitumen viscosity and facilitate separation of fine mineral particles and dispersed water. An important part of the bitumen clean-up directly depends on the kinetics of the bitumen concentrate dissolution in kerosene. The Whiterocks oil sand bitumen concentrate originating from the hot-water separation experiments was dissolved in kerosene prior to removal of dispersed water and fine mineral particles, and results of the kinetics of dissolution of bitumen concentrate in kerosene are presented. It was observed that dissolution of bitumen in kerosene can be rendered into a very fast process with a judicious use of the dissolution maps presented in this work.

The process flow sheet for the hot-water separation process as well as preliminary mass and energy balances for both 100 and 2000 tpd oil sand pilot plants are presented. A processing strategy which requires less energy and which leads to higher grade bitumen concentrates and higher bitumen recovery has been developed. The processing strategy is based on four features: 1) feed preparation, involving size reduction and pretreatment with diluent; 2) bitumen separation from sand, achieved by digestion, gravity separation, and flotation; 3) tailings disposal and water recycle; and 4) bitumen concentrate clean-up and solvent recycle. This water-based process development has been aided by fundamental research on the surface chemistry of bitumen-sand mixtures, the natural porosity of the oil sands accessible by various hydrocarbon diluents, the identification of natural surfactants released from the bitumen during processing, and the FTIR microscopic studies of oil sands,

as well as laboratory-scale experiments of bitumen separation from Utah oil sands. Based on the results from process development work, it is concluded that the modified hot-water process proposed by the University of Utah is now ready for pilot plant testing.

Preliminary studies with a blend of sand, water and plastic platelets to simulate the sand, water and bitumen feed stream were conducted in a laboratory scale three-product separator. The results were encouraging. Ninety nine plus % of plastic platelets used to simulate the bitumen were recovered in the overflow and middlings product streams.

Specifications for a 3-product classifier for use at the North Salt Lake pilot plant have been established and plans for assembling, installing and testing the equipment have been developed. Representative sample material will be obtained from the pilot plant studies which will permit the testing of three-product classifiers and two product cyclones and at the same time develop proper sample material for flocculation and thickening of fine solids products.

Precise temperature control of a coupled two-reactor system is difficult because of a relatively large thermal interaction and the nonlinear nature of the process. Controllers must account for the thermal coupling effect and the effect of changing operating conditions on the controller design to control the reactor temperatures precisely. The coupled fluidized-bed study shows that the internal model control strategy provides a means to directly use process knowledge and a process model to make a control decision. However, the major drawback of the internal model control tuning technique is that it is difficult to determine the optimal value of its only tuning parameter, τ_c. Even though some typical τ_c values have been suggested before, this study shows those recommended values might not be appropriate for the process investigated here. Instead, the relative gain array was used in this study to help determine the proper τ_c value, which provides a simple approach to extend the internal model control strategy to multi-input/multi-output systems.

A 15.2 cm diameter fluidized-bed reactor was designed, built, and operated to study the pyrolysis of oil sands at pressures slightly less than ambient. Fluidizing gas flow through the reactor was caused by reducing the pressure above the bed with a gas pump operating in the vacuum mode. Pyrolysis energy was supplied by a propane burner, and the hot propane combustion gases were used to fluidize the bed.

The fluidized bed pyrolysis at reduced pressure using combustion gases allowed the reactor to be operated at significantly lower temperatures than previously reported for equivalent liquid yields. At 723 K over 80 wt% of the bitumen fed was recovered as a liquid product, and the spent sand contained less than 1 wt% coke. The liquid product recovery system, by design, yielded three liquid streams with distinctly different properties.

As a result of the pyrolysis experiments with Whiterocks oil sands, modifications to the reactor heating system were required. A new burner system using refractory materials was designed. Pyrolysis of Whiterocks oil sands in a combustion gas environment led to the following conclusions:

1. Pyrolysis of bitumen would appear to give higher liquid yields, and make less gas and coke (carbonaceous residue), when compared to previous ambient pressure, nitrogen fluidization, studies. Maximum liquid products were produced when the pyrolysis temperature was 748 K.

2. There was no new evidence to suggest that U/U_{mf} has any influence on product yields for the ratios investigated.[134]

3. In contrast to previous observations by Wang,[172] residence times from 29 to 70 minutes were found to give similar yields and product distributions.

4. Hot combustion gases from a propane (LPG) burner, regulated to avoid excess oxygen, can be used to fluidize the spent sand as part of the fluidized bed pyrolysis of oil sands.

5. This work has verified the observation of previous workers using TGA that bitumen pyrolysis rates peak at temperatures below 775 K.[144] It has also provided experimental evidence that, when coke formation is suppressed, increased liquid yields are favored over increased gas yields at pyrolysis temperatures below 775 K.

Continuous, reproducible solids feeding has been a problem associated with oil sands surface mining-recovery process development studies. Commercial Acrison bin-discharge feeders were tested for oil sand feeding in rotary kiln and fluidized bed

pyrolysis reactors and in spent sand combustion reactors. Feeder calibration experiments were conducted using spent sands, oil sands and mixtures of fresh and spent sands. Three types of feeder, nine different sized augers, and three different auger types were tested. Experimental data included average feed rates and cumulative weight delivered from the feeder. The factors which were determined to affect oil sands feeding were: (1) bitumen content of the oil sand, (2) moisture content of the oil sand, (3) temperature rise in the auger and auger housings during the operation of the feeder, (4) auger rotation speed which was controlled by motor speed controller, (5) level of oil sand in the feeder hopper, (6) auger size and type, (7) ratio of spent sand to oil sand in the feed mixture, and (8) effect of shear in the auger and auger housing. A larger size auger running at low speed with a water jacketed auger housing gave the best feeding performance.

The successful application of an auger-type dry materials feeder for feeding oil sands to a process reactor or vessel requires careful consideration of the following findings:

1. Fast auger speeds did not give constant or reproducible feed rates.

2. Small diameter augers are less likely to give constant oil sands feed rates than large-diameter augers.

3. Dilution of the oil sands with spent sands improved feeder performance, however, small diameter augers still did not give constant feed rates.

4. Compaction of oil sand feed in the hopper appeared to temporarily increase feed rates with small augers.

5. Oil sand feed rates are directly proportional to the oil sand moisture content (on an air-dry basis).

6. Reducing the clearance between the feed auger and auger housing with a sleeve did not improve the feeder performance with oil sands.

7. A helical auger offers no advantage in feeder performance using oil sands.

8. Augers with special coatings gave no significant improvement with regard to reducing the tendency of the oil sands to adhere to the auger flights.

9. Large diameter augers, running at slow speeds and low temperatures, are most likely to yield linear and reproducible feed rates.

Based on the theory and practice of circulating fluidized bed combustors, a laboratory scale dense phase transport reactor has been designed and constructed for the study of combustion of carbonaceous residues on spent or coked sand. Both hydrodynamic and combustion experiments have been conducted with the reactor. Fluidization and defluidization experiments gave a minimum fluidization velocity of 1.7 cm/s which is close to the predicted minimum fluidization velocity of 1.5 cm/s. The transition velocities were determined in flow regime transition studies: (a) plug slugging (U_{ms}) = 20 cm/s; (b) turbulent fluidization (U_c) = 50 cm/s; and (c) refluxing pneumatic transport (U_k) = 75 cm/s. Particle residence time distribution experiments indicated that the fine particles tend to bypass the bed especially at higher superficial gas velocities which negatively impacts the combustion efficiency. The initial combustion experiment gave a combustion efficiency of 54% at an equivalence ratio of 0.56 which indicated that longer combustion residence times in the combustion zone are required. Type I and Type II curves were observed for the multisized coked sand under both fluidization and defluidization conditions.

The supercritical fluid extraction of bitumen from the PR Spring oil sand deposit (Utah) was studied using commercial propane as the solvent. The bitumen volatility (<617 K) was 36.3 wt % and its asphaltene content was 19.3 wt %. Experiments were performed at five different operating conditions which included three pressures (5.6 MPa, 10.4 MPa and 17.2 MPa) and temperatures (339 K, 380 K and 422 K) .

The extracted phase yield increased as the extraction pressure increased at constant temperature. This effect was directly related to the increase in the pure solvent density with pressure. It was also observed that at higher extraction pressures, relatively heavier hydrocarbons were extracted. The asphaltene content of the residual fraction was compared with the asphaltene content of the bitumen and was observed to be higher, even on an absolute weight basis.

The extraction process was modeled using the Peng-Robinson cubic equation of state and Lee-Kesler pseudocomponent characterization correlations. The experimental extraction results

were in reasonable agreement with the predicted phase compositions based on a flash calculation using seven pseudocomponents.

Pure solvent density was the governing factor for the extraction of PR Spring bitumen with propane. The extraction yield increased with an increase in pure solvent density. The asphaltene content of the residual fractions was higher than the original bitumen on an absolute basis assuming all the asphaltene stayed in the residue. This indicates the depletion of cosolubilizing agents during the extraction process. The H/C ratio of the residual fractions was lower than the original bitumen, thus establishing that paraffinic and naphthenic hydrocarbons were preferentially extracted leaving the residue richer in aromatic compounds. Reasonable agreement between the experimental and predicted phase compositions was observed at the highest solvent density.

A Uinta Basin bitumen was hydrotreated over a sulfided commercial Ni-Mo on alumina hydrodemetallation catalyst. The catalyst was on-stream continuously for over 1,000 hours. The extent of heteroatom removal, residuum conversion and molecular weight reduction were investigated as a function of process variables. The fixed bed reactor was operated in the upflow mode to insure complete wetting of the catalyst and to maintain isothermal operation. The primary process variables studied were reactor temperature (620-685 K), weight hourly space velocity (0.24-1.38 h^{-1}) and total reactor pressure (11.3-16.7 MPa). The hydrogen/oil ratio was fixed in all experiments at 890 m^3/m^3 (=5000 scf H_2/bbl).

The effect of process variables on the extent of denitrogenation, desulfurization, demetallation, residuum (>811 K) conversion and the product distribution and yields are reported. The apparent activation energies for desulfurization and denitrogenation were 91 and 98 kJ/mol, respectively. A molecular weight reduction-model for hydrotreating over the HDM catalyst was proposed using four reactant lumps.

The HDM catalyst was effective for nickel and sulfur removal during hydrotreating of the Whiterocks bitumen. However, it was ineffective for denitrogenation. HDN, HDS and CCR conversion of the Whiterocks bitumen over the HDM catalyst were correlated by first order kinetics. The HDM catalyst deactivation rate was about 0.18°C/day during bitumen hydroprocessing. Sulfur conversion appeared to be linked to residuum conversion because residuum conversion facilitates conversion of sulfur in higher molecular weight moieties.

Uinta Basin bitumen has been hydrotreated under varying conditions to determine the effect of catalyst on heteroatom conversion and molecular weight reduction. The process variables investigated included total reactor pressure (11.0-16.9 MPa); reactor temperature (618-711 K), feed rate (0.29-1.38 h^{-1} WHSV) and catalyst. A hydrodenitrogenation catalyst was more active for nitrogen and sulfur removal and residuum conversion than a hydrodemetallation catalyst. Residuum conversion was sensitive to the catalyst surface area, metal loading and phosphorus promoter indicating that a certain portion of residuum conversion obtained during hydrotreating results from catalytic reactions. Differences between nitrogen and sulfur removal and residuum conversion and product yields are reported for bitumen hydrotreated over the hydrodenitrogenation and hydrodemetallation catalysts.

Catalyst selection influences the conversion of residuum. A high surface area/high metal content HDN catalyst was more effective for residuum conversion than a low surface area/low metal content HDM catalyst.

The bitumen-derived heavy oil used in the BDL-HDN study was much more amenable to hydrotreating than the bitumen in the BIT-HDN study. Thus, it was concluded that molecular weight reduction should be stressed prior to heteroatom removal for upgrading high nitrogen content bitumens.

Residuum conversion was less sensitive to catalyst selection than heteroatom removal because it proceeds, in part, via a thermal pathway which, for the most part, is not available for heteroatom removal. Residuum conversion can be represented by lumping residuum into two lumps: a reactive or facile portion and a less reactive or refractory fraction. Facile residuum conversion was presumed to involve dealkylation of naphthenic/aromatic/polar ring structures forming a volatile or nonvolatile nucleus and a volatile alkyl fragment. Refractory residuum conversion is presumed to occur via a reaction sequence in which nonvolatile dealkylated nuclei undergo hydrogenation/ring opening/side chain cleavage reactions.

A large-pore hydrodemetallation catalyst was treated with anthracene and/or a Uinta Basin bitumen in a mineral oil solvent to obtain coke levels up to 12% wt% carbon. In some runs, carbazole was added to the anthracene-coking solution and in others, a nickel porphyrin compound was added to the bitumen-coking solution. Physical properties of the coked catalysts were determined. The catalyst activities for hydrogenation and for hydrodenitrogenation

were determined using a mixture of naphthalene and indole in n-heptane, respectively.

The coke produced from the bitumen appeared to be porous, while that produced from anthracene was non-porous. A significant enhancement of nitrogen in the coke on the catalyst over that in the bitumen was observed. Catalytic activities of the coked catalysts decreased with increasing coke content, with hydrodenitrogenation activity being more deactivated than hydrogenation activity. Neither the nature of the coke precursor, nor the presence of nitrogen or nickel on the catalyst, affected the extent of deactivation. Apparent activation energies decreased with increasing coke content. The role of coke on catalyst deactivation is discussed in terms of its effect on the distribution of different catalytic active sites for the reactions. Coke deposited from bitumen was found to be different from that deposited from anthracene. The former appears to be porous in contrast to a consolidated non-porous coke for the latter. A significant enhancement in nitrogen content of the coked catalysts over that in the feed was found. Catalytic hydrogenation activity decreased almost linearly with carbon content, while hydrodenitrogenation activity was more deactivated, but appeared to line out above about 10% carbon on the catalyst. Nickel deposits up to 5 wt% had no noticeable effect on catalytic activities over that of the coke deposits. Decrease in apparent activation energies of coked catalysts is ascribed to a distribution of active sites in the sulfided catalyst, in which strong sites of high hydrogenation activity effectively prevent coke formation, while weak sites of low hydrogenation activity allow formation and deposition of coke on the catalysts.

The generalized wake model was used to calculate phase holdups in three-phase ebullieted bed reactor systems. Existing correlations for the terminal velocity of a single bubble rising through a column of liquid, u_{tb} (for the determination of the bubble rise velocity, u_{br}); the ratio of the wake volume to the bubble volume, κ; and the ratio of the solid holdup in the bubble wake to the solid holdup in the liquid-solid region, x; were used for these calculations. The phase holdups predicted from these calculations were in reasonably good agreement with the experimental holdup data available in the literature.

A comprehensive dimensional analysis was carried out to arrive at criteria that would ensure identical phase holdups for commercial and laboratory scale reactors. It was determined that for similarity, six dimensionless groups would have to be the same

for the commercial and laboratory units. Given the commercial system dimensions and parameters, the values of the parameters for the laboratory unit were determined using the established similarity criteria. The phase holdups for the commercial and the laboratory units, calculated from the generalized wake model were equal, thus validating the similarity criteria.

Manipulating the system parameters to keep all of the six dimensionless groups constant was impractical for the reacting systems and the criteria could only be applied to nonreacting systems. A simplified set of criteria were developed for reacting systems to ensure the similarity of holdups in the two units by the manipulation of the parameters, d_p, u_l and u_g. Again, given the values of the parameters for the commercial unit and assumed values of d_p for the scaled-down laboratory reactor, the values of u_l and u_g for the laboratory scale unit were calculated using the simplified criteria. The phase holdups for the two units calculated using these values of d_p, and u_l and u_g and the generalized wake model were almost identical, thus validating the concept of using the reduced set of similarity criteria for scaling down three-phase ebullieted bed reactors.

Since high pressure three-phase ebullieted reactors operate in a dispersed bubble regime, a scaled down reactor will have the same flow regime and similar bubble size as the high pressure commercial reactor, resulting in a closer hydrodynamic similarity.

Lost work analysis shows that incremental economic improvements can be made through carefully designed heat and energy management. Overall, the economics are highly sensitive to product price. Not unexpectedly, the product price needed is greater than the prevailing price of crude oil but not outside of the range of foreseeable prices, taking into account the premium quality of the resulting syncrude. The high process yields translate into a lower requirement for feedstock than alternative processes such as coking and hydrotreating.

INFORMATION REQUIRED FOR THE NATIONAL ENVIRONMENTAL POLICY ACT

Principal Investigator: A.G. Oblad
Co-Principal Investigators: M.D. Deo
F.V. Hanson

INTRODUCTION

The information required for compliance with the National Environmental Protection Act (NEPA) has been documented in this section. This final report has been prepared to reflect the research and development activities performed under the cooperative agreement 89MC26268 between the University of Utah, Department of Chemical and Fuels Engineering and the U.S. Department of Energy. Detailed descriptions of the individual projects, process flow diagrams for the various oil sand recovery technologies, laboratory locations, environmental impacts, health and safety procedures, etc. have been documented in detail in the 1991-92 final report for the cooperative agreement 89MC26268. [1]. The proposed program for the current contract does not include any experimental activity which would result in the generation of additional gaseous, liquid and solid wastes over and above those indicated in the detailed report submitted previously [1]. All liquid and solid waste materials produced during the course of the experimental program will be processed through the EPA approved University of Utah Safety Services disposal system.

This section includes an NEPA checklist and a brief description of the program and its overall environmental impact. The information provided essentially qualifies the program for CX-B exclusion determination.

NEPA CHECKLIST

1. Date: 7-22-92 NEPA Number

2. Activity/Project Name Tar Sand Program/University of Utah Cooperative Agreement DE-FC21-89MC26268, "RECOVERY OF BITUMEN FROM WESTERN TAR SAND."

3. Project Manager/Branch/Division J.D. Westhoff, LFT Br., FRM Div

4. Project/Activity Description Include purpose, location, site map (proved figure or map if appropriate) construction requirements, schedule, operation processes.

This action is in response to a renewal application for a cooperative agreement with the University of Utah Fuels Engineering Department that has been in place since 1989. A memo to file (dated 20 Nov. 1990) was written, submitted and provided NEPA approval for the program and proceeding operations conducted under the cooperative agreement. This program is a continuation of effort to develop commercially viable oil sand processes to utilize the extensive resource base in Utah. During the past 15 years the program has produced a comprehensive body of scientific and engineering data related to Utah oil sand recovery and characterization and has evaluated numerous options for bitumen upgrading.

The program is composed of twelve projects, of which ten are laboratory bench or laboratory pilot scale processes that are operated in existing facilities on the University of Utah campus in northeast Salt Lake City. The processes are as indicated below:

- Coupled Fluidized Bed/Heat Pipe/Coke Combustor

- Rotary Kiln Pyrolysis Reactor
- Small Diameter Fluidized Bed Reactor
- Large Diameter Fluidized Bed Reactor
- Water Assisted Recovery Process
- Dense Gas Phase Solvent Extraction (Butane and Propane)
- Hydropyrolysis Reactor
- Hydrotreater
- Hydrocracker
- Three Phase Gravity Classifier

A site map showing the location of the project laboratories on the Utah campus is attached as Figure 1. There are no earth moving or construction requirements for the program or its projects. The Fuels Engineering and Chemical Engineering Departments operate under the University of Utah, Department of Safety Services, which is responsible for compliance with the U.S. EPA, state and city permits. The office of Safety Services provides a Hazardous Waste management program and contract and a Chemical Hygiene Program. The University air and water effluents are monitored by the state and city. The hazardous waste program is monitored by the U.S. EPA and the chemical hygiene program is monitored by OSHA.

5. Brief Description of Affected Environment State if previously disturbed, occupied, or vacant. Indicate in a few words the type of cover (e.g., grasslands, woods, natural, landscaped), or habitat types known.

The program and all the projects are located at the University of Utah campus in northeast Salt Lake City, Utah, in existing facilities assigned to the Departments of Fuels Engineering, Chemical Engineering and Metallurgy. The

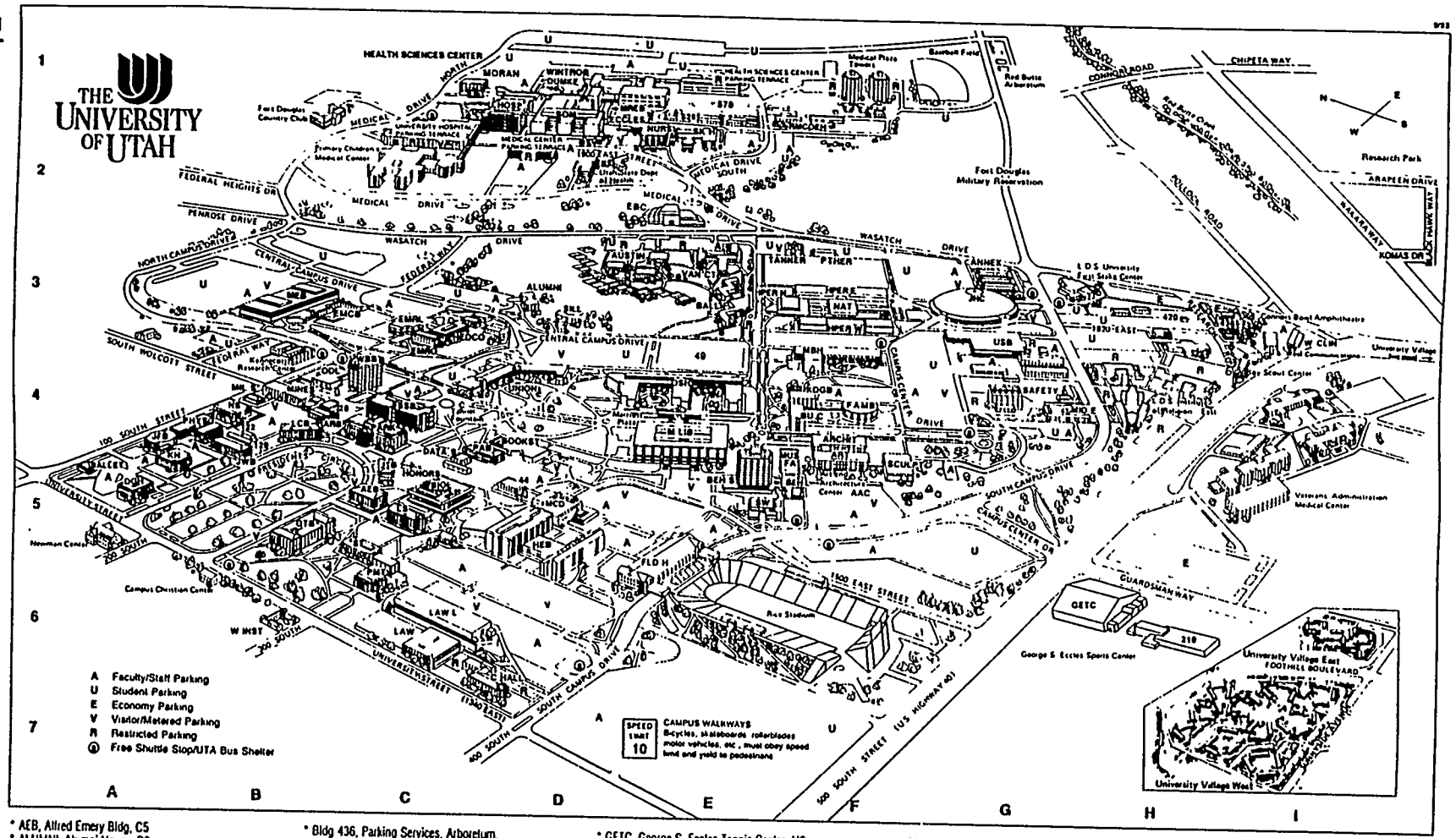

* AEB, Alfred Emery Bldg, C5
* ALUMNI, Alumni House, D3
* ANNEX, Annex Bldg, G3
ARB, Applied Research Bldg, B4
* ARCHIT, Architecture Bldg, F4
* ART, Art Bldg, F4
* AUSTIN, Austin Hall, E2
OPERA, Opera Studio, A5
* BALLR, Ballrd Hall, E3
* BEH L, Social & Behavioral Science Lecture Hall, F5
* BEH S, Social & Behavioral Science Tower, E4
* BIOL, Biology Bldg, C5
Bldg 20, Physics Offices/Lab, B4
* Bldg 44, Office Annex, D5
* Bldg 49, Language/Communications Bldg (under construction), E4
Bldg 122, Math Office Bldg, B4
* Bldg 129, Math Offices, Communication Lab, B4
* Bldg 210, O Glenn Smith Athletic Center, H6
* Bldg 420, Outdoor Program Bldg, I3
* Bldg 436, Parking Services, Arboretum, Fire Marshal, H3
* Bldg 528, Health Sciences Bookstore, Credit Union, E1
* Bldg 570, Biomedical Polymers Research Bldg (under construction), E1
* BOOKST, University Bookstore, D4
* BU C, Business Classroom Bldg, F4
C HALL, Carlson Hall, D6
* DATA S, Data Services Bldg, C4
* DGH, David Gardner Hall, A5
* DUMKE, Dumke Biomedical Engr Research Bldg, D1
* EBC, Dolores Dore Eccles Broadcast Center, E2
* ECCLES, Eccles Health Sciences Library, D1
* EHG, Eccles Institute of Human Genetics, D1
* EMCB, Engineering & Mines Classroom Bldg, C3
* EMRL, Energy & Minerals Research Lab, C4
* EMRO, Energy & Minerals Research Office Bldg, C3
* FAMB, Francis A Madsen Bldg, F4
* FLD H, Eimar Nielsen Field House, E5
* GETC, George S Eccles Tennis Center, H6
* GTB, George Thomas Bldg (Museum of Natural History), B5
* HEB, Henry Eyring Bldg, D5
* HEDCO, Hedco Bldg, C4
HONORS, Honors Program, C4
* HPER E, Health, Physical Education & Recreation East Bldg, F3
* HPER N, Health, Physical Education & Recreation North Bldg, F3
* HPER W, Health, Physical Education & Recreation West Bldg, F3
* JFB, James Fletcher Bldg, A4
* JHC, Jon Huntsman Center, G3
JTB, James Talmage Bldg, C4
* JWB, John Widstoe Bldg, B4
* KDGB, Kendall D Garff Bldg, F4
KH, Kingsbury Hall, A5
* LAW, Law Bldg C6
* LAW L, Law Library, C6
LCB, LeRoy Cowles Bldg, B4
* LS, Life Science Bldg, C5
* MBH, Milton Bennion Hall, F3
* MCD, Marriott Center for Dance, D5
* MEB, Merrill Engineering Bldg, B3
MIDE, Middle East Center, G4
MIL S, Military Science Bldg, B4
MINES, Mines Bldg, B4
* M LIB, Marriott Library, E4
* MORAN, John A Moran Eye Center, C1
* MREB, Medical Research & Education Bldg, D1
* MUS FA, Museum of Fine Arts, Utah, F4
* NAT, Natatorium, F3
NS, Naval Science Bldg B4
* NURS, Nursing Bldg, E1
ODL, Ore Dressing Lab B4
* OSH, Orson Spencer Hall E3
* PAB, Performing Arts Bldg, D4
* PARK, Park Bldg C4
PHYS, Physics Bldg B4
* PMT, Pioneer Memorial Theatre, C6
* P THER, Physical Therapy Bldg, F2
* RMCOEH, Rocky Mountain Center for Occupational & Environmental Health, E2
SAFETY, Public Safety, H3
* SCULPT, Sculpture Bldg, F4
* SILL, Sterling Sill Home Living Center, D3
* SK H, Skaggs Hall, E1
* SOM, School of Medicine Bldg, D1
* SSB, Student Services Bldg, C4
ST, Stewart Bldg C5
* SW, Social Work Bldg, E5
TANNER, Virginia Tanner Dance Bldg, F2
* U HOSP, University Hospital, D1
* UNION, Olpin Union D3
* USB, University Services Bldg, G3
* VAN CT, Van Cott Hall, E2
* WBB, William Browning Mineral Science Bldg C4
* W CLIN, University Wasatch Clinics, I3
W INST, LDS Institute of Religion (West), B6
* WINTRO, Wintrobe Research Bldg, D1

Figure 1. Location site map University of Utah

University of Utah is a major public educational and research institution located in Salt Lake City at the foothills of the Wasatch mountain range. University enrollment is 26,000 students with 3,400 full-time faculty, for a total of more than 30,000 people in its facilities. The campus has 233 buildings, including 1,400 research laboratories, all of which are located on 1,480 acres.

6. Environmental Concerns Will the project/activity, either during construction or operation, result in changes or disturbances to the following entities? Provide brief explanations to any "yes" answers.

6.1 Threaten a violation of applicable statutory, regulatory, or permit requirements for environment, safety, and health requirements o DOE orders?
Yes_____ No__X__ Unknown_____

6.2 Require siting and construction or major expansion of waste storage, disposal recovery, or treatment facilities?
Yes_____ No__X__ Unknown_____

6.3 Uncontrolled or unpermitted releases resulting from hazardous substances, pollutants or CERCLA-excluded petroleum and natural gas products that preexist in the environment?
Yes_____ No__X__ Unknown_____

6.4 Adversely affect environmentally sensitive resources, including:

4.a Threatened/Endangered Species or Critical Habitat Areas
Yes_____ No__X__ Unknown_____

4.b Flood Plains/Wetlands
Yes_____ No__X__ Unknown_____

4.c Archaeological/Cultural Resources
Yes_____ No__X__ Unknown_____

4.d Prime, Unique or Important Farmland
Yes_____ No__X__ Unknown_____

4.e Special sources of Groundwater (sole source aquifer, etc.)
Yes_____ No__X__ Unknown_____

4.f Tundra, Coral Reefs, Rain Forests, Coastal Zones
Yes_____ No__X__ Unknown_____

4.h National Parks, Wild and Scenic Rivers, Waters of the State, etc.
Yes_____ No__X__ Unknown_____

4.i CAA Criteria Pollutants (7)
Yes_____ No_____ Unknown__X__

Under the projected optimum operating conditions, the cumulative gaseous releases will be 755 Kg per year (Optimum operating intensity is highly improbable due to equipment failure or modification). All gaseous effluents are vented to the exhaust of the individual laboratory buildings where they are flared with natural gas. As a result, an estimated 96 percent of the gaseous emissions are CO_2 and H_2O. The chemical form and fate of the remaining 4% or 30.2 Kg is speculative.

7. Additional Information Will the project/activity...

7.1 affect water use and quality, including sedimentation, and discharge of point/nonpoint source pollutants to surface or ground water?
Yes_____ No__X__ Unknown_____

7.2 control or modify the water, streambed, or shoreline of any stream or water body?
Yes_____ No__X__ Unknown_____

7.3 result in the generation, transportation, and disposal of any hazardous or toxic materials as defined by Federal or applicable state regulations?
Yes__X__ No_____ Unknown_____

Both solid and liquid hazardous wastes are collected by the University Department of Safety Services along with other research wastes generated on campus and are disposed of according to state and federal guidelines by their contractor APTUS Environmental. Product liquids from process experiments

are stored in plastic lined drums for upgrading research. The waste sand is stored for combustion and residual carbon research.

The Office of Safety Services provides a hazardous waste management program including a clear and concise flow-chart for management of hazardous materials from the point of identification to disposal. The office has a U.S. EPA number for hazardous waste handling and disposal and it monitors University waste management activity.

7.4 affect any aspect of the human environment besides those mentioned above either directly or indirectly (e.g. visibility, noise, aesthetic and socioeconomic impacts; public facilities and services or exposure to toxic and hazardous material)?
Yes_____ No_____ Unknown__X__

All processes are located in existing buildings, visibility and aesthetic effects due to the processes are nonexistent. Noise effects are limited to no more 75 to 85 db and hearing protection is provided in all laboratory areas. Socioeconomic effects are limited to those resulting from financial support of 20 plus graduate students and there are no personnel displacements or housing, schooling, hospital, etc., requirements beyond those provided through the University and Salt Lake City. Exposure to hazardous and toxic substances is monitored by the Office of Safety Services under their Chemical Safety and Hygiene Plan. Safety Services is monitored in turn by the Salt Lake City Office of the Occupational Safety and Health Administration. In a reactor testing and development environment there are always

unforeseen errors in judgment and, therefore, dangers exist. These conditions have been reviewed, safeguards emplaced and educational procedures instituted to minimize the potential for accident or exposure occurrence.

7.5 generate public controversy?

Yes_____ No__X__ Unknown_____

Please write all explanations of any "yes" answer on an attached page.

8. Is the Project/Activity specifically called out in the procedures as a categorical exclusion?

Yes__X__ No_____ Unknown_____

State Specific category _____Cx-B 3.10_____

9. Recommended NEPA Determination: CX_A_____ CX-B__X__ EA___

EIS_____ None needed_____

_____original signed_____ _____

Signature of Project Manager Date

_____original signed_____ _____

Signature of Environmental Project Manager Date

_____original signed_____ _____

Signature of METC NCO Date

CATEGORICAL EXCLUSION (CX-B) DETERMINATION

RECOVERY OF BITUMEN FROM WESTERN TAR SANDS

Proposed Action: Renewal of existing cooperative agreement 89MC26268 with the University of Utah, Fuels Engineering Department

Location: University of Utah
Department of Fuels Engineering,
306 W.C. Browning Bldg.
Salt Lake City, Utah, 84112-1183

Proposed by: Morgantown Energy Technology Center, U.S. Department of Energy (DOE).

Description of the proposed action:

The U.S. DOE and the University of Utah, Department of Fuels Engineering, entered into cooperative agreement 89M26268 to conduct research and development advancing the body of scientific and engineering data necessary to develop viable oil sand processes and enhance the commercial potential of extensive U.S. Tar Sand resources. The current cooperative agreement was initiated on 7 July 89. With this renewal the cooperative agreement is planned for expiration on 7 July 1993.

All research, development, small-scale fabrication and test activities will be conducted in existing facilities and operated under University permits, inspections and monitoring procedures responsive to U.S. EPA, state and local regulation. The ten projects are composed of four thermal, two water assisted, a closed solvent and three upgrading processes, all of which are located in laboratory facilities. There are no earth moving or construction requirements for the program or its projects. Hazardous wastes are segregated and manifested in the individual laboratories under

guidance, implementation procedures and contracted disposal (APTUS ENVIRONMENTAL) provided by the University Department of Safety Services.

Operating experimental equipment located in university laboratory facilities includes the following processes:

- Coupled fluidized Bed/Heat Pipe/Coke Combustor
- Rotary Kiln Pyrolysis Reactor
- Small Diameter Fluidized Bed Reactor
- Large Diameter Fluidized Bed Reactor
- Water Assisted Recovery Process
- Dense Gas Phase Solvent Extraction (Butane and Propane)
- Hydropyrolysis Reactor
- Hydrotreater
- Hydrocracker
- Three Phase Gravity Classifier

The experimental program involves extraction, upgrading and product development testing. The experiments use crushed and sized oil sand in laboratory scale extraction equipment, and the bitumen product in upgrading and product development research. Feedstock use, product fate, and cumulative waste management are discussed below:

A. Feedstock: In a year of tests a maximum of 14.2 tons of oil sand are processed (it is likely that the quantity processed will actually be less than one-half this amount). Oil sand feedstocks are approximately 7 - 9% hydrocarbon and 91 - 93% inorganic support matrix (silica sand).

B. Produced Bitumen: Production from all processes will be approximately 7.6 barrels of bitumen. The bitumen will be stored in polyethylene-lined barrels and used for upgrading research or it will be disposed of as a hazardous waste and incinerated by the University Hazardous Waste Contractor, Aptus Environmental. Process hydrocarbon capture is conservatively estimated in the range of 95+ %. During any one year experimental period, hydrocarbon losses are less than thirty-five kilograms. Hydrocarbon losses are disposed to building flares or the solids and liquids are disposed through the hazardous waste management program.

C. Off-Gas Wastes: All the pyrolytic processes (fluidized beds, and rotary kiln, etc.) vaporize the bitumen and, therefore, must recover the liquid product in a collection system. This involves extensive filtration and cleanup of off-gases. Off-gases leaving the collection systems are incinerated. The processes will generate a maximum of 756 Kg of off-gases at the cited maximum operating conditions and all will be flared with natural gas. At least 96% of the off-gases will be oxidized to CO_2 and H_2O.

D. Water Wastes: The water-assisted process and the three-phase gravity classifier use water in the process studies. The classifier is in design development stage at laboratory bench scale and its waste is generated under controlled conditions and disposed of as hazardous or solid waste. The water assisted process uses approximately 22 gallons of water per experiment (1,300 gallons per year). The water is recycled ten times after which it is pumped to

a water-tight sump and is disposed of as a hazardous waste and is incinerated. All other processes use cooling water which is isolated from the process feed, products and waste streams and, as such, is not contaminated.

E. Solid and Liquid Hazardous Wastes: All spent sand from the reactors is stored in polyethylene-lined barrels for use in fluidization or spent sand combustion research. None of the disposed sand is a hazardous material. Bitumen produced from the water-assisted process is not used for upgrading research and the total estimated production of 0.8 barrels per year will be disposed of as a hazardous waste. Small quantities of analytical and cleaning solvents from the upgrading and solvent extraction processes are manifested and disposed of by the Office of Safety Services hazardous waste disposal contractor for incineration.

F. CX to Be Applied: The proposed action is within the threshold limits of the DOE National Environmental Policy Act (NEPA) Implementing Procedures, 10 CFR 1021, effective date May 26, 1992, Subpart D, Appendix B. {site number of classification (i.e., B.1.16)} {site the CX-B classification as found in the partial list of CX's in this file or the section of the regulations noted above}. This action meets all of the eligibility requirements for categorical exclusions as set forth in 10 CFR 1021, Section 410, and all of the integral elements of the Classes of Actions in Appendix B.

CHARACTERIZATION OF UINTA BASIN OIL SAND DEPOSITS AND ACQUISITION OF MINED ORE SAMPLES

Principal Investigator
Consulting Geologists

F.V. Hanson
K.M. Clem
C. Sanders

INTRODUCTION

The Oil Sand Research and Development program at the University of Utah has as a primary objective the development of a comprehensive database with which technical and economic evaluations of recovery and upgrading processes can be made. The program also requires significant quantities of mined and crushed oil sand ores with which recovery process development studies are conducted. The bitumens are also extracted from the ores for use in the various upgrading studies. Drum quantities of ore from the PR Spring oil sand deposit were acquired during the 1992-1993 contract period and the Sunnyside oil sand deposit was reconnoitered for future ore acquisition.

PR SPRING OIL SAND DEPOSIT

Deposit Location

The PR Spring oil sand deposit is located in the southeastern region of the Uinta Basin in the state of Utah, Townships 11 through 17 South, Ranges 21 through 26 East (Salt Lake Meridian), Uintah and Grand Counties.

Deposit Description

The PR Spring oil sand deposit is located on the southeast flank of the Uinta Basin, about 50 miles northwest of Grand Junction, Colorado, and about 50 miles south of the town of Vernal, Utah. The deposit extends along the length of the Book Cliffs, with

an eastern boundary along Willow Creek and a western boundary along Atchee Ridge. The deposit is wholly within the state of Utah and does not appear to extend into Colorado. The elevations of the outcroppings range from about 6,500 feet to 8,800 feet.

Access to the deposit is by either of two routes: one from the south and the other from the north. The area may be approached from the north by heading east from Vernal, turning off U.S. Highway 40 onto Highway 45, and heading south past the town of Bonanza. There are two roads serving the area from the south: San Arroyo Canyon road, which joins Interstate Highway 70 near the Utah-Colorado state line; and the Hay Canyon road, which joins Interstate Highway 70 3 miles northeast of Haley Dome, Utah. There are numerous oil well maintenance roads that connect the canyons and ridges upon which the deposit outcrops.

Geology

The deposit is located on the eastern portion of the southern limb of the Uinta Basin. A general geology map of the PR Spring deposit is presented in Figure 2[2,3]. Regional dip is northwest at 2 to 6 degrees. The deposit also lies on top of the Uncompahgre Uplift, a major northwest trending, subsurface structural feature. While numerous anticlinal features related to the Uplift are present on the surface, it appears that they did not exert significant influence on the emplacement or migration of the bitumen within the deposit.

The oil-impregnated sandstones are found in the Eocene Green River Formation. The Green River Formation in this area is

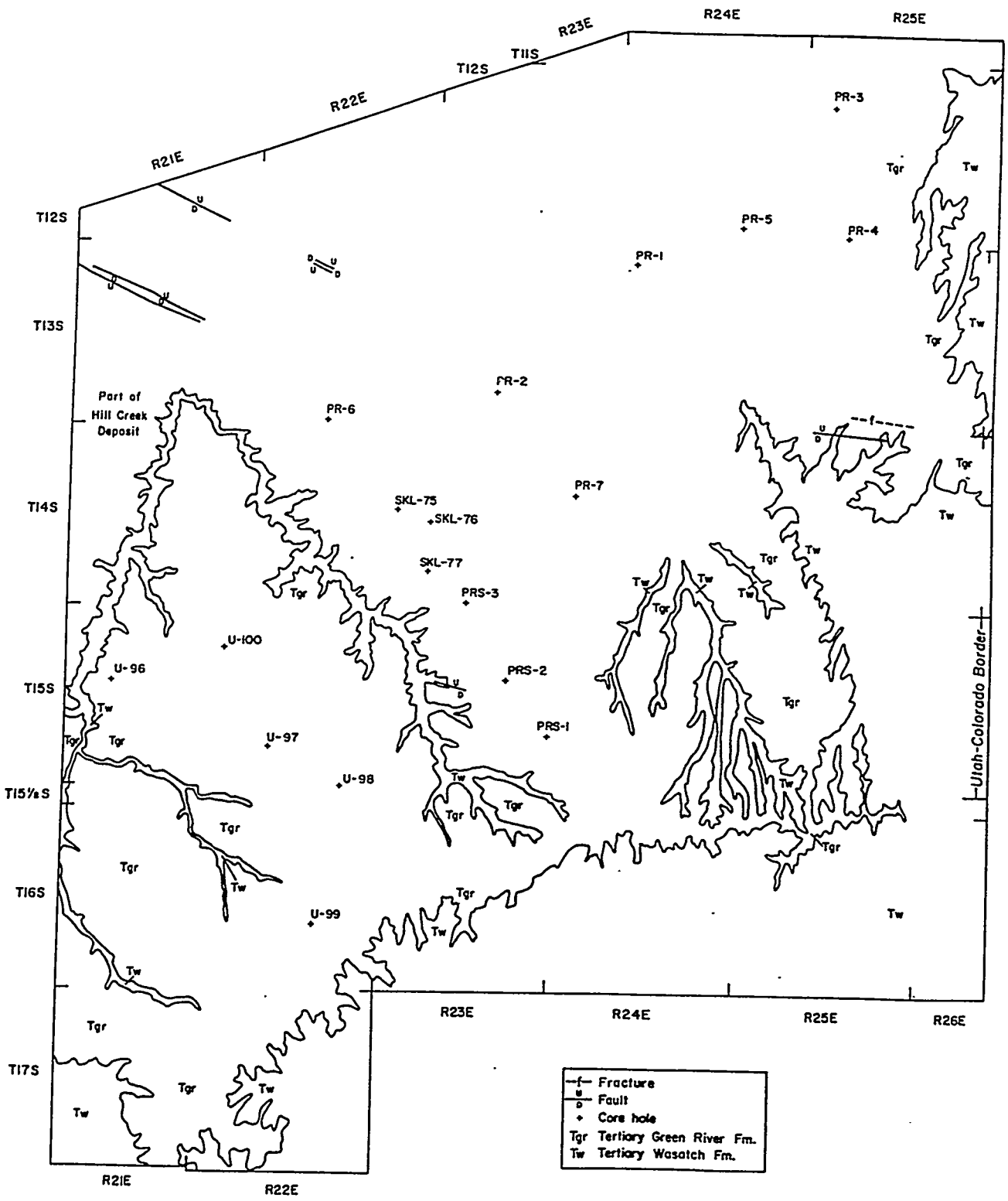

Figure 2. General Geology Map of the PR Spring Oil Sand Deposit

composed of oil shale beds, marlstones, shales, siltstones, sandstones, limestones, and tuffs. These were deposited in a lacustrine environment. The majority of the clastic sediment is related to the Uncompahgre Uplift to the south. This is evidenced by an increase in grain size and number of sandstone beds extending southward.

Lithology - Character of Reservoir

The bitumen saturation occurs in five distinct zones located within the Eocene age Green River Formation. The four lower zones lie within the Douglas Creek Member, and the highest zone lies in the Parachute Creek Member[3]. The Mahogany Oil Shale in the lower part of the Parachute Creek member divides these two members. The zones are designated from bottom to top as "A", "B", "C", "D", and "E", and can be correlated throughout the area (Figures 3 through 7)[3]. The zones consist of one or more oil-impregnated lenticular beds separated by barren strata. The impregnation is controlled by the lateral extent of the bed, its porosity and permeability, and the distance the oil has migrated within the bed. Correlation of individual rock units throughout the area is difficult, even over short distances. Individual sandstone beds range from 6 inches to 30 feet in thickness. The sandstones vary extremely in size and shape of grains and in type and degree of cementing.

The degree of saturation varies both laterally and vertically. Vertically, all degrees of saturation are visible in an individual bed at any one locality. Horizontally, variations from slight to rich[4] may occur within a distance of a few hundred feet along the

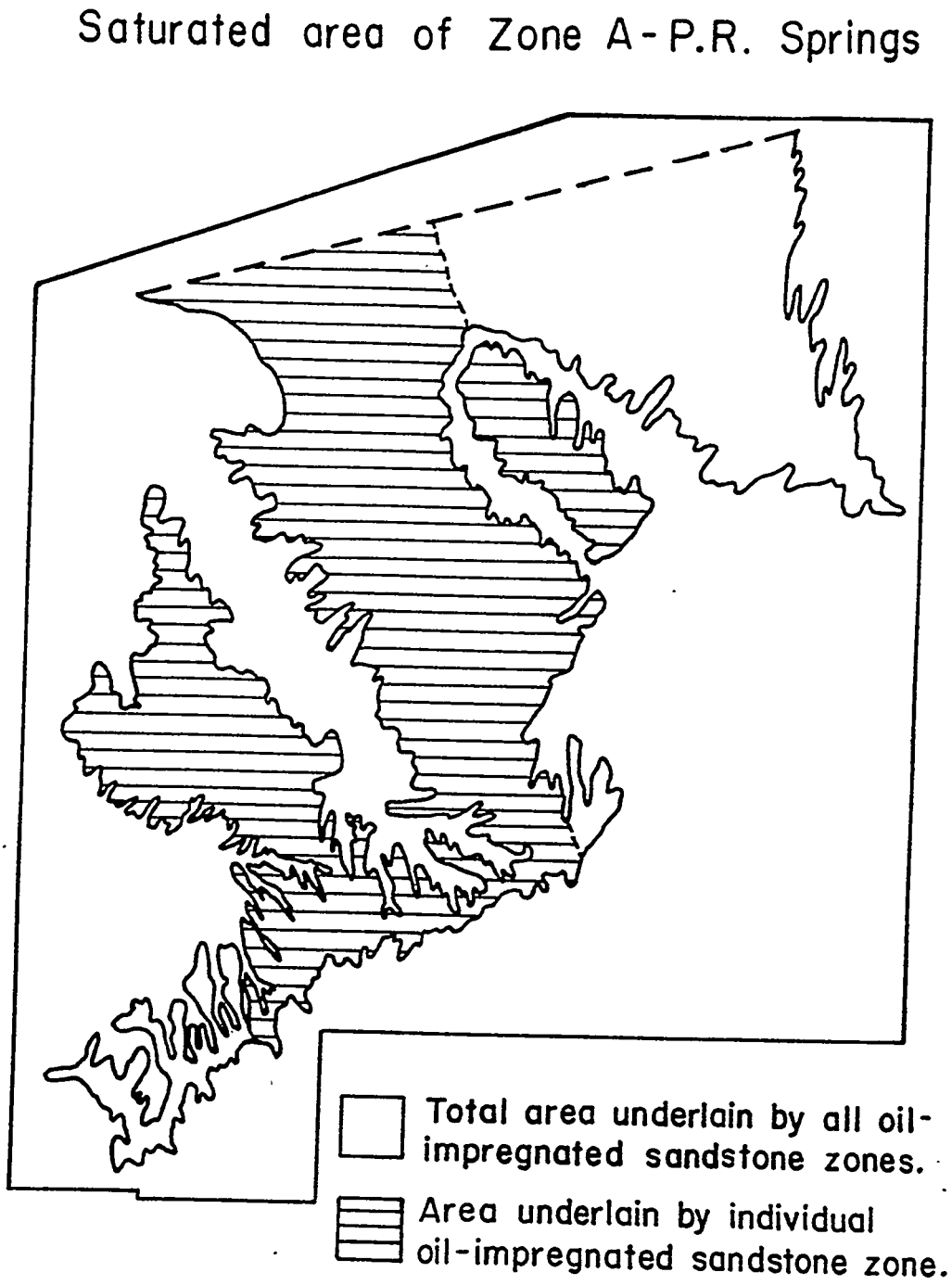

Figure 3. Oil Impregnated Zone A in the Douglas Creek Member, PR Springs Oil Sand Deposit

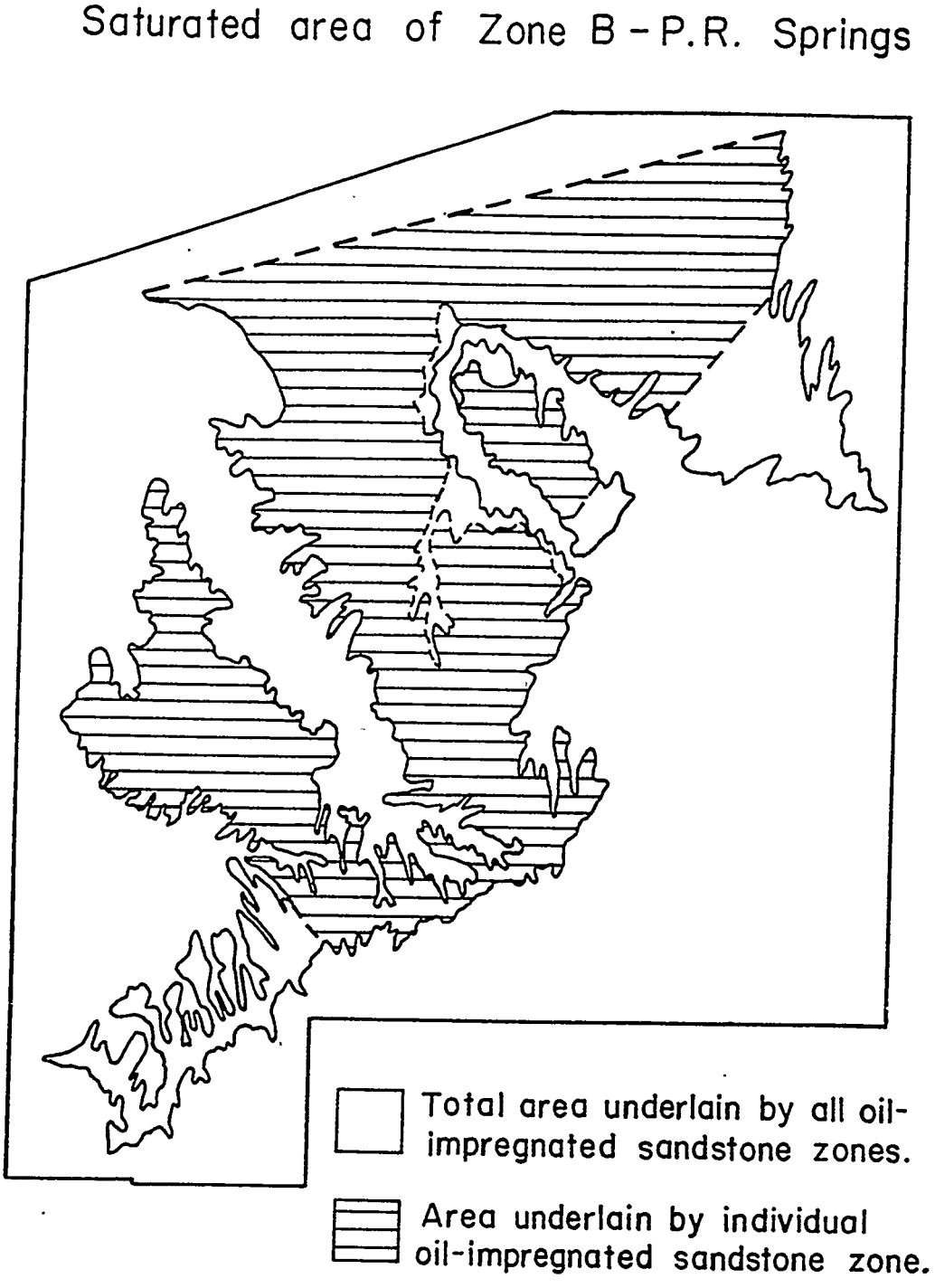

Figure 4. Oil Impregnated Zone B in the Douglas Creek Member, PR Springs Oil Sand Deposit

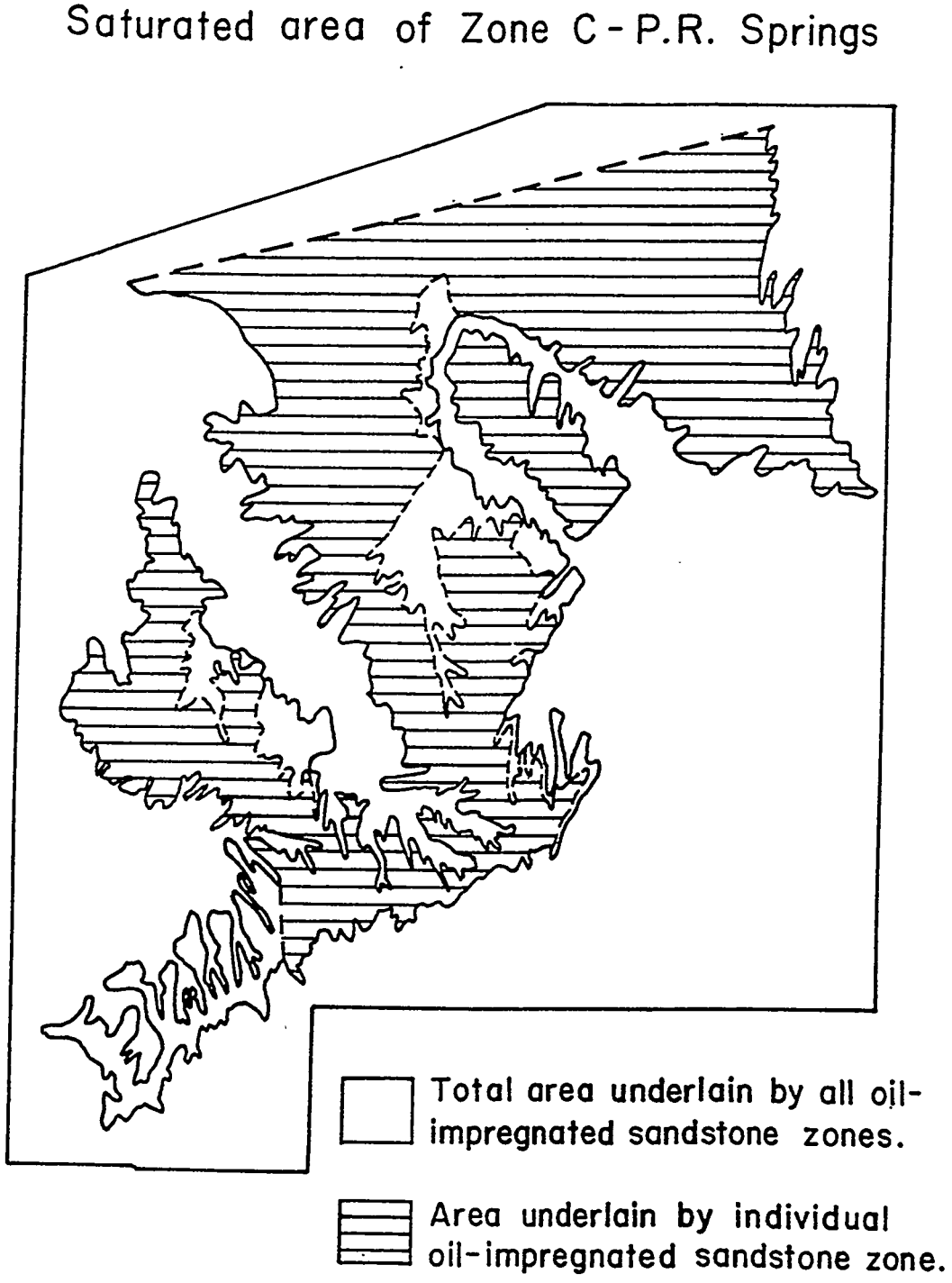

Figure 5. Oil Impregnated Zone C in the Douglas Creek Member, PR Springs Oil Sand Deposit

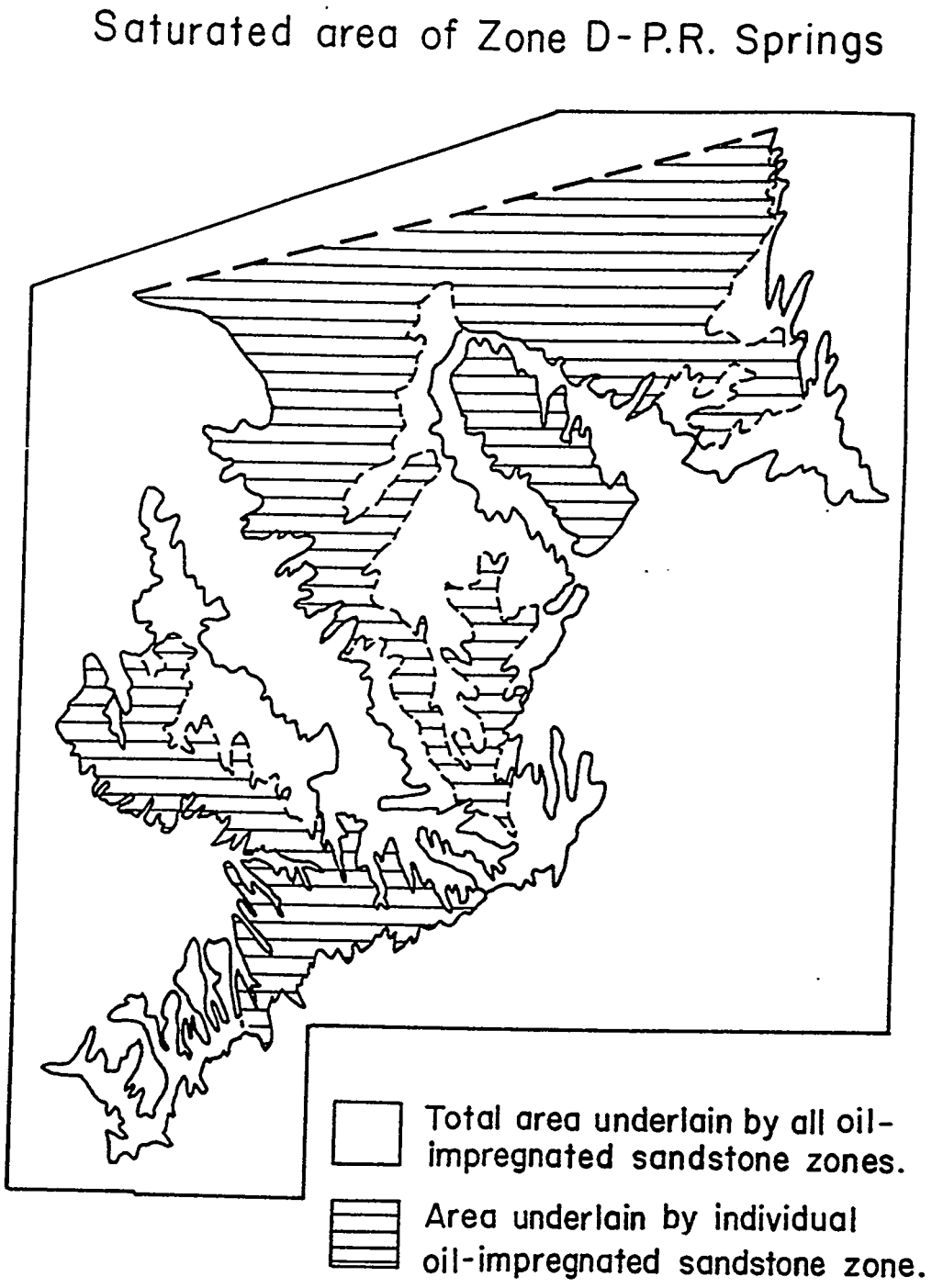

Figure 6. Oil Impregnated Zone D in the Douglas Creek Member, PR Springs Oil Sand Deposit

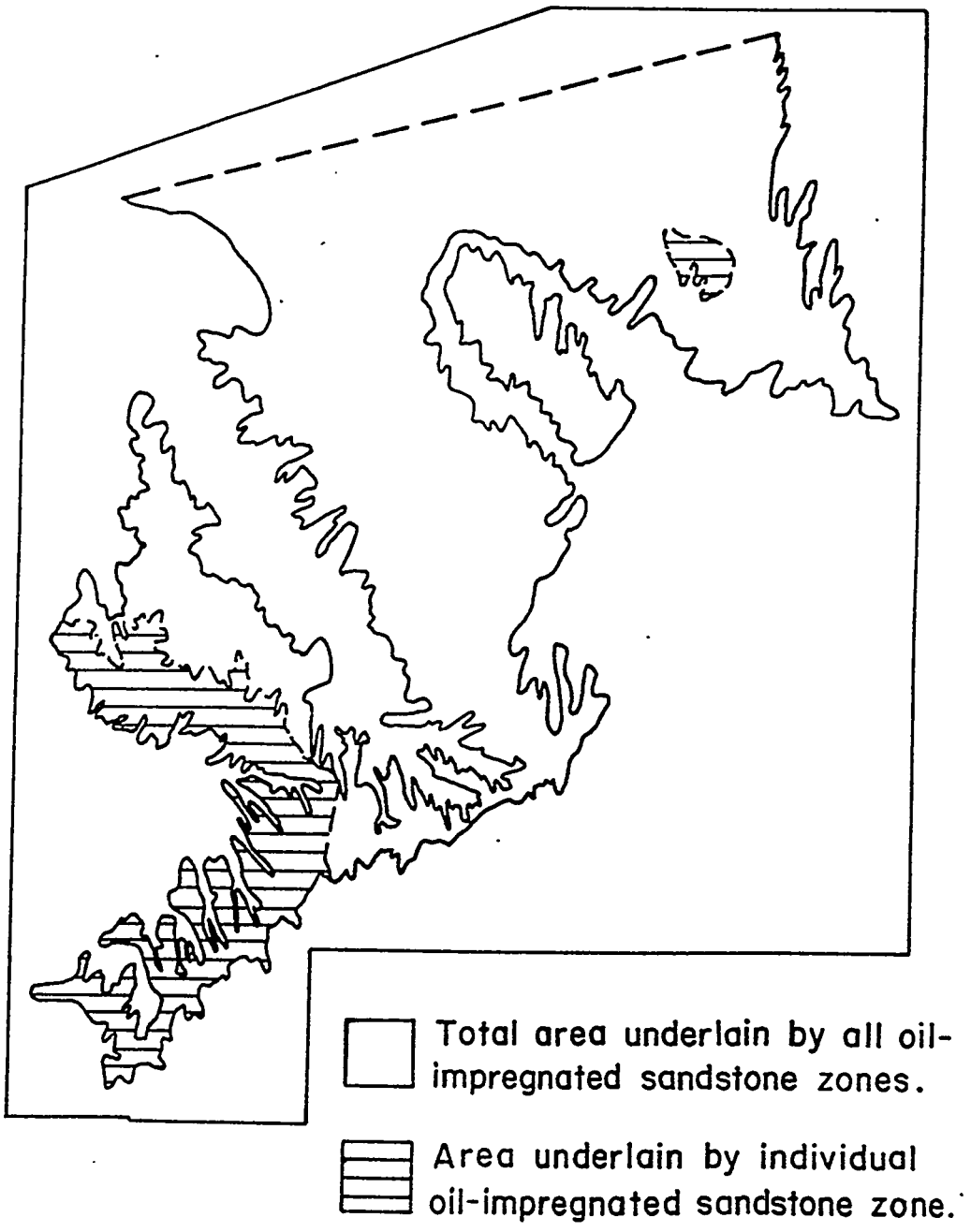

Figure 7. Oil Impregnated Zone E in the Parachute Creek Member, PR Springs Oil Sand Deposit

outcrop. Numerous heavy oil seeps occur in the PR Spring deposit with the Main Canyon seep being the largest. Bitumen movement has been determined to be caused by water pressure from the hydrostatic head of the Roan Cliffs pushing the bitumen downdip into the canyons. During wet seasons, the seeps become active and large amounts of water flows in addition to the bitumen. During dry seasons, both bitumen and water cease to flow.

Resource Estimates

Resource estimates have been prepared by a number of investigators [5-10]. Byrd[5] estimated the total resource at 3.7 billion barrels of bitumen in place. Ritzma[6] and Campbell and Ritzma[7] estimated the total resource at 4.0 to 4.5 billion barrels, Dahm[8] estimated the resource underlying state-owned lands at 1.9 billion barrels and Clem[9] estimated the resource at 3.3 billion barrels. Sinks[10] chose not to report a revised resource estimate despite compiling an exhaustive recitation of the available core data on the PR Spring deposit. The Utah Geological and Mineral Survey classified the PR Spring oil sand deposit as a Giant deposit.

Characterization and Analysis of the Bitumen

Three outcrop samples were collected by Ritzma and Gwynn during the 1967 and 1969 field seasons[11]. The UGS 69-13E (1969) sample is from the Douglas Creek Member, located in the SW/4 of the NE/4 of section 8, Township 12 South, Range 25 East. The UGS 69-14E (1969) sample is from the Parachute Creek Member, located in the NW/4 of the NW/4 of section 5, Township 12 South, Range 25

East. The UGS 67-1A (1967) is from the Main Canyon seep in the Douglas Creek Member, located in the center of NE/4 of section 5, Township 16 South, Range 24 East. The analyses of the three samples as reported by Wood and Ritzma[11] are presented in Table 1.

Table 1

Analyses of PR Spring Bitumen Samples[11]

	Weight Percent					Specific	API
Sample No.	Tar	C	H	N	S	Gravity	Gravity
UGS 69-13E	12.4	80.0	9.5	1.0	0.45	1.012	8.3
UGS 69-14E	14.8	88.0	10.0	1.8	0.35	1.031	5.7
UGS 67-1A	97.6	86.0	10.9	0.67	0.36	0.969	14.5

The bitumen contents of samples UGS 69-13E and UGS 69-14E are in reasonable agreement with core saturation data reported by Byrd[5].

A freshly mined sample of the ore from the UTAR pit (SE 1/4 NE 1/4, Section 5, Township 16 South, Range 24 East) was analyzed at the University of Utah in 1982[12]. The analyses are reported in Table 2. Three additional samples were acquired by the oil sand research and development group at the University of Utah in 1981. The drum quantity samples were identified as PR Spring Rainbow I, PR Spring Rainbow II and PR Spring South. The sample sites are identified in Figure 8 and the analyses of the bitumens are reported in Table 3. The crushed ore was used in fluidized bed process research and development studies.[4] The analyses of the

Table 2

Analysis of PR Spring Bitumen Sample
from UTAR Pit Circa 1982

Bitumen Content, wt. % (Toluene Extraction)	11.2
Specific Gravity (293 K/293 K)	0.9785
API Gravity, °API	13.1
Pour Point, K (°F)	318.7 (114)
Conradson Carbon Residue, wt. %	7.9
Viscosity, cp	1,806 @ 363 K 3,588 @ 353 K 9,162 @ 343 K 21,086 @ 333 K 63,210 @ 323 K
Simulated Distillation, wt. %	
IBP - 478 K	1.3
478 - 617 K	6.3
617 - 811 K	23.4
Volatility, wt. %	31.0
Resid., wt. %	69.0

bitumens and the bitumen-derived heavy oils produced from the three different ore samples at a temperature of 823 K, a solids retention time of 20 minutes and a fluidization gas flow rate of 144 LPH [STP] are presented in Tables 4, 5 and 6.

Development History

The earliest known petroleum recovery operation in the PR Spring area was an oil test well drilled in Section 35, Township 15 South, Range 23 East, by John Pope in 1900. Another early venture consisted of an adit of more than 50 feet located in Section 34, Township 15 South, Range 23 East A steel pipe ran from the adit

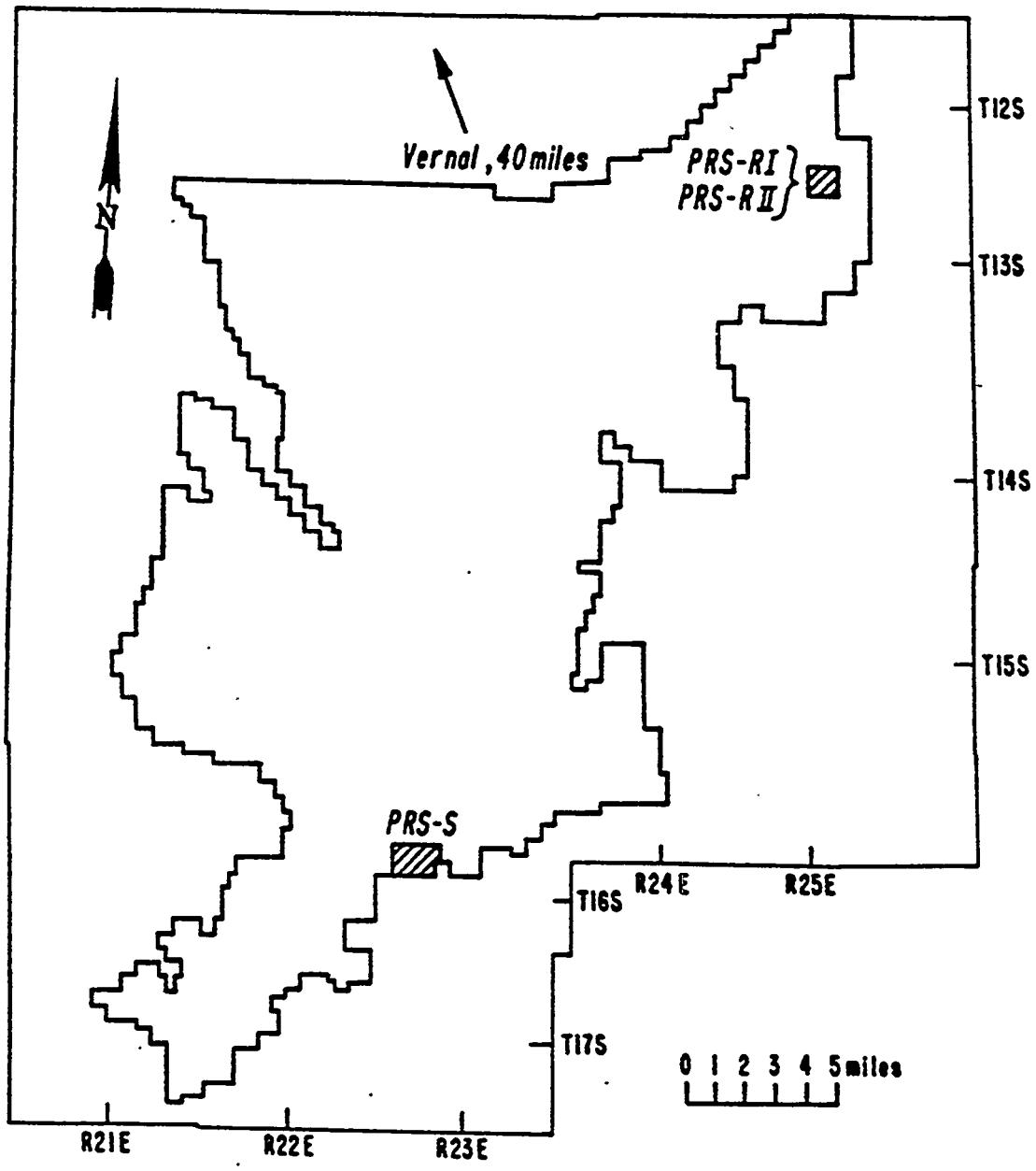

Figure 8. Sample Locations from the PR Spring Oil Sand Deposit

Table 3 - Analysis of Native Bitumens from the PR Spring (Utah) Oil Sand Deposit

Source	Rainbow I	Rainbow II	South
Bitumen Content, wt. %	14.1	8.5	6.45
Specific Gravity	1.016	0.987	1.008
API Gravity, °API	7.8	11.8	8.8
Conradson Carbon, wt. %	14.0	17.4	24.0
Ash, wt. %	3.3	1.4	1.9
Simulated Distillation			
Volatility, wt. %	31.9	22.8	14.3
IBP - 400° F, wt. %	1.3	0.5	0.7
400 - 650° F, wt. %	5.1	2.2	1.3
650 - 1000° F, wt. %	25.6	20.1	12.3
1000° F_+, wt. %	68.1	77.2	85.7
Elemental Analysis			
C, wt. %	84.7	81.4	81.7
H, wt. %	11.3	10.3	9.3
N, wt. %	1.3	1.4	1.4
S, wt. %	0.5	0.4	0.4
O, wt. %	1.8	6.3	7.2
H/C Atomic Ratio	1.61	1.52	1.36
Molecular Weight, g mol_{-1}	702.	1381.	1561.
Gradient Elution Chromatography			
Saturates, wt. %	9.5	15.8	4.1
MNA/DNA Oils, wt. %	10.2	3.5	5.3
PNA Oils, wt. %	11.4	9.0	1.0
Soft Resins, wt. %	13.9	5.8	4.0
Hard Resins, wt. %	1.1	2.3	1.8
Polar Resins, wt. %	2	3.6	1.1
Asphaltenes, wt. %	31.3	35.9	55.7
Noneluted Asphaltenes, wt. %	20.6	24.1	27.1
Ni, ppm	110.	116.	102.
V, ppm	10.	3.	8.

Table 4 - Analysis of the Liquid Product from the Fluidized-Bed Pyrolysis of the PR Spring Rainbow I Oil Sand

Reactor Temperature, K	823
Solids Residence Time, min.	20
Fluidizing Gas Velocity, LPH (STP)	144
Product Yields, wt. %*	
Gas	20.1
Liquid	70.4
Coke	9.5

Property	P.R. Spring Rainbow I	Pyrolysis Liquid Product
API Gravity, °API	7.8	17.3
Viscosity, cps	8268.8 (@373 K)	396.2 (@298 K)
Pour Point, K (°F)	372.1 (210 °F)	274.7 (35 °F)
Conradson Carbon Residue, wt. %	14.0	4.25
Ash, wt.%	3.3	0.01
Simulated Distillation		
Volatility, wt. %	31.9	79.0
IBP - 400° F, wt. %	1.3	2.7
400 - 650° F, wt. %	5.1	23.1
650 - 1000° F, wt. %	25.6	53.2
1000° F plus Residue, wt. %	68.1	21.0
Gradient Elution Chromatography		
Saturates, wt. %	9.5	13.9
MNA/DNA Oils, wt. %	10.2	32.9
Soft Resins, wt. %	13.9	13.7
Hard Resins, wt. %	1.1	1.6
Polar Resins, wt. %	2.0	2.3
Asphaltenes, wt. %	31.3	16.8
Noneluted Asphaltenes, wt. %	20.6	1.3

* Normalized to 100%

Table 5 - Analysis of the Liquid Product from the Fluidized-Bed Pyrolysis of the PR Spring Rainbow II Oil Sand

Reactor Temperature, K	823
Solids Residence Time, min.	20
Fluidizing Gas Velocity, LPH (STP)	144
Product Yields, wt. %*	
Gas	20.6
Liquid	60.5
Coke	18.9

Property	PR Spring Rainbow II	Pyrolysis Liquid Product
API Gravity, °API	11.8	18.3
Viscosity, cps	9,000. (@473 K)	158.4 (@298 K)
Pour Point, K (°F)	433. (320 °F)	271.9 (30 °F)
Conradson Carbon Residue, wt. %	17.4	3.6
Ash, wt.%	1.4	0.01
Simulated Distillation		
Volatility, wt. %	22.8	82.9
IBP - 400° F, wt. %	0.5	7.6
400 - 650° F, wt. %	2.2	23.1
650 - 1000° F, wt. %	20.1	52.2
1000° F plus Residue, wt. %	77.2	17.1
Gradient Elution Chromatography		
Saturates, wt. %	15.8	13.4
MNA/DNA Oils, wt. %	3.5	37.1
PNA Oils, wt. %	9.0	5.7
Soft Resins, wt. %	5.8	17.4
Hard Resins, wt. %	2.3	3.5
Polar Resins, wt. %	3.6	2.6
Asphaltenes, wt. %	35.9	15.7
Noneluted Asphaltenes, wt. %	24.1	4.6

* Normalized to 100%

Table 6 - Analysis of the Liquid Product from the Fluidized-Bed Pyrolysis of the PR Spring South Oil Sand

Reactor Temperature, K	823
Solids Residence Time, min.	20
Fluidizing Gas Velocity, LPH (STP)	144
Product Yields, wt. %*	
Gas	30.6
Liquid	49.3
Coke	20.1

Property	PR Spring South	Pyrolysis Liquid Product
API Gravity, °API	8.8	10.2
Viscosity, cps	10,071. (@373 K)	548.5 (@298 K)
Pour Point, K (°F)	433. (320 °F)	283. (50 °F)
Conradson Carbon Residue, wt. %	24.0	7.2
Ash, wt.%	1.9	0.01
Simulated Distillation		
Volatility, wt. %	14.3	97.7
IBP - 400° F, wt. %	.07	4.9
400 - 650° F, wt. %	1.3	36.4
650 - 1000° F, wt. %	12.3	56.4
1000° F plus Residue, wt. %	85.7	2.3
Gradient Elution Chromatography		
Saturates, wt. %	4.1	7.4
MNA/DNA Oils, wt. %	5.3	35.6
PNA Oils, wt. %	1.0	3.9
Soft Resins, wt. %	4.0	17.8
Hard Resins, wt. %	1.8	2.4
Polar Resins, wt. %	1.1	2.7
Asphaltenes, wt. %	55.7	26.4
Noneluted Asphaltenes, wt. %	27.1	3.8

* Normalized to 100%

and where it hung over a metal trough which collected the gravity drained oil.

This deposit, as well as the Asphalt Ridge deposit, was the subject of intense activity during the late 1970s-early 1980s. While very few on-site operations were conducted, numerous companies and government agencies studied the resource and assessed the recovery potential. During 1983, the UTAR Division of Bighorn Oil Company, Salt Lake City, operated a 200 barrel-per-day plant, located in section 5, Township 16 South, Range 24 East. The recovery process utilized diesel fuel as a solvent to extract the bitumen. As of 1985, with the release of the draft environmental impact statement for the PR Spring oil sand deposit, nine companies proposed development operations. Beartooth Oil Company proposed two in-situ operations intended to produce 150 barrels per day each. Bradshaw, Duncan, Enserch, Farleigh, and Thompson also proposed 150 BPD in-situ operations. Kirkwood Oil and Gas Exploration and Production proposed a 16,000 BPD in-situ operation. Two surface mining and extraction plant operations were also proposed, one by Enercor to produce 5,000 BPD and the other by Mobil Oil to produce at 40,000 BPD.

Maxwell Quarry: Section 17, T12S, R25E

The Maxwell Quarry was an operating pit as recently as of July 1991. The operator, James Maxwell of Provo, was experimenting with a steam extraction method. Water was trucked from an unspecified location to the site of the pit. The source of water may have been the White River.

Uintah County Quarry: Section 32, T14S, R23E

Uintah County excavated a surface oil sand occurrence to determine the feasibility of using the PR Spring oil sand ore for road paving material. The site did not prove suitable and was reclaimed.

Wasatch Tar Sands Quarry: Section 32, T14S, R23E

John B. Fairbanks, Jr., and Wasatch Tar Sands, of Salt Lake City, excavated a surface oil sand occurrence for "development" purposes. Apparently Wasatch Tar Sands did not have permission to develop the lease and the site was reclaimed.

Enercor Quarry: Section 32, T12S, R25E

Enercor Company, of Salt Lake City, excavated a surface oil sand occurrence in 1981. The pit, two acres in size, was developed in the "E" Zone, with 3,500 tons of material extracted. The site was reclaimed in 1985 and additional remedial work was conducted in 1990. As the reclamation work was minimal (very thin to no overburden soil), permission to acquire samples from the site can be obtained without extensive permitting.

U-Tar Quarry: Section 5, T16S, R24E

During 1983, the UTAR Division of Bighorn Oil Company, Salt Lake City, operated a 200 barrel-per-day plant, located in SE1/4 of NE1/4 of Section 5, Township 16 South, Range 24 East. The process involved solvent extraction of the bitumen.

Kerr-McGee Quarry: Section 36, T15S, R22E

Byrd[5] indicated the existence of a pit located in Section 36, Township 15 South, Range 22 East. which was operated by Kerr-McGee

Company. Nothing else is known regarding the operation conducted at this pit.

Kamp Kerogen: Section 2, T14S, R22E

Kamp Kerogen was the site of the field camp which supported the in-situ oil shale retorting experiments of Geokinetics, Inc., in the PR Spring oil sand area. A technology for producing crude shale was developed, tested, and evaluated here, and more than 135,000 barrels of shale oil were produced and used as potential refinery feedstock for the production of aviation turbine fuels under programs directed by the U.S. Departments of Energy and Defense.

The technology was adapted to thick, rich oil shales with moderate dip (few to <8°) at overburden depths of less than 100 feet. Rectangular plots of shale were extensively fractured by slurry explosives set in varying patterns. The shale was ignited and air was injected downdip to sustain a combustion front. As the front advanced up dip, oil produced by in-situ retorting flowed down dip to sumps and was pumped to the surface for storage.

The process, known as LOFRECO (Low Front End Cost) or "fluff'n puff", produced quality crude shale oil which was refined into a number of products, notably jet fuel which was tested extensively by the Air Force. Operations ceased in 1984. Geokinetics, Inc. did not attempt to apply LOFRECO to the PR Spring oil sand zones.

OWNERSHIP

Maxwell Quarry

The quarry is located in Section 17, Township 12 South, Range 25 East, a state-administered section. The quarry is being operated by James F. Maxwell of Provo, Utah.

Uintah County Quarry

The quarry is located in NW SE Section 32, Township 14 South, Range 23 East, a state administered section. As the site has been reclaimed, it cannot be disturbed without extensive permitting.

Wasatch Tar Sands Quarry

The quarry is located in NE SW Section 32, Township 14 South, Range 23 East, a state administered section. The lease was held by Celsius Corporation (Mountain Fuel). As the site has been reclaimed, it cannot be disturbed without extensive permitting.

Enercor Quarry

The quarry is located in Section 32, Township 12 South, Range 25 East, a state administered section. The lease was held by Texaco, and subleased to Enercor. The Texaco lease expired in 1990, and in 1991 leased to Maxus Exploration Company. Geokinetics had the oil shale lease on same lands.

U-Tar Quarry

Ownership of NE1/4 quarter is split between D.J. Johnson Family Trust (75%) and Richard Peasmont (25%). The site has not been reclaimed and might be available for pilot plant siting.

Additional Information

The PR Spring deposit is stratigraphically related to the westward lying Hill Creek deposit. The separation of these deposits is strictly erosional, with Willow Creek separating the two.

Report on the September 1992, Uinta Basin Field Trip of the Department of Fuels Engineering, University of Utah

A field trip was conducted on the 10th and 11th of September 1992 by the oil sand research and development group of the Fuels Engineering Department, University of Utah. Two sites in the PR Springs area were visited to collect oil sand samples. The locations are referred to as the UTAR Pit and the Enercor Pit. Permission to obtain samples was obtained from the Johnson Family Trust and the Maxus Exploration Company, respectively.

UTAR Pit. NWSENE Sec. 5. T16S. R24E Natural outcrops of oil sand form resistant ledges in a gully just east of the location at approximately the same stratigraphic level as the pit. A cursory study of the slopes surrounding the location did not turn up any other outcrops of oil sand, but an oil seep can be seen in the bottom of the canyon below the pit, near the mouth of the gully containing the oil sand outcrops. Twenty four, polyethylene lined 55-gallon drums of oil sand ore were mined and transported to Salt Lake City for use in process research and development studies at the University of Utah.

Enercor Pit. CW/2 NWSW Sec. 32. T12S. R25E. This location, which had been bulldozed over as part of a reclamation effort, occurs at the point of a ridge. An apron of rock debris surrounds the

location itself and blankets the uppermost 15 feet or so of the slope, concealing any outcrops that may originally have occurred in that interval (Unit 8 of the attached stratigraphic section, Figure 9). Oil sand outcrops are visible immediately downsection from this covered interval (Unit 7). It is impossible to say how much of Unit 8 may consist of oil sand, but there is no reason to doubt that the oil sand of Unit 7 continues upward under the cover of Unit 8.

Unit 6 is mostly covered, but shale can be seen here and there in washes. Underlying Unit 6 is a conspicuous and distinctive ledge-forming stromatolitic limestone (Unit 5). The underlying 15 feet or so (Unit 4) consists of fine-grained clastic rocks interbedded with oil sand, and the two lithologies appear to intertongue. The base of Unit 4 is marked by the disappearance of the fine-grained interbeds, and the underlying 20 feet or so (Unit 3) consist of massive oil sand.

Unit 2 is a resistant cross-bedded sandstone unit without any appreciable hydrocarbon content. The contact between Unit 2 and Unit 3 is interesting: it is very irregular and appears to be defined solely by the presence of oil in the pore spaces of the sandstone of Unit 3. This is to say that the contact appears to cut across primary sedimentary structures and is probably more an accident of hydrocarbon emplacement than a reflection of pre-existing differences in the rock. There are obviously substantial petrographic differences between the units now, however, as a result of their divergent diagenetic histories. Unit 3 is less

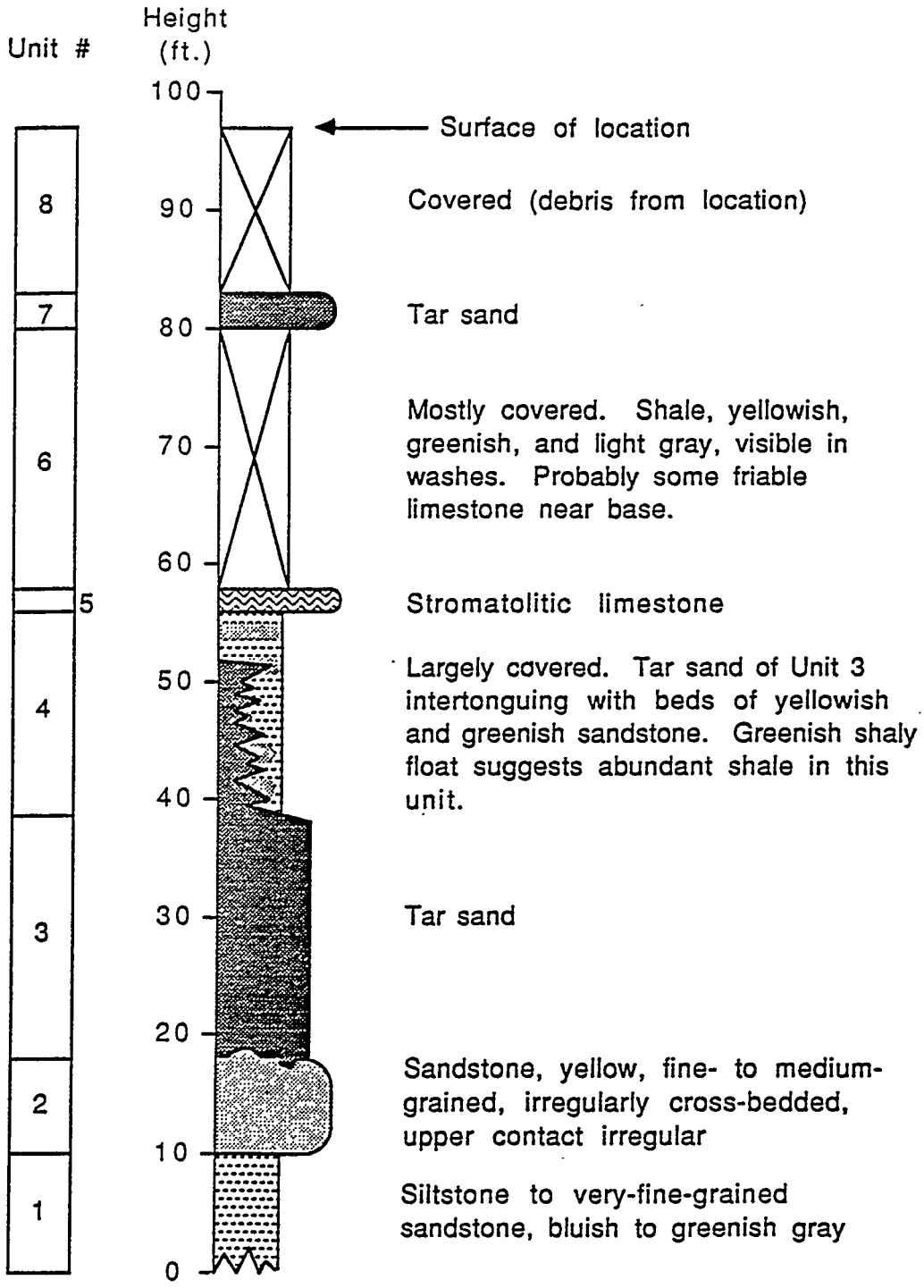

Stratigraphic Section underlying Intercor Site

c w/2 nw sw Sec. 32, T12S, R25E,

Figure 9. Stratigraphic Section Underlying the Enercor Site on the PR Springs Oil Sand Deposit.

resistant than Unit 2 and appears to be nearly structureless, although there are traces of what may be deformed bedding near the contact with Unit 2. The structureless appearance of Unit 3 may be the result of deformation within the oil sand, which is quite malleable. Approximately 5 polyethylene 55-gallon drums were loaded with the best available material from the floor of the partially restored pit. This material was reserved for analysis purposes and was not used in process studies.

Stratigraphy This report relies upon the stratigraphy and mapping of Cashion[2], and the stratigraphic units are as defined by Cashion[2].

Both the UTAR and Enercor locations are underlain by rocks of the uppermost ("A") tongue of the Douglas Creek Member of the Green River Formation. In the area of the UTAR Pit, Cashion[2] places the base of the overlying Parachute Creek Member at the Mahogany oil-shale bed, a distinctive regional marker bed. In the area of the Enercor site, on the other hand, Cashion[2] places the contact appreciably below the Mahogany bed. It is difficult to know, therefore, what to make of the fact that the Enercor Pit, but not the UTAR Pit, is shown on the map as being close to the overlying Parachute Creek Member. Cashion[2] stated, referring to the oil sands of this region, "The thickest, most continuously impregnated bed or beds occurs in the Douglas Creed Member in a zone about 100 feet below the Mahogany oil-shale bed." Although Cashion's measured sections I and L lie near the UTAR and Enercor sites, respectively, those sections do not yield any additional

information about the stratigraphic position of the oil sands.

Figure 12 in Cashion's report[2] suggests that the oil-impregnated interval in the area of the UTAR site is about 40 feet thick, while the oil-impregnated interval in the vicinity of the Enercor site is about 30 feet thick. The same figure gives the amount of oil in the oil sands as between 5 and 15 gallons per ton.

SUNNYSIDE OIL SAND DEPOSIT

Deposit Location

The Sunnyside oil sand deposit is located in Townships 12 and 13 South, Ranges 13, 14, and 15 East; Township 14 South, Ranges 14 and 15 East (Salt Lake Meridian), Carbon County.

Reconnaissance of the Sunnyside Oil Sand Deposit

A reconnaissance of the Sunnyside oil sand deposit was made during the 1992-1993 contract period to identify potential sample acquisition sites. The consolidated nature of the exposed bitumen saturated zone led to the conclusion that the exposed face would have to be drilled and shot in order to obtain drum quantity samples. There was a stockpile of mined ore in the vicinity of the northern pit; however, there appeared to be a large amount of overburden material dispersed in the ore which may obviate its use. A photographic record of the site was made to provide additional insight as to the potential for sample acquisition during the 1993-1994 contract period.

FUTURE ACTIVITIES

Drum quantity samples will be obtained from the Sunnyside oil sand deposit in the spring of 1994. The characterization of the Asphalt Ridge and PR Spring oil sand deposits will be continued.

CHARACTERIZATION OF CIRCLE CLIFFS TAR SANDS OF UTAH

Principal Investigator:	J.D. Miller
Co-Principal Investigator:	F.V. Hanson
PostDoctoral Fellow:	K. Bukka

INTRODUCTION

Bitumen impregnated sandstone deposits are known to occur in a variety of stratigraphic and climatic environments throughout the world. However, nowhere else can such a diversity among the desposits be observed as in the United States. A recent estimate of the total U.S. oil sand resources was reported to be at 54 billion barrels of in-place bitumen[13]. Although this resource is small in comparison to the Canadian oil sand resources, which amount to 1.7 trillion barrels,[14] their variety may offer an excellent opportunity for some fundamental understanding with regard to the nature of the resource and its diagenesis. The largest of these U.S. deposits are found in Utah, and are mainly situated in the eastern one-half of the State. They are widely scattered among nine major and thirteen minor deposits. The estimated and speculated oil sand resources contained in the major deposits are listed in Table 7[13]. Since the combined estimates of the minor deposits amount to about 3% of the total Utah oil sands, they are not believed to be viable for commercial exploitation under the prevailing circumstances.

Among the major deposits, a relatively large body of data has been obtained for the Asphalt Ridge and Sunnyside deposits. Recently, significant efforts have been directed to the study of

Table 7. Estimated Major Oil Sand Deposits of Utah.[13]

Major Deposits	Measured (MMB)	Speculative (MMB)
Uinta Basin		
P.R. Spring	2,140	2,230
Hill Creek	320	560
Sunnyside	4,400	1,700
Whiterocks	60	60
Asphalt Ridge	830	310
Paradox Basin		
Tar Sand Triangle	2,500	420
Nequoia Arch	730	160
Circle Cliffs Uplift		
Circle Cliffs	560	1,140
San Rafael Uplift		
San Rafael Swell	300	250
Total	11,840	6,830

the Whiterocks deposit[15-17]. Apparently, the high bitumen saturation values or the relative ease of accessibility to the above-mentioned three major deposits were the main reasons for these extensive studies.

At the Univerity of Utah sustained efforts have been made in areas such as the estimation of the resource, chemical characterization of the bitumen, development of bitumen separation technologies and bitumen upgrading strategies. The results of characterization studies on the Circle Cliffs oil sand deposit are presented here. This activity focused on the determination of mineral composition and chemical characterization of the bitumen present in the oil sand. The effect of mineral composition on the bitumen recovery, and the quality of the bitumen product that can be expected from the modified hot-water process are discussed. Finally, the influence of chemical composition on bitumen viscosity is discussed with respect to the earlier reported empirical relationship between the carboxylic acid content and the viscosity of the bitumen[18].

EXPERIMENTAL

The Circle Cliffs oil sand sample was obtained through Kirkwood Oil and Gas Exploration & Production of Casper, Wyoming. The extent of this deposit and a clear description of the location was presented by Ritzma.[19] Initially, an outcrop of the deposit was located (in the NW quarter of the SE quarter of Section 32, Township 34 south, Range 7 east), and a section of the outcrop was dynamited to expose the unweathered bitumen-bearing sandstone from

a depth of approximately 4-6 feet. The exposed oil sand sample was collected into six 55-gallon drums which were sealed to prevent interaction with the ambient air during the transportation and storage.

The large chunks of oil sand samples were ground in two different stages for the purpose of extracting bitumen from them. In the first stage a jaw-crusher was used to reduce the sample size to 1-2 inches, and in the second stage a roll crusher was used to reduce the sample to less than one-quarter inch size. The crushed oil sand samples were extracted in several batches to obtain bitumen by the Dean-Stark toluene extraction method. In these extractions, the bitumen and water contents of the samples were noted. The toluene extracts of the bitumen were subjected to vacuum distillation on the rotary evaporator, and the final traces of the solvent were removed at high vacuum and temperature (20 torr and 363 K).

The residual sand, obtained after the extraction of bitumen, was analyzed to determine the mineralogical composition. A 120 g representative sample was obtained from a 2 kg oil sand sample by fractionation using a sample riffler. This sample was wet sieved using a VECO #254 Eerbeak (Holland) precision sieve with a circular opening of 45 μ. The oversize particles were dried in the oven at 383 K, and ground to a finer size in a micro-pulverizer (Fritsch, Pulverisette) for 10 minutes. Thus, sieving and grinding were repeated several times until more than 95% of the sand passed through the sieve. The finely ground sand sample (particle size <

45 μ) was analyzed for mineralogical composition by X-ray diffraction. Identification and quantification of the constituent minerals of the oil sand were made as described earlier.[20]

The viscosity of the extracted bitumen was measured on a Brookfield Cone/Plate Viscometer using 3° cone spindle CP #42. These measurements were made in the temperature range 323-363 K. The elemental composition of the bitumen was determined using LECO-600 and LECO-SC132 analyzers.

In an attempt to characterize the bitumen sample, it was quantitatively separated into saturates, aromatics, resins, and asphaltenes (SARA) fractions following a procedure described previously[21,22]. Each fraction was further characterized in terms of elemental and FTIR spectroscopic analyses.

The FTIR spectroscopic analysis of the Circle Cliffs oil sand bitumen and its separated fractions was performed on a Digilab FTS-40 spectrometer equipped with liquid nitrogen cooled MCT (mercury-cadmium telluride) detector, and 3240-SPC data processing station. The less viscous saturate and aromatics fractions were analyzed in the standard transmission mode. The viscous resin fraction and the solid asphaltene fraction were analyzed using a specular reflectance accessory. Sample preparation and the details of the technique have been described previously[22]. The spectra of the samples were obtained from 256 scans in the mid-infrared region with a nominal resolution of 4 cm^{-1}.

RESULTS AND DISCUSSION

Mineralogical Analysis.

The bitumen content of the Circle Cliffs oil sand was low (2.8 wt%) in comparison to the other oil sand deposits of Utah, which were observed to be in the range 5-14 wt%. [23,24] The moisture content was also lower (0.3 weight percent) than that reported for other oil sands.[22,25] The physical properties and the chemical characteristics of the Circle Cliffs oil sand bitumen obtained from the same location were recently reported.[26] Shun[26] also determined the fractional composition of the bitumen based on the method of gradient elution chromatography. Since the fractional composition of bitumen is dependent on the method of fractionation, the results presented here are notably different from those reported by Shun.[26] The results of bitumen fractionation based on a SARA type analysis are presented in this report. This task was undertaken in an attempt to compare the chemical characteristics of the Circle Cliffs bitumen to the Uinta basin (Utah) bitumens such as Asphalt Ridge, Sunnyside, and Whiterocks[21,22].

The mineralogical composition of the Circle Cliffs oil sand is presented in Table 8. The analysis indicated that the Circle Cliffs mineral matter consisted of comparably low silicious material[20] with a significant proportion of carbonate minerals such as calcite and dolomite. Kaolinite and K-feldspar were observed to be relatively high in comparison with the Uinta basin oil sands.[20] In addition, a small amount of pyrite (3%), which was absent in the Uinta Basin oil sands, was also detected. The differences in the

Table 8. Mineralogical Composition of the Dry and Bitumen Free Circle Cliffs Oil Sand.

Mineral	Weight Percent
Quartz	44
Calcite	18
Dolomite	11
Kaolinite	10
K-Feldspar	7
Plagioclase	4
Pyrite	3
Illite	3
Amorphous Material	1

other observed minerals were relatively small. The minerals such as quartz, K-feldspar, plagioclase are considered to be inert and are not expected to interfere with hot-water processing of Circle Cliffs oil sands. However, the other minerals such as kaolinite and carbonate minerals may potentially interfere with the separation of bitumen, particularly in the flotation step of the hot water processing of oil sands. It has also been reported that kaolinite influences the thermal recovery of bitumen from these oil sands by functioning as a catalyst, thus, affecting the ratio of liquid and gaseous product yields.[26]

Viscosity of Bitumen

The viscosity of the toluene extracted bitumen from Circle Cliffs oil sand was measured in the temperature range 318-363 K. A linear relationship was observed between log [viscosity] and 1/T, in which T (temperature) was expressed in degrees Kelvin (Figure 10). From this relationship, the viscosity value of the bitumen at 323 K was determined, and the data are presented in Table 8 for the purpose of comparison with the Uinta Basin oil sand bitumens. The viscosity at 323 K indicates that the Circle Cliffs bitumen has a moderately high value, and occupies an intermediate position among the bitumens listed in Table 9.

Table 9. Comparison of Circle Cliffs Bitumen Viscosity with Those of the Uinta Basin Bitumens.

Bitumen Source	Viscosity,(Pa.S) At 323 K
Whiterocks	33
Asphalt Ridge	43
Circle Cliffs	258
Sunnyside	1260

Elemental Analysis of the Bitumen

The elemental analysis of the Circle Cliffs oil sand bitumen along with those of the Uinta Basin bitumens are presented in Table 10. Several distinct features of the Circle Cliffs bitumen are apparent from examination of Table 9. Unlike the other bitumens listed in

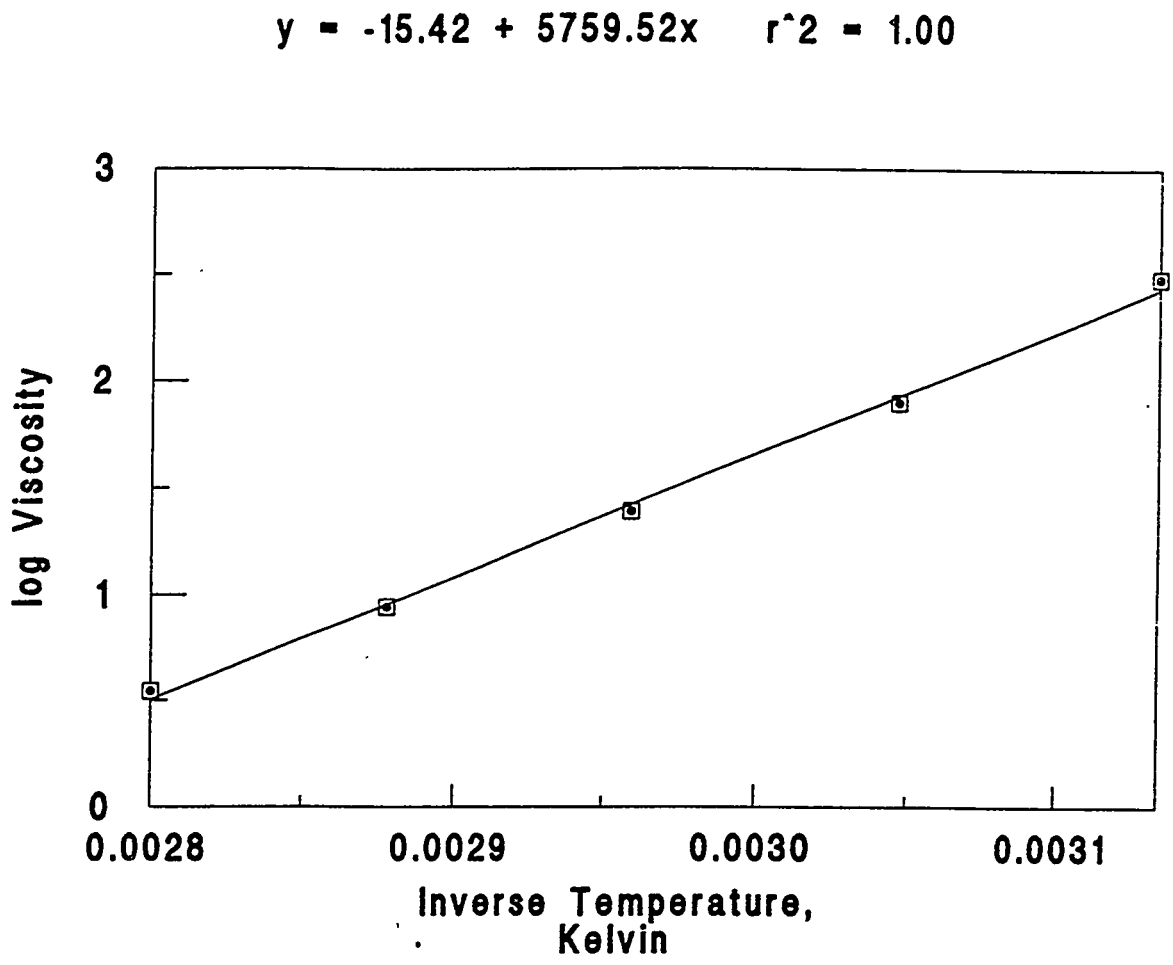

Figure 10. Variation of Circle Cliffs bitumen viscosity with temperature.

Table 10. A Comparision of Elemental Composities of Circle Cliffs and Uinta Basin Oil Sand Bitumens of Utah.

Bitumen Source	Weight %					Atomic Ratio				Mol. Wt.	Empirical Formula
	Carbon	Hydrogen	Nitrogen	Sulfur	Oxygen	H/C	N/C	S/C	O/C		
Whiterocks	86.4	11.5	1.1	0.4	0.5	1.60	0.011	0.002	0.004	500	$C_{36}H_{58}N_{0.39}S_{0.06}O_{0.16}$
Asphalt Ridge	84.5	11.0	1.1	0.4	3.0	1.56	0.011	0.002	0.027	490	$C_{34}H_{54}N_{0.37}S_{0.07}O_{0.93}$
Sunnyside	84.9	10.3	0.9	0.5	3.4	1.45	0.009	0.002	0.030	588	$C_{42}H_{73}N_{0.52}S_{0.64}O_{2.08}$
Circle Cliffs	83.0	9.5	0.5	4.9	2.1	1.37	0.005	0.022	0.019	744	$C_{51}H_{51}N_{0.27}S_{1.14}O_{0.98}$
Athabasca[18]	83.2	10.1	0.5	4.7	1.5	1.46	0.005	0.021	0.014	407[26]	$C_{28}H_{41}N_{0.14}S_{0.60}O_{0.38}$

the Table 10, Circle Cliffs bitumen has almost an order of magnitude higher sulphur content than the Uinta Basin bitumens. Only one other Utah oil sand bitumen, viz., that derived from Tar Sand Triangle deposit is known to contain comparable amounts of sulphur.[27] The Circle Cliffs bitumen resembles the Athabasca bitumen with regard to sulphur content, thus, the elemental analysis of the Athabasca bitumen is also included in Table 10. Bitumens with high sulphur contents are believed to have marine origins. On the other hand, the low sulphur bitumens such as those occurring in the Uinta basin are believed to be of lacustrine or of fresh water origin. Considering that the Utah oil sands are situated in the eastern one-half of the State, it is interesting to note that the sulphur content of the bitumens appears to increase from the deposits in the north to the deposits in the south, as shown in Table 11. In other words there appears to be a well defined boundary between the marine origin and lacustrine bitumens in Utah. The second notable feature of the Circle Cliffs bitumen, as noted from the data presented in Table 10, is indicated by the atomic ratio H/C. As seen from Table 10, Circle Cliffs bitumen has the lowest H/C ratio indicating the highly unsaturated or aromatic nature of the bitumen. In this respect, Circle Cliffs bitumen is more aromatic than the Athabasca bitumen. Finally, the molecular weight of the Circle Cliffs bitumen, as determined by the vapor pressure osmometry method, was significantly higher than the Uinta Basin bitumens and nearly twice that of the Athabasca bitumen.

Table 11. Trends in the Sulphur Content Among the Utah Oil Sand Bitumens.

Location of The Deposit	Bitumen Source	Sulphur Content, Wt. %
North	Whiterocks	0.4
North	Asphalt Ridge	0.4
Central	Sunnyside	0.5
Central	PR Spring	0.8
South	Tar Sand Triangle	4.4
South	Circle Cliffs	4.9

Fractional Analysis of Bitumen

The fractional composition of the Circle Cliffs bitumen, as determined by the modified SARA analysis, is presented in Table 12 The composition of the Uinta Basin bitumens, obtained in the similar manner, are also included in Table 12 for comparison. The composition of the Circle Cliffs bitumen resembles the Sunnyside bitumen, particularly with regard to asphaltene, saturate, and resin contents. Although the viscosity of the Circle Cliffs bitumen is much lower than that of the Sunnyside bitumen (see Table 9), its asphaltene content is higher. This observation further underscores the assertion reported earlier that the viscosity does not depend solely on the asphaltene content of the bitumen.[18,21]

In order to determine the distribution of sulphur containing

Table 12. Quantitative Fractional Composition of the Circle Cliffs Oil Sand Bitumen Based on SARA Type Analysis.

Bitumen Fraction	Athabasca	Weight Percent			
		Circle Cliffs	Uinta Basin Bitumens		
			White Rocks	Asphalt Ridge	Sunnyside
Saturates	34.6	23.8	30.2	32.4	24.9
Aromatics-I	21.9	17.0	14.6	22.4	18.1
Aromatics-II	3.1	1.4	6.8		
Aromatics-III	1.7	0.8	3.4	0.5	0.5
Resin-I	24.7	28.2	38.8	37.6	30.0
Resin-II	0.7	0.6	1.3		0.6
Asphaltenes	15.0	28.1	3.6	7.3	23.7

compounds among the fractions, elemental analyses were performed on the SARA fractions from the Circle Cliffs and Athabasca bitumens. The results are presented in Tables 13 and 14. The results clearly show some differences between these two bitumens. In the case of Circle Cliffs bitumen the aromatic fraction was shown to contain greater amounts of sulphur than the resin fraction, whereas in case of Athabasca bitumen the resin fraction contained more sulphur than the aromatic fraction. Although oxygen contents were not determined directly, the values presented in Table 13 and 14 indicate that the polar fractions may have incorporated oxygen from the ambient air. It is quite probable that some of the compounds present in these fractions are susceptible to oxidation. This can be clearly demonstrated by assembling the separated fractions in their appropriate proportions into respective bitumens and comparing these calculations with the bitumens' original elemental composition. In general, most bitumens have been noted to increase their oxygen content during the course of fractional separation.[18]

Infrared Spcetroscopic Analysis

The SARA fractions from the Circle Cliffs bitumen were analyzed by FTIR spectroscopy to determine the chemical differences among the fractions. The saturates fraction is predominantly a mixture of paraffinic and naphthenic hydrocarbons with very small amounts of unsaturated compounds. The infrared spectrum of the saturates fraction, as shown in Figure 11, gave a simple profile consisting of stretching and bending vibrations of the C-H bonds. As indicated in the elemental analysis of this fraction (Table 13)

Table 13. Elemental Analyses of the Fractions Derived from Circle Cliffs Oil Sand Bitumen.

	Weight Percent							
	C	H	N	S	O	H/C	N/C	S/C
Saturates	84.9	12.4	0.0	1.4	1.3	1.75	-	0.00
Aromatics-I	81.9	9.1	0.0	6.4	2.6	1.33	-	0.02
Resin-I	73.7	8.6	0.5	4.2	13.0	1.40	0.00	0.02
Asphaltenes	81.3	7.6	1.0	6.7	3.4	1.12	0.01	0.03

Table 14. Elemental Analyses of the Fractions Derived from Athabasca Oil Sand Bitumen.

	Weight Percent							
	C	H	N	S	O	H/C	N/C	S/C
Saturates	86.1	12.3	0.1	1.4	0.0	1.72	0.00	0.00
Aromatics-I	86.3	9.5	0.7	2.4	1.1	1.33	0.00	0.01
Resin-I	76.4	9.2	0.9	5.2	8.3	1.45	0.01	0.02
Asphaltenes	79.3	7.8	1.2	8.0	3.7	1.18	0.01	0.03

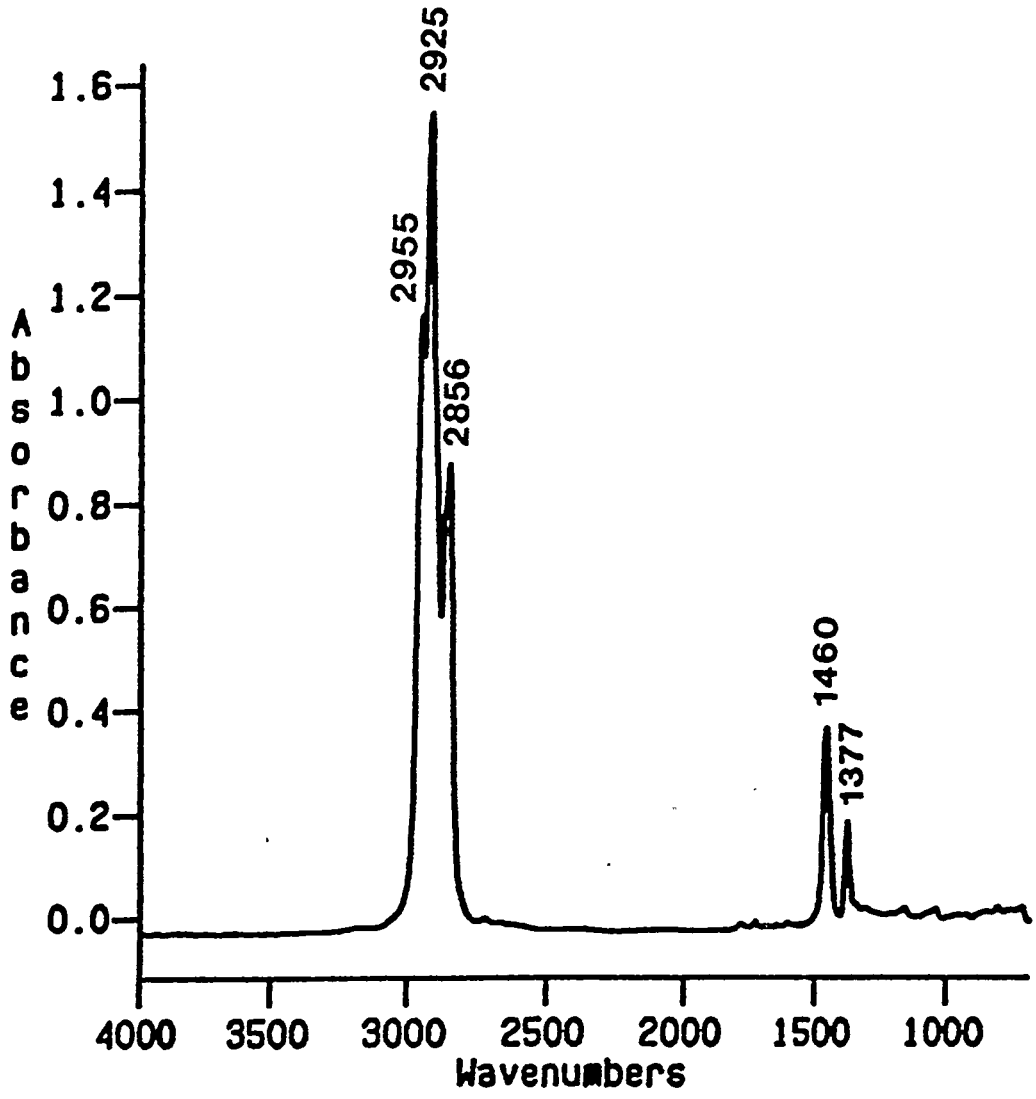

Figure 11. Infrared Spectrum of the Saturates Fraction of the Circle Cliffs Bitumen.

there may be some sulphur-containing compounds. However, their abundance is relatively low. The infrared spectrum of the aromatic-I fraction is presented in Figure 12. Typically, the spectral features of the aromatic fractions include aromatic C-H stretching, conjugated -C=C- stretching and C-H bending vibrations at 3650 cm^{-1}(broad shoulder on the aliphatic C-H stretching band), at 1600 cm^{-1}, and in the region 950-750 cm^{-1} respectively. The appearance of an absorbance band at 1037 cm^{-1}, indicates the presence of sulphur compounds in this fraction as noted from the elemental analysis (Table 12). This band is generally attributed to the sulfoxides. The other bands in the spectrum are relatively weak and may represent other of the functional groups.

Earlier work has shown that the resin fractions are most characteristic of the oil sand bitumens.[18,21] The spectroscopic analyses of the resin fractions have been used to establish the relationship between physical properties and chemical composition. It has been shown previously that the carboxylic acids present in the bitumen accumulate in the resin fraction, and an empirical relationship between the viscosity of the bitumen and the amount of carboxylic acids was demonstrated. The infrared spectrum of the Circle Cliffs resin fraction is presented in Figure 13. In comparison with the spectra of resin fractions derived from the other U.S. and Canadian oil sand bitumens,[18] that of the Circle Cliffs bitumen shows some unique characteristics. The principal feature of the spectrum is the presence of an extremely sharp absorbance band at 1727 cm^{-1}, which has been attributed to the

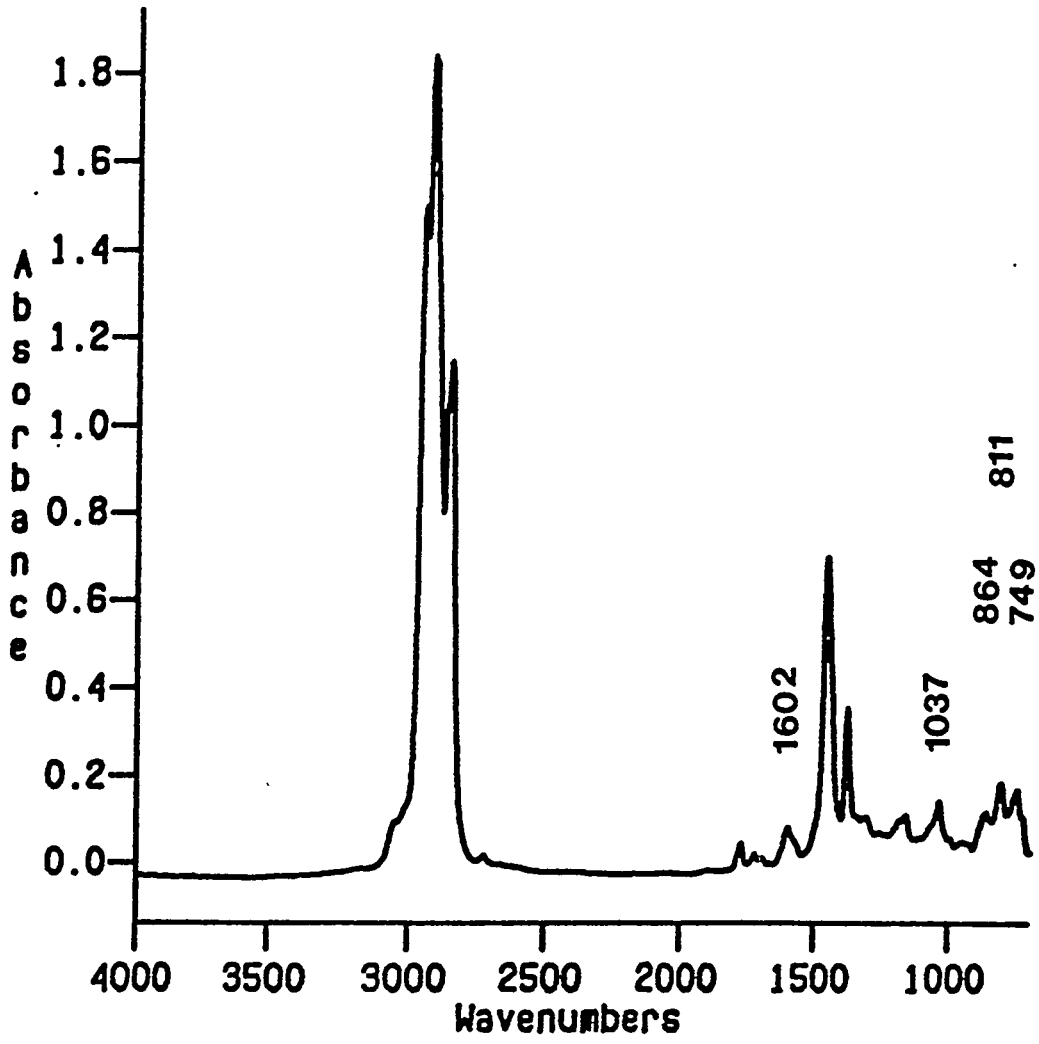

Figure 12. Infrared Spectrum of the Aromatics-I Fraction of the Circle Cliffs Bitumen.

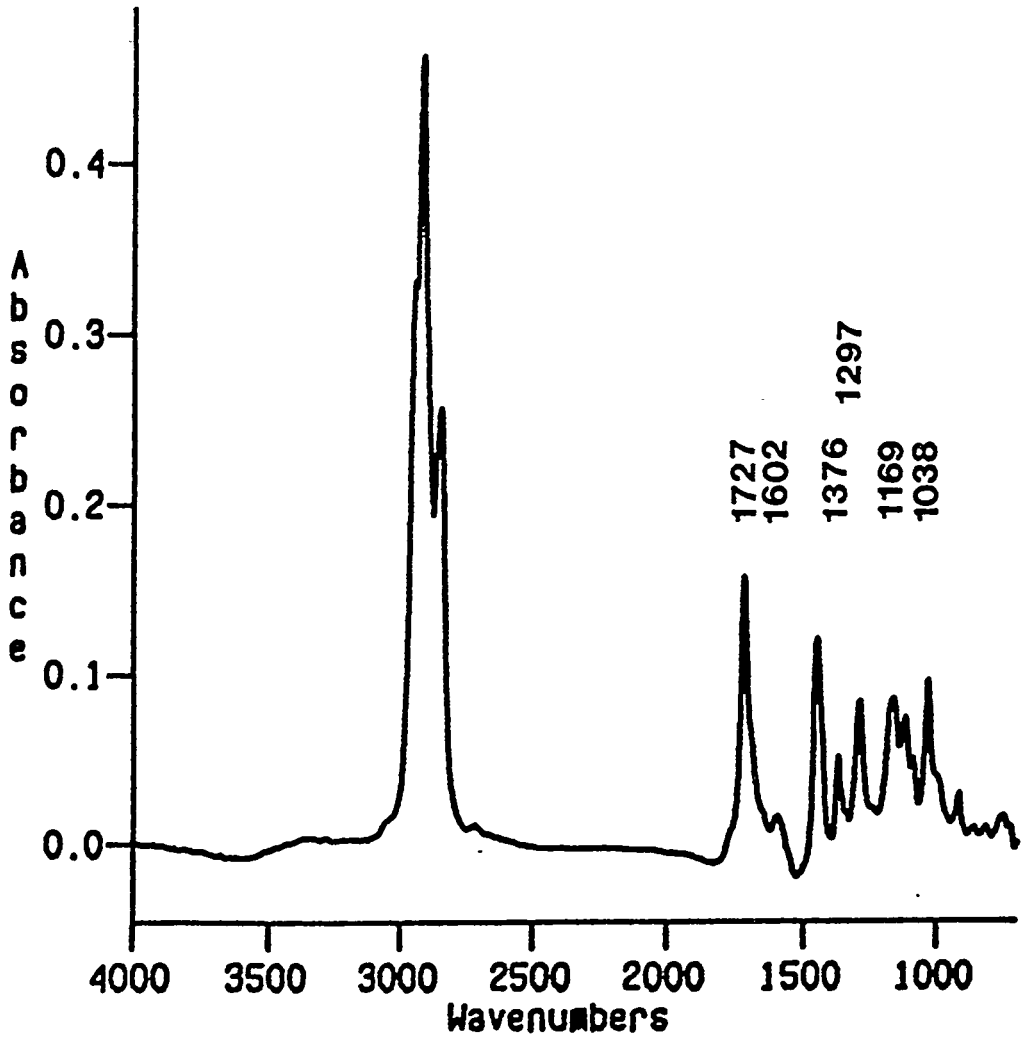

Figure 13. Infrared Spectrum of the Resin-I Fraction of the Circle Cliffs Bitumen.

carbonyl group present in an ester.[28] In the course of the analysis of U.S. oil sand bitumens, it was observed that carboxylic acids were present in the resin fractions, and occasionally, a small amount of esters were found, as noted in the case of Oklahoma bitumen.[18] On the other hand, it has been reported that the Athabasca bitumen resin fraction contained predominantly esters and a small amount of carboxylic acid.[18] In the case of Circle Cliffs bitumen, as shown in Figure 13, the infrared spectrum of the resin fraction indicates an exclusive band for the esters with no apparent indication of the carboxylic acid band, which is usually found at 1700 cm^{-1}. It is possible to have a low concentration of carboxylic acid such that its aborbance band may have been eclipsed by the ester band. As noted earlier with regard to the sulphur content the Circle Cliffs bitumen resembles the Athabasca bitumen in terms of chemical composition. The origin of an intense band observed at 1297 cm^{-1} is uncertain, but it is presumed to arise from a sulfur containing functional group. This speculation is based on the fact that no such band was observed in the resin fractions of other U.S. oil sand bitumens studied in our laboratory.[18] Furthermore, a similar band was observed in Athabasca bitumen, and both these bitumens contain significant amounts of sulphur. The band at 1169 cm^{-1} is believed to be due to the -C-O-C- linkage in the ester group. Evidence for this band assignment comes from the observation that when the esters in the resin fraction were hydrolyzed the band at 1169 cm^{-1} disappeared. Finally, the infrared spectrum of the asphaltene fraction is presented in Figure 14. In

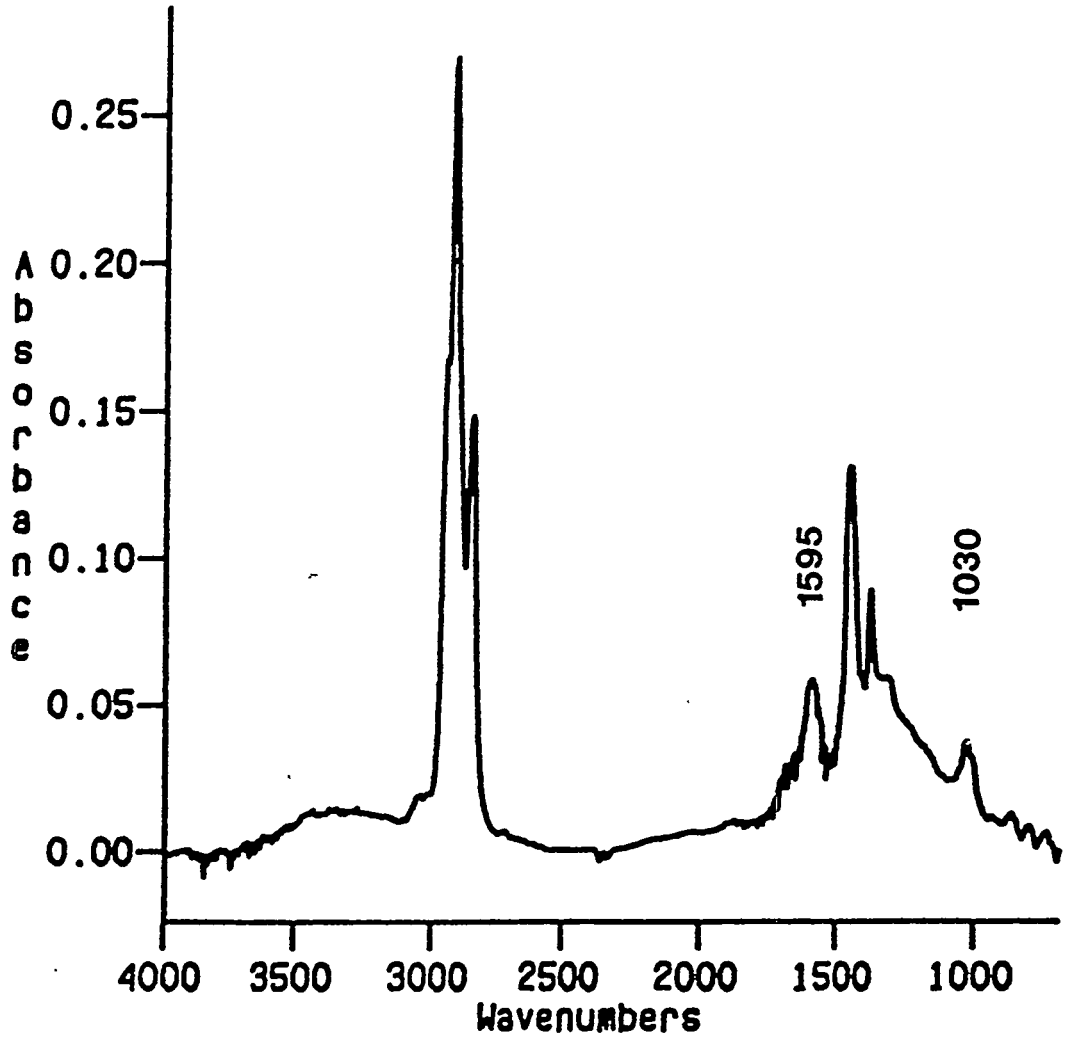

Figure 14. Infrared Spectrum of the Asphaltene Fraction of the Circle Cliffs Bitumen.

most cases the asphaltene fraction presents a featureless spectrum; hence, not much information can be derived from it.

The analysis of Circle Cliffs oil sand bitumen provides an example of the complementary role played by the asphaltene and carboxylic acid contents in the determination of bitumen viscosity. This bitumen, which is high in asphaltene content, does not exhibit a high viscosity due to the low concentration of carboxylic acids; that is, the concentration is below the threshold required to suspend the solid asphaltenes. The presence of 28.1% of asphaltenes renders Circle Cliffs bitumen more viscous than the Whiterocks, Asphalt Ridge, and Athabasca bitumens which contain 3.6%, 7.3%, and 15% asphaltenes, respectively. The Sunnyside bitumen, because of its high carboxylic acid content, exhibits higher viscosity despite its lower asphaltene content (23.7%). This is explained by the enhanced interaction of the asphaltenes with the carboxylic acids present in resin and aromatic fractions through hydrogen bonding which results in a stabilized suspension.

Oil Sand Processing Considerations

The hot-water processing technology developed for the Canadian oil sand deposits has been found to be inadequate for the U.S. oil sand bitumens.[23] This is mainly attributed to the inherent differences in the physical and chemical properties of the U.S. deposits. The main differences are the oil-wet nature and relatively high viscosity of the U.S. oil sand bitumens. These differences necessiated the development of a modified hot-water process for application to U.S. oil sands. This process includes a

diluent pretreatment step to reduce the viscosity of the bitumen prior to digestion. [29,30] However, it has been observed that the mineralogical composition of the oil sand also plays an important role in the overall recovery and in the quality of the bitumen obtained in the primary (gravity separation) and secondary flotation products.[20] The presence of minerals such as carbonates, kaolinites and other fine particles have an adverse impact on the recovery of bitumen. Since the Circle Cliffs oil sands contains a significant amount of these minerals, the recovery of bitumen would not be expected to be efficient. Shun[26] has noted that these same minerals appear to function as catalysts in thermal processing of oil sands leading to extensive cracking of the bitumen-derived heavy oil resulting in higher yields low-molecular hydrocarbons (C_1-C_4) and lower yields of the liquid product.

Although Circle Cliffs oil sand deposits constitute a major hydrocarbon resource in Utah, they present several drawbacks to commercial development as a viable energy source: (i) the deposit is remote and difficult to access for development, (ii) the bitumen saturation values are low and considered to be uneconomical for surface mining and recovery, and (iii) the mineralogical composition, as presented in Table 8, indicates a very high proportion of fine particles such as kaolinite and carbonate minerals which have adverse effect on the recovery of bitumen by either the hot-water or the thermal processes.

FUTURE ACTIVITIES

Characterization studies will focus on the PR Spring oil sand deposit. The mineralogical composition and the chemical composition of the constituent bitumen will be examined. In addition, fundamental studies involving the aggregate nature of asphaltenes as a function of bitumen composition will be conducted on Utah oil sand bitumens. Finally, the relative affinities of the constituent minerals in the oil sand towards various fractions of the bitumen and their subsequent changes in surface properties will be investigated.

AQUEOUS SEPARATION/RECOVERY OF UINTA BASIN BITUMENS

Principal Investigator:	J. D. Miller
Res. Assoc. Professor:	J. Hupka
Visiting Professor:	N. Chakraborti
Research Associate:	M. Hupka
Graduate Students:	J. Drelich
	D. Lelinski

SURFACE CHARACTERIZATION OF WHITEROCKS BITUMEN

INTRODUCTION

Chemical composition affects the interfacial properties of bitumen, such as surface tension, interfacial tension, and surface charge at the bitumen/water interface, which are of importance in water-based separation processes. A survey of the literature indicates that very little attention has been paid to the study of surface properties and that which has been done has been mainly concerned with the Athabasca bitumen. High viscosity and density (density close to that for water) make the measurements of surface and interfacial tension very difficult or even impossible for most bitumens. Bowman[31], and Isaacs and Smolek[32] measured the surface and interfacial tensions of bitumen recovered from the Athabasca oil sand. Results presented by Bowman[31] have little practical significance as they were obtained for non-equilibrium systems and the procedure used was not well defined. Isaacs and Smolek[32] reported the surface tension of the Athabasca bitumen to be 29.6 mNm^{-1} at 64°C which decreased to 25 Mnm^{-1} at 112°C. They found that the interfacial tension between bitumen and water is about 18 Mnm^{-1} at 23°C and about 15.4 mNm^{-1} at 50°C (with an accuracy of 12%). They further reported that the interfacial tension decreased with

increasing concentration of sodium chloride and/or surfactant (sodium dodecyl sulfate, TRS 10-80: a petroleum sulfonate, or Suntech 5: a synthetic sulfonate). Potoczny et al.[33] measured the surface tension of several Canadian bitumen samples from different sites using the Wilhelmy plate technique. The surface tension of these samples varied from about 23 mNm^{-1} to about 32 mNm^{-1} at 40°C, depending on the bitumen sample, the solvent type used for bitumen extraction from oil sand, and the residual solvent content of the bitumen. Vargha-Butler et al.[34] proposed that the surface tension of bitumen at room temperature can be determined from contact angle measurements on films of bitumen together with Neumann's equation-of-state.[35] They obtained a good agreement between surface tension values calculated from contact angle data, for the water/bitumen film and glycerol/bitumen film systems, and those measured by means of the Wilhelmy plate technique. The surface tension of bitumen was determined to be from 24.4 mNm^{-1} to 33.8 mNm^{-1} depending on the sample and the experimental procedure for bitumen preparation.

Electrophoretic mobilities for Athabasca bitumen have been reported by Schramm and Smith.[36,37] The measurements have been performed for bitumen droplets dispersed in processing water with differing amounts of NaOH. Electrophoretic mobility changed from $-18 \cdot 10^{-5}$ $cm^2s^{-1}V^{-1}$ to $-84 \cdot 10^{-5}$ $cm^2s^{-1}V^{-1}$ depending on the bitumen sample and the amount of NaOH added to the emulsion.[36,37] It was found that electrophoretic mobilities of the dispersed bitumen varied with the free carboxylate-surfactant concentration.[37] Also, it was shown that sulfate/sulfonate surfactants can significantly contribute to

the surface charge at the bitumen/water interface.[36] It was further noted that the electrophoretic mobility reaches a maximum value at a critical surfactant concentration.

Electrophoretic mobilities of two Utah oil sand bitumens, Asphalt Ridge and Sunnyside, were analysed by Hupka and Miller.[38] Toluene-extracted bitumens were dispersed in tailings water or distilled water at various pH values and the zeta potentials of bitumen droplets were measured. It was found that the zeta potential (negative) increased with a decrease in the concentration of hydrogen ions up to pH=5-6. At pH values higher than pH 5-6, zeta potential was observed to have reached a constant negative value. However, the plateau value of the zeta potential was observed to vary from -25 mV to -65 mV, depending on the tailings water used. It was concluded that the zeta potential correlated with the free surfactants content, and the experimental data further indicated the presence of other surface-active compounds more polar than carboxylate surfactants.

The surface and interfacial tension data for bitumen recovered from the Whiterocks oil sands are presented in this chapter. Experimental data from direct measurements of bitumen surface tension using the Wilhelmy plate method are compared with surface tensions calculated from Neumann's equation-of-state using contact angle measurements and with Zisman's critical surface tensions of wetting. Further, interfacial tension data, which were measured at several temperatures and for varying pH and electrolyte concentration (NaCl, $Na_5P_3O_{10}$) are presented. Finally, zeta

potentials at the bitumen/water interface are reported for varying pH and electrolyte concentration (NaCl, $Na_5P_3O_{10}$). These experimental data are used for the explanation and understanding of the bitumen disengagement mechanism discussed in the next part of this report.

EXPERIMENTAL

Reagents

All chemicals used in these experiments, unless stated otherwise, were of analytical grade. Reagents used were: distilled water with specific conductivity less than $10^{-6}\Omega^{-1}cm^{-1}$ and pH=5.8±0.1; spectroscopic grade methanol and spectroscopic grade toluene (EM Science); ethylene glycol (Mallincrodt, Inc.); propanol (J.T. Baker, Inc.); sodium carbonate (Mallincrodt, Inc.); sodium chloride (EM Science); 37% Hcl hydrochloric acid (Mallincrodt, Inc.); technical grade sodium tripolyphosphate (GFS Chemicals); formamide with purity > 98% (Mallincrodt, Inc.); glycerol with purity > 99.5% (EM Science); diiodomethane with purity more than 99% (Aldrich Chemical Co.).

The bitumen was extracted with toluene from oil sand samples received from the North West (NW) and West Central (WC) sites of the Whiterocks deposit.[22,39] A map of Whiterocks deposit and its sample locations were presented by Bukka et al.[22] The residual toluene in the bitumen was less than 0.2 wt% as determined by gas chromatography. The elemental analyses of the Whiterocks bitumen showed:[22] 86.4 wt% carbon, 11.5 wt% hydrogen, 1.1 wt% nitrogen, 0.6 wt% oxygen, 0.4 wt% sulphur. Fractional compositions of the

Whiterocks bitumens are presented in Table 15, and physical properties in Table 16.

Table 15. Fractional Compositions of Bitumens[22,32]

Bitumen Fraction	Whiterocks North West	Whiterocks West Central	Athabasca
saturates	29.5	30.2	24.6
aromatics	22.2	24.8	26.2
resins	42.4	40.2	32.5
asphaltenes	3.3	3.6	14.7

Table 16. Physical Properties of the Whiterocks Bitumen Samples[22]

Physical Property	Bitumen North West	Bitumen West Central
specific gravity (60°F/60°F)	0.981	0.976
API gravity	12.7	13.5
Conradson carbon, wt.%	8.82	9.45
ash, wt.%	0.24	0.16
heat of combustion, Btu/lb	18512	18470
viscosity at 323 K, Pa·s	32	32

Surface and Interfacial Tension Measurements

The surface and interfacial tensions were measured on a Digital-Tensiometer K10T (KRUSS, GmbH; Germany). The ring method was applied for surface tension measurements of pure liquids, and the Wilhelmy plate method for surface/interfacial tension measurements of bitumen. The absolute accuracy for the ring method

with the Digital-Tensiometer K10T is 0.1 mNm^{-1}, and the accuracy for the Wilhelmy plate technique is 0.2 mNm^{-1}. The tensiometer was calibrated using distilled water with a surface tension of 72.8 mNm^{-1} at 294 K. The pH of the aqueous phase was adjusted by hydrochloric acid or sodium carbonate.

The dynamic surface tension of a selected number of liquids in contact with bitumen was measured. The measurement consisted of the following procedure: 30 mL of the liquid was poured into the sample container (diameter of 40 mm) of the tensiometer. The Wilhelmy plate was brought into the contact with liquid and the surface tension was measured. A drop of bitumen with volume of 5 μL to 15 μL was placed on the inside wall of the container, at a level of the liquid surface, such that about 30% of the bitumen drop was immersed in the liquid (see Figure 15). After contact of the liquids, the bitumen was allowed to spread over the liquid surface affecting the liquid surface tension, and the dynamic surface tension was again recorded as a function of time.

The interfacial tension at the bitumen/aqueous phase boundary was measured by Wilhelmy plate method according to the following procedure: First, the aqueous phase samples were saturated with bitumen by contact of the phases over a day at room temperature, and an additional 1.5-2 h in the tensiometer at a temperature of 333 K ± 1 K before measurements were made. A clean platinum plate was immersed into the warm aqueous phase 333 K and zero adjustment of the tensiometer was carried out. This adjustment should be performed for the plate immersed into the bitumen but bitumen's

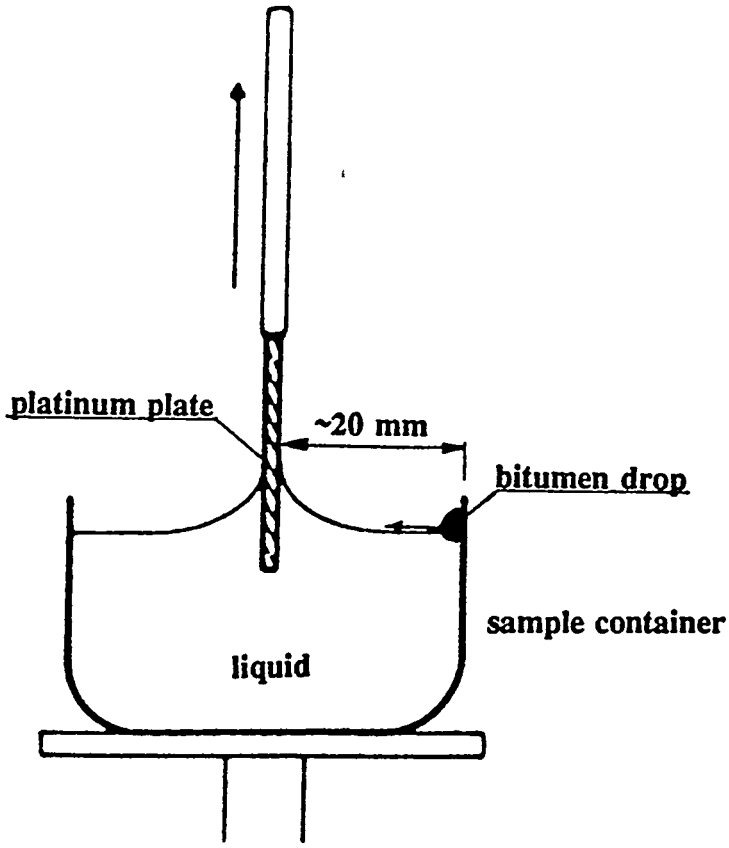

Figure 15. Illustration of the Dynamic Surface Tension Measurements.

high viscosity makes this operation difficult. There is only a small difference in the specific gravity of water and bitumen (see Table 16), and thus, the error for such procedure, calibration of the instrument in the aqueous phase instead of in bitumen, is less than 0.2 mNm^{-1}. In the next step, the plate was pulled up to such a position as required by the surface tension measurement, and a warm bitumen (338-348 K) was poured over the surface of the aqueous phase. The volume ratio of the bitumen to aqueous phase was maintained in the range of 0.8-1.2. After 1.5-2 h of equilibration at 333 K the measurement was performed. The system was equilibrated for 30 min at each lower temperature. Measurements were made only after careful cleaning of the platinum plate so that there was preferential wetting of its surface by the aqueous phase rather than by bitumen. Also, it was important to keep the platinum plate wetted by the aqueous phase before the bitumen was accommodated. Reported interfacial tension data for bitumen and a bitumen-kerosene (10 wt.%) mixture are for various pH values, which were recorded at the end of the interfacial tension measurements. The pH of the aqueous phase was measured using an ICM pH-meter (Hillsboro, U.S.A.) with an accuracy of 0.1 mNm^{-1}. For selected systems, changes in the interfacial tension with time were recorded (aging of the interface). In these experiments, "fresh" aqueous phase samples, not saturated with the bitumen before measurements, were used.

Contact Angle Measurements

A film of bitumen was deposited on a clean glass slide by two different techniques. First, a few drops of bitumen solution (0.5

g bitumen in 2 mL of toluene) were placed on the glass slide, and kept for partial evaporation of solvent at ambient temperature. Residual toluene was evaporated by placing the glass slide in an oven at 80°C for 4 h. The thickness of bitumen film was less than 1 μm as was calculated from a difference in the weight of a clean glass slide and that covered by the bitumen film. In the second method, a bitumen film was spread mechanically on a clean and warm (313-318 K) glass slide to form a thickness of about 0.005 mm in one case, and 0.2 mm in the second case.

A water drop was placed on the bitumen film and the contact angle was measured with the NRL Goniometer (Rame-Hart Inc., U.S.A.) with an accuracy of 2°.

Zeta Potential Measurements

Zeta potential measurements were carried out by the laser-Doppler electrophoresis technique using Zetasizer 3 (Malvern Instruments, Ltd., Great Britain) with the AZ4 standard circular cell, and experiments were performed at ambient temperature, 295 ± 1 K. Bitumen emulsions were prepared using a homogenizer. Warm distilled water (323-333 K) with specified ionic strength, and hot bitumen (353-363 K) were used in the emulsion preparation. The pH of cooled emulsion was adjusted by HCl or Na_2CO_3, and samples were equilibrated 30-40 min before measurements. Bitumen droplets being analysed had a diameter of 2-10 μm. The reproducibility of the measured zeta potential values was good and uncertainties were less than 10% of the measured values.

RESULTS AND DISCUSSION

Surface Tension from Direct Measurements - Wilhelmy Plate Technique

Results of the temperature dependence of surface tension for the Whiterocks bitumens (γ_B) performed using the Wilhelmy plate technique are presented in Figure 16. It was observed that the surface tension of both the bitumens decreased with an increase in temperature (T). The results can be described by the following equations:

- for the sample from the North West location:

$$\gamma_B = -(0.077 \pm 0.002)T + (25.13 \pm 0.06) \quad (1)$$

- for the sample from the West Central location:

$$\gamma_B = -(0.082 \pm 0.001)T + (25.83 \pm 0.04) \quad (2)$$

The surface tension of bitumen increased after addition of kerosene. The surface tension/ temperature relationship for the mixture consisting of 90 wt% bitumen and 10 wt% kerosene is expressed as follows:

$$\gamma_{BK} = -(0.095 \pm 0.001)T + (28.73 \pm 0.01) \quad (3)$$

The values of $d\gamma_B/dT = -0.077$ mNm^{-1} (NW), $d\gamma_B/dT = -0.082$ mNm^{-1} (WC), and $d\gamma_{BK}/dT = -0.095$ mNm^{-1} (bitumen-kerosene mixture) represent the temperature coefficients for the surface tension in the temperature range from 313 K to 350 K. The observed negative value of the temperature coefficient is in agreement with that reported for most liquids,[40-42] and a negative value indicates that as the temperature increases there is a gain in the energy of molecules located at the surface compared to those remaining in the bulk phase.

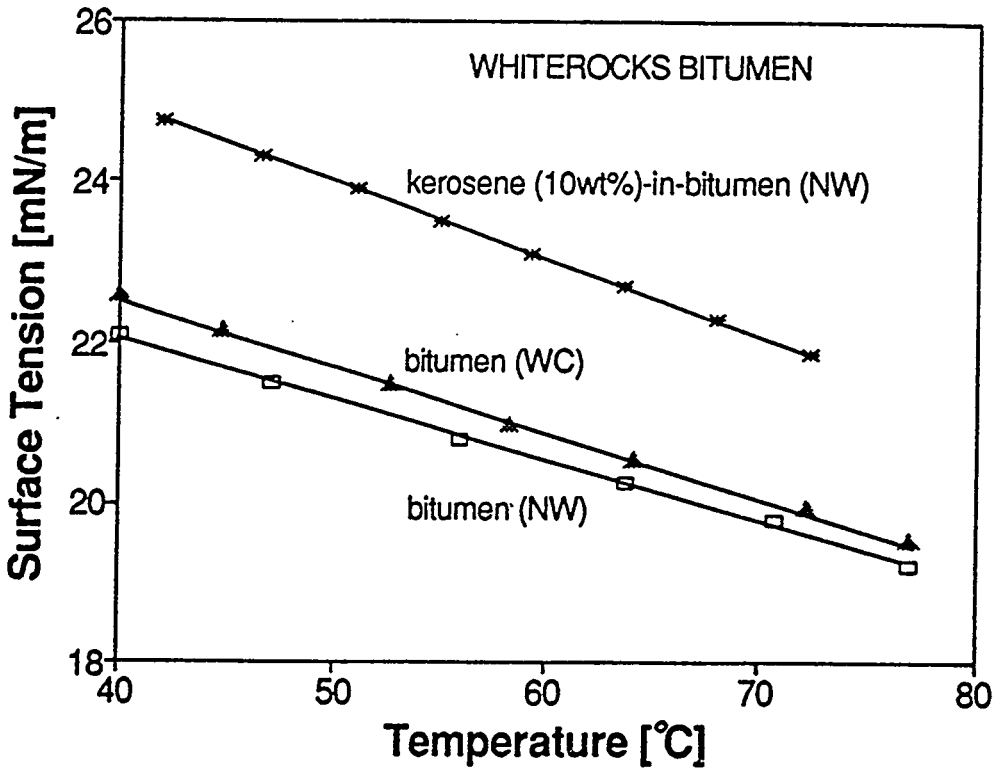

Figure 16. Effect of Temperature on the Surface Tension of Whiterocks Bitumen

The surface tension values for bitumen samples were not reproducible at lower temperatures, T<313 K and were recorded to be always higher than that expected from the linear relationship of $\gamma_B=f(T)$. Thus, the experiments were limited to the examination of the surface tension at 313 K and higher. The viscosity of Whiterocks bitumen is high, especially at low temperatures, which may contribute to the experimental error in surface tension measurements when the Wilhelmy plate technique is applied. The surface tension of high viscosity bitumen is known to give higher values.[33] It is also known that the preparation technique for the bitumen sample can affect the surface tension value as was suggested by Potoczny et al.[33]

The surface tension of bitumen at ambient temperature can be obtained by extrapolation of the experimental data. These values were determined to be 23.5 mNm^{-1}(NW) and 24.1 mNm^{-1}(WC).

Data on the surface tension of bitumens are very limited, and that available from the literature are presented in Table 17. The surface tension of Whiterocks bitumen is 5 mNm^{-1} to 9 mNm^{-1} lower than that reported for the Canadian bitumens. The composition of bitumen also differs from one deposit to another. For example, the fractional compositions of Whiterocks and Athabasca bitumens are presented in Table 15. There is a significant difference in the ratio of aromatics to saturates and for Whiterocks bitumens this ratio varies from 0.75 to 0.82 whereas for Athabasca bitumen is 1.07. Also, the Athabasca bitumen contains more asphaltenes and less resins. The Athabasca bitumen tends to be more aromatic than

Table 17. Surface Tensions for Bitumens

Bitumen Coefficient	Surface Tension Literature mNm^{-1}	Temperature $mNm^{-1}deg^{-1}$	
Whiterocks (U.S.A.)			
North-West	22.1 (313 K) 23.5 (294 K)	-0.077±0.002 (313 to 350 K)	This work
West-Central	22.6 (313 K) 24.1 (294 K)	-0.082±0.001 (313 to 351 K)	This work
Athabasca (Canada)	~31 (313 K) 29.6 (337 K)	~ -0.19 (313 to 368 K) -0.095±0.004 (337 to 385 K)	(16) (17)
Peace River (Canada)	26.5±2.7 (313 K) 27.5±2.7 (296 K)	-0.063±0.010 (313 to 363 K)	(18) (19)
Pelican Lake (Canada)	28.0±2.6 (313 K) 29.1±2.7 (296 K)	-0.063±0.012 (313 to 363 K)	(18) (19)
Fort McMurray (Canada)	27.5±2.9 (313 K) 26.4±1.3 (296 K)	-0.063±0.010 (313 to 363 K)	(18) (19)

the Whiterocks bitumen. Generally, it is known that surface tensions of aromatic and cyclic hydrocarbons are larger than those for normal hydrocarbons.[43]

Surface Tension from Contact Angle Measurements

1. Bitumen Film Preparation for Contact Angle Measurements

The accuracy of contact angle measurements for a liquid drop placed on a bitumen film depends on the technique of bitumen film preparation. Three bitumen films of varying thicknesses were prepared on glass slides using two different techniques (as described in the experimental procedure). A drop of distilled water was placed on the surface of each bitumen film and the contact angle was measured by the Rame-Hart goniometer as a function of time. Results are presented in Figure 17. The most stable contact angle value was observed for a system in which the bitumen film was deposited from the solution (curve 1), and the contact angle decreased slightly from 96.5° to 94° during the first 10 min of observation. However, the advancing contact angle observed at the very beginning (15 s) was approximately three degrees lower than that observed for the bitumen films prepared by direct coating of the glass slide. The effect of residual toluene in the bitumen film, accumulation of fine particles (dust from air environment) on the bitumen surface, and/or oxidation of bitumen at elevated temperature (363 K) could influence the surface properties of the bitumen film (problems associated with the oxidation of bitumen and collection of dust particles would remain with the bitumen films obtained by direct coating but to a smaller extent). In order to

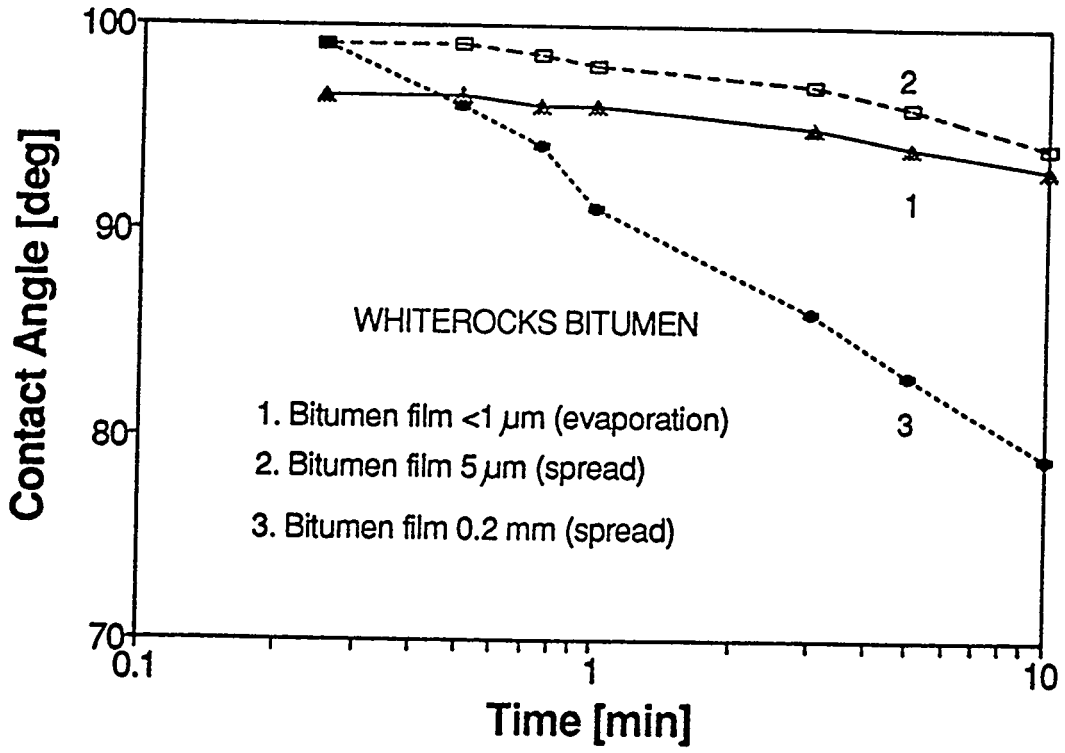

Figure 17. Contact Angle Data for Water Drops Placed on the Bitumen Film Formed from the Bitumen-in-Toluene Mixture (Curve 1: Thickness of Bitumen Film <1 μm), and from the Bitumen Mechnaically Spread on Glass Slide (Curve 2: 5 μm, Curve 3: 0.2 mm)

eliminate some of these difficulties, bitumen film deposition by solution coating was abandoned in the later experiments.

As is shown in Figure 17, the thickness of the bitumen film is a significant factor which affects the contact angle measurement. A bitumen film should be as thin as possible, and a thickness of about 5 μm was considered adequate. However, it was important to measure the contact angle in the shortest possible time (15 to 30 s) (see Figure 17). For the sample with a 0.2 mm bitumen layer, deformation of the bitumen film at the point of contact of the three phases, and spreading of bitumen over the liquid drop surface, were observed. Thus, only the bitumen film with a thickness of 5 μm (or less) was used in further experiments. With respect to experimental data presented in Figure 17, the time during which the contact angle was measured did not exceed 1 min.

Spreading of bitumen over the liquid drop surface during contact angle measurements was observed in some experiments. This phenomenon can significantly change the contact angle value and lead to incorrect characterization of the bitumen surface. In this regard, spreading of bitumen or at least diffusion of some components of the bitumen at the surfaces of different liquids was recorded in the dynamic surface tension measurements, for liquids which are in partial contact with the bitumen phase (for experimental details see Figure 15). The results of dynamic surface tension measurements for water, formamide, glycerol, ethylene glycol and diiodomethane are presented in Figure 18. For all five liquids examined, the bitumen spreading significantly affected the

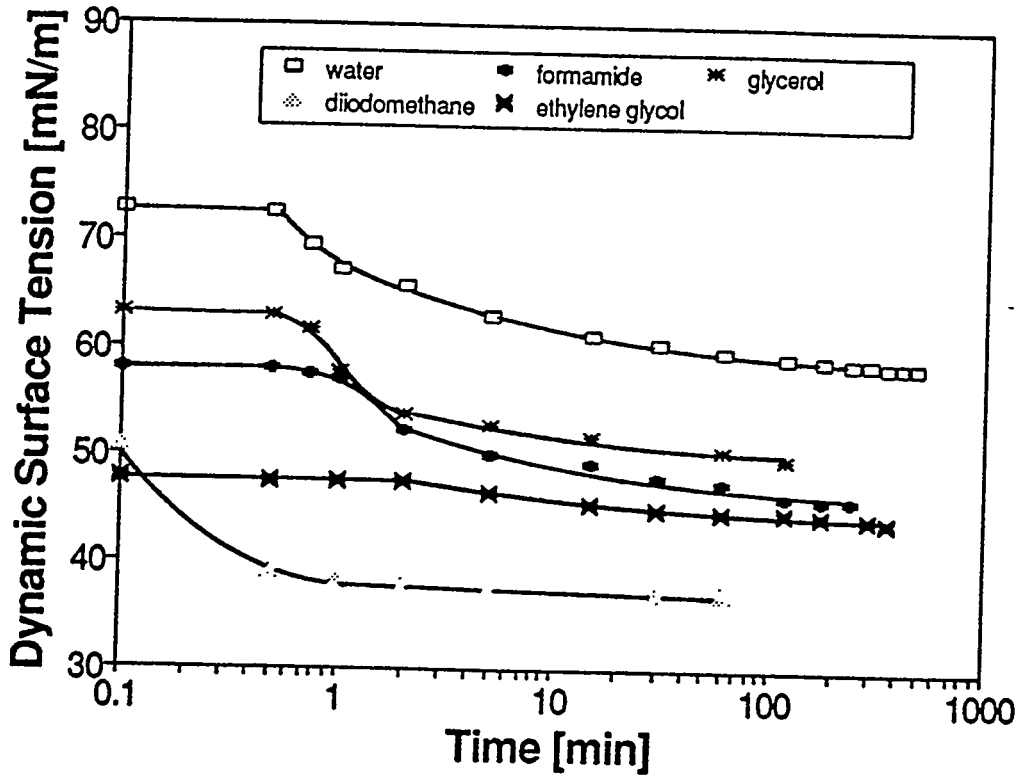

Figure 18. Dynamic Surface Tension of Water, Glycerol, Formamide, Ethylene Glycol, and Diiodomethane, in Contact with Bitumen Drop

surface tension values. The smallest decrease in surface tension was recorded for ethylene glycol. The surface tension of diiodomethane decreased rapidly, from about 50 mNm^{-1} to 38 mNm^{-1}, in the first 30 s, and remained almost constant afterwards. Results of the dynamic surface tension for the other four liquids indicate that in the first 15-30 s there is no significant decrease in the surface tension value and these liquids can be used for contact angle measurements in the characterization of the bitumen surface.

2. Bitumen Surface Tension Based on the Equation-of-State

Girifalco and Good[44] suggested that if two phases are immiscible and interact only through additive dispersion forces the interfacial free energy can be expressed by the following equation:

$$\gamma_{SL} = \gamma_S + \gamma_L - 2\phi(\gamma_S\gamma_L)^{\frac{1}{2}} \qquad (4)$$

where γ_S, γ_L, γ_{SL} are the surface free energy of solid, liquid, and the interfacial free energy of solid/liquid interface, respectively; Φ is the correction factor called the interaction parameter.

According to Neumann et al.[35], there is a relationship between the surface free energy of the solid, γ_S, of the liquid, γ_L, and the solid/liquid interfacial free energy, γ_{SL}:

$$\gamma_{SL} = f(\gamma_S, \gamma_L) \qquad (5)$$

It is assumed that the interaction parameter, Φ, is a function of the interfacial free energy of the solid/liquid interface, γ_{SL}. The empirical dependence of Φ on γ_{SL} was determined from the contact angle data for hydrophobic surfaces and was expressed as follows:

$$\Phi = -\alpha\gamma_{SL} + 1 \qquad (6)$$

where α is a constant with a value of 0.0075 m^2/mJ.

Substituting the value of Φ and introducing the Young equation (7),

$$\gamma_S - \gamma_{SL} = \gamma_L \cos\theta \qquad (7)$$

into equation (4), the Neumann equation takes the form:

$$\cos\theta = \frac{2(\alpha\gamma_S - 1)(\gamma_S\gamma_L)^{\frac{1}{2}} + \gamma_L}{\gamma_L[2\alpha(\gamma_S\gamma_L)^{\frac{1}{2}} - 1]} \qquad (8)$$

where θ is the contact angle.

The equation (8) is referred to as the equation-of-state.

Vargha-Butler and others[34] have suggested that the equation-of-state (8) can be used for a determination of the surface tension of bitumens at ambient temperature. Advancing contact angles for water and glycerol drops placed on Canadian bitumen films were measured. They found that for most bitumens the surface tension data calculated from the equation-of-state are in agreement with that obtained from direct measurements using the Wilhelmy plate technique. However, in a few cases the difference in the surface tension values by these methods exceeded 2 mNm^{-1}.

A disadvantage of the equation-of-state (8) calculation lies in the discontinuity of the dependence of $\cos\theta = f(\gamma_S)$ when $2\alpha(\gamma_S\gamma_L)^{1/2}$ approaches 1. In order to overcome this disadvantage the above equation-of-state was revised and a new equation was recently derived by Li and Neumann:[45]

$$\cos\theta = 2\left(\frac{\gamma_s}{\gamma_L}\right)^{\frac{1}{2}} e^{-\beta(\gamma_L - \gamma_s)^2} - 1 \qquad (9)$$

where β is a constant with a value of 0.0001247 $(m^2/mJ)^2$.

The equation-of-state is semiempirical and does not allow for correct characterization of all solids.[46] However, as long as intermolecular interactions remain unexplained the evaluation of the surface tension of solids is made possible only with such an empirical approach (an excellent review and discussion on the equation-of-state is given by Kloubek[47]). The experimental data presented in the literature[34,35,48-52] prove that Neumann's approach is valid for most low energy solids. The principal advantage of the equation-of-state is that it allows for the determination of γ_s from a measurement of the contact angle using only one liquid..

The applicability of the equation-of-state (9) for bitumen surface characterization was examined, and the advancing contact angle was measured for water, formamide, glycerol, ethylene glycol, and n-propanol drops resting on a bitumen film (Whiterocks bitumen). The contact angle and calculated bitumen surface tension values are collected in Table 18. The surface tension of bitumen differs in a narrow range of values from 23.3 mNm^{-1} to 24.1 mNm^{-1} (NW) and from 23.7 mNm^{-1} to 25.4 mNm^{-1} (WC). For the system involving ethylene glycol the values were lower for both the bitumens viz., 21.2 mNm^{-1} (NW) and 21.3 mNm^{-1} (WC). As shown in Table 18, the average values for the surface tension of bitumens, 23.2 mNm^{-1} (NW) and 23.9 mNm^{-1} (WC), calculated from the data set are close to that

Table 18. Comparison of Bitumen Surface Tension Calculated from i) Contact angle Measurements, ii) Wilhelmy Plate Measurements and iii) by Critical Surface Tension Analysis (21°C)

Liquid	Surface Tension of Liquid	Dispersion Component for Surface Tension of Liquid	Contact Angle for Liquid Drop at Bitumen Film		Bitumen Surface Tension Calculated from Equation-of-State	
			North-West Bitumen	West-Central Bitumen	North-West Bitumen	West-Central Bitumen
	[mNm^{-1}]	[mNm^{-1}]	[degree]		[mNm^{-1}]	
water	72.8	21.8[53]	98.3±1.8	97.4±2.3	24.1±1.1	24.7±1.4
formamide	58.0	39.5[53]	84.8±1.1	83.1±2.1	23.3±0.6	24.2±1.2
glycerol	63.4	37.0[53]	89.2±3.5	86.7±1.8	24.0±1.8	25.4±1.4
ethylene glycol	47.7	30.9[54]	77.2±2.8	76.9±1.9	21.2±1.3	21.3±0.8
n-propanol	23.9	20.8[55]	8.8±1.5	6.9±2.9	23.6±0.1	23.7±0.2
		Average:			23.2±1.2	23.9±1.6
Bitumen Surface Tension Determined by Wilhelmy Plate Technique:				23.5	24.1	
Bitumen Critical Surface Tension of Wetting:				22.7	23.3	

determined directly by the Wilhelmy plate method, 23.5 mNm^{-1} (NW) and 24.1 mNm^{-1} (WC).

Vargha-Butler et al.[34] used only two liquids, water and glycerol, for the determination of the surface tension of bitumen. They noted a discrepancy between the direct experimental value of surface tension for bitumen and that calculated from the older version of the equation-of-state (8); the difference varied from 0.4 mNm^{-1} to 5.3 mNm^{-1}. There was no systematic trend in this discrepancy and the values of bitumen surface tension calculated from the equation-of-state varied at random from those determined by tensiometry. In the case of Whiterocks bitumens, the surface tensions calculated from the equation-of-state when contact angles were measured using water or glycerol drops, are in good agreement with the values from direct measurements (see Table 12), and for both samples the observed difference was only 0.6 mNm^{-1} (about 2.5% error).

Further, Vargha-Butler et al.[34] suggested that the presence of clay particles in bitumen can affect the energetic state of the bitumen surface, and thus, may be responsible for the difference in the surface tension measured directly and that calculated based on the contact angle data. However, based on the results of this research, it is believed that some interaction between molecules of different liquids and bitumen occurs rapidly during the contact angle measurement (10-20 s). This may involve reorientation of molecules or some groups of molecules of bitumen at the bitumen/liquid interface which can affect the contact angle. Also,

such factors as solubility of bitumen compounds in liquid and/or liquid in the bitumen, deformation of bitumen film at the three-phase contact line, and spreading of bitumen or bitumen constituents at the liquid drop surface, can affect the contact angle measurements.

A disadvantage of the contact angle technique is its limitation in the determination of bitumen surface tension at ambient or lower temperature when the bitumen becomes a semi-solid. In practice, oil sand is processed at elevated temperatures, from 323 to 358 K, and thus, the bitumen surface tension at elevated temperature is of practical importance. Nevertheless, it is also true that technological practice often requires much less precise data on the physicochemical properties of bitumen. The 10-20% uncertainty is considered as acceptable for some calculations. Thus, the bitumen surface tension at ambient temperature can be determined from contact angle data and using the equation-of-state. Further, adopting the temperature coefficient of surface tension for bitumens from the literature, -0.05 $mNm^{-1}deg^{-1}$ to -0.10 $mNm^{-1}deg^{-1}$ (see Table 17), the surface tension of bitumen at elevated temperature can be reasonably estimated.

3. Critical Surface Tension of Wetting of Bitumen

Fox and Zisman[56] observed that the cosine of the advancing contact angle, $\cos\theta$, often has a linear correlation with surface tension, γ_L, for a homologous series of liquids:

$$\cos\theta = 1 + b(\gamma_c - \gamma_L) \qquad (10)$$

where γ_c is the critical surface tension of wetting of solid, which is the highest value of the surface tension for a liquid which spreads over the solid surface; and b is a characteristic constant for a given set of liquids.

The critical surface tension of wetting for a given solid can vary according to the homologous series of liquid used.[57] Greater differences in γ_c were obtained when aqueous solutions of different compounds were used[58,59] due to a specific interaction or adsorption of molecules at solid-liquid interface. Thus, it was recommended[60] that only pure liquids of homologous series should be used for the determination of the value of γ_c. Nevertheless, the concept of a critical surface tension of wetting has been found to be very useful in the analysis of mineral flotation, even when only aqueous surfactant or alcohol solutions are used (as reviewed by Finch and Smith[61]).

Some attempts have been made to correlate the critical surface tension of wetting with the surface free energy of solid.[44,62-64] Girifalco and Good[44,64] found that the ratio between γ_c and γ_s depends on the interaction parameter, Φ:

$$\gamma_s \Phi^2 = \gamma_c \qquad (11)$$

The interaction parameter is close to one ($\Phi \approx 1$) when the cohesive forces in both phases, liquid and solid, are of the same type as the adhesive forces. It means that in order to determine γ_c of bitumen, a homologous series of hydrocarbon liquids are required for contact angle measurements. Unfortunately, for alkanes, commonly used in this method, mutual solubility with bitumen, that

is, bitumen-in-alkane and alkane-in-bitumen, was observed, and contact angle measurements could not be performed. The alternate possibility consisted in using aqueous solutions of surfactants or alcohols for determination of γ_c. Methanol-water solutions were prepared in ratios of 0 to 100 vol% which resulted in surface tensions of liquids from 72.8 mNm^{-1} to 22.6 mNm^{-1}. Drops of these methanol-water solutions were placed on a bitumen film and contact angles were measured. Results are presented in Figure 19. A nonlinear relationship between $\cos\theta$ and γ_L was observed which can be attributed to hydrogen-bonding[59] or methanol adsorption at bitumen-aqueous phase interface.[60] The critical surface tension of wetting of bitumen was obtained by extrapolation of experimental results to $\cos\theta=1$, and it was determined to be $\gamma_B^c=22.7$ mNm^{-1} and $\gamma_B^c=23.3$ mNm^{-1} for North West and West Central samples, respectively. These values are smaller than the values of surface tension of the bitumens determined from direct measurements, $\gamma_B=23.5$ mNm^{-1} (NW) and 24.1 mNm^{-1} (WC), and those calculated using the equation-of-state, $\gamma_B=23.2$ mNm^{-1} (NW) and 23.9 mNm^{-1} (WC). Nevertheless, the differences did not exceed 5 %. It has been found for other systems that the value of γ_c is often lower when surfactant solutions are used rather than the use of a homologous liquid series.[58,59]

4. Dispersion Component of Bitumen Surface Free Energy

As already shown, the interfacial free energy between solid and liquid can be expressed by equation (4). Fowkes[65] has suggested that the Van der Waals dispersion interaction should be dominant at the interface of two immiscible liquids, as applied to the water-

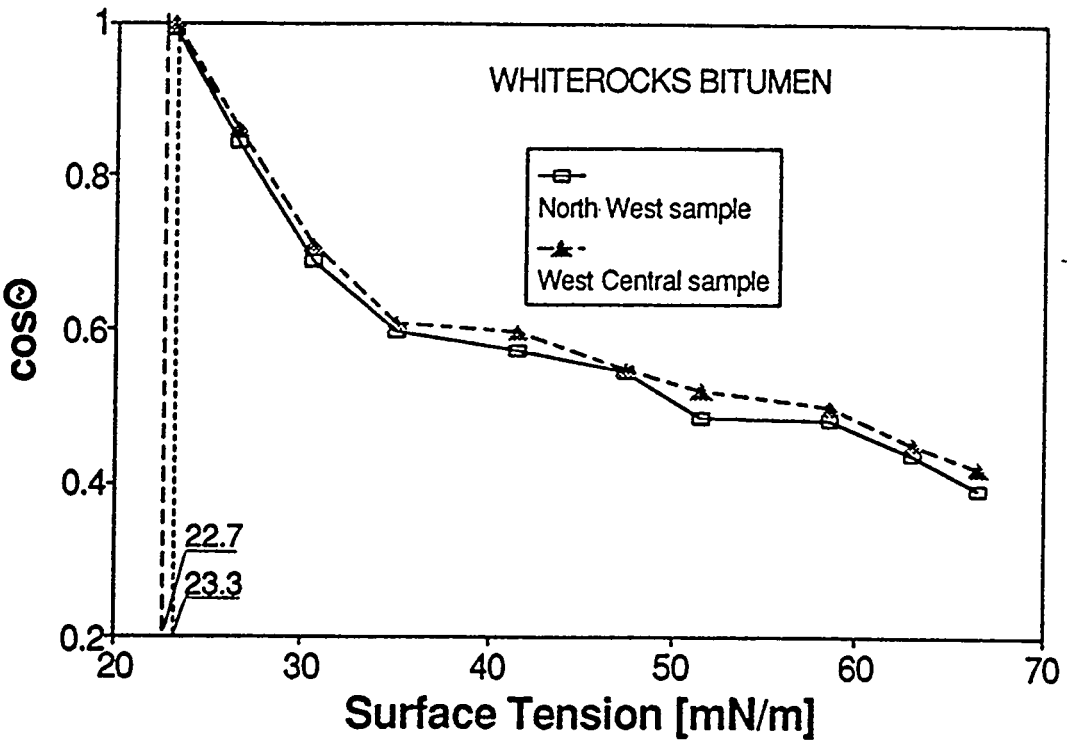

Figure 19. Determination of the Critical Surface Tension of Wetting of the Whiterocks Bitumens Using Methanol-Water Solutions

hydrocarbon system, and equation (4) for a nonpolar solid can be modified as follows:

$$\gamma_{SL} = \gamma_S + \gamma_L - 2(\gamma_S^d \gamma_L^d)^{\frac{1}{2}} \qquad (12)$$

where γ_s^d and γ_L^d are the dispersion contributions to the surface free energy of solid and liquid, respectively.

This enables the calculation of the dispersion component of the surface tension of any liquid or the dispersion component of the surface free energy of any solid. After substituting the Young equation into equation (12), the contact angle, θ, and the dispersion components of surface free energy of solid, γ_s^d, and liquid, γ_L^d, are shown to be related according to the following equation:

$$\cos\theta = 2(\gamma_S^d)^{\frac{1}{2}} \frac{(\gamma_L^d)^{\frac{1}{2}}}{\gamma_L} - 1 \qquad (13)$$

According to this equation the value of γ_s^d is determined based on the contact angle measurement with a liquid having a dispersion nature. As was already mentioned, the solubility of alkanes in bitumen and bitumen in alkanes makes the measurements of contact angle impossible for such systems. Only contact angles for liquids, which have both dispersion and nondispersion components of surface tension (see Table 18), were measured. When nondispersion interaction takes place at the interface an additional component, the excess interaction term (I^p_{SL} - energy term due to the stabilization at the interface by the nondispersion forces, such as

hydrogen bonding and dipole interactions), should be included in equation (13):[66]

$$\cos\theta = 2(\gamma_S^d)^{\frac{1}{2}} \frac{(\gamma_L^d)^{\frac{1}{2}}}{\gamma_L} + \frac{I_{SL}^P}{\gamma_L} - 1 \qquad (14)$$

It has been postulated[53] that this equation can be applied for the characterization of surface properties of distillation residues from heavy oils. Experimental data for contact angle measurements expressed as $\cos\theta = f((\gamma_L^d)^{1/2}/\gamma_L)$ should approach a straight line relationship as defined by equation (13) when the nondispersion component of the surface tension of liquid, used to examine the organic surface, decreases. A deviation from the linear relationship allows the calculation of the nondispersion excess interaction, I^P_{SL}. Experimental data are presented in Figure 20. As mentioned earlier, for liquids with a fully dispersive nature the measurements were not successful. Alkanes, diiodomethane and tetrabromoethane were tested and it was found that bitumen was readily soluble in these organic solvents. As a result of rapid dissolution, the measurement of contact angle, even at the moment of contact, was impossible. Nevertheless, a rough estimation of the dispersion component of the bitumen surface tension from results presented in Figure 20 is still possible. A small amount of nondispersion bitumen-liquid interaction is expected for the bitumen/propanol system because the nondispersion component of propanol surface tension is only 3.1 mNm^{-1} (see Table 18). Thus, a straight line behavior described by equation (13) should cross a

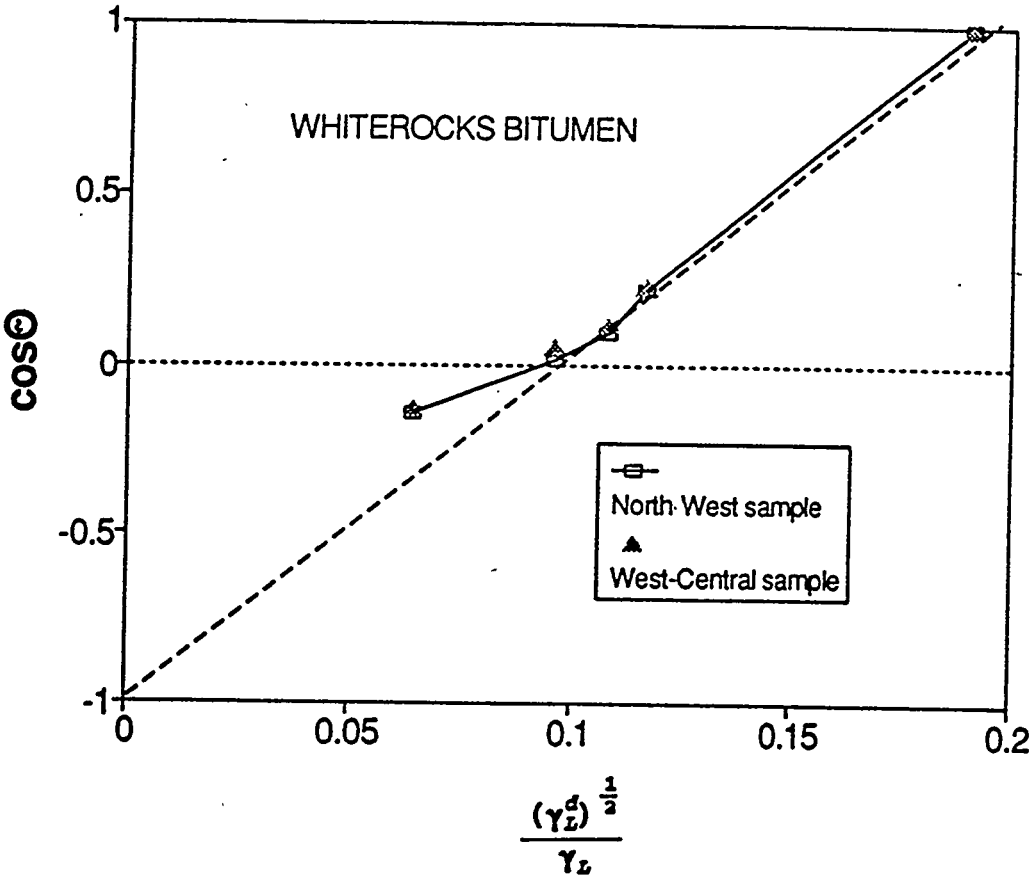

Figure 20. Determination of the Dispersion Componenet of the Surface Tension of Whiterocks Bitumen

point close to the experimental data for the bitumen/propanol system. Using data presented by Papirer et al.[67] for a wide variety of distillation residues from heavy oils, it is expected that the nondispersion excess interaction, I^{p}_{SL}, for the bitumen/propanol system would be in the range of 1.3 mNm^{-1} to 3.0 mNm^{-1}. Adopting these values, the dispersion component of surface tension of bitumen, based on equation (14), has been calculated to be γ_B^d=23.8 - 25.7 mNm^{-1}, for both samples. This value compared with the surface tension of bitumen, 23.5 mNm^{-1} (NW) and 24.1 mNm^{-1} (WC), indicates that the nondispersion component to the surface tension of bitumen is insignificant.

Interfacial Tension

1. Dynamic Interfacial Tension

A very small density difference between bitumen and water and a very high viscosity of the bitumen at low temperatures make the measurement of bitumen-aqueous phase interfacial tensions difficult. Additionally, when bitumen or crude oil and the aqueous phase are in contact, the interfacial tension invariably falls to an equilibrium value or falls precipitously to a minimum and then slowly rises by almost an equal amount.[32,68-70] Such a decline of the interfacial tension (sometimes called the dynamic interfacial tension) is typically accounted for by the rate and kinetics of molecular diffusion from the bulk phase to the interface, adsorption/desorption, and reaction at the interface.[69] The dynamic behavior of the interfacial tension for alkaline solutions is well known in the literature for crude oils and can be described as

follows:[71,72] during contact of the organic and aqueous phases the organic acids in the oil and the base (sodium carbonate in our system) in the aqueous phase migrate to the interface where they react to form surface-active species called petroleum soaps. The dynamic concentration of the soaps at the interface depends, among other factors, on the rate of adsorption and desorption, and the dynamic interfacial tension decreases significantly when there is much slower desorption than adsorption. However, increasing concentration of the active species at the interface causes a higher concentration gradient and thus the rate of desorption increases, and the interfacial tension increases to higher values.

The time required for equilibration of the bitumen-aqueous phase system is impossible to predict based on experimental data presented in the literature, and should be determined for each individual system examined.

The dynamic interfacial tension of the Whiterocks bitumen (North West)/aqueous phase system is presented in Figure 21 for varying initial concentrations of hydrogen ion. At each pH value the interfacial tension decreased to a minimum with time of contact between bitumen and the aqueous phase and increased slightly thereafter for curves 1, 2, 5, and 6, or remained constant for curves 3 and 4 (see Figure 21). The shapes of the interfacial tension vs. time curves (curves 5 and 6) are similar to those reported for Athabasca bitumen[32] and a large number of crude oils[68-70], when bitumen is in contact with an alkaline solution. Nevertheless, there are several examples in the literature where

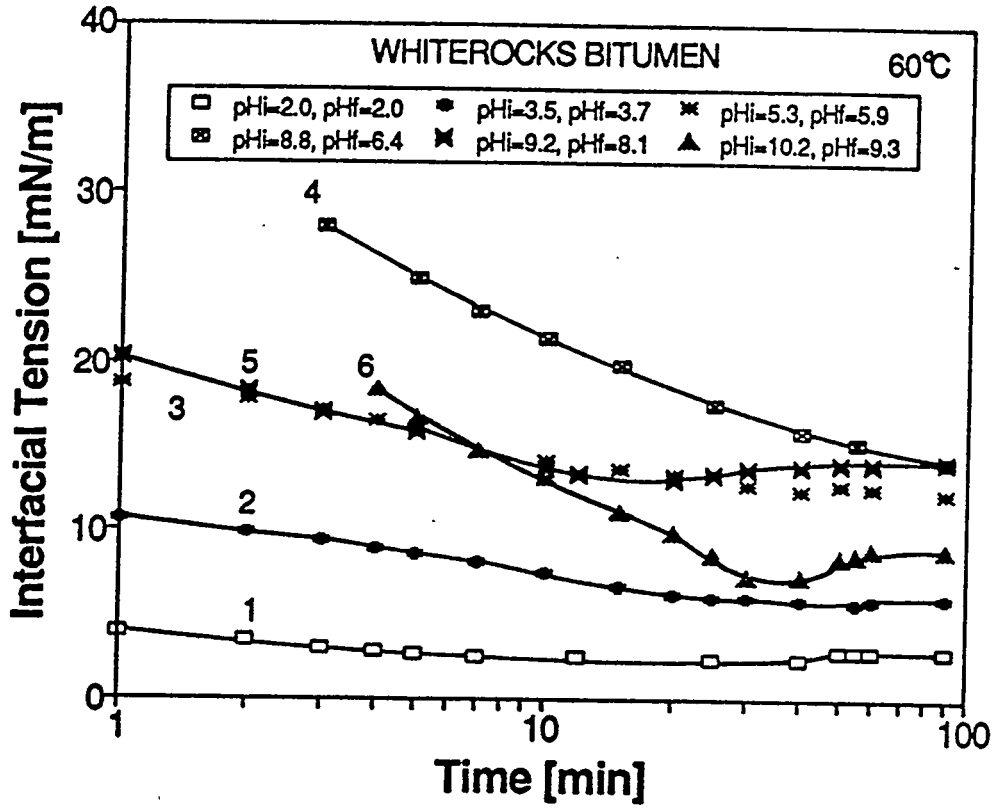

Figure 21. Dynamic Interfacial Tension for the Bitumen/Aqueous Phase Systems (Subscripts 'i' and 'f' Correspond to Initial pH Value of Aqueous Phase and that Measured after Experiment, Respectively)

the relationship between the interfacial tension of crude oils and time differs from those presented in Figure 16, especially for highly alkaline solutions.[69,73,74]

The minima for the interfacial tension values appear after 10-30 min for acidic solutions (curves 1 and 2; Figure 21). In agreement with the published data,[32] more distinct minima values were observed for alkaline solutions (curves 5 and 6; Figure 21) and these were also observed after 10-30 min. Isaacs and Smolek[32] reported more pronounced minimum in the interfacial tension for elevated alkalinity of the aqueous phase, in the pH range of pH=11-13. The interfacial tension vs.time relationship recorded in this work for pH_i=10.2 (Figure 21) is similar in both shape and value to that presented by Isaacs and Smolek[32] for pH=10. Also, the time required to reach a minimum in interfacial tension is similar to that reported in the literature.[32] However, different bitumens were used and the technique used for interfacial tension measurements (Isaacs and Smolek[32] used the spinning drop method) was also different. The minima in the interfacial tensions were extensively discussed by Rubin and Radke[69] and a physical model, which includes the effects of bulk phase mass transfer resistances, interfacial sorption kinetics, and finite phase volumes, have been formulated. Based on this model it is expected that lowering of the interfacial tension is a function of the rates of adsorption and desorption of surface-active species at the oil-water interface. As described in the caption of Figure 21, there is a significant change in hydrogen ion concentration for aqueous phases at the beginning and after

exposure to bitumen for most examined aqueous phases, and instability in pH can also affect the interfacial tension/time relationship. There was no minimum in the interfacial tension for the system at pH_i=5.3 (curve 3; Figure 21) and pH_i=8.8 (curve 4); however, there is also a time-dependent change in the hydrogen ion concentration.

2. Hydrogen Ion Concentration Effect

It has been demonstrated several times in the technical literature that the interfacial tension of crude oils is a function of the aqueous phase pH,[75-79] and a similar correlation is expected for bitumens.[31] The interfacial tension data for Whiterocks bitumen, pure and 10 wt.% solution of kerosene in bitumen, are shown in Figure 22. The largest values of interfacial tension were recorded in the pH range 4.8-8.7, and the interfacial tension was found to decrease sharply for more alkaline or more acidic solutions, as observed for crude oils.[78,79] Generally, it has been accepted that acids present in the crude oil, mainly carboxylic acids, are primarily responsible for the interfacial activity in alkaline solutions.[77,80,81] Interfacial activity of long-chain, polynuclear, aromatic, and naphthenoaromatic carboxylic acids, and porphyrin-metal chelate complexes has been reported in the literature.[76,82] The presence of carboxylic acids in bitumen has been well established.[31,83] It is believed that interfacial activity of carboxylates promotes bitumen separation from oil sands.[,84]

Which compounds are responsible for the lowering of the interfacial tension in acidic solutions is not clear, but it is

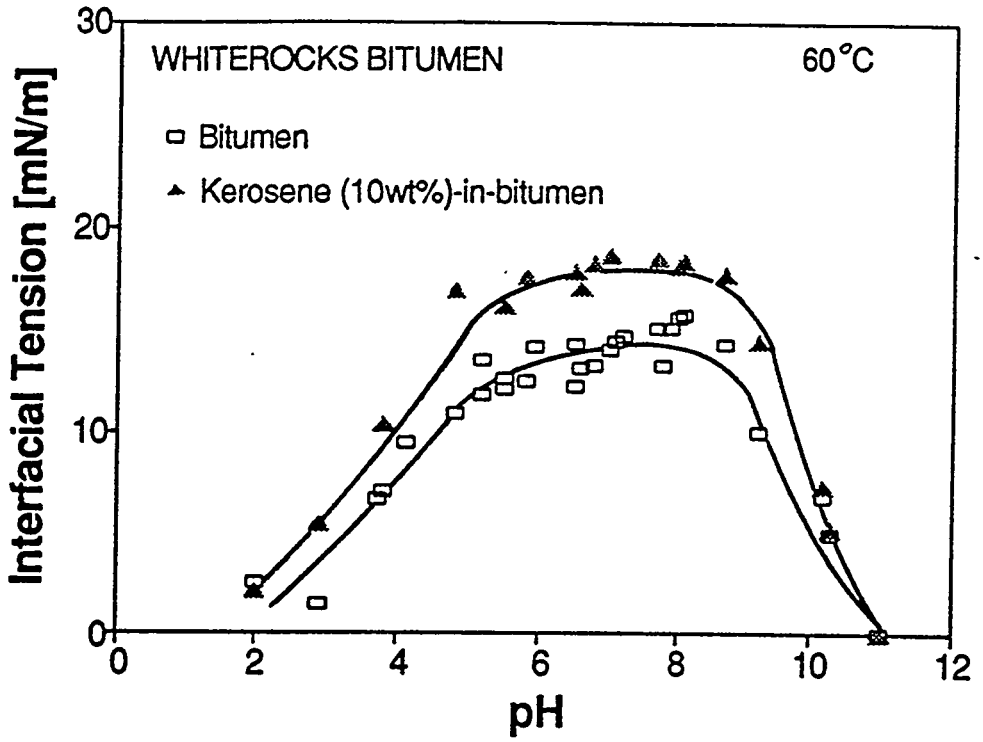

Figure 22. Effect of pH on the Interfacial Tension of Whiterocks Bitumen as Determined by the Wilhelmy Plate Technique

expected that amines/amides could be the surface active compounds which influence interfacial tension at low pH.[75,79] Cratin and Dean[85] suggested that some compounds of crude oils, such as aminoacids, are amphoteric in nature, and these compounds are highly active in alkaline as well as in acidic solutions.

The common technological strategy for hot water processing of Utah oil sands requires a reduction in the bitumen viscosity to a value of 0.5-1.5 Pa·s before digestion.[29,30] The bitumen viscosity in the Whiterocks oil sand is sufficiently reduced with the pretreatment of oil sand by a suitable diluent. Thus, the determination of the physico-chemical properties of the kerosene-in-bitumen mixture becomes equally important. Interfacial tension data for the Whiterocks bitumen diluted with kerosene (10 wt%) are also presented in Figure 22. The shape of the interfacial tension/pH relationship is similar to that of bitumen, and the interfacial tension values are 2-3 mNm^{-1} greater than for the pure bitumen (Figure 22).

3. Electrolyte Concentration Effect

Separation of bitumen from oil sand can be more effective when other reagents are used, such as silicates or phosphates, in addition to NaOH or Na_2CO_3 (for review see de Malherbe et al.[86]). Laboratory hot-water processing experiments for Whiterocks oil sands have showed that the addition of sodium tripolyphosphate improved the efficiency of bitumen separation.[87,88] Polyphosphates are also widely used as complexing agents for polyvalent cations in detergency[89] and as dispersants in mineral processing.[90]

Interfacial tension data of Whiterocks bitumen as a function of $Na_5P_3O_{10}$ and NaCl concentration are shown in Figure 23.

As shown in Figure 23, an increase in the concentration of electrolyte causes lowering of the interfacial tension. The effect of salt concentration on interfacial tension of the crude oil-water systems has been reported in the literature.[78,91,92] It is generally believed that the presence of salt alters the distribution of soluble components of crude oil between two phases. According to Ruckenstein and Rao[92] the activity coefficient of the solute increases with increasing salt concentration. Consequently, the solute molecules are gradually transferred to the oil with increasing salinity (salting-out effect). There is an increase in the chemical potential of the solute in both oil and aqueous phases, and the interfacial tension is reduced, for a positive interfacial excess of the solute.[92]

It is believed that the tripolyphosphate ions form complexes with polyvalent metal ions,[89] and thus, may intensify the activity of surface-active species of bitumen. With respect to the experimental data presented in Figure 23B, there appears to be no difference in the bitumen/aqueous phase interfacial tension for both systems, viz., $Na_5P_3O_{10}$ and NaCl solutions. This observation indicates that the beneficial effect of sodium tripolyphosphate in the separation of bitumen is not related to the interfacial tension.

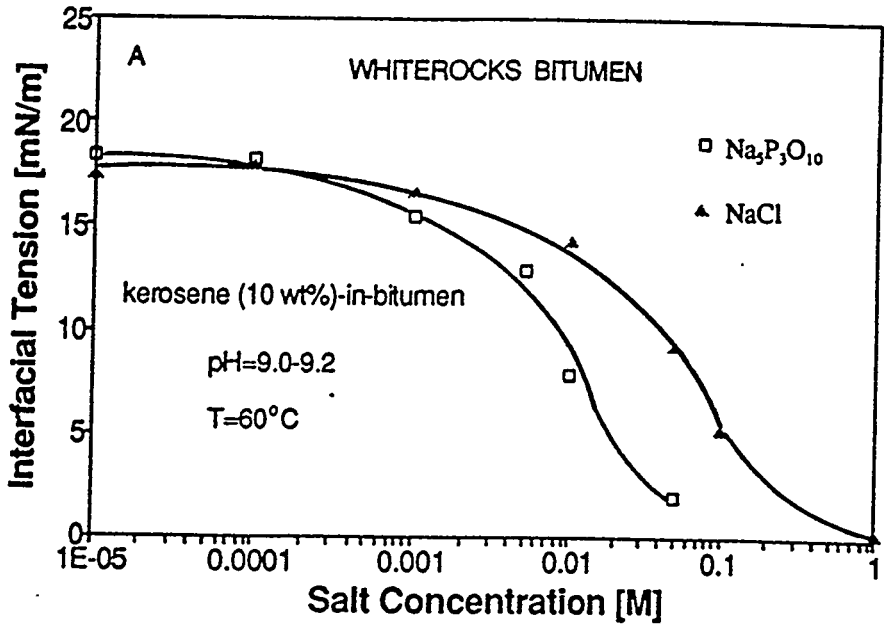

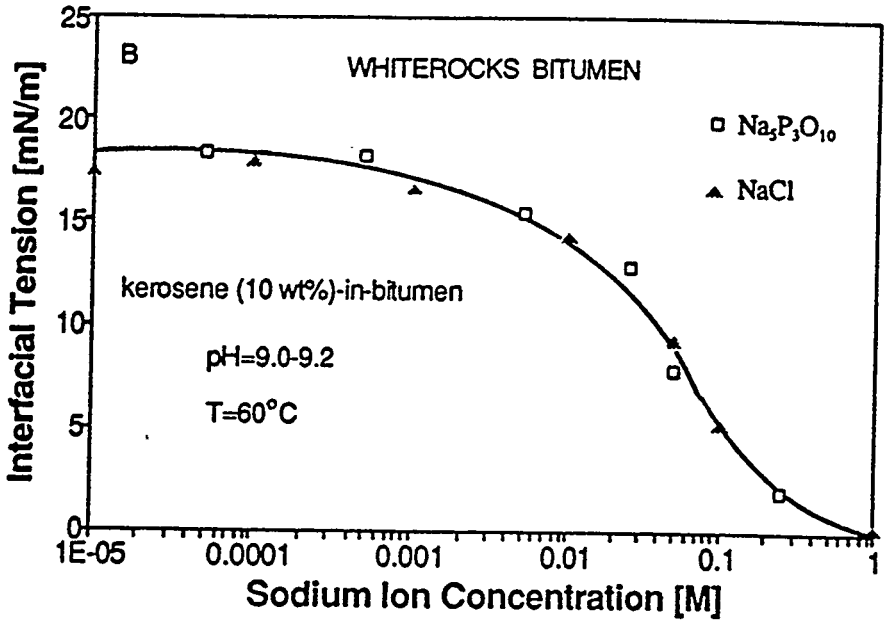

Figure 23. Effect of $Na_5P_3O_{10}$ and NaCl Concentration on Interfacial Tension for the Bituminous/Aqueous Phase Systems; Presented as a Function of Salt (A) or Sodium Ion (B) Concentration

4. Temperature Effect

The interfacial tension measurements were performed at several temperatures (308-333 K) At each pH value and electrolyte concentration, there was a linear correlation between the interfacial tension and temperature. The examples of the interfacial tension/temperature plots are presented in Figure 24. The temperature coefficients of interfacial tension ($d\gamma/dT$), calculated from the slope of the interfacial tension vs. temperature relationship, are shown in Figure 25 for varying pH values of the aqueous phase. The temperature coefficients of the bitumen/water interfacial tension were found to be negative in the pH range pH=2-9, and positive for systems with pH>9. The temperature coefficient of the interfacial tension is interpreted to represent excess entropy arising from the formation of the unit area of interface. For most liquids, this corresponds to the gain in the entropy of molecules located at the interface compared to those dissolved in the bulk phases, and thus, the temperature coefficient of the interfacial tension is negative.[40,42,93] A positive temperature coefficient for interfacial tension implies excess order at the interface and such has been observed for liquid crystals.[94] Also, positive values of $d\gamma/dT$ were reported for higher concentrations of alcohols in the water-dodecane and water-hexadecane systems.[93] The excess order of liquid crystals was attributed solely to the degree of alignment of molecules at the interface.[94] Caminati and co-workers[93] suggested that anomalous

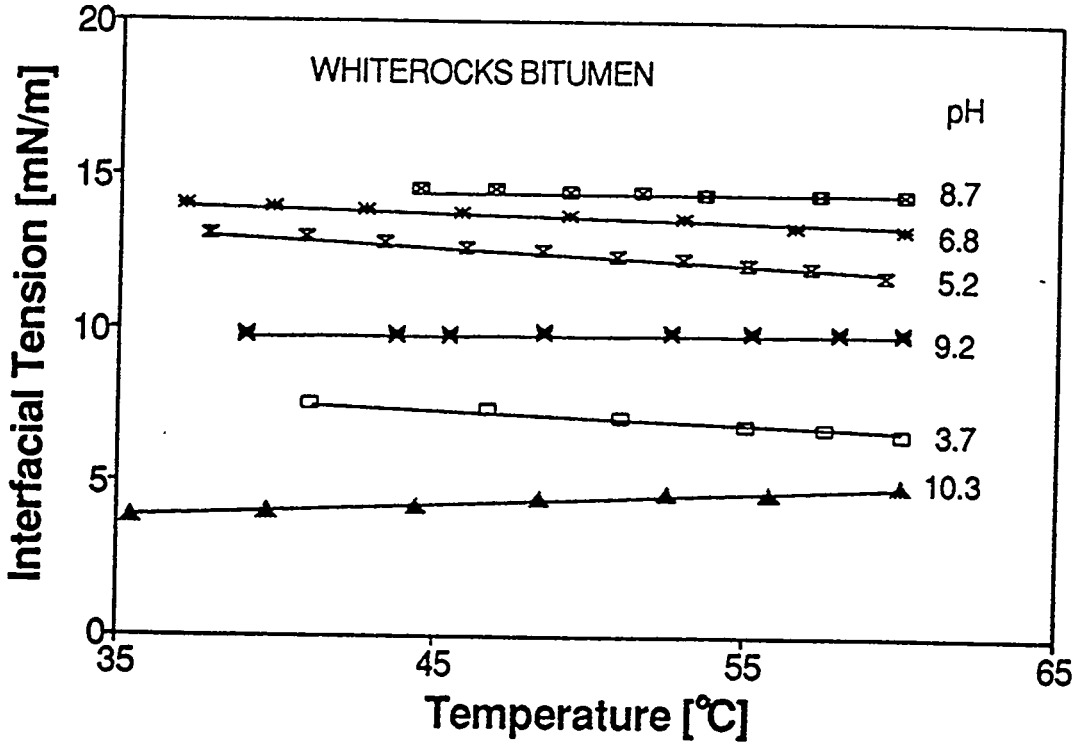

Figure 24. Effect of Temperature on the Interfacial Tension for the Bitumen/Aqueous Phase System, Measured at Various pH Values

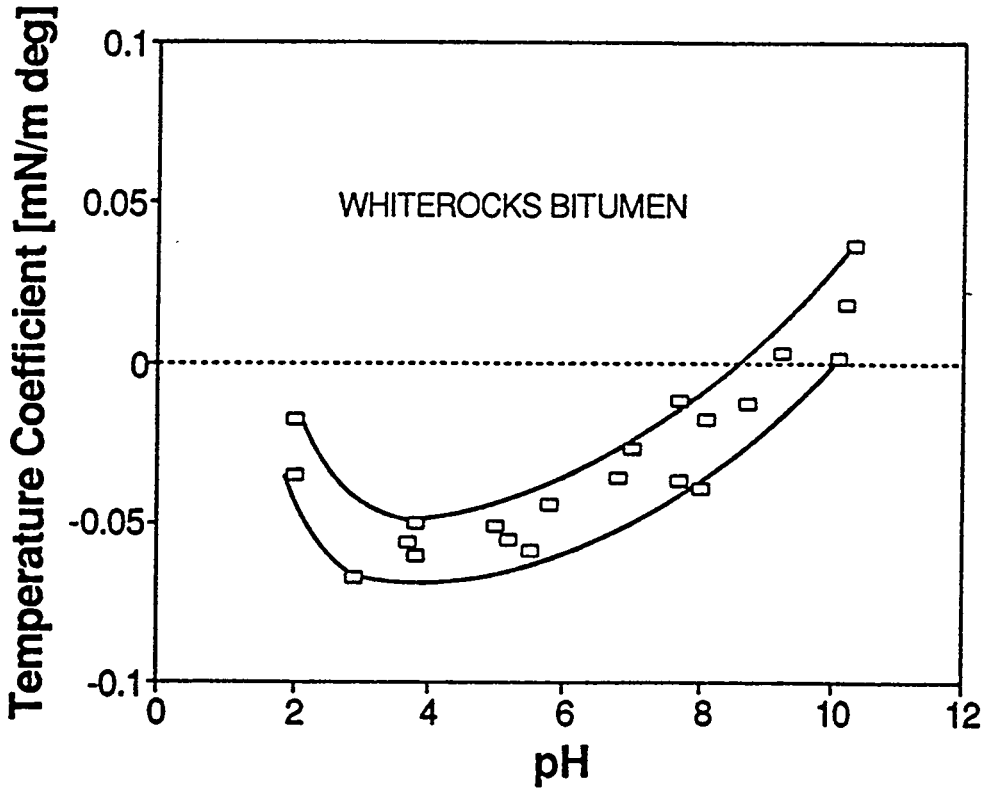

Figure 25. Effect of pH on the Temperature Coefficient of the Bitumen/Aqueous Phase Interfacial Tension

properties of the interfacial water layer are responsible for the positive temperature coefficient of the interfacial tension at the oil-water interface in the presence of alcohols. In both these cases the interpretation was not adequately supported by the experimental data and this phenomenon remains enigmatic.

Electrical Properties of Bitumen Emulsions

Surface charge at the bitumen/aqueous phase as well as mineral/aqueous phase interfaces play a significant role in the hot water processing of oil sands, especially, in the separation of bitumen droplets from digested oil sand pulp by air bubbles (flotation). Several sets of experimental data on the electrical properties of Athabasca, Asphalt Ridge, and Sunnyside bitumens have been reported in the literature.[36-38,95]

Zeta potentials of Whiterocks bitumen (from West Central) droplets dispersed in the aqueous phase containing $Na_5P_3O_{10}$ or NaCl (10^{-3}M) were measured as a function of pH (adjusted by using HCl or Na_2CO_3) and are presented in Figure 26. The bitumen droplets were negatively charged when dispersed in the aqueous phase with pH>4.5-4.6, and the negative zeta potential increased with an increase in hydrogen ion concentration. The isoelectric point was observed at pH=4.5-4.6, and the zeta potential of bitumen/water interface was positive in acidic solutions, pH<4.5.

The shape of the zeta potential/pH curve is similar to that reported for several crude oils, fuel and heavy oils,[96-98] Athabasca bitumen,[95] and pure alkanes,[96,99] and differ slightly from that reported for Asphalt Ridge and Sunnyside bitumens.[38] The observed

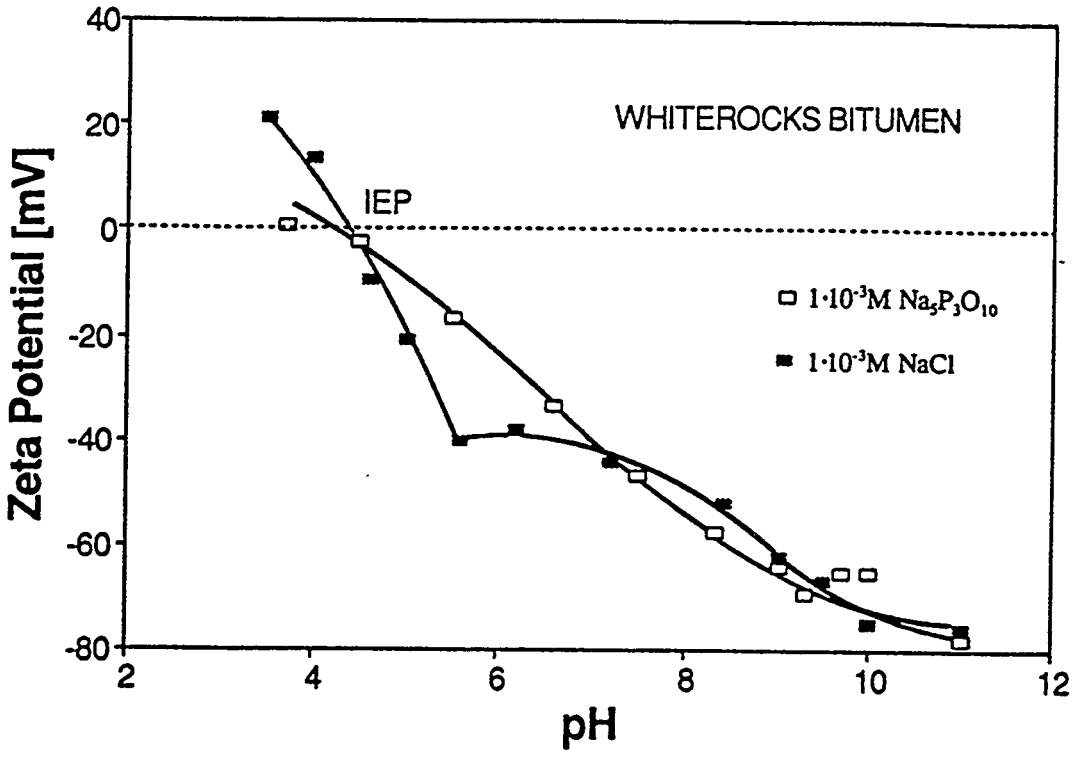

Figure 26. Zeta Potential of Whiterocks Bitumen Dispersed in Aqueous Solutions of $Na_5P_3O_{10}$ and NaCl ($1 \cdot 10^{-3}$M) with Varying pH

isoelectric point for Whiterocks bitumen was at higher pH (pH=4.5-4.6) than the isoelectric points reported for other bitumens; Athabasca bitumen pH~2,[95] Asphalt Ridge bitumen pH<3.5 (undetermined),[38] Sunnyside bitumen pH<3 (undetermined).[38]

The origin of the negative charge at the pure alkane/water interface has been postulated to be due to preferential adsorption of OH^- ions in comparison to H_3O^+ ions.[96,99] It is believed that the bitumen surface is charged due to dissociation of carboxyl groups of fatty acids which are favorably located at the interface.[95]

The zeta potential/pH relationship for the system with 10^{-3} M NaCl shows a small local maximum at pH=4.8-5.5 (Figure 21). A similar maximum was recorded for hydrocarbons, and it is believed that the adsorption at the interface of Cl^- ions, present in the solution, is responsible.[96] Below the maximum at pH≈5, there occurs an increasing competition between H_3O^+ and Cl^- ions to be located at the interface. This explanation seems reasonable, as there is no local maximum observed in the case of sodium tripolyphosphate (Figure 26).

Experimental measurements of zeta potential presented in Figure 18 have been performed for bitumen droplets dispersed in an aqueous phase of low ionic strength. In practice, processing water contains a high concentration of ions not only due to the addition of chemicals (Na_2CO_3 and $Na_5P_3O_{10}$) but also due to the accumulation of dissolved species in the recycled water. Zeta potential values for Whiterocks bitumen at higher salt concentrations are presented in Figure 27. Increasing the concentration of electrolytes lowers

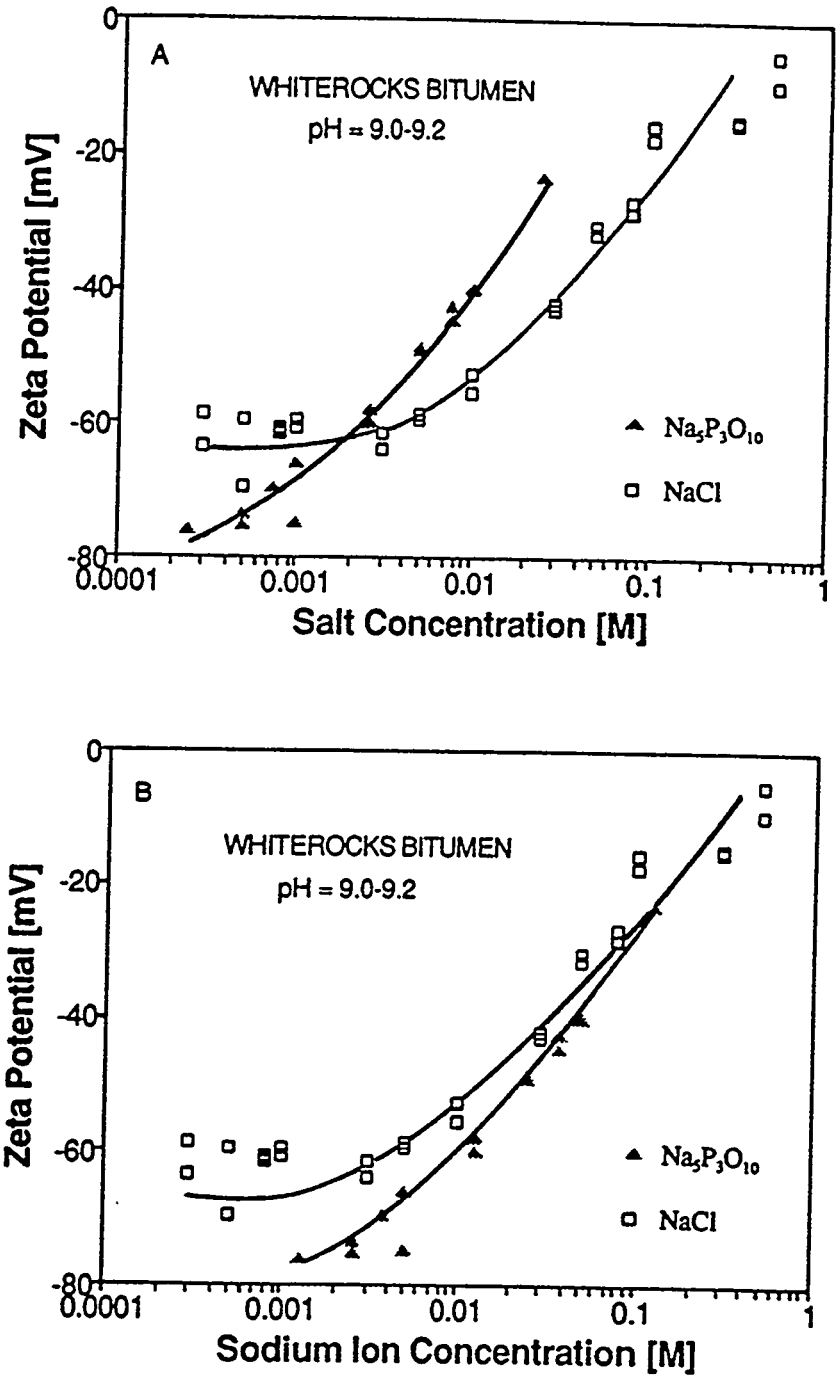

Figure 27. Effect of $Na_5P_3O_{10}$ and NaCl Concentration on the Zeta Potential of Bitumen Droplets; Presented as a Function of Salt (A) and Sodium Ion (B) Concentration

the zeta potential (Figure 27) due to compression of the double layer at the droplets surface.[100]

SUMMARY AND CONCLUSIONS

Bitumens from Whiterocks oil sands (North West and West Central sites of deposit) were extracted with toluene and recovered by solvent evaporation. The surface tension of the bitumens was measured using the Wilhelmy plate method, and it was found that there is a linear decrease in surface tension from 22.1 mNm^{-1} at 313 K to 19.2 mNm^{-1} at 350 K for the North West sample, and from 22.6 mNm^{-1} at 313 K to 19.6 mNm^{-1} at 350 K for the West Central sample. Negative temperature coefficients for surface tension were calculated to be -0.077 $mNm^{-1}deg^{-1}$ and -0.082 $mNm^{-1}deg^{-1}$ for the North West and West Central samples, respectively. A deviation from a linear relationship of surface tension vs. temperature was observed at low temperatures, below 313 K; increasing bitumen viscosity is believed to be primarily responsible for this deviation. Dilution of bitumen (North West sample) by 10 wt% kerosene increased the surface tension from 20.5 mNm^{-1} to 23.0 mNm^{-1} at a temperature of 333 K and the negative temperature coefficient of surface tension increased to a value of -0.095 $mNm^{-1}deg^{-1}$.

Contact angle measurements were also used for the determination of the bitumen surface tension. The surface tension values, for both bitumen samples, determined at ambient temperature (294 K) based on Neumann's equation-of-state, were found to be in agreement with the values extrapolated from data obtained by the Wilhelmy plate technique. The advantages in the calculation of

bitumen surface tension from contact angle measurements with Neumann's equation-of-state are that only a small amount of bitumen is required for a measurement (only a few miligrams of bitumen is needed for the bitumen film preparation), and the contact angle measurement can be limited to only one liquid. A disadvantage of this technique is its limitation in the determination of bitumen surface tension at ambient or lower temperature when the bitumen becomes a semi-solid.

Critical surface tensions of wetting for bitumens were determined using methanol-water solutions, and found to be in close agreement with Wilhelmy plate surface tension measurements. The determination of the critical surface tension of wetting using a homologous series of alkanes was impossible due to the solubility of alkanes in bitumen and of bitumen in alkanes. Also, for this reason, a dispersion component of the surface tension of bitumen was approximated, and it was found that the surface of Whiterocks bitumen is of dispersion nature when exposed to the air.

The effect of aqueous phase composition on interfacial tension between bitumen or 90 wt% bitumen in kerosene and water was examined at 333 K by the Wilhelmy plate technique. Equilibration and saturation of the bitumen/aqueous phase system required at least 90 minutes at an elevated temperature of 333-338 K. Bitumen compounds reacted with aqueous phase resulting in pH changes. The bitumen/water interfacial tension decreased in time reaching a minimum in the first 10-30 minutes, and then slowly increased slightly, for alkaline and acidic solutions. In the region 9>pH>5,

the interfacial tension decreased to a constant value in the first 40-90 minutes.

When the pH of the aqueous phase was varied, a maximum interfacial tension of γ=13-15 mNm^{-1} was obtained between pH=4.8 and pH=8.7. Interfacial tension values close to zero were obtained at both low pH (pH=2, γ_{BW}<2 mNm^{-1}) and at high pH values (pH=11, γ_{BW}<0.2 mNm^{-1}). The interfacial tension values for the 90 wt% bitumen in kerosene were recorded to be 2-4 mNm^{-1} larger than for pure bitumen. Increasing the concentration of sodium tripolyphosphate or sodium chloride (>0.1 M) in the aqueous phase at pH=9.0-9.2 lowered the interfacial tension significantly, reaching a value of less than 5 mNm^{-1}.

The temperature coefficient of the interfacial tension has been calculated to be negative for 1.9<pH<9. A maximum negative value was observed in the pH region 2.5-6. With an increase in the alkalinity of the aqueous phase the temperature coefficient of interfacial tension decreased (in absolute value) to a value close to zero at pH=9 and increased with positive values at higher pH.

The measurements of the zeta potential at the bitumen-water interface were done by the laser-Doppler electrophoresis technique. The isoelectric point has been found to be at pH=4.5-4.6, and zeta potentials of bitumen droplets were negative at pH>4.6 and positive for pH<4.5. The negative value of the zeta potential increased up to -(73-78) mV as the pH was increased to pH=9.5-10 ($1 \cdot 10^{-3}$M NaCl or $Na_5P_3O_{10}$). Zeta potential decreased with increasing concentration of electrolytes, NaCl or $Na_5P_3O_{10}$. A similar relationship between

zeta potential and sodium ion concentration was found for both salts, sodium chloride and sodium tripolyphosphate.

FUTURE ACTIVITIES

Surface tension, interfacial tension and zeta potential of bitumen play a significant role in the hot water process. These properties will be examined for bitumens from other Utah deposits. These data will establish the surface chemistry criteria for efficient bitumen separation from oil sands using the water-based technology.

BITUMEN RELEASE FROM OIL SAND DURING STAGNANT DIGESTION

INTRODUCTION

Oil sand digestion methods in which mechanical energy is introduced during the process (either by mechanical agitation or by sonic stimulation) do not reach equilibrium with respect to bitumen release from sand, therefore, are less adequate to study the bitumen-sand interactions. The importance of surface phenomena in the separation of bitumen from oil sand is stressed throughout the literature, but suprisingly no reference is made to the bitumen viscosity as the hot water process efficiency determining factor. Such an approach is acceptable when the Athabasca oil sand is investigated for which the bitumen viscosity at 323 K is 5 Pa·s). But most U.S. oil sand deposits contain bitumen with viscosity values several orders of magnitude higher than that of the Canadian oil sand bitumen.

In the earlier descriptive models of bitumen separation the oil sand was represented by only a few mineral grains covered with a bitumen film of a varying thickness.[101-103] In reality, the oil sand feed consists of mechanically sturdy porous aggregates containing numerous mineral grains. These grains are bound together not only by the bitumen but also by carbonaceous or silicious cementing material. Therefore, the bitumen displacement and disengagement mechanism involves both surface wetting and capillary phenomena.

It is understandable that microscopic examination should play a key role in the determination of the mechanism of bitumen separation from oil sand. In view of this, 2 mm oil sand aggregate microdisintegration experiments were conducted under an optical microscope and observations were recorded using video camera at magnifications of 150x and 400x.[102] Such large magnification have allowed for the investigation of the receding contact line, but the behavior of larger oil sand fragments was not considered. Our own work using a thorough microscopic scrutiny of the oil sand surface is in progress,[104,105] and further study is required.

In our current study a stagnant digestion technique was developed, involving oil sand immersed in an alkaline solution, which allows simultaneous determination of some physical and surface properties of the system, such as the oil sand natural porosity, the wetting ability of the aqueous phase based on the kinetics of air and bitumen displacement from the oil sand, the droplet size of released bitumen, the bitumen-bitumen droplet coalescence time, the extent of bitumen dilution (when diluent was used), the size and electrophoretic mobility of particulates released from the oil sand sample to the aqueous phase, and in-situ IR analysis. In this section the stagnant digestion laboratory setup is described and the experimental data are discussed.

EXPERIMENTAL TECHNIQUE

The laboratory setup used to investigate the behavior of the oil sand sample placed in an alkaline solution is shown in Figure 28. The mass of the oil sand sample was adjusted to maintain a

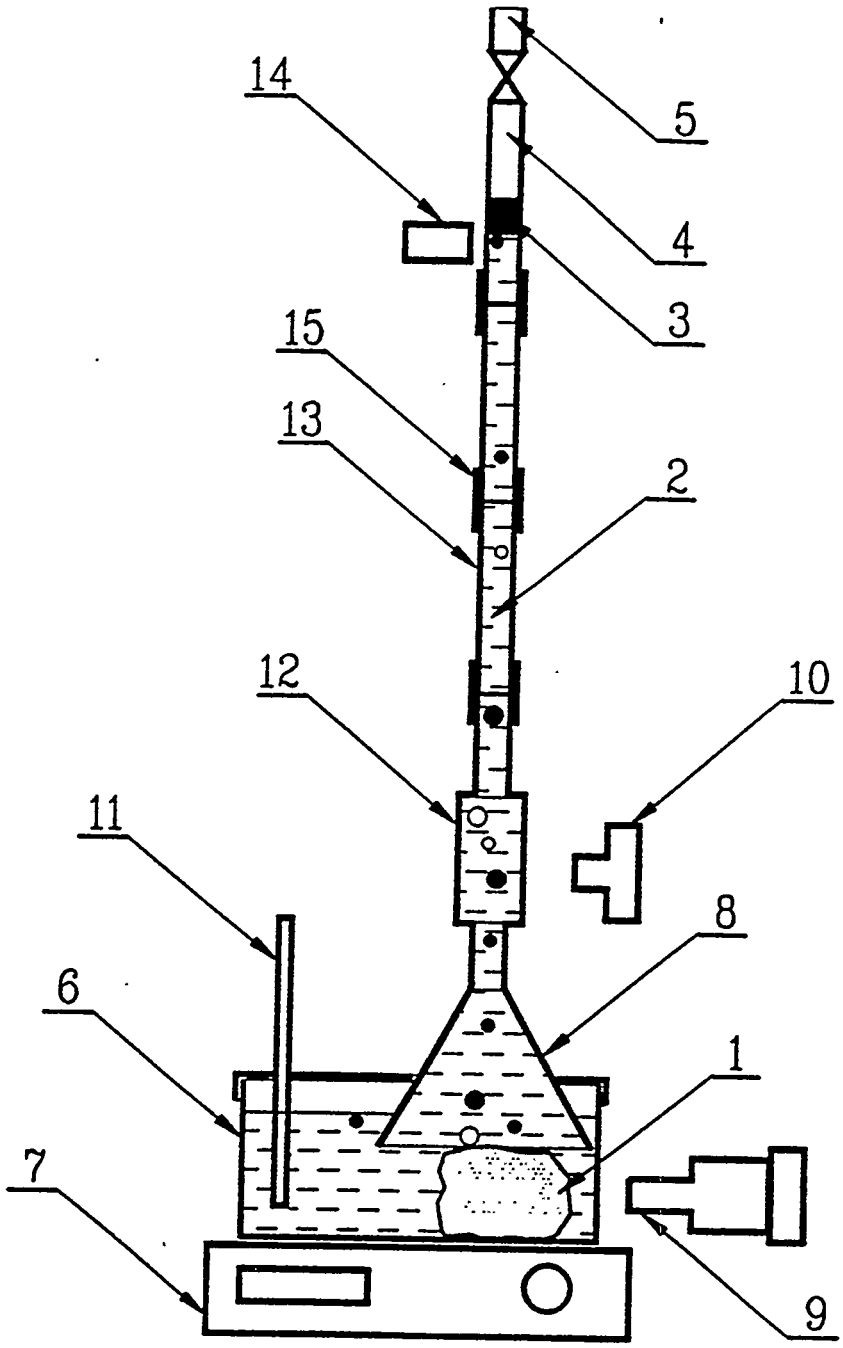

Figure 28. Experimental Set-up used for Stagnant Digestion of Oil Sand. 1 - oil sand; 2 - aqueous phase; 3 - bitumen; 4 - air/gas phase; 5 - to vacuum; 6 - digestion vessel; 7 - hot plate; 8 - funnel; 9 - microscope with photo camera or video camera; 10 - photo camera; 11 - sensors (pH, temperature, in situ IR spectr.); 12 - cell with flat wall; 13 - calibrated tube composed of segments; 14 - magnifying lens; 15 - transparent tubing joining tube segments

constant weight of bitumen at 5 grams. 500 mL of sodium carbonate, providing initial pH = 10, was used in each experiment. Both, as received and diluent pretreated oil sand samples were used. Due to the differences in natural porosity, pore size, and pore wetability by the aqueous phase, the extent of bitumen surface in contact with the aqueous phase varied according to the oil sand origin. Despite its simplicity, the technique has allowed for the following information to be collected.

1) Based on the gas phase release:

- the kinetics of the aqueous phase migration into the oil sand,
- oil sand natural porosity, including closed porosity inaccessible to diluent,
- wetting ability of the aqueous phase,

2) Based on bitumen release:

- droplet size and density (including entrapped air, water and mineral fines in bitumen),
- extent of bitumen dilution - when diluent is used (by viscosity measurements of released bitumen),

3) By analysis of the aqueous phase:

- size and electrophoretic mobility of particulates released to the aqueous phase from the oil sand sample,
- pH and change of chemical composition of the aqueous phase by in-situ IR analysis,

4) By continuous microscopic examination and photomicrography:

- coalescence time of bitumen droplets:
  - at water/air interface
  - at water/bitumen interface,
- bitumen and gas phase behavior at oil sand surface,
- rough estimate of water/bitumen interface tension,
- rough estimate of contact angle of bitumen droplets on mineral particles.

RESULTS

Oil sand samples from the following deposits were used in the stagnant digestion experiments: Asphalt Ridge, Athabasca, PR

Spring, Sunnyside and Whiterocks. Our current report pertains mainly to the microscopic examination of oil sand samples remaining in contact with the alkaline solution for up to 3 weeks. Such an extended contact time would allow the system to equilibrate. It was observed that:

- all examined oil sands released bitumen for the experimental conditions used (temperature 323 K initial pH=10 controlled by Na_2CO_3 addition, bitumen/aqueous phase weight ratio 1:100); however, at different rates and to different extents of release,
- the bitumen film spontaneously retracted from the sand surface in less than 3 minutes regardless of oil sand origin provided that the bitumen viscosity was less than the critical value. However, many sand grains exhibited residual bitumen (as tiny droplets or invisible patches) at certain spots. The invisible spots were evidenced by FTIR microscopy.
- later, the bitumen was released by capillary displacement at a rate depending on the bitumen viscosity and the magnitude capillary forces. The size of bitumen drops forming at the mouth of a capillary was between 0.5 to 5 mm, depending on bitumen-water interface tension and bitumen wettability of mineral particles. The minute bitumen droplets (<100 μm) originated from bitumen film rollup on sand grains (exposed to the aqueous phase from the very beginning of the process), and as satellite droplets formed during detachment of large bitumen drops.

- bitumen release took place at several sites. Generally, the lower the number of bitumen release sites the larger were the bitumen drops. For oil sand exhibiting multi-strata morphology (e.g., Whiterocks oil sand) bitumen release could be attributed to certain strata.
- the release of the gas phase took place from the very moment of oil sand sample submersion in the alkaline solution. At the initial stage of the process the gas bubbles were covered with only a thin film of bitumen. However, when the capillary displacement occurred bitumen droplets encapsulated smaller and larger gas bubbles.
- all air/gas entrapped in bitumen drops was of natural origin (already contained in the oil sand). The diameter of air bubbles displaced from oil sand was from below 1 mm to about 5 mm. This observation may support speculation that during aeration of digested oil sand slurry air bubbles attach to the bitumen-sand aggregates rather than to the already separated bitumen droplets.
- the coalescence time of bitumen droplets at the water/air interface was 1 to 10 s and varied with pH (time of digestion). The coalescence time of bitumen droplets at the water/bitumen interface was from a few minutes to 30 min.
- for some oil sands, bitumen initially retracted from the surface into the pores and later was displaced from the pores by the aqueous phase forming large, sessile droplets (2 to 5

mm) which never detached from the surface due to the lack of buoyancy force.

- addition of diluent to the oil sand (10 to 15 wt% with respect to bitumen) prior to digestion accelerated bitumen release. Lower viscosity improved the kinetics of the bitumen film rollup, and the released bitumen generally floated due to the reduced density of the diluted bitumen drop.

A sequence of typical photographs, taken during stagnant digestion of PR Spring oil sand, pretreated with kerosene is shown in Figure 29. The photographs marked A,B,C depict the initial stage of digestion - the bitumen retracts to pores and the gas phase is released. The photographs D,E,F represent oil sand surface after 2 days, when the pH dropped from 10 to 9 and stable bitumen drops reside at the surface of sand grains. The bitumen drops were detached when the pH is increased (see section on bitumen/water interfacial tension).

DISCUSSION

The results obtained from stagnant digestion experiments can be interpreted in the following details:

- The wide range of the bitumen droplets size found in the digested oil sand indicates that efficient gravity separation of bitumen from oil sand cannot be explained by the "single particle oil sand model". This model assumes that bitumen disengages from oil sand grains which have already detached from oil sand fragments. Coalescence time of bitumen droplets

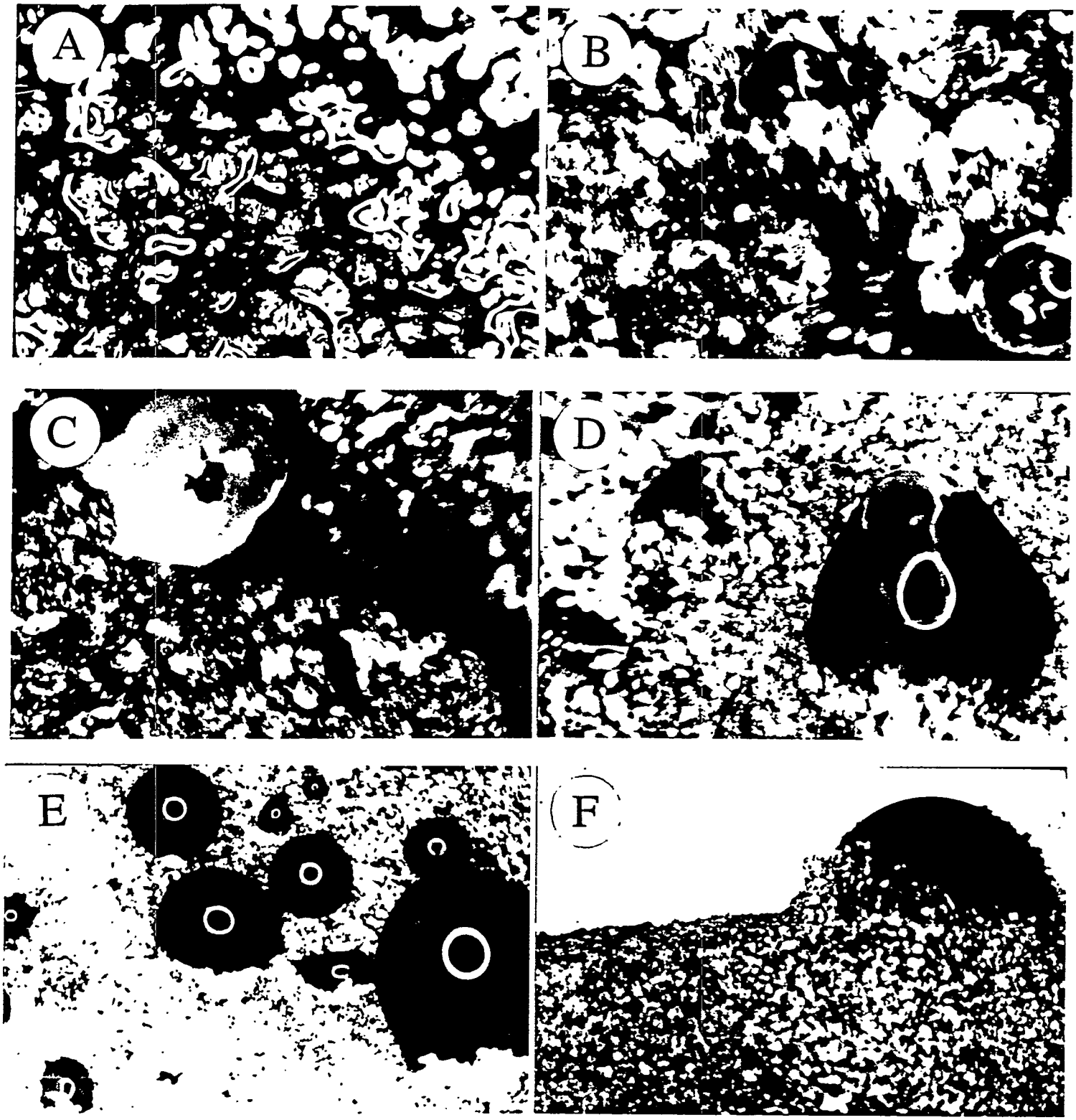

Figure 29. Stagnant Digestion of PR Spring Oil Sand Pretreated with Kerosene.

is too long for satisfactory droplet size growth in the digested oil sand slurry.

- Neither the consolidated nature of the oil sand nor bitumen viscosity (diluent application) altered the capillary release of bitumen. Bitumen viscosity had a clear impact on bitumen retraction rate from the sand surface.
- Depending on the buoyancy force available (resulting mainly from air entrapment and diluent addition), the bitumen can be released as free drops (e.g., Asphalt Ridge bitumen) or can form sessile droplets which never detach from the surface (e.g., Sunnyside bitumen). In the shear stress field bitumen droplets will be smaller.
- Various sites or strata in oil sands exhibit different wettability with regard to bitumen.
- The smaller the size of oil sand feed, the larger the contribution of small bitumen droplets in the digested oil sand slurry.
- The bitumen phase collected during stagnant digestion did not contain water or minerals unlike bitumen concentrate obtained in routine digestion and separation experiments.

Mechanism of Separation

The postulated mechanism of oil sand digestion for water-based processing of oil sand is presented in Figure 30. At the initial stage of digestion bitumen film retracts to the pores leaving only tiny bitumen droplets on the surface of most of the sand grains. Simultaneously, some gas bubbles are released. The gas bubbles are

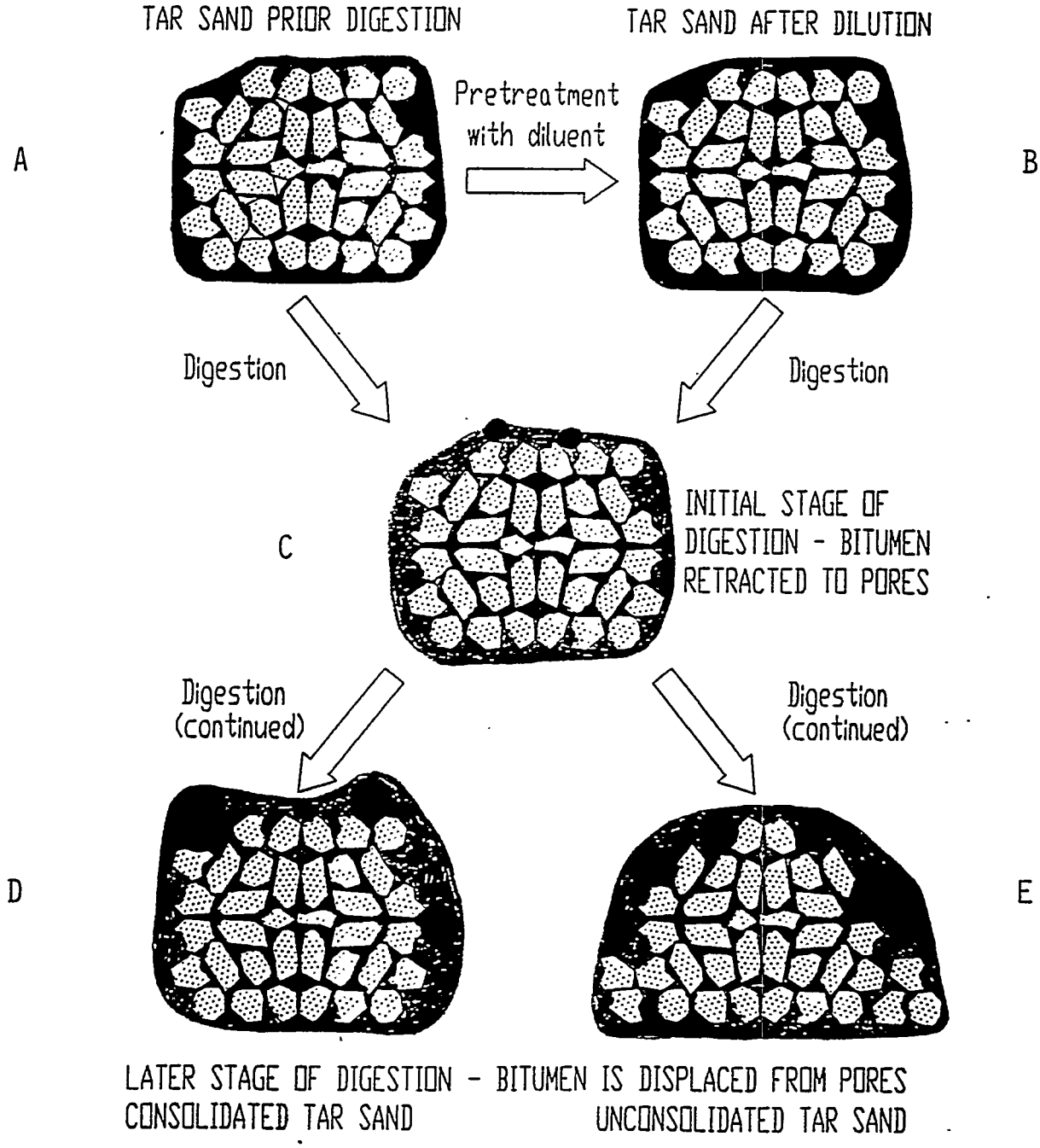

Figure 30. Postulated Mechanism of Oil Sand Digestion for Water-based Processing of Oil Sand. (A) Oil Sand Prior Digestion; (B) Oil Sand after Treatment with Diluent; (C) Initial Stage of Digestion, Bitumen has Retracted to Pores, some Gas Bubbles are Released; (D) Later Stage of Digestion, Bitumen is Displaced from Pores of Consolidated Oil Sand; (E) Later Stage of Digestion - Bitumen is Displaced from Pores of Unconsolidated Oil Sand; Oil Sand Aggregate Falls Apart. White - Mineral; Blue - Gas; Green - Aqueous Phase; Black - Bitumen

covered with a very thin film of bitumen (and diluent, when used). In the later stage, bitumen is displaced from pores by the aqueous phase and released as droplets. For the capillary flow the viscosity of the organic phase is of paramount importance, as was demonstrated in our experiments. Some bitumen droplets, released due to capillary displacement, contain gas bubbles which were still present in the pores. Bitumen droplets will be smaller when mechanical energy is supplied into the system.

Oil Sands of Low Natural Porosity

Certain oil sands exhibit very low natural porosity which limit the diluent penetration into pores.[106] The natural porosity of oil sand accessible to diluent has a crucial impact on the reduction of bitumen viscosity, and influences the penetration time required for successful bitumen separation from the oil sand. In the processing of oil sands diluent, access to the bitumen can be enhanced by more extensive oil sand size reduction. However, in underground processing low natural oil sand porosity can limit diluent application, thus, reducing the number of oil sand deposits available for underground water-based processing. The impact of the natural porosity on the amenability of the diluent-assisted hot water process can be illustrated with the Sunnyside oil sand. The natural porosity of that oil sand is only 1.2 %, and the bitumen is very viscous (18 Pa•s at 363 K) resulting in a high demand for diluent. Thus, the amount of diluent required to reduce its viscosity is 24 wt% with respect to the bitumen content, but its low porosity can accommodate only 4.7 wt%. diluent. [106]

Low natural permeability (less than 10 mD) - and low porosity of the formations containing petroleum deposits - can be attributed to such deposits being carbonate reservoirs.[107] The stimulation of oil production from such reservoirs is achieved through acid-fracturing operations.[92] A similar technique may be used for in situ process for the Sunnyside oil sand which contains about 10% of carbonates, as determined by HCl leaching of toluene extracted sand. Dissolution of carbonates not only will enlarge the oil sand porosity but may also weaken cementing bonds among sand grains which can lead to an easier underground slurrying. Sunnyside oil sand belongs to well consolidated oil sands.

CONCLUSIONS

A new experimental technique - the stagnant digestion - has been developed to study the bitumen release from oil sand. The stagnant digestion method is intended to test and predict separation amenability of oil sand to the hot water processing. Regardless of oil sand origin, the mechanism of bitumen separation involved the following two stages:

- spontaneous retraction of the bitumen film from the sand surface into the pores in less than 3 minutes provided that the bitumen viscosity was less than the critical value (which is controlled by diluent addition). For more viscous bitumens the retraction time was observed to be about 1 hour. Even after extended period of observation, many sand grains exhibited residual bitumen at certain spots.

- subsequent bitumen release from the pores due to the preferential wetting of sand by the aqueous phase. Depending on the buoyancy force available (resulting mainly from air entrapment and diluent addition), the bitumen was released as free drops (Asphalt Ridge bitumen) or formed sessile droplets on the sand grains which never detached from the surface (Sunnyside bitumen).

FUTURE ACTIVITIES

In our 93-94 annual report detailed analyses of the kinetics of the bitumen and the gas phase release from all oil sand samples mentioned in this section will be presented. The behavior of model oil-sand aggregates during stagnant digestion and acid treatment of consolidated oil sands will also be included. The investigation will help to formulate a mathematical model for bitumen displacement from sand which later may allow computer process visualization.

Attempts will be made to correlate asphaltene concentration at bitumen/water interface with respect to asphaltene and resin content of the oil sand bitumen, and diluent application. The diluent may enhance asphaltene mobility to the interface and, thus, stimulate surface activity.

ENHANCED BITUMEN RECOVERY FROM WHITEROCKS OIL SANDS BY CONTROL OF THE BITUMEN/WATER INTERFACIAL TENSION

INTRODUCTION

The hot-water processing technology for the Whiterocks oil sand has been well-described in previous contributions but our understanding of the mechanisms of bitumen separation from oil sand is incomplete. Three physico-chemical properties of bitumen: viscosity, surface tension and interfacial tension, are expected to be of great importance in the bitumen release from oil sand. The effect of bitumen viscosity on the hot water processing of oil sands has been discussed extensively in the literature[29,30,108] but little information is available regarding the significance of surface/interfacial tension on the recovery of bitumen from oil sands.

Bowman and Leja[31,109] analysed the thermodynamic equilibria in the hot water process for the bitumen/water/sand and air/bitumen/water systems. They indicated that the interfacial properties of bitumen (surface tension, interfacial tension, surface charge) should play an important role in bitumen release from mineral particles during oil sand digestion and bitumen spreading at the gas bubble surface during the flotation of oil sand pulp. However, this analysis was only partially confirmed with hot water processing experiments.[31] There was no attempt to correlate the interfacial properties of bitumen with bitumen separation from oil sands during hot water processing (an exception is the discussion by Schramm and Smith[36] who have observed a correlation between the

concentration of natural surfactants, which are released from bitumen during the hot water process, and bitumen recovery).

The surface and interfacial tension data for the bitumen recovered from Whiterocks oil sand are presented in the previous section. The bitumen release from mineral particle surfaces under stagnant conditions has been observed through a microscope and mechanisms of bitumen separation from the mineral surface are discussed with respect to surface/interfacial tension data. The spreading coefficient for bitumen at the water surface has been calculated from surface/interfacial tension data to be positive for all pH values of practical significance, and for all $Na_5P_3O_{10}$ and NaCl concentrations considered. Finally, a good correlation of interfacial tension with bitumen release from Whiterocks oil sand was found and such a correlation could provide the basis for improved separation efficiencies.

EXPERIMENTAL

Reagents

The bitumen was extracted with spectrograde toluene from representative oil sand samples received from the North West site of the Whiterocks deposit.[39] The residual toluene in the bitumen was less than 0.2 wt% as determined by gas chromatography in the Department of Fuels Engineering at the University of Utah. The significance of residual solvent has been discussed in another publication.[39] The elemental analyses, fractional composition, and physical properties of Whiterocks bitumen have been presented by Bukka et al.[21] (see Tables 15 and 16).

The basic chemicals used in these experiments were as follows: distilled water with specific conductivity less than $10^{-6}\Omega^{-1}cm^{-1}$ and pH=5.8±0.1, analytical grade sodium carbonate (Mallincrodt, Inc.), analytical grade hydrochloric acid (Mallincrodt, Inc.), analytical grade sodium chloride (EM Science), technical grade sodium tripolyphosphate (GFS Chemicals), and a commercial grade kerosene (Chevron).

Microscopic Observations of Bitumen Release from Oil Sand

Samples of the Whiterocks oil sand were submerged in alkaline solutions (pH=8.0-11.5) in a glass cell and the changes in sample structure were observed through a stereoscopic microscope (Carl Zeiss Jena, Germany) and recorded by making photographs of the sample. The contact angle for the bitumen drops formed on the mineral particle surfaces were measured from the photographs. The temperature of the system in the glass cell was maintained at a constant level (±3°C) by using a hot plate, and the pH of the aqueous phase was measured using a pH-meter (model 520, Orion Research, Inc.).

Hot Water Processing

Oil sand samples from the North West location of the Whiterocks oil sand deposit (7.6 wt% bitumen) were crushed, screened, and sprayed with kerosene (10 wt% based on the bitumen content). The kerosene pretreated oil sand was allowed to equilibrate for 2 hours. Batch aqueous digestion (328-333 K, 75 wt% solids) experiments were conducted in a baffled stirred-tank reactor (3.8 L) equipped with a double blade turbine impeller.

After 5 minutes the digested pulp was discharged into a gravity cell and diluted with water (50°C, 40 wt% solids) for sand sedimentation and separation of released bitumen concentrate. The system was gently stirred and the bitumen concentrate was skimmed from the surface of the process water. Batch flotation (15 wt% solids) was conducted in a Denver flotation cell (38 L) followed by gravity separation. The air flowrate was 5 L/min. The bitumen concentrate was removed for 2 minutes.

The grade of the bitumen concentrates was determined by Dean-Stark analysis. Samples of processing water were withdrawn from the digestion pulp and the pH was measured using a pH-meter (model 520, Orion Research, Inc.). Also, interfacial tension between bitumen-10 wt% kerosene mixture and processing water was measured using the ring method (Digital-Tensiometer K10T: KRUSS GmbH, Germany).

RESULTS AND DISCUSSION

Bitumen Release from Oil Sand

Samples of the Whiterocks oil sand were submerged in an alkaline solution (pH of aqueous phase was adjusted by sodium carbonate at pH=8.0 to pH=11.5) in a glass cell and the changes in sample structure were observed under a stereoscopic microscope (magnification about 50). Based upon microscopic examination the following observations were made in sequence for the Whiterocks oil sand immersed in alkaline water: rupture of bitumen film surrounding mineral particles and bitumen lens formation, gas bubble formation on the oil sand surface, bitumen spreading over the gas bubble surface, rupture of the particle-bitumen-particle

aggregates, and release of bitumen-enveloped gas bubbles and bitumen drops (Figure 31). Several photographs illustrating these events have been presented in our previous contributions.[104,105]

1. Bitumen film rupture and bitumen rollup (lens formation). A viscous bitumen film envelops the mineral particles (mainly quartz) which is thermodynamically unstable in the alkaline water at elevated temperature. The bitumen film rupture for the Whiterocks oil sand (diluted by 10 wt% kerosene during pretreatment) was observed in the temperature range 318 to 323 K. The bitumen lenses (drops) at the surface of mineral grains equilibrated to reach a stable state as defined by the Young equation:[40]

$$\gamma_{MW} - \gamma_{MB} = \gamma_{BW} \cos\theta \qquad (15)$$

where γ_{MW}, γ_{MB}, γ_{BW} are the interfacial tensions between mineral particle surface and water, mineral particle surface and bitumen, bitumen and water, respectively; θ is the contact angle for bitumen drop at the mineral particle surface. The value of the "thermodynamic equilibrium" contact angle (θ) depends on the pH and concentration of dissolved species in the processing water. However the true equilibrium, as defined by Young's equation (15), may never be reached due to the heterogeneity of mineral particle surfaces. The stable contact angle, which was observed after 2-3 minutes of equilibration of this model system, corresponds to a receding contact angle (θ_R). When the oil sand sample was immersed in an alkaline solution direct microscopic observations of the bitumen droplets located on the mineral particle surfaces were

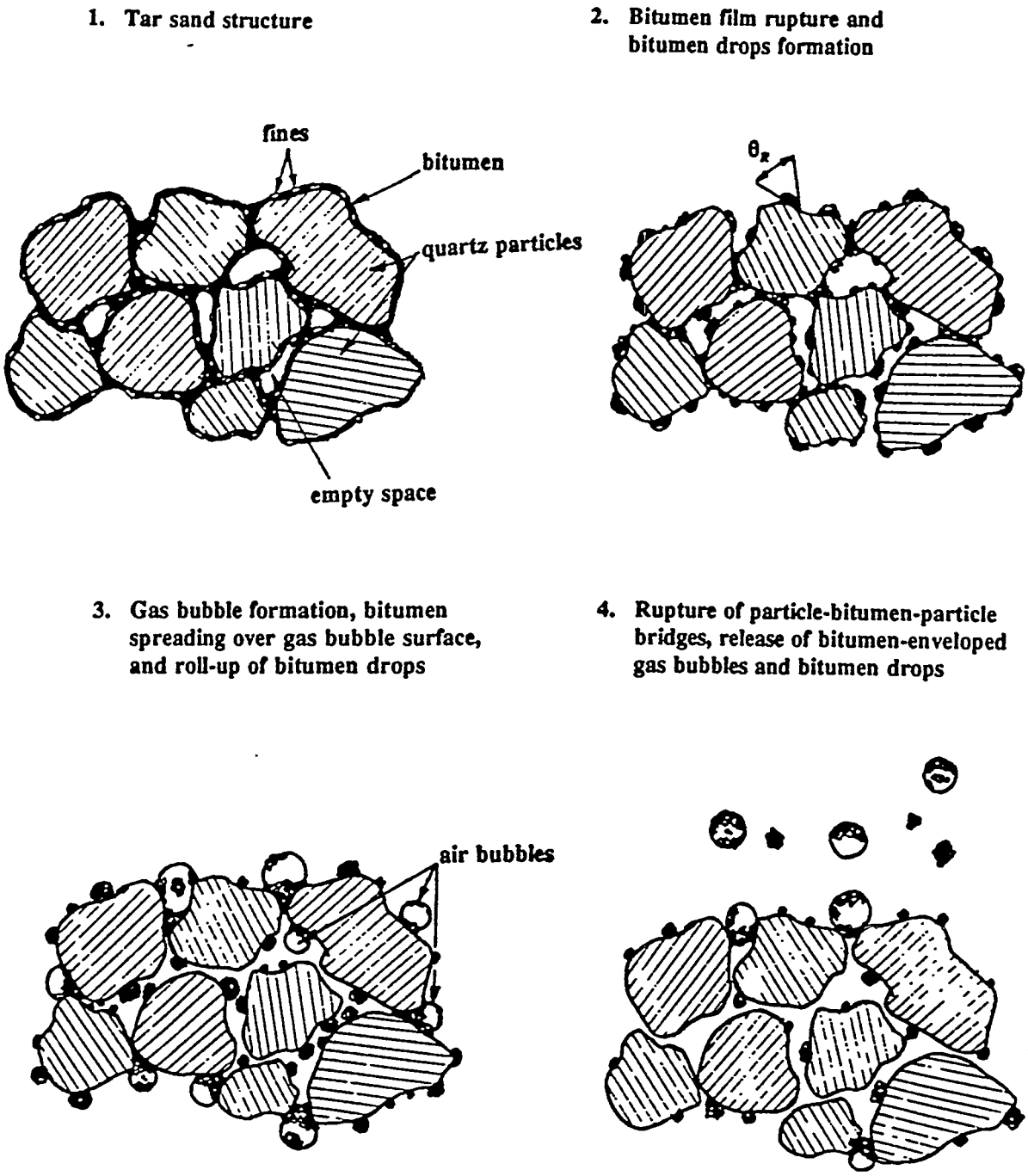

Figure 31. Illustration of Mechanisms of Bitumen Release from Whiterocks Oil Sands as Observed by Stereoscopic Microscopy

possible and the receding contact angles were measured from photographs (Figure 31 illustrates the receding contact angle for a bitumen drop at the mineral surface). The receding contact angle data, which are presented in Figures 32-34, are believed to be very reasonable but still must be regarded as having poor accuracy for measurements of tiny bitumen lenses (droplets) which were observed from different directions. Experimental data represent 85-90% of the observed population of bitumen droplets, and there were bitumen droplets with contact angles beyond the ranges shown in Figures 32-34, including drops with both smaller and larger contact angles. The wide range of experimental contact angle data (Figures 32-34) was due mainly to the randomly distributed surface heterogeneity of the mineral particles and also due to the poor accuracy of the measurements. On the other hand, any model bitumen/water/quartz system with the heterogeneity and roughness of the mineral surface such as observed for real systems is difficult to duplicate. Thus, the experimental procedure of contact angle measurements presented in this contribution has a poor accuracy but describes reasonably well the actual oil sand behavior.

The receding contact angle increased from 30-60 degrees at pH=7.5-9.0 to 120-150 degrees at pH=10.8 (Figure 32). There was no formation of bitumen-kerosene drops at pH≥11.0, and patches of the bituminous phase, differing in a shape, were formed on the surfaces of the mineral particles. These patches were easy to detach if sheared by the motion of the aqueous phase from stirring (the bituminous phase/water interfacial tension at pH=11 is close to

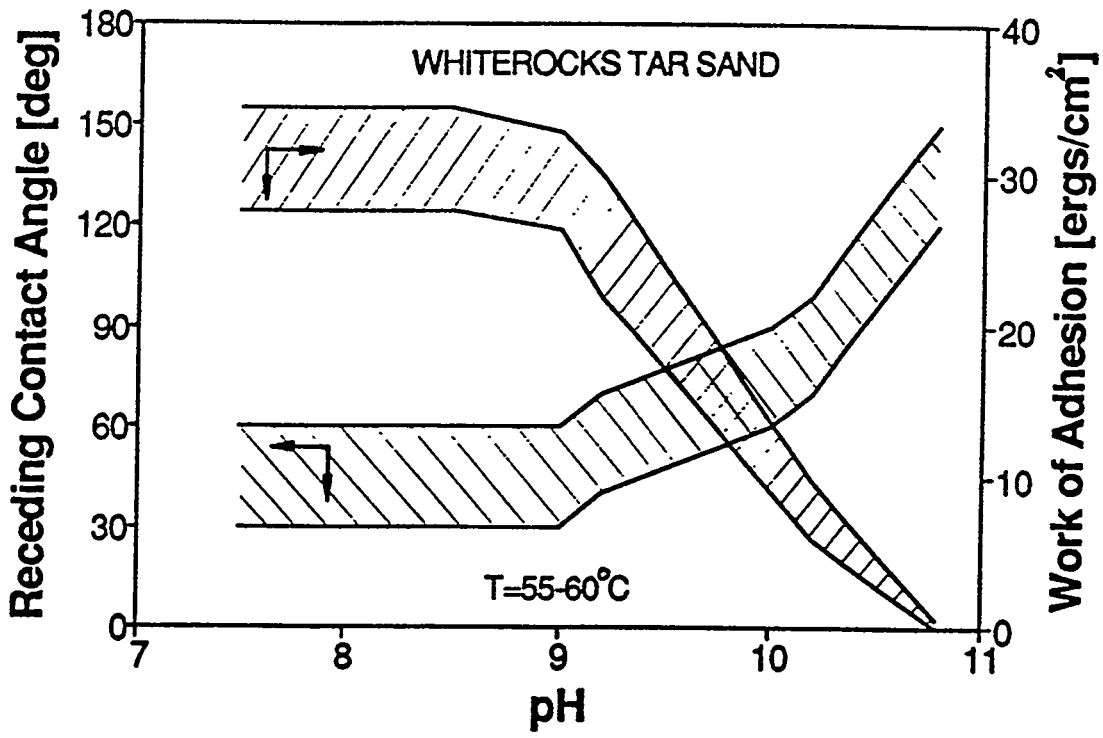

Figure 32. The Receding Contact Angle Measured for Bitumen (Containing 10 wt% Kerosene) Drops at Particle Surfaces and the Calculated Bitumen-Solid Work of Adhesion for Varying pH Values

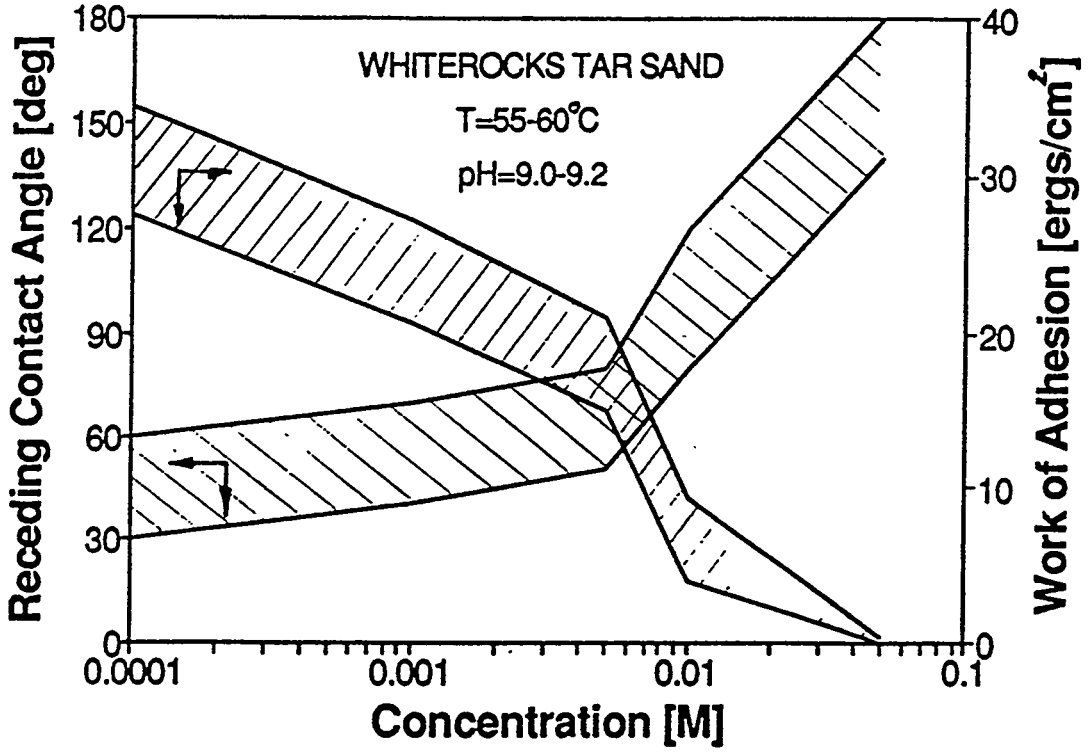

Figure 33. The Receding Contact Angle Measured for Bitumen (10 wt% Kerosene) Drops at Particle Surfaces and the Calculated Bitumen-Solid Work of Adhesion for Varying $Na_5P_3O_{10}$ Concentration

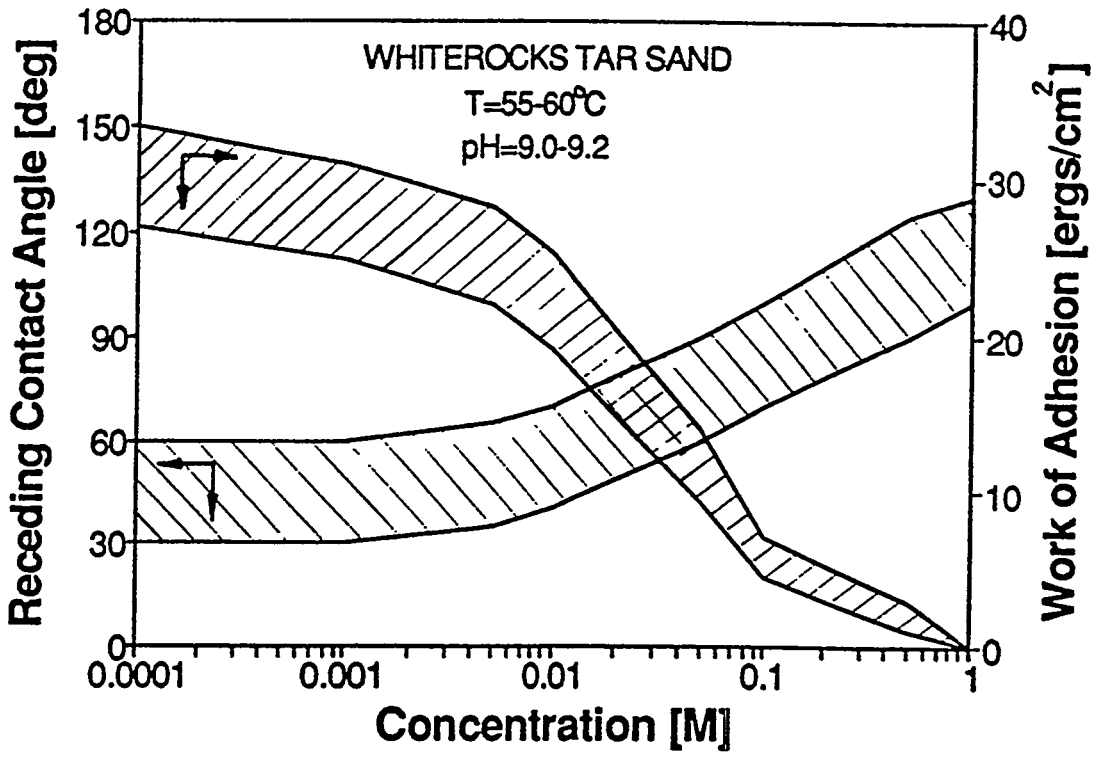

Figure 34. The Receding Contact Angle Measured for Bitumen (10 wt% Kerosene) Drops at Particle Surfaces and the Calculated Bitumen-Solid Work of Adhesion for Varying NaCl Concentration

zero, see Figure 22). The receding contact angle increased significantly in the presence of electrolyte ($Na_5P_3O_{10}$ concentration of 0.05 M; Figure 33, or NaCl concentration of 1 M; Figure 34) and reached a value of close to 180 degrees. Experimental data for the receding contact angle together with interfacial tension data, shown in Figures 22 and 23, allowed for the calculation of the work of adhesion (W) defined by the Young-Dupre equation as follows:[40,110]

$$W = \gamma_{BW}(1 + \cos\theta_R) \qquad (16)$$

The calculated values for the work of adhesion are presented in Figures 32-34. The work of adhesion between the bituminous phase (bitumen diluted with 10 wt% kerosene) and the mineral surface decreases drastically for pH>9, from about 30-35 ergs cm^{-2} at pH=7.5-9.0 to almost 0 ergs cm^{-2} for pH=10.8 (Figure 27). The adhesion forces are weakened in systems with higher $Na_5P_3O_{10}$ or NaCl concentration, and are close to zero for 0.05M $Na_5P_3O_{10}$ concentration (Figure 33) or for 1 M NaCl concentration (Figure 34). Importantly, it was found that a value of the work of adhesion, as calculated from equation (16), decreases significantly with a decrease in the bituminous phase/aqueous phase interfacial tension and only slightly depends on the change in contact angle value. Further, based on the work of adhesion calculations presented in Figures 32-34 it can be expected that only a small amount of energy will be required for the separation of bitumen drops from mineral surfaces for systems with pH>10.2 or for systems with $Na_5P_3O_{10}$ concentration >0.01 M (pH=9) or NaCl concentration ≥0.1 M (pH=9).

2. Air bubble formation and bitumen spreading at the air bubble surface. Observations made in the glass cell indicated that rollup of the bitumen film was accompanied by the release of gas bubbles from the oil sand. It is supposed that gas (mainly air) entrapped in the empty inter-particle space of the oil sand and in the pores of mineral particles was displaced by penetration of the aqueous phase. Gas displaced by the aqueous phase formed bubbles at the surface of oil sand which adhered to mineral particle surfaces via bitumen bridges. It was observed that gas displacement was facilitated with increasing pH and electrolyte ($Na_5P_3O_{10}$, NaCl) concentration.

In time, bitumen spreads over the gas bubble surface (this phenomenon is often called "filming") indicating that there is a positive spreading coefficient (S), expressed by the dependence:[40]

$$S = \gamma_W - (\gamma_{BW} + \gamma_B) > 0 \qquad (17)$$

where γ_W, γ_B are the surface tension of water and bitumen, respectively.

The experimental data for surface and interfacial tension presented in Figures 16, 22, and 23, allowed for the calculation of spreading coefficients, and the results are shown in Figures 35-37. The surface tension of the alkaline water was assumed to be 45-55 mNm^{-1}, as is expected for process water in the hot water processing of oil sands.[31,105] Surface-active species (natural surfactants) of bitumen are dissolved in the aqueous phase and lower the surface tension of the aqueous phase.[31,105] As is shown from Figures 35-37, the spreading coefficient is positive for all pH values and

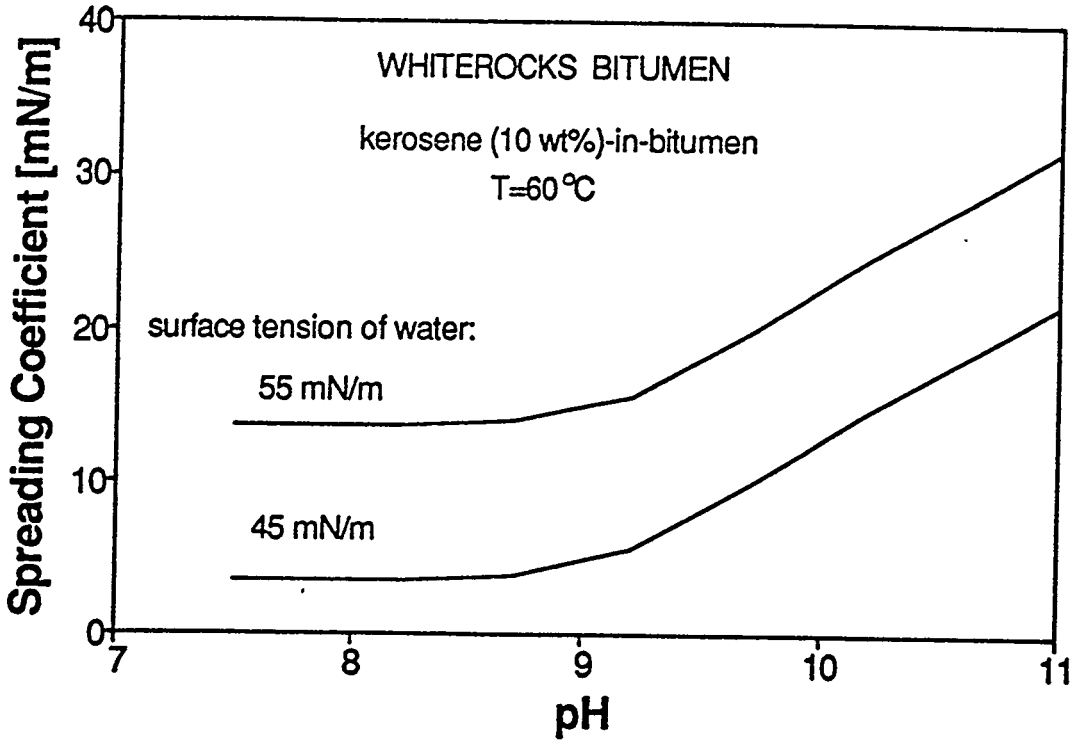

Figure 35. Spreading Coefficient of Bitumen (10 wt% Kerosene) at the Water Surface

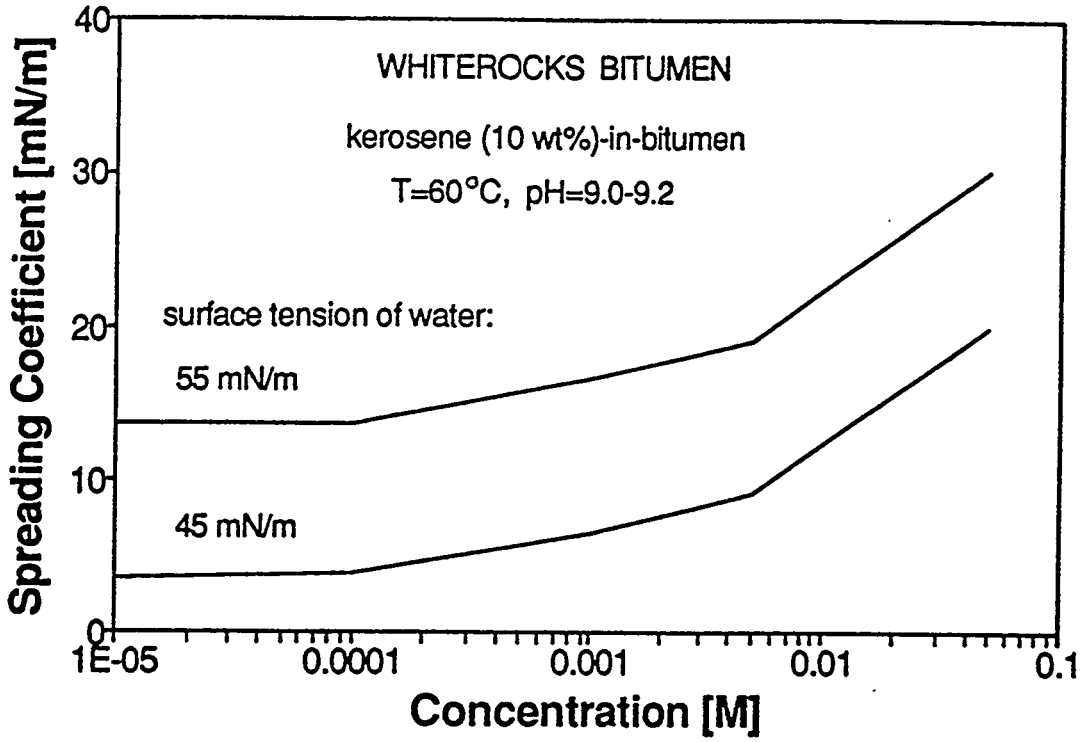

Figure 36. Spreading Coefficient of Bitumen (10 wt% Kerosene) at the Water Surface for Varying $Na_5P_3O_{10}$ Concentration

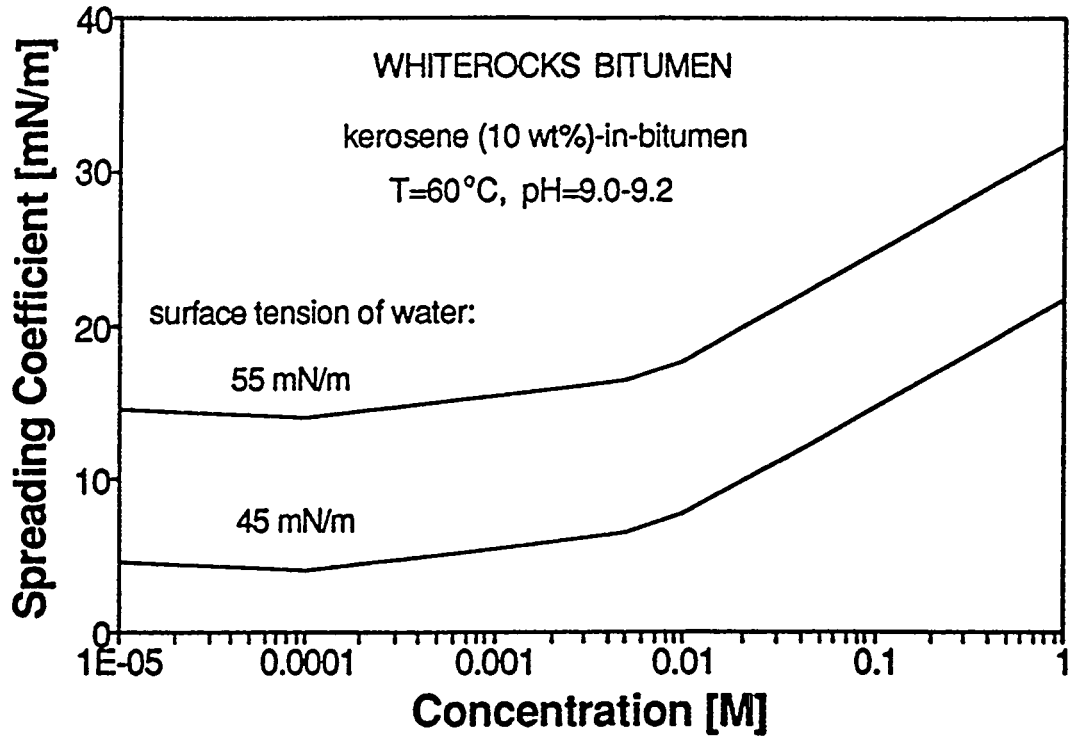

Figure 37. Spreading Coefficient of Bitumen (10 wt% Kerosene) at the Water Surface for Varying NaCl Concentration

electrolyte ($Na_5P_3O_{10}$, NaCl) concentrations and increases significantly for systems with pH>9.2 (Figure 35) and for the systems with a high concentration of sodium tripolyphosphate (Figure 36) or sodium chloride (Figure 37). Large values of the spreading coefficient for the bituminous phase are desired in hot water processing, and efforts to appropriately control bitumen filming at gas bubbles should facilitate separation and recovery of bitumen.

3. Rupture of particle-bitumen-particle bridges, and release of oily gas bubbles and bitumen drops. The bitumen film rupture and the formation of small bitumen lenses reduces the sand-bitumen contact area and weakens the force of adhesion in the unconsolidated Whiterocks oil sand. When the receding contact angle for the bitumen drop was close to or larger than about 90 degrees, there was rupture of particle-bitumen-particle bridges. The oil sand sample disintegrated into individual mineral particles with the attached bitumen almost immediately. Such was the case after contact of the oil sand sample with aqueous phase of high pH values, pH>10.2-10.3, or for systems with highly concentrated solution of $Na_5P_3O_{10}$, >0.01 M at pH=9.1-9.2, or NaCl, >0.5 M at pH=9.1-9.2.

The buoyancy force stimulated the detachment of gas bubbles, covered by the bituminous phase and associated fines, from the coarse mineral particle surfaces. The amount of bitumen carried with the gas bubbles depended on the aqueous phase used in the experiment, and generally the amount of bitumen covering the gas

bubble increased with increasing pH and electrolyte ($N_5P_3O_{10}$, NaCl) concentration.

Correlation of Interfacial Tension with Bitumen Recovery

Calculations of the work of adhesion based on the interfacial tension and contact angle data for model systems presented in the previous section (see Figures 32-34) suggest that a decrease in energy required for bitumen separation from mineral particle surfaces should be observed with an increase in pH and/or an increase in electrolyte ($Na_5P_3O_{10}$, NaCl) concentration. Only a small energy may be required to separate the bitumen from Whiterocks oil sand immersed in the alkaline solutions with pH>10.2-10.3, or pH=9 and electrolite (NaCl or $Na_5P_3O_{10}$) concentration >0.01 M, based on the calculation of the work of adhesion data obtained from contact angle measurements (Figures 32 to 34). The bitumen (10 wt% kerosene)/water interfacial tension measured in such systems corresponds to a value less than 5-7 mNm^{-1} (compare Figures 22 and 23 with Figures 32 to 34). Also, it was presented in Figures 35 to 37 that the spreading coefficient increases for increasing pH and/or electrolyte ($Na_5P_3O_{10}$, NaCl) concentration in the aqueous phase. A positive and large value for the spreading coefficient is desired in oil sand systems to facilitate the bitumen separation from oil sands when bitumen is removed from mineral particles by air bubbles[104] (spreading of bitumen at gas bubbles, as discussed in a previous section).

It should be noted that both parameters, the work of adhesion between bitumen and mineral particle and the spreading coefficient

for bitumen at the air bubble surface, significantly depend on the bitumen/water interfacial tension (see equations 16 and 17). There are other additional properties of the three-phase system such as the surface tensions of bitumen and the aqueous phase or the sand/water and sand/bitumen interfacial tensions which contribute to the spreading coefficient (see equation 17) and the work of adhesion (see equation 16). As demonstrated in a the previous section, the interfacial tension can be modulated by the pH and/or the inorganic salt ($Na_5P_3O_{10}$ or NaCl in our case) concentration. Thus, it was concluded that if bitumen separation from oil sands in the hot water process is governed by adhesion forces between the bitumen and the mineral surface as well as the kinetics of bitumen spreading over the gas bubble surface, the efficiency of bitumen recovery should be improved by decreasing the bitumen/water interfacial tension.

To correlate the interfacial tension with the effectiveness of bitumen disengagement from Whiterocks oil sand, several hot water processing experiments were performed, as described in the experimental procedure. Experimental results are presented in Table 19 and are illustrated for the gravity separation step in Figure 38. A different interfacial tension between the bituminous and aqueous phases was obtained by changing the concentration of Na_2CO_3, $Na_5P_3O_{10}$, and NaCl in the process water (according to the effect of pH and electrolyte ($Na_5P_3O_{10}$, NaCl) concentration on the interfacial tension, see Figures 22 and 23). In the hot water processing experiments for Whiterocks oil sands either fresh tap water or

Table 19. Recovery of Bitumen from Whiterocks Oil Sands

Exp. No.	Reagents [per kg tar sand]	pH	Interfacial Tension (60^{o})[A] [mNm^{-1}]	Recovery Gravity Separation [wt%]	Recovery Flotation (2 min) [wt%]
1.	fresh water 0.5g Na_2CO_3	7.8	9.3	13	33
2.	fresh water 0.5g Na_2CO_3	7.7	10.6	12	29
3.	fresh water 1g Na_2CO_3	8.0	8.1	14	36
4.	fresh water 0.5g Na_2CO_3 0.75g NaCl	7.7	11.0	15	42
5.	fresh water 1g Na_2CO_3 1g NaCl	8.3	7.9	16	55
6.	fresh water 2g Na_2CO_3 2g NaCl	8.7	3.8	39	34
7.	fresh water 1g Na_2CO_3 0.5g $Na_5P_3O_{10}$	8.2	7.2	22	48
8.	fresh water 1g Na_2CO_3 1g $Na_5P_3O_{10}$	8.5	6.3	43	21
9.	recycled water[B] ~1.5g Na_2CO_3 ~1.5g $Na_5P_3O_{10}$	8.7	<3	51	21
10.	recycled water[B] ~2g Na_2CO_3 ~2g $Na_5P_3O_{10}$	8.8	<3	59	20
11.	recycled water[B] ~2g Na_2CO_3 ~1g $Na_5P_3O_{10}$ 1.5g NaCl	8.6	<2	57	23

A) the accuracy of interfacial tension measurements was $\pm$1.2-1.8 mNm^{-1}

B) the amount of sodium carbonate and sodium tripolyphosphate reported includes that total amount dissolved in water in subsequent cycles. The amount of reagents which may have precipitated during the course of the experiment could not be determined at experimental conditions.

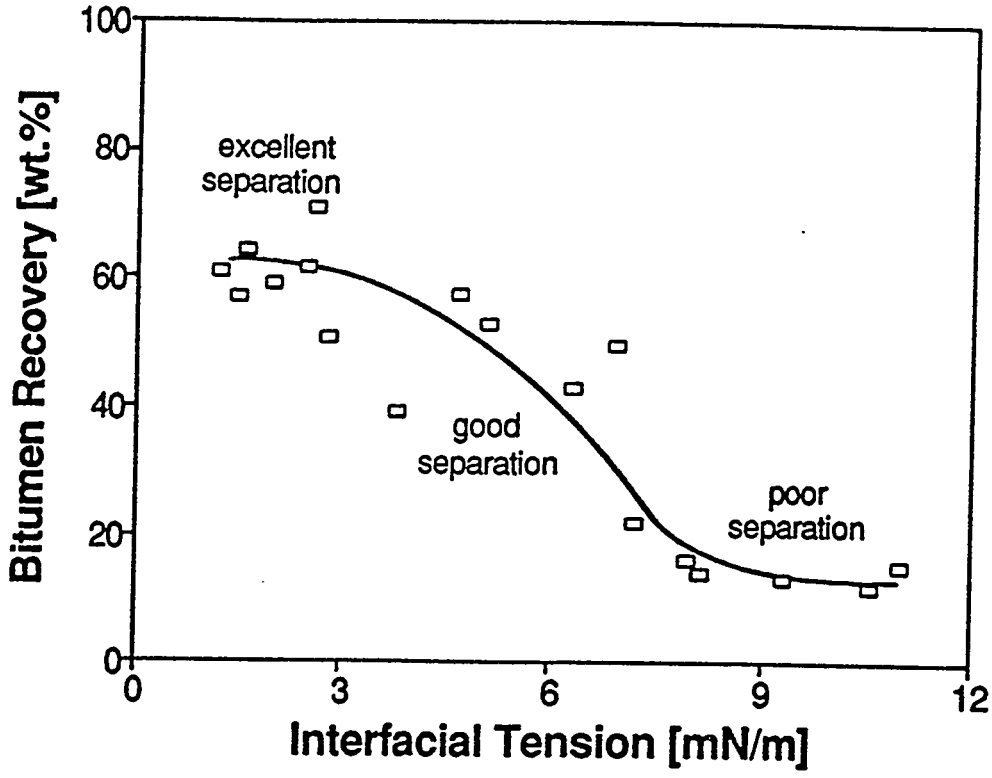

Figure 38. Relationship Between Bitumen Recovery from Gravity Separation and the Bitumen (10 wt% Kerosene)/Process Water Interfacial Tension

recycled water (process water recovered from tailings after hot water experiments) was used. An increase in bitumen recovery by gravity separation was observed with decreasing interfacial tension, as is shown in Table 19. Also, the advantageous influence of a decrease in interfacial tension on bitumen recovery during flotation can be deduced from the experimental data presented in Table 19. The results presented in Table 19 are limited to data for the first 2 minutes of flotation, and continuation of this operation allow for the separation of 20-30 wt% of bitumen which remained in the pulp, depending on the time of flotation and the experimental conditions.

Based on these experiments the following correlation of interfacial tension (γ_{BW}) with bitumen recovery has been identified:

1. $\gamma_{BW} > 7\text{-}9$ mNm^{-1} poor separation
2. $3\text{-}4$ $mNm^{-1} < \gamma_{BW} < 6\text{-}7$ mNm^{-1} good separation
3. $\gamma_{BW} < 2\text{-}3$ mNm^{-1} excellent separation

Of course, these criteria are based on the separation of bitumen from Whiterocks oil sand, and a complete generalization requires the examination of oil sands from other deposits. Also, these criteria are mainly applied for bitumen release under the specified digestion procedure.

SUMMARY AND CONCLUSIONS

Samples of the Whiterocks oil sand were submerged in alkaline solutions in a glass cell and the bitumen release from samples was observed using an optical microscope. Microscopic observations allowed for the description of macroscopic phenomena associated

with bitumen release from oil sand samples and for the determination of reasonable values of the receding contact angle for the bitumen droplets located on mineral particle surfaces. Bitumen phase disengagement under stagnant conditions involved bitumen layer rupture and bitumen lens formation, gas bubble formation on the surface of oil sand samples, bitumen spreading over the gas bubble surface, rupture of the particle-bitumen-particle bridges, and release of bituminous gas bubbles and bitumen drops. Generally, release of bitumen from the mineral particle surfaces was facilitated at high pH and at higher concentrations of $Na_5P_3O_{10}$ and/or NaCl. Almost spontaneous separation of bitumen from oil sand was observed for the system at pH=9.0-9.2 and 0.05M $Na_5P_3O_{10}$ or 1 M NaCl. Also, adhesion forces between bitumen and mineral particle surfaces were weakened to a value of close to zero in the system with pH=10.8. Based on the surface/interfacial tension data, the spreading coefficient for the bitumen-10 wt% kerosene mixture at the water surface was calculated and found to be positive under all experimental conditions.

In addition to bitumen viscosity considerations, bitumen/water interfacial tension plays an important role in the hot water processing of oil sands. Microscopic observations of the bitumen release from the Whiterocks oil sands under stagnant conditions for varying composition of aqueous phase (varying pH and/or electrolyte concentration) showed that bitumen release from mineral particles strongly depends on the bitumen/water interfacial tension. Importantly, in accordance with these observations, it was found

that bitumen recovery from oil sands may be enhanced by appropriately controlling the bitumen/water interfacial tension, which can be accomplished for the Whiterocks oil sands by increasing the pH and/or electrolyte concentration in the process water. Excellent bitumen disengagement from the Whiterocks oil sand was observed for systems in which the interfacial tension between the bituminous and aqueous phases is lowered to a value of less than 2-3 mNm^{-1}. A somewhat reduced but satisfactory separation efficiency was found when the interfacial tension was from 4 mNm^{-1} to 7 mNm^{-1}. At higher interfacial tensions, poor bitumen recovery from the Whiterocks oil sand was observed.

FUTURE ACTIVITIES

The interfacial tension criteria for the effective bitumen separation from the Whiterocks oil sands have been determined in this research program. Nevertheless, the examination of oil sands from other deposits is required to determine similar criteria for separation of bitumen from other oil sand resources. Additional effort will be undertaken to correlate the pH and specific conductivity of the process water with bitumen/water interfacial tension. Also, further experiments are required to specify other physico-chemical properties for hot-water separation of bitumen from oil sands.

BUBBLE SIZE DISTRIBUTIONS GENERATED DURING OPERATION OF AN AIR-SPARGED HYDROCYCLONE

INTRODUCTION

Bubble size is a important factor which may control the rate and the efficiency of flotation separation. It is generally known that bubble size distribution generated in the flotation machine depends on the technique of gas injection. Bubble generation techniques are as follows:[111]

- mechanical shear contacting (conventional mechanical flotation cells),
- static shear contacting (i.e., Davcra cell, packed column),
- sparging through porous media: without high external shear (column flotation),

  sparging through porous media: with high external shear (i.e., (Bahr cell, air-sparged hydrocyclone),
- jetting: bubble generation occurs when either a gas stream is jetted from an orifice into liquid or when a liquid (or slurry) is jetted from an orifice into a pool.

A comparison of the typical size distributions produced by different generators was presented by Yoon et al.,[112] and Benett.[113] The size of the bubbles generated in mechanical flotation cells is typically from 400 μm to 2.1 mm. Porous materials used as gas distributors may generate such small microbubbles as less than 300 μm. The bubble size distribution is narrow in the flotation cell equipped with porous gas sparger in contrast to that obtained in the mechanical cell.

In the air-sparged hydrocyclone (ASH), the bubbles are generated in the high shear field. Only a few studies were conducted for similar conditions. Sada et al.[114] examined a bubble formation mechanism under dynamic conditions in an intensified flow rate of liquid. Two nozzles of 0.86 and 3.05 mm diameter were used. The gas flow rate and the superficial liquid velocity ranged from 0.33 to 36.2 cm^3/s and from 0 to 154.9 cm/s, respectively. The bubble size formed in such conditions decreased with decreasing gas flowrate and with increasing superficial liquid velocity. Tsuge et al.,[115] examined the effect of the velocity (0.13 cm/s) of a horizontal liquid flow on the size of the bubbles (gas flowrate 0.1 to 12 cm^3/s) generated at a single orifice (range of diameters: 0.95 to 2.52 mm). The bubble volume decreased as the liquid velocity was increased at constant gas flow. Johnson et al.,[116,117] developed a gas distributor which was able to produce microbubbles with a diameter of 30 to 200 μm. The distributor consisted of a cylindrical glass disperser (4 to 5.5 μm pore size) placed concentrically inside a glass sleeve. In operation, emerging bubbles were sheared from the frit by water flowing through the narrow annular space (150 μm) between the frit and the sleeve. A similar microbubble distributor was presented by Yoon et al.[112] It is, essentially, a Venturi tube made of porous material whose pore size may be 2.5 to 60 μm. As a slurry containing frother flows through the generator, the fluid velocity increases as the tube narrows. This, in turn, decreases the pressure according to Bernoulli's principle. The reduced pressure draws air into the

annular chamber around the porous tube. Air bubbles are nucleated on the inner wall of the porous tube and sheared off by the high fluid velocity. If the fluid velocity is fast enough, the bubbles are sheared off their nucleation sites before they grow in size, thereby containing microbubbles. At a given frother addition, the size of the bubbles produced by this generator is a function of fluid velocity, length and diameter of the Venturi tube, air flow rate, and the pore size of the material used to make the Venturi. Unfortunately, Yoon and co-authors[112] did not present the bubble size distribution generated by this new gas sparger. They only mentioned that the size of bubbles was over a magnitude smaller than that observed in most industrial columns and the distribution is much narrower than that found in conventional mechanical cells.

The force field generated in the spargers invented by Johnson et al.,[116,117] and Yoon et al.[112], is expected to be similar to that in the ASH. The bubble size distribution generated in ASH was analysed theoretically in a previous contribution, and a theoretical formula for the bubble dimension was derived as follows:[118]

$$r_b = \left[\frac{3Q_a}{2V_t}\sin^{-1}\left(\frac{r_o+r_b}{2(R_c-r_b)}\right)(R_c-r_b)\right]^{\frac{1}{3}} \qquad (18)$$

where: Q_a =volumetric flowrate of air

R_c = hydrocyclone radius

r_b = bubble radius

r_0 = capillary radius

V_t = tangential velocity of the fluid at the point of bubble formation

Experimental verification of this formula was examined for systems with single capillaries in a plexiglass hydrocyclone.[119] The tangential velocity of water was controlled at 2.8 m/s, and a diameter of single capillary was 0.64 mm. It was observed that the bubble diameter was comparable in size to the capillary diameter and does not change appreciably with the air flowrate (or flow ratio). Surface tension of water did not have a significant effect on the bubble size under these conditions. A similar correlation was observed by Yoon et al.[112]

In these current studies, high-speed photography has been used to examine the nature of bubble formation in the swirl flow of the ASH and the corresponding bubble size distributions. On this basis, it is expected that these fundamental measurements will help to establish design features and operating conditions for efficient flotation separations of dispersed bitumen from tailings water.

EXPERIMENTAL

A number of techniques have been developed over the years to measure bubble size in liquids and liquid-solid dispersions. These include: photographic methods, optical probe measurements, and electrical conductivity (resistivity) probe methods. A detailed description of these methods can be found in the literature.[120]

In our experiments the photographic technique was selected. A conventional 35 mm camera (Pentax K1000) with special magnifying lens (Samyang 28-200 mm) and an electronic flash (Vivitar 283) were

used to capture moving fluid with bubbles. The ideal place to capture bubbles on the film for examination of the size distribution is inside the ASH. Even in a specially designed and constructed hydrocyclone with transparent windows, it was impossible to photograph the bubbles because of difficulties with lighting and focus. In this regard, measurements were carried out to determine the bubble size distributions in the underflow stream during water-only operation of actual ASH units of different diameter and length. The effect of pore size has not yet been studied in detail. A high-speed photographic technique coupled with a reflecting screen allowed for a 30 μs exposure time. The froth pedestal of the ASH was replaced by a 90° Plexiglas cone to improve resolution of the bubbles. Nevertheless, the velocity of discharge (~1 m/sec) and the limitations of the photographic system, the diameter of bubbles smaller than 300 μm diameter was estimated with increasing error. The photographs of the underflow stream were taken just as the water discharged from the ASH. The significance of bubble coalescence was evaluated from variations in the length of the ASH. The effect of frother, 4-methyl-2-pentanol (MIBC), was studied at concentrations from 0 to 20 mg/L.

RESULTS AND DISCUSSION

Frother Concentration

Typical air bubble size distributions for different frother concentrations are presented in Figure 39. When the frother concentration increases the size distribution becomes narrower and shifts towards smaller average bubble diameters. These results

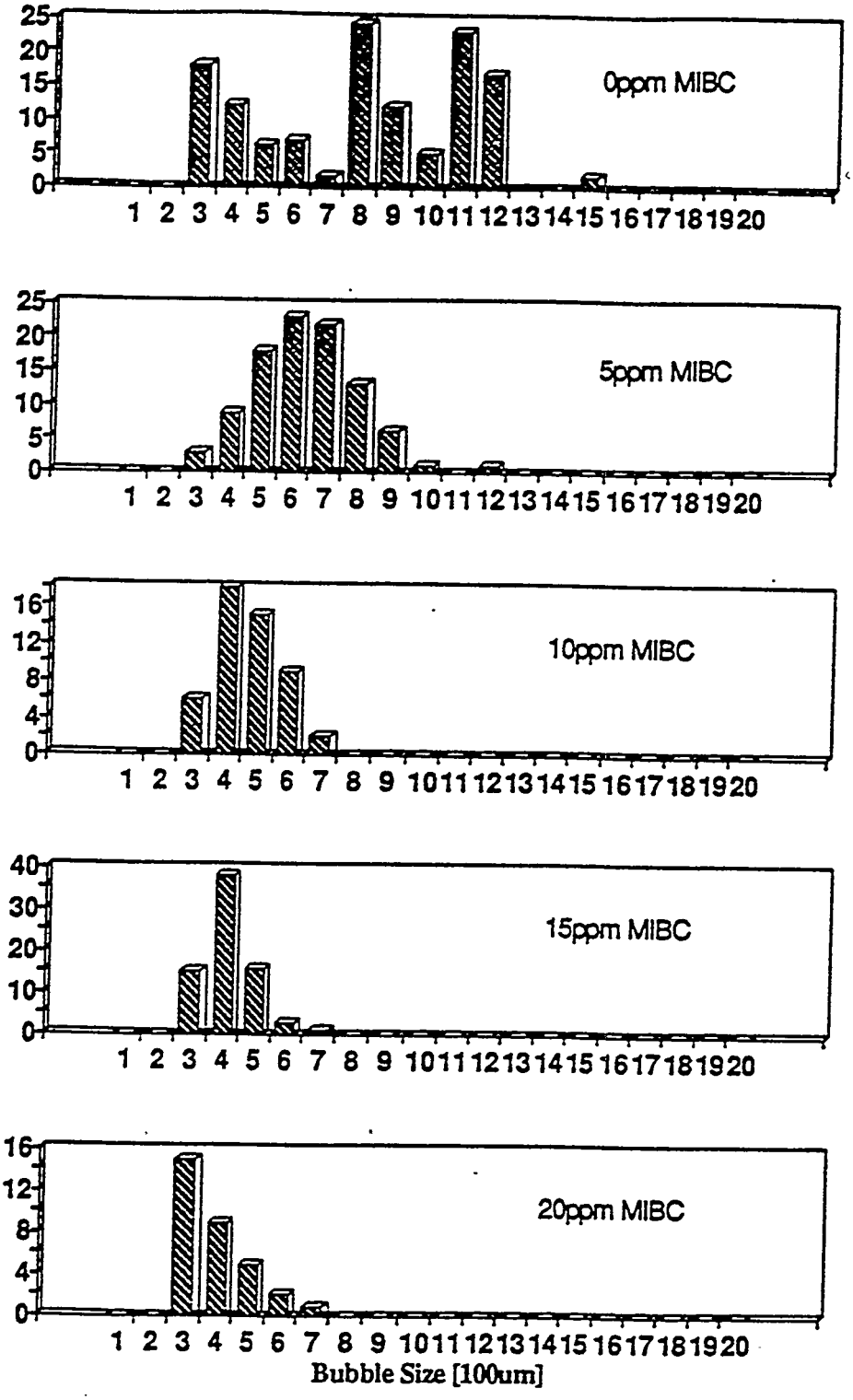

Figure 39. The Size Distribution for Air Bubbles Leaving the ASH in the Underflow as a Function of MIBC Concentration, Measurements Were Made for 5 cm Diameter, 16 cm Long ASH

confirm earlier predictions for bubble generation from a porous wall under significant shear.[112,119] In the absence of frother the distribution shows a characteristic contribution from both large and small bubbles. It is believed that the large bubbles were formed by coalescence, and that the small bubbles are, in part, the satellite bubbles, released during the formation and/or coalescence process.

The concentration of frother had the most pronounced effect on the average bubble size as calculated from each size distribution (Figure 40). The average bubble size dropped from almost 1000 μm to below 500 μm with an increase in frother concentration for 0 ppm to 20 ppm. Such a change in the bubble size was not observed during the single capillary studies.[119] It may be that the major role of the frother is to prevent coalescence of bubbles as they form at adjacent pores on the porous tube wall. Also, it was observed that with an increase in frother concentration the bubble concentration in the underflow increased, presumably due to smaller bubble diameter and larger retention in the swirl layer.

ASH Diameter

The average diameter of bubbles generated in the 15 cm ASH unit was approximately 25 % larger than in the 5 cm ASH unit when frother was absent, as is evident from the data presented in Figure 35. With an increase in MIBC concentration the bubble size decreased in both ASH units, and the difference in the average bubble size diminished. For example; for the 5 cm unit (47 cm in length, $Q^* = 2$) the average bubble size dropped from 780 μm at 0 ppm

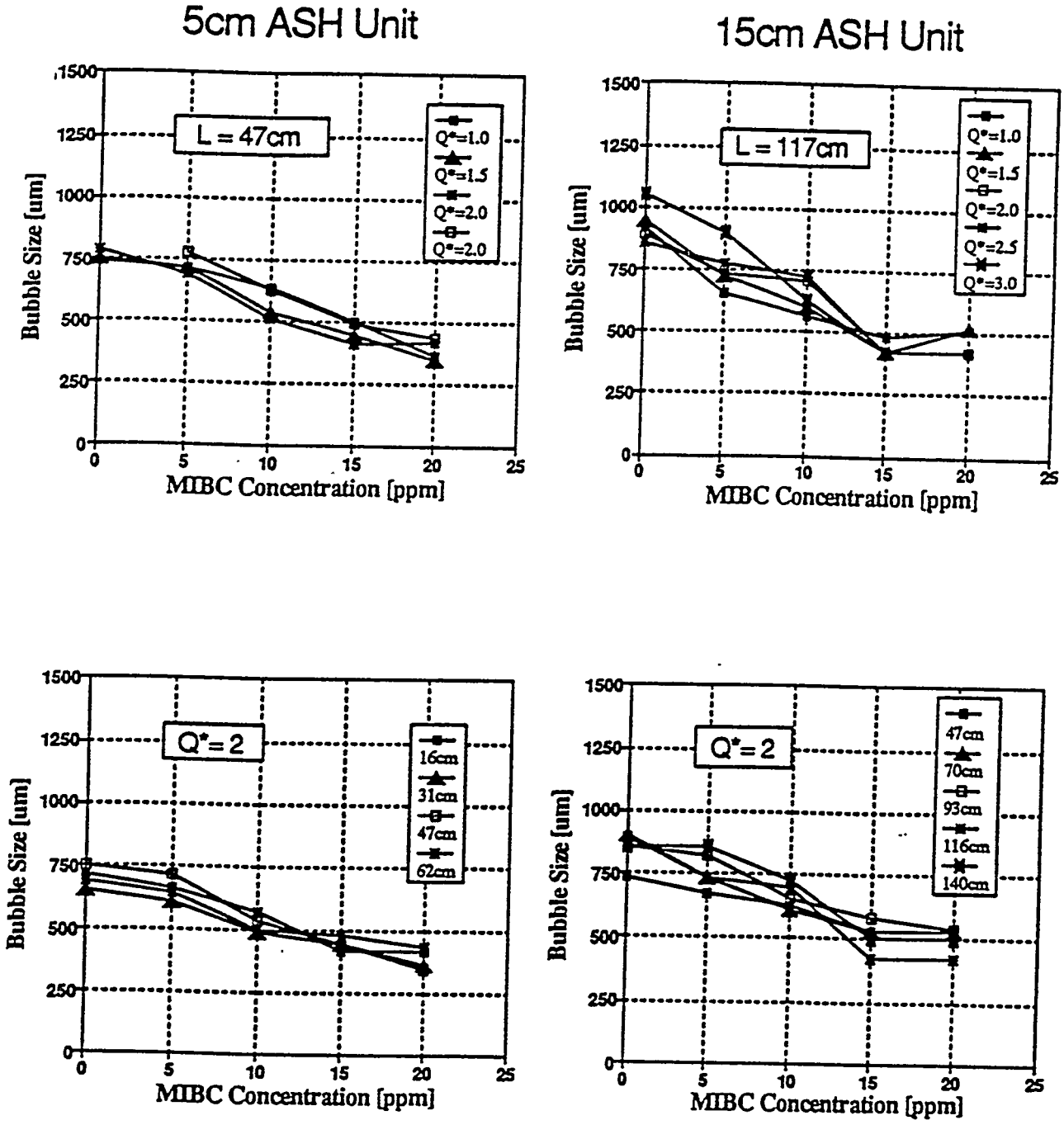

Figure 40. Average Bubble Size in the Underflow as a Function of MIBC Concentration for 5 cm ASH and 15 cm ASH Units of Different Lengths (L) and Different Dimensionless Flowrate Ratios (Q^*)

MIBC to 420 μm at 20 ppm MIBC, whereas for the 15 cm unit (117 cm in length, $Q^* = 2$) the average bubble size dropped from 890 μm at 0 ppm MIBC to 440 μm at 20 ppm MIBC. At higher frother concentration the bubble size is almost independent of ASH diameter and from one perspective this might be attributed to the fact that as the bubbles become smaller the thickness of the effective hydrodynamic boundary layer for the swirl flow is no longer of significance. In the absence of frother the bubble size is sufficiently large that the bubble extends beyond the effective boundary layer into the shear flow. In this way, the shear velocity which, of course, is greater for the 5 cm ASH unit leads to smaller bubbles in the absence of frother. On the other hand in the presence of sufficient frother bubble, release occurs at a smaller size in the boundary layer due to a reduced surface tension. Under these circumstances, the boundary layer thickness (ASH diameter), does not significantly influence bubble size. In addition, the presence of frother tends to stabilize these smaller bubbles and prevent coalescence. Of course, the effect of frother is of considerable significance and quite different from the results reported for single capillary experiments.[118] Finally, it should be noted that the "average pore size" of the porous wall, (another factor which might affect bubble size) was 25 to 50 μm for the 5 cm ASH unit, and approximately 60 μm for the 15 cm ASH unit, as specified by the manufacturer and independently confirmed by microscopic examination in our laboratory.

ASH Length

The data presented in Figure 35 indicate that, as expected, the length of the ASH unit has no influence on the measured bubble size for both 5 cm and 15 cm ASH units. These results suggest that coalescence after formation is not significant and that the measured bubble size in the underflow is probably close to the bubble size in the swirl layer.

Flowrate Ratio

Of equal importance from these results is the observation that the bubble size distribution is independent of the dimensionless flowrate ratio (Q^* = air flowrate / water flowrate) for both the 5 cm ASH unit and the 15 cm ASH unit for all concentrations of MIBC as shown in Figure 41. Strictly speaking, the water flowrate remained constant (at 70 lpm for the 5 cm ASH unit and at 700 lpm for the 15 cm ASH unit) and only the air flowrate was changed. The lack of influence of the air flowrate on the bubble size was already predicted for air-sparged hydrocyclone flotation,[119] and regarding bubble generation from orifices, these findings support the findings from previous research for orifice air velocities exceeding 0.1 m/s.[120]

The experimental results can be discussed in terms of frother stabilization of bubbles formed at individual pores and the effective thickness of the hydrodynamic boundary layer relative to bubble size. Such an analysis has been mentioned previously.

On the other hand it is conceivable that the sparged air creates a blanket, or cushion, of air which covers the inside wall

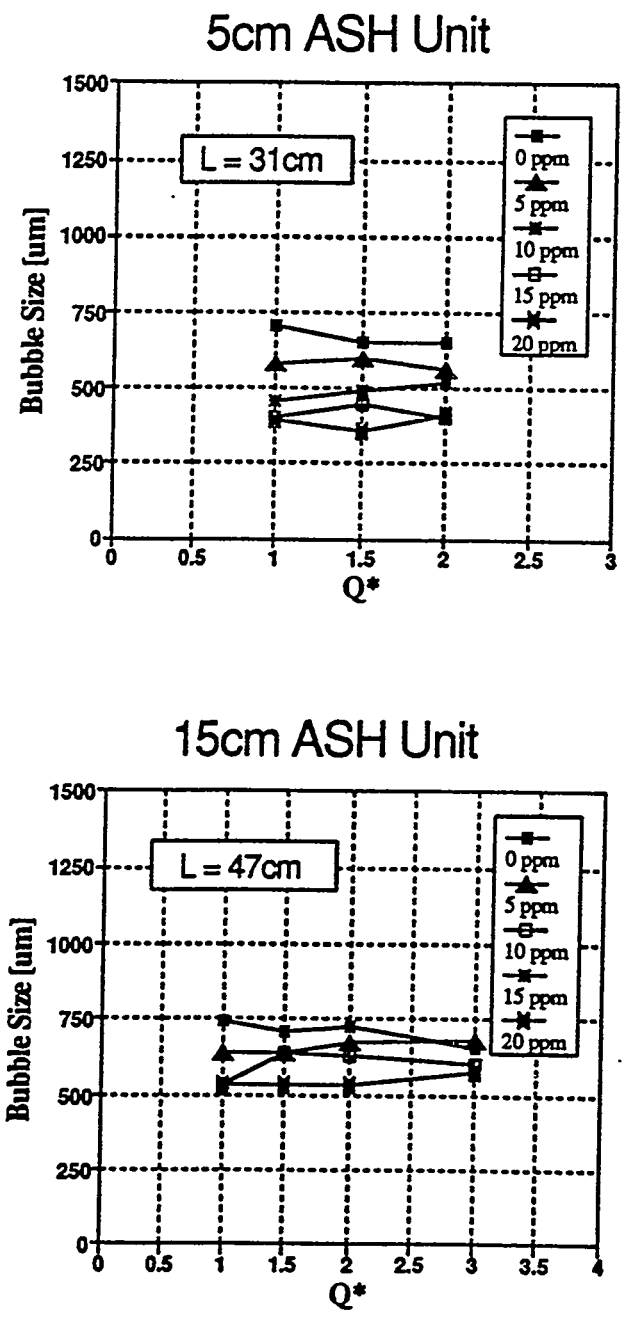

Figure 41. Average Bubble Size in the Underflow as a Function of the Dimensionless Flowrate Ratio (Q^*) for 5 cm ASH and 15 cm ASH Units of Different Lengths (l) and for Different MIBC Concentrations

of the porous tube and, thus, creates a "frictionless" surface. Evidence for this phenomenon was found from the radial density gradients as determined by X-ray CT experiments.[121] From this perspective the blanket of air is sheared or broken into bubbles the size of which might simply be controlled by the size of turbulent eddies. In this case the pore size of the porous tube would have little effect on the bubble size distribution and the bubble size would only be expected to become dependent on Q^* at low air flowrates where the air blanket would became unstable.

FUTURE ACTIVITIES

The measurements of the bubble size of less than 100 μm were not possible with the equipment used in these studies. Further research must be undertaken with an improved photographic system. The effect of bubble size on the efficiency of bitumen droplet separation from the hot-water process tailings stream will be investigated in order to improve the quality of recycle water.

A DIMENSIONAL ANALYSIS OF CLEANUP OF A BITUMEN CONCENTRATE DERIVED FROM UTAH OIL SAND

INTRODUCTION

The ever-increasing dependence of the global economy on petroleum and its derivatives and the rather limited nature of conventional sources have rendered research on nonconventional oil sources of practical importance, and the research efforts pertinent to processing bitumen-rich Utah oil sands can be considered an important step in this direction. The major aspects of the oil sand processing program at the University of Utah are described in a review article by Oblad et al.[24] In a number of recent research papers,[38,87,88,106] the various aspects of water-based processing of Utah oil sand have been described in detail. The bitumen produced in this way contains a significant amount of water along with residual sand particles. Also, its high viscosity hinders subsequent processing steps. An organic solvent like kerosene, therefore, needs to be added to the bitumen concentrate to facilitate separation of fine mineral particles and emulsified aqueous phase from preceding operations. An important part of the bitumen cleanup directly depends on the kinetic aspects of dissolution of the bitumen concentrate in kerosene.

Although solvent extraction has been recommended as a highly efficient technique for the separation of bitumen from oil sands,[122] its efficacy and the subsequent scaleup of the dissolution process calls for a systematic analysis of the process variables, and so far, very few studies in the oil sand literature have addressed this engineering aspect of the problem in sufficient

depth and detail. The process variables that influence bitumen dissolution in a solvent such as kerosene are large in number. Variation of each of the variables individually would constitute a rather enormous task of experimentation which might be difficult to accomplish in a finite period of time. A better strategy, however, is to incorporate the variables in the form of dimensionless groups pertinent to the system, so that the same analysis can be performed on the basis of a substantially fewer number of experiments.

During this study a systematic dimensional analysis of the bitumen dissolution in a stirred tank was performed as detailed in the subsequent section.

EXPERIMENTAL

During this work the dissolution of bitumen was studied in a cylindrical, stainless steel, baffle-less vessel, fitted with a mechanical stirrer (six straight-blade, 5.2 cm dia and 1.0 cm high turbine), type IKA-RW 15 Janke & Kunkel, Germany. The turbine diameter (d) per mixer diameter (D) ratio was d/D = 0.394. The rotational speed of the stirrer was measured accurately with a phototachometer manufactured by Cole Parmer Instrument Co. Stirring a highly viscous liquid like bitumen is an extremely cumbersome task, and limited success is possible with the screw agitators used by Swainsky et al.[123] During this study, however, no attempts were made to agitate the bitumen phase, as it was possible to obtain a very high rate of bitumen transfer by stirring the solvent near the liquid/diluent interface. The distance between the stirrer and the initial bitumen surface was kept

constant at 1.5 cm. The reactor was immersed in a water bath where the temperature was controlled using a heating-plus-controller assembly. A constant temperature of 327±4 K was used in all the experiments. A total of sixteen experiments was performed, the basic conditions of which are presented in Table 20.

Table 20
EXPERIMENTAL CONDITIONS

Expt. #	Initial Mass of Bitumen Concentrate* (g)	Volume of Kerosene (cm^3)	Stirrer rpm (min^{-1})
1	542	1084	680
2	516	516	680
3	295	885	680
4	539	1078	780
5	297	891	780
6	492	492	308
7	300	900	308
8	310	930	402
9	517	1034	402
10	498	498	402
11	500	1000	503
12	502	502	503
13	375	1125	503
14	502	502	150
15	498	1000	150
16	400	1200	150

*Bitumen concentrate contained 64 wt% bitumen.
All the experiments were performed at a temperature of 327±4 K.

Prior to the dissolution tests the bitumen concentrate and the solvent were heated to the desired temperature. When the preparatory activities were complete, the required volume of kerosene was poured into the stirred tank on top of the bitumen concentrate, and the stirrer was turned on. After 1, 2, 5, 10, 20,

30 and 60 minutes, 2 mL samples were withdrawn with a pipette (1 cm below the liquid surface) to be analysed for bitumen content.

The bitumen concentrate used in the dissolution tests originated from water-based bitumen recovery experiments described previously.[87,88] The oil sand was sampled from two locations at the Whiterocks deposit (Uintah Basin, Utah; containing 7.6 wt% bitumen content). In each experiment 20 kg oil sand in a 75 wt% slurry was used. Before digestion at 328 K, a total amount of 15 wt% kerosene with respect to bitumen was added to the oil sand. Six subsequent hot water batch experiments yielded 25 kg of bitumen concentrates from the gravity cell. Free water was allowed to percolate on a filter paper for 3 days, and after that the concentrates were mixed together and stored in a tight container prior to the dissolution experiments. The Dean-Stark analysis of the combined concentrates showed 64 wt% bitumen, 2.4±0.4 wt% solids, and 34±1 wt% water. The composition did not change within the analytical error through the entire storage time, as the concentrate did not stratify. The average diameter of the emulsified water droplets was about 5 μm, while most of the fine mineral particles were below 3 μm, as revealed by optical microscopy. The bitumen concentrate originally contained more than 30 vol% of entrapped gas (air) bubbles; however, that content dropped gradually to less than 10 vol% when the bitumen was used in the dissolution experiments. Dissolved bitumen withdrawn periodically during the dissolution tests was centrifuged, dilluted with toluene (1:1000), and analyses in the Klett-Summerson photoelectric colorimeter, Model 900-3,

equipped with 520-580 nm transmission filter. The analytical error (±10%) resulted mainly from a high dilution ratio.

DIMENSIONAL ANALYSIS

In the case of isothermal dissolution of bitumen in a stirred-tank reactor, the mass of bitumen transferred to a solvent like kerosene can be expressed through the following functional relationship:

$$M_d^b = f(M_I^b,\ t,\ N,\ \mu_b,\ D_b,\ \rho_b,\ \rho_d,\ M_d) \qquad (19)$$

where:

a	Unknown exponent
b	Unknown exponent
c	Unknown exponent
D	Tank diameter
D_b	Diffusivity of bitumen
d	Impeller diameter
f	Function
M	Fundamental quantity of mass
M_d^b	Mass of bitumen in diluent
M_d	Mass of diluent added
N	rpm
t	Time
μ_b	Viscosity of bitumen
ρ_b	Density of bitumen
ρ_d	Density of diluent

Subscripts

b Bitumen phase

d Diluent phase

I Initial value

The important dimensionless groups affecting the process can be determined by applying Buckingham's Pi theorem, as described by Geiger and Poirier[124] in their well-known text on transport phenomena. The major steps involved in the analysis are as follows:

i) The first step constitutes a dimensional representation of all the parameters in terms of the fundamental quantities of time (θ), mass (M) and length (L), so that we obtain:

$$M_I^b \equiv M \equiv M_d \tag{20}$$

$$t \equiv \theta \tag{21}$$

$$N \equiv \theta^{-1} \tag{22}$$

$$\mu_b \equiv ML^{-1}\theta^{-1} \tag{23}$$

$$D_b \equiv L^2\theta^{-1} \tag{24}$$

$$\rho_b \equiv ML^{-3} \equiv \rho_d \tag{25}$$

where:

M_I^b Initial mass of bitumen

L Fundamental quantity of length

θ Fundamental quantity of time

ii) Next, since we have three fundamental units in the present problem, we need to specify three primary quantities which in this analysis are conveniently taken as M_I^b, t, ρ_b. This leaves behind the quantities M_d^b, μ_b, D_b, ρ_d, N, and M_d, so that

a maximum of six dimensionless groups can be determined for the process. We seek to determine the pi groups as described in the following step.

iii) We define the first pi group as:

$$\pi_1 = \frac{M_d^b}{(M_I^b)^a (t)^b (\rho_b)^c} \tag{26}$$

which, in terms of the fundamental units, can be stated as:

$$\pi_1 = \frac{M}{M^a \theta^b (ML^{-3})^c} \tag{27}$$

In order to keep the group dimensionless, we can equate the exponents of various fundamental quantities in the numerator and the denominator, so that, from the exponents of M:

$$a + c = 1 \tag{28}$$

from the exponents of L:

$$-3c = 0 \tag{29}$$

and from the exponents of θ:

$$b = 0 \tag{30}$$

Solving eqs. (26-28) we obtain the unknown exponents as

$$a = 1 \tag{31}$$

$$b = 0 \tag{32}$$

$$c = 0 \tag{33}$$

and hence the first pi group is formed as

$$\pi_1 = \frac{M_d^b}{M_I^b} \tag{34}$$

which essentially denotes the fraction of bitumen dissolved in the diluent.

iv) Proceeding in an analogous manner, the remaining pi groups are obtained as:

$$\pi_2 = \frac{\mu_b\, t}{(M_I^b)^{2/3}\, \rho_b^{1/3}} \tag{35}$$

$$\pi_3 = \frac{D_b\, t\, \rho_b^{2/3}}{(M_I^b)^{2/3}} \tag{36}$$

$$\pi_4 = \frac{\rho_d}{\rho_b} \tag{37}$$

$$\pi_5 = Nt \tag{38}$$

and

$$\pi_6 = \frac{M_d}{M_I^b} \tag{39}$$

v) The experimental data, therefore, can be expressed as:

$$\pi_1 = f[\pi_2, \pi_3, \pi_4, \pi_5\, \pi_6] \tag{40}$$

where π_1 through π_6 are dimensionless pi groups which for a constant density ratio between the bitumen and the diluent reduce to

$$\pi_1 = f[\pi_2, \pi_3, \pi_5, \pi_6] \tag{41}$$

Analysis of the experimental data was performed in terms of the pi groups included in equation 41, as detailed in the following section.

RESULTS AND DISCUSSION

It should be pointed out that the dimensionless groups presented in equation 41 are by no means unique. Changing the so-called "primary quantities", one can arrive at perhaps several other sets of dimensionless groups, each representing the process in its own way. Similarly, a number of other external variables like impeller diameter or tank diameter could be included in the analysis, resulting in a few additional pi groups. Bird et al.,[125] for example, presented the classical problem of prediction of vortex depth in an agitated tank where Reynolds Number (Re) and Froude Number (Fr), defined using the impeller diameter as the characteristic length, were used for establishing dynamic similarity between a small and a large tank. Since the present study was not conducted for any such scaleup, impeller diameter, tank diameter, etc., variables, and the groups like Re and Fr were not used.

Using the experimental data obtained in this study, the values for the various pi groups were obtained. The physical parameters used in the calculation are listed in Table 21. Among the dimensionless groups obtained in this analysis, the first pi group actually determines the fraction of bitumen dissolved in the diluent, and, therefore, for an efficient process design one needs to determine the conditions leading to a high value of π_1. One of

the major objectives of the present analysis is to identify how the other pi groups influence the magnitude of the pi group one.

Table 21

PHYSICAL PARAMETERS

Average viscosity of the feed	1.4 Pa·s
Density of bitumen concentrate	1010 kg/m^3
Density of kerosene	800 kg/m^3
Diffusivity of bitumen	10^{-9} m^2/sec

Since for the present set of experiments the fourth pi group is effectively a constant, it can be excluded from the analysis as mentioned earlier. Among the remaining dimensionless quantities, the second and third pi groups, by definition, are directly proportional to each other, at all points in time, and that proportionality has been satisfied in virtually all the experimental conditions. Consequently, conditions leading to the optimum value of the first pi group, in all practical purposes, need to be specified in terms of either the second or the third group, and no meaningful correlation should attempt to include both of them. Alteration of the values of the second and third pi groups significantly affects the values of pi group one, and hence the extent of bitumen dissolution, as shown in Figures 42 and 43. A similar response is also obtained with pi group five, as shown in Figure 44.

The data scatter shown in Figures 42-44 is rather expected, because of the fact that the values of the remaining pi groups were not held constant for the points plotted in these diagrams. These

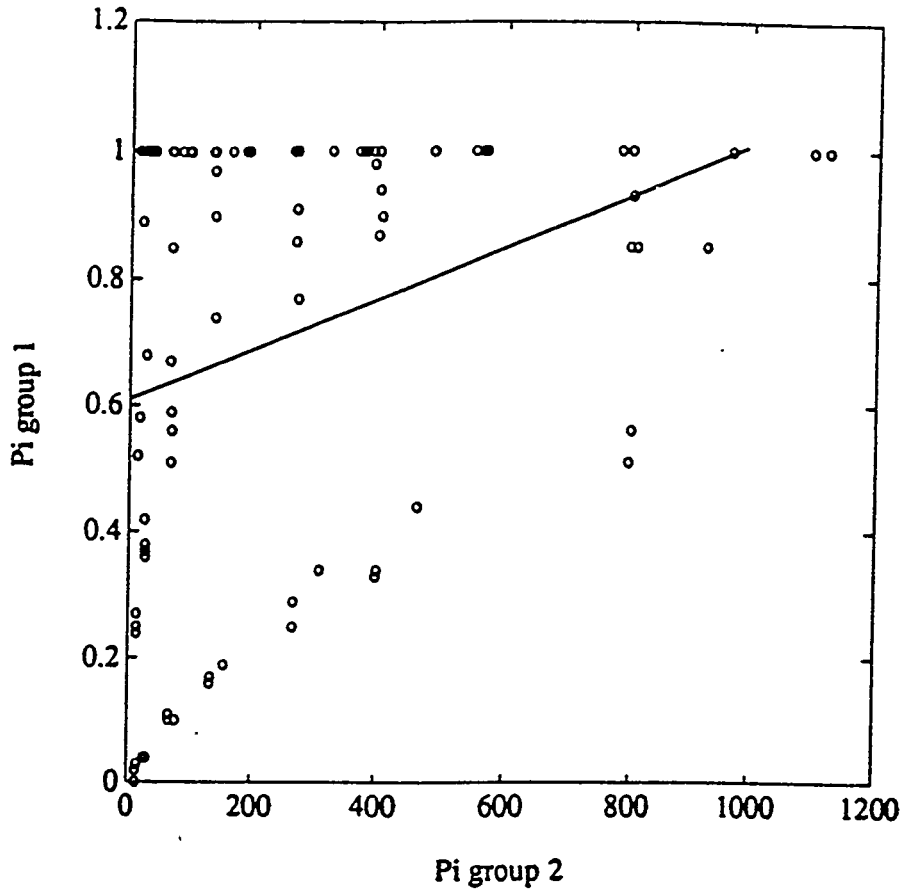

Figure 42. Influence of the Second pi Group on pi Group 1

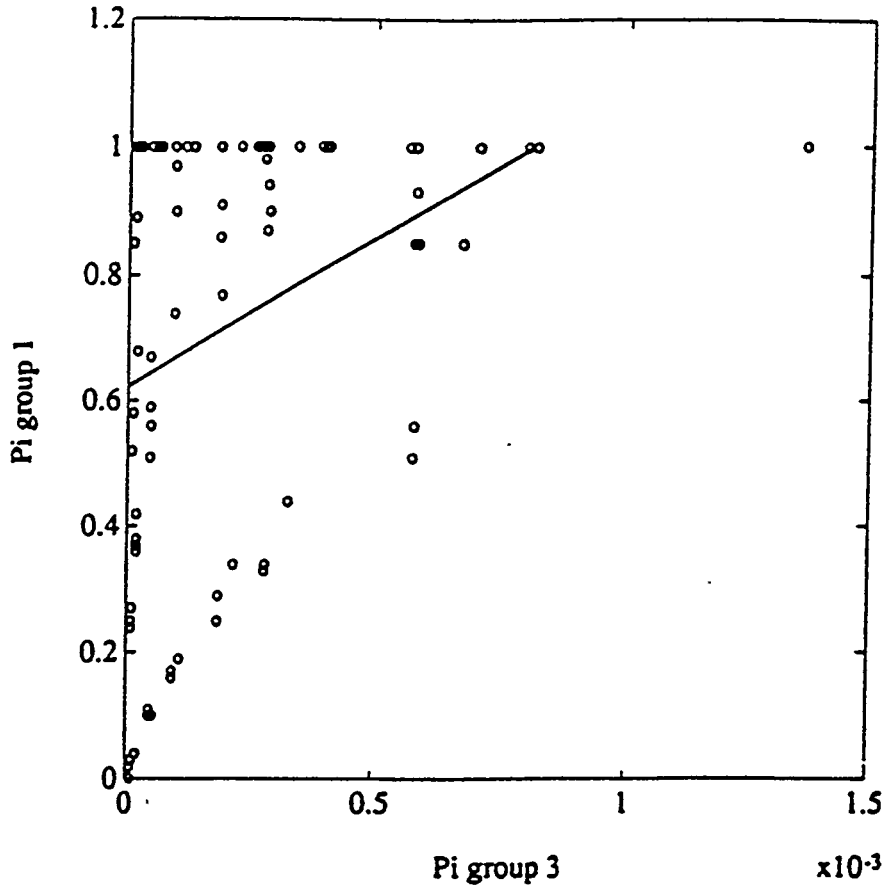

Figure 43. Influence of the Third pi Group on pi Group 1

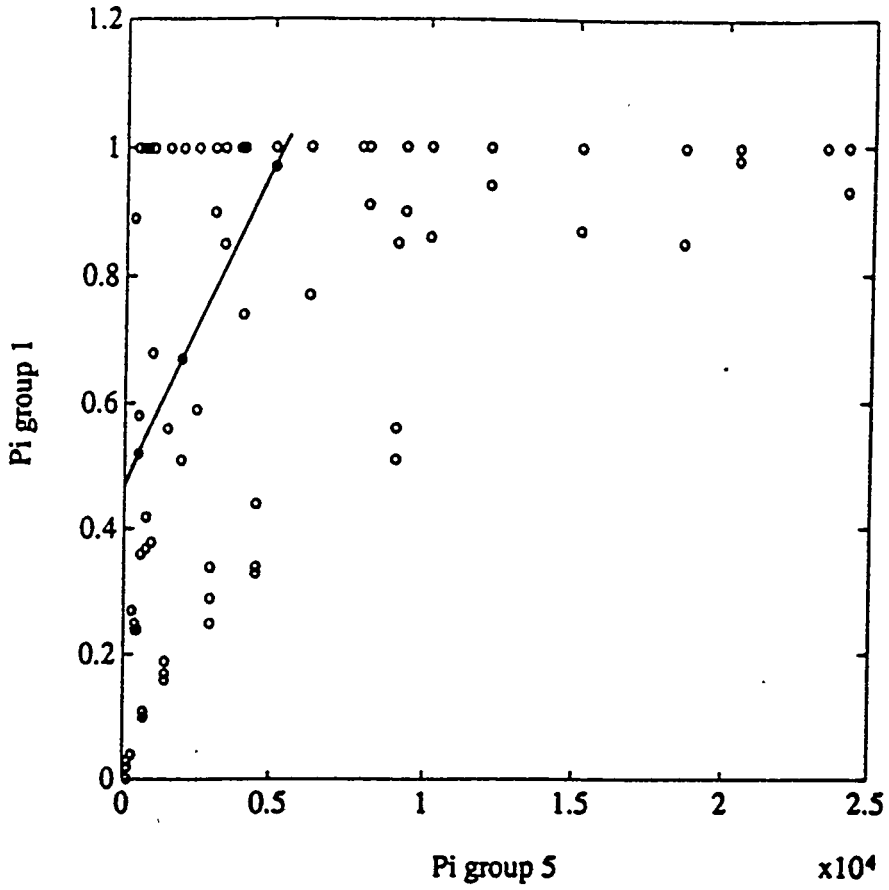

Figure 44. Influence of the Fifth pi Group on pi Group 1

diagrams, however, demonstrate satisfactorily that the second, third and fifth pi groups indeed influence the dissolution process, and the fitted solid lines shown in these plots indicate the approximate nature of that influence. Based upon a similar type of argument, we conclude that the sixth pi group has no significant effect on the dissolution process within the applied range of bitumen-solvent ratio, since virtually any possible value of the first pi group was obtained at all the values of the sixth group used in these experiments, as evidenced by Figure 45.

An obvious extension of the above arguments is that, based upon the present findings, the oil sand dissolution data can be correlated either in terms of pi groups 1, 3 and 5 or in terms of pi groups 1, 2 and 5, and the remaining groups need not be included in the analysis. This allows us to construct the oil sand dissolution maps presented in Figures 46 and 47, which can potentially be used for an efficient experiment design.

The major features of the oil sand dissolution maps can be summarized as follows. Each diagram consists of a series of Π_1 isopleths, the least square representation of the constant values of this group, shown as solid lines. These isopleths divide the diagram into a number of regions, marked as A, B and C in the present case. If the experimental conditions are adjusted in the region A, a low value of bitumen dissolution (less than 25%) will result. If the experiments are conducted in region B, the recovery may be higher than 25%, but it cannot exceed 50%, and in a similar fashion, in region C, bitumen dissolution can become higher than

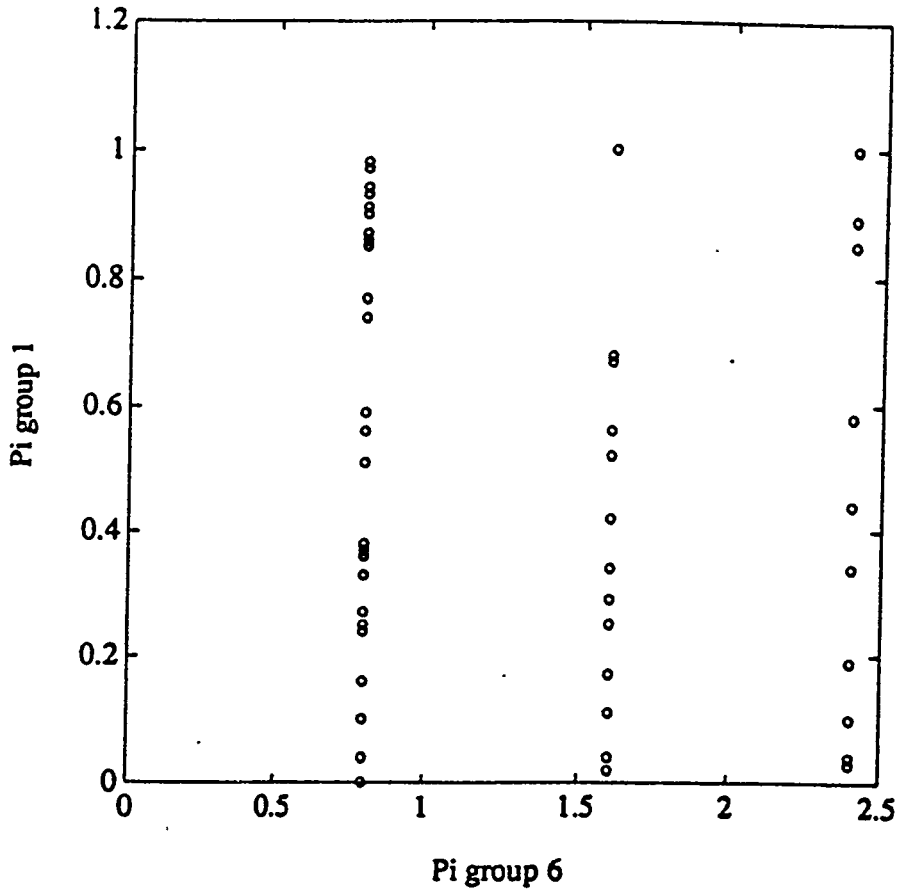

Figure 45. Influence of the Sixth pi Group on pi Group 1

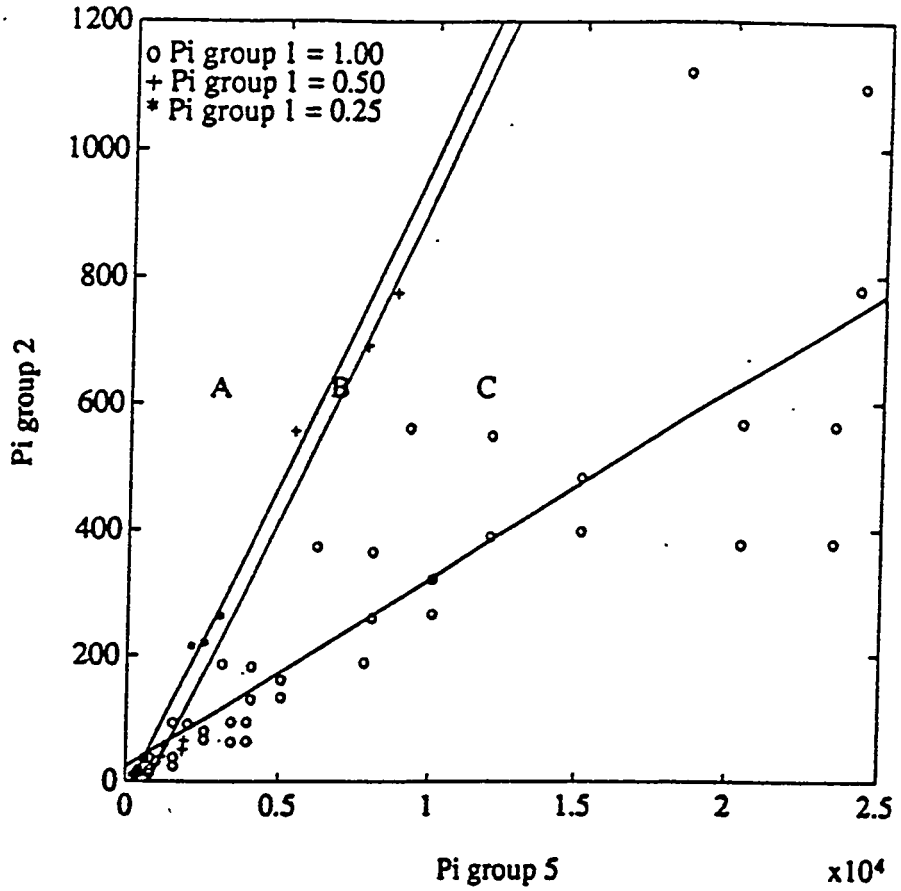

Figure 46. Oil Sand Dissolution Map Based upon pi Groups 2 and 5

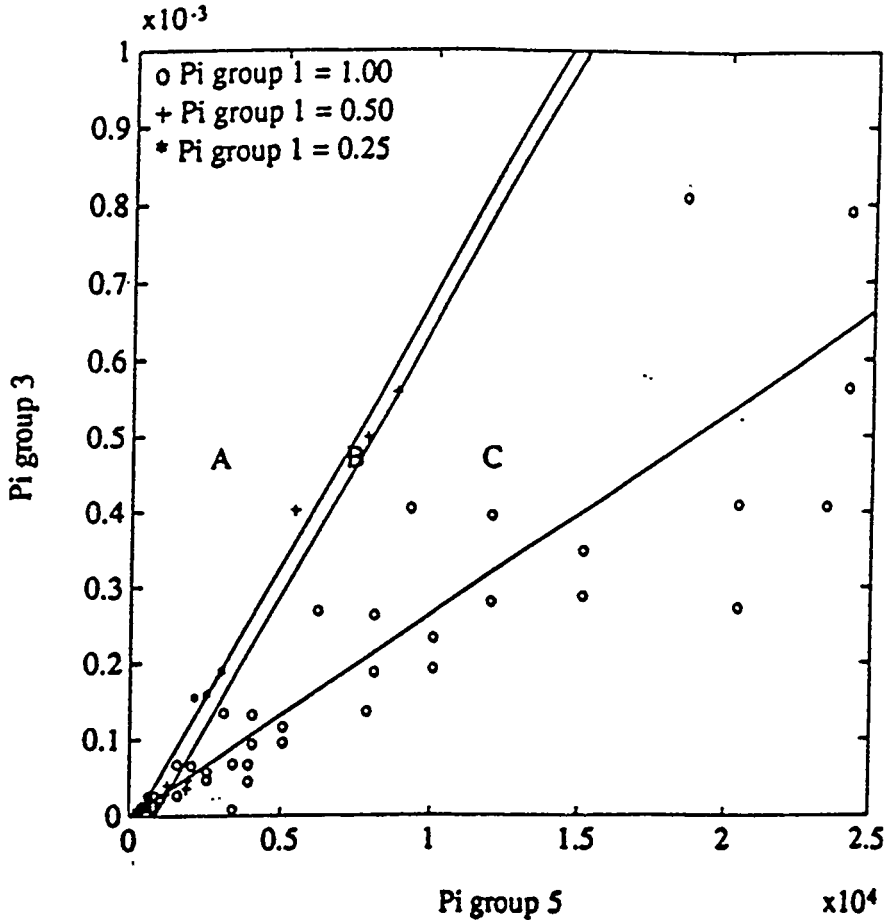

Figure 47. Oil Sand Dissolution Map Based upon pi Groups 3 and 5

50%. Almost complete dissolution will result if the experimental conditions are adjusted near the right-hand boundary of this region; furthermore, operating beyond region C will only constitute a waste of resources (e.g., extra energy consumption associated with the higher stirring speed), as it cannot possibly improve the extent of dissolution.

SUMMARY AND CONCLUSIONS

The Whiterocks oil sand bitumen concentrate, originating from the hot-water separation experiments, was dissolved in kerosene in order to remove dispersed water and fine mineral particles. It was observed that dissolution of bitumen in kerosene can be rendered rapidly with a judicious use of the dissolution maps presented in this work. During this study a quick, nearly complete dissolution of the bitumen concentrate was obtained in 80% of the experiments, so that the right-hand boundary of region C may, in fact, represent a physical reality.

FUTURE ACTIVITIES

The bitumen concentrate cleanup method and its efficiency is critical with respect to the size of the equipment, and determines further processing strategy. Residual water left in the bitumen may cause foaming during diluent and lightends distillation, while fine solids (mostly clay particles) may influence the process of bitumen upgrade or the treatment aimed at obtaining modified asphaltic binders. In this regard, our efforts to minimize water and solids content in the final product will be continued.

WATER-BASED SEPARATION PROCESS DESIGN AND DEVELOPMENT FOR UTAH OIL SANDS

Principal Investigator:	J.D. Miller
Co-Principal Investigator:	F.V. Hanson
Res. Assoc. Professor:	J. Hupka
Research Associate	R. White
Graduate Students:	G.Gopalakrishnan
	Y.Yang

INTRODUCTION

Over the past two decades, University of Utah researchers have developed both water-based separation process and several thermal processing approaches for recovering bitumen from the vast oil sand deposits in Utah. The energy-efficient, moderate temperature water-based process developed in the research group headed by Dr. J.D.Miller, Professor of Metallurgical Engineering - is ready for testing and further development at the pilot plant level. Although similar to the hot water process successfully applied in two large commercial plants in Alberta, Canada, the University of Utah technique has been worked-out for high viscosity bitumen and "oil wet" type bitumen-sand interactions which are common in Utah oil sands. Several U.S. patents for the new process were granted. The contribution to the advancement of oil sand processing was also recognized by the SME Taggart Award. Until now, however, water-based processing was mainly considered for surface-mined material. However, recent results indicate that underground processing can provide high quality bitumen concentrate if an appropriate rubbelizing technique is adopted.

Another contribution to process design and development was associated with a scaleup research of the hot water process for the Whiterocks oil sand. Beside DOE financial support, this research was supported in a significant degree by private funds, and was directed by Dr. Francis V. Hanson, Professor of Fuels Engineering. As a consequence, process flowsheets were developed and preliminary mass and energy balances for various plant sizes were prepared.

PROCESS STEPS AND PROCESSING STRATEGY

A flowsheet of the hot water separation process for a 100 to 2000 tpd oil sand pilot plant is shown in Figure 48. Four basic technological circuits can be distinguished in the schematic:

- feed preparation, involving size reduction and pretreatment with diluent,
- bitumen separation from sand, achieved by digestion, gravity separation, and flotation,
- tailings disposal and water recycle, and
- bitumen concentrate cleanup and solvent recycle.

In the first step, the oil sand is crushed to minus 3/4", if necessary, followed by diluent (kerosene or naphtha) treatment for an appropriate period of time to ensure complete penetration of the bitumen by the diluent. In this case, the diluent must be added to reduce the bitumen viscosity to below 1.5 Pa•s (15 Poise) at the temperature of digestion. The amount of diluent required to lower the digestion-separation temperature to 323-328 K for most U.S. oil sands is from 10 to 35 wt% with respect to the bitumen content and can be predicted from the bitumen viscosity curves.

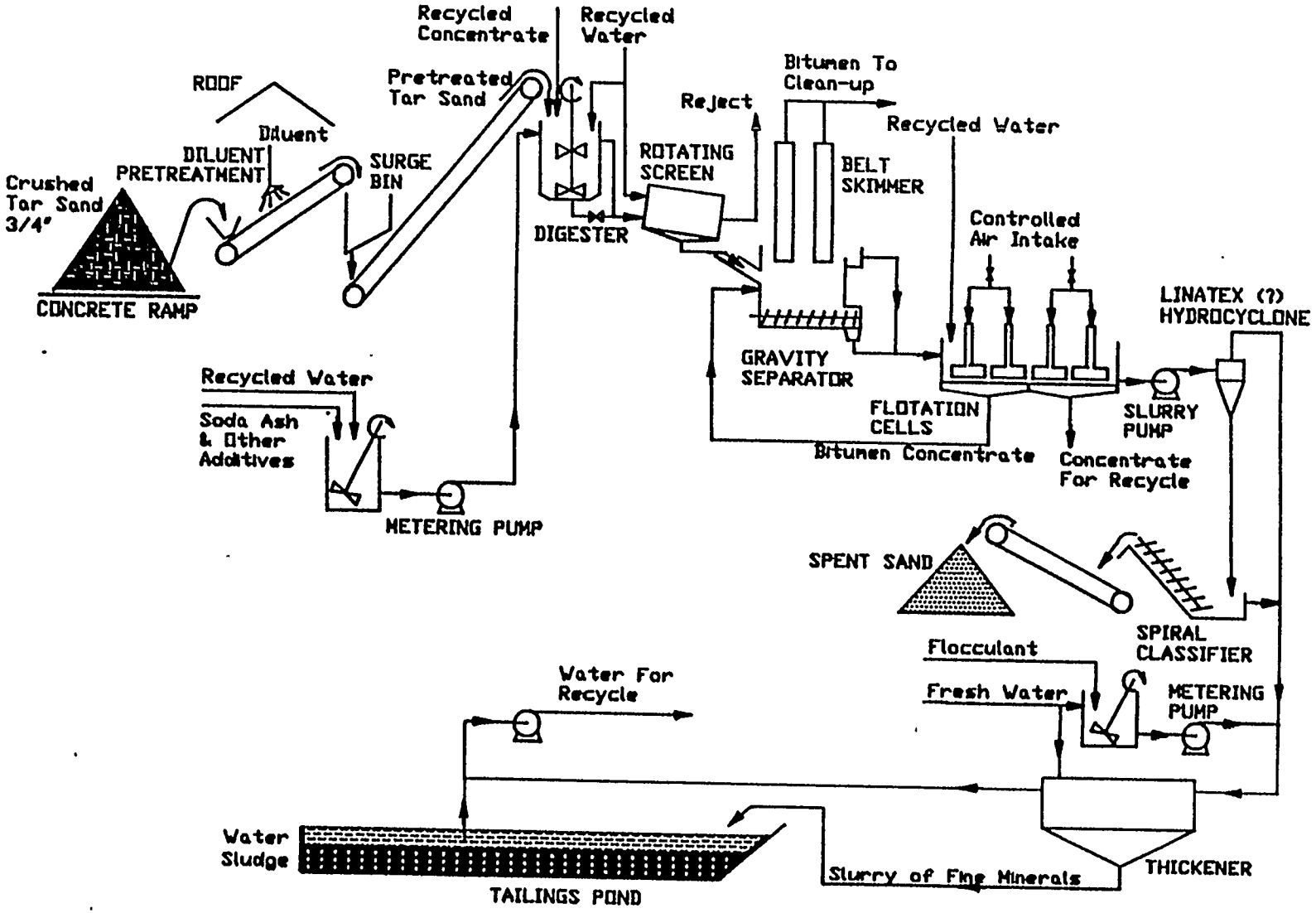

Figure 48. Pilot Plant Flow Chart for Bitumen Recovery from Utah Oil Sands

In the second step the diluent treated oil sand is subjected to digestion in an alkaline solution to displace bitumen from the surface of mineral matter (~ 90% quartz). Negative charges at the bitumen droplet and sand particle interfaces facilitate disengagement during digestion. The exceptional role of sodium tripolyphosphate has been shown to be advantageous in promoting bitumen displacement from the sand particles and the creation of sand-free bitumen droplets in the digested slurry. Tripolyphosphate acts also as complexing agent for multivalent cations, particularly calcium, and controls their concentration in the aqueous phase. Another characteristic impact of the addition of sodium tripolyphosphate is the enhanced bitumen filming of air bubbles. Air bubble filming has been recognized as being beneficial for subsequent separation and recovery steps.

For water-based separation processes large quantities of oil sand slurry have to be handled, therefore, bitumen gravity separation after digestion is most desired from technical point of view. Unlike Athabasca oil sand processing, gravity separation of bitumen from U.S. oil sand deposits may not be effective even after diluent pretreatment. However, when tripolyphosphate is used, gravity separation for partial bitumen recovery can be accomplished successfully. A fluorescence microscopic examination of digested oil sand slurry (containing 75 wt.% solids, as typically obtained during water-based separation process) revealed that bitumen droplets exist with a broad size distribution from a few microns to 1 mm in size. The large bitumen droplets can be rapidly separated

in a gravity cell when sodium tripolyphosphate was used. Fine bitumen droplets and bitumen-sand aggregates require flotation for fast and complete recovery. Flotation of bitumen (20 wt.% solids) produces a concentrate containing about 55 wt.% (dry basis) bitumen in the first minute, and subsequently, lower grade concentrate products as the flotation continues. These results can be described in terms of the electrophoretic mobility of suspended particles and droplets both of which exhibit negative surface charges. After gravity separation only small bitumen droplets (<0.3 mm) remain in suspension. When compared to gravity separation the flotation of negatively charged mineral particles competes with the flotation of negatively charged bitumen droplets resulting in an inferior bitumen concentrate quality. Flotation kinetics indicate a first order rate equation with respect to bitumen recovery.

The tailings sand is subjected to size separation in a spiral classifier from which coarse sand is stockpiled, and the turbid tailings water is pumped to a thickener. The use of sodium tripolyphosphate does not impede sedimentation of fines, yielding almost the same volume of clarified supernatant compared to the experiments in which sodium tripolyphosphate was not used. In fact the content of suspended matter in the supernatant was clearly lower in the case when polyphosphates were used, both for fresh water and recycled water experiments. Sodium tripolyphosphate hydrolysis to orthophosphate, which acts as a mild flocculating agent, certainly contributes to the favorable sedimentation characteristics. It was also observed that the recycle of process

water containing 4 to 5 wt.% suspended matter had no deleterious effect on the process separation efficiency, which indicates that the sedimentation time of the tailings in the thickener can be significantly reduced.

The combined bitumen concentrate, i.e., from the gravity cell and from flotation, contains 20 to 60 wt.% dispersed water and fine minerals. Up to 40% of the fine mineral particles pass a 38 μm (400 mesh) screen. Larger sand grains, most of which have undigested or residual bitumen on the surface, report to the concentrate during flotation. Cleaning of the bitumen concentrate can be accomplished by dilution and subsequent sedimentation by gravity and centrifugation (bitumen-diluent ratio was 1:2). Stable water-in-oil emulsions have been encountered in our concentrate cleaning experiments, even when microscopic investigation revealed almost a lack of mineral particles at the water-oil interface. In this case, surface active asphaltenes are responsible for the emulsion stability. Sedimentation tests have shown that in order to reduce water and solids content below 5 wt.% in a reasonable period of time, centrifugation or other separation techniques will have to be used.

Comments on Oil Sand Pretreatment with Diluent

The beneficial impact of the oil sand pretreatment step involving diluent spraying on the oil sand feed prior to digestion has to be emphasized. The bitumen from almost all U.S. deposits is more viscous than from the Athabasca oil sands. The dissolution of the bitumen concentrate from the U.S. oil sands in an organic

solvent, necessary for the cleanup operation, may require much higher temperature than the Athabasca bitumen. In fact, because of the high bitumen viscosity, our cleanup experiments (see preceding section of the report) could not be carried out at moderate temperature if solvent-pretreated oil sand was not used in the hot water separation process. From the bitumen concentrate cleanup point of view, the more diluted the bitumen is the more favorable dissolution kinetics in the solvent can be expected. Assuming that the diluent loss in the process is not dependent on the degree of bitumen dilution within the oil sand, two other important factors limit the amount of diluent used in the pretreatment step:

- extensive bitumen emulsification (and/or formation of multiphase emulsions) during digestion due to reduced cohesion energy of the diluted bitumen, resulting in inferior separation characteristics by gravity and flotation. The lower range of bitumen viscosity amounts to 500 mPa·s and less,
- gradual caesurae of the importance of bitumen viscosity in the mixing process with diluent with the shift to the hydrodynamic effects. In this regard, the critical bitumen viscosity needs to be determined.

MASS BALANCE AND ENERGY BALANCE

The expected steady-state mass balance for 2000 tons per day Whiterocks oil sand pilot plant is presented in Table 22, while simplified energy balance is given in Table 23. Both balances were

Table 22. Steady State Mass Balance for 2000 Tons Per Day of Whiterocks Oil Sand Pilot Plant

Assumptions	Process Stream
Feed composition is: 7% bitumen, 92.5% sand and 0.5% water.	1
Bitumen density = 8.34 lbs/gallon. (1 g/cc)	
Diluent density = 7.09 lbs/gallon. (0.85 g/cc)	
Diluent dosage:	
15% by weight of bitumen in dilution pretreatment;	1
200% by volume of bitumen in dilution for bitumen concentrate cleanup	21
Sodium carbonate addition = 1 g/1 kg of tar sand.	47
Sodium phosphate addition = 0.5 g/1 kg of tar sand.	48
Diluent follows bitumen.	
Salts follow water.	
Bitumen product contains up to 3% sand and 0.1% water.	30
Bitumen recovery is about 90%.	30
Coarse sand tailings contain 1% bitumen, 84% sand and 15% water.	42
Fine sand tailings contain 60% sand and 40% water.	39
The ratio of the amount of bitumen in stream from gravity separation to dilution and in stream from froth flotation to dilution is 2:1.	17,19
Composition of the stream from gravity separation to dilution is: 40% bitumen, 20% sand and 40% water.	17
Composition of the stream from froth flotation to dilution is: 25% bitumen, 35% sand and 40% water.	19

Table 22. Steady State Mass Balance for 2000 Tons Per Day of Whiterocks Oil Sand Pilot Plant (continued)

Assumptions	Process Stream
Composition of the stream recycled from froth flotation to digestion is: 10% bitumen, 50% sand and 40% water.	8
Solids concentration during digestion is 75% by weight. Bitumen is considered as solids at this stage. Bitumen becomes liquid after digestion stage.	(9)
Solids (sand) concentration during gravity separation is 40%. Solids concentration during froth flotation is 20%.	
Final cleanup and storage are bypassed.	
Sludge from the thickener is directed to slime dewatering and not to the tailings pond.	35
Mass flowrates in the following streams are neglected:	
Pebbles disposal from screening after digestion.	11
Skimmed bitumen from thickener and tailings ponds.	14,37,41
Sands from gravity separation to sand dewatering. (i.e., Oil sand undergoes flotation).	16
Demulsifier addition into sedimentation.	23
Flocculants addition into thickener.	33
Water flow from tailings pond. This might compensate water loss due to evaporation. Water from the tailings pond would be pumped into a recycled water tank periodically and reused.	45

Table 22. Steady State Mass Balance (lbs/hour) for 2000 Tons Per Day Whiterocks Oil Sand Pilot Plant (continued)

	PROCESS STREAM							
No.	FROM	TO	TOTAL	BITUMEN	SAND	WATER	DILUENT	SALT
1	Input	Diluent Pretreatment	166666.7	11666.7	154166.7	833.3	0.0	0.0
2	Recycled Diluent	Diluent Pretreatment	1750.0	0.0	0.0	0.0	1750.0	0.0
3	Diluent Pretreatment	Digestion	168416.7	11666.7	154166.7	833.3	1750.0	0.0
4	Wetting Soln. Prep.	Digestion	870.6	0.0	0.0	621.9	0.0	248.7
5	Recycled Water	Digestion	40254.9	0.0	544.6	39573.3	0.0	136.9
7	Recycled Sludge	Digestion	24921.3	1108.3	8131.4	13405.8	2229.4	46.4
8	Froth Flotation	Digestion	12681.4	1108.3	5049.1	6157.4	345.2	21.3
9	Digestion	Screening	247144.9	13883.3	167891.8	60591.7	4324.7	453.3
10	Recycled Water	Screening	118836.2	0.0	1607.8	116824.2	0.0	404.1
11	Pebbles	Disposal	0.0	0.0	0.0	0.0	0.0	0.0
12	Screening	Gravity Separation	365981.0	13883.3	169499.6	177415.9	4324.7	857.5
13	Makeup Water	Gravity Separation	70451.7	0.0	0.0	70451.7	0.0	0.0
14	Skimmed Bitumen	Gravity Separation	0.0	0.0	0.0	0.0	0.0	0.0
15	Gravity Separation	Froth Flotation	411801.8	5133.3	165124.6	239117.6	1599.0	827.2

Table 22. Steady State Mass Balance (lbs/hour) for 2000 Tons Per Day Whiterocks Oil Sand Pilot Plant (continued)

	PROCESS STREAM							
No.	FROM	TO	TOTAL	BITUMEN	SAND	WATER	DILUENT	SALT
16	Gravity Separation	Sand Dewatering	0.0	0.0	0.0	0.0	0.0	0.0
17	Gravity Separation	Dilution	24630.9	8750.0	4375.0	8750.0	2725.6	30.3
18	Recycled Water	Froth Flotation	453609.4	0.0	6137.2	445929.6	0.0	1542.6
19	Froth Flotation	Dilution	12591.4	2916.7	4083.3	4666.7	908.5	16.1
20	Froth Flotation	Sand Size Separation	840138.5	1108.3	162129.4	674223.1	345.2	2332.4
21	Diluent Storage	Dilution	19833.3	0.0	0.0	0.0	19833.3	0.0
22	Dilution	Sedimentation	57055.6	11666.7	8458.3	13416.7	23467.5	46.4
23	Demulsifier	Sedimentation	0.0	0.0	0.0	0.0	0.0	0.0
24	Sedimentation	Final Clean-Up,Storage	32134.2	10558.3	326.9	10.9	21238.1	0.0
25	Recycled Sludge	Digestion	24921.3	1108.3	8131.4	13405.8	2229.4	46.4
26	Sedimentation	Distillation	32134.2	10558.3	326.9	10.9	21238.1	0.0
27	Recycled Sludge	Digestion	0.0	0.0	0.0	0.0	0.0	0.0
28	Distillation	Bitumen Storage	10948.9	10558.3	326.9	10.9	52.8	0.0

Table 22. Steady State Mass Balance (lbs/hour) for 2000 Tons Per Day Whiterocks Oil Sand Pilot Plant (continued)

	PROCESS STREAM							
No.	FROM	TO	TOTAL	BITUMEN	SAND	WATER	DILUENT	SALT
29	Recycled Diluent	Heat Exchange	21185.3	0.0	0.0	0.0	21185.3	0.0
29	Recycled Diluent	Diluent Storage	21185.3	0.0	0.0	0.0	21185.3	0.0
30	Bitumen Storage	Output	10948.9	10558.3	326.9	10.9	52.8	0.0
31	Sand Size Separation	Thickener	698535.4	0.0	59719.4	636613.7	0.0	2202.3
32	Sand Size Separation	Sand Dewatering	141603.1	1108.3	102410.0	37609.4	345.2	130.1
33	Flocculants	Thickener	0.0	0.0	0.0	0.0	0.0	0.0
34	Sand Dewatering	Thickener	15538.1	0.0	9310.0	6206.7	0.0	21.5
35	Thickener	Slime Dewatering	256650.5	0.0	65382.5	190608.6	0.0	659.4
	Thickener	Tailings Pond	0.0	0.0	0.0	0.0	0.0	0.0
36	Thickener	Water Recycling	457423.0	0.0	3646.9	452211.8	0.0	1564.4
37	Skimmed Bitumen	Gravity Separation	0.0	0.0	0.0	0.0	0.0	0.0
38	Slime Dewatering	Water Recycling	15277.4	0.0	4642.7	150115.4	0.0	519.3
39	Slime Dewatering	Fine Sand Disposal	101373.1	0.0	60739.8	40493.2	0.0	140.1
40	Sand Dewatering	Storage-Stock Pile	126065.0	1108.3	93100.0	31402.8	345.2	108.6

Table 22. Steady State Mass Balance (lbs/hour) for 2000 Tons Per Day Whiterocks Oil Sand Pilot Plant (continued)

	PROCESS STREAM							
No.	FROM	TO	TOTAL	BITUMEN	SAND	WATER	DILUENT	SALT
41	Run-off Water	Tailings Pond	14828.9	0.0	0.0	14777.8	0.0	51.1
42	Storage-Stock Pile	Coarse SAnd Disposal	111236.1	1108.3	93100.0	16625.0	345.2	57.5
43	Misc. Discharges	(For Contingency)						
44	Skimmed Bitumen	Gravity Separation	0.0	0.0	0.0	0.0	0.0	0.0
45	Tailings Pond	Water Recycling	0.0	0.0	0.0	0.0	0.0	0.0
46	Make-up Water	Wetting Soln. Prep.	621.9	0.0	0.0	621.9	0.0	0.0
47	Sodium Carbonate	Wetting Soln. Prep.	165.8	0.0	0.0	0.0	0.0	165.8
48	Sodium Phosphate	Wetting Soln. Prep.	82.9	0.0	0.0	0.0	0.0	82.9
49	Makeup Diluent	Diluent Storage	398.0	0.0	0.0	0.0	398.0	0.0

Table 23. Steady State Energy Balance (Heat Units/Hour) for 2000 Tons Per Day Whiterocks Oil Sand Pilot Plant

Ambient Temperature (Degree Centigrade): 20

	Kcal	BTU
Digestion:		
Heat Reqd. for Feed:	681000	2702426
Heat Reqd. for Wetting Soln:	15811	62741
Total Heat Requirement	696811	2765167
Heat from Recycled Water:	180779	717389
Heat input from Steam:	516032	2047778
Heat from Recyc. Water into Screening:	533677	2117799
Heat from Makeup Water to Gravity Sep.	959552	3807808
Heat from Recycled Water to Flotation	2037097	8083851
Heat Loss during Sand Size Separation	1611038	6393113
Recycled Water Heat Requirement:	8254656	32757118
Heat Loss in Coarse Sand Tailing:	936689	3717082
Total Heat Losses:	6258830	24837041
(Dilution Heat Losses - From Gravity)	105078	416982
(Dilution Heat Losses - From Flotation)	117778	467381
	6481686	25721404
Dilution Heat Requirement:	209654	831973
From Gravity Sepn.	100953	400612
From Froth Flotation	310606	1232585
Heat Input From Diluent Storage		
Heat Requirement for Distillation	1624002	6444560

prepared based on the block diagram depicted in Figure 49. The block diagram was already incorporated in our 1990-91 annual oil sand report and served as the foundation for the flow diagram presented in Figure 48. Each stream in Figure 49 is specified in Table 22, and its composition is given with respect to bitumen, sand, water, diluent and inorganic salts. A short, nevertheless detailed, description of the process is provided below. All the assumptions, some of them accepted arbitrary because of lack of data from large scale tests, follow Table 22.

Oil sand, which undergoes size reduction (stream number (1) in the diagram, Figure 49) is conditioned with diluent (2) and fed (3) into the digester together with: steam (6), recycled water (5), wetting solution (4) [which was prepared from fresh water (46), sodium carbonate (47), and sodium tripolyphosphate (48)], recycled sludge (25 and 27) combined into stream (7), and recycled low-grade bitumen concentrate (8). Digested slurry (9) is diluted with recycled water (10), screened to -1/4" (11), and transferred (12) to the gravity cell, yielding three products: bitumen concentrate (17), slurry and/or middlings (15), and coarse sand (16). The slurry/middlings stream (15) undergoes flotation. The bitumen-rich concentrate (19) is directed to cleanup, while the low-grade concentrate (8) is recycled for digestion.

The tailings sand (20) is subjected to size separation in a spiral classifier from which coarse sand (40) is stockpiled, and the turbid tailings water (31) is pumped to a thickener. An

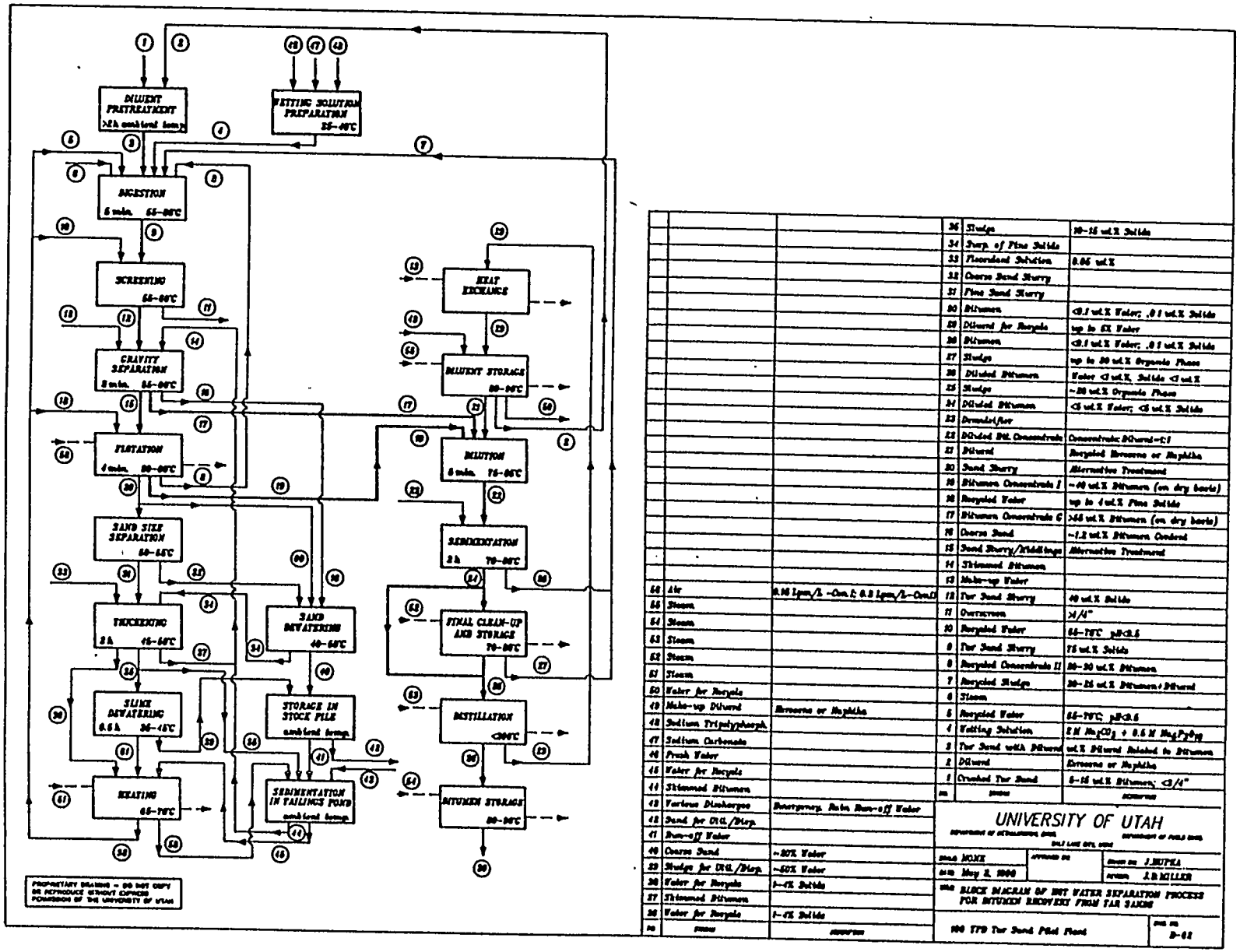

Figure 49. Block Diagram of Hot Water Separation Process for Bitumen Recovery from Oil Sands

alternative to this treatment is direct size separation of the coarse sand (16) from the gravity cell in the spiral classifier, recycle of the aqueous phase with suspended matter (32) into the flotation cell and bypassing the size separation after flotation (34). The supernatant from the thickener (36) is heated and recycled (38). Makeup water (13), serving also as a cooling medium during diluent removal from bitumen, is added to the recycled water prior to heating. Periodically, sediment (58) has to be pumped from recycled water tank to a tailings pond. The runoff water (41), thickened sludge (35), and various discharges (43) are also collected in the tailings pond. The bitumen skimmed from the thickener (37) and from the tailings pond (44) is combined in one stream (14) and recycled.

The bitumen concentrates (17 and 19) are mixed with diluent (21), and subjected to sedimentation and to a final cleanup, if necessary, as indicated by streams (24) and (26). When removal of fine mineral particles and fine water droplets is not required, diluted bitumen concentrate (39) is directed to distillation. After distillation, the bitumen (28 and 30) can be utilized or further processed, while the diluent (29) is recycled. Water precipitated during diluent storage (50) is recycled. Other stream numbers in the schematic stand for the following media: demulsifier (23), air (56), optional flocculant (33), makeup diluent (49), and heating steam (51 to 55). Depending on oil sand properties, different versions of the processing strategy are available and will be tested in a pilot plant operation.

COST OF BASIC CHEMICALS FOR BITUMEN RECOVERY FROM OIL SAND USING HOT WATER TECHNOLOGY

Price of Bulk Reagents

Caustic Soda (beads); NaOH (Ashland Chem.)	$0.34/lbs
Sodium Tripolyphosphate (light or heavy); $Na_5P_3O_{10}$ (Ashland Chem.)	0.38/lbs
Soda Ash (light); Na_2CO_3 (Ashland Chem.)	0.08/lbs
Kerosene (Dunn Oil)	1.60/gal
Flocculant; polyamine, 50% active (Thatcher Chem.)	1.25/lbs
Demulsifier; polyamine, 50% active (Thatcher Chem.)	1.25/lbs

Table 24. Cost of Chemicals for 100 tpd of Oil Sand Pilot Plant

Chemicals Used for Processing of Oil Sand	Asphalt Ridge* Pounds per Ton	Asphalt Ridge* Total lbs/day	Asphalt Ridge* Cost $/day	Whiterocks** Pounds per Ton of Oil Sand	Whiterocks** Total Amount lbs/day	Whiterocks** Cos $/day
Na_2CO_3[1]	4	400	32	2	200	16
Kerosene Loss[2]	3(0.5 gal)	300	80	2(0.3 gal)	200	48
Flocculant	0.02	2	3	0.05	5	6
Demulsifier	0.08	8	10	0.06	6	8
Total Cost, $ per						
-ton of oil sand		1.6[3]			1.2[4]	
-bbl of bitumen		2.6[3]			3.2[4]	

* 12 wt.% bitumen
** 7.5 wt.% bitumen
[1] demand for both alkalies may be reduced in a continuous mode of operation
[2] kerosene loss of 0.75 gal per bbl of bitumen has been accepted assuming that sludge resulting from bitumen concentrate clean-up is recycled to the process
[3] assumes 90% recovery (62 bbl/day)
[4] assumes 85% recovery (36 bbl/day

COMMENTS AND CONCLUSIONS

1) Considerable progress has been made in the water-based recovery of bitumen from Utah's oil sands. A processing strategy which require less energy and which lead to higher grade bitumen concentrates and higher bitumen recovery has been developed.

2) The processing strategy is based on diluent addition to the oil sand prior to digestion. As a result, the 323 K modified hot water process was conceived, patented in 1982 and continues to be evaluated.

3) It was observed that the recycle of process water containing 4 to 5 wt.% suspended matter had no deleterious effect on the process separation efficiency, which indicates that the sedimentation time of the tailings in the thickener can be significantly reduced.

4) Pilot plant testing should now be undertaken to examine the process strategy under continuous plant operations in order to optimize the system. A complete flowsheet has been prepared with heat and material balances of the principal steps in the process.

5) This water-based process development has been aided by fundamental research on the surface chemistry of bitumen-sand mixtures, the natural porosity of the oil sands accessible by various hydrocarbon diluents, the identification of natural surfactants released from the bitumen during processing and the FTIR microscopic studies of oil sands, as discussed in our

previous reports and in the preceding sections of the present report.

FUTURE ACTIVITIES

Based on the results from our process development work, pilot plant testing should now be undertaken to examine the process strategy under continuous plant operations in order to optimize the system. The revival of the 50 bbl/day bitumen pilot plant located in North Salt Lake City, successfully operated a decade ago, and actually owned by the University of Utah, seems to be most appropriate. On the other hand, important fundamental studies on oil sand properties and surface chemistry, forming the foundation for process development, need to be continued.

EXTRACTION OF BITUMEN FROM WESTERN OIL SANDS BY AN ENERGY-EFFICIENT THERMAL METHOD

Principal Investigator:	J.D. Seader
Graduate Students:	C.J. Coronella
	A.S. Bhadkamkar
	K.R. Khot

INTRODUCTION

During the year ending July 1993, significant progress was accomplished in the development of an energy-efficient process for the extraction of cracked bitumen from oil sands by a thermal method. The process and apparatus described below involve advanced technology based on the use of thermally coupled fluidized beds. The cracked bitumen, following hydrotreating for removal of nitrogen and sulfur, is a high-grade synthetic crude oil. The process is characterized by the absence of a need to provide process water or solvents and does not require the recycle of large amounts of sand.

The extraction equipment, shown in Figure 50, and descibed by Coronella and Seader[126], consists of a vessel segregated into a pyrolysis reaction zone, a first-stage combustion zone, and a second-stage combustion zone. Each zone operates as a fluidized-bed reactor. Oil sand feed at ambient temperature and pressure is fed by a conveyor from a hopper down into the pyrolysis reactor, which operates at 723-798 K and where bitumen is thermally cracked to about 80 weight percent vapor and 20 weight percent coke that remains deposited on the sand particles. The vapor is sent to a condensing system, where almost 90 weight percent of the vapor is

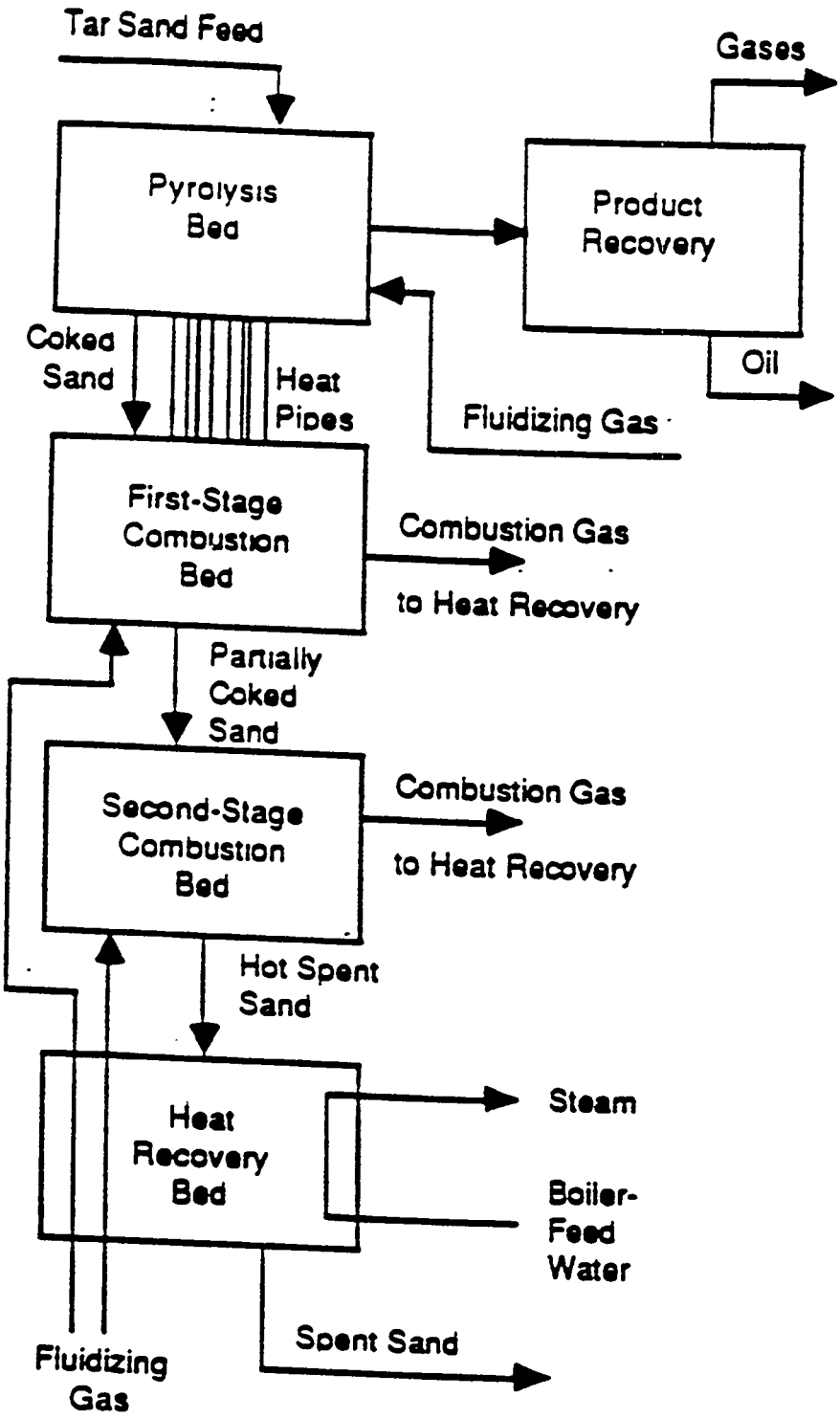

Figure 50. Schematic Diagram of Coupled Thermal Fluidized-Bed Oil Sands Extraction Process.

condensed to oil. The coked sand flows downward to the first-stage combustion reactor, where approximately 90% of the coke is combusted with air or oxygen-enriched air at 823 to 873 K. The heat of combustion is transferred to the pyrolysis zone by heat pipes. The remaining coke is combusted adiabatically with air in the second-stage combustion zone. Energy remaining in the sand is used to preheat the combustion air and produce steam from boiler feed water. The clean sand can then be returned to the environment or used for other purposes, such as for drilling or for making glass.

In other fluidized-bed thermal processes for extraction of bitumen from oil sands, energy requirements in the pyrolysis zone, including preheating of oil sands and heat of pyrolysis, are provided by recycling large amounts of hot sand from the combustion zone to the pyrolysis zone, with recycle ratios of 4-to-1 being typical. In the process being developed here, sand recycle is eliminated by transferring the heat between the two zones with heat pipes, which are closed tubes that contain a heat transfer medium that boils at the lower end and condenses at the upper end. Heat pipes can transfer heat at extremely high rates so that the pipes operate almost isothermally.

In large-scale applications of the process, a large number of heat pipes would be provided for transferring the thermal energy from the first-stage combustion zone to the pyrolysis zone. The equipment may also include additional heat exchangers for heating the incoming combustion air for the combustion zone and cooling the

sand. The combustion air serves as the fluidizing medium for the fluidized bed reactors of the combustion zones while flue gases from the combustion zone can serve as the fluidizing medium for the fluidized bed reactor of the pyrolysis zone. Alternatively, recycled light hydrocarbon gases produced from the bitumen and/or steam may be used to fluidize the pyrolysis zone.

During the year ending July, 1993, four tasks were completed:

1. The experimental coupled reactor system was modified and some troubleshooting was accomplished.
2. A pyrolysis model was completed and tested.
3. An internal-model-control tuning method was developed for improved temperature control of the coupled reactor system.
4. A method was determined for estimating the heat of pyrolysis of bitumen.

Details of these four tasks are given in the following four sections.

REACTOR MODIFICATIONS AND TROUBLESHOOTING

An Acrison volumetric feeder, Model BDF-1, was purchased to supply oil sands at a constant rate to the coupled-reactor system built by Smart[127] and being used in the present study. The Acrison volumetric feeder was connected to the reactor by a vertical 1.5-inch stainless steel pipe. In between the feeder and this vertical pipe there is a 4-inch diameter compressible fixture, to allow for the thermal expansion of the reactor at high temperature. This fixture has a conical end that connects it to the vertical

1.5-inch pipe. During the course of a test run, the oil sand got stuck in this conical section and did not flow into the reactor, causing the auger in the feeder to get twisted. To help alleviate this problem, the conical end of the compressible fixture was eliminated and the vertical 1.5-inch pipe was replaced by a 4-inch diameter pipe. The reactor has been successfully run with this modification, using Whiterocks oil sand.

The discharge cylinder from the feeder is wrapped in copper tubing to allow for cooling, to keep the oil sand feed cool and, thus, to reduce agglomeration and plugging of the feedstock. A nitrogen purge was introduced at the top of the downspout to help prevent oil vapors, leaving the pyrolysis section, from rising into the feedstock and initiating plugging.

The feeder was built to withstand pressures of up to 0.5 psi. The hopper is made of mild steel; augers and cylinder are made of 304 SS. The feeder is powered by a 0.5 hp, 115V DC motor that is controlled by an Acrison model 050-1A controller with a 30:1 speed range from maximum speed.

Three augers were purchased so that an optimal feeding configuration could be identified. Auger A is a typical screw, size D/2, about 1 inch in diameter. Auger B is an open helix without a center solid bar, size F/2, and about 2 inches in diameter. Auger C is a typical screw (flights encircling a solid bar), size F/2, about 2 inches in diameter, but coated with a stick-free "Release Coat" offered by Acrison. Averaged over 30

minutes for oil sand and 15 minutes for clean sand, calibration curves are as follows:

Auger	Material	m	b	Setting Range
A	Oil Sand	0.012	-3.9	500 - 999
A	Clean Sand	0.190	-0.87	50 - 999
B	Oil Sand	1.97	-62.4	40 - 100
B	Clean Sand	1.62	-12.8	10 - 100
C	Oil Sand	0.454	2.2	40 - 100
C	Clean Sand	1.59	-4.2	10 - 100

where, the feed rate is linear with controller setting, and is fitted to the equation: m(setting)+b, (in g/min).

In general, feed rate is quite nearly linear when feeding clean sand, but is not nearly so when feeding oil sand. Auger A completely failed to deliver oil sand at a constant rate; however, augers B and C were somewhat more successful.

A small screen was bolted inside the end of the discharge cylinder and mounted so that the feed is pushed through the screen at the end of the flights of the auger. The openings in the screen are diamond shaped, 4 mm × 22 mm, and the wire is approximately 2 mm thick. The purpose of this screen is to break up any clumps of oil sand that might have agglomerated in the feeder before dropping into the pyrolysis bed.

A computer control system, consisting of an HP Vectra personal computer and a data acquisition unit, was installed for data logging and process control. The data acquisition unit is an HP-E1301A unit featuring several different-sized slots. This unit can be easily configured with a variety of plug-in cards to meet data acquisition needs. It also handles communications of control

signals and data between the computer and the process via an HP-IB (Hewlett-Packard) interface. The following plug-in cards were installed in the data acquisition unit: 1) A 16-bit digital multimeter (HP E1326B) for measuring various electrical signals such as DCV, ACV, and resistance with extremely high precision. 2) Two 16-channel thermocouple relay multiplexers (HP E1347A) providing the basic analog-to-digital conversion capability for data logging. One of the multiplexers is used to measure temperatures, i.e., the voltage signals from 16 K-type thermocouples. Another multiplexer is used to read the output signals of the four pressure transmitters, which monitor the pressure drops across the fluidized beds and maximum pressures below the gas distributors. 3) A 4-channel D/A converter (HP E1328A) to provide four independent, isolated channels of digital-to-analog output capability. In this research, two output channels send variable voltage signals to the two pressure transducers, which control the solid flow valves for level control of the pyrolysis and combustion reactors. The other two output channels are used to control temperatures in the two reactors by sending 0 to 10 volt signals to the single-phase, phase-angle-fired (SCR) power controllers. Then, the SCR power controllers regulate power into the heating wires wrapped around the reactors. 4) A 16-channel form C switch (HP E1364A) is used for an emergency situation. This module consists of 16 independent single-pole, double-throw relays, allowing a wide variety of devices and signals to be switched. In case of emergency, the data acquisition/control

system detects the problem and energizes appropriate relays to turn off the power supply or perform other procedures.

Several runs were made with clean sand at high temperature 713 K to see if the bed levels could be well-controlled. The pressure drop across the pyrolysis bed fluctuated as shown in Figure 51. A number of factors were investigated to determine which one of them caused these fluctuations. The tuning parameters, of the control valve; viz., the Proportional and Integral values of the PI control, were varied. It was thought that if the control valve did not open or close as frequently, the fluctuations would stop. This, however, did not stop the fluctuations.

The instrumentation was then checked to see if it were faulty. The D.P. cell for the pyrolysis bed was interchanged with the D.P. cell for the combustion bed. No improvements were observed. The pressure transducers of the two beds were then exchanged. This did not make any difference in the results either.

The feed rate was then measured. The fluctuations in the feed rate were approximately 7 gm per 6 seconds. On the other hand, the pressure drop fluctuations observed across the pyrolysis bed were approximately 580 gm per 6 seconds. Thus, it was thought unlikely that the feeder could cause the fluctuations.

The combustion bed was operating normally and without pressure drop fluctuations. The bed level in the combustion bed is twice that in the pyrolysis bed; hence, for the same gas flowrate, slugging would have first occurred in the combustion bed; but since the combustion bed operated in the bubbling regime, so did the

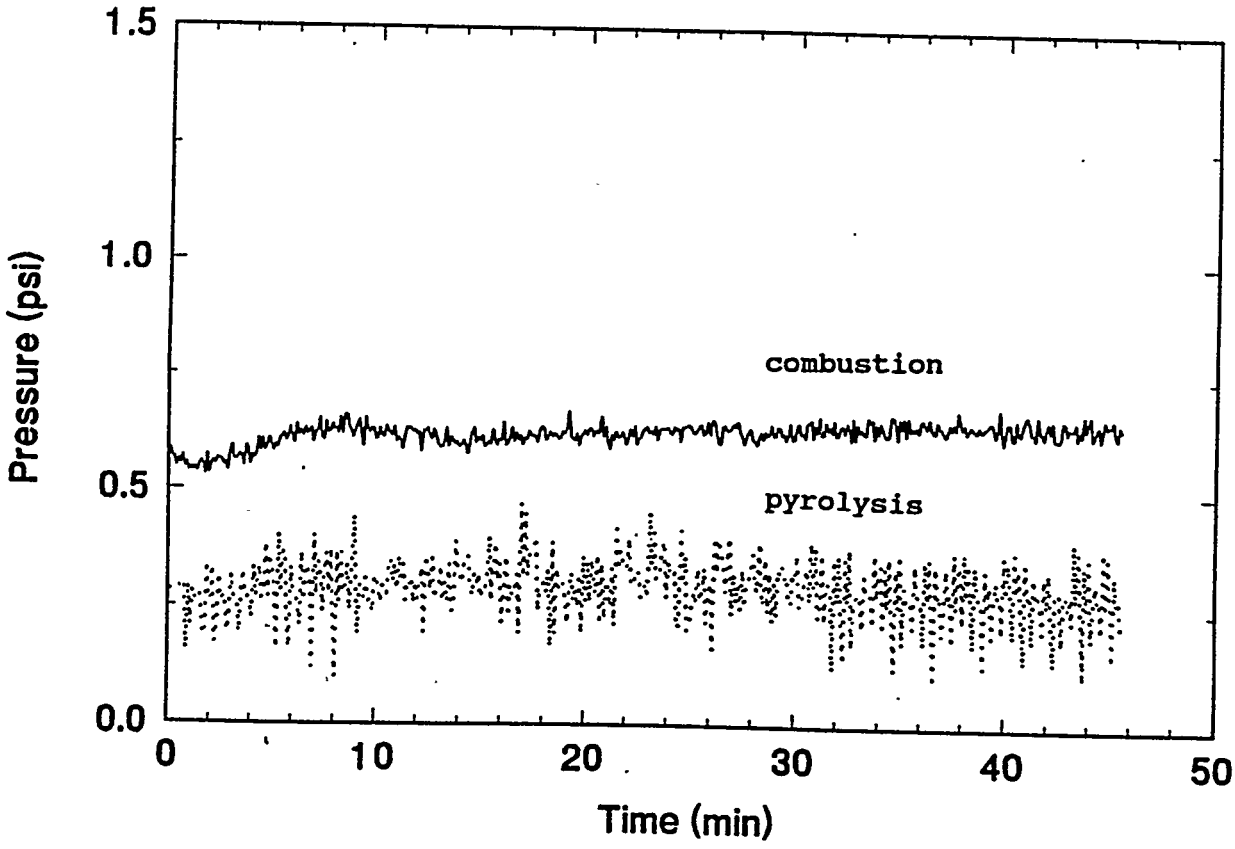

Figure 51. Run With Clean Sand (Pyrolysis Pressure Drop Oscillates)

pyrolysis bed. Hence the fluidization was in the bubbling regime and could not be the cause of the pressure fluctuations.

All the above runs were made with auger C which is a typical screw (flights encircling a solid bar), size F/2. This auger was removed and auger B, which is an open helix without a center solid bar, was put in place. When the reactor was run with this auger in place, no pressure fluctuations were observed. Hence, it was concluded that it was fluctuation in the feed that caused the pressure fluctuations. The fluctuations in the feed were amplified when they were recorded by the D.P. cells. Thus, the bed levels were finally well-controlled as seen in Figure 52.

PYROLYSIS REACTOR MODEL

A promising process for extracting and upgrading Utah tar-sand bitumen is a thermal, fluidized-bed process, first proposed by Peterson and Gishler.[128] for processing the richer Athabascan oil sands. An energy-efficient version of this concept is the coupled fluidized-bed process for the thermal pyrolysis of oil sand bitumen developed over the last several years by Seader and coworkers in the Chemical Engineering department at the University of Utah.[126,127,129-133] Three consecutive fluidized beds in series are used to process crushed oil sands. A schematic diagram of the process is presented in Figure 50. Thermal pyrolysis occurs in the first, which is generally fluidized by nitrogen or light ends, and typically operates at 723 K. Bitumen evaporates and cracks and is carried out with the fluidizing gas to a product recovery system, where oils are condensed. Coked sand, the residue after the

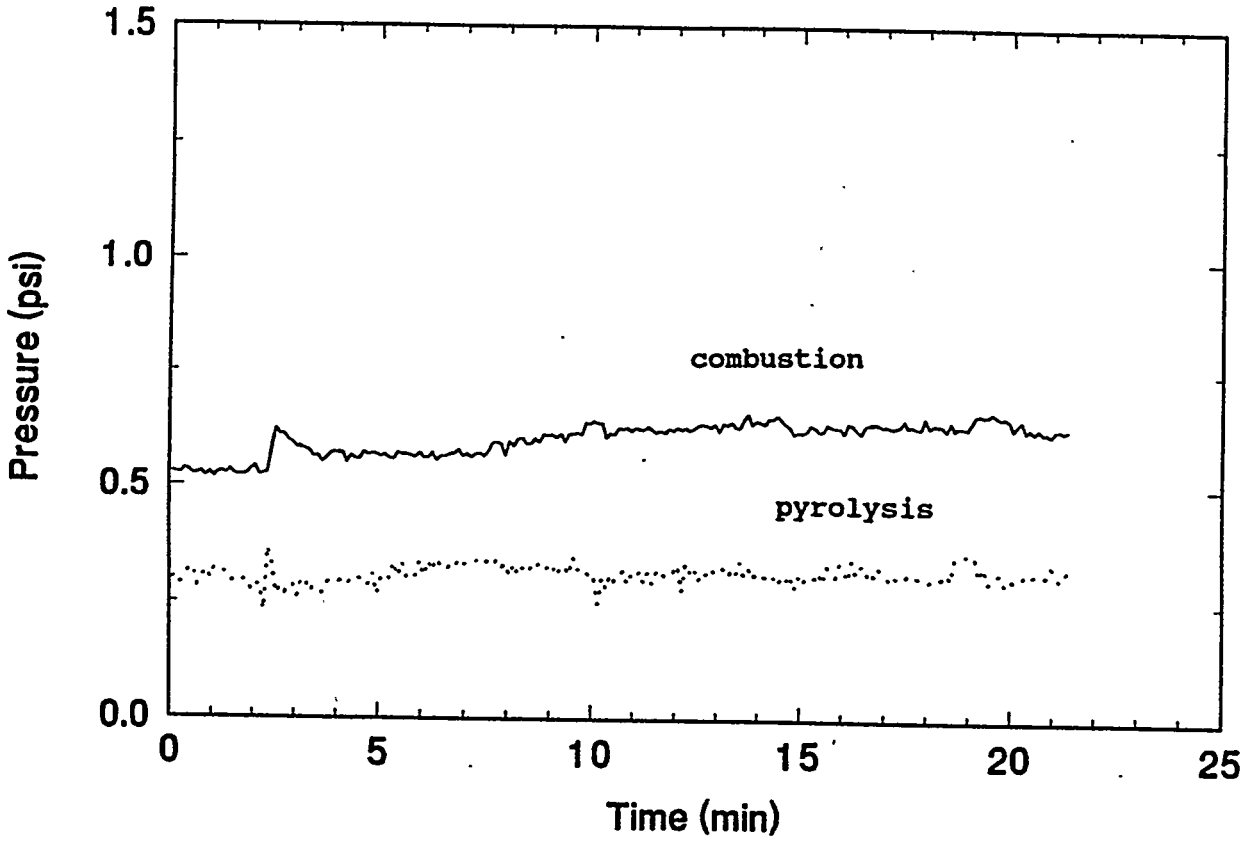

Figure 52. Run With Clean Sand

pyrolysis, is passed into the second bed by way of a standpipe. This bed is fluidized by air and operates at a higher temperature causing the coke to combust. Heat pipes, mounted vertically between and extending into both beds, transfer this heat of combustion from the combustion bed to the pyrolysis bed. A heat pipe is essentially an extremely good conductor of heat that can rapidly transfer heat from a warm zone to a cooler zone. Sand then is transferred from the combustion bed to a third fluidized bed that operates adiabatically and is fluidized by air where the remaining coke is burned off. The heat transferred via heat pipes into the pyrolysis reactor supplies all the heat required there for both heating the raw oil sand feed to the pyrolysis-bed operating temperature and for the endothermic pyrolysis reactions.

Oil yield is defined to be the fraction of the native bitumen that is converted to condensible oils and has been found to depend primarily on the pyrolysis-bed temperature, T_p, and the average solids-residence time in the pyrolysis bed, $\bar{t}_p$. Additionally, the source of the specific oil sand influences the oil yield. Physical properties of the oil, such as viscosity, °API (density), or simulated distillation, vary with the operating conditions as well. Unfortunately, the level of reproducibility between different workers is quite significant, and at this time, it is difficult to draw precise conclusions regarding optimal operating conditions. Figure 53 shows oil yields found by Fletcher[134] in a 6-inch diameter bed and by Smart[127] in a 4-inch diameter bed. No trends are readily apparent from these data. Since the experimental data

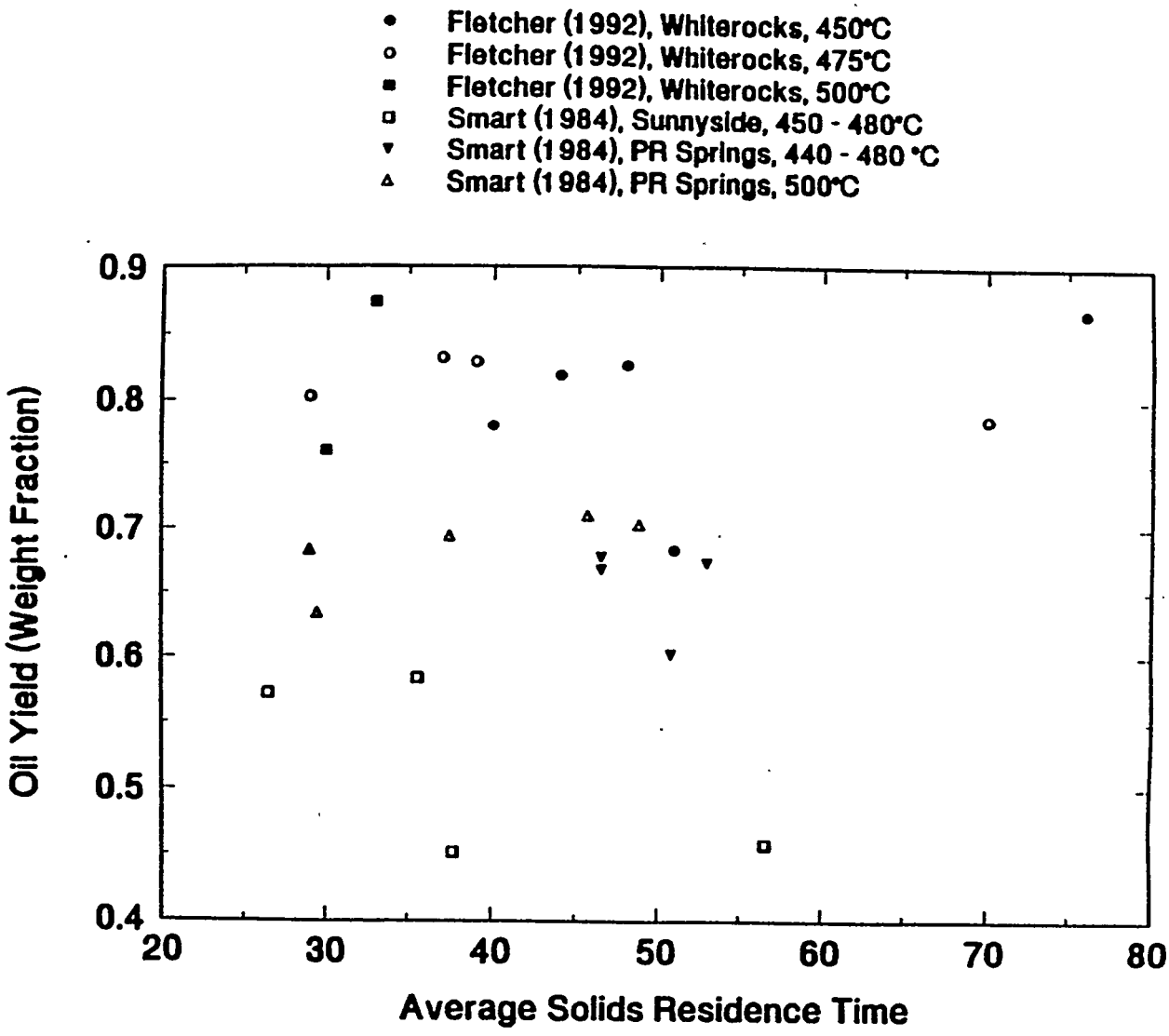

Figure 53. Some Typical Experimental Oil Yields from Fletcher[134] and Smart.[127]

to date do not clearly and objectively point to these optimum operating values, another strategy must be used in order to find them so that design, optimum energy efficiency, and economic viability of a commercial scale reactor can be investigated. Mathematical modeling and computer simulation are gradually becoming more widely accepted for design and optimization of industrial-scale chemical processes because an accurate model can be used to conduct low cost computational "experiments". Thus, an in-depth mathematical simulation of the operation of the coupled fluidized-bed reactor for the thermal pyrolysis of oil sands was carried out.

PREVIOUS MODELING WORK

Models of the two coke-combustion beds have been completed.[126, 133] Since there are many similarities between the pyrolysis zone and the combustion zones, a summary of the relevant work is presented here.

The two-phase bubbling bed model of Grace[135] was adopted to model the fluidization hydrodynamics and the mass balances of the gas-phase species. This model assumes: 1) that the bed is operating in the bubbling regime, 2) that the bed is operating isothermally, 3) that the bed is operating at steady state, 4) that solids are well-mixed in the bed, 5) that the bed is made up of two phases, a bubble phase containing very few solids and a dense phase containing most of the solids, 6) that all of the net gas flow is through the bubble phase in plug flow while continuously exchanging with the dense phase, 7) that the void

fraction of the dense phase is constant at ϵ_{mf}, and 8) at any axial position z, properties are independent of radial position. In addition, bubble growth is accounted for by the model of Darton et al.[136] as modified by Stubington et al.[137] A mass balance for gas species in the bubble and dense phase may be derived in light of these assumptions as follows:

$$S\frac{-d\ (u\ C_b)}{dz} + k_q\ a_b\ \varepsilon_b\ (C_d - C_b) + r_b\ \varepsilon_b = 0 \qquad (42)$$

$$k_q\ a_b\ \varepsilon_b\ (C_b - C_d) + r_d\ (1 - \varepsilon_b) = 0. \qquad (43)$$

C_b and C_d are the bubble-phase and dense-phase gaseous concentrations (mass or molar), respectively. In Equation 42, the first term represents convection, the second term represents mass transfer between the dense and bubble phases, and the last term accounts for chemical reaction. Under assumption 6 above, the bubble-phase concentration of a species at the top of the bed, $C_b(L)$, corresponds to the amount of that particular component leaving a bed. Likewise, $C_b(0)$ corresponds to gas inlet conditions.

Equations 42 and 43 contain a term describing the rate of mass transfer between the bubble and dense phases. Grace[135] recommends the following relationship for k_q, the mass-transfer coefficient:

$$k_q = \frac{u_{mf}}{3} + \frac{\sqrt{4D_i\ \varepsilon_{mf}\ u_b}}{\pi\ d_b}. \qquad (44)$$

Thus, mass transfer includes a convective component and a diffusive component.

Results of the combustion-zone simulation have been reported previously.[126] The most important conclusion of that work was a consequence of assumption 4 above, that the solid particles (sand) are well mixed throughout the bed. As a result, particles leave the bed at a wide distribution of residence times, with a residence-time-distribution (RTD) function
of

$$E(t) = \frac{1}{\bar{t}} \exp\left(\frac{-t}{\bar{t}}\right). \qquad (45)$$

Thus, at any finite average residence time, complete conversion of solids is impossible, because there will always be some particles leaving before adequate time has passed. Nearly all coke should be oxidized if the sand is to be returned to the ground, due to environmental considerations. Therefore, it was proposed to conduct the coke oxidation in two sequential beds, where more than 90% of the coke is burned in the first bed, to achieve high coke conversion. In this manner, high coke conversion can be achieved with significantly reduced total residence time, at small expense of heat required in the pyrolysis bed.

HYDRODYNAMICS

Many hydrodynamic parameters needed in a comprehensive model can be found from correlations resulting from the two-phase theory of fluidization proposed by Davidson and Harrison.[138]

$$L = L_{mf} \; / \; (1 - \overline{\varepsilon_b}) \tag{46}$$

$$L_{mf} = \frac{4 \; W \; \overline{t}}{\pi \; (1 - \varepsilon_{mf}) \; D_B^2} \tag{47}$$

$$\overline{\varepsilon_b} = \frac{1}{L} \int_0^L \varepsilon_b \; (z) \; dz \tag{48}$$

$$\varepsilon_b = \frac{\varepsilon - \varepsilon_{mf}}{1 - \varepsilon_{mf}} \tag{49}$$

$$\varepsilon = \frac{u_b \; \varepsilon_{mf} + u - u_{mf}}{u_b + u - u_{mf}} \tag{50}$$

$$u_b = 0.71 \; \sqrt{g} \; d_b. \tag{51}$$

In addition, bubble growth may be modeled by the correlation of Darton et al.,[136] amended for high-temperature operation by Stubington et al.:[137]

$$d_b = 0.43 \; (u - u_{mf})^{0.4} \; (z + 4 \; \sqrt{A_0})^{0.8} \; g^{-0.2}. \tag{52}$$

A value for u_{mf}, the minimum fluidization velocity, can be found from the Ergun equation. The following relationship is valid only for low Reynolds Numbers:

$$Re_{mf} = \frac{\overline{d_p}\, u_{mf}\, \rho_g}{\mu} = \frac{Ar\, \phi_s^2\, \varepsilon_{mf}^3}{150\ (1 - \varepsilon_{mf})} \tag{53}$$

where the Archimedes number is defined as

$$Ar = \frac{g\, \overline{d_p^3}\, \rho_g\, (\rho_s - \rho_g)}{\mu^2}. \tag{54}$$

Gas density ρ_g can be found from the ideal gas law. The shape factor ϕ_s, minimum-fluidization void fraction ϵ_{mf}, and average particle diameter $\bar{d}_p$ are properties of the solids being fluidized and must be measured.

Reviewing Equations 42 through 52, it is apparent that the superficial gas velocity u is an extremely important parameter in many of the above relations. Therefore, it is important to have an accurate relation to describe the dependence of u on all of the important physical phenomena that affect it. There are only three phenomena influencing the gas velocity: initial inlet gas velocity, the pressure gradient through the bed caused by supporting a reduced amount of solids at higher positions in the bed, and volumetric changes in gas due to either chemical reaction or phase change. Obviously, u is directly proportional to u_o, the velocity at the base of the bed-barring volumetric changes. At operating pressures of most fluidized beds, the pressure dependence is inverse by the ideal gas law.

The influence of volumetric changes is far more difficult to characterize, and has not been adequately addressed in the literature. Volumetric changes in the bubble phase should have a direct influence on u; u will proportionally increase or decrease with changes in volume. However, volumetric changes in the dense phase are less easily resolved. For gas-solid reactions or sublimation, dense-phase volumetric changes may be quite significant, and consequential effects on u need to be carefully quantified. Consider a small volume of the dense phase. Gas produced at the surfaces of particles will increase the volumetric ratio of gas to solids in the differential volume, i.e., increase the void fraction ϵ. This would contradict assumption 7 of the two-phase bubbling-bed model, that the dense phase has a constant void fraction of ϵ_{mf}. The only way that this can be true is if the excess volume produced at the particle surfaces is actually transferred directly into the bubble phase causing an increase in u (or a decrease in u if volume is consumed at the particle surface).

The following expression accounts for each of the three dominant physical phenomena influencing u:

$$u = u_o \frac{P(0)}{P} (\varepsilon_B \sigma_b + (1 - \varepsilon_b) \sigma_d) . \qquad (55)$$

The terms σ_b and σ_d account for molar gas flow produced or consumed in the bubble and dense phases, respectively.

$$\sigma_{b,\,or\,d} = \frac{u}{u_o}\,\frac{R\,T}{P(0)}\sum_{i=1}^{N}\frac{C_{i,b,\,or\,d} - C_{i,\,b}(0)}{M_i} \qquad (56)$$

The summation is taken over all gas-phase species present in the reactor. If most of the fluidizing gas in a bed is made up of some "carrier gas," then the following form of Equation 56 may be simpler to use, where the summation is taken over reacting species only:

$$\sigma_{b,\,or\,d} = 1 + \frac{u}{u_o}\,\frac{R\,T}{P(O)}\sum_{i=1}^{N}\frac{C_{i,\,d} - C_{i,\,b}\,(0)}{M_i}\,. \qquad (57)$$

The pressure changes with height, and is proportional to the amount of solids being supported above. Pressure P(z) can be found by integrating the following ordinary differential equation:

$$\frac{dP(z)}{dz} = (\rho_s - \rho_g)\;g\;(1 - \varepsilon)\,. \qquad (58)$$

PYROLYSIS REACTION SCHEME AND KINETICS

Bitumen consists of a wide range of compounds, from high molecular weight asphaltenes to light gases. The thermal pyrolysis of oil sand bitumen consists of the volatilization and cracking of both gaseous and liquid/solid compounds. The number of simultaneous reactions may be quite large. To efficiently model bitumen pyrolysis, both the number of lumped component fractions or pseudocomponents and the number of group reactions must be reduced to a small finite number.

Several workers have attempted to derive an efficient bitumen pyrolysis reaction scheme consisting of only two or three reactions. Recognizing the inherent error associated with this goal, various degrees of success have been achieved. Of course, it may not be possible to define a pyrolysis reaction network universally applicable to all bitumens, because of the very different physical nature of various bitumens, characterized by average molecular weight, aromaticity, asphaltenic content, or boiling-point distribution. Figure 54 shows several first-order rate constants as a function of temperature used to model various pyrolysis reactions.[139-144] Note that the use of first-order rate constants implies that bitumen pyrolysis can never be complete.

The reaction network presented by Hayashitani et al.[140] has been used to model the rotary kiln pyrolysis of Utah oil sands[145] and is presented here:

$$\text{Asphaltene} \rightarrow s_A \text{ Coke} + s_B \text{ Gas}$$

$$\text{Maltene} \rightarrow s_C \text{ Heavy Oil} + s_D \text{ Gas}$$

$$\text{Heavy Oil} \rightarrow s_E \text{ Light Oil} + s_F \text{ Gas}$$

In this model, bitumen is said to consist of asphaltene and maltene only. The work of Hayashitani et al.[140] was done on raw bitumen, first extracted from Athabascan oil-sand by solvent extraction. Since that time, it has been shown that sand serves as a catalyst in the pyrolysis reactions.[141] Thus, Hayashitani's reaction rate constants are probably too slow to accurately model tar-sand pyrolysis. Figure 54 shows that these rate constants are indeed slower than those measured by most other workers.

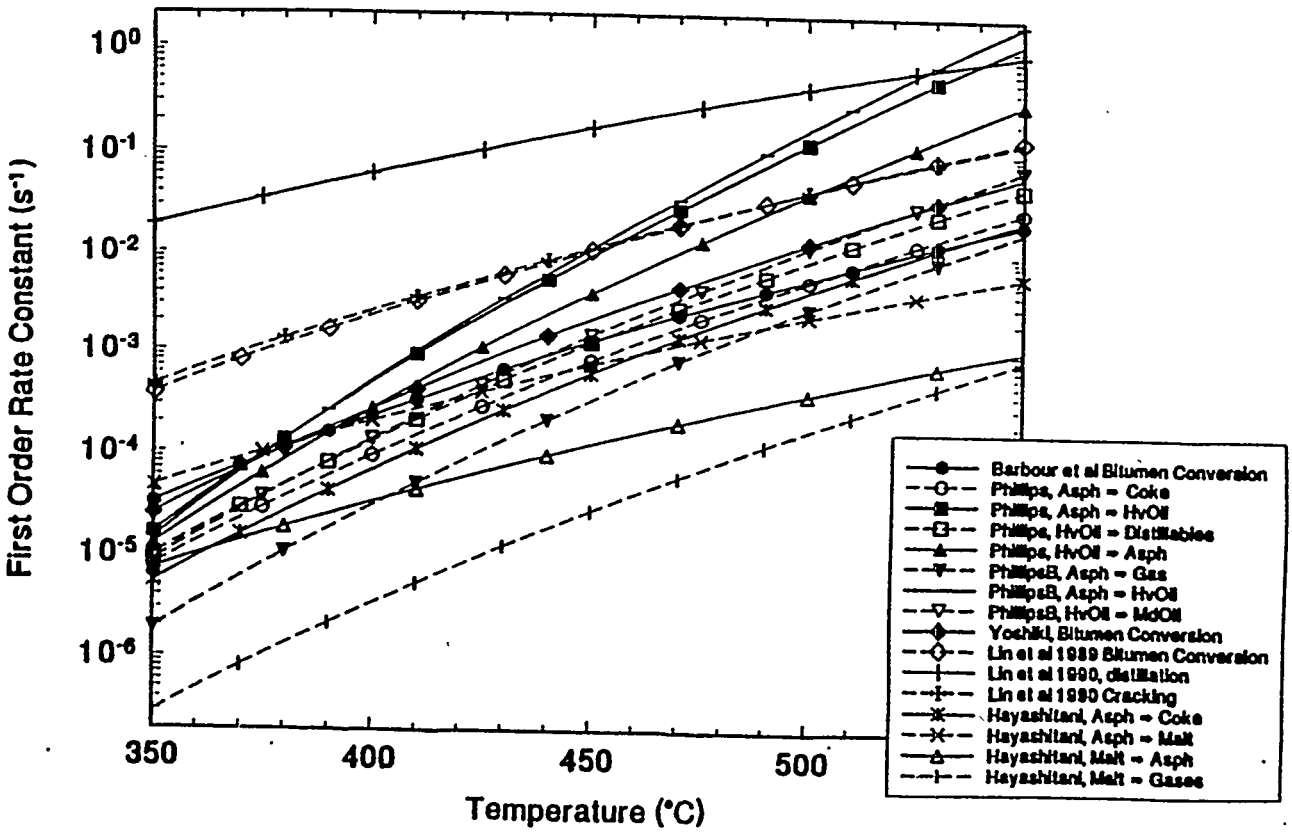

Figure 54. First-Order Rate Constants Used to Model Bitumen Thermal Pyrolysis as a Function of Temperature.

Lin et al.[143] studied the rate of bitumen evolution by ramped-temperature TGA studies of Whiterocks (Utah) oil sand. They showed that the rate of bitumen conversion could be modeled by a low-temperature "distillation" reaction and by a high-temperature "cracking" reaction. One possible interpretation of this is the following heterogeneous reaction scheme:

Heavy Bitumen → Light Bitumen	$k_{cracking}$
Light Bitumen → Volatiles	$k_{distillation}$

Unfortunately, they made no attempt to describe what was produced, nor did they describe any gas-phase cracking reactions that might be important. They did conclude that the weight ratio of heavy bitumen-to-light bitumen was approximately 1:1 in raw oil sand.

Phillips et al.[141] derived two complete reaction networks from constant temperature TGA studies of Athabascan oil sands, one of which is shown below.

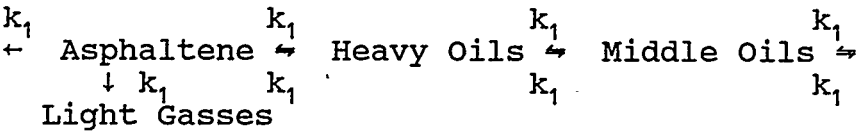

Each reaction in this scheme is said to be first order.

Each of the oil products was defined in terms of a boiling-point range, with light oils having a boiling point ≤453 K, heavy oils boiling at temperatures > 693 K and middle oils falling in the intermediate range. Since all of the studies were done at temperatures less than 693 K, little of the heavy oil in these

studies was vaporized, so the heavy-oil cracking reaction was a "solid-phase" reaction.

A pyrolysis reaction network can be derived by combining the results of Lin, et al., with the results of Phillips et al.[141] All bitumen pyrolyzes either by a "cracking" reaction or a "distillation" reaction, as proposed by Lin, et al. Heavy bitumen (asphaltene) produces light gases, coke, and heavy oils. Light bitumen (heavy oils) produces lighter oils. In the vapor phase, heavy and middle oils will crack to form lighter oils and light gas. Gas-phase reforming reactions proposed by Phillips, et al.[141], are considered to be insignificant. Consider the reaction scheme shown below:

$$\text{Heavy Bitumen} \xrightarrow{k_1} s_A \text{ Coke} + s_B \text{ Light Gas} \quad (59)$$

$$\text{Heavy Bitumen} \xrightarrow{k_2} s_C \text{ Light Bitumen} + s_D \text{ Coke} \quad (60)$$

$$\text{Light Bitumen} \xrightarrow{k_3} \text{Heavy Bitumen} \quad (61)$$

$$\text{Light Bitumen} \xrightarrow{k_4} s_E \text{ Heavy Oil} + s_F \text{ Middle Oil} + s_G \text{ Light Oil} + s_H \text{ Light Gas} \quad (62)$$

$$\text{Heavy Oils} \xrightarrow{k_5} s_I \text{ Middle Oil} + s_J \text{ Light Oil} + s_K \text{ Light Gas} \quad (63)$$

$$\text{Middle Oil} \xrightarrow{k_6} s_L \text{ Light oil} + s_M \text{ Light Gas.} \quad (64)$$

Reaction 1 (Equation 59) accounts for the production of coke and light gas from heavy bitumen or asphaltenes. Phillips, et al.[141], derived separate rate constants for the production of coke

and light gas, but clearly, the production of coke must be accompanied by the simultaneous production of light gas, since coke generally has a higher C:H ratio than does asphaltene. Reaction 2 (Equation 60) is akin to the high-temperature "cracking" reaction of Lin, et al.[143]. The solid-phase reforming reaction, reaction 3, was reported to be significant by Phillips, et al.[141] Reaction 4 might be thought of as a "distillation" reaction, described by Lin, et al.[143] The products of this reaction are distributed over a wide range and might represent the maltene fraction content of raw bitumen. Finally, reactions 5 and 6 (Equations 63 and 64) are gas-phase cracking reactions, as predicted by Phillips, et al.[141] Each forms a distribution of products, although Phillips, et al.[141], model only one lighter product from each reaction. The products coke, light gas, and light oil are each said to be inert in this reaction scheme. Rate constants can be taken directly from the values predicted by Lin, et al.[144], and by Phillips, et al.,[141] and are given Arrhenius-type temperature dependence (Table 25).

Table 25
First-Order Kinetic Rate Constants

	PreExponential Constant (s^{-1})	Activation Energy (kJ/Mol)	Temperature Range (C°)	Reference
k_1	6.78×10^9	176.7	360-420	(144)
k_2	6.5×10^6	125.9	100-500	(141)
k_3	1.56×10^{13}	215.8	360-420	a
k_4	1.7×10^5	82.97	100-500	(141)
k_5	1.05×10^{15}	230.0	360-420	a
k_6	1.05×10^{15}	230.0	360-420	a

a Derived from Phillips, et al.[141]

Stoichiometric constants for the reaction network above are assigned with some knowledge of the reactions, although the exact values are somewhat arbitrary and are given in Table 26. Note that these values refer to weight fractions, rather than molar ratios. The relative rates of coke and gas formed by reaction 1 can be found by comparing the two rate constants given for coke and gas formation from asphaltenes, evaluated by Phillips, et al.[141] They predict that the ratio of gas-product formation to coke-product formation increases with temperature.

$$s_A = 1 - s_B = \left[1 + 12.2 \exp\left[\frac{-20.3\ kJ/mol}{R\ T}\right]\right]^{-1} \qquad (65)$$

Table 26

Stoichiometric Constants

Stoichiometric Constant	Value (wt / wt)
s_A	See Equation 24
s_B	See Equation 24
s_C	0.80
s_D	0.20
s_E	0.70
s_F	0.20
s_G	0.07
s_H	0.03
s_I	0.70
s_J	0.20
s_K	0.10
s_L	0.60
s_M	0.40

In order to characterize product oil and raw bitumen, each of the pseudo-components must be assigned physical characteristics.

Table 27 gives these descriptions. The physical properties of

Table 27

Physical Characteristics of Pseudocomponents

Pseudo-Component	Boiling Point Range (K)	Molecular Weight	Density (°API)	Phase in Reactor
Heavy Bitumen	> 823			Solid
Light Bitumen	≤ 823			Solid
Heavy Oil	693 - 823	400	9	Vapor
Middle Oil	453 - 693	240	19	Vapor
Light Oil	293 - 453	160	70	Vapor
Light Gas	≤ 293	28		Vapor

ethylene have been used to characterize the light gas product, although all compounds up through nC5 are considered in the boiling-point range. The boiling point ranges of the three oil products were taken to be the same as those used by Phillips et al.[141] The molecular weights were selected somewhat arbitrarily, and the densities were found from API charts,[146] using the known boiling points and molecular weights. Any component in liquid or solid form, i.e., not evaporated, is called bitumen in this scheme. Although a compound residing on sand may be a product of thermal cracking, it cannot be recovered with the product oil and should not be considered as a product.

ENERGY BALANCES

To find the operating temperature of the three fluidized-bed reactors, an energy balance is written around each. The operating

temperature is then found by setting the steady-state balance equal to zero and finding the value of the temperature that satisfies the balance.

Pyrolysis bed

A steady-state energy balance around the pyrolysis bed is:

$$Q_{hp,p} - \Delta H_{sand,p} - \Delta H_{Bitumen} - \Delta H_{fg,p} - Q_{loss,p} = 0. \qquad (66)$$

The first term accounts for heat transfer from the heat pipes; $\Delta H_{sand,p}$ is the sensible heat required to heat the sand portion of the tar-sand feed; $\Delta H_{Bitumen}$ includes the sensible heat required to heat the bitumen feed and the heat of the thermal pyrolysis reactions; $\Delta H_{fg,p}$ is the sensible heat of the fluidizing gas; and $Q_{loss,p}$ accounts for heat loss through the bed walls due to imperfect insulation. In a large bed, the Q_{loss} term would be significantly smaller than the other terms.

The rate of heat transfer from the heat pipe to the bed is found from

$$Q_{hp,p} = \overline{h_p}\, n_{hp}\, \pi\, d_{hp}\, L_p\, (T_{hp} - T_p). \qquad (67)$$

This equation assumes that heat transferred from the heat pipes to the freeboard (open area above the bed consisting of gas) is small relative to the heat transferred directly to the bed. It also assumes that heat pipes extend through the full height of the bed, L_p. If the heat pipes did not extend the entire bed height, L_p in Equation 67 would be replaced with the height into the bed that

they do extend. Implicit in Equation 67 is the assumption that the heat pipe is isothermal, and that the only resistance to heat transfer is from the outside wall of the heat pipe to the fluidized bed.

Fluidized-bed heat transfer is an extremely complex phenomenon, as it is influenced by considerations of gas properties, fluidized solids properties, gas velocity, and tube geometry. Thus, convection coefficients, $\bar{h}$, are notoriously difficult to predict. Although two rather complete reviews of fluidized-bed heat transfer have been published recently,[147,148] there is no reason a priori to believe that more recent relations are more accurate than the older as empirically-derived correlations that are so much simpler to utilize. A correlation developed by Wender and Cooper[149] was derived from experimental data taken from heat transfer between vertical tubes and various beds, and is given by:

$$\bar{h} = 3.5 \times 10^{-4} \frac{k_g}{d_p} \alpha_g^{-0.43} (1 - \varepsilon) Re^{0.23} \left(\frac{C_s}{C_g}\right)^{0.8} \left(\frac{\rho_s}{\rho_g}\right)^{0.66} . \qquad (68)$$

This is a dimensional equation, with $\bar{h}$ in $(W/m^2 \cdot °C)$ and α_g in m^2/s.

The heat absorbed by the sand, ΔH_{sand}, can be evaluated rather simply by integrating sand specific-heat, C_{sand}, over temperature, from the tar-sand-feed temperature to T_p. However, SiO_2, which makes up a large part of the sand, changes phase from α-quartz to β-quartz at 847 ± 1.5 K,[150] so the sensible heat of this phase change must be included, if T_p is greater than 847 K.

The term $\Delta H_{Bitumen}$ includes the sensible heat of the bitumen from feed temperature to the bed temperature and the heat of pyrolysis. The heat capacity of bitumen can be estimated from a correlation for any hydrocarbon:[146]

$$C_p = [0.681 - 0.308\ s + (8.15 - 3.06\ s)\ T \times 10^{-4}] \times (0.055\ K + 0.035) \qquad (69)$$

where C_p is the heat capacity in Btu/lb, s is the specific gravity at 60°F, T is temperature in °F, and K is the Watson characterization factor.

The second component in $\Delta H_{bitumen}$, heat of the pyrolysis reaction, can be estimated from the heats of combustion as follows:

$$\Delta H_{pyr} = m_{pyr} \left[\int_{T_p}^{T_o} C_{p,Bitumen}\, dT + \Delta h^{\circ}_{pyr} + \sum_{products} \nu_i \int_{T_o}^{T_p} C_{p,i}\, dT\right] \qquad (70)$$

$$\Delta h^{\circ}_{pyr} = \sum_{products} \nu_i\, \Delta h^{\circ}_{c,i} - \Delta h^{\circ}_{c,bit}. \qquad (71)$$

In the above expressions, ν_i represents the yield (w/w) of a pyrolysis product, $\Delta h^{\circ}_{c,i}$, is the standard heat of combustion of a compound, and m_{pyr} is the mass rate of bitumen pyrolysis. The two summations are over products of thermal pyrolysis, i.e., light gas, synthetic crude oil, and coke.

The energy balance, Equation 66, includes a term to account for loss of heat from the reactor to the outside environment, Q_{loss}, which may be evaluated as follows:

$$Q_{loss} = U_o A_{Bo} (T_p - T_\infty) . \qquad (72)$$

The overall heat-transfer coefficient can be evaluated by the usual resistance-in-series method, including wall thicknesses and thermal conductivities, as well as convection and radiation coefficients.

Combustion Bed

In a similar manner, a steady-state energy balance can be written about the combustion bed.

$$\Delta H_{Coke,c} - Q_{hp,c} - \Delta H_{sand,c} - \Delta H_{fg,c} - Q_{loss,c} = 0 . \qquad (73)$$

The terms $Q_{hp,c}$, ΔH_{sand}, $\Delta H_{fg,c}$, and $Q_{loss,c}$ can be evaluated in a manner similar to the way they were evaluated in the pyrolysis-bed energy balance. The main differences are that the sand is entering the bed at T_p, that $Q_{hp,c}$ is energy going out of the bed (into the heat pipes,) and that the fluidizing gas is air, which reacts with coke at T_c.

The term ΔH_{Coke} in Equation 73 includes the sensible heat required to heat the coke from T_p to T_c and the exothermic heat of coke oxidation, ΔH_{comb}, evaluated at T_c:

$$s\text{-}\Delta H_{Comb} = m_{Coke} \overline{\overline{x_c}} \left[\sum_{reactants} \nu_i \int_{T_c}^{T_o} C_{p,i}\, dT + \Delta h_c^\circ + \sum_{products} \nu_i \int_{T_o}^{T_c} C_{p,i}\, dT \right] . \qquad (74)$$

In this equation, m_{coke} is the rate that coke enters the combustion bed from the pyrolysis bed, and $\overline{\overline{x}}_c$ is the total conversion of the coke in the first combustion bed. The reactants in Equation 74 are

coke and oxygen; the products are carbon dioxide and carbon monoxide. Again, ν_i represents the mass stoichiometric constant of each reactant or product. Because of the wide distribution of residence times of oil sand in the pyrolysis bed, there may be unreacted bitumen entering the combustion bed. This analysis lumps together unreacted bitumen and coke formed by the pyrolysis reaction. The term Δh°_{c} gives the negative exothermic heat of the coke combustion at a standard temperature, and may be found in standard references.

Second-Stage Combustion Bed

Finally, a steady-state energy balance may be written about the second-stage combustion bed:

$$\Delta H_{Coke,a} - \Delta H_{Sand,a} - \Delta H_{fg,a} - Q_{loss,c} = 0. \qquad (75)$$

This bed operates adiabatically, without heat removed by heat pipes. Each term can be evaluated in a manner similar to the way it was evaluated in the first combustion-bed energy balance.

Heat Pipes

For most purposes, the surface temperature of a heat pipe can be assumed spatially constant within the appropriate working-temperature range.[151] Consequently, an energy balance can be written about the heat pipes as follows:

$$Q_{hp,c} - Q_{hp,p} = 0. \qquad (76)$$

This equation assumes that the rate of heat transfer between the heat pipes and the fluidizing gas in the freeboard is much smaller

than the rate of heat transfer between the beds and the heat pipes, and that the section between the combustion and pyrolysis beds is essentially adiabatic. Each of the terms Q_{hp} can be evaluated by Equation 67.

METHOD OF SOLUTION

The underlying physical phenomena influencing the coupled fluidized-bed reactor are mathematically described above and in Coronella and Seader.[126] The mathematical treatment of these submodels and their incorporation into a single comprehensive model is described next.

Solid-Phase Products

From the pyrolysis reaction model above, it is possible to estimate the conversion of bitumen and the coke yield. Equations describing the disappearance of the two components of bitumen, HB and LB are:

$$\frac{dw_{HB}}{dt} = k_3\, w_{LB} - (k_1 + k_2)\, w_{HB} \tag{77}$$

$$\frac{dw_{LB}}{dt} = s_c\, k_2\, w_{HB} - (k_3 + k_4)\, w_{HB}. \tag{78}$$

where w gives the weight fraction of a component with respect to the original bitumen, and clearly depends on, among others, time. Initial conditions for w_{HB} and w_{LB} are $w_{HB,0}$ and $w_{LB,0}$, and depend on the characterization of the raw bitumen. This is a system of two simultaneous first-order, ordinary differential equations, which

may be readily converted to a single second-order ordinary differential equation. Their solutions are

$$W_{HB}(t) = \gamma_1 e^{x_1 t} + (W_{HB,o} - \gamma_1) e^{x_2 t} \tag{79}$$

$$W_{LB}(t) = \gamma_2 e^{x_1 T} + (W_{LB,o} - \gamma_2) e^{x_2 t} \tag{80}$$

where x_1 and x_2 are the eigenvalues of the differential equations, and γ_1 and γ_2 are integration constants:

$$x_1 = \alpha + \beta \tag{81}$$

$$x_2 = \alpha - \beta \tag{82}$$

$$\gamma_1 = \frac{k_3 - W_{HB,o}\,(x_2 + k_1 + k_2 + k_3)}{2\beta} \tag{83}$$

$$\gamma_2 = \frac{s_c k_2 - W_{LB,o}\,(x_2 + s_c k_2 + k_3 + k_4)}{2\beta} \tag{84}$$

$$\alpha = \frac{-1}{2}\,(k_1 + k_2 + k_3 + k_4) \tag{85}$$

$$\beta = [\alpha^2 + s_c k_2 k_3 - (k_1 + k_2)(k_3 + k_4)]^{\frac{1}{2}}. \quad (86)$$

Here, $w_{HB,0}$ and $w_{LB,0}$ refer to content of heavy and light bitumen, respectively, in native bitumen, and must sum to one. The coke yield can be found by a similar method:

$$w_c(t) = (s_A k_1 + s_D k_2) \left[\frac{\gamma_1}{x_1}(e^{x_1 t} - 1) + \frac{w_{HB,o} - \gamma_1}{x_2}(e^{x_2 t} - 1)\right]. \quad (87)$$

The average solids concentration in a fluidized bed is found by integrating the conversion over the solids residence-time distribution given in Equation 45. Thus,

$$\overline{w_{HB}} = \int_o w_{HB}(t)\, E(t)\, dt \quad (88)$$

$$\overline{w_{LB}} = \frac{\gamma_2}{1 - \bar{t}\, x_1} + \frac{w_{LB,o} - \gamma_2}{1 - \bar{t}\, x_2} \quad (89)$$

$$\overline{w_{LB}} = \frac{\gamma_2}{1 - \bar{t}\, x_1} + \frac{w_{LB,o} - \gamma_2}{1 - \bar{t}\, x_2} \quad (90)$$

$$\overline{w_c} = \bar{t}\,(s_A k_1 + s_D k_2)\,\overline{w_{HB}}. \quad (91)$$

These expressions for $\bar{w}_{HB}$, $\bar{w}_{LB}$, and $\bar{w}_c$ can be used for an accurate first estimate of the bitumen conversion of each of these "solid-phase" species, i.e., those residing on the sand.

Gas-Phase Products

The yield of a gas-phase product, i.e., one that is transported from the bed with the fluidizing gas, can be found from knowledge of its concentration profile, or more specifically, from its bubble-phase concentration at the top of the bed, $C_{i,b}(L)$. This, in turn, comes from integration of its bubble-phase mass balance, Equation 42. This equation requires the volumetric rate of production of a species in the bubble phase, $r_{i,b}$. Different strategies are used for homogeneous gas-phase reactions and heterogeneous solid-phase reactions.

Homogeneous reactions are the heavy- and middle-oil gas-phase cracking reactions given in Equations 63 and 64. As an example, the volumetric rate of production of light gas by the middle-oil cracking reaction is

$$r_{LG,b}(z) + s_M k_6 C_{MO,b}(z) . \qquad (92)$$

The rate of production of a gas-phase species by a solid-phase reaction is related to the local particle concentration $(1 - \epsilon)$ and to the quantity of bitumen present on the sand particles. By assumption 7 of the two-phase bubbling-bed model, the quantity of both heavy and light bitumen will be the same on all sand present in the bed, and can be found from the initial bitumen content of the oil sand, x_{BO}, and from the fractions of unconverted bitumen, $\bar{w}_{HB}$ and $\bar{w}_{LB}$.

Assumption 4 of the fluidization model gives the void fraction in the dense phase as ϵ_{mf}, so the volume fraction of solids is simply $(1 - \epsilon_{mf})$. The bubble phase is said to contain little solids, but it does contain some and should be considered. Grace[135] characterizes this volume fraction by ϕ_b / ϵ_b, and says it lies between 0.1% and 1%. The volumetric rate of production of light gas by heavy bitumen can now be characterized by

$$r_{LG,b} = s_B \, k_1 \, \overline{w_{HB}} \, x_{BO} \, \rho_{TS} \, \frac{\phi_b}{\epsilon_b} \, \frac{1}{1 - x_{BO} + x_{BO} \, w_s} \qquad (93)$$

in the bubble phase, and

$$r_{LG,d} = s_B \, k_1 \, \overline{w_{HB}} \, x_{BO} \, \rho_{TS} \, \frac{1 - \epsilon_{mf}}{1 - x_{BO} + x_{BO} \, w_s} \qquad (94)$$

in the dense phase. The fraction $1/(1 - x_{BO} + x_{BO} \, w_s)$ gives the volume fraction of oil sand in the pyrolysis bed that is actually bitumen, where w_s is the fraction of the bitumen still residing on the sand:

$$w_s = \overline{w_{HB}} + \overline{w_{LB}} + \overline{w_c}. \qquad (95)$$

The term ρ_{TS} in these expressions refers to the density of the oil sand in the bed, and becomes closer to the value of ρ_{sand} as most of the bitumen cracks and vaporizes.

With appropriate reaction-rate expressions, a bubble-phase and a dense-phase mass balance equation can be solved for each gaseous

species. However, the number of differential equations to be solved can be limited by first summing the two mass balance equations for a species.

$$\frac{d(u\, C_{i,b})}{dz} = \varepsilon_b\, r_{i,b} + (1 - \varepsilon_b)\, r_{i,b} \qquad (96)$$

If this species is produced by a heterogeneous, solid-phase reaction, then this may be written, after substituting for ϵ_b and some algebra and integration, as:

$$u\, C_{i,b} = (s_i\, k_i\, \overline{w_i})\, V_1(z) \qquad (97)$$

$$V_1(z) = \frac{x_{BO}\, \rho_{TS} \left[\int_0^z \varepsilon\, dz \left(\frac{\phi_b}{\varepsilon_b} + \varepsilon_{mf} - 1\right) - z \left(\varepsilon_{mf}\, \frac{\phi_b}{\varepsilon_b} + \varepsilon_{mf} - 1\right)\right]}{(1 - \varepsilon_{mf})\, \left([1 - x_{BO}\, (1 - w_s)\right]}. \qquad (98)$$

The terms in parentheses on the right-hand side of Equation 97 refer to the appropriate kinetic rate expression. Since the term $(\int \epsilon\, dz)$ in Equation 98 is evaluated in order to find L and P, (cf. Equations 46-49 and 58), no additional integration needs to be performed to evaluate $C_{i,b}$ and $C_{i,d}$.

However, in our reaction scheme, many products are formed from homogeneous cracking reactions. Nonetheless, under close scrutiny, we can see that no additional integration is required to evaluate concentrations of these species either. As an example, let us consider light gas formed from the cracking of heavy oil. Had no heavy oil cracked in the bed, the flux of heavy oil passing any

point would be given by Equation 97, written here in terms of a hypothetical concentration C:

$$u(z)\ C_{HO,b}(z) = s_E\, k_4\, \overline{w_{LB}}\, V_1(z)\,. \qquad (99)$$

The difference between this hypothetical flux and the flux found by integrating the heavy-oil mass-balance equation represents oil that was cracked to lighter products. Thus,

$$u(z)\ C_{LG,b}(z) = s_K\ (s_E\, k_4\, \overline{w_{LB}}\, V_1(z) - u(z)\ C_{HO,b}(z)) \qquad (100)$$

and still no integration is required.

In fact, integration of the bubble-phase mass-balance equation is required only for products that undergo reactions themselves. In addition to $(\int \epsilon\ dz)$, integration is required to evaluate $C_{HO,b}$ and $C_{MO,b}$, only.

During the course of the integrations, it is necessary to evaluate u by Equation 55, which is written in terms of the bubble-phase concentrations $C_{i,b}$ by way of σ_b. Unfortunately, the integrator does not give us the values of $C_{i,b}$ directly, but gives the flux, $(u\ C_{i,b})$. By substituting for $C_{i,b}$ from this flux into σ_b and for $C_{i,d}$ (from Equation 43) into σ_d, a single nonlinear equation in terms of u alone can be solved for the value of u at any position z that satisfies Equation 55. Little difficulty was encountered solving this equation by a secant method, using u_0 and $1.1\ u_0$ for the initial guesses. Then, at each step, all bubble- and dense-phase concentrations could be evaluated.

Mass Balance

Upon integration through the top of the bed, yields of each gaseous product were added to the already-determined yields (conversions) of coke and unreacted bitumen. This sum should equal exactly the rate of bitumen fed into bed to satisfy a mass balance. After one iteration of all the integrations, the mass balance was typically close to 95%. This problem is analogous to a similar problem encountered with results from experiments conducted on the reactors[134] where mass balances are never totally closed. At this point, a few options exist:

1) Scale the yields to 100%[134]

2) Add the error to one of the products, typically oil, or subtract a positive error from one of the products, typically light gas.[152]

3) Find values of $\bar{w}_{HB}$, $\bar{w}_{LB}$, and $\bar{w}_{C}$ that, after subsequent integration, close the mass balance.

Obviously, the third option is not available to those conducting experimental studies. This is one advantage that mathematical modeling has over experimental work. The important issue to be resolved is how to adjust the solid-phase yields. Perhaps the simplest way is to adjust each so that their relative magnitudes are unchanged. Note that $\bar{w}_{LB}$ in particular must be adjusted carefully, since oil and light-gas yields are highly dependent on this parameter.

A methodology may be outlined for closing the mass balance. First, evaluate $\bar{w}_{i}$ by Equations 89 to 91, perform the integrations,

and check for closure on the mass balance. Then add a small fraction of the error, perhaps 1%, to $\bar{w}_{HB}$ and adjust $\bar{w}_{LB}$ and $\bar{w}_{C}$ in direct proportion. Again, perform the integrations, calculate the yields, and check for closure on the mass balance. From these first two iterations, a secant method may be applied to find the value of $\bar{w}_{HB}$ that satisfies the mass balance requirement. With this technique, convergence was rapid and always to a value that was quite close to the initial estimates of $\bar{w}_{i}$ that assumed CSTR behavior.

Physical Properties

Throughout the model, physical properties of the fluidizing gas, including viscosity, average molecular weight, density, and diffusivity, must be evaluated. Each of these properties will naturally depend on local concentrations, and so is not constant through the bed. However, the increased accuracy in model predictions from using variable properties must be weighed against increased computational effort, and, with the exception of density, taking an average value was assumed sufficient.

The gas density is found by the ideal gas law and is evaluated from a constant average molecular weight.

The viscosity of the fluidizing gas is found from Wilke's approximation for mixtures, as cited in Reid et al.,[153] considering a mixture of nitrogen, heavy oil, and light gas. In all cases, properties of ethylene were used to evaluate properties of the light gas hydrocarbon product. Cha[145] claimed that ethylene made up the largest fraction of the light gas. Individual viscosities

were found from the Chapman-Enskog theory using a Lennard-Jones collision integral.[153]

Diffusivities are required to evaluate the interphase mass-transfer coefficient, as shown in Equation 44. Diffusivities of light gas, light oil, and heavy oil were each estimated for transport through pure nitrogen and were estimated by the Chapman-Enskog theory using a Lennard-Jones collision integral for diffusivity.

Both the diffusivity correlation and the viscosity correlation require Lennard-Jones potentials for each compound; a characteristic length σ and a characteristic energy ϵ. These were easily available for nitrogen and light gas (ethylene) but needed to be estimated for the oil products. They were evaluated by rough approximations from Reid et al:

$$\frac{\varepsilon}{K} \cong 1.15\ T_b \tag{101}$$

$$\sigma \cong 1.18\ V_b^{\frac{1}{3}}. \tag{102}$$

In Equation 101, k is Boltzmann's constant and T_b is absolute temperature.

Coding

The previously described mathematical submodels of the physical phenomena transpiring in the pyrolysis bed were subsequently translated into FORTRAN code. With the exception of

upper/lower case letters, the code was standard FORTRAN 77. The domain of the fluidized bed was divided into 500 discrete cells in the axial (vertical) direction, and the pressure profile, void fractions, superficial gas velocity, all the concentrations, etc., were calculated at each of these points. An algorithm of the code for the pyrolysis-bed model is shown in Figure 55.

RESULTS

Default values used for the pyrolysis-bed "base-case" simulation are listed in Table 28. In all cases, the bed diameter was taken to be the same as that in the reactor built by Smart.[127] For most of the simulations, pyrolysis temperature was taken as a predetermined value (rather than that determined from solving the energy balance). The default fluidizing-gas flow rate and tar-sand feed rate were taken as the values typically used by Smart. Default sand properties are those values measured from clean sand coming from a Whiterocks tar-sand deposit. Bitumen content of oil sand was taken as 10%, and the fraction of bitumen consisting of heavy bitumen, w_{HBO}, was taken as 50%, as advocated by Lin et al.[144]

Solutions to the pyrolysis model using the pyrolysis reaction scheme shown in Equations 59-64 predicted coke yields as high as 50% at high pyrolysis temperatures, such as 823 K. Dorius[152] showed that coke yield is relatively independent of temperature. Since all coke is produced from the heavy bitumen fraction, rapid production of heavy bitumen from light bitumen by the reaction given in Equation 61 is a likely source of the error. The rate constant for this reforming reaction was taken from the work of

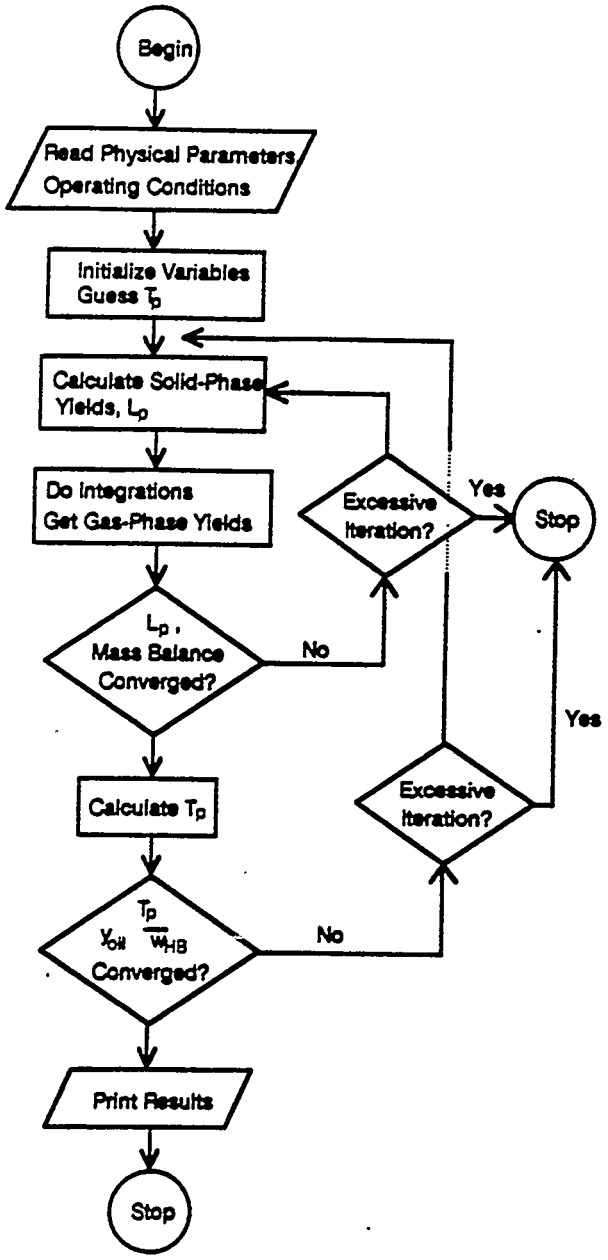

Figure 55. Flow Chart of Pyrolysis-Bed Model.

Table 28

Base-case Simulation Parameters

Parameter	Description	Value
D_B	Bed Diameter	0.1082 m
T_T	Pyrolysis-Bed Temperature	475 °C
$\bar{t}_p$	Average Sand Residence Time in Pyrolysis Bed	20 min.
G	Fluidizing-Gas Flowrate	45 SCFH
W	Oil-Sand Feed Rate	10 lb/hr
$\bar{d}_p$	Average Particle (Sand) Diameter	155 μm
ϕ_s	Particle Shape Factor	0.8
ϵ_{mf}	Void Fraction at Minimum Fluidization Condition	0.46
x_{BO}	Weight Fraction of Bitumen in Native Oil Sand	0.10
w_{HBO}	Weight Fractin of "Heavy Bitumen" in Bitumen	0.50

Phillips et al.[141] that was done at temperatures less than 693 K and, therefore, may be inaccurate at higher temperatures. All the work presented subsequently set k_3 to zero.

Predicted pyrolysis products are shown in Table 29 along with values found by Smart[127] in experiments with PR Springs oil sand. Note that Smart's yields were normalized to 100% for this presentation, and that individual oil fractions were interpolated from simulated distillation data reported by Smart.[127] With the

exception of light oil and middle oil fractions, the model is in excellent agreement with the experimental data.

Table 29

Best Fit for Adjustable Model Parameters-Combustion Bed Only

Parameter (Units)	Model 1	Model 2	Model 3
Q_c (kcal/min)	15.9	15.5	15.4
$h_{h,c}$ $A_{h,c}$ (kcal/min·K)	0.29	0.29	0.29
$M_{r,c}$ (kg)	0.95		

Typical product yields are shown in Figure 56 as a function of bed temperature. A maximum oil yield of about 75% occurs when $T_p \cong 738$ K, with all other parameters taking their default values. A single curve is shown for coke plus unreacted bitumen, since they cannot be distinguished from the perspective of the reactor. That is, they simultaneously exit the pyrolysis bed and are oxidized simultaneously in the combustion bed. The oil product is composed of three separate products, and the yield of each is given in Figure 57 as a function of pyrolysis temperature. At lower temperatures, the oil is dominated by heavy oil, but, as T_p increases above approximately 733 K, the heavy oil undergoes a cracking reaction, producing both middle and light oils. The synthetic crude oil density is shown in the same figure, which predicts a much lighter oil produced at higher pyrolysis temperatures.

The combined effects of bed temperature and average solids residence time on product yields and quality is shown in Figures 58-63. Figures 58 and 59 show that an optimum pyrolysis

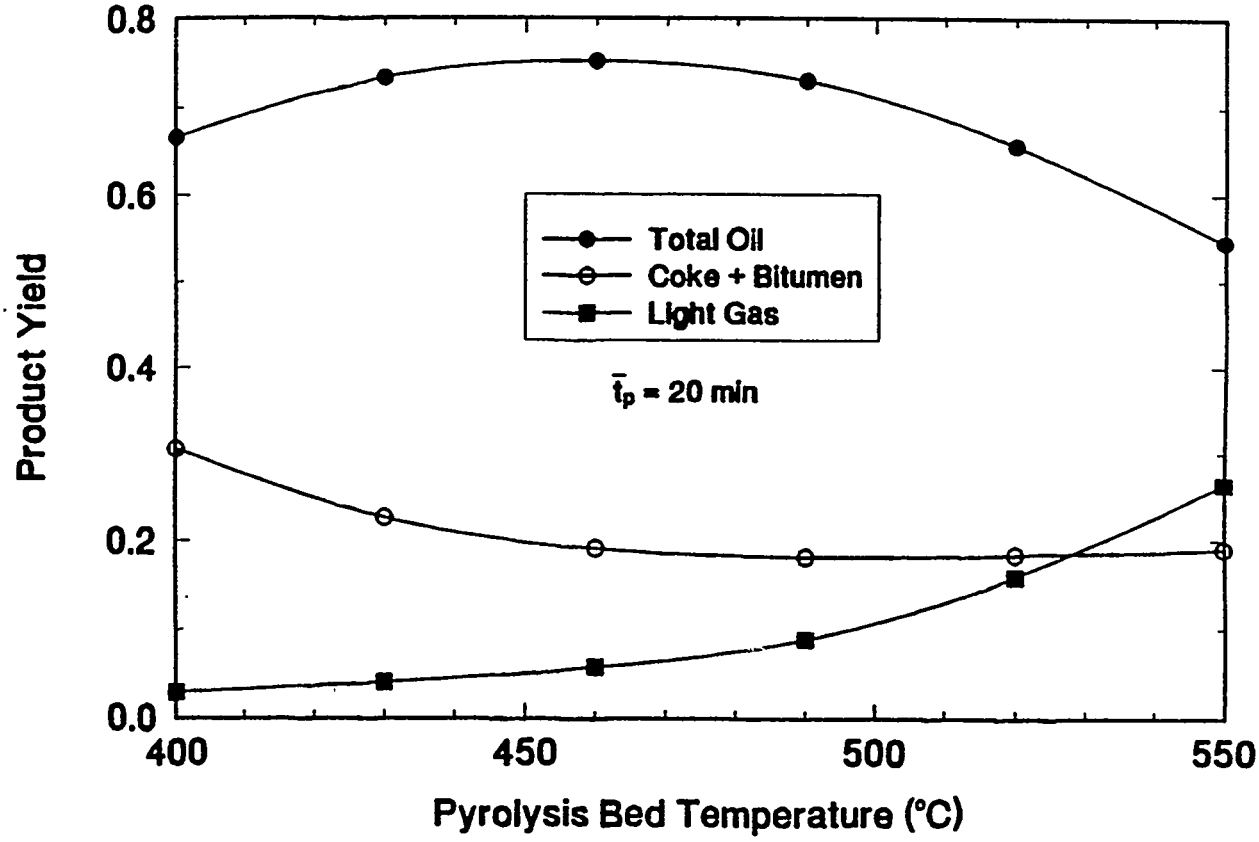

Figure 56. Predicted Product Yields of Bitumen Pyrolysis as a Function of Pyrolysis Temperature; $\bar{t}_p$= 20 Min.

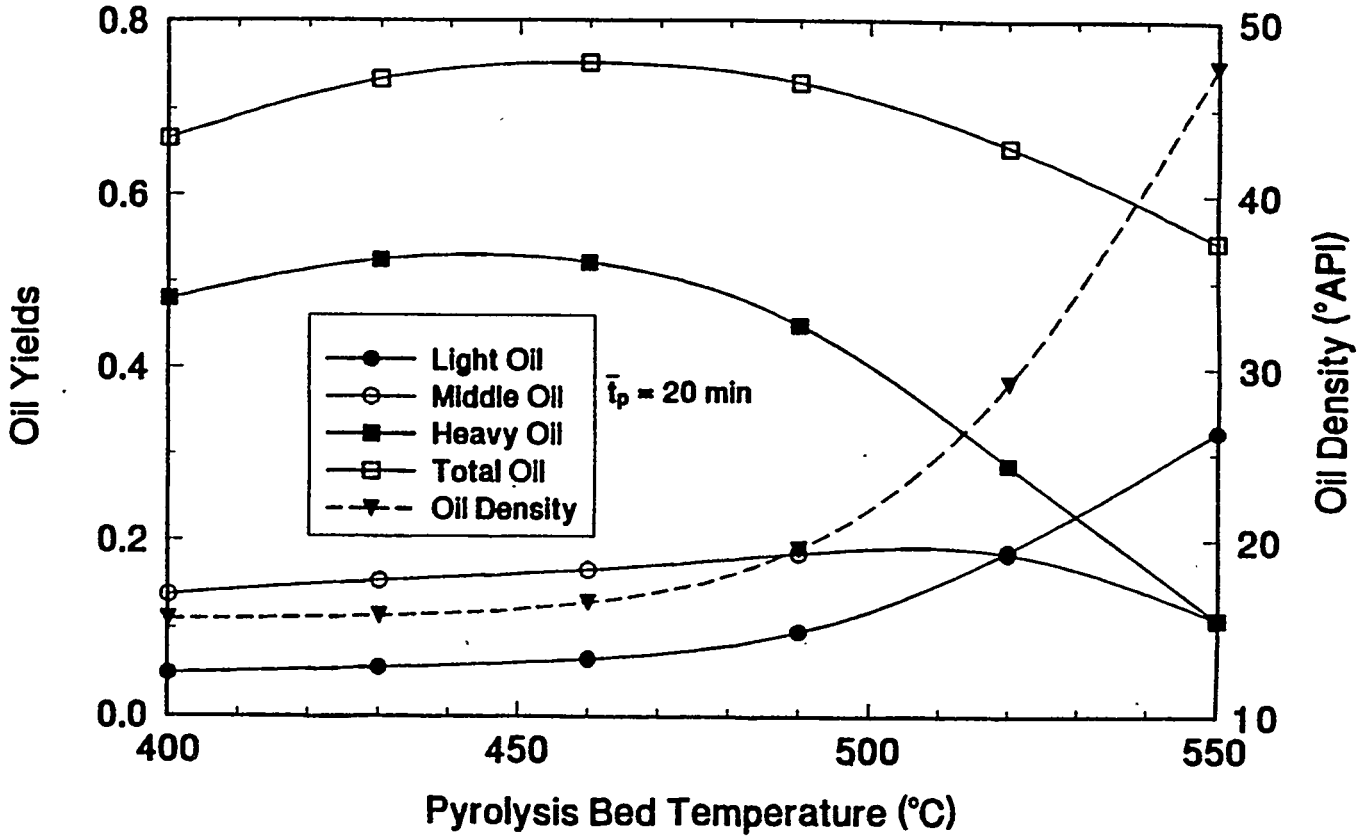

Figure 57. Predicted Oil Yields and Condensed Oil Density from Bitumen Pyrolysis as a Function of Pyrolysis Temperature; $\bar{t}_p$ = 20 Min.

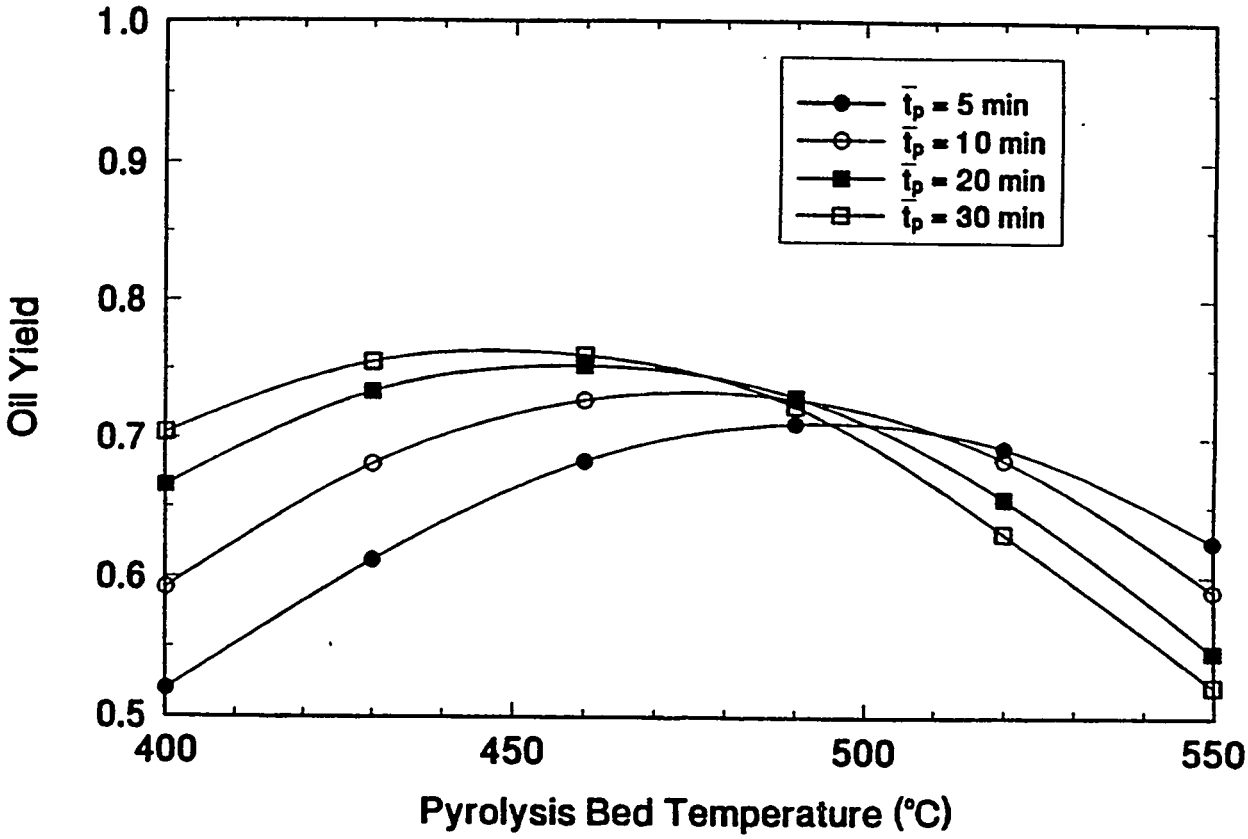

Figure 58. Predicted Oil Yield as a Function of Pyrolysis Temperature and Average Solids Residence Time.

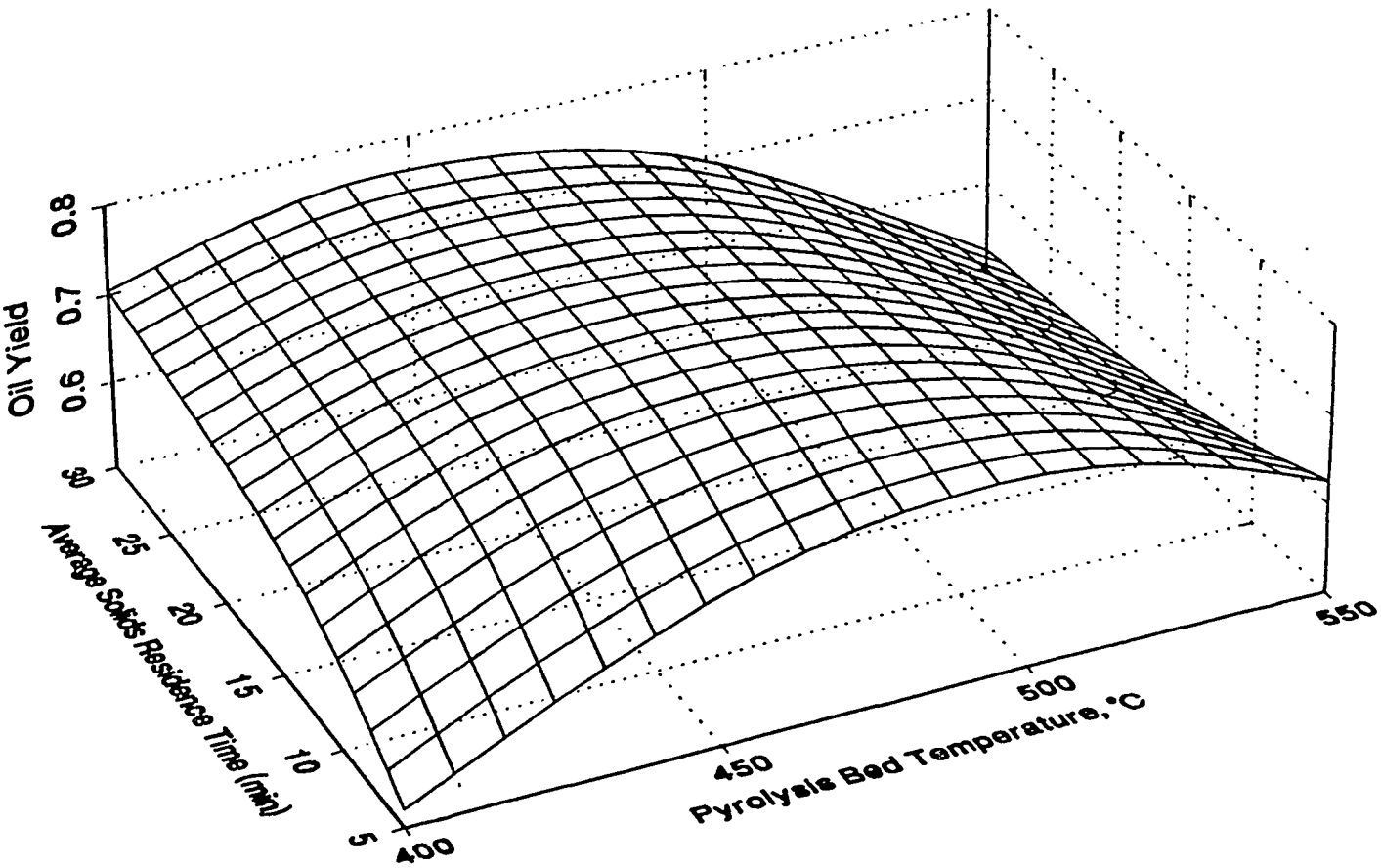

Figure 59. Predicted Oil Yield as a Function of Pyrolysis Temperature and Average Solids Residence Time.

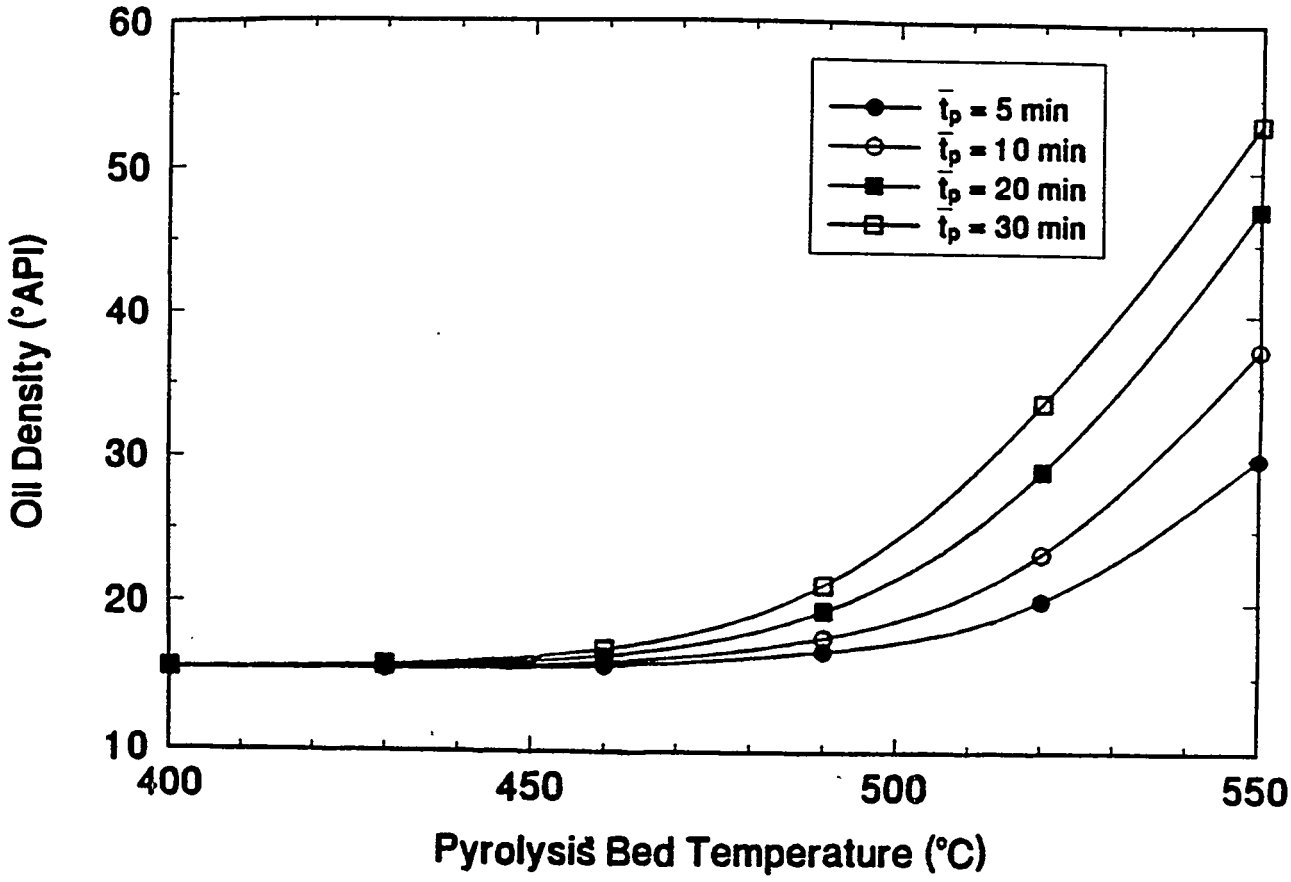

Figure 60. Predicted Oil Density as a Function of Pyrolysis Temperature and Average Solids Residence Time.

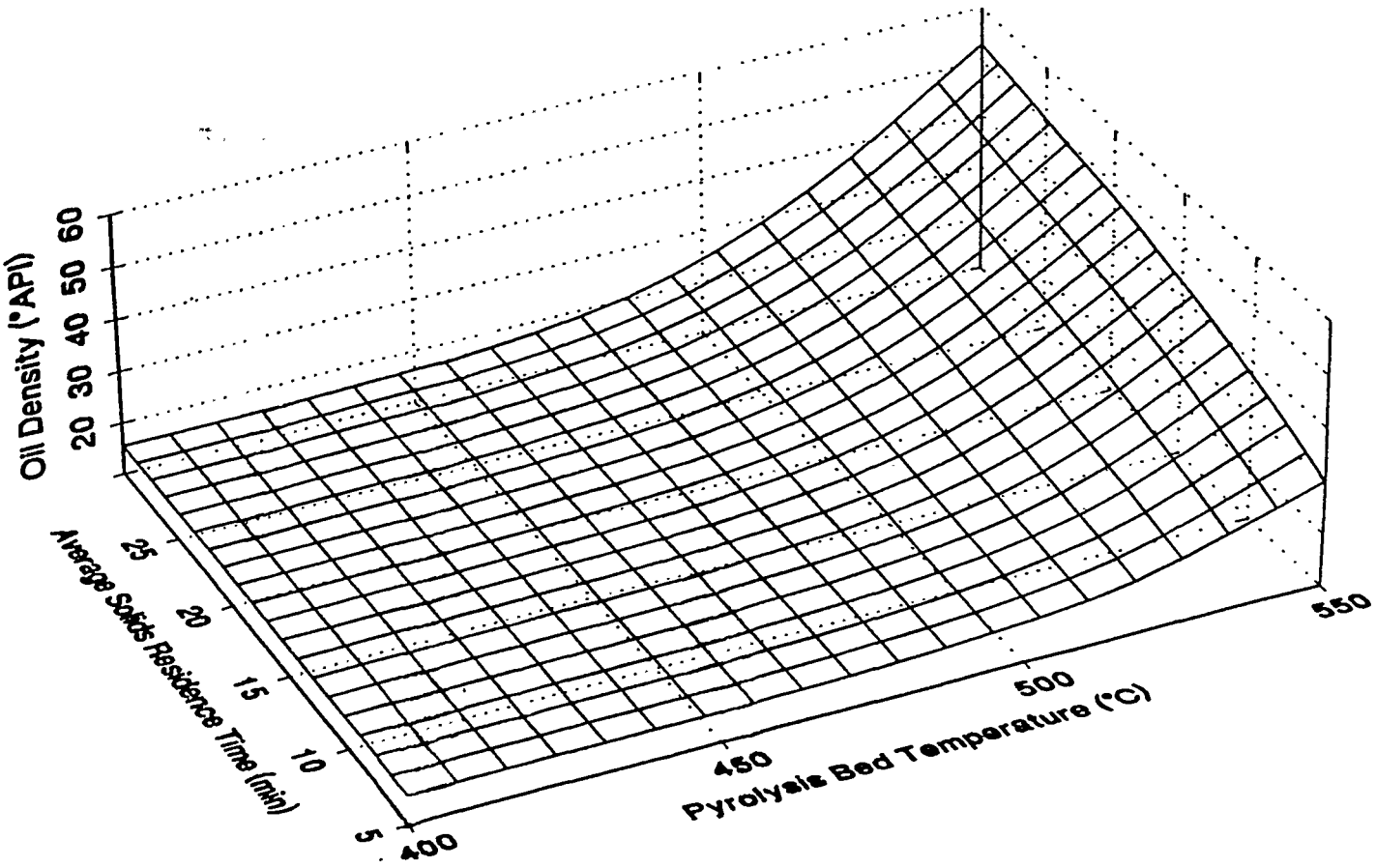

Figure 61. Predicted Oil Density as a Function of Pyrolysis Temperature and Average Solids Residence Time.

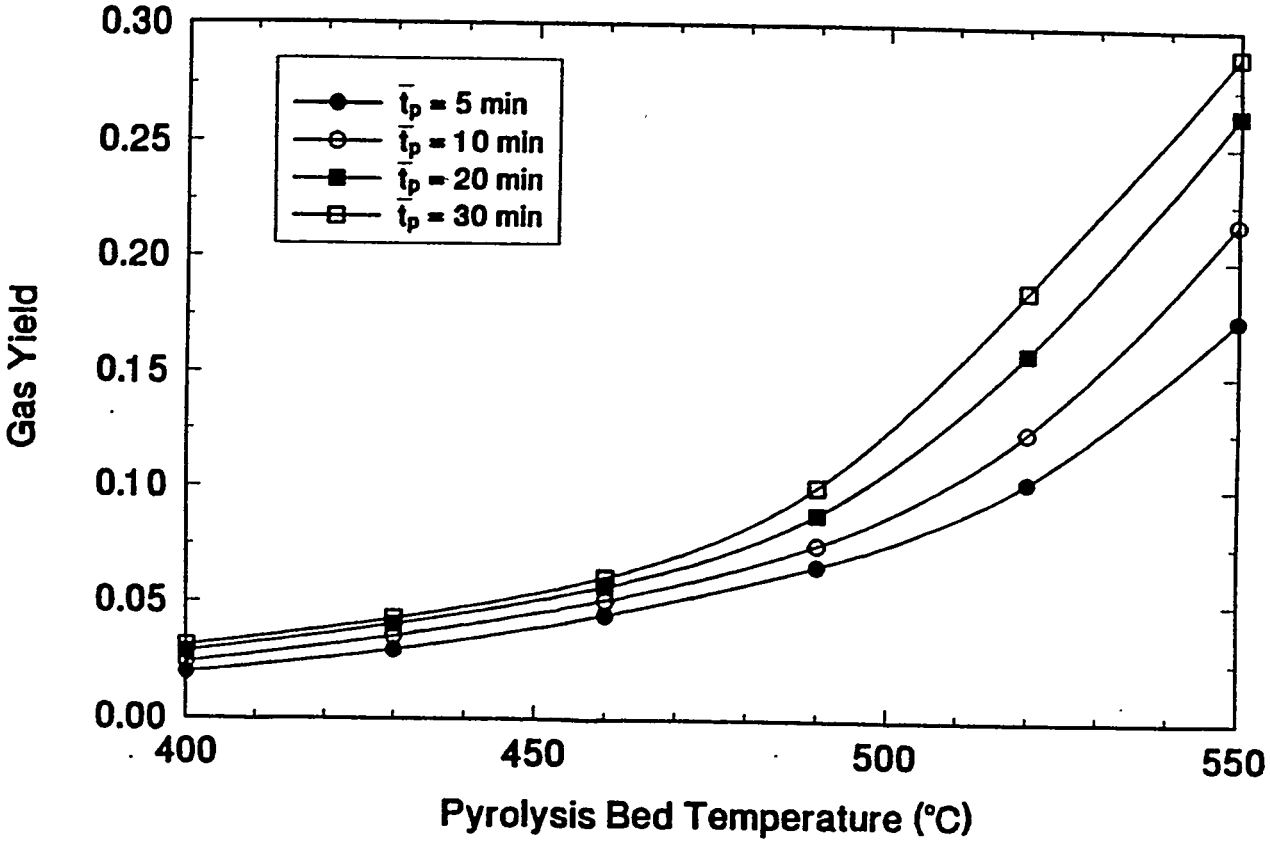

Figure 62. Predicted Light Gas Yield as a Function of Pyrolysis Temperature and Average Solids Residence Time.

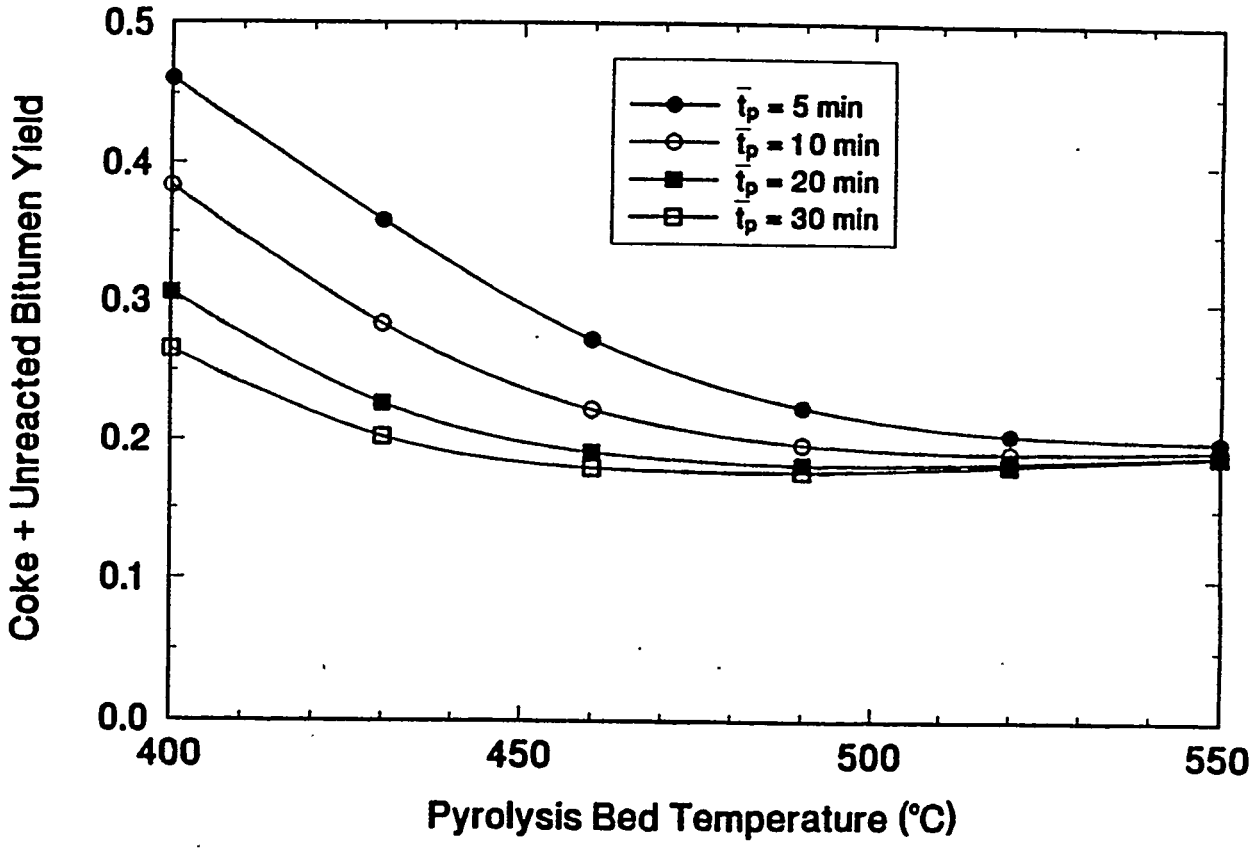

Figure 63. Predicted Yield of Coke + Unreacted Bitumen as a Function of Pyrolysis Temperature and Average Solids Residence Time.

temperature exists for all residence times, and decreases with increasing residence time. The overall maximum oil yield is realized at T_p = 713 K and $\bar{t}_p$ = 30 minutes. We see that increasing residence time causes an increase in oil yield at low temperatures, and at high temperatures, increasing residence time causes a decrease in oil yield. The combined effects of pyrolysis temperature and sand residence time on product oil density are shown in Figures 60 and 61. Oil density decreases with both increasing residence time and increasing pyrolysis temperature, although the effect of residence time is slight at lower temperatures.

Vapor-phase cracking reactions (Equations 63 and 64) apparently are slow, except at higher temperatures. Even at high temperatures, vapor-phase cracking is quite slow at small sand residence times. However, as sand residence time is increased, gas-phase residence time also increases, since the gas has a deeper bed to travel through. Thus, vapor-phase cracking becomes more significant with a deeper bed.

Light gas is produced both by solid-phase cracking reactions and by vapor-phase cracking reactions. However, it is produced in greater quantity by the vapor-phase reactions. For example, compare s_H and s_M in Table 26. Thus, we expect greater light gas yield under the same circumstances listed above for inducing a lighter oil product: high pyrolysis temperature, coupled with high gas-residence time caused by a deeper bed, caused by a high solids

residence time. This is borne out by the results shown in Figure 62.

The yields of unreacted bitumen and coke are shown in Figures 63 and 64. Conversion of bitumen is quite high except for both low T_p and low $\bar{t}_p$, a result of the solids in the bed being well mixed. It is interesting to note that at temperatures above 723 K, the total of coke + unreacted bitumen is nearly independent of both residence time and temperature.

The effect of fluidizing gas flowrate on oil yield and oil density is shown in Figure 65. At high pyrolysis temperature, increasing fluidizing gas velocity causes a modest increase in oil product yield, and a simultaneous increase in oil density. Again, this is related to the residence time of the gas phase.

The effects of changing oil sand feed rate, while holding sand residence time constant, are shown in Figures 66-69. Changing the feed rate is conceptually similar to adjusting bed height, while holding all other parameters constant, as shown in Figure 66. Thus, we expect that a deeper bed will not affect coke yield and bitumen conversion and will influence oil yield and density only at the high temperatures at which the vapor-phase cracking reactions become significant. This is verified in Figures 67-69.

Note that gas-phase cracking reactions may continue in the freeboard, the open region in the reactor above the sand bed. After the gas exits the bed, but before the oil vapors are condensed, it is still at the same pyrolysis temperature characterizing the bed, and so is subject to the same gas-phase

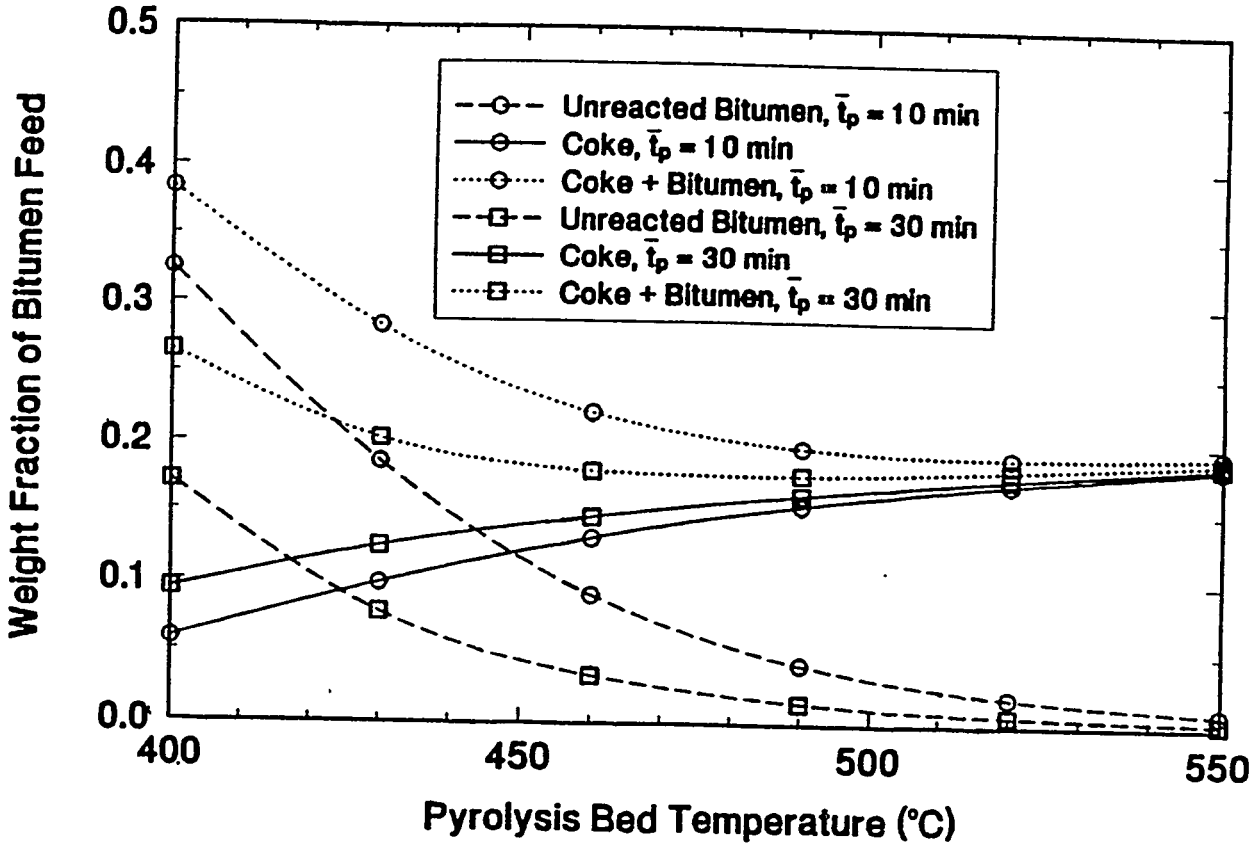

Figure 64. Predicted Coke Yield and Bitumen Conversion as a Function of Pyrolysis Temperature and Average Solids Residence Time.

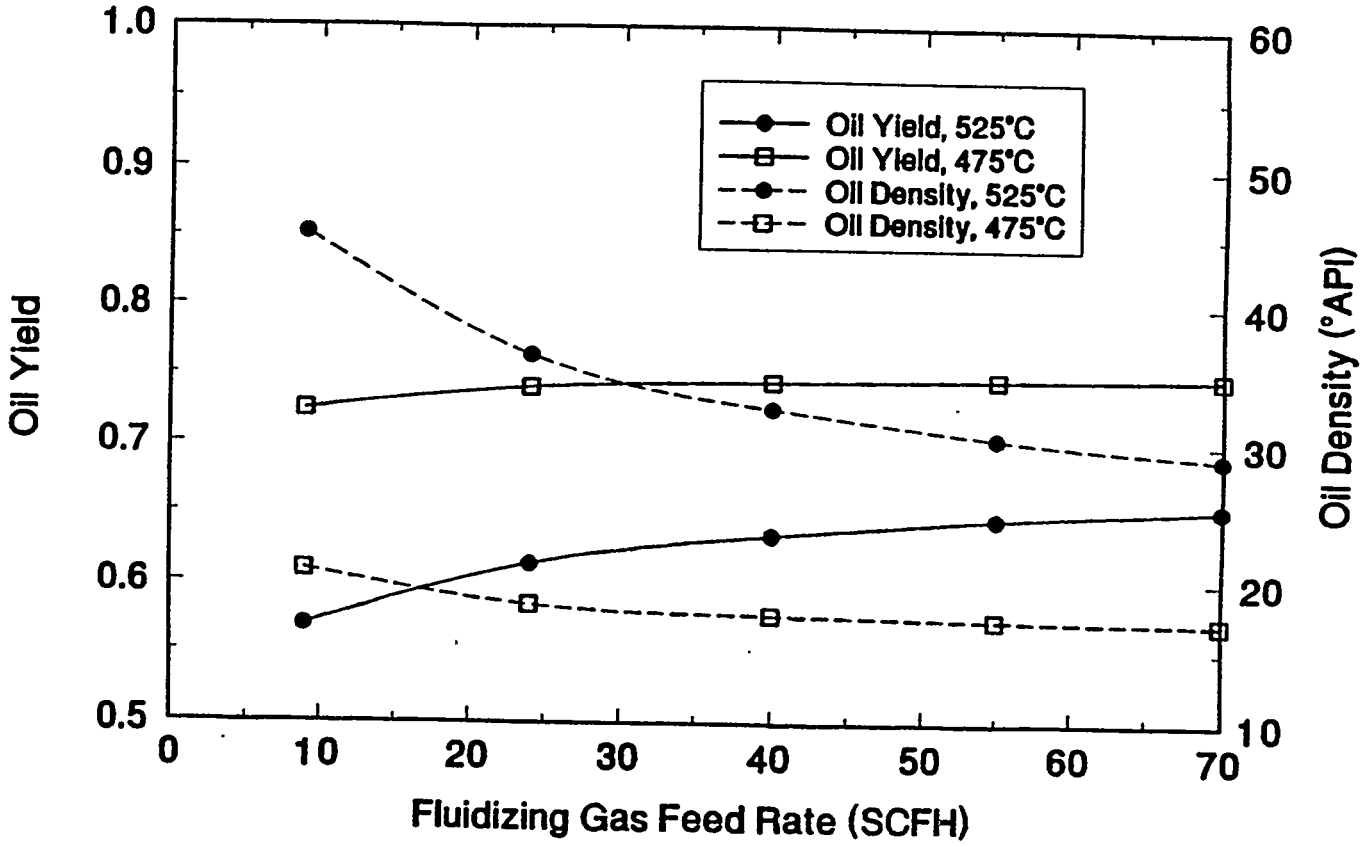

Figure 65. Predicted Oil Yield and Density as a Function of Pyrolysis Temperature and Fluidizing-Gas Flow Rate; $\bar{t}_p$= 20 Min.

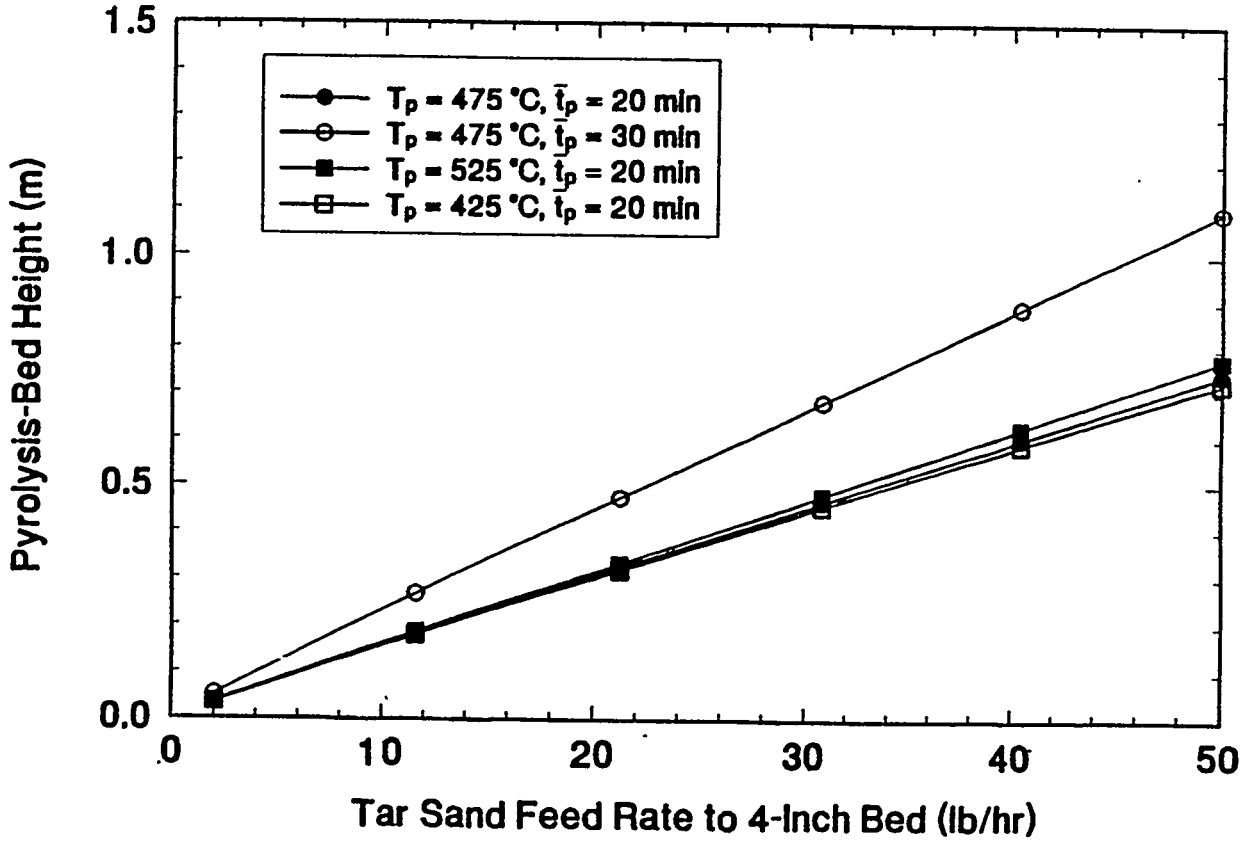

Figure 66. Predicted Bed Height as a Function of Oil-Sand Feed Rate, Pyrolysis Temperature, and Average Solids Residence Time.

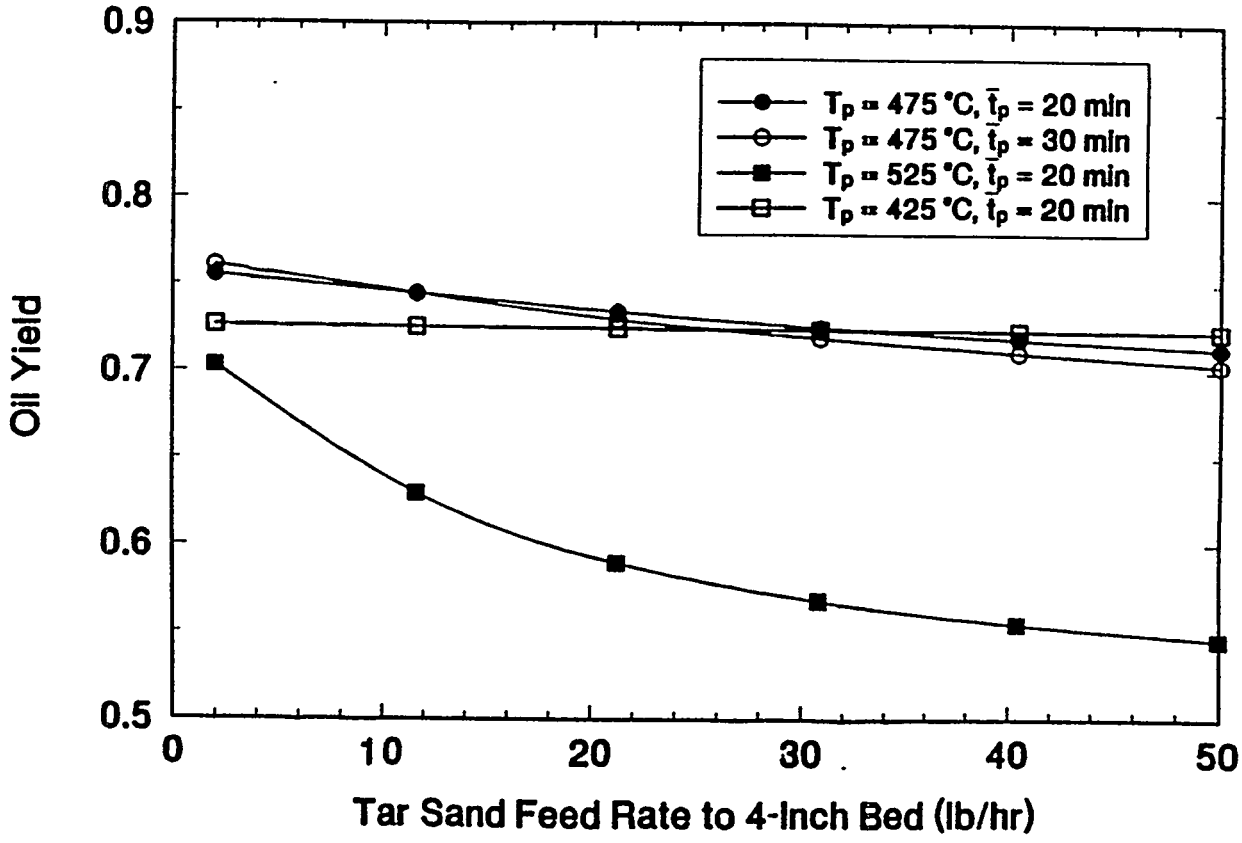

Figure 67. Predicted Oil Yield as a Function of Oil-Sand Feed Rate, Pyrolysis Temperature, and Average Solids Residence Time.

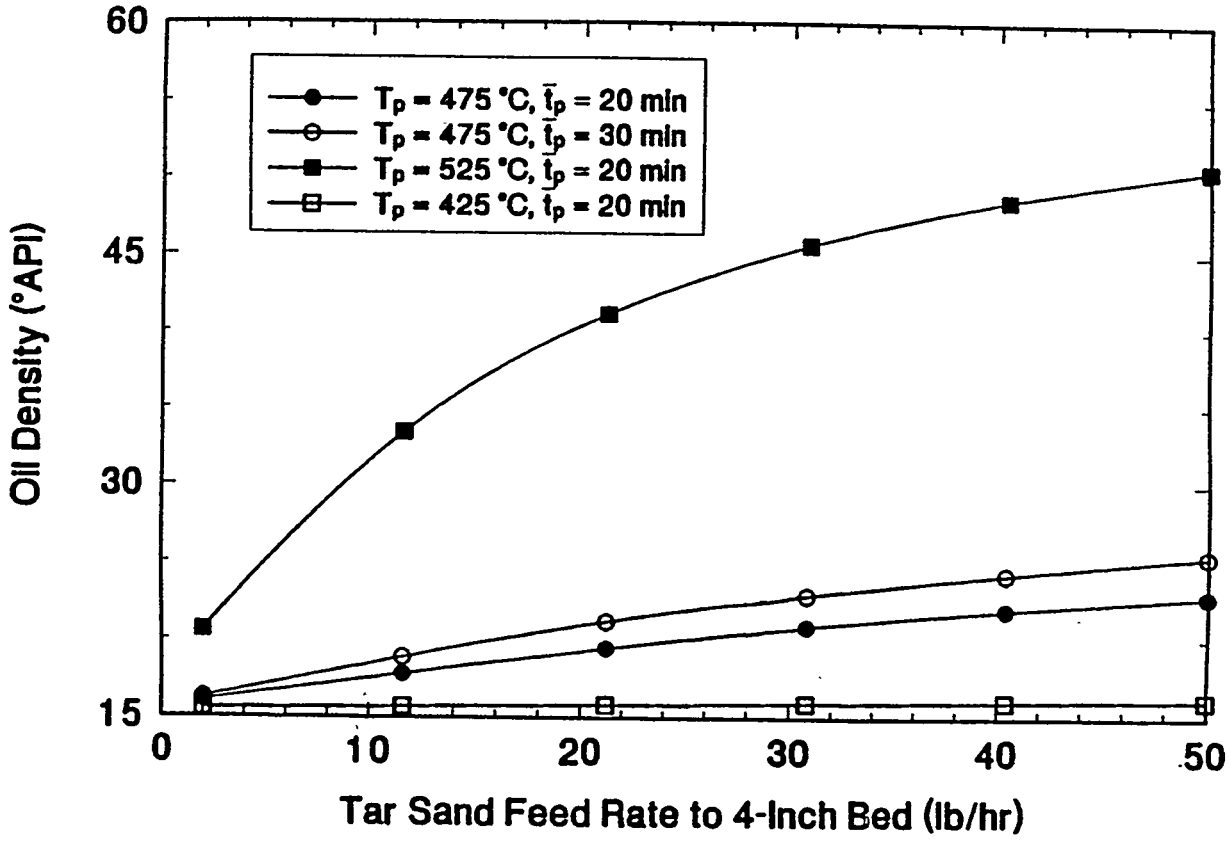

Figure 68. Predicted Oil Density as a Function of Oil-Sand Feed Rate, Pyrolysis Temperature, and Average Solids Residence Time.

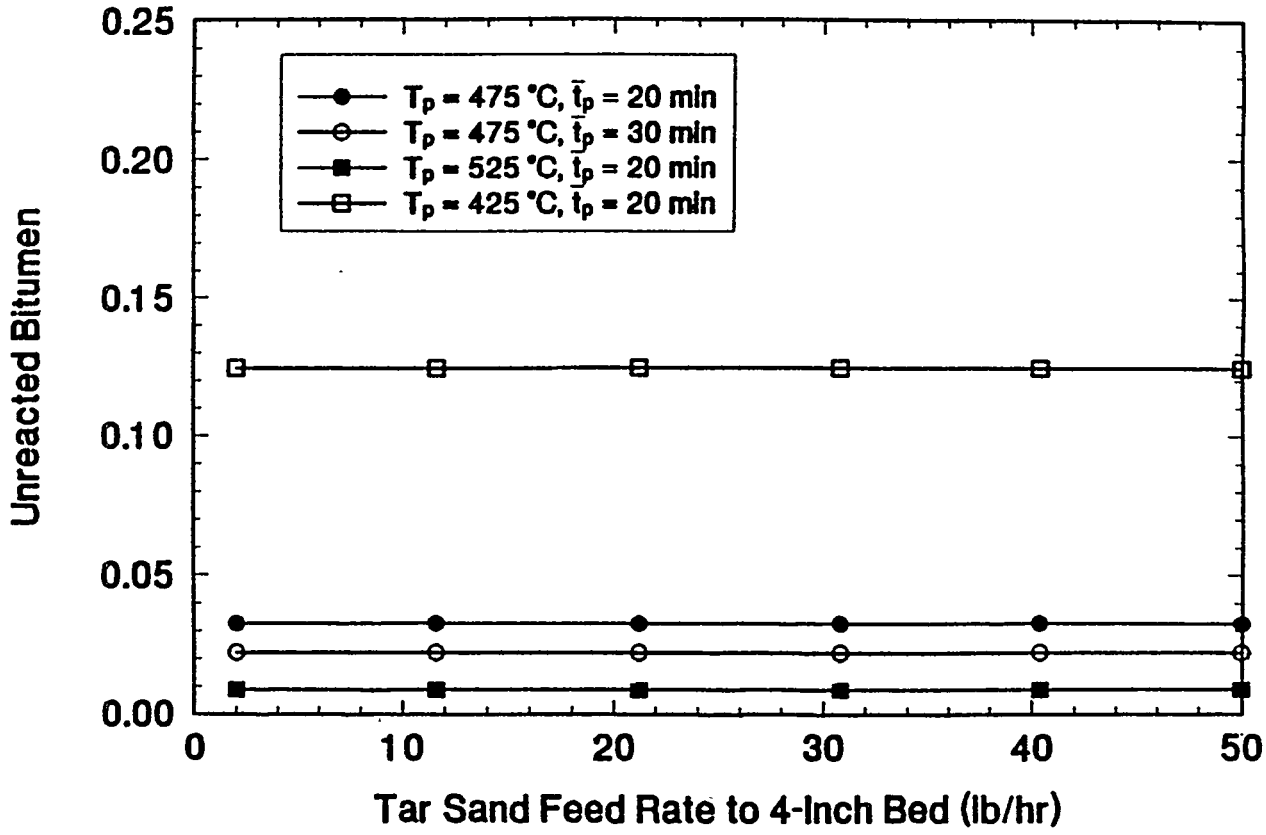

Figure 69. Predicted Bitumen Conversion as a Function of Oil-Sand Feed Rate, Pyrolysis Temperature, and Average Solids Residence Time.

reactions that may occur in the bed. If we assume that the reactor vessel is of a constant height, then gas-phase cracking reactions observed in deeper beds may well occur in the freeboard above shallow beds. Thus, the decreased oil yield and oil gravity shown in Figures 67 and 68 at T_p = 798 K may be misleading. Quite possibly, the condensed oil product may be independent of the pyrolysis-bed depth, although the oil product at the top of the bed is dependent on bed depth. If gas-phase cracking reactions continue throughout the freeboard, the condensed oil product will most resemble that of the deepest bed.

Thus far, the parameters considered have been related to the operation of the pyrolysis bed: T_p,$\bar{t}_p$, F, and W. However, it is well-known that the characteristics of the different tar-sand bitumens can have a significant effect on the pyrolysis products. The only two physical characteristics of the oil sand considered in this model are x_{BO} and w_{HBO}. According to the reaction network described in Equations 62-67, the bitumen content of oil sand, x_{BO}, does not affect the reactions. Its only influence on the hydrodynamical model is the influence on the solids density. Thus, it is not surprising that x_{BO} has no appreciable effect on pyrolysis product yields or quality.

On the other hand, w_{HBO} directly influences the reaction rates by determining $\bar{w}_{HB}$ and $\bar{w}_{LB}$ by Equations 89 and 90. This parameter characterizes the bitumen itself in terms of boiling point and should determine the relative rate of production of heavy oil, light gas, and coke. Figure 70 shows that oil yield decreases with

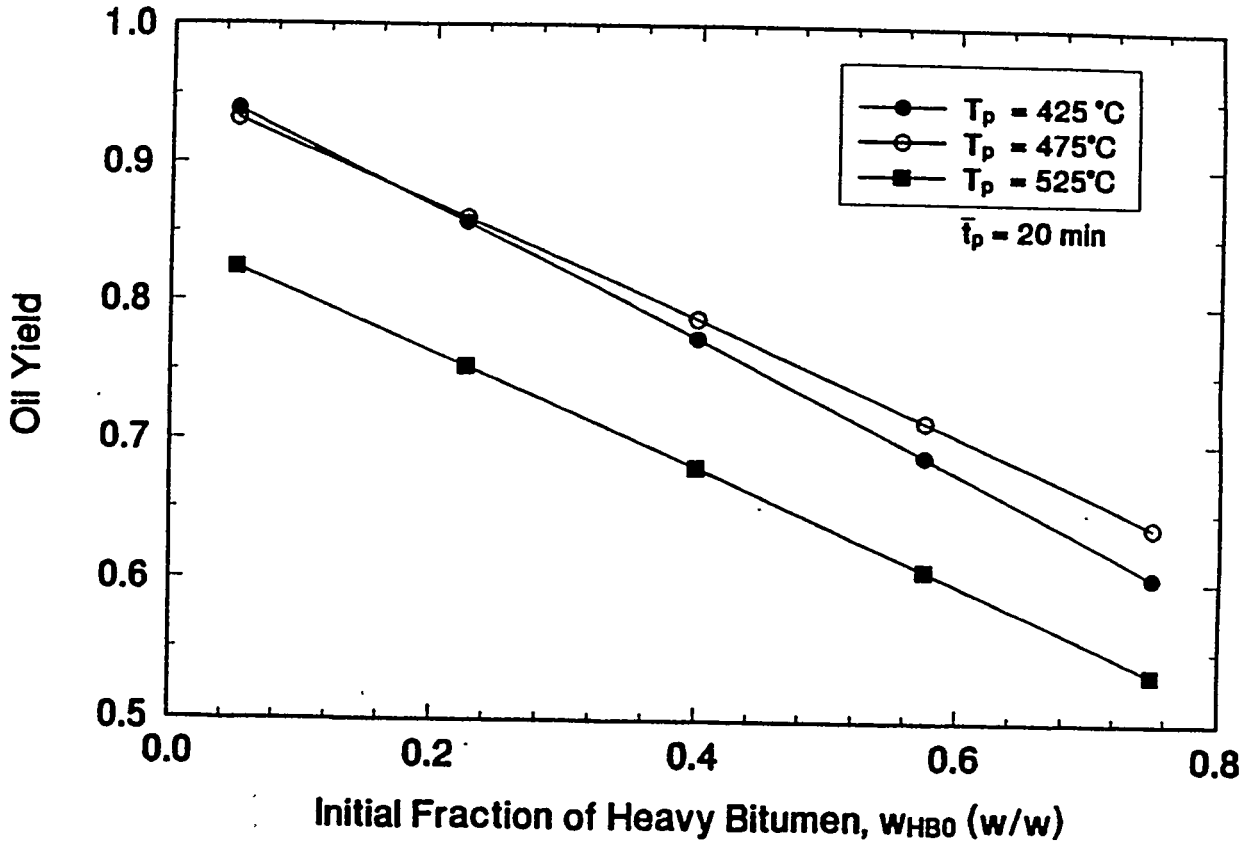

Figure 70. Predicted Oil Yield as a Function of Bitumen Quality and Pyrolysis Temperature; $\bar{t}_p$= 20 Min.

increasing w_{HBO} at three pyrolysis temperatures. The rate of decrease is greatest at the lowest temperature. This is because the formation of light bitumen from heavy bitumen, reaction 2 or Equation 60, takes place at a relatively higher temperature than reaction 4. Thus, as w_{HBO} increases, a greater fraction of the bitumen must go through this higher-temperature reaction pathway. On the other hand, oil yield is greatest at low w_{HBO} for the lowest temperature considered. This is because reaction 4, the "distillation" reaction, occurs quite quickly even at lower temperatures, so that as w_{HBO} decreases, nearly all of the bitumen is volatilized. All the bitumen is volatilized at the higher temperatures as well, but the gas-phase cracking reactions become more significant, and consequently, reduce oil yield. The combined effects of bed temperature and average solids residence time on oil yield is shown in Figures 71 and 72 at a very low w_{HBO} and a very high w_{HBO}, respectively. It is interesting to compare these with Figure 59, where $w_{HBO} = 0.5$. In general, as the fraction of heavy bitumen increases, oil yield is maximized at higher temperatures.

It is remarkable that oil yields in excess of 90% are predicted for very low w_{HBO} and temperatures $\leq$ 748 K. This coincides well with the recent experimental work done by Fletcher[134] who found oil yields as high as 90% for experiments done on Whiterocks oil sands. Whiterocks stands out among the various deposits as the one with the lowest overall asphaltenes content; it has been reported to be as low as 5%.[134] Thus, there may be some relationship between asphaltenes content and w_{HBO}.

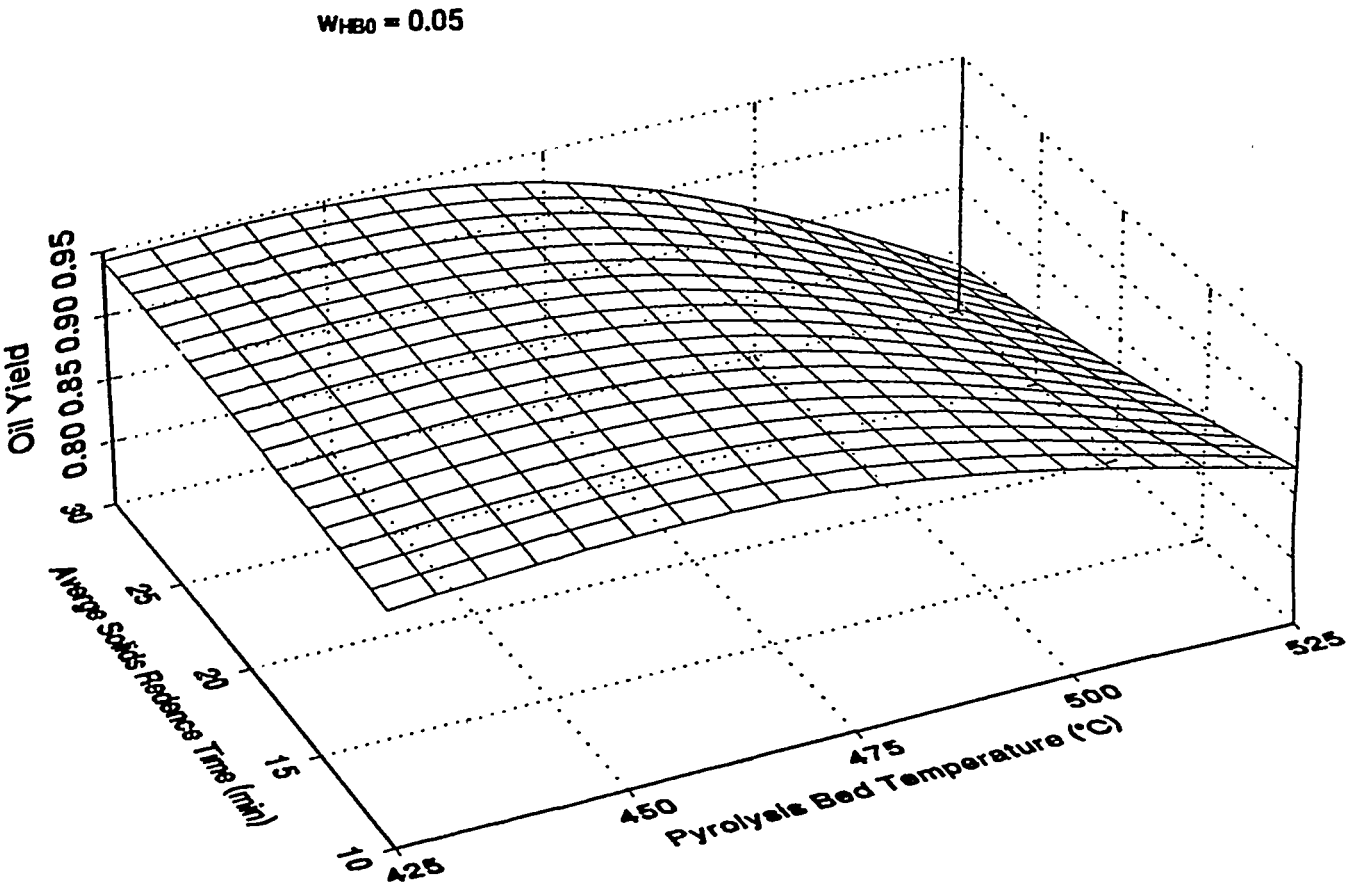

Figure 71. Predicted Oil Yield as a Function of Pyrolysis Temperature and Average Solids Residence Time; w_{HBO} = 0.05.

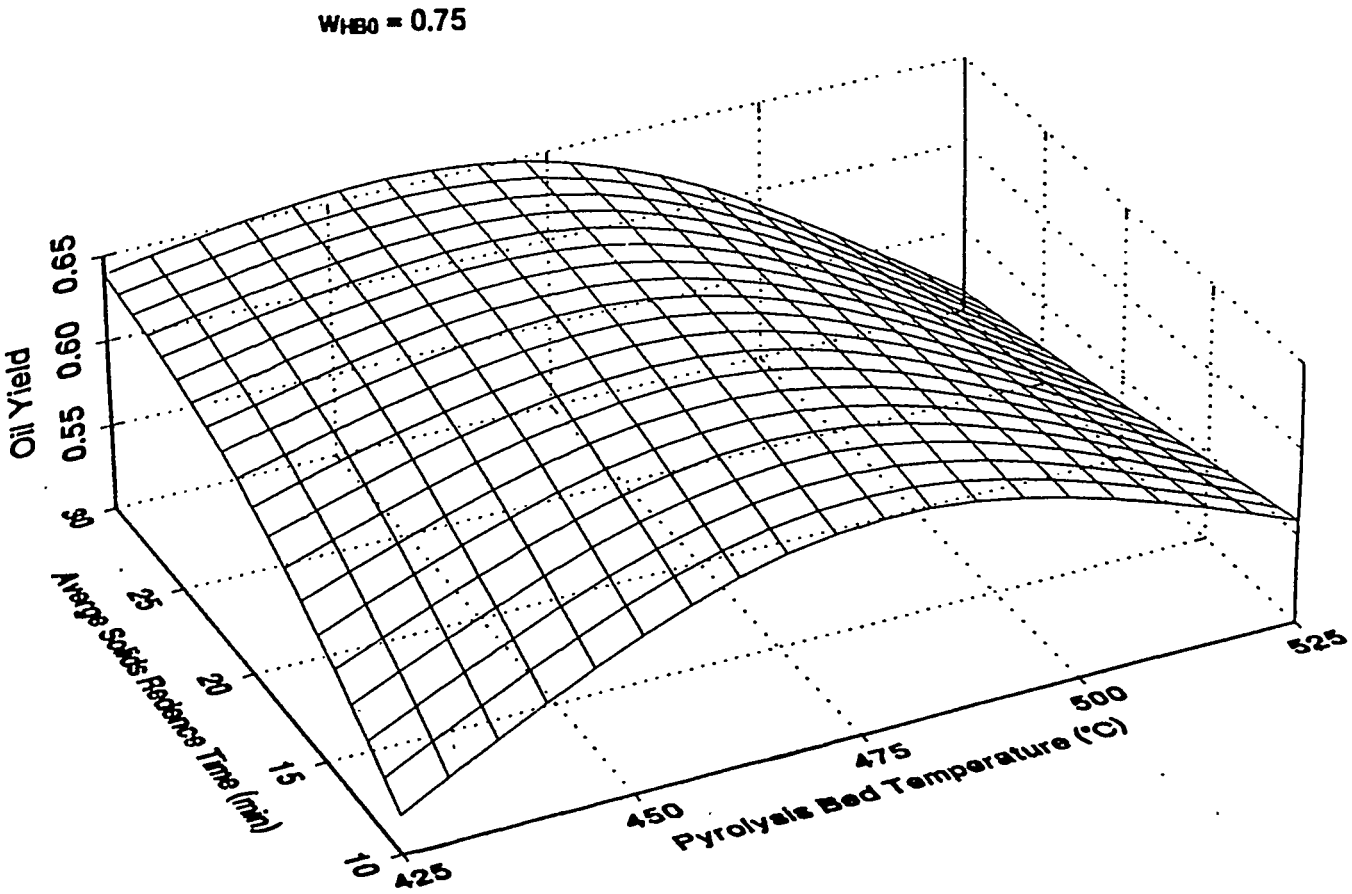

Figure 72. Predicted Oil Yield as a Function of Pyrolysis Temperature and Average Solids Residence Time; W_{HBO} = 0.75.

Based on the discussion above regarding the influence of w_{HBO} on the pyrolysis product distribution, one would expect that increasing w_{HBO} would increase product oil density. However, predicted oil density is independent of initial bitumen heavy fraction. At a constant temperature and residence time, the reaction network allows no provision for influencing the relative fractions of oil produced. This clearly illustrates a deficiency in the reaction network presented above. Perhaps stoichiometric coefficients s_E through s_H should have some dependence on bitumen quality. Alternatively, and more simply, the "distillation" of the light bitumen produced from cracking heavy bitumen by reaction 1 might produce an oil biased more towards heavy oil, and the "distillation" products of the light bitumen in the raw oil sand might be biased more in favor of light oil and light gas.

CONCLUSIONS

A mathematical model of a thermally coupled fluidized-bed tar-sands extraction process is developed here. The model incorporates hydrodynamic considerations, mass transport phenomena, and reaction kinetics.

A relationship for the superficial gas velocity is developed, and accounts for the pressure gradient through the bed as well as volumetric changes due to chemical reaction.

A new pyrolysis reaction scheme is developed. It predicts total bitumen conversion, coke production, light gas production, oil yield and oil density. Raw bitumen is characterized by the fraction of "heavy bitumen" that has a boiling point greater than

823 K and may be related to the fraction of asphaltenes present in the bitumen.

The model predicts bitumen yields in general accord with trends observed experimentally. Maximum oil yields are observed at pyrolysis temperatures of approximately 733 K. Oil yield increases monotonically with average sand residence time at low temperatures, but at higher temperatures, first increases, and then decreases with residence time. This high-temperature phenomenon is explained by the increased gas-phase residence time, allowing gas-phase cracking reactions to become significant, which is not a consideration at lower temperatures. This model does not account for gas-phase reactions that may occur in the freeboard, which may be important at pyrolysis temperatures greater than about 773 K.

The fraction of heavy bitumen has a pronounced effect on pyrolysis products. If the bitumen consists of primarily light bitumen, then oil yield is maximized at long sand residence times and low pyrolysis temperatures. However, if the bitumen is dominated by a heavy fraction, then oil is recovered only by first cracking the heavy bitumen. This reaction has a modestly higher activation energy, so a higher temperature is required, and consequently, oil vapors may crack to light gas. To maximize oil yield from heavy bitumens, it may be necessary to use a higher fluidizing gas velocity, in order to limit the oil cracking reactions.

The kinetic model does not predict any dependence of oil density on bitumen quality. This seems to be a deficiency of the

pyrolysis reaction model. This shortcoming may be addressed by making the product stoichiometry of reaction 4 (Equation 62) dependent on either the source of the light bitumen (native or product of reaction 2) or on w_{HBO}.

It remains to solve the four energy balances in Equations 66, 32, 34, and 35 for T_p, T_c, T_a, and T_{hp}, respectively. The solution of the pyrolysis model determines the quantity of unreacted bitumen and coke that will enter the first combustion bed. The amount of coke burned in the first combustion bed (and in the second combustion bed) is determined in large part by the amount of coke entering, which then affects T_c, T_{hp}, and finally T_p. Thus, an iterative procedure is indicated, where at first, a pyrolysis temperature is assumed. Then the pyrolysis model is solved, the first-stage combustion model is solved, the heat-pipe temperature is found, and again, the pyrolysis model is solved, this time finding a new T_p. The second-stage combustion model would be solved after the coupled model has iterated to convergence.

Finally, the completed coupled model may be submitted to a rigorous optimization procedure. An objective function to be optimized might be oil yield, or revenues from oil sales, where oil quality is a concern, or perhaps operating or capital costs, or plant profitability.

INTERNAL MODEL CONTROL STRATEGY FOR TEMPERATURE CONTROL

A two-stage, thermally coupled fluidized-bed reactor system has been developed for energy-efficient conversion of tar-sand bitumen to synthetic crude oil.[24,126] In the first reactor, the

bitumen is pyrolyzed at 723-823 K to condensible crude oil and a light gaseous product. Coke, formed as a byproduct from the pyrolysis reaction, and left behind on the sand, flows into the second reactor and is combusted with air at 823-923 K. Excess energy generated by the combustion reaction is then transferred by liquid-potassium-containing heat pipes to the first reactor, providing the energy required by the pyrolysis reaction and the preheat for bringing the tar-sand feed to operating temperature. The use of the heat pipes causes significant thermal interaction between the two reactors with a relatively large time constant. As a result, precise regulation of the reactor temperatures becomes a complicated control problem.[132]

Despite many advanced control strategies proposed in the last 20 years, the majority of controllers used in the chemical industry are still of proportional-integral-derivative (PID) type. It is recognized that most of the major advanced feedback control algorithms to date can be converted into some form of the PID algorithm.[154-156] Also, a well-tuned PID controller can do better than most advanced control algorithms for unmeasured load disturbances.[157] Hsu and Seader[132] employed various control schemes, including PID control, deadbeat algorithm, Dahlin's method,[158] and Kalman's approach[159] to regulate temperatures of a tar-sands processing system. They found that the PID algorithm yielded the best control performance, although it was difficult to determine the optimum tuning settings. Even though several tuning techniques, such as continuous cycling and reaction curve

methods,[160] are widely used to determine controller settings, the best settings are normally difficult to obtain and, thus, lengthy on-line tuning may be necessary.

In recent years, Rivera et al.[155] introduced a PID tuning technique based on an Internal Model Control (IMC) structure that has received much attention.[161-163] The IMC scheme has a number of advantages over conventional PID tuning methods. For example, it uses only one tuning parameter (closed-loop time constant, τ_c) that can be adjusted to yield the best compromise between performance and robustness.[164] A larger value of the tuning parameter results in more robust control which, in turn, makes the designed controllers insensitive to model error. Thus, the concept of the IMC structure provides a way to include robustness as a design criterion in an explicit manner. In addition, a simulation study by Chien[165] showed that the IMC-based tuning method was superior to the Ziegler-Nichols and Cohen-Coon tuning methods for set-point responses in deadtime dominant processes; also, it worked very well under severe model mismatch conditions. Chien and Fruehauf[161] also indicated that this tuning technique minimizes controller interactions and enhances overall process disturbance rejection, resulting in no oscillation or overshoot of the closed-loop load response. Therefore, it appeared that a better temperature control of the tar-sands processing system might be obtained via the IMC-based tuning technique.

Although IMC has been studied extensively, most studies are based on simulation or theoretical analysis; very little laboratory

experimental work has been conducted. The study reported here presents digital PID controllers, tuned by the IMC technique, that are used to control temperatures of the oil sands reactor when processing clean sand (not oil sand). Dynamic simulation of the thermal behavior of the reactor system was also carried out at various levels of complexity to illustrate the effect of model error on the control performance. Because the reactor system is thermally coupled and the temperatures are interrelated, this study provides a better understanding of the application of the IMC tuning technique to systems involving process interactions.

EXPERIMENTAL

Reactor system

As shown in Figure 73, the laboratory reactor system consists of two four-inch-diameter fluidized-bed reactors thermally coupled by three potassium-containing heat pipes. In this work, ambient-temperature silica sand was continuously fed into the upper fluidized-bed (i.e., pyrolysis reactor), transported to the lower fluidized-bed (i.e., combustion reactor) by gravity through a standpipe, and then discharged from the bottom of the combustion reactor. Solids retention times (or sand holdups) in the two reactors were regulated by two solids control valves employing a digital PID control algorithm in conjunction with a valve linearization method.[132] Both reactors were equipped with independent electrical heaters to allow for separate temperature control of each reactor. In all test runs, temperatures in the combustion reactor (T_c) were always maintained higher than those in

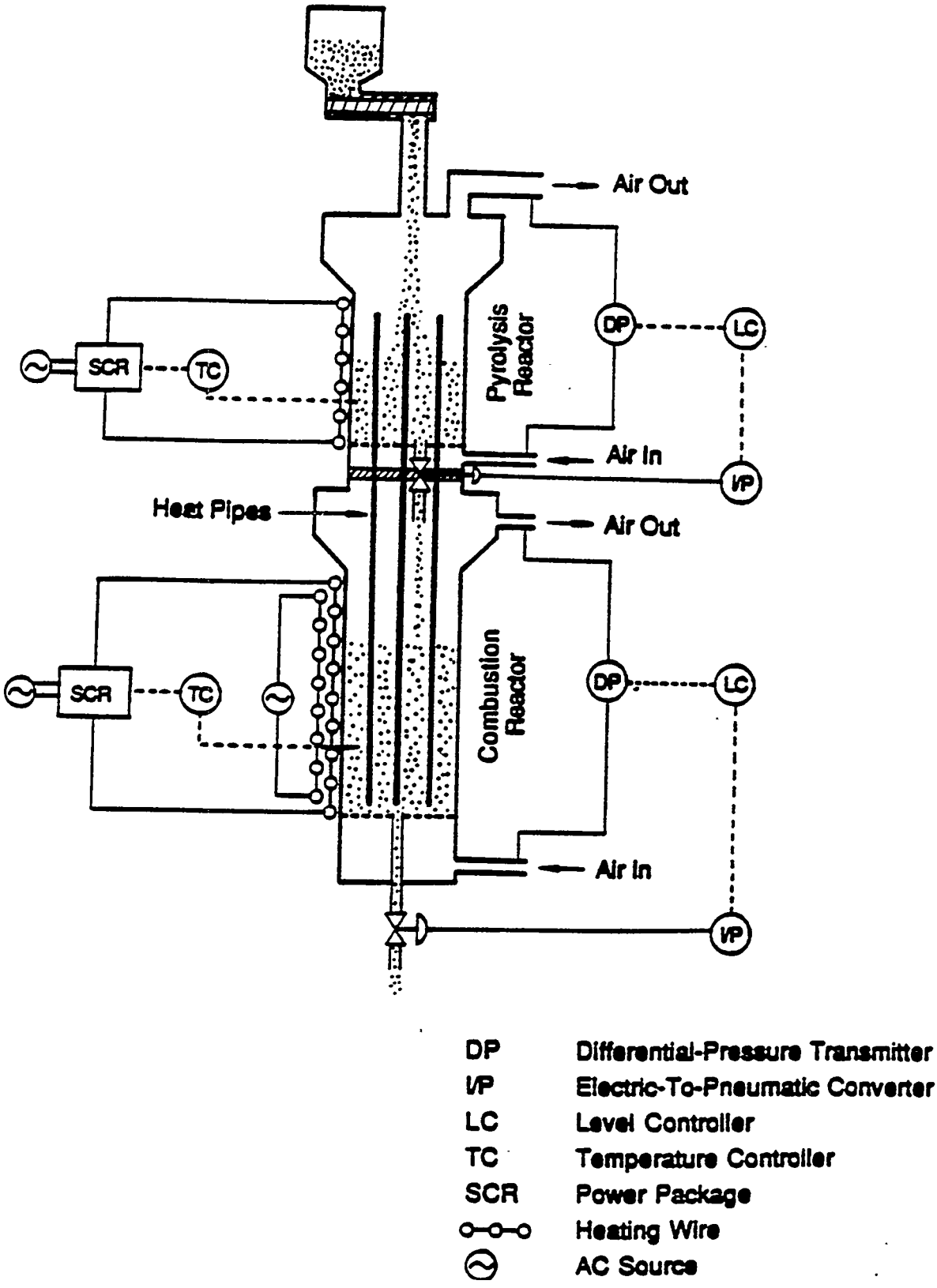

Figure 73. Experimental Apparatus and Instrumentation.

the pyrolysis reactor (T_p). Ambient-temperature compressed air was employed as the fluidizing gas. In the work presented here, only clean sand was fed to the reactor. Thus, no pyrolysis or combustion reaction occurred in the beds.

Control system

A computer control system, consisting of an HP Vectra personal computer and a data acquisition unit, was used for data logging and process control. The system handled communications of control signals and data between the computer and the process via an HPIB (Hewlett-Packard Interface Bus) interface. Two 16-channel thermocouple relay multiplexers (HP E1347A) were employed to provide basic analog-to-digital conversion capability for data logging. One of the multiplexers was used to measure temperature and the other was used to read output signals from four pressure transmitters, which measured the pressure drops across the fluidized beds and maximum pressures below the gas distributors. A 4-channel D/A converter (HP E1328A) was used to provide four independent, isolated channels of digital-to-analog output capacity. Two output channels sent variable voltage signals to the pressure transducers for regulating the two solids control valves. The other two output channels were used to control temperatures in the two reactors by sending variable DCV (direct current voltage) signals to single-phase, phase-angle-fired (SCR) power controllers, which, in turn, regulated ACV (alternating current voltage) to the electrical heaters. All manipulated variables were sent to the process through a zero-order hold.

A computer code was developed for data acquisition and execution of control algorithms. Typical procedures for the process control included: acquisition of online data, noise rejection of the pressure-drop data, comparison of process variables and set points, calculation of appropriate control signals, and transfer of the control signals to the process. Because the sampling period was taken as only 5 seconds, much less than the dominant time constants, the digital control algorithms provided good approximations to continuous controllers. Therefore, the transfer function in Laplace transform notation was used in this control study. Detailed control strategy will be discussed later. The control system was evaluated from the point of view of its ability to handle servo problems. Prior to all test runs, the reactor system was maintained at "hot" conditions (approximately 293 K less than the initial temperature setpoints) overnight to yield better reproducibility.

MATHEMATICAL MODEL

A rigorous mathematical model of the fluidized-bed reactor system has been under development[126]. Although the model can provide a detailed description of the reactor system, it is relatively complex and, thus, is not considered suitable for online control applications of the type discussed here. Instead, a linear time-invariant model was developed for the control study reported here. Since the major purpose of a control model is to provide a basis for evaluating temperature controller settings, only thermal characteristics of the process are of concern.

The primary mechanisms of heat transfer through the three heat pipes are conductive evaporation and condensation. When the heat pipes are in operation, the lower end of each heat pipe is heated to a relatively high temperature causing liquid potassium to vaporize. The vapor then moves at speeds approaching sonic velocity from the lower end to the upper end of the heat pipe, where it condenses at a lower temperature, releasing its latent heat of vaporization. The condensed liquid is then returned to the lower end along a wick on the inside pipe wall by gravity for re-evaporation. Obviously, for the heat pipes to function properly, the temperature of the lower section must be high enough to vaporize the liquid potassium. A test was carried out by slowly increasing the temperature in the lower combustion reactor. It can be seen in Figure 74 that a time delay is generated by the heat pipes before energy is transferred to the pyrolysis reactor. The heat transfer rate through the heat pipes increased rapidly only when the temperature in the combustion bed was above 723 K. Accordingly, initial temperatures in the combustion reactor were at least 723 K for all experiments studied here so that the time-delay behavior at low temperatures was irrelevant. This practice assured that the thermal coupling effect of the reactor system could be adequately addressed.

With the above-described evaporation-condensation cycle, heat pipes can rapidly transport a large amount of heat from the lower section to the upper section with an extremely small temperature gradient[151]. Therefore, it is assumed that the temperature of the

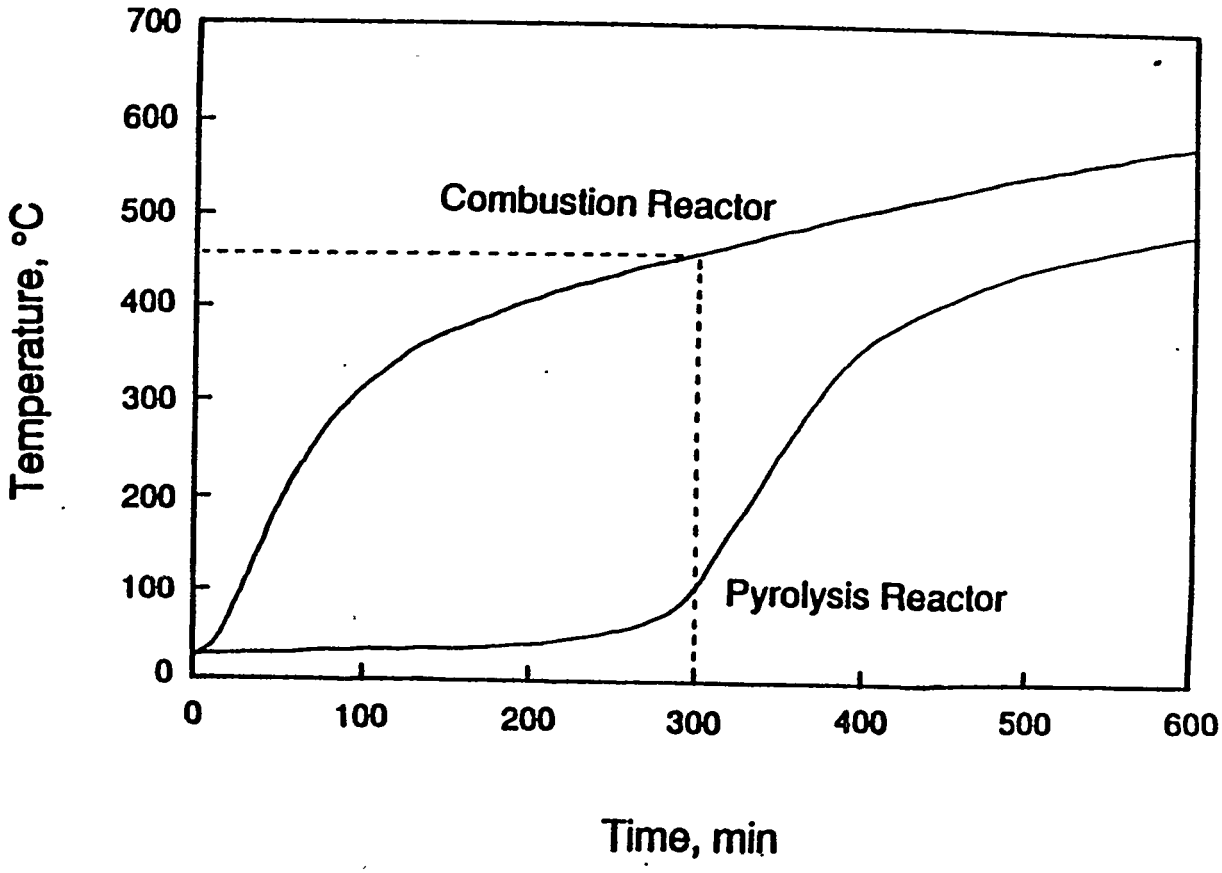

Figure 74. Temperature Responses for Slowly Heating the Combustion Bed from Ambient Temperature.

three heat pipes is uniform. It may be assumed that, within a specific temperature range, the effective thermal conductivity of the heat pipes was greater than that for an equivalent copper rod. In addition, each fluidized bed can be viewed as a continuous stirred tank operated under isothermal constant-holdup conditions with respect to sand flowing through the reactor system. As a result, the whole reactor system can be schematically represented by Figure 75. Thermal resistances to convective and radiative heat transfer between the inside wall of a reactor and its fluidized bed and between the outer surface of a heat pipe and the surrounding fluidized bed were thought to be the most significant and, thus, equivalent convection is the only heat-transfer mechanism considered here. Accordingly, the dynamic energy balances for the two-reactor system are given by

$$M_{s,p}\, C_s\, \frac{dT_{s,p}}{dt} = h_p\, A_p\, (T_{r,p} - T_{s,p}) + h_{h,p}\, A_{h,p}\, (T_h - T_{s,p}) - W\, C_s\, (T_{s,p} - T_{s,o}) - F_{a,p}\, C_a\, (T_{a,p} - T_{a,o}) \tag{103}$$

$$M_{s,c}\, C_s\, \frac{dT_{s,c}}{dt} = h_c\, A_c\, (T_{r,c} - T_{s,c}) - h_{h,c}\, A_{h,c}\, (T_{s,c} - T_h) - W\, C_s\, (T_{s,c} - T_{s,o}) - F_{a,c}\, C_a\, (T_{a,c} - T_{a,o}) \tag{104}$$

$$M_{r,p}\, C_r\, \frac{dT_{r,p}}{dt} = Q_p - h_p\, A_p\, (T_{r,p} - T_{s,p}) \tag{105}$$

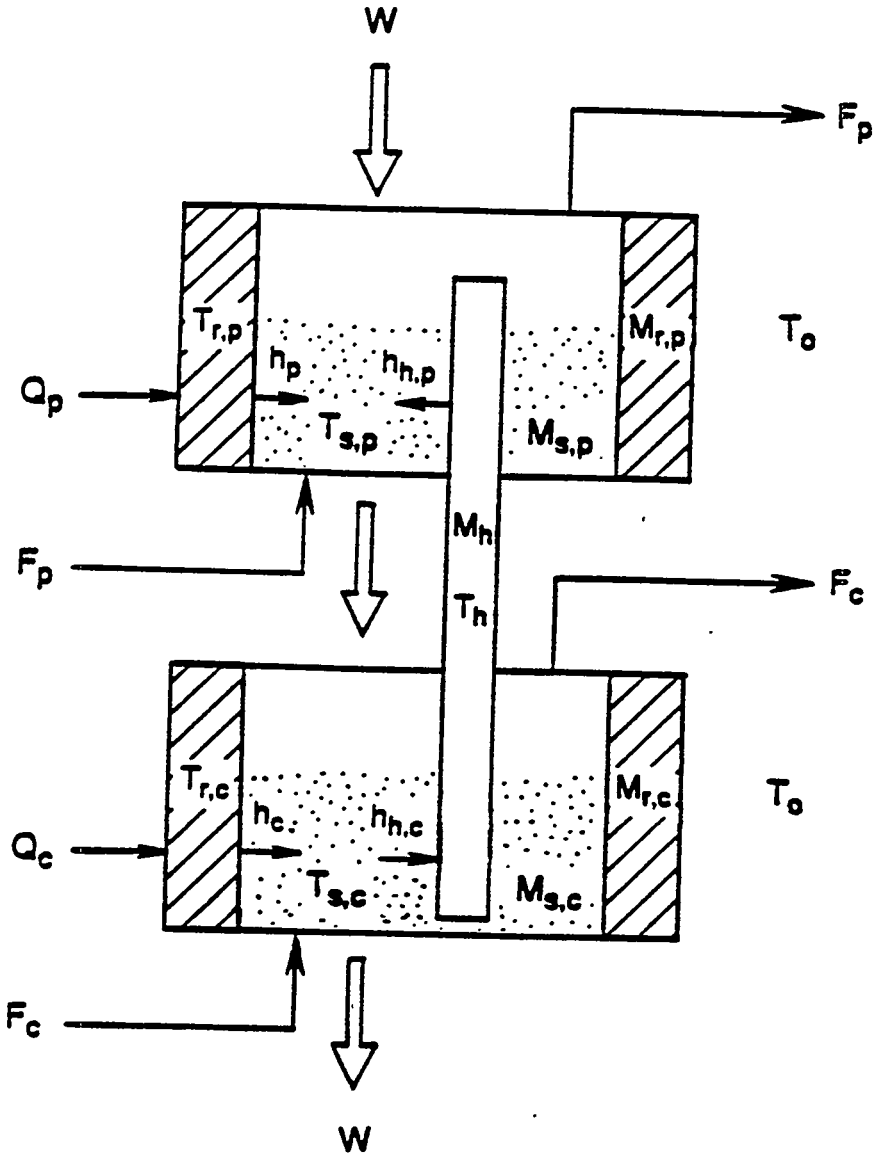

Figure 75. Schematic Representation of the Reactor System for an Energy Balance.

$$M_{r,c}\, C_r\, \frac{dT_{r,c}}{dt} = Q_c - h_c\, A_c\, (T_{r,c} - T_{s,c}) \qquad (106)$$

$$M_h\, C_h\, \frac{dT_h}{dt} = h_{h,c}\, A_{h,c}\, (T_{s,c} - T_h) - h_{h,p}\, A_{h,p}\, (T_h - T_{s,p}). \qquad (107)$$

The energy balances of Equations 103 to 107 represent a relatively rigorous model (called Model 1), and describe in detail the temperature response of two beds, two vessel walls, and the heat pipes. The model is relatively complex making it difficult to incorporate it directly into control algorithms. Since controllers tuned by the IMC tuning method have been found to perform well even with severe model error,[164] a simplified model was sought. Such a model should allow for easy implementation into a control strategy without sacrificing control performance.

Energy conservation Equations 103 to 107 can be simplified by neglecting the reactor energy conservation equations, Equations 105 and 106, and assuming a constant heat input into the beds. Consequently, a simpler reactor model (called Model 2) is formed from Equations 103, 104, and 107, where the first terms on the right hand side of Equations 103 and 104 are replaced by Q_p and Q_c, respectively. In a similar manner, the energy conservation Equation 107 for the heat pipes can be simplified by assuming negligible heat accumulation. Thus, a further simplified model (called, Model 3) is derived from Model 2, with T_h evaluated by the following expression:

$$T_h = \frac{h_{h,c}\, A_{h,c}\, T_{s,c} + h_{h,p}\, A_{h,p}\, T_{s,p}}{h_{h,c}\, A_{h,c} + h_{h,p}\, A_{h,p}}. \qquad (108)$$

Each of the three models, with appropriate parameter values, was used to simulate transient behavior of the reactor system -- the simplest of which was adopted for the control study.

TRANSIENT RESPONSE

Model parameters were determined by best-fitting experimental open-loop step response curves to the model predictions. To obtain the response curves, step changes in electric power inputs, Q_p and Q_c, to the system were made, allowing reactor temperatures to seek new steady-state values. An effort was made to reduce the number of adjustable parameters by exploring the relationship between effective heat-transfer coefficients in the two reactors. Although there have been many empirical correlations proposed to estimate fluidized bed-to-surface heat-transfer coefficients, most of them are not reliable or require knowledge of parameters that are not generally available[159]. Under bubbling fluidization conditions with silica sands, the maximum heat transfer coefficient between an immersed surface (e.g., heat-pipe surface) and a fluidized bed can be estimated by[166]:

$$h_{max} = 35.8\, \rho_s^{0.2}\, k_f^{0.6}\, d_p^{-0.36}. \qquad (109)$$

However, Equation 109 is seldom used directly to calculate a heat-transfer coefficient because the maximum heat-transfer coefficient is normally difficult to realize [166] due to, for example, the disturbance caused to the local fluidization condition

when immersing a tube in the bed. Thus, the proportionality constant, 35.8, might not be appropriate. In this study, the sand-particle density and particle diameter in the two reactors are the same. Thus, the heat-transfer coefficient is mainly affected by air thermal conductivity, which, at near-atmospheric pressure is proportional to the absolute temperature raised to an exponent of 0.84. By substituting this temperature effect into Equation 109 and recognizing that gas and particle temperatures are equal in fluidized beds, the following useful relationship is derived:

$$\frac{h_p}{h_c} = \frac{h_{h,p}}{h_{h,c}} \cong \left[\frac{T_{s,p}}{T_{s,c}}\right]^{0.5}. \qquad (110)$$

Surface area of heat pipes immersed in a fluidized sand bed, vessel wall heat-transfer area, and the mass of the reactor vessel are each assumed to be proportional to sand holdup, i.e.,

$$\frac{A_p}{A_c} = \frac{A_{h,p}}{A_{h,c}} = \frac{M_{r,p}}{M_{r,c}} = \frac{M_{s,p}}{M_{s,c}} \qquad (111)$$

where sand mass holdups $M_{s,p}$ and $M_{s,c}$ can be determined by the set points of bed-level controllers. For a base case, the feed rate of silica sand is about 2.5 kg/hr and the fluidizing air velocities are 45 and 90 SCFH (standard cubic feet per hour) for pyrolysis and combustion reactors, respectively. The sand holdups in the two laboratory reactors are approximately 1.8 and 3.6 kg.

In a typical experiment, electric power to the combustion reactor was suddenly increased by about 18 kcal/min after the system reached a steady state ($T_{s,c}$ = 743 K) at a time arbitrarily

called zero. Reactor temperatures responded rapidly to the small amount of additional heat input and gradually moved to another steady state, as shown in Figure 76 (closed circles and squares). The process dead time was observed to be only about 1 minute, and is negligible in comparison with the process time constant. Therefore, digital PID control algorithms without any dead-time compensation were used throughout this study.

Various adjustable parameters were used, depending on the model selected, to fit the experimental data. The major drawback of the step-response technique is that it assumes the system to be time-invariant. In reality, the two-reactor system is subjected to variations in parameters. For instance, the heat-transfer coefficient is a function of temperature and should not be a constant as temperature changes with time. Nevertheless, time-invariant parameters were assumed and found by fitting data using the maximum-likelihood method. The calculated parameter values are summarized in Table 29, where only those associated with the combustion reactor are presented. The corresponding values in the pyrolysis reactor can be estimated by Equations 110 and 111. The calculated heat input is only about 87% of the electric power to the system, implying a 13% heat loss, despite the heavy insulation used. Nevertheless, Figure 76 shows that all three models give reasonably satisfactory results, with Model 1 fitting the data most closely, and Model 3 fitting the data least closely, as might be expected.

The data points in Figure 77 characterize the response of the two-reactor system to two step increases in heat input, i.e., a

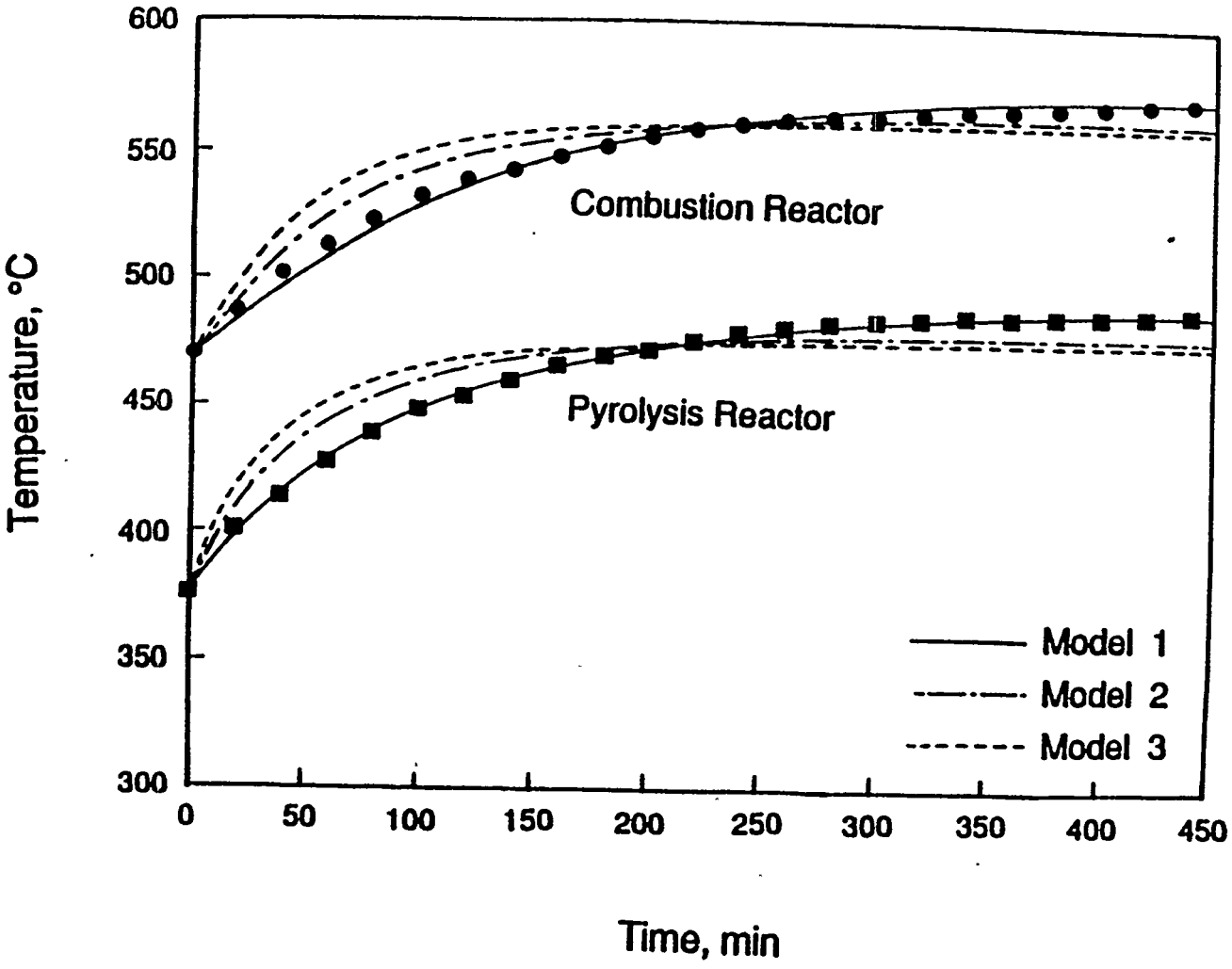

Figure 76. Comparison of Three Models with Experimental Results.

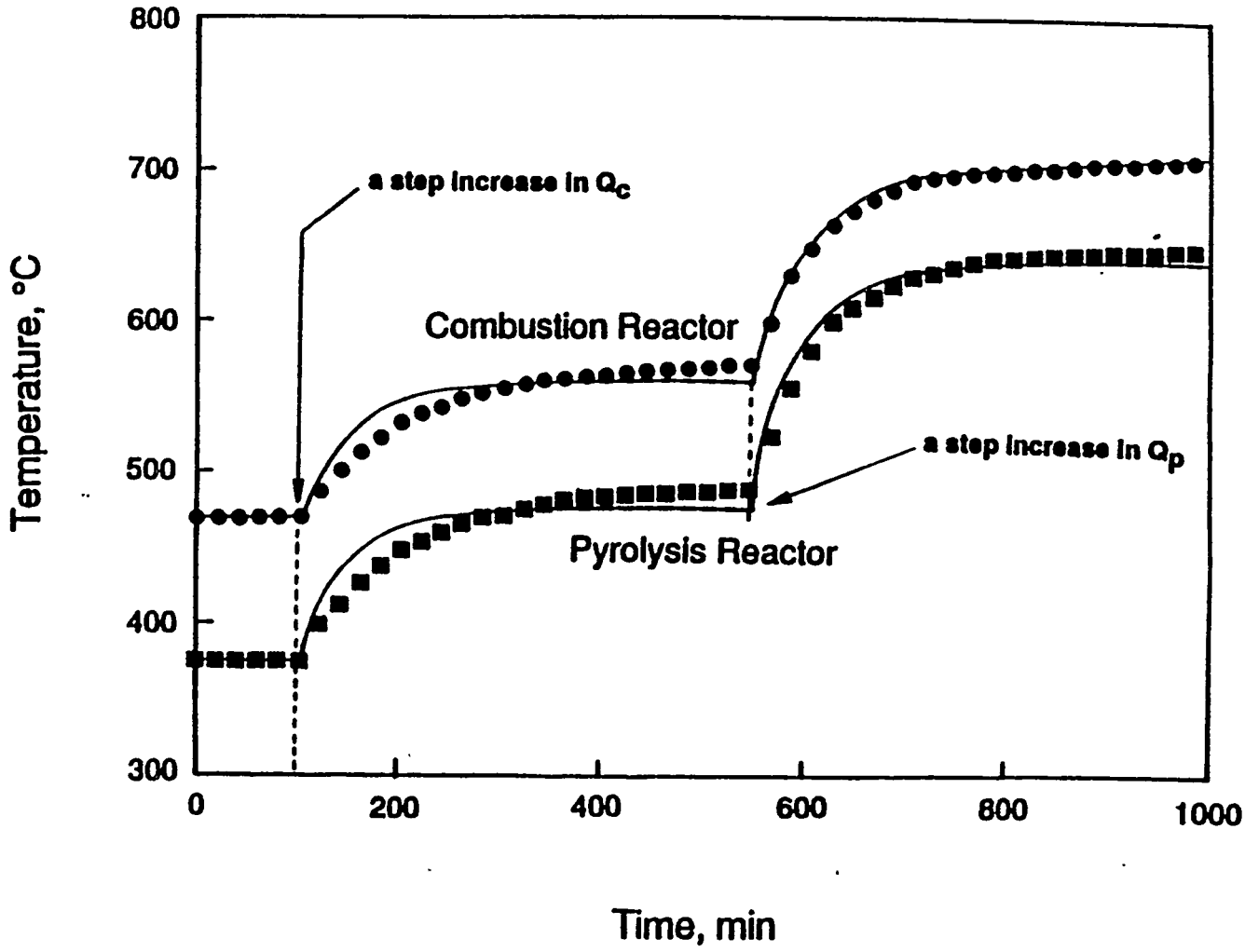

Figure 77. Comparison of Model 3 to Experimental Results for Step Increases in Electrical Power.

step increase in electric power to the combustion reactor at 100 minutes, followed by an electric-power increase to the pyrolysis reactor at approximately 550 minutes. The solid lines in Figure 69 were calculated by Model 3. As can be seen, although heat transfer in the heat pipes is limited to the upward direction from the combustion bed to the pyrolysis bed, an increase in electric power to the pyrolysis reactor not only increases the temperature in the pyrolysis reactor but also the temperature in the combustion reactor. This is possible because a higher temperature in the pyrolysis reactor lowers the rate of energy transfer from the combustion reactor, resulting in an increase in the combustion-reactor temperature. Because the models developed in this study are independent of the direction of heat transfer in the heat pipes, the significance of this test was to evaluate the validity of the proposed models. It was found that Model 3, the simplest of the three models developed above, could, with appropriate adjustable parameter values, predict satisfactorily the dominant static and dynamic behavior of the system. As a result, Model 3 was chosen for the control study reported next.

CONTROL STRATEGY

Transfer function

In this study, individual power input to a reactor is the manipulated variable to control the reactor temperature (i.e., controlled variable). By combining Equation 108 with Equations 103 and 104 to eliminate T_h, Model 3 can be converted to the following mathematical forms:

$$a_1 \frac{dT_{s,p}}{dt} = b_{11}\, T_{s,p} + b_{12}\, T_{s,c} + Q_p' \qquad (112)$$

$$a_2 \frac{dT_{s,c}}{dt} = b_{21}\, T_{s,p} + b_{22}\, T_{s,c} + Q_c' \qquad (113)$$

where a_i and b_{ij} are functions of process variables and model parameters, e.g., $b_{11} = (h_{h,p}\, A_{h,p})^2 / (h_{h,p}\, A_{h,p} + h_{h,c}\, A_{h,c}) - h_{h,p}\, A_{h,p} - WC_s - F_{a,p}\, C_a$. The process variables and model parameters are dependent upon operating conditions. Laplace transforms of Equations 112 and 113 are taken and solved simultaneously resulting in the following process transfer function:

$$t(s) = G_p(s)\, M(s) \qquad (114)$$

where

$$T(s) = \begin{bmatrix} T_{s,p}(s) \\ T_{s,c}(s) \end{bmatrix} \qquad (115)$$

$$M(s) = \begin{bmatrix} Q_p'(s) \\ T_c'(s) \end{bmatrix} \qquad (116)$$

$$G_p(s) = \begin{bmatrix} \frac{a_2\, s - b_{22}}{\Delta} & \frac{b_{12}}{\Delta} \\ \frac{b_{21}}{\Delta} & \frac{a_1\, s - b_{11}}{\Delta} \end{bmatrix} \qquad (117)$$

where $\Delta = a_1a_2s^2 - (a_2b_{11} + a_1b_{22})s + b_{11}b_{22} - b_{12}b_{21}$. T(s) and M(s) are perturbation variables, which represent controlled variables and manipulated variables, respectively. The transfer function is typical of a multiinput/multioutput system (MIMO), i.e., a reactor temperature can be affected by both heat inputs (Q_p and Q_c) to the system. If a_i and b_{ij} are assumed to be constants and the parameter values given in Table 29 are used, Equation 115 becomes

$$G_p(s) = \begin{bmatrix} \frac{295\ s + 37}{133\ s^2 + 48\ s + 1} & \frac{30}{133\ s^2 + 48\ s + 1} \\ \frac{33}{133\ s^2 + 48\ s + 1} & \frac{148\ s + 35}{133\ s^2 + 48\ s + 1} \end{bmatrix} \qquad (118)$$

Based on this example, the process transfer function is second-order lag with time constant $\tau \cong 12$ minutes and damping coefficient of 2 (overdamped system). Due to the relatively large time constant and the significant thermal coupling effect, precise temperature regulation of the process becomes difficult.

Controller design

The presence of process interactions generally leads to a degradation of the control system performance. The classic approach to MIMO control problems is to incorporate decouplers into the control system. However, the success of the decoupler design largely relies on the accuracy of a process model and, thus, is very sensitive to the mismatch between the model and the real process[167]. This feature seriously limits its application because an exact process model is normally difficult to obtain. Other multivariable control schemes based on IMC have been proposed,[164,168] but are difficult to apply to the system of this study.

Alternatively, the velocity form of the PID control algorithm, with settings determined by the IMC tuning technique, was adopted. It was anticipated that with this control strategy, the requirements of an exact process model and complicated decoupling design could be avoided, providing a simple control strategy for MIMO control. The detailed procedure and the justification are as follows:

1. Two separate digital PID controllers are used for the temperature control. The Relative Gain Array (RGA) of the system in Equation 118 is:

$$\text{RGA} = \begin{bmatrix} 0.56 & 0.40 \\ 0.44 & 0.56 \end{bmatrix} .$$

Based on this RGA, it is determined that $T_{s,p}$ and $T_{s,c}$ should be paired with Q_p and Q_c, respectively.

2. The changes in reactor temperatures resulting from heat transfer through the heat pipes are not controllable and, thus, are regarded as load disturbances. Accordingly, the thermal coupling effect (i.e., off-diagonal elements in the RGA) is treated as an unmeasured disturbance in developing the control algorithm.

3. By neglecting the off-diagonal elements in Equation 117, the transfer function becomes a second-order-lag-plus-first-order lead model:

$$G_p(s) = \begin{bmatrix} \dfrac{k_p\ (\beta_p\ s + 1)}{\tau^2\ s^2 + 2\ \tau\ \zeta\ s + 1} \\ \dfrac{k_c\ (\beta_c\ s + 1)}{\tau^2\ s^2 + 2\ \tau\ \zeta\ s + 1} \end{bmatrix} \qquad (119)$$

The constants k_c, k_p, β_c, β_p, τ, and ζ are defined here by comparison with the elements on the main diagonal in Equation 118. This

decoupling, of course, causes serious modeling errors. However, a major advantage of the IMC tuning technique is that it can perform well despite serious model mismatch conditions. Therefore, satisfactory control performance might be achieved despite this simplification.

4. The transfer function of the digital PID controllers is based on the following form, which includes an "optimal" roll-off element[164].

$$G_c(s) = K_c \frac{1 + (\tau_i s)^{-1} + \tau_d s}{\tau_f s + 1} \qquad (120)$$

By following the straightforward two-step IMC controller design procedure[155], the digital PID controller settings can be calculated from the process model, i.e., Equation 119, via

$$K_c = \frac{2\tau\zeta}{k\tau_c} \qquad \tau_i = 2\tau\zeta \qquad \tau_d = \frac{\tau}{2\zeta} \qquad \tau_f = \beta. \qquad (121)$$

5. Controller tuning settings can be calculated from Equation 121, provided that the value of τ_c is known. This so called closed-loop time constant is the only tuning parameter, specified by the user, which determines the closed-loop speed of response. A smaller τ_c gives a faster return to the temperature set point while a larger τ_c results in slower response. Although a larger τ_c sacrifices performance, it can tolerate greater modeling errors and minimize control-loop interactions. Thus, with a proper choice of τ_c, the PID controllers can satisfy performance requirements, but still allow some modeling errors as well as

process interactions. Thus, even though the thermal coupling effect is not explicitly considered in developing the control algorithm (see procedure 2) the effect is indeed taken into account by adjusting the controller tuning settings.

6. The RGA is employed here to help determine the proper value of τ_c. When the model error and process interactions are significant, which is indicated by large off-diagonal elements in the RGA, the value of τ_c should be increased to enhance the controller robustness. Thus, depending on the magnitude of RGA, a proper τ_c value might be chosen.

7. The parameters of the process model are automatically adjusted based on operating conditions to account for the nonlinear and time-variant nature of the reactor system. The idea is very similar to predetermined adaptive controllers, where the adaptation rule is determined as part of the control system design. One example is the electric power (i.e., V^2/R) to the reactor system, which is regulated by SCR power controllers. At low output voltage (ACV), a small change in DCV signal to the SCR produces only a modest change in the electric power while the same DCV change will produce a relatively large change in the power in the high voltage range. Thus, the process gain, in this case the ratio of a change in the electric power to a change in the DCV signal, increases rapidly as the ACV increases to its maximum value (i.e., 110 V). Since their relationship is reasonably well understood, it is possible to compensate for this change in process gain in a predetermined manner.

PROCESS TEST

Control performance was evaluated based on transient responses of the two reactor temperatures to set-point changes. Temperatures in the pyrolysis (T_p) and combustion (T_c) reactors were controlled according to the following sequence over a 6-hour period:

1. T_p=748 K, T_c=773 K
2. T_p=748 K, T_c=823 K
3. T_p=798 K, T_c=823 K
4. T_p=848 K, T_c=873 K

The control objective was to force the reactor temperatures to track their setpoints quickly and smoothly.

For IMC-based controllers, the choice of a closed-loop time constant, τ_c, has a strong influence on the control results. Chien and Fruehauf[161] suggested τ_c values between the open-loop dominant time constant and the process dead-time. On the other hand, Morari and Zafiriou[164] indicated that τ_c should be selected at least greater than one-tenth of the process time constant τ. For our study purposes, the tuning parameter, τ_c, was selected to be one-half of the process time constant (i.e., ~6 minutes). Then, PID controller settings were calculated by Equation 121. The resulting PID control with the calculated settings is shown in Figure 78, where the reactor temperatures fluctuate and cannot reach steady-states values within the test period. Small, but vigorous, temperature fluctuations (i.e., within ±3°C) were observed during the test run, caused by one or more of a number of possible causes (e.g., oscillatory sand holdups,

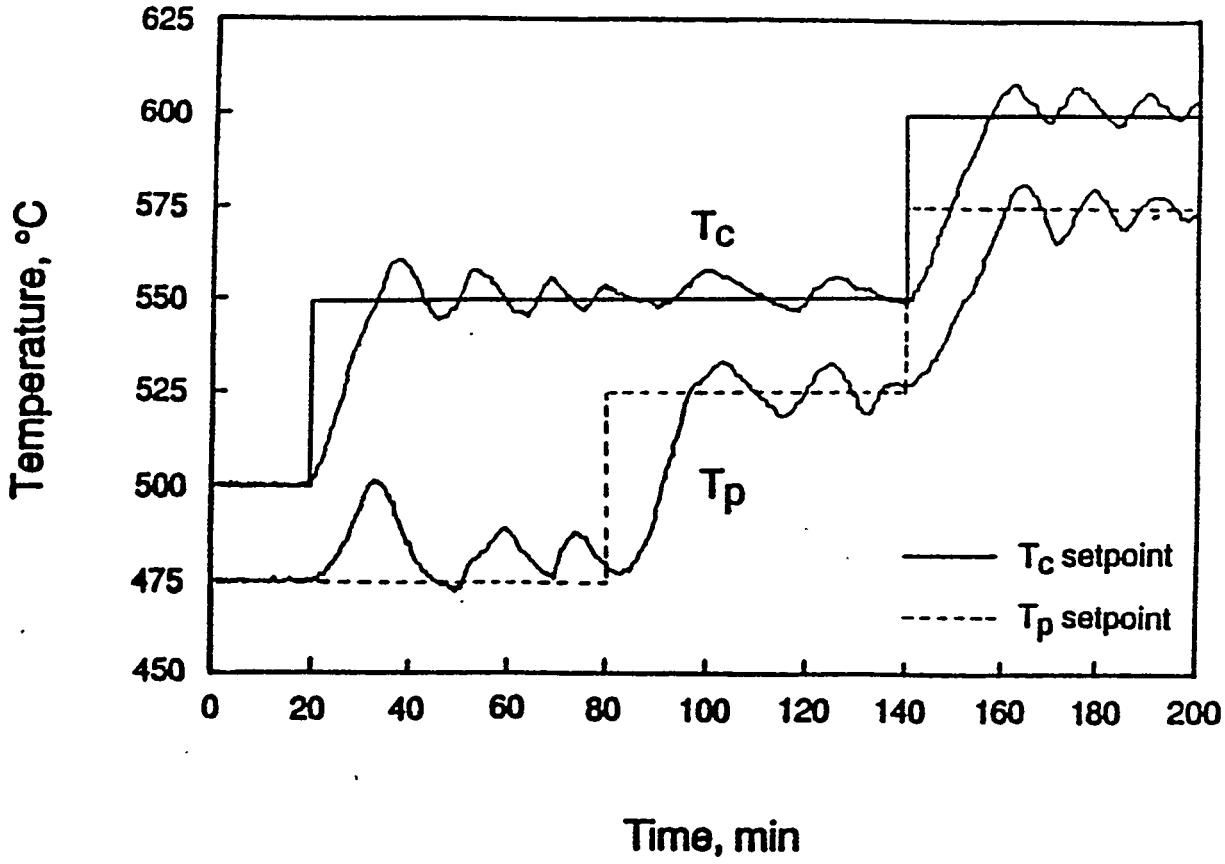

Figure 78. Temperature Responses to the Setpoint Changes of PID Controllers that are Tuned by IMC Strategy with τ_c = 6 Min.

derivative-dominated control caused by noisy temperature signals, etc.) To avoid this problem, the derivative control action was nullified by setting τ_d to zero. Subsequently, significant improvement in control performance was achieved by using the PI controllers, as shown in Figure 79. Thus, PI controllers were used in all of the subsequent tests.

As observed in Figure 79, sufficiently good controller settings were obtained through the IMC tuning method without lengthy online tuning. At least, the settings obtained here can be used as the initial values for an online tuning operation. However, the settings may not be optimal values, which is indicated by the relatively long settling time. This imperfection is likely due to the inaccurate system transfer function, which results from the process/model mismatch. There are two dominant sources of model error. The first, due to the inherent assumptions in Model 1 (e.g., constant heat capacities, ambient heat loss,) is relatively small, as can be seen in Figure 76. However, the error resulting from neglecting the thermal coupling between the two beds is significant and dominates the model mismatch. The different types of model error may require a design procedure not provided for in the IMC tuning method.

According to E119. 80, the IMC tuning method incorporates the tuning parameter, τ_c, into the controller design, which in turn decreases the controller proportional constants. As a result, the control system is sluggish, but relatively insensitive to model error. In principle, this feature should improve control

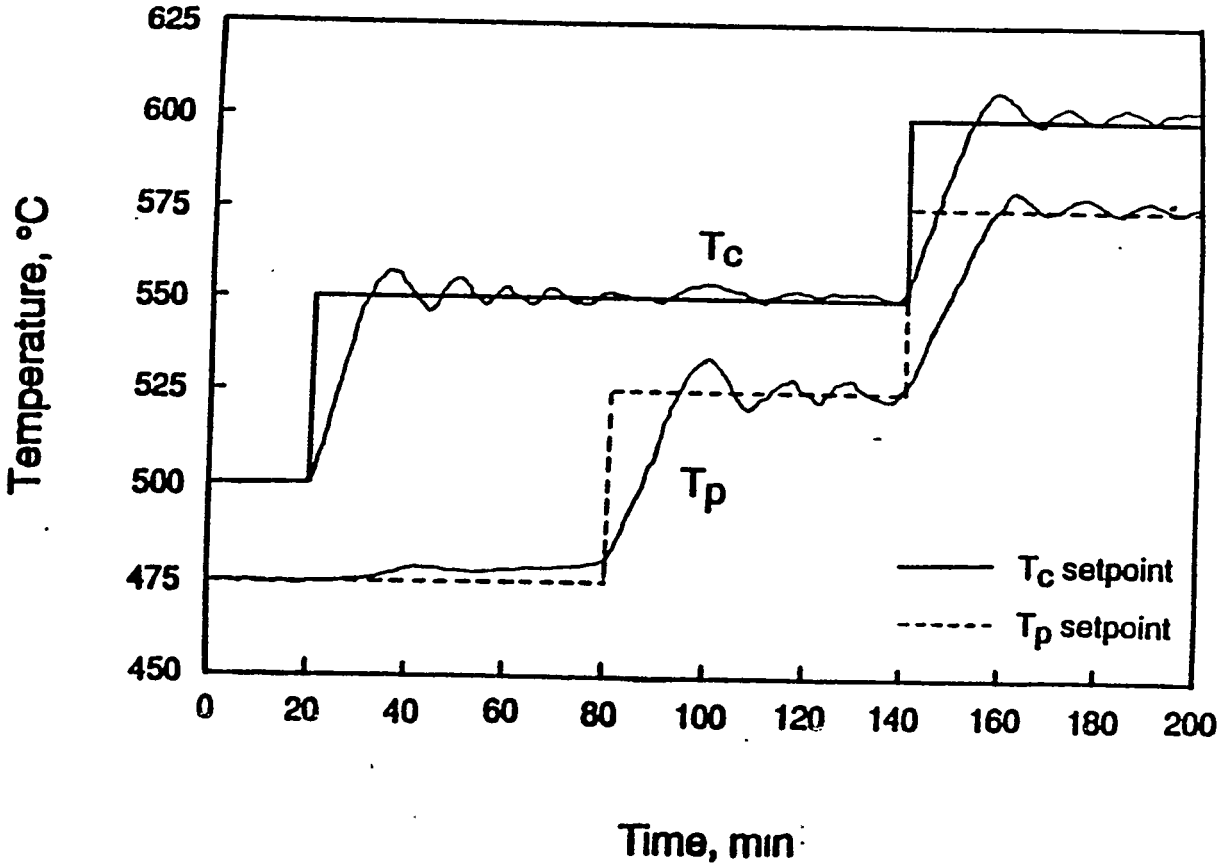

Figure 79. Temperature Responses to the Setpoint Changes of PI Controllers that are Tuned by IMC Strategy with τ_c = 6 Min.

performance when an exact process model is not available. However, the process studied here is strongly influenced by thermal interaction, and the sluggish control action cannot quickly counteract the temperature disturbances caused by the interaction. Consequently, good control performance cannot be achieved. IMC theory suggests that τ_c should increase with increasing model error. Because the transfer function developed here has a relatively large model error resulting from the neglect of the thermal coupling effect, a large τ_c value should be used according to the IMC control strategy. Obviously, this guideline is not valid for the study reported here. Instead, to quickly respond to thermal disturbances, a small τ_c should be used. Thus, depending on the sources of model error, different control strategies or τ_c values should be adopted.

An advantage of the IMC tuning method is that control performance or robustness can be achieved simply by adjusting the sole tuning parameter, τ_c. The effect of τ_c on IMC-based control was studied with the reactor system using PI controllers, with results given in Figures 80 and 81 for τ_c = 40 min and 0.5 min, respectively. IMC theory predicts that a larger τ_c increases control robustness, but sacrifices control performance. As expected, in Figure 80 the control performance becomes worse with increasing τ_c, and a smaller τ_c gives the much better control result in Figure 81. The optimal τ_c values obtained here are less than the recommended values[161,164]. The recommended τ_c values do not work well because this system, which is inherently highly coupled, as

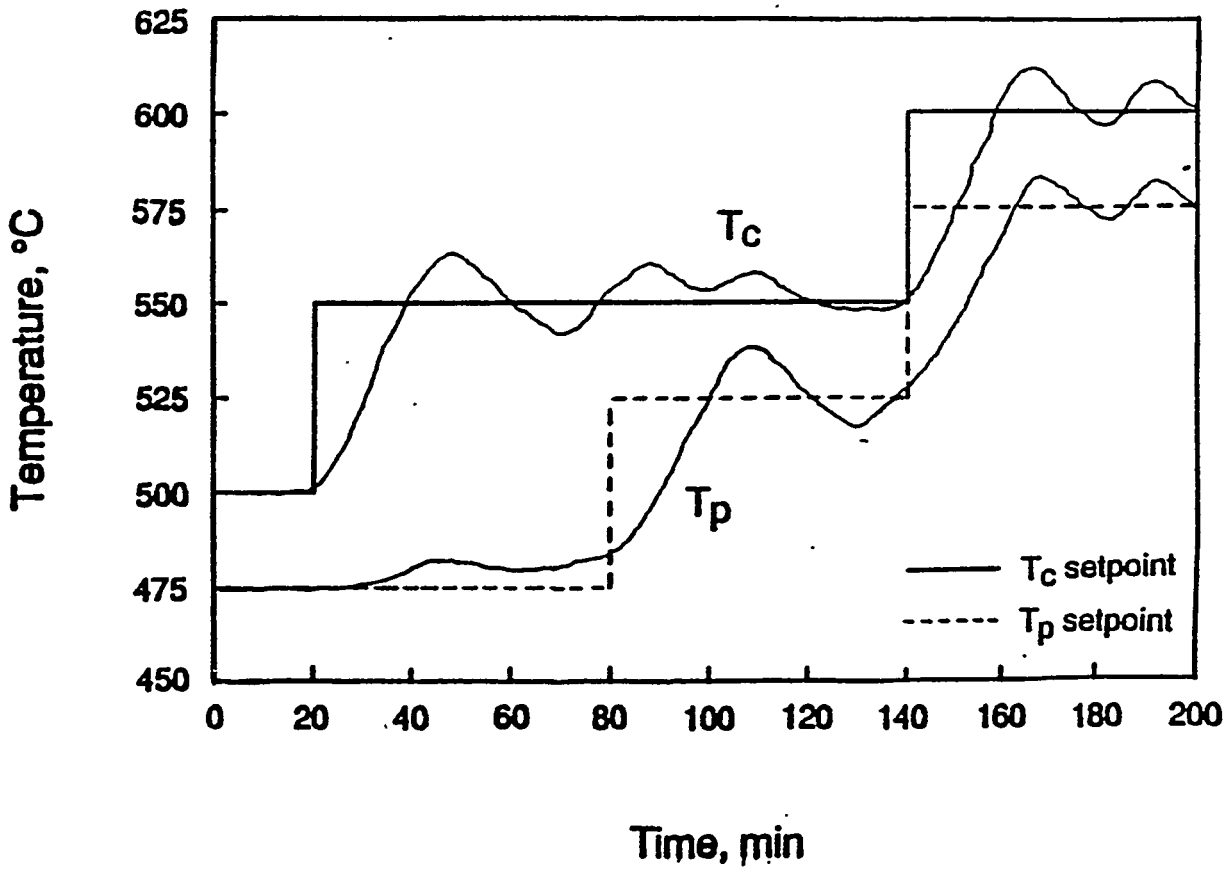

Figure 80. Temperature Responses to the Setpoint Changes of PI Controllers that are Tuned by IMC Strategy with τ_c = 40 Min.

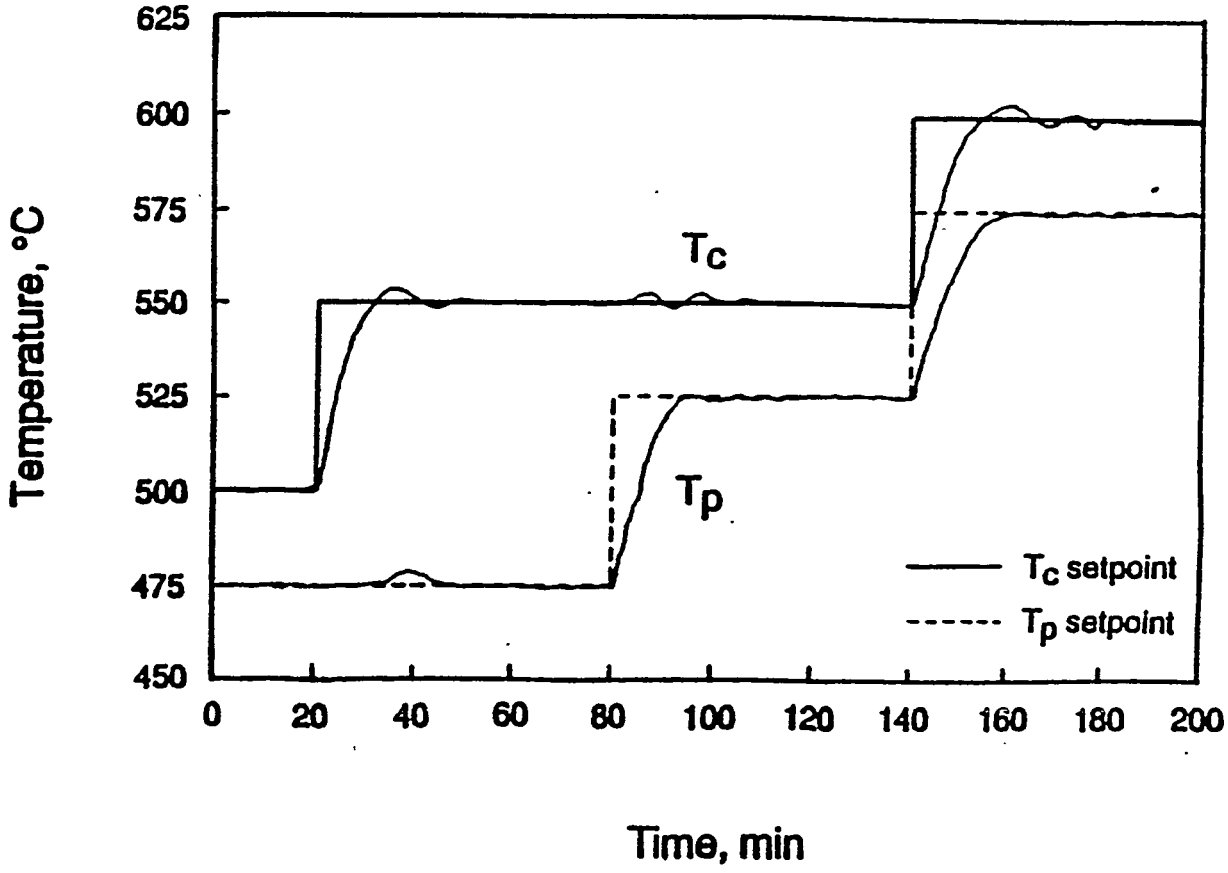

Figure 81. Temperature Responses to the Setpoint Changes of PI Controllers that are Tuned by IMC Strategy with τ_c = 0.5 Min.

seen in the RGA, has essentially been decoupled. In principle, when τ_c decreases below some value, the control system will become unstable, and then control robustness becomes an important issue. However, in this study, this unstable situation was never observed, even with a relatively small τ_c value. Since the electric heaters of the reactor system have a limited maximum heat duty, the process instability is precluded. As a result, the consideration of control robustness by the IMC tuning technique becomes irrelevant.

The control test of Figure 79 was repeated using the same PI controllers and settings but increasing the sand holdup in the combustion reactor from 3.6 to 7.2 kg to investigate the effect of changing operating conditions on controller settings. Figure 74 shows the closed-loop control result for τ_c = 6 min. By carefully comparing Figures 79 and 82, for the same τ_c, it was found that with the same controller settings, control performance is less satisfactory for the case of larger sand holdup in the combustion reactor. To achieve the same control performance the τ_c value should be decreased. This finding suggests that the value of τ_c should be adjusted with changing operating conditions. Because most chemical processes are nonlinear in nature, adjusting controller settings to cope with changing operating conditions is a common practice for a better process control. However, most conventional tuning techniques[160] require more than one tuning parameter, which makes tuning very difficult.

Based on the formula to calculate the RGA, it is known that the thermal interaction increases with increasing surface area of

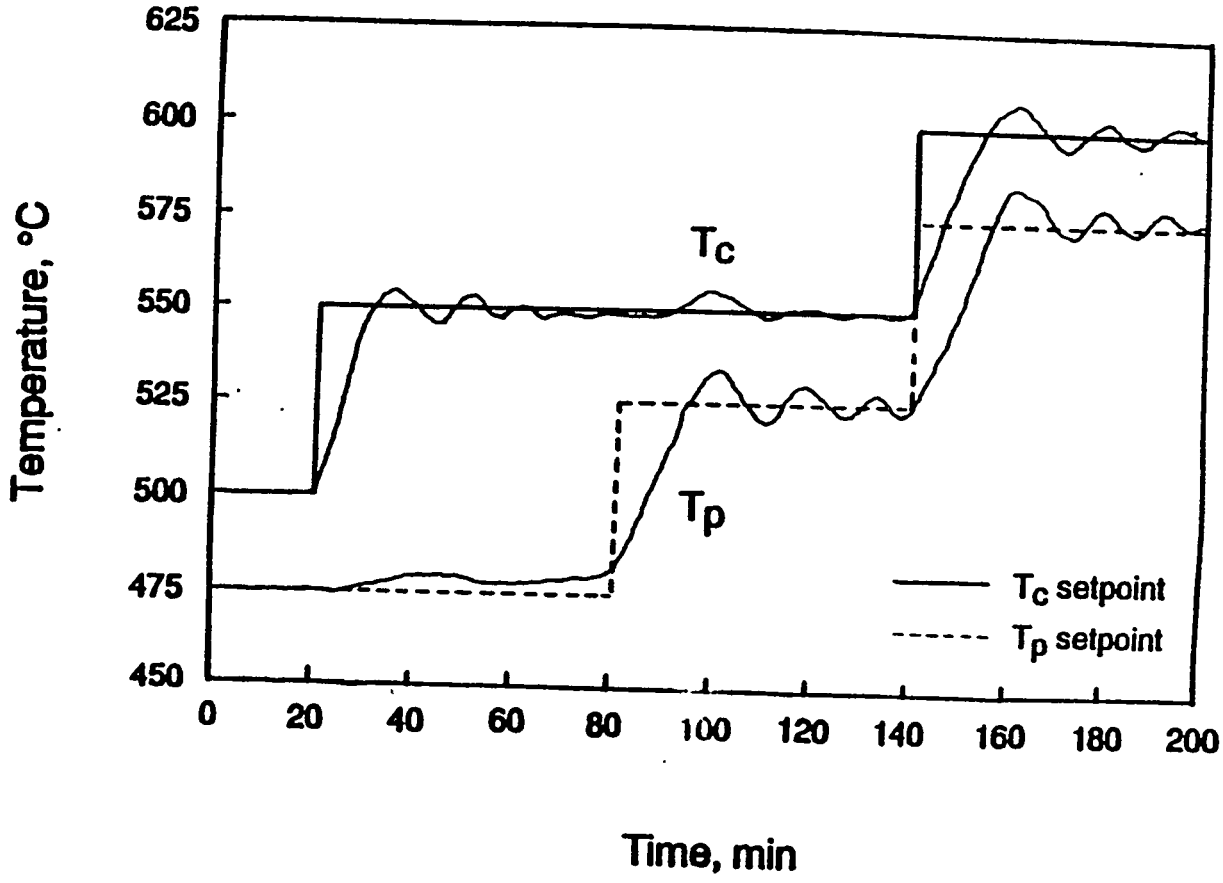

Figure 82. Temperature Responses to the Setpoint Changes of PI Controllers that are Tuned by IMC Strategy with τ_c = 6 Min.; Sand Holdup in Combustion Bed = 7.2 kg.

heat pipes immersed in sand. Thus, the least satisfactory control performance with increasing sand holdup might be due to an increasing thermal coupling effect. It has been concluded that a small τ_c value should be used when the thermal coupling effect is large. In other words, depending on the significance of the thermal interaction, the τ_c value should be adjusted accordingly. IMC theory does not reveal a method for determining a value for τ_c. However, because the IMC tuning method uses only one tuning parameter, it generally can yield a straightforward relationship between the parameter and the nature of the process. For instance, in this study, the magnitude of off-diagonal elements in the RGA, which is proportional to the thermal interaction, was used to help determine a value for τ_c. A simple tuning guideline was developed on the basis of the above studies, i.e., the value of τ_c should decrease with increasing magnitude of off-diagonal elements in the RGA. With this approach, satisfactory control performance was obtained regardless of operating conditions. It is believed that by carefully studying the nature of processes, the IMC tuning procedure used in this study can be applied to many chemical processes, providing a simple way to tune PID controllers not only for SISO (single-input/single-output) but also for MIMO systems.

CONCLUSIONS

Precise temperature control of a coupled two-reactor system is difficult because of a relatively large thermal interaction and the nonlinear nature of the process. To control the reactor temperatures precisely, controllers must account for the thermal

coupling effect and the effect of changing operating conditions on the controller design. This study shows that the IMC strategy provides a means to directly use process knowledge and a process model to make a control decision. However, the major drawback of the IMC tuning technique is that it is difficult to determine the optimal value of its only tuning parameter, τ_c. Even though some typical τ_c values have been suggested before, this study shows those recommended values might not be appropriate for the process investigated here. Instead, the relative gain array was used in this study to help determine the proper τ_c value, which provides a simple approach to extend the IMC strategy to multiinput/multioutput systems.

HEAT OF PYROLYSIS OF BITUMEN

The thermal pyrolysis of oil sands involves a pyrolysis step during which the bitumen gets volatilized and cracked. This pyrolysis step is endothermic requiring energy to be supplied for this process. In order to carry out an energy balance for the process it is necessary to estimate the heat requirement of the pyrolysis reaction. A method for estimating the heat of pyrolysis of oil sands bitumen is developed here.

The overall pyrolysis reaction can be written as follows:

$$\text{Bitumen} \rightarrow \text{gas} + \text{oil condensate} + \text{coke}$$

$$\text{or} \quad A \rightarrow x_1 B + x_2 C + x_3 D$$

where x_1 , x_2 , x_3 are the weight fractions of bitumen reacting to form gas, oil and coke, respectively.

The heat of pyrolysis at any temperature TC can be calculated as follows:

$$
\begin{array}{ccccccc}
 & & \Delta H & & & & \\
A(T^{\circ}C) & \rightarrow & x_1\ B & + & x_2\ C & + & x_3\ D \\
\Delta H_1 \downarrow & & & & \uparrow \Delta H_3 & & \\
A(298\ K) & \rightarrow & x_1\ B & + & x_2\ C & + & x_3\ D \\
 & & \Delta H_2 & & & &
\end{array}
$$

Since the heat of pyrolysis at any temperature T°C is not a path function it can be written as

$$\Delta H = \Delta H_1 + \Delta H_2 + \Delta H_3. \qquad (122)$$

The standard heat of reaction for any given reaction is given by

$$\Delta H^0_{rn} = -\sum \nu_i \Delta H_{comb_i} \quad or \quad \Delta H^0_{rn} = \sum \nu_i (HV)_i \qquad (123)$$

where HV is the heating value, which is numerically the same as the heat of combustion but has the opposite sign. Gross heating values for bitumen, oil and coke can be calculated, if the elemental composition is known, using the formula of Bunger[169] in terms of weight fraction of the elements (C, H, N, S, and O).

$$HV(Btu/lb) = 15120\,(C) + 49977\,(H) + 2700\,(N) + 4500\,(S) - 4770\,(O). \qquad (124)$$

The gas formed during the reaction consists of C_1 - C_5 compounds with a higher percentage of the lower-molecular-weight compounds. For simplicity of calculations, it is assumed that the average properties of the gas can be approximated by those of ethylene.

The formula for calculating the heating values suggests that it is independent of the structure of the compound and depends only on the elemental composition. The veracity of this suggestion has

been tested by comparing the heats of combustion of compounds with the same molecular formula, but different structures. The heat of combustion was calculated by first estimating the free energy of formation for each compound using Benson's Group Contribution method[153] and then using it in the combustion reaction for that compound.

The results are given in Table 30. It is found that the

Table 30: Comparison of the Predicted and Calculated Values of the Heat of Combustion. (All values in Btu/lb)

Compound	$\Delta H°f$ (estimated)	$\Delta H°$ comb (estimated)	$\Delta H°$ comb from (170)
C_5H_{10}			
cyclopentane	-474.27	-20367	
1-pentene	-127.01	-20715	-20100
2-methyl-2-butene	-290.81	-20551	
C_2H_4O			
Acetaldehyde	-1603.07	-11659	-11056
Ethylene oxide	-502.72	-12760	

predicted values of the heat of combustion for different compounds are in agreement with each other and with the value predicted by the formula above.

The following expression for the standard heat of pyrolysis is thus obtained :

$$\Delta H_2 (Btu/lb) = x_1 (HV)_A + x_2 (HV)_C + x_3 (HV)_D. \qquad (125)$$

ΔH_1 is the sensible heat required to cool the reactant to 25°C (77°F) from the reaction temperature, while ΔH_3 is the sensible

heat required to take the products back to the reaction temperature.

$$\Delta H_1 = T\int_{T}^{77} (C_p)_A \, dT \tag{126}$$

$$\Delta H_3 = 77\int_{77}^{T} [x_1 (C_p)_B + x_2 (C_p)_C + x_3 (C_p)_D] \, dT \tag{127}$$

At the temperature at which the pyrolysis reaction takes place the bitumen and oil are in vaporized form and hence H_1 and H_3 should strictly include the heat of vaporization of the bitumen and oil condensate, respectively. For simplicity of calculation the differences between these two are assumed to be negligible. The errors caused by this assumption in the calculation of ΔH_1 and ΔH_3 nullify each other and hence the overall error is small.

The expressions for the heat capacities of gas and coke are available in Perry's Chemical Engineer's Handbook[170]. The heat capacities for bitumen and oil are available in API[146] tables. These are given by

$$C_p(\text{Btu/lb°F}) = [0.6811 - 0.308s + (0.000815 - 0.000306s)T]$$
$$(0.053K + 0.035)$$

where s is the specific gravity (60°F/60°F), T is the temperature (°F), and K is the Watson characterization factor.

The following expressions are obtained for ΔH_1 and ΔH_3.

$$\Delta H_1(\text{Btu/lb}) = [(0.6811 - 0.308s_A)(77 - T) - (4.075 - 1.53s_A)$$
$$(77^2 - T^2) \times 10^{-4}](0.053K_A + 0.035) \tag{128}$$

$$\Delta H_3(\text{Btu/lb}) = x_1[(0.1348)(\{(T - 32)/ 1.8 + 273\} - 298) + (1.1457 \times 10^{-3})(\{(T - 32)/1.8 + 273\}^2 - 298^2) - (2.21 \times 10^{-7})(\{(T - 32)/1.8 + 273\}^3 - 298^3)]$$
$$x_2 [(0.6811 - 0.308s_c)(T - 77) - (4.075 - 1.53s_c)(T^2 - 77^2) \times 10^{-4}](0.053K_c + 0.035)] + x_3 (0.359)(T - 77) \quad (129)$$

From Equations (122), (125), (128), and (129) the heat of pyrolysis can be calculated.

Using the expression obtained above, the heat of pyrolysis for PR springs oil sands deposits was calculated to be about 450 Btu/lb of bitumen reacted. This is of the same order as the approximate value of 200 Btu/lb given by Bezama[131]. Since oil sands typically contain about 8-10% bitumen the heat of pyrolysis in terms of the oil sand fed to the reactor would be about 36 Btu/lb.

The total heat requirement for the pyrolysis step includes the heat of pyrolysis and the sensible heat required to heat the feed oil sand to the reaction temperature. This was calculated to be about 450 Btu/lb. Thus it is clear that the heat of pyrolysis is a small fraction of the total heat requirement of the pyrolysis step.

NOMENCLATURE

a_b Volumetric area of interphase transport

A Surface area of heat pipe immersed in fluidized bed

A_0 "Catchment Area" of distributor = Cross sectional area / number of holes

Ar Archimedes number defined in Equation 52

Ar	Archimedes number defined in Equation 52
C	Heat capacity; Gas-phase mass concentration
C_p	Thermal heat capacity
d_b	Equivalent diameter of bubble
d_{hp}	Heat-pipe diameter
$\bar{d}_p$	Average particle diameter
d_p	Particle diameter
D	Diffusivity
D_B	Bed diameter
E	Residence-time distribution
F	Fluidizing air flowrate
g	Acceleration of gravity
G	Fluidizing gas flowrate
$\bar{h}$	Average heat transfer coefficient
h	Effective convective heat transfer coefficient
k	Reaction rate constant; process steady gain
k_g	Gas thermal conductivity
k_q	Mass transfer coefficient between bubble and dense phases
K_c	Proportional constant of a PID controller
L	Bed height
m_{coke}	Feed rate of coke into first combustion bed
M	Molecular Weight; Mass of sand holdup in a bed, reactor vessel, or heat pipe
n_{hp}	Number of heat pipes
N	Total number of species present in gas phase
P	Pressure
Q	Heat transfer rate or heat input rate
Q'	$Q + F\ C_a\ T_{a0}$

r Rate of production by chemical reaction

R Electric resistance; Gas constant

Re Reynolds number defined in Equation 53

s Stoichiometric coefficient; Laplace transform variable

t Time

$\bar{t}$ Average sand residence time

T Temperature

T_b Normal boiling temperature

T_o Standard temperature of reaction

T_p Pyrolysis temperature

u Superficial fluidizing gas velocity

u_o Velocity of fluidizing gas at $z = 0$

u_b Velocity of bubble rising through a fluidized bed

V Voltage

V_b Molar volume at boiling point

V_1 A continuous function of z defined in Equation 98

w Weight fraction relative to total bitumen fed

$\bar{w}$ Weight fraction leaving fluidized bed relative to total bitumen fed

W Sand feedrate; Oil sand feed rate

x_{BO} Bitumen weight fraction of oil sand

$\bar{\bar{x}}_c$ Total conversion of coke in first combustion bed

z Axial bed position

Greek

α Thermal diffusivity

β time constant of a first-order lead system

ΔH Change in enthalpy per time

Δh Change in enthalpy per mass

ϵ Void fraction

ϵ_b Volume fraction of bubble phase

ϕ_b Volume fraction of bubble phase occupied by solids

υ Stoichiometric coefficient

ρ_p particle density

ρ_g Density of fluidizing gas

ρ_s Density of fluidized solids

τ process time constant

τ_c closed-loop time constant

τ_d derivative constant of a PID controller

τ_i integral constant of a PID controller

τ_f parameter of optimal roll-off element in Equation 120

σ Volumetric correction factor used in Equation 55

π 3.14159...

μ Viscosity

ζ damping coefficient

Subscript

a Air; property in second combustion bed

b Property in bubble phase

c Property in first combustion bed; Property of coke; combusion reactor

d Property in dense phase

g Property of fluidizing gas

h Heat pipe

HB Heavy Bitumen

LB Light bitumen

mf Property at minimum fluidization conditions

o	ambient conditions
p	Property in pyrolysis bed; pyrolysis reactor
r	reactor vessel
s	Silica sand; Property of fluidized solid
TS	Property of bulk oil sand

FLUIDIZED-BED PYROLYSIS OF OIL SANDS IN A LARGE DIAMETER REACTOR

Principal Investigator	F.V. Hanson
Graduate Students	J.V. Fletcher
	S. Nagpal

INTRODUCTION

Fluidized-bed pyrolysis of mined Utah oil sands has been part of the process research development programs of the Chemical Engineering and Fuels Engineering departments at the University of Utah for approximately 15 years. A history of the oil sands research and development studies was reported by Oblad et al.[24] The results of the thermal process development efforts offer some interesting contrasts in terms of the influence of process variables on product yields when oil sands are pyrolyzed in a fluidized-bed reactor.[127,130,131,152,171-174] For example, liquid yields appeared to be a maximum at 773-798 K, but the effect of residence time on liquid yields was not at all clear.[152,172,174,175]

Studies of Utah oil sand pyrolysis in fluidized beds have led to the conclusion that pyrolysis liquid yields were a maximum near 798 K.[24,175] Pyrolysis studies on Nigerian oil sands found liquids to be a maximum at 773 K[176]. Fluidized-bed pyrolysis of Canadian oil sands yielded maximum liquid products near 783 K[177]. Spouted bed pyrolysis of oil shales also showed that liquid yields may be greatest in the 753-773 K range.[178] Coke yields in the Utah oil sand studies did not vary appreciably with pyrolysis temperature or retention time but were sensitive to oil sand source.[131,172,174,178] The effect of residence times greater than or less than 30 minutes was not consistent in the University of Utah studies, but the

majority of data seemed to favor a conclusion that liquid yields would decrease as average residence times increased.[24,127,130,131,152,171-175] Recent pyrolysis studies on vacuum residues suggest that 30 minutes may be the appropriate residence time for maximum liquid yields when pyrolysis temperatures are less than 773 K[180,181] Gas yields (C_1 - C_4) in previous pyrolysis studies, including oil sands, increased with pyrolysis temperature.[145,175,182,183] Gases were usually reported as C_1 - C_4 yields. The effect of fluidizing gas velocity has also been studied, with the conclusion that the fluidizing gas velocity did not appear to affect product distribution and yields or product quality.[152,174] Finally, 723 K appeared to be the lower temperature limit for oil sand pyrolysis.[172,180,181]

The objectives of this work included an evaluation of the relative merits of thermal recovery of bitumen at reduced pressures as compared to previous ambient pressure studies. The effect of relative fluidizing gasflow, U/U_{mf}, on product yields, and the effect of residence time on liquid product yields was to be reexamined. It was also an objective to demonstrate experimentally that hot flue gases from the reactor heat source can be used as the process fluidizing media, and that lower pyrolysis temperatures are possible using a reduced pressure fluidized-bed reactor.

EXPERIMENTAL

The fluidized-bed reactor and support systems used in this investigation were designed and constructed specifically for the purposes outlined in the research objectives. The processing system constitutes a small pilot-scale continuous flow pyrolysis

reactor, and consists of an oil sand feeder, a fluidized-bed reactor, pyrolysis products withdrawal and recovery systems, and various process monitoring and support systems. A process flow diagram is presented in Figure 83.

Oil sand from the Whiterocks deposit of Northeastern Utah, crushed and screened through a 6.35×10^{-3} m square mesh, was fed to the reactor with an Acrison BDF-1.5 dry materials feeder. Spent sand was withdrawn from the reactor using an L valve as described by Knowlton but modified to discharge sands with a diameter range from less than 0.1 mm to over 3 mm.[184] Liquids were recovered at three points in the recovery train (Figure 83) using strainers and traps modified for water cooling.

The fluidized-bed reactor was designed to allow hot combustion gases to be pulled into the windbox for use as the fluidizing media. The pressures in a traditional "Push" reactor are contrasted with this "Pull" reactor design in Figure 84. A "Pull" configured reactor (Figure 84) must have, by design, a pressure above the distributor that is less than the sum of the windbox pressure and the distributor pressure drop in order for gas to flow through the distributor. This configuration established the sub-atmospheric (i.e., less than ambient) requirement in the bed and facilitated an easy transfer of the hot combustion gases to the windbox. A detailed description of the reactor and the operating system has been reported by Fletcher et al.[185]

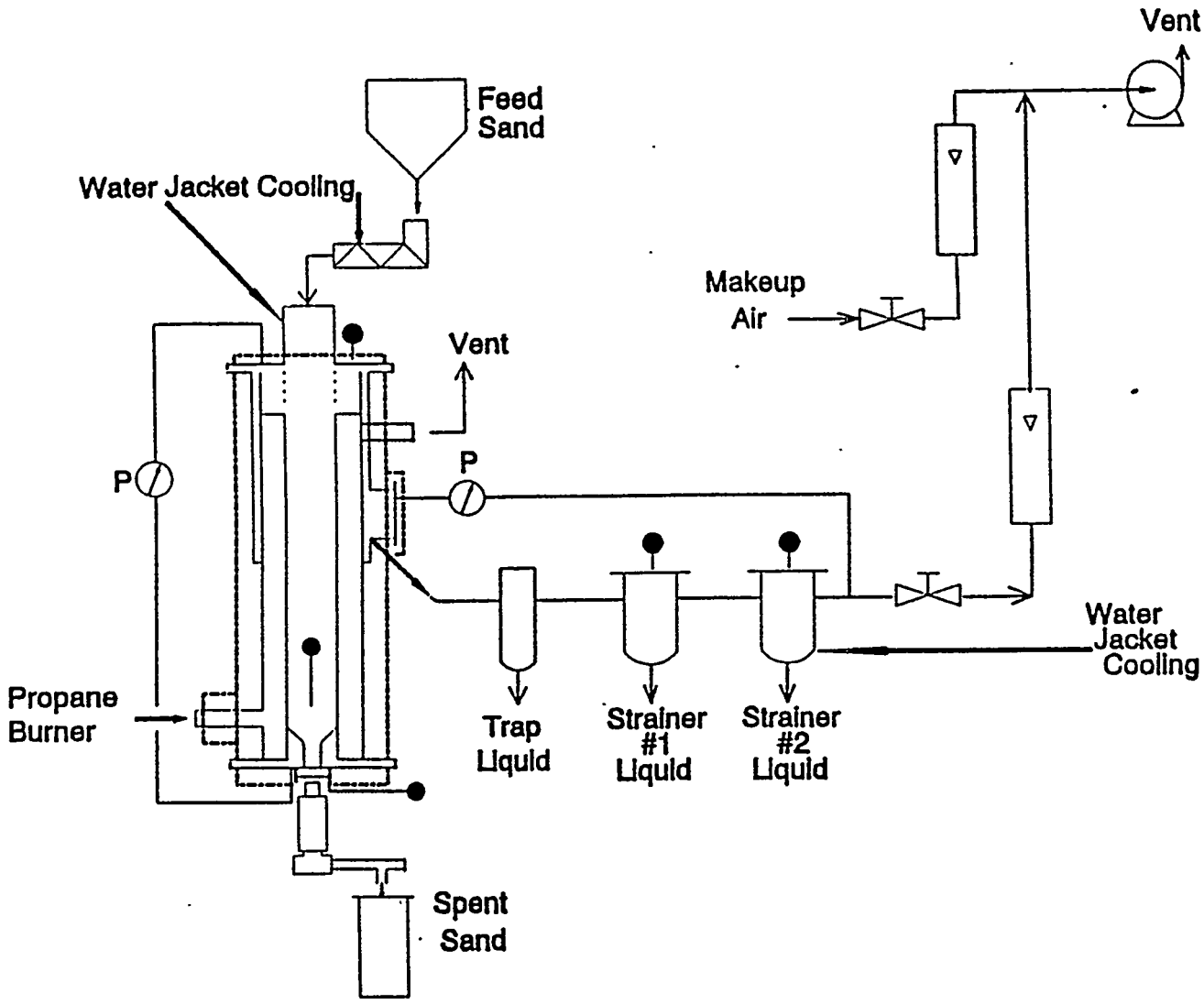

Figure 83. Process Flow Diagram

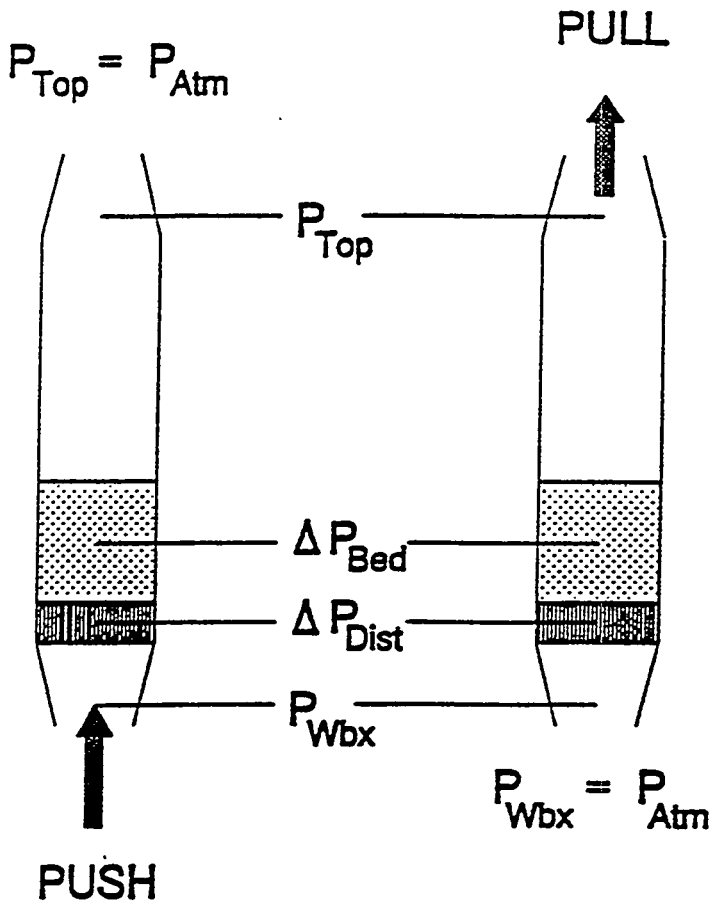

Figure 84. Pressure Description for Push and Pull Configurations

RESULTS AND DISCUSSION

After confirming that the "Pull" configured fluidized-bed reactor could be operated in the bubbling regime at temperatures necessary for pyrolysis, the system was used for the study of oil sand pyrolysis process variables. Based on the results of previous investigations, three reactor temperature ranges (±10 K) were targeted, 733 K, 748 K, and 773 K.[175] Oil sand pyrolysis products included liquids, gases, and a spent sand which contained a carbonaceous residue referred to as coke in previous investigations.[24,127,130,131,152,171-175]

Product Distribution and Yields

Results from a total of eleven pyrolysis experiments at the three target temperatures were presented by Fletcher.[134] Four of these runs, with material balances of 90-93%, were selected for this analysis and discussion. Process data for those runs are presented in Table 31. Reported hydrocarbon gases, including C_5 and C_6 products recovered in the gas trap, were analyzed using gas chromatography. Based on the data in Table 31, the distribution of product liquids and gases appeared insensitive to pyrolysis temperatures below 748 K. Above 748 K, product gases increased at the expense of liquids. Coke production appeared to be insensitive to pyrolysis process temperatures in this range.

Comparison of product distributions in Table 31 suggests that, for the system and conditions of this study, retention times greater than 30 minutes are not a significant process variable. This is in contrast to the observation of Smart who reported that

Table 31
Summary of Product Distributions

Run #	709	619	812	721
Average Bed Temperature, T_B, (K)	720	731	746	773
Products Recovered, wt%				
Prestrainer trap	7.6	9.3	5.9	4.3
Strainer #1	52.6	38.7	54.1	69.3
Strainer #2	39.8	51.9	40.0	26.4
Total Liquids	88	89	88	84.5
Coke	9	9	9	9
Gas	3	2	3	6.5
Average Retention Time, t_{Res}, (min)	44	48	29	30
U/U_{mf}	2.5	2	2.5	2.5

liquid yields increased as retention times increased above 30 minutes.[127] Also, the previously reported loss in liquid yields for Whiterocks oil sands at these lower pyrolysis temperatures may have been offset by the longer average residence times of this study.[24]

Runs #709 and #619 (Table 31) were very similar in average solids residence times and pyrolysis temperatures, yet the weight distributions of liquids recovered at the three liquid collection points (Figure 83) were very different. At the lower gas velocity, with U/U_{mf} equal to 2.0 (Run #619), more liquid was found in strainer #2 at the expense of strainer #1. Total liquid yields were comparable for the two runs and comparison of simulated

distillation data suggested that there was no significant difference in liquid products boiling point distributions. Therefore, the liquid weight distribution difference is probably related to the gas velocity in the liquid product collection system. At lower velocities (U/U_{mf} = 2.0) the liquids stay entrained in the gas. whereas at the higher velocities (U/U_{mf} = 2.5) the liquids appear to drop out of the gas at points of impact on the strainer walls.

From Table 31 it would appear that the Whiterocks oil sands can be pyrolyzed at 723-748 K to yield 88 wt% liquids, 9% wt% coke, and 3 wt% gases. These liquid yields are significantly greater than those previously reported for the pyrolysis of Whiterocks oil sands in either a fluidized bed or a rotary kiln at any temperature.[145,172,175] The pyrolysis of Whiterocks oil sands was studied in a fluidized bed and a rotary kiln by Wang[172] and Cha[145]. Their yields at 773 K are presented in Table 32 along with the yields from this study at 773 K. Comparison of their yields at 773 K with yields from this study at 773 K indicates that reactor design or process variables other than pyrolysis temperature also has an influence on product yields. It is interesting to note that no residuum was reported by Cha.[145] However, the product liquids, corrected for residuum, are still greater in this investigation (72.3 wt% versus 65.5 wt%) than reported for the rotary kiln at 773 K.[145]

The recovery of more liquids in this work could be the result of the reduced pressure above the bed and/or the use of combustion

Table 32
Whiterocks Oil Sands Pyrolysis Product Yields at 773 K

	Rotary[145] Kiln	Fluidized Bed[172]	This Study
From Product Weights			
Liquids, wt%	65.5	61.2-67.6	84.5
Gases, wt%	13.0	Not Reported	6.5
Coke, wt%	21.5	9-13	9.0
From Sim D of Liquids			
Volatility, wt%	100	69.1	85.6
Naphtha, wt%	7.7	3.1	1.3
Middle Distillate, wt%	24.3	22.4	33.8
Gas Oil, wt%	68.0	43.6	50.5
Residuum, wt%	0.0	30.9	14.4
t_{Res}, min	20	25	30

gases for fluidization. The fact that pyrolysis temperatures were also lower than traditional suggests that one or both of these reactor conditions has a potential application for process scaleup. Based on the modest pressure reductions above the bed (about 7 kPa) for most of these experiments, it is more likely that the presence of CO_2 and/or H_2O in the fluidizing gas was responsible for the improved liquid yields. Confirmation of the contribution of fluidizing gas composition to improved liquid yields is the subject of future work with this reactor system.

The carbonaceous residue (coke) produced as a byproduct of the pyrolysis reaction has been previously reported to be independent

of pyrolysis temperature but sensitive to oil sand source.[152,172,174,175,179] The results of the experiments in this study support the conclusion that pyrolysis temperature has no significant effect on coke yield for the Whiterocks oil sand. Average wt% coke on the sand (±1 σ) for 11 runs was 0.615 (±0.072) which was about 8.2 wt% of the bitumen fed.

The coke yields of less than 9 wt% are lower than any previously reported coke yields regardless of oil sand source.[127,130,131,152,171-175] Although trace amounts of oxygen may have been present in the fluidizing gas, there was no supporting evidence for partial combustion of the carbonaceous residue either visually or in terms of LPG fuel consumed. It is more likely that the water content of the fluidizing gas suppressed the coke formation. The water content of the product gas was at least 2 wt%; however, based on CO_2 in the gas, stoichiometric combustion water should be 7 wt% of the fluidizing gas. The difference between 7 wt% water from combustion and the 2 wt% found by GC analysis of the products is the water condensate found in the product recovery system (Figure 83). Condensible hydrocarbon gases present in the reactor caused only about 1% (vol/vol) dilution. It, therefore, seems reasonable that the fluidizing gases contained 5-7 wt% steam. Steam, it should be noted, is used commercially to mitigate coke formation in processes involving the pyrolysis of heavy hydrocarbons.[186]

Hydrocarbon gas yields in this study were slightly less than reported by Cha and, as noted previously, any C_5 or C_6 found in the

gas stream was reported as gas in this investigation.[134] Cha,[145] on the other hand, reported C_5 and C_6 as part of the liquid product yield. Gas yields at 500°C from one pyrolysis run reported by Cha were compared to a similar run (#721) from this study in Table 33.[145,177] For the sake of uniformity, the results for Run #721 were also normalized after subtracting C_5 and C_6 wt%.

Table 33
Whiterocks Oil Sands Pyrolysis Gas Product Yields at 773 K

	Rotary Kiln[145]	This Study Run #721[a]	This Study Run #721[b]
Product Species	wt% (gas basis)	wt% (gas basis)	wt% (gas basis)
H2	0.4	0.4	0.4
CH_4	10.6	14.0	17.7
C_2H_4	4.7	7.2	9.2
C_2H_6	7.0	10.1	12.8
C_3H_6	46.1	14.0	17.7
C_3H_8	12.9	10.6	13.4
$i\text{-}C_4H_{10}$	1.0	1.2	1.5
$n\text{-}C_4H_8$	10.3	13.0	16.4
$n\text{-}C_4H_{10}$	5.8	7.7	9.7
$i\text{-}C_4H_8$	1.1	1.3	1.6
C_5	Not	15.3	---
C_6	Reported	5.8	---
t_{Res}, min	21	30	30

[a] $C_1 - C_6 = 100$ wt%
[b] $C_1 - C_4 = 100$ wt%

The gas analysis trends are very similar for the fluidized bed at reduced pressure and the rotary kiln. Products are normal alkanes and alkenes, with little isobutane or isobutene. One

noticeable difference is the unusually high propene content in the kiln gaseous product, a trend seen in all of the data reported by Cha.[145] Propene was not found at a high wt% in any analysed gas sample from the fluidized bed operated at reduced pressure in this work. Based on the lower overall hydrocarbon gas yields in these experiments, the lack of propene would seem consistent with less thermal cracking which tends to produce alkenes in a low hydrogen environment. It is also possible that more hydrogen was available at the time when C_3 chains were created in the fluidized bed due to cracking reactions, even though the H_2 in the product gas streams was low and the same for the rotary kiln and the fluidized bed.[134,145]

Pyrolysis gas product yields in these experiments (Table 31) are reported in Table 34. Gas analysis showed low iso-C_4 gases in all the runs. Run #709, with the lowest pyrolysis temperature (720 K), had more hydrogen product than the other runs. Run #619 is again a noticeable contrast to the others, with a higher CH_4 and lack of C_5 - C_6 in the gas, which would appear to be the result of the lower relative fluidizing gas velocity and longer gas residence time of that run. The sweep gas residence time in the fluidized bed is estimated to be between 0.5 minutes (U/U_{mf} = 2.5) and 1.4 minutes (U/U_{mf} = 2.0), and its temperature is assumed constant until rapid quenching occurs at the reactor exit. Another interesting contrast observed in this study was the relative wt% of C_4 hydrocarbons (Table 33). The rotary kiln produced 18.2 wt% C_4 and the fluidized bed produced 29.2 wt% C_4.

Table 34
Reduced Pressure Pyrolysis Gas Product Yields Using Whiterocks Oil Sands

Run #	709	619	812	721
U/U_{mf}	2.5	2.0	2.5	2.5
T_B, K	720	731	746	773
Product Species	wt% (gas basis)	wt% (gas basis)	wt% (gas basis)	wt% (gas basis)
H_2	1.1	0.4	0.4	0.4
CH_4	15.7	23.9	14.0	14.0
C_2H_4	4.6	6.6	14.1	7.2
C_2H_6	11.7	15.4	10.4	10.1
C_3H_6	17.4	14.6	13.0	14.0
C_3H_8	17.2	16.2	12.7	10.6
$i\text{-}C_4H_{10}$	1.2	0	2.7	1.2
$n\text{-}C_4H_8$	13.6	14.0	13.5	13.0
$n\text{-}C_4H_{10}$	10.1	9.2	9.1	7.7
$i\text{-}C_4H_8$	0.6	0	1.2	1.3
C_5	7.0	0	7.7	15.3
C_6	0.8	0	1.6	5.8

Liquid Products Quality

As mentioned above, the liquid products were collected in three separate collectors. These liquids were visibly different in physical properties. The weight percent of the liquids at 720 K, 746 K and 773 K (Table 31) are plotted versus temperature in Figure 85. It was apparent that the liquids distribution in the recovery system was dependent on the process temperature.

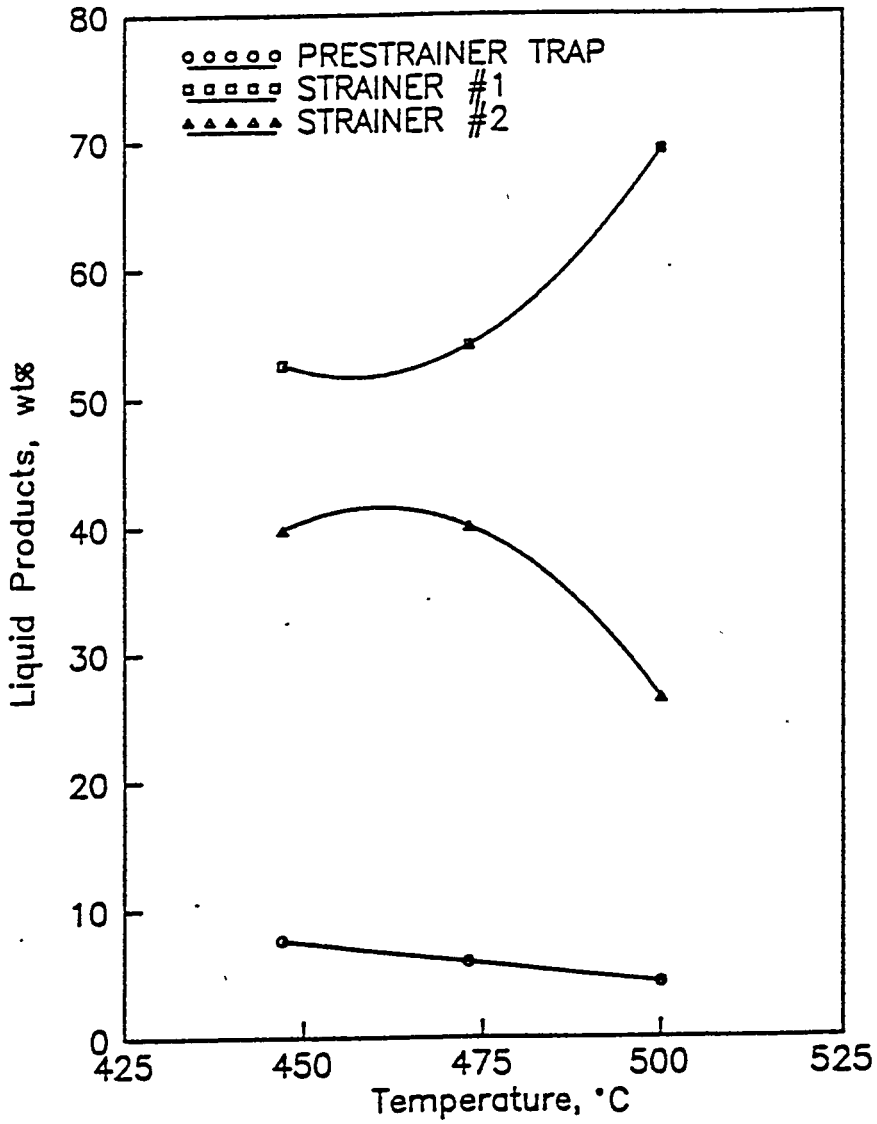

Figure 85. Liquid Product Yield vs Temperature for Recovery Streams

The variation in pour points for the three liquids produced at various process temperatures is shown in Table 35. Pour points of the two strainer liquids exhibited a marked change toward lower values above 748 K. Liquids recovered in the prestrainer trap seemed to be similar at all process temperatures and independent of temperature variations at this uncooled area.

Table 35
Pour Point of Liquid Products

	Pour Point (K)			
T_B (K)	Pre-Strainer Trap	Strainer #1	Strainer #2	Run #
720	287	281	266	709
731	286	282	260	619
746	293	287	248	812
773	291	267	214	721

The asphaltene contents (pentane insolubles) of the liquid products are presented in Table 36. Below 748 K, it appeared that the asphaltenes were either concentrated in the prestrainer trap or evenly distributed in all three liquid streams. At 773 K, the asphaltenes appear to have shifted to strainer #1, possibly because the prestrainer trap operated at a higher temperature when the pyrolysis temperature was higher.

Table 36
Asphaltenes Content of Liquid Products

	Asphaltene Content (wt%)			
T_B (K)	Pre-Strainer Trap	Strainer #1	Strainer #2	Run #
720	7.8	1.3	2.2	709
731	4.6	4.8	5.5	619
746	4.8	0.7	1.1	812
773	1.7	4.8	0.8	721

Conradson carbon residues (CCR) for the three pyrolysis liquid products are presented in Table 37. No clear trend with temperature was observed. However, there was a drop in the CCR for each successive downstream liquid, consistent with heavier materials condensing first in the liquid product recovery train.

Table 37.
Conradson Carbon Residue of Liquid Products

	Conradson Carbon Residue (wt%)			
T_B (°C)	Pre-Strainer Trap	Strainer #1	Strainer #2	Run #
447	3.7	3.1	1.4	709
458	3.6	3.2	3.0	619
473	4.0	3.9	2.8	812
500	4.7	2.6	1.3	721

Viscosities were only measured for the liquids recovered in strainer #2 due to the sand content of the other liquid products. Viscosities and API gravities for the liquids from strainer #2 are presented in Table 38. As expected, liquid product viscosity

Table 38.
Viscosity and API Gravity of Strainer #2 Liquids

T_B (K)	Viscosity (cp) at 296 K	API Gravity (°API)	Run #
720	470	17.6	709
731	490	14.3	619
746	210	21.3	812
773	70	26.4	721

decreased with increasing pyrolysis temperature. An increase in pyrolysis temperature from 720 to 746 K reduced the viscosity by more than 50% for these liquids.

The average calculated specific gravities for the three liquid product streams are presented in Table 39. The specific gravity was calculated using the apparent specific gravity measurements from a pycnometer or hydrometer and the wt% inerts as determined

Table 39
Calculated Specific Gravity of Liquid Products

T_B (K)	Pre-Strainer Trap	Strainer #1	Strainer #2	Weighted Average
720	1.02	1.00	0.95	0.99
731	1.02	0.95	0.97	0.98
746	1.01	0.96	0.93	0.96
773	0.98	0.90	0.90	0.94

with the asphaltenes. Volumes of oil and inerts were assumed to be additive. The trends in Table 39, which must be viewed with caution due to the sand correction, are consistent with other findings in this study. The specific gravity of the liquids was greatest in the prestrainer trap and the least in strainer #2. The specific gravity of the liquids also decreased as pyrolysis temperatures increased. The specific gravity of extracted bitumen has been reported as 0.99.[145] The calculated average specific gravity for the liquids (Table 39) recovered from pyrolysis at 723 K is similar to the extracted bitumen. The trend of decreasing specific gravity with increasing pyrolysis temperature is opposite to that reported for pyrolysis in a rotary kiln by Cha.[145] In the rotary kiln, lower pyrolysis temperatures produced lower specific gravity liquids, the range being from 0.91 at 748 to 0.94 at 848 K.

In this study, a 0.94 specific gravity liquid was produced at 773 K.

An increase in specific gravity of hydrocarbon liquids is usually attributed to an increase in aromaticity. An increase in aromatics with their lower H/C ratio can also result in greater coke formation. In this work, however, the specific gravity trends (Table 39) suggest an absence of aromatization and/or dealkylation reactions. Lower aromaticity would also be consistent with the low coke (Table 31) yields from the experiments.

Moisture and sand-free samples from each of the three liquid collectors were analyzed using a simulated distillation gas chromatograph. Simulated distillation data for liquid products were reported by Fletcher[134] who reported that each of the liquid products exhibited similar features. At pyrolysis temperatures of 748 K or less, there was very little difference in liquid composition. Liquids produced by pyrolysis above 748 K were clearly lighter, with lower boiling point ranges.

The calculated simulated distillation cuts for the combined liquid products are plotted as a function of pyrolysis temperature in Figure 86. The distribution of weight percents among the various cuts was consistent with visual observations and measured properties. Pyrolysis at 720 K produced a heavier liquid product with a higher residuum fraction than pyrolysis at higher temperatures. The most striking feature of this plot is the drop in residuum from 26.4 wt% at 748 K to 14.4 wt% at 773 K. Overall trends are consistent with greater cracking rates and lower

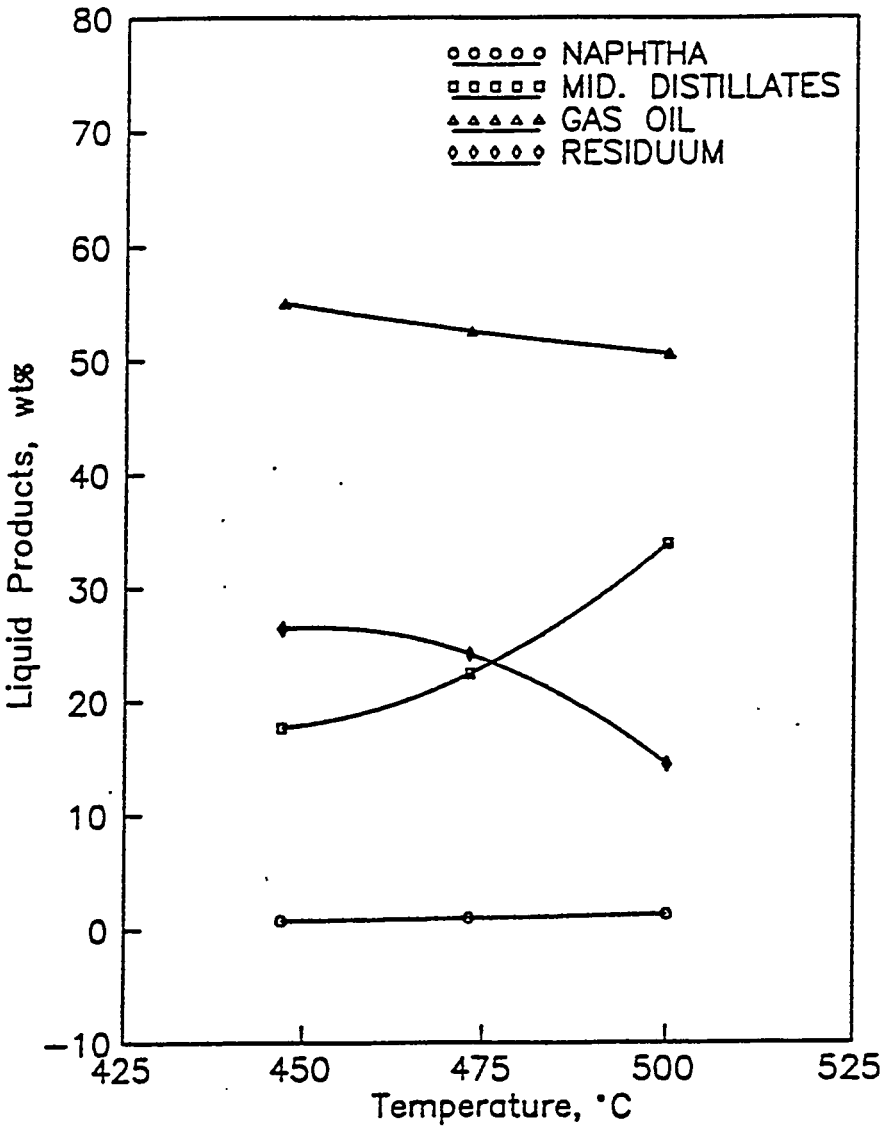

Figure 86. Simulated Distillation Cuts versus Temperature

molecular weight products at the higher pyrolysis temperatures. Recalling that product yields and solid/liquid/gas distributions were unchanged from 723 K to 748 K, the 748 K pyrolysis temperature is seen to yield a better quality liquid product.

SUMMARY AND CONCLUSIONS

A 15.2 cm diameter fluidized-bed reactor was designed, built, and operated to study the pyrolysis of oil sands at pressures slightly less than ambient. Fluidizing gas flow through the reactor was caused by reducing the pressure above the bed with a gas pump operating in the vacuum mode. Pyrolysis energy was supplied by a propane burner, and the hot propane combustion gases were used to fluidize the bed.

The fluidized-bed pyrolysis at reduced pressure using combustion gases allowed the reactor to be operated at significantly lower temperatures than previously reported for equivalent liquid yields. At 723 K over 80 wt% of the bitumen fed was recovered as a liquid product, and the spent sand contained less than 1 wt% coke. The liquid product recovery system, by design, yielded three liquid streams with distinctly different properties.

As a result of the pyrolysis experiments with Whiterocks oil sands, modifications to the reactor heating system were required. A new burner system using refractory materials was designed.

Using a 15.2 cm fluidized-bed reactor operating at less than ambient pressure, pyrolysis of Whiterocks oil sands in a combustion gas environment led to the following conclusions:

1. Pyrolysis of bitumen would appear to give higher liquid yields, and make less gas and coke (carbonaceous residue), when compared to previous ambient pressure, nitrogen fluidization, studies. Maximum liquid products were produced when the pyrolysis temperature was 748 K.
2. There was no new evidence to suggest that U/U_{mf} has any influence on product yields for the ratios investigated.[134]
3. In contrast to previous observations by Wang, residence times from 29 to 70 minutes were found to give similar yields and product distributions.[172].
4. Hot combustion gases from a propane (LPG) burner, regulated to avoid excess oxygen, can be used to fluidize the spent sand as part of the fluidized-bed pyrolysis of oil sands.
5. This work has verified the observation of previous workers using TGA that bitumen pyrolysis rates peak at temperatures below 775 K.[144] It has also provided experimental evidence that, when coke formation is suppressed, increased liquid yields are favored over increased gas yields at pyrolysis temperatures below 775 K.

FUTURE ACTIVITIES

The prototype nature of the 6 inch I.D fluidized-bed reactor resulted in a failure of the burner area metal structure near the end of the above studies. Therefore, it was necessary to reconsider the burner function and develop an improved burner design. The new design call for two burners in order to reduce the heat load believed to be part of the cause of metal failure

using the former one burner design. The new burners were also designed to contain refractory, which will be cast on site. The new burners will be stainless steel and attached to the reactor with flanges and, will thus, be useable on the new stainless steel reactor when it is built.

ROTARY KILN PYROLYSIS OF OIL SANDS

Principal Investigator: F.V. Hanson
Graduate Student: H. Zheng

PERFORMANCE AND CALIBRATION OF DRY MATERIALS FEEDERS WHEN FEEDING OIL SANDS

INTRODUCTION

The commercial development of the Uinta Basin oil sands will most likely involve a central processing facility fed by satellite recovery operations on the major deposits: Asphalt Ridge, Hill Creek, PR Springs, Sunnyside and Whiterocks. The bitumen and/or bitumen-derived heavy oil recovery processes will include a combination of in-situ thermal enhanced oil recovery and mining-surface recovery schemes. The mining-surface recovery process concepts investigated for potential application to Uinta Basin oil sands deposits are aqueous bitumen separation [23,30,87,187,188], solvent extraction of the bitumen [189-193], and oil sands pyrolysis to produce a bitumen-derived heavy oil[26,127,130,134,145, 152, 171,175,194,195]. Fluidized-bed [26,127,130,134,171,175] and rotary kiln [145,194,195] reactors have been used to develop the product distribution and yields, and liquid product quality data base in the pyrolysis studies.

Materials feeding has historically been a problem in the laboratory and pilot-scale development studies of oil sands pyrolysis processes.[152,171] Typical feeding problems included: (1) oil sands agglomeration and plugging of the feeder and in the auger housing; (2) feed rates tended to decrease with time; (3) feed

rates were not reproducible; and (4) feed rates were not consistent during a run. Cha[145] circumvented feeder problems by using the spent sands produced in the rotary kiln pyrolysis reactor to dilute the oil sands feed. The overall objective of this study was to determine the conditions required to feed undiluted oil sands to a reactor at a constant mass flowrate.

The specific objectives of this study included the following: (a) determine the effect of the oil sands moisture content on feed rate; (b) determine the effect of auger speed on feed rate; (c) determine the effect of auger-housing clearance sleeves on auger performance; (d) evaluate and compare helical and coated or non-coated solid flight augers; (e) determine the effect of hopper fill level on the feed rate; and (f) evaluate feeder performance at various oil sand/diluent ratios.

EXPERIMENTAL

Feed Materials

The mined and crushed ores from the Whiterocks and PR Spring oil sand deposits were used in this study. The spent sand produced during rotary kiln pyrolysis of the Whiterocks oil sand was used as a solid diluent in some experiments. The carbonaceous residue content of the spent sands was 0.8 wt%. Bitumen saturations and moisture contents of the feed sands are presented in Table 40. The oil sands samples were spread-out in a thin layer in a polyethylene box and allowed to air-dry to evaporate gravitational water.

Table 40

Bitumen Saturation and Moisture Content of Oil Sand Samples used for Feeder Calibration Studies

Oil Sand Source	Bitumen Saturation (wt%)	Moisture Content (wt%)
Whiterocks	5.0/7.0	0-12.0
P. R. Spring	10.8	0-6.8

Note: Moisture content is on an air-dried basis.

Experimental Apparatus

A schematic of a typical Acrison bin-discharge, dry materials feeder is presented in Figure 87. The Acrison feeder consists of a solids feed hopper fitted with an intromitter to prevent slumping, bridging and agglomeration of the feed in the hopper, a feed auger fitted with an end bearing, a jacketed auger and a gear box driven by a DC motor. The bulk material in the hopper was mixed by the intromitter. The cooling jacket was intended to cool the auger housing during the course of a run. The temperature rise (1 to 5°C) was due to frictional heating of the oil sand as it moved through auger housing. The bins were purged with nitrogen to prevent oxidative degradation of the bitumen during the course of an experiment. Feeder models and augers used in this study are listed in Table 41. Three types of auger were tested: solid flight augers, a special fluorocarbon polymer-coated solid flight auger and a helical auger.

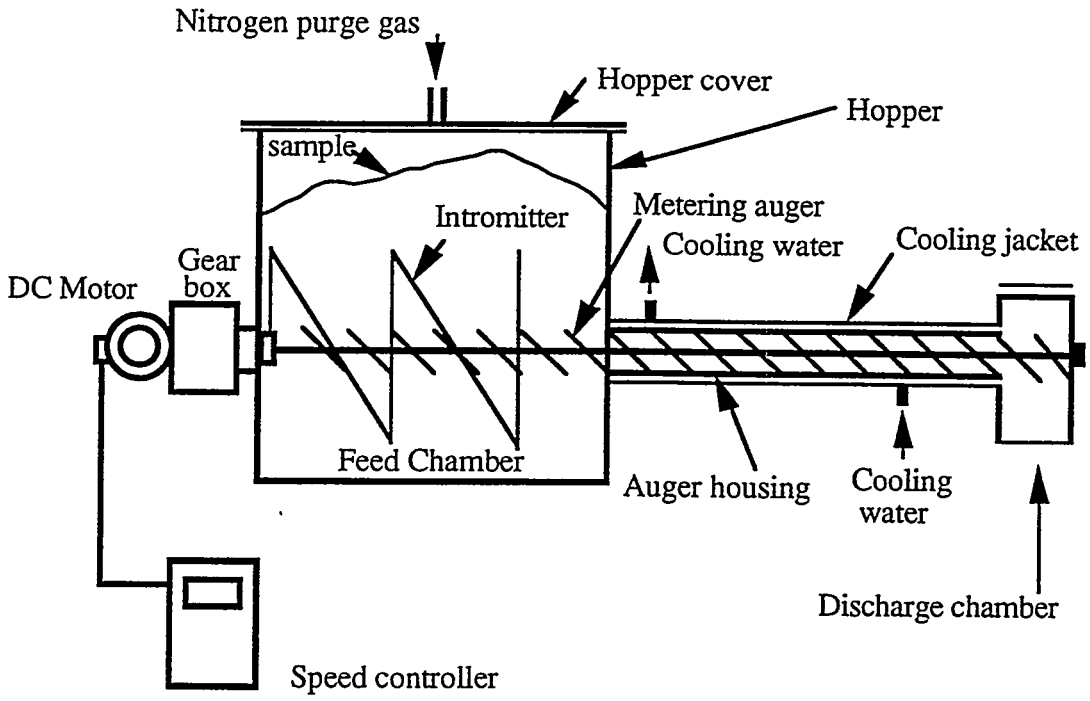

Figure 87. Acrison Dry Materials Feeder Schematic

Table 41

Feeder and Auger Designations

Feeder Models	Feeder Capacity (ft^3)	Auger Size Code	Auger Configurations
105Z	2.0	D, G	Solid flight
BDF-1.0	1.0	C, D, E, F, G	Solid flight, helical, and coated
BDF-1.5	2.0	E, H	Solid flight

Methodology

Preparation of feed mixtures

The mined PR Spring and Whiterocks oil sand ores were crushed and screened through a 1/2-inch screen with square openings. Feed mixtures of Whiterocks oil sand and spent sand were prepared by mixing the appropriate amount of each in a portable concrete mixer for approximately 20 minutes. Undiluted oil sands and spent sand feeds were also mixed prior to use.

Feeder calibration procedures

Ten to fifty kilograms of oil sand feed were placed in the feed hopper for each experiment depending on the size of the feeder selected for study. The feeder was started and the weight of sample discharged from the feeder was determined as a function of time. The cumulative weight delivered from the feeder was measured at 5-minute intervals. The average feed rate (g/min) was calculated from the cumulative weight delivered (g or kg) during specific time intervals. The temperatures in the hopper, on the auger and in the auger housing were measured before and after each run.

RESULTS AND DISCUSSION

Performance data for the various feeders, auger sizes and configurations provided insight regarding the use of Acrison feeders to feed oil sands to process units. Using spent sands as a diluent or increasing the auger rotation speed failed to improve the performance of the smaller augers (C, D, E). The larger size augers (F, G, H), with cooling jackets, gave the most consistent feeding. The factors found to affect feeding were: (1) bitumen content of the oil sand, (2) moisture content of the oil sand, (3) temperature rise in the auger and auger housing during the operation of the feeder, (4) motor speed of the feeder controller, (5) the level of oil sand in the feeder hopper, (6) the auger size and auger configuration, (7) ratio of spent sand-to-oil sand, and (8) effect of shear in the auger auger housing.

Feeding performance with small augers

The performance of D-size solid-flight augers installed on the BDF-1.0 and 105 Z feeders using the Whiterocks oil sand is shown in Figures 88 and 89. The auger plugged with the oil sands after 1.5, 3 and 4 hours operation at controller set points of 10, 90 and 50%, respectively (BDF-1.0 feeder, D auger, Figure 88). Inspection revealed that oil sand was building up on the auger at the outlet to the auger housing. Installation of a sleeve to minimize the space between the solid flight of the auger and the auger housing gave no improvement.

The inconsistent average feed rates are indicated in Figure 89 (105Z-D auger feeder) at controller set points of 10, 30, 50 and

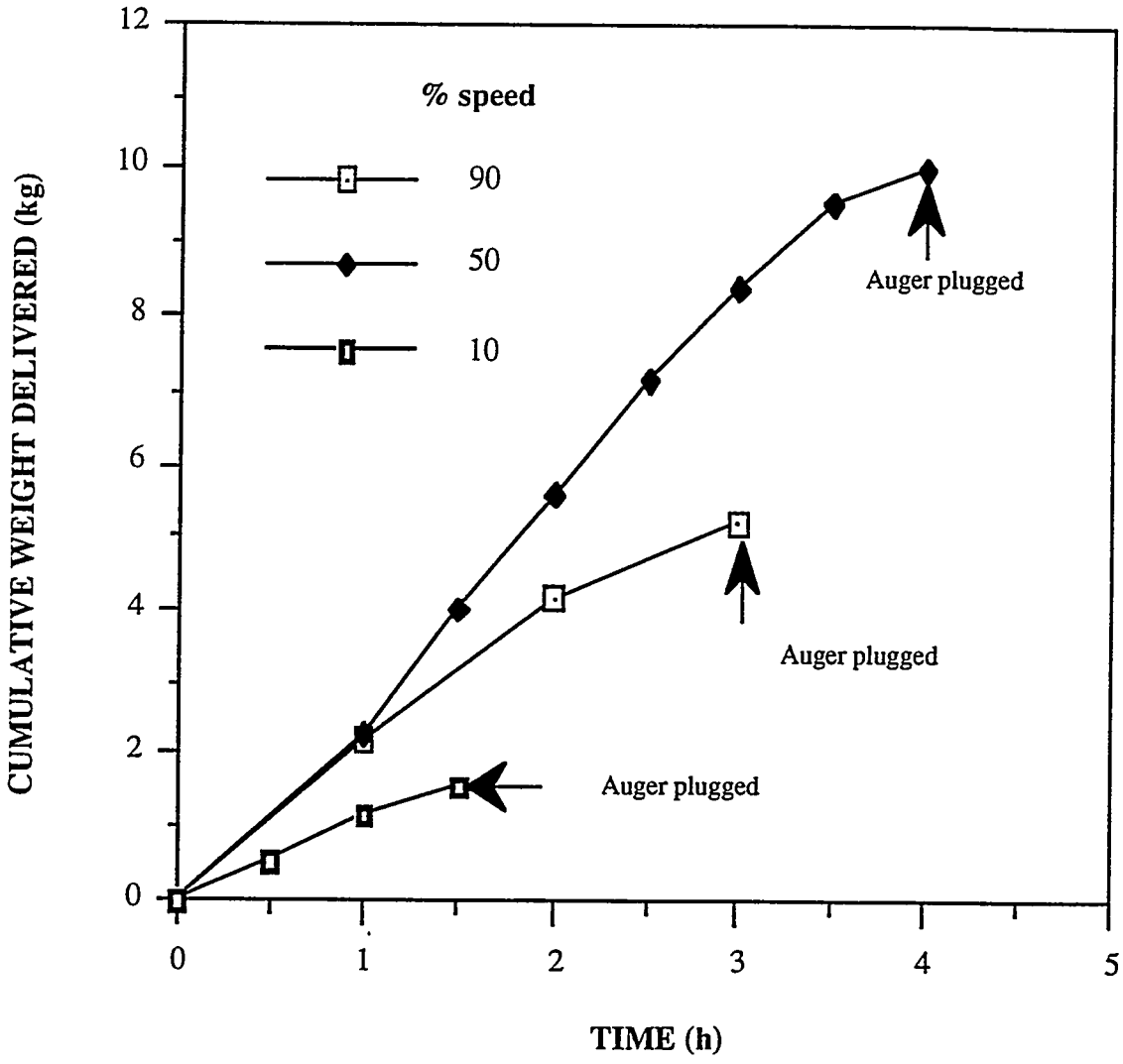

Figure 88. Average Feed Rate Vs. Time for 105Z-D feeder using 100% Whiterocks Oil Sand

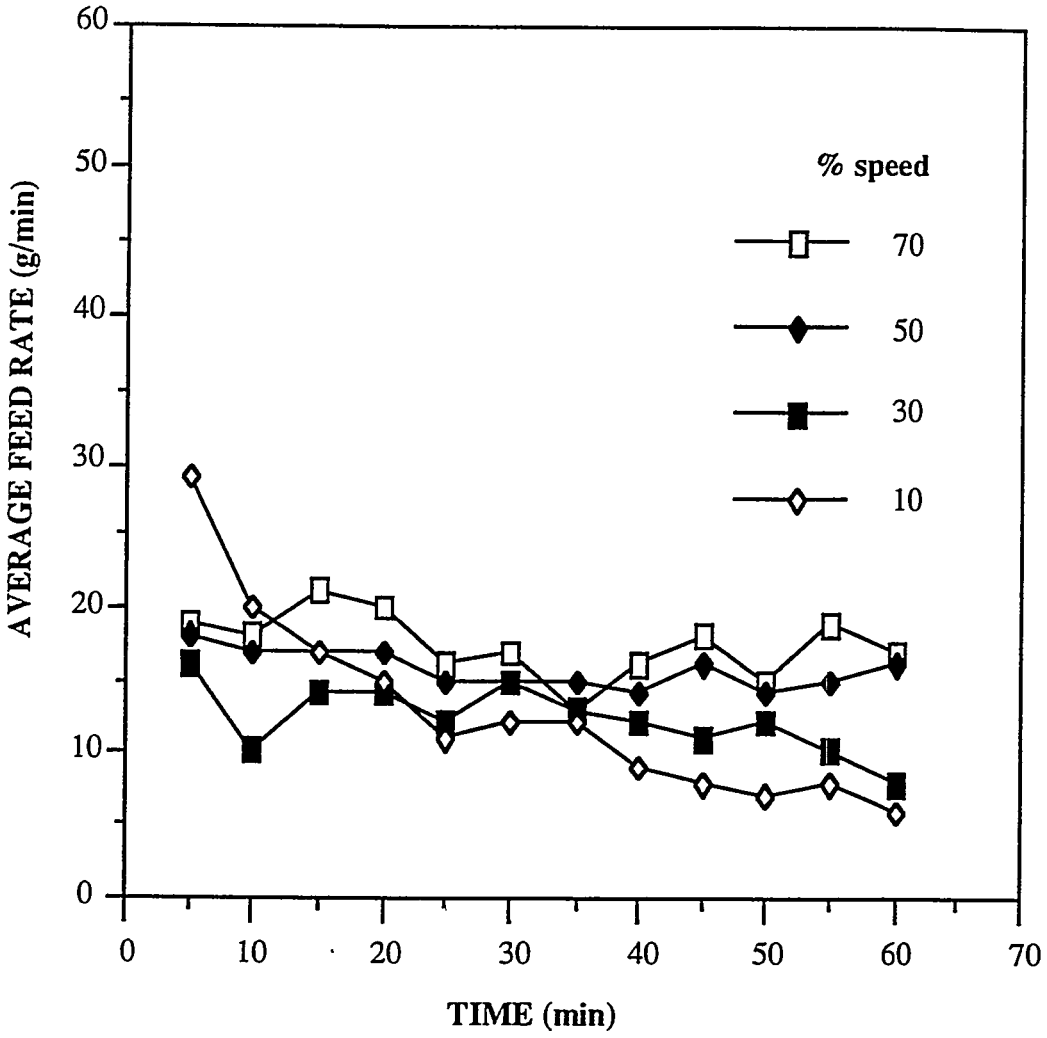

Figure 89. Average Feed Rate Vs. Time for 10Z-D Feeder Using 100% Whiterocks Oil Sand

70% of full range. These inconsistencies are caused by the nature of the bitumen on the oil sands fed. The average feed rate at a set point of 10% was the same as the average feed rate at 30% (see Table 42). This may have been the result of reusing the oil sand sample in successive tests. The oil sands changed visibly with each use thus the practice was discontinued.

Table 42

Statistical Analysis of Average Feed Rates (Figure 89.)

Set Point % Full Range	10	30	50	70
No. of points	12	12	12	12
F_{AVG}(g/min)	12.9	12.3	15.8	17.4
σ_{n-1}	6.6	2.3	1.3	2.2
σ_{n-1}/F_{AVG}(%)	51.6	18.8	8.2	12.8

F_{AVG} -- average feed rate (g/min)

σ_{n-1} — standard deviation

σ_{n-1}/F_{AVG}— relative deviation (%)

Whiterocks Oil sand and spent sands were mixed in ratios of 2:1, 3:1 and 4:1 for use as feed material with a 105Z feeder. The feed rate increased at lower oil sand-to-spent sand ratios(2/1) (Figure 90). However, the average feed rates were significantly less during the runs with the 4/1 and 3/1 mixtures. These observations may be related to a number of factors: temperature increase of oil sands during feeding; the fill-level of crushed ore in the feed hopper; and shear-working of the oil sand ore during

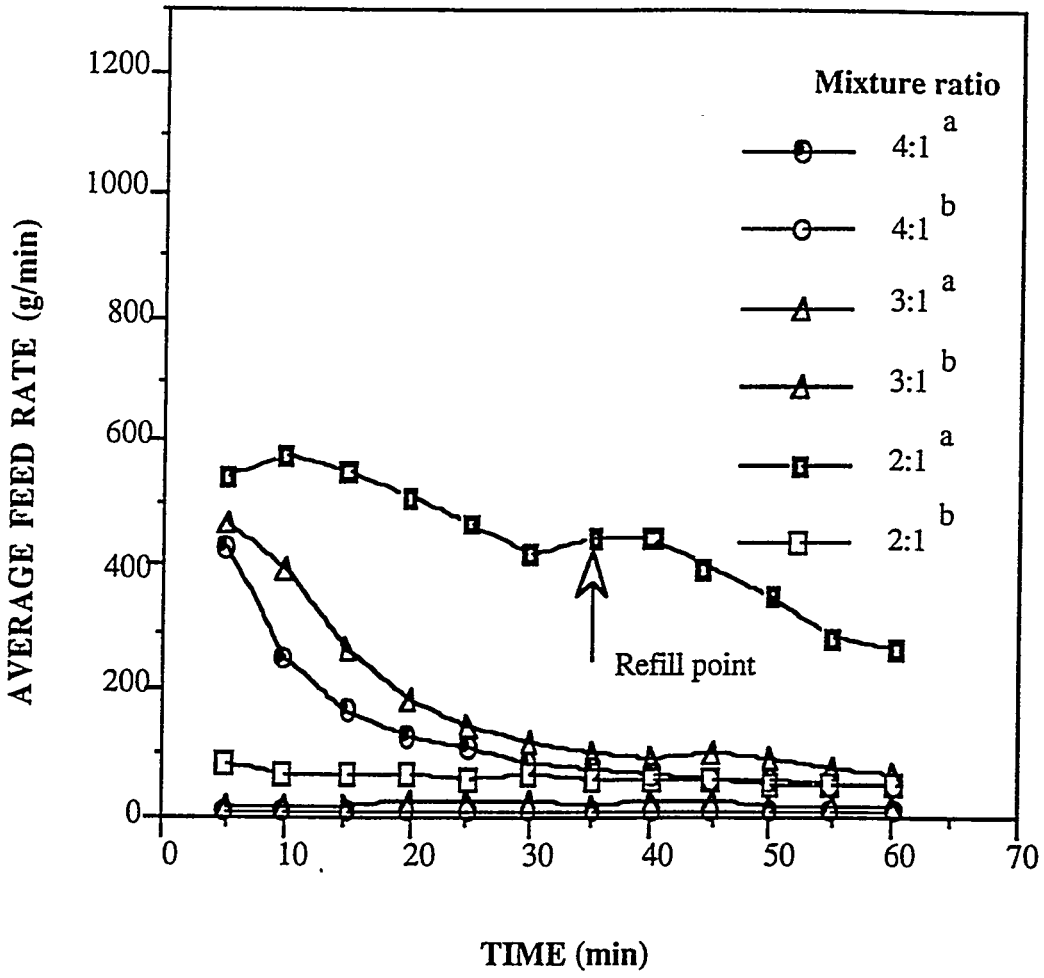

Figure 90. Average Feed Rate Vs. Time for 105Z-D Feeder Using Oil Sands and Spent Sands Mixtures at 70% Speed a--Fresh Sample; b--Reused Sample

feeding. The temperature increases in the feed hopper, the auger and the auger housing were 1°C, 5°C and 2°C, respectively, after a 1-hour run at a motor controller set point of 70% of full range. The temperature rise caused the bitumen to soften which caused the crushed ore to agglomerate and clump, leading to a decrease in the feed rate.

Refilling the feed hopper during the course of an experiment appeared to influence the feed rate with smaller sized augers: the decline in the feed rate with time was arrested for a period of time (10-15 minutes) after which the decline resumed. This effective increase in feed rate with the addition of feed to the hopper was most likely due to compaction of the ore in the hopper, thus, increasing the "packed" density of the ore being delivered by the auger. The decrease in feed rate with time resumed once the intromitter had completely mixed and "fluffed" the ore in the hopper thus reducing its "packed" density and, concomitantly, the feed rate. This effect is illustrated in Figure 90 for the experiment with fresh oil sands with an oil sand-to-spent sand ratio of 2:1 and a motor controller set point of 70% of full range.

It became apparent during the course of this investigation that the recent rheological history of the oil sands ore being fed influenced the feed rate with the small augers. The feed rates of ore sample which had been previously fed through the auger(four, 4-hour passes through the feeder system at a controller set point of 70% of full range) gave feed rates significantly below those obtained with a fresh oil sand sample. Inspection of the ores which

had passed through the auger revealed a distinctive color change. That is, they were much darker when compared to the fresh ore. The reduced feed rate and color change are presumed to be related to the compaction and frictional interaction of the bitumen-impregnated sandstone granules during passage through the auger. The shear forces acting between bitumen-coated granules and between bitumen-coated granules and the metal surfaces of the auger and housing produces significant local thermal gradients. These thermal gradients soften the bitumen and cause agglomeration and compaction leading to reduced feed rates and to a spreading or "working" of the bitumen on the granules as well as transfer of bitumen from the oil sand granules to the spent sand granules thus giving rise to the color change. Immediate reuse of the used sand as feed sand does not allow sufficient time for the agglomerates to "break-down" to their previous state even though the intromitter constantly mixed the feed material in the hopper. Thus, upon feeding, it is possible that agglomerates grow in size further reducing feed rates.

An F-size coated auger and a helical auger were also tested. Neither showed significant improvement during feeding when compared to an uncoated, solid flight auger.

Feeding performance with large augers

The effect of moisture content on feeding was tested using the Whiterocks oil sand ore (7.0 wt% bitumen saturation) in a BDF-1.5 feeder with an H-size auger.

Moisture contents were based on an air dry sample being 0.0 wt%. The cumulative mass of oil sands fed in 8 minutes is plotted vs. wt% moisture in Figure 91. A higher oil sands moisture content resulted in a lower feed rate.[14] 100% Whiterocks (5.0 wt% bitumen content) and PR Spring (10.8 wt% bitumen content) oil sands were fed with a G auger from a 105Z feeder (Figures 89, 92 and 93). The average feed rate was much more stable with the G-size auger than that with the D-size auger. This can be seen by comparing Figures 89 and 90 with Figures 92 and 93. The relative deviation shown in Table 45 and 46 is also much smaller than in Table 42 and 43. As

Table 43

Statistical Data for Fresh Mixture Sample Feeding at 70% Speed (Figure 90).

Feed Ratio* (kg/kg)	2:1	3:1	4:1
No. of data	12	12	12
F_{avg} (g/min)	438.1	176.5	128.0
σ_{n-1}	99.87	132.39	110.65
σ_{n-1}/F_{avg} (%)	22.8	75.0	86.7

* Note: Ratio is the weight ratio of oil sands to spent sands.

expected, the higher bitumen content PR Spring sample gave a lower feed rate than the Whiterocks oil sands. No significant hydrodynamic effect was found with the G-size auger (see Figure 93) at the refill point. A correlation was established between the set point of the motor speed controller (% full range) and the feed rate for the model 105 Z-G feeder (Figure 94) .

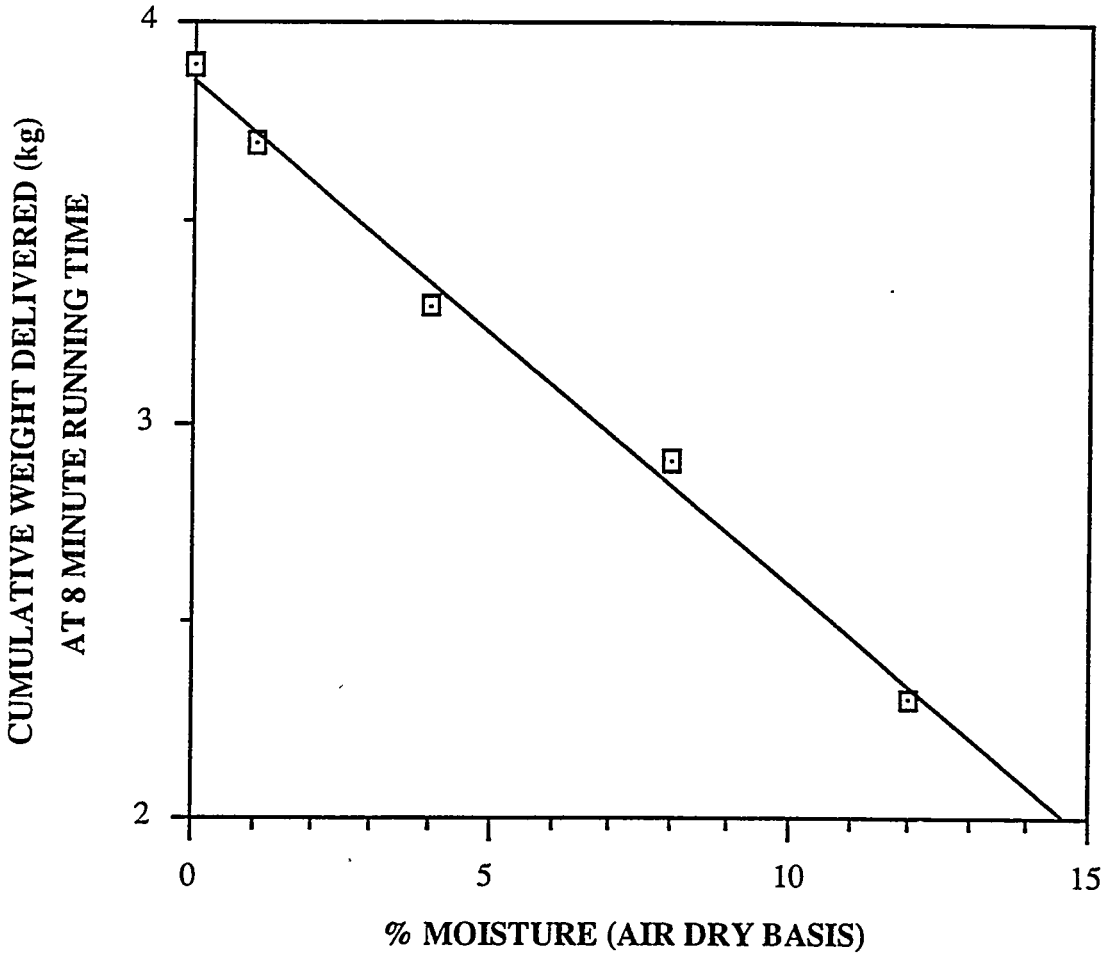

Figure 91. Moisture Content Effect on Feed Rate from a BDF-1.5 Feeder (H-Auger Using 100% Whiterocks Oil Sands)

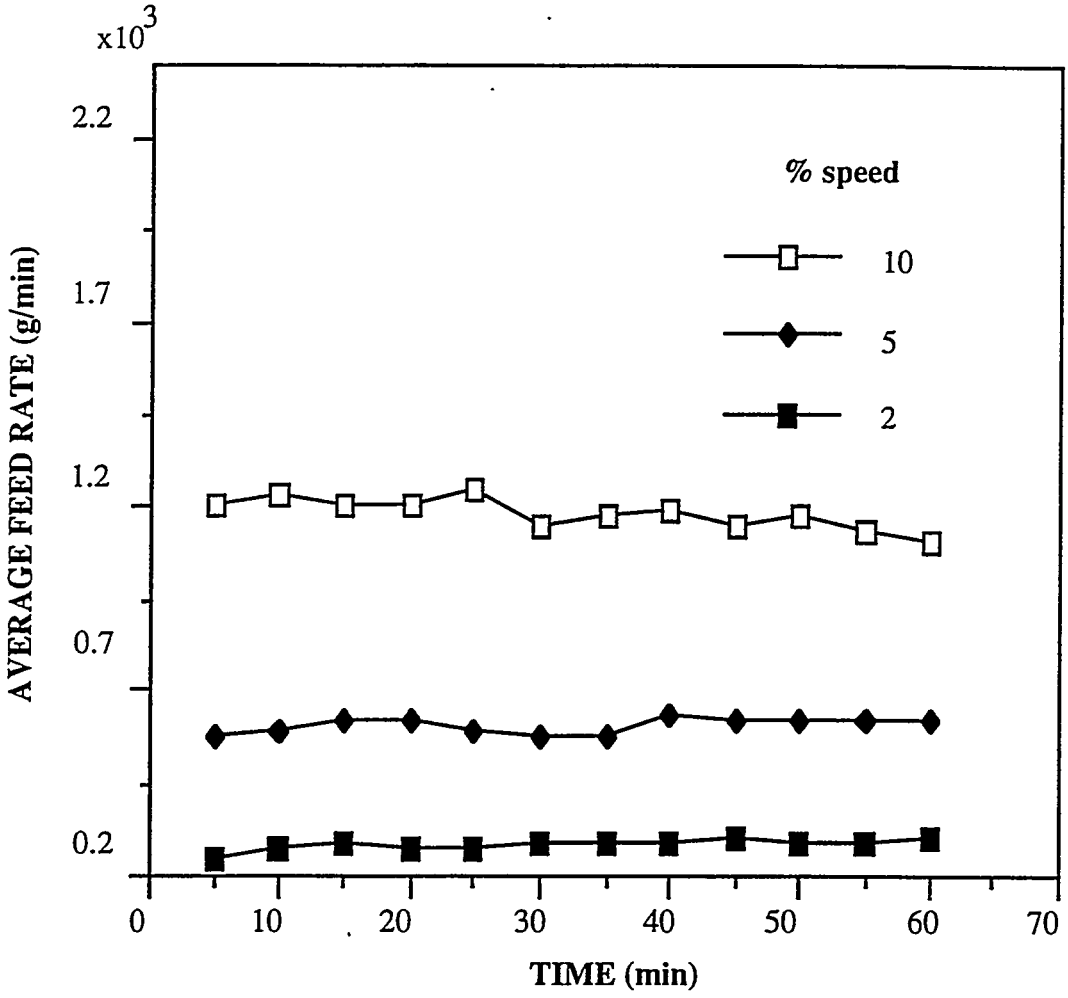

Figure 92. Average Feed Rate vs. Time for 105Z-G Feeder Using 100% Whiterocks Oil Sands

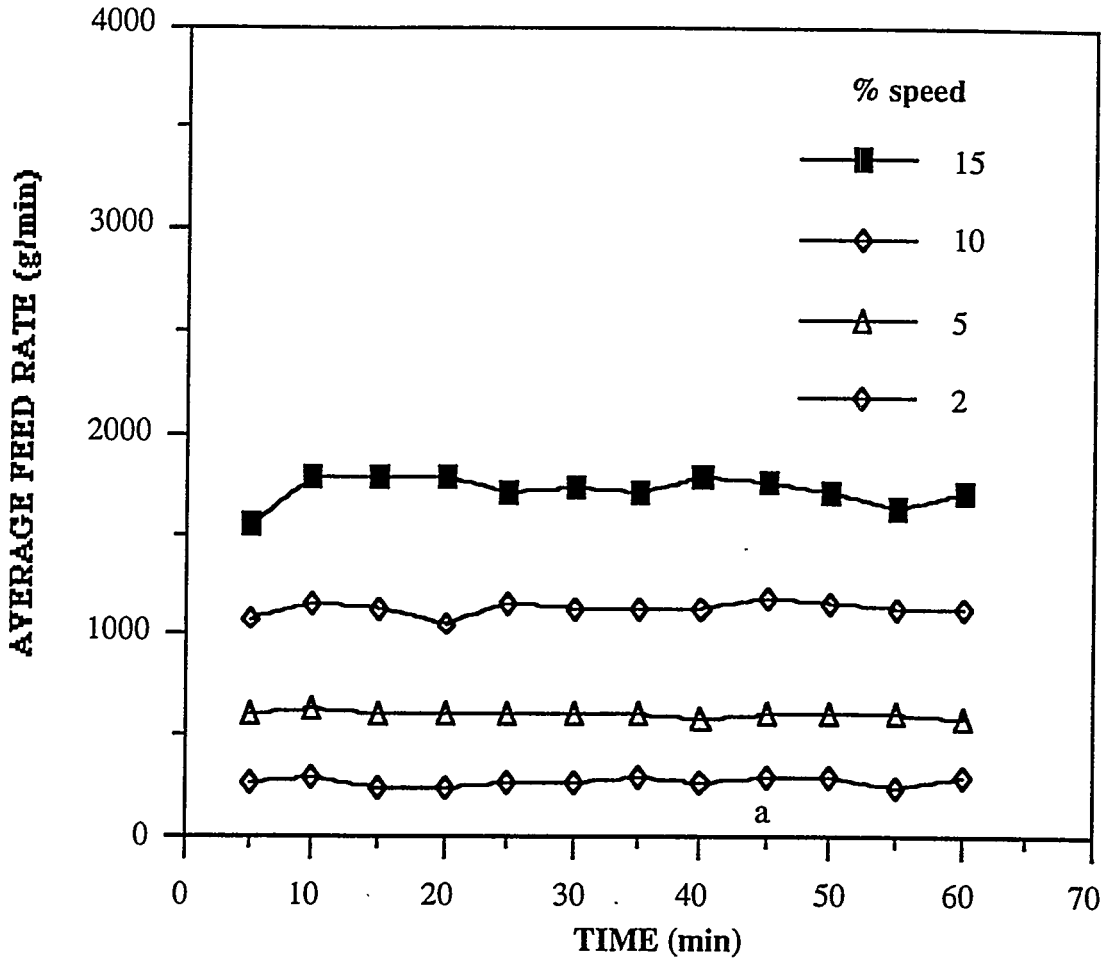

Figure 93. Average Feed Rate vs. Time for 105Z-G Feeder Using 100% PR Spring Oil Sands; a--Refill Point

Table 44

Statistical Data for Used Mixture† Feeding at 70% Speed (Figure 90).

Feed Ratio (kg/kg)	2:1	3:1	4:1
No. of points	12	12	12
F_{avg} (g/min)	62.0	21.4	8.8
σ_{n-1}	9.4	1.5	1.7
σ_{n-1}/F_{avg} (%)	15.1	7.0	19.4

† Note: Used oil sands were used for 4-hour runs and four times through the auger housing.

Table 45

Statistical Data for 100% Whiterocks Oil Sand Feeding (Figure 92.)

Set Point % Full Range	10	5	2
No. of data	12	12	12
F_{AVG}(g/min)	1181.6	604.6	282.5
σ_{n-1}	42.0	21.4	16.2
σ_{n-1}/F_{AVG}(%)	3.6	3.5	5.7

The correlation for the Whiterocks oil sand (5 wt% bitumen saturation) was given by:

$F = 43.2 + 110.6S$

The correlation for the PR Spring oil sand (10 wt% bitumen saturation) was given by:

$F = 51.0 + 112.7S$

where F is the average feed rate (g/min)

S is the motor speed set point(% full range).

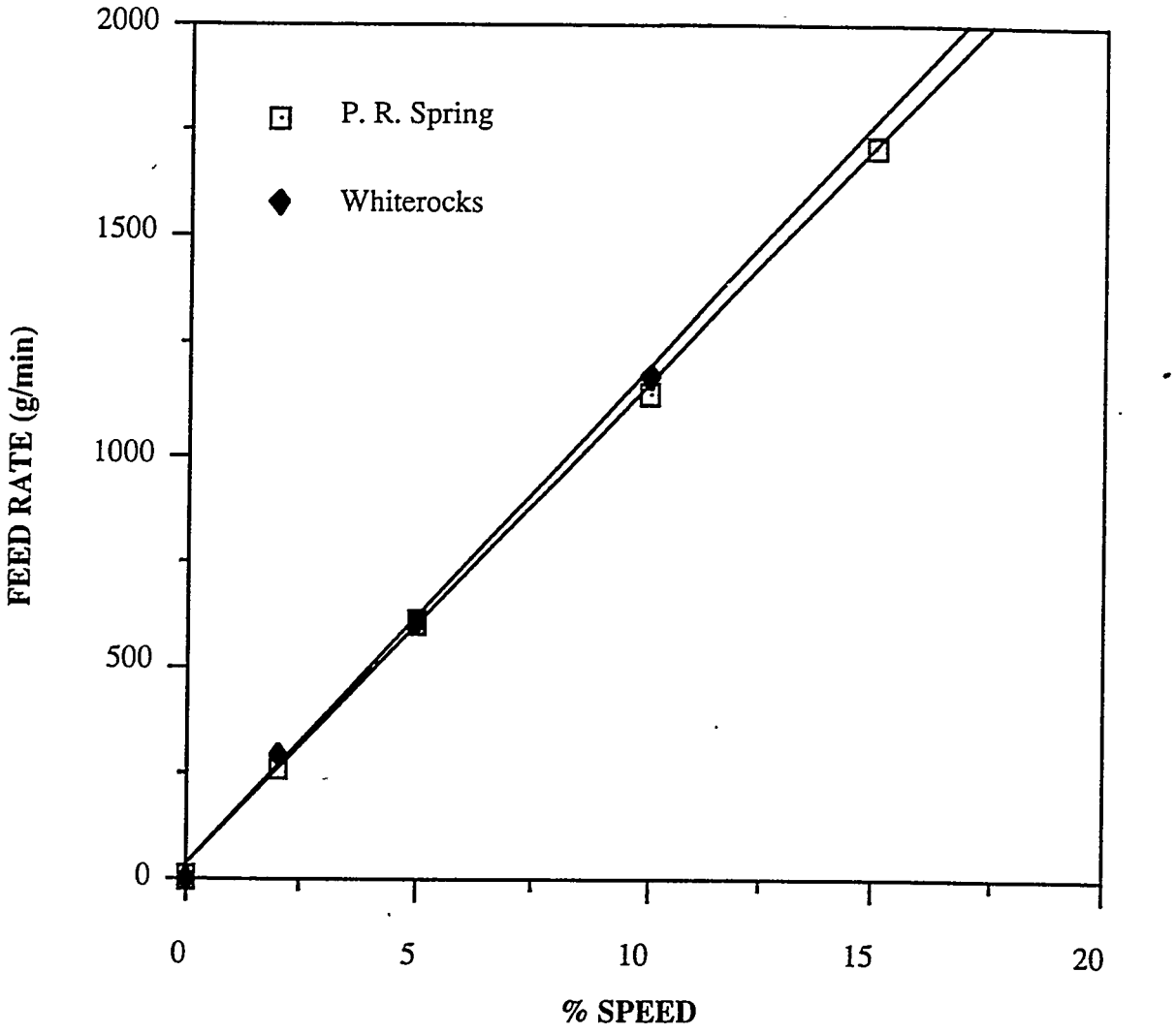

Figure 94. Feed Rate vs. Motor Speed (%) for 105Z-G Feeder Using 100% Oil Sands

Table 46

Statistical Data for 100% PR Spring Oil Sand Feeding (Figure 93).

Set Point % Full Range	15	10	5	2
No. of data	12	12	12	12
F_{AVG}(g/min)	1709.1	1137.1	600.1	266.2
σ_{n-1}	74.3	27.7	16.1	23.5
σ_{n-1}/F_{AVG}(%)	4.4	2.4	2.7	8.8

SUMMARY AND CONCLUSIONS

Continuous, reproducible solids feeding has been a problem associated with oil sands surface mining-recovery process development studies. Commercial Acrison bin-discharge feeders were tested for oil sand feeding in rotary kiln and fluidized-bed pyrolysis reactors and in spent sand combustion reactors. Feeder calibration experiments were conducted using spent sands, oil sands and mixtures of fresh and spent sands. Three types of feeder, nine different sized augers, and three different auger types were tested. Experimental data included average feed rates and cumulative weight delivered from the feeder. The factors which were determined to affect oil sands feeding were: (1) bitumen content of the oil sand, (2) moisture content of the oil sand, (3) temperature rise in the auger and auger housings during the operation of the feeder, (4) auger rotation speed which was controlled by motor speed controller, (5) level of oil sand in the feeder hopper, (6) auger size and type, (7) ratio of spent sand to oil sand in the feed mixture, and (8) effect of shear in the auger and auger

housing. A larger size auger running at low speed with a water jacketed auger housing gave the best feeding performance.

The successful application of an auger-type dry materials feeder for feeding oil sands to a process reactor or vessel requires careful consideration of the following findings:

1. Fast auger speeds did not give constant or reproducible feed rates.
2. Small diameter augers are less likely to give constant oil sands feed rates than large-diameter augers.
3. Dilution of the oil sands with spent sands improved feeder performance, however, small diameter augers still did not give constant feed rates.
4. Compaction of oil sand feed in the hopper appeared to temporarily increase feed rates with small augers.
5. Oil sand feed rates are directly proportional to the oil sand moisture content (on an air-dry basis).
6. Reducing the clearance between the feed auger and auger housing with a sleeve did not improve the feeder performance with oil sands.
7. A helical auger offers no advantage in feeder performance using oil sands.
8. Augers with special coatings gave no significant improvement with regard to reducing the tendency of the oil sands to adhere to the auger flights.

9. Large diameter augers, running at slow speeds and low temperatures, are most likely to yield linear and reproducible feed rates.

NOMENCLATURE

F_{avg} -- average feed rate (g/min) (based on 5 minute sample collection)

σ_{n-1} -- standard deviation

σ_{n-1}/F_{avg} -- relative deviation (%)

F--average feed rate (g/min) (based on 1-hour sample collection)

S--motor speed (% speed)

FUTURE ACTIVITIES

The solids residence time distribution studies will be completed in an attempt to develop a modified operating procedure so that all the bitumen-derived liquid produced during oil sands pyrolysis moves countercurrent to the solids. The rotary kiln pyrolysis process variable study with the PR Spring oil sands will be conducted after the modified operating procedure has been developed.

COMBUSTION OF CARBONACEOUS RESIDUES ON SPENT OIL SANDS IN A LABORATORY SCALE DENSE PHASE TRANSPORT REACTOR

Principal Investigator: F.V. Hanson
Graduate Student: H.Q. Tang

INTRODUCTION

The pyrolysis of oil sands in rotary kilns and fluidized beds results in the formation of a carbonaceous residue on the spent or coked sand. Combustion of the coked sand can provide sufficient energy to drive the oil sand pyrolysis reactions. A laboratory-scale dense phase transport reactor has been designed and constructed based on the theory and practice of circulating fluidized-bed combustors[196,197] to investigate the combustion of coked sand. Compared to bubbling fluidized-bed reactors, these reactors have the advantage of greater fuel flexibility, higher combustion efficiency, and higher throughputs based on combustor cross-sectional area. A thorough understanding of the bed hydrodynamics is necessary to evaluate the performance of the reactor. Both hydrodynamic and combustion experiments are discussed in this section.

EXPERIMENTAL APPARATUS

A schematic of the experimental apparatus is presented in Figure 95. The system consists of (a) a D-size auger, solids screw feeder; (b) an air supply and a preheating system; (c) a 3.81 cm ID 53 cm high gas-solid heating and an ignition furnace; (d) a 5.72 cm ID 71 cm high combustor on top of the gas-solid ignition furnace; and (e) a two-stage cyclone gas-solid dry-separation system. There

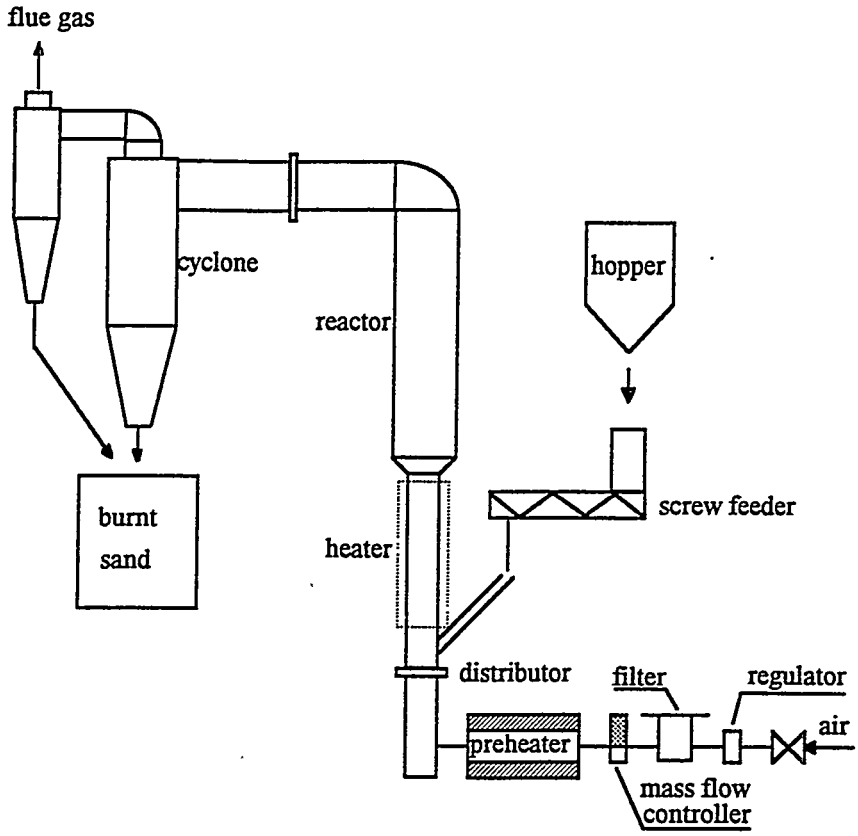

Figure 95. Schematic of the Dense Phase Transport Reactor Apparatus

are five thermocouples mounted in the combustion section to monitor the temperature variation during combustion. A sixth thermocouple is mounted underneath the distributor to measure the air temperature entering the reactor. There are also three pressure monitoring taps to measure the differential pressure across the combustion section and across the entire reactor. The distributor is a 20 μm porous metal plate, which has the advantage of easy machining, low cost, low pressure drop and better gas distribution. The temperatures and differential pressures are recorded by an IBM-XT computer through a HOTMUX temperature data logger. The reactor is supported by a three leg metal stand which is anchored to a leveled pad (Figure 96). The burnt sand and flue gas pass into the first cyclone where the primary gas-solid separation takes place. Fine particles entrained by the flue gas enter a second cyclone where these fines are recovered. The burnt sands recovered in the two cyclones are collected in a burnt sand receiver and the flue gas is vented. The solid particles used in these studies were a wide particle size distribution (0-1000 μm) coked sand produced by a 4-inch fluidized-bed oil sand pyrolysis reactor. The average particle size was 130 μm.

HYDRODYNAMIC STUDIES

Fluidization and Defluidization

Two different bed pressure drop versus superficial gas velocity curves are often observed in fluidization and defluidization of multisized particles.[134] These curves are illustrated in Figure 97. Although there are many different

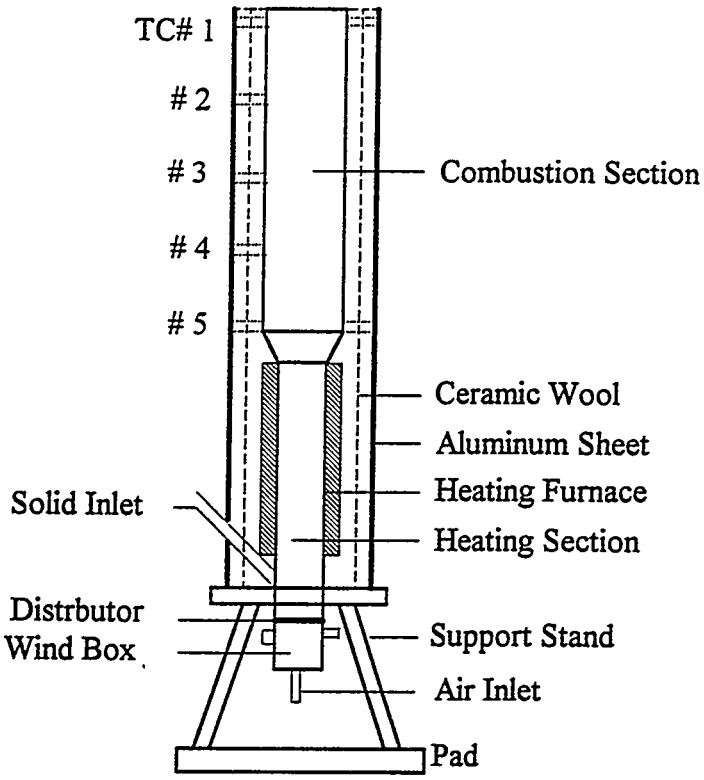

Figure 96. Reactor Schematic

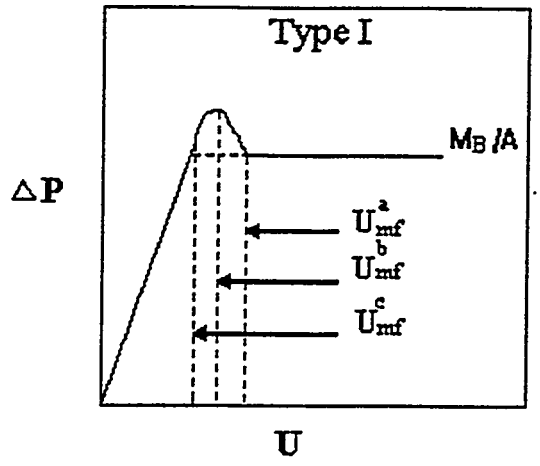

(a)

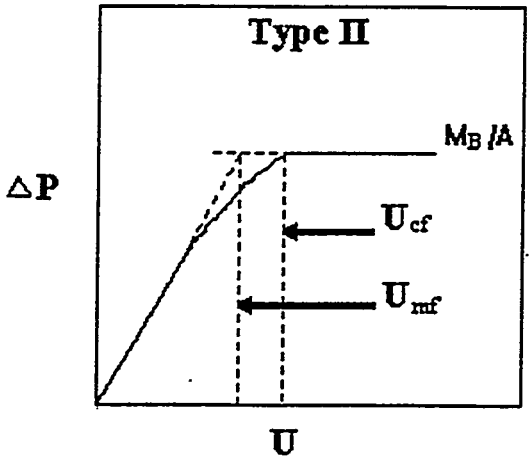

(b)

Figure 97. Typical Bed Pressure Drop vs. Gas Superficial Velocity

interpretations for minimum fluidization velocity,[198,199] U_{mf}^{b} was adopted as the minimum fluidization velocity in this study.

The fluidization-defluidization pressure drop as a function of air superficial velocity with the bed height (H) / bed diameter (D) ratio as a parameter is presented in Figures 98(a) and 98(b) (H/D ratios of 2.5 and 3.5, respectively). The fluidization pressure drop versus air superficial velocity with H/D ratios of 2.5, 3.0, and 3.5 is presented in Figure 99. It is seen (Figures 98 and 99) that both Type I and Type II curves (Figure 97) were observed for the multisized coked sand under both fluidization or defluidization conditions. As expected, Type I curves were observed when a bed of coked sand was fluidized by gradually increasing the gas flow through the bed. Type II curves were observed for the defluidization mode. Furthermore, Type II curves were also observed when the gas flow was increased stepwise in the fluidization mode. The experimental minimum fluidization velocity (U_{mf} = 1.7 cm/s) was determined from the curves in Figures 98 and 99.

Fletcher, et al,[200] reported that at ambient conditions, the following equations:

$$Remf = Ar/1400 \qquad Ar < 1400 \tag{130}$$

where

$$Re_{mf}=\frac{\overline{d_p}\rho_g U_{mf}}{\mu_g}. \tag{131}$$

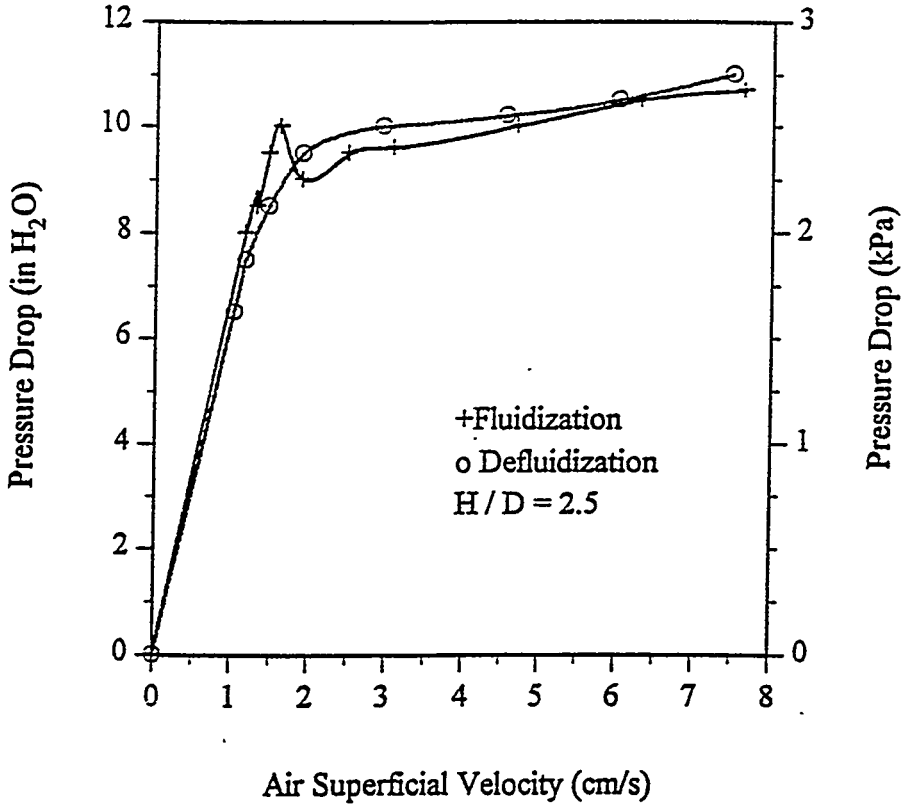

Figure 98(a). Pressure Drop vs. Air Superficial Velocity

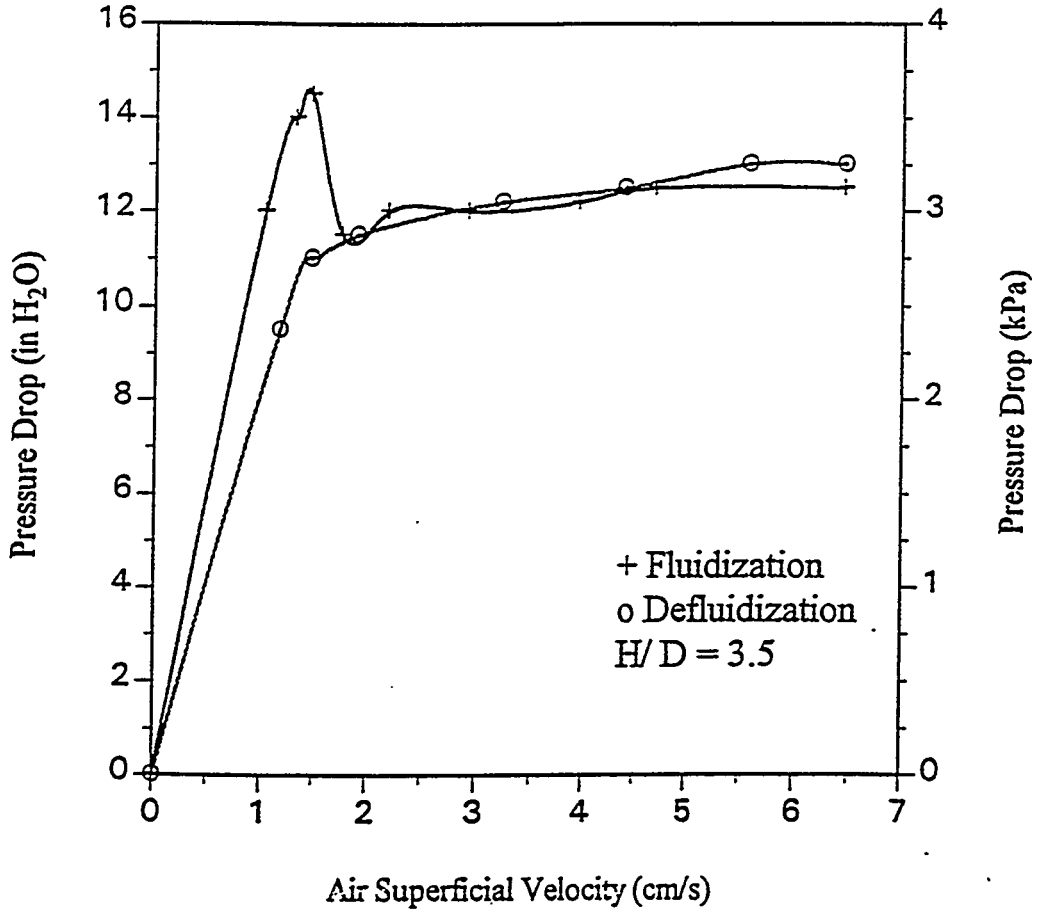

Figure 98(b). Pressure Drop vs. Air Superficial Velocity

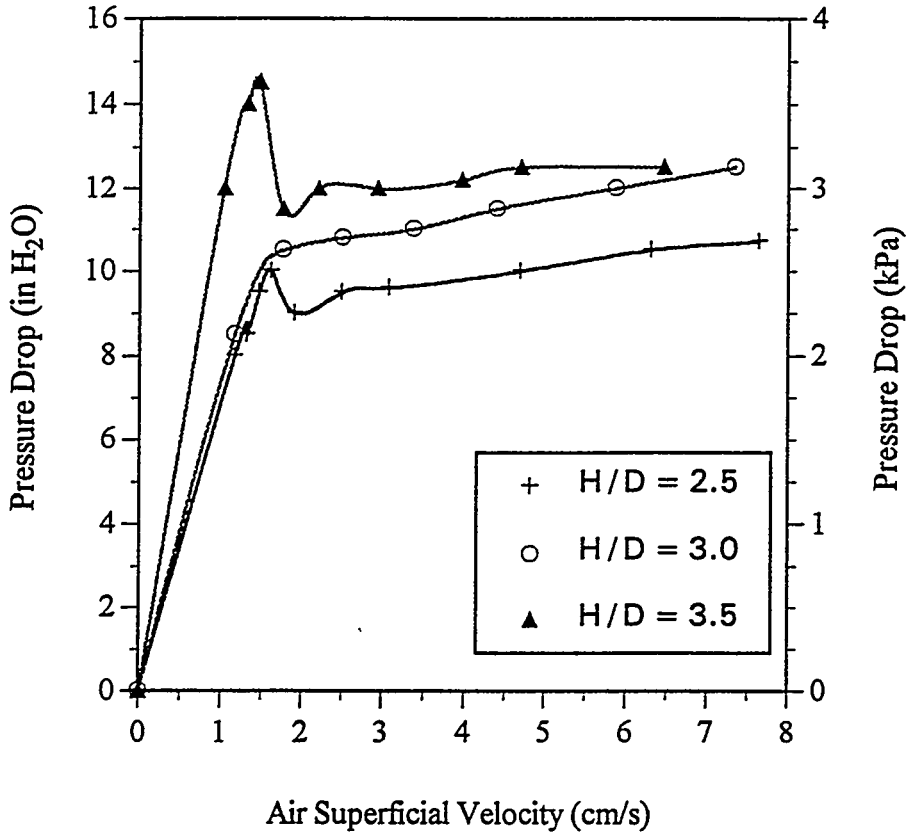

Figure 99. Fluidization Pressure Drop vs. Superficial Velocity

and the Archimedes number, Ar, is given by

$$Ar=\frac{\overline{d_p^3}g\rho_g(\rho_s-\rho_g)}{\mu_g^2} \qquad (132)$$

can predict Remf, and hence Umf, for some group B sands including coked sands. The predicted Umf calculated using equation 1,2 and 3 was 1.5 cm/s, which was very close to the experimental value (1.7 cm/s).

Flow Regime Transition Studies

Gas-solid contacting modes vary as the fluidization regime changes, thus, results obtained for one regime for a particulate material or reactor cannot be applied to another.[201] Specific reactor experiments in each fluidization regime are necessary to determine the transition velocities from one regime to another to establish the appropriate operating conditions. The purpose of the flow transition studies was to quantitatively characterize the flow dynamics of gas/solid fluidized beds for the transition from a fixed or settled bed to the transport mode with a wide-size distribution coked sand.

Pressure fluctuations are related to gas-solid contacting modes, or flow regimes. Thus, the flow regimes and their transition characteristics can be determined by monitoring the pressure fluctuation across the bed.[202] The pressure drop across the bed was

monitored and recorded with a HOTMUX data logger every 2 seconds. Starting from high superficial velocity (about 100 cm/s), the gas flow was decreased so that the superficial velocity was adjusted stepwise, until bubbling fluidization was attained.

The differential pressure across the bed (including the distributor) versus operation time or gas superficial velocity is presented in Figure 100. It is seen that the largest pressure fluctuation was observed at a superficial velocity of 49 cm/s. Nevertheless, it is difficult to distinguish the flow regimes directly from this figure.

The differential pressure data (Figure 100) was converted to the standard deviation of the pressure and plotted versus air superficial velocity in Figure 101. Ums is defined as the superficial velocity at the onset of plug slugging[203]. U_c is defined as the superficial gas velocity at which the differential pressure fluctuations begin to decrease from the maximum value marking the onset of a flow transition to a regime generally identified as turbulent fluidization.[204] Bubble coalescence and growth are predominant below U_c, while above U_c the bubbles (or voids) become unstable and break down frequently.[205] Uk is defined as the superficial velocity at which the differential pressure fluctuations have decayed to a minimum and begin to level out marking the onset of turbulence or refluxing pneumatic transport.[196] It can be seen from Figure 101 that U_{ms} is about 20 cm/s. As the gas superficial velocity increases, the standard deviation of the bed differential pressure fluctuation also

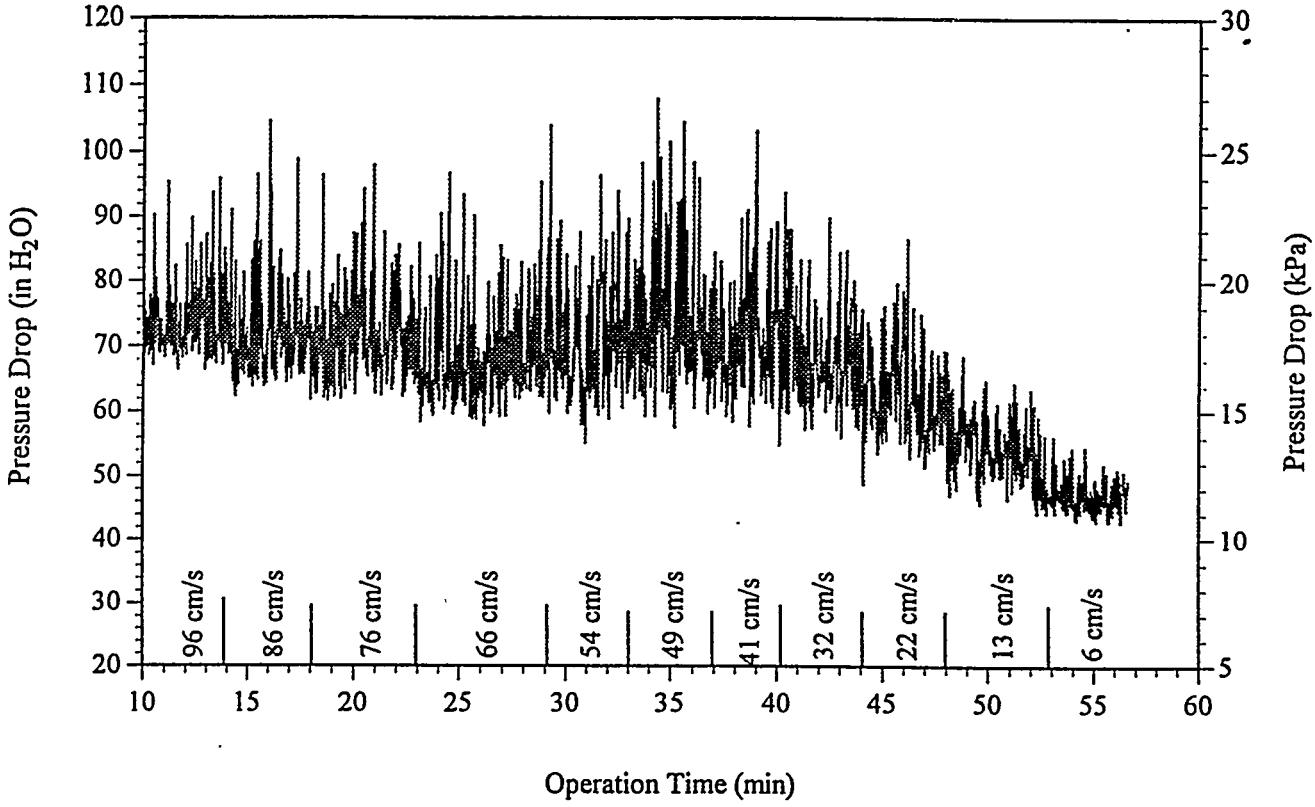

Figure 100. Pressure Drop vs Operation Time and Air Superficial Velocity

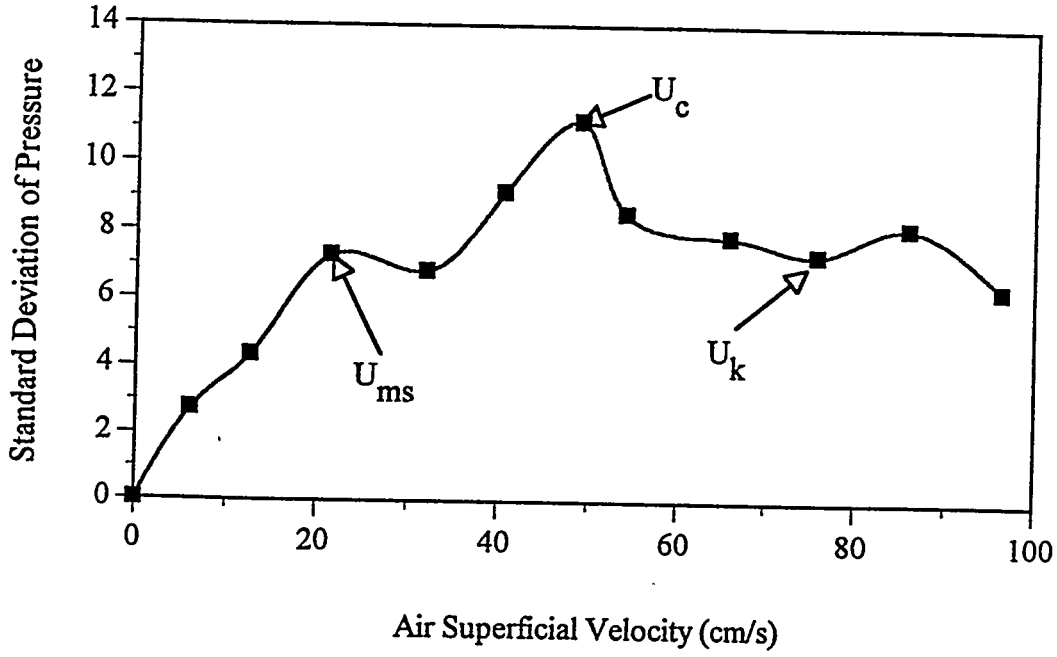

Figure 101. Standard Deviation of Pressure vs Air Superficial Velocity

increases up to a gas superficial velocity of 50 cm/s which is U_c. The decay in pressure fluctuation is primarily due to the holdup of solids in the free board region. At a gas velocity of 75 cm/s, the bed differential pressure fluctuation had decayed to a minimum value which is U_k (75 cm/s). At the transition velocity, U_k, the bed height approaches zero, which means that all of the solids are suspended as individual particles in the free board region.

Particle Residence Time Distribution Studies

Different sized particles have different residence times in a fluidized bed, especially at high superficial gas velocities. Thus, it is important to determine the particle residence time distribution for multisized coked sand to ensure high combustion efficiency.

In this study KMnO4 was used as the tracer material since it has the same average particle size and particle density as the coked sand (130μm and 2.6 g/cm3 respectively). Six grams of the tracer was mixed with six grams of coked sand and injected into the reactor with the spent sand fed through the outlet of the solids feeder. The time was started at the injection time and a sand sample was collected at the outlet of the gas-solid separation cyclone every 30 seconds for 17 minutes. The sample was dissolved in water, the solution was filtered and the filtrate was diluted to volume. An ultraviolet-visible spectrophotometer was used to analyze for the KMnO4 concentration in the solution. The KMnO4 concentration was converted to KMnO4 content per gram of sample collected.

The tracer concentration in the samples versus solids residence time is plotted in Figure 102 for superficial gas velocities of 65 and 85 cm/s. At both superficial velocities, there are two maxima. The first maximum is presumed to be related to fine particles by-passing the bed, especially for the case when Uo is 85 cm/s (the peak is higher and appears earlier).[12] The second peak is likely due to particle diffusion and back mixing.

Despite the fact that the average particle size and density are similar, it does not mean that the transit of the tracer and coked sand through the bed will be the same, since the coked sand size distribution is different from that of the tracer (Figure 103). In a second experiment, coked sand coated with KMnO4 was used as the tracer material. Following the same experimental procedure at a gas superficial velocity of 65 cm/s, the tracer concentrations in the solid samples were obtained and plotted versus residence time (Figure 104). It is seen that the coated coked sand tracer exhibited the same residence time trend as was observed with the KMnO4 granuler as the tracer except that the first large peak caused by fine particle bypassing comes a little later because of the difference in the particle size distributions.

COMBUSTION EXPERIMENT

A combustion experiment was carried out with preheated air entering the reactor at 653 K and a superficial velocity of 75 cm/s. The screw feeder was set to feed 170 g/s of coked sand to the reactor. The carbon content of the coked sand was 0.85 wt%, which gave an equivalence ratio for this experiment of 0.56 (fuel-lean).

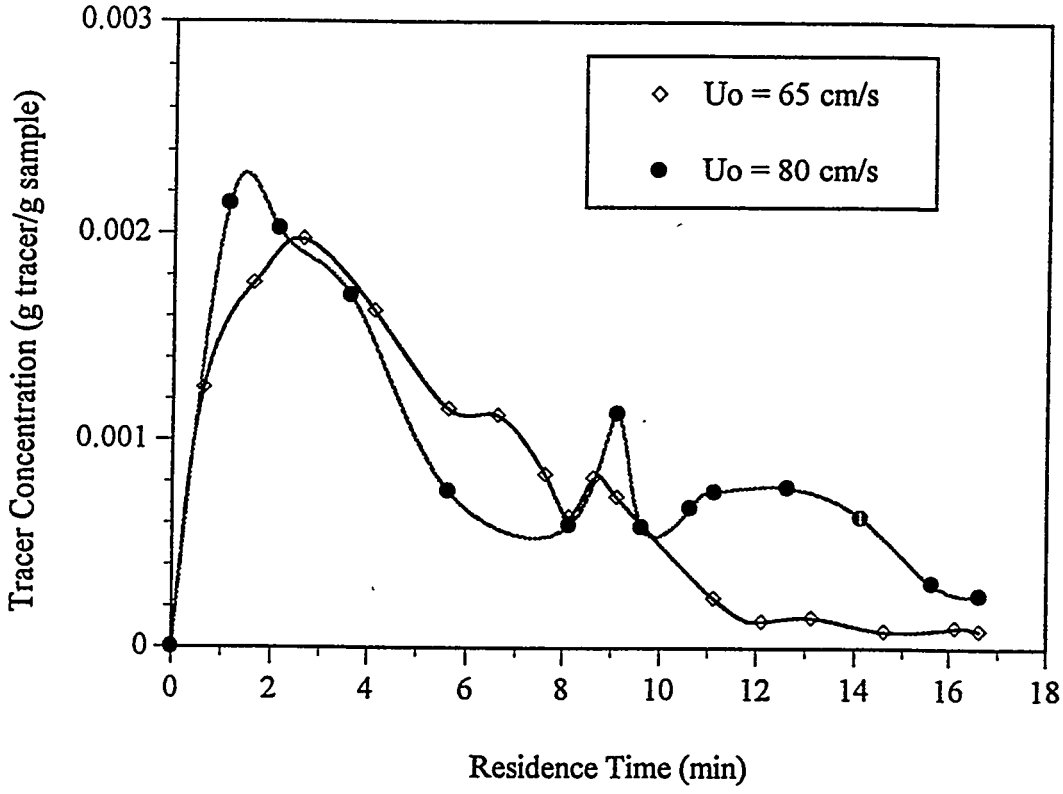

Figure 102. Tracer Concentration vs Residence Time

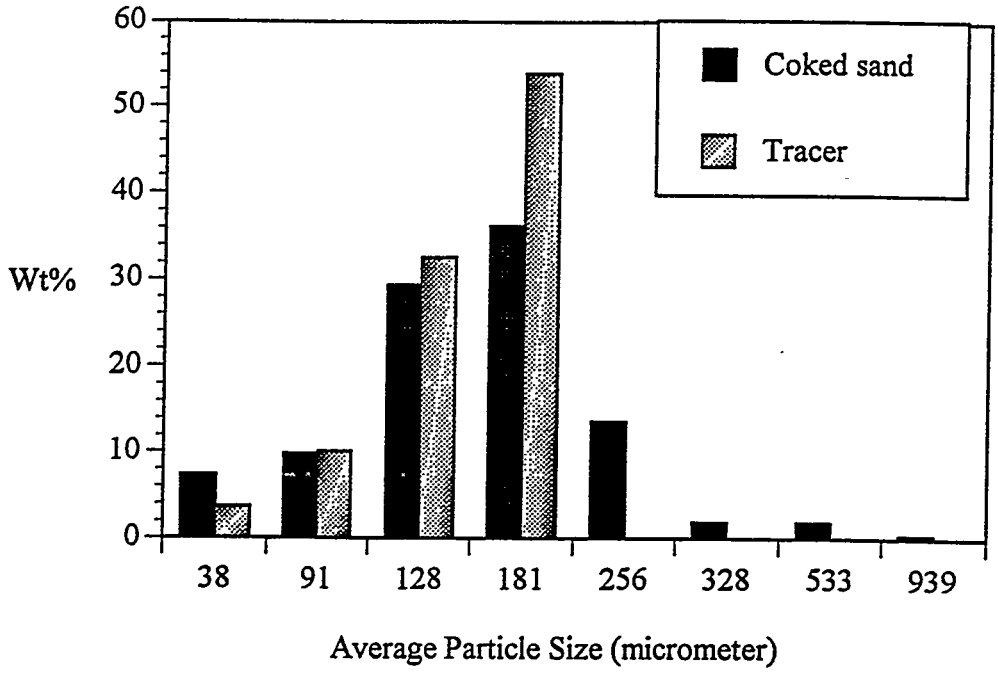

Figure 103. Coked Sand and Tracer Particle Size Distribution Comparison

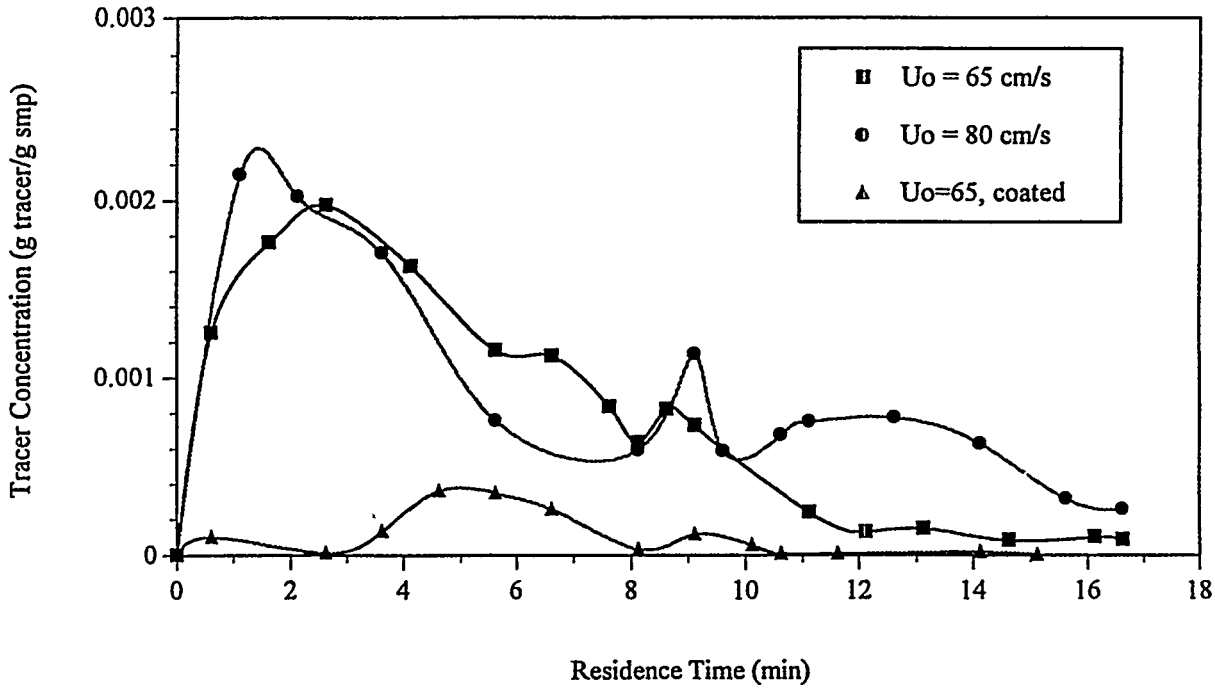

Figure 104. Tracer Concentration vs Residence Time

The temperature controllers for the air-coked sand heating and ignition furnace were set at 1073K. The time-temperature profiles for the six thermocouples before and after the solid feeding starts are presented in Figure 105. After the feeding started, thermocouples 1 and 2 rose, while the other three thermocouples in the lower region of the combustion section were unchanged. A comparison of the elemental analyses of the coked sand (feed) and the burnt sand (product) is presented in Table 47.

Table 47. Comparison of Elemental Analysis of Coked Sand and Burnt Sand

Elements	Coked Sand	Burnt Sand
C, wt%	0.85	0.39
H, wt%	0.06	0.00
N, wt%	0.03	0.00
S, wt%	0.08	0.01

The combustion efficiency of the experiment was calculated ato be 54% from the data in Table 47. The low combustion efficiency was a result of insufficient residence time in the combustion zone, especially for the fine particles which bypass the reactor. This can also be observed from the temperature profile plot (Figure 105). After feeding started, the temperature in the lower part of the combustion section actually decreased, then increased in the upper part of the section, which means that ignition took place at the middle of the combustor, instead of, as expected, at the bottom of the combustor.

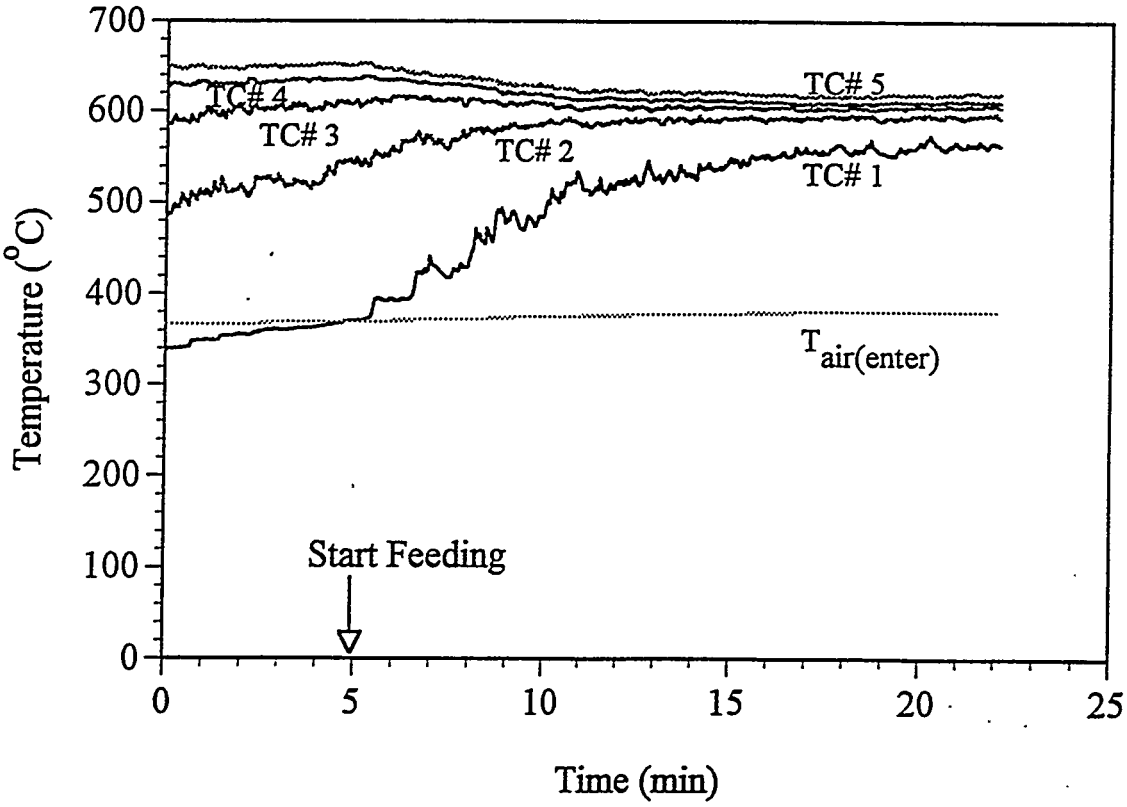

Figure 105. Temperature Variation vs Time

CONCLUSIONS

Based on the theory and practice of circulating fluidized bed combustors, a laboratory scale dense phase transport reactor has been designed and constructed for the study of combustion of carbonaceous residues on spent or coked sand. Both hydrodynamic and combustion experiments have been conducted with the reactor. Fluidization and defluidization experiments gave a minimum fluidization velocity of 1.7 cm/s which is close to the predicted minimum fluidization velocity of 1.5 cm/s. The transition velocities were determined in flow regime transition studies: (a) plug slugging (U_{ms}) = 20 cm/s; (b) turbulent fluidization (U_c) = 50 cm/s; and (c) refluxing pneumatic transport (U_k) = 75 cm/s. Particle residence time distribution experiments indicated that the fine particles tend to bypass the bed especially at higher superficial gas velocities. The initial combustion experiment gave a combustion efficiency of 54% at an equivalence ratio of 0.56.

1. Both Type I and Type II curves were observed for the multisized coked sand under both fluidization or defluidization conditions.
2. The experimental minimum fluidization velocity was reasonably close to the predicted minimum fluidization velocity, 1.5 cm/s and 1.7 cm/s, respectively.
3. Flow regime transition experiments indicated that the transition velocity for plug slugging flow was 20 cm/s, for turbulent fluidization it was 50 cm/s and for refluxing pneumatic transport it was 75 cm/s.

4. Particle residence time distribution experiments indicated that the fine particles tend to bypass the reactor which negatively impacts the combustion efficiency.
5. The combustion efficiency was 54% in the initial combustion experiment, which indicated that longer combustion residence times in the combustion zone are required.

NOMENCLATURE

Ar Archimedes number

d_p Particle size, cm

g Acceleration due to gravity, cm/s2

Re_{mf} Reynolds number at minimum fluidization velocity, cm/s

U_{mf} Minimum fluidization velocity, cm/s

ρ_g Gas density, g/cm3

ρ_s Solid density, g/cm3

μ_g Gas viscosity, g/cm s

FUTURE ACTIVITIES

The combustion efficiency will be evaluated with and without the introduction of secondary air to induce swirl. The influence of oxygen-enriched air on combustion efficiency will be investigated. The spent sand combustion process variable study will be conducted.

SUPERCRITICAL FLUID EXTRACTION OF OIL SAND BITUMEN

Principal Investigator: F.V. Hanson
Graduate Student: M. Subramanian

INTRODUCTION

Supercritical extraction (SFE) is normally carried out at or above the critical pressure (P_c) and critical temperature (T_c) of the solvent. SFE has found numerous applications in the food and petroleum processing industries.[207-209] Chevron[210] is reportedly using propane for in-situ recovery of oil sand bitumen from one of their Canadian reservoirs on a pilot scale.

The objectives of this study, SFE of PR Spring bitumen with propane, included the following:

a) determination of the effect of pressure and temperature on extract yields and on the composition of the extract phases;

b) determination of the chemical composition of the residual fractions; and

c) determination of the extent of asphaltene rejection during SFE.

This work was a continuation of the SFE study with the Whiterocks bitumen reported previously[211-214].

EXPERIMENTAL

Experimental Apparatus and Procedure

The SFE system was built by Autoclave Engineers and has been described in previous publications[211-214]. A positive displacement pump was used to measure the volume change of mixing which was then used to calculate the initial overall composition. An online

densitometer was used to measure extract phase densities. A schematic of the SFE system is presented in Figure 106. The system is composed of three major subsystems: the supercritical fluid supply system, the extractor, and the separator assembly.

The fluid supply system consisted of a gas cylinder, and vacuum, positive displacement and circulation pumps. The extractor assembly was a 280 cc autoclave rated for 37.2 MPa at 616 K, and was equipped with a temperature controller and a magnetic packerless stirring system. The densitometer was mounted downstream of the extractor to measure the extracted phase densities. The separator assembly consisted of a heated metering valve, a separator vessel, and a flow meter and a flow totalizer.

In each experiment, a known quantity of solute was charged to the extractor and a measured quantity of supercritical solvent was pumped into the extractor using the positive displacement pump. Temperature and pressure control was achieved using the controllers provided with the system. After the initial solvent charge, a circulating pump was used to supply replacement solvent during continuous, extraction experiments[211].

Solvent and FeedStocks

The hexadecane(99.9 wt %) used for preliminary studies was obtained from Aldrich Chemicals. The properties of the PR Spring bitumen are presented in Table 48. The bitumen was extracted from oil sand using toluene in a conventional Dean Stark extraction apparatus. The toluene in the extracted bitumen solution was rotoevaporated until the final toluene content was reduced to less

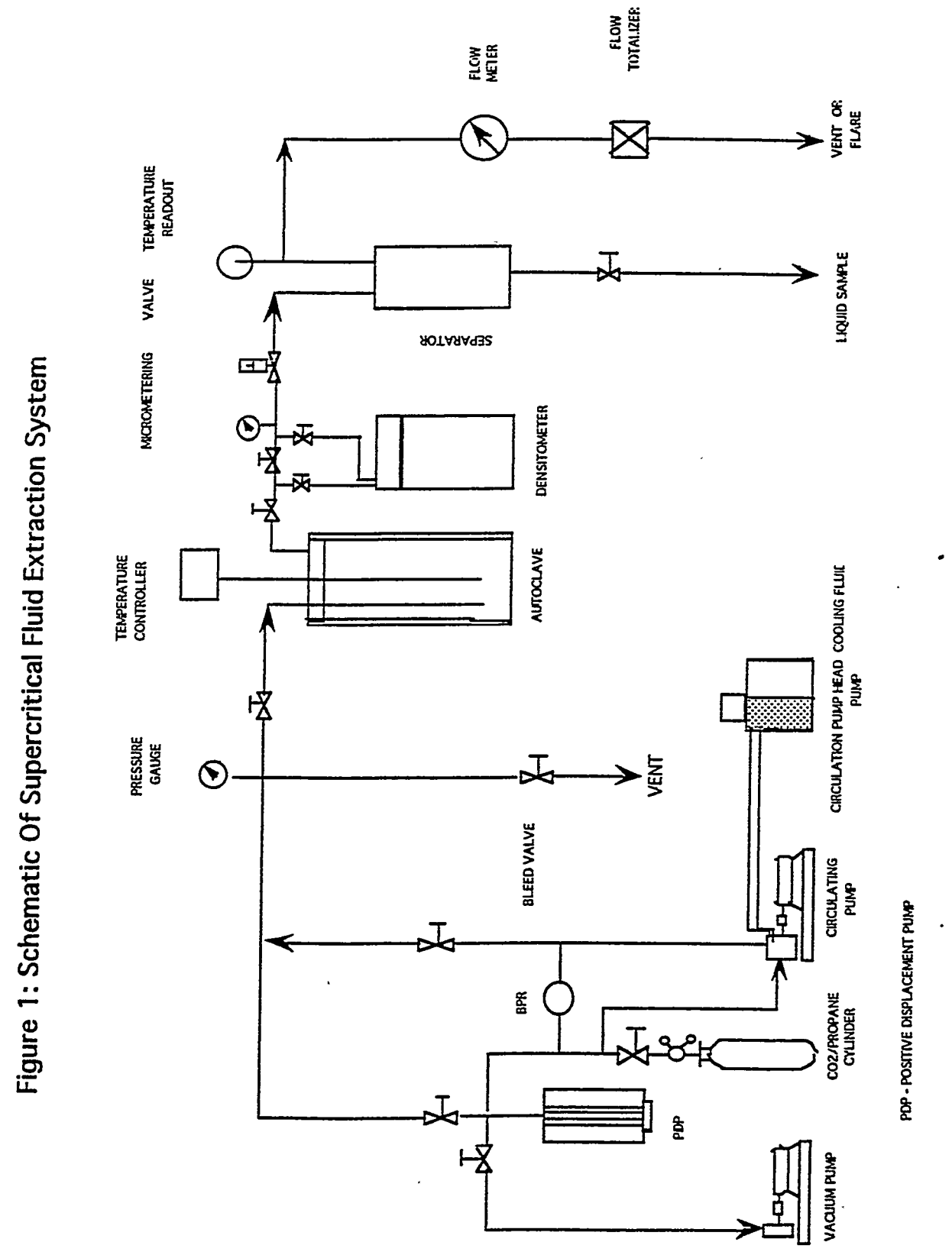

Figure 106. Schematic of Supercritical Fluid Extraction System

Table 48

Chemical and Physical Properties of the PR Spring Bitumen

Specific Gravity (288/288 K)	1.01
Conradson Carbon, wt.%	14.2
Pour Point, K	319
Viscosity, cps @325K	65,000
Asphaltenes[a], wt%	19.3
Saturates & Aromatics, wt%	37.0
Resins, wt%	43.8
Elemental Analysis[b]	
C, wt%	87.5
H, wt%	11.5
N, wt%	0.5
S, wt%	0.5
H/C Atomic Ratio	1.56
Simulated Distillation	
Volatility, wt%	36.3
Boiling Point Distribution, wt%	
< 477 K	1.5
477 - 616 K	6.5
617 - 811 K	28.4
> 811 K	63.6

a) Pentane Insolubles
b) C,H,N,S normalized to 100%

than 0.1 wt %. The boiling point distributions were determined up to 993 K. The carbon number distribution, based on SIMDIS, of the PR Spring bitumen is presented in Figure 107.

The carbon dioxide and propane used for extraction were commercial grade gases. The purity of the carbon dioxide was 99.5 wt % while the C_3 content in the propane was 93.9 wt %.

RESULTS AND DISCUSSION

Extraction of Hexadecane

Preliminary experiments were conducted with hexadecane using carbon dioxide as a solvent at a constant reduced temperature of 1.02 and reduced pressures of 1.4 and 2.3. The close match of measured extracted phase compositions and densities with the published data[212,215] and Peng-Robinson EOS[216] predictions demonstrated that the system operated at thermodynamic equilibrium and was capable of producing reliable thermodynamic data.

Reproducibility experiments were carried out at a reduced pressure of 3.8 and a reduced temperature of 1.03. The results for two extraction runs are plotted in Figure 108, and indicate that the experimental results are reproducible.

Extraction of PR Spring Bitumen

Bitumen extractions were carried out at five different operating conditions using propane as the solvent. Three different pressure and temperature combinations (Figure 109) resulted in four conditions in the critical region and one with $P_r>1.0$ and $T_r<1.0$. Deviations observed for the extraction yields for the first window were due to the equipment configuration.

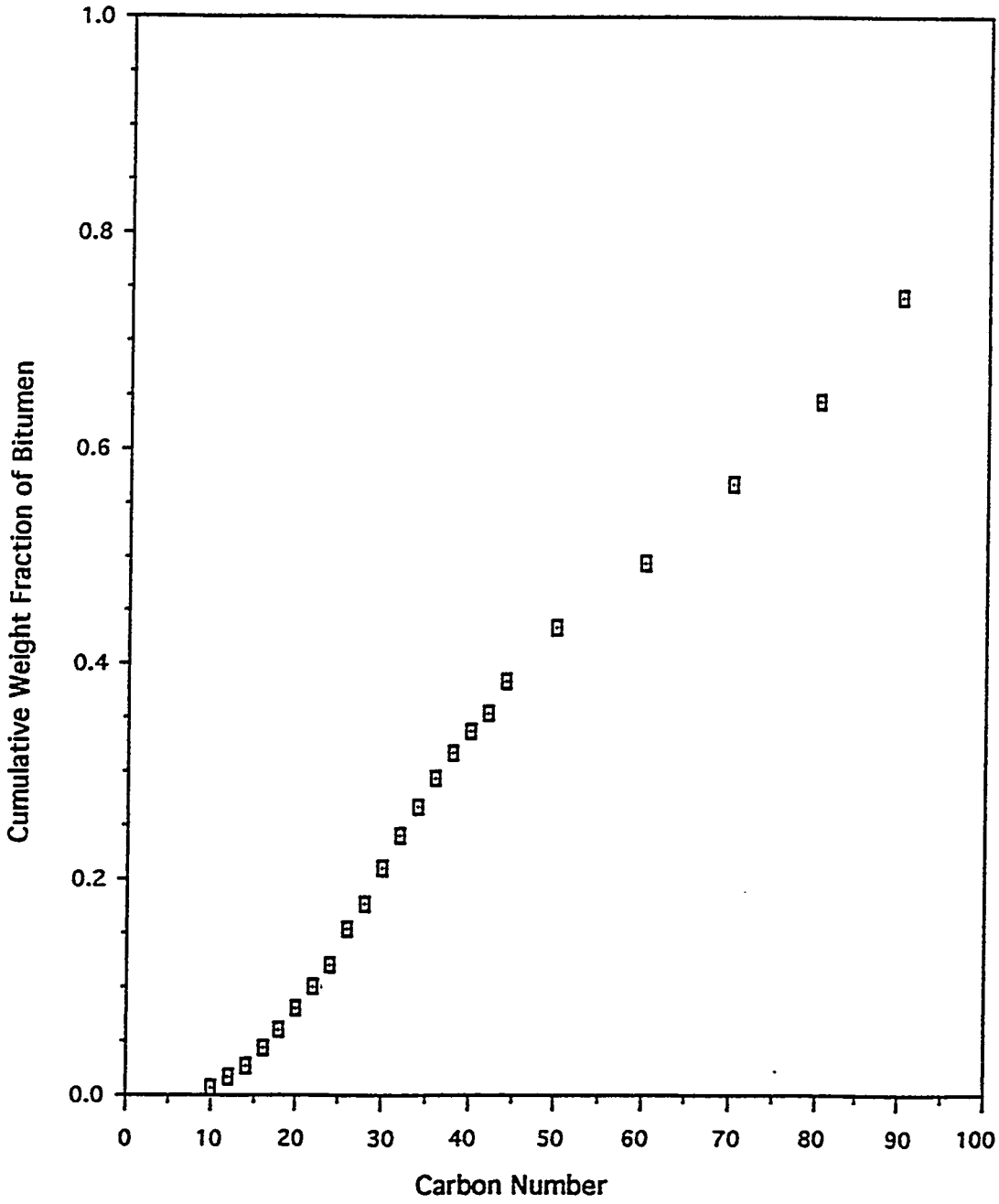

Figure 107. Carbon Number Distribution for PR Spring Bitumen

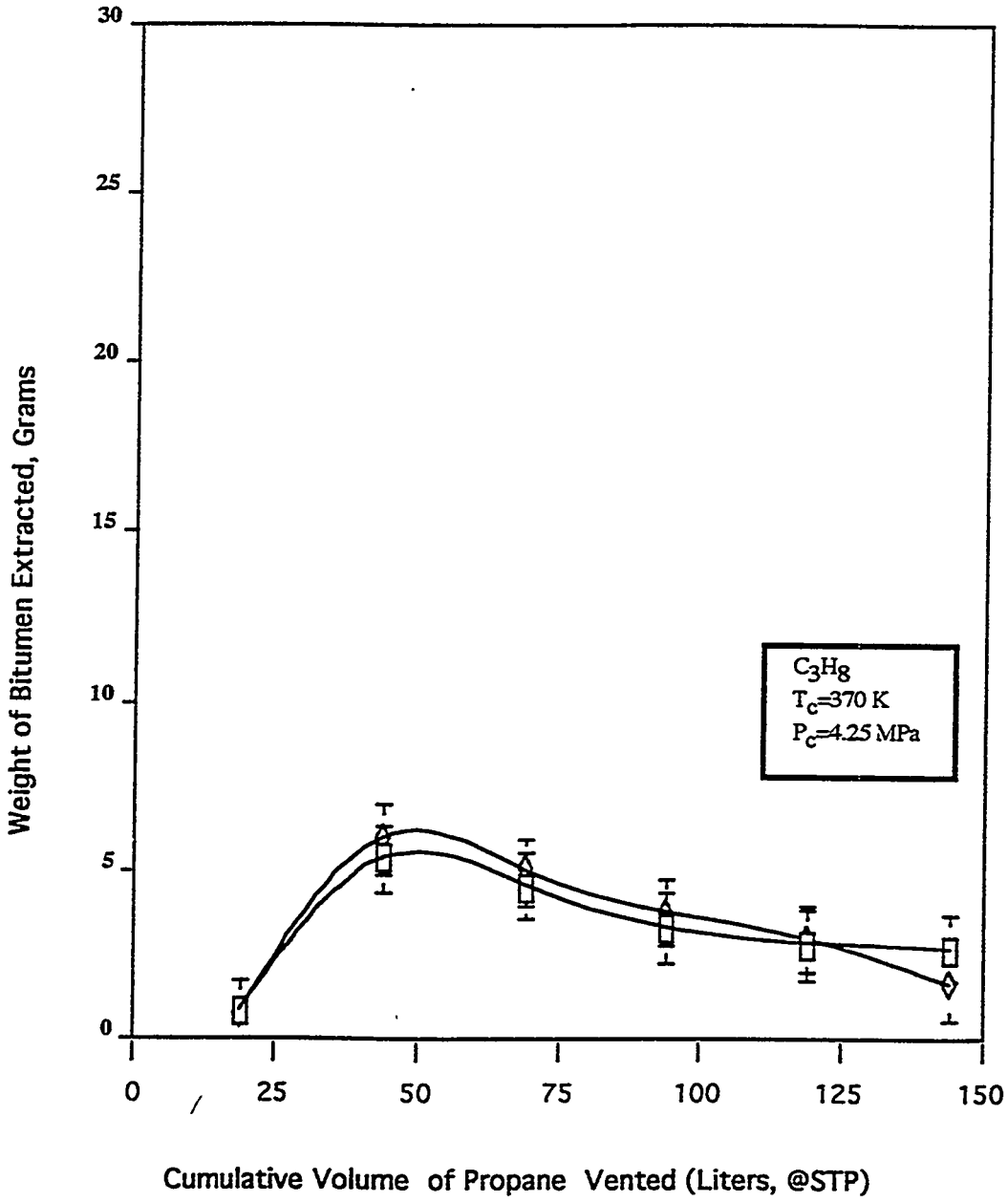

Figure 108. Reproducibilty of SFE of PR Spring Bitumen by Propane at a P_r of 3.8(P=17.3 MPa) and a T_r of 1.03 (T=380 K)

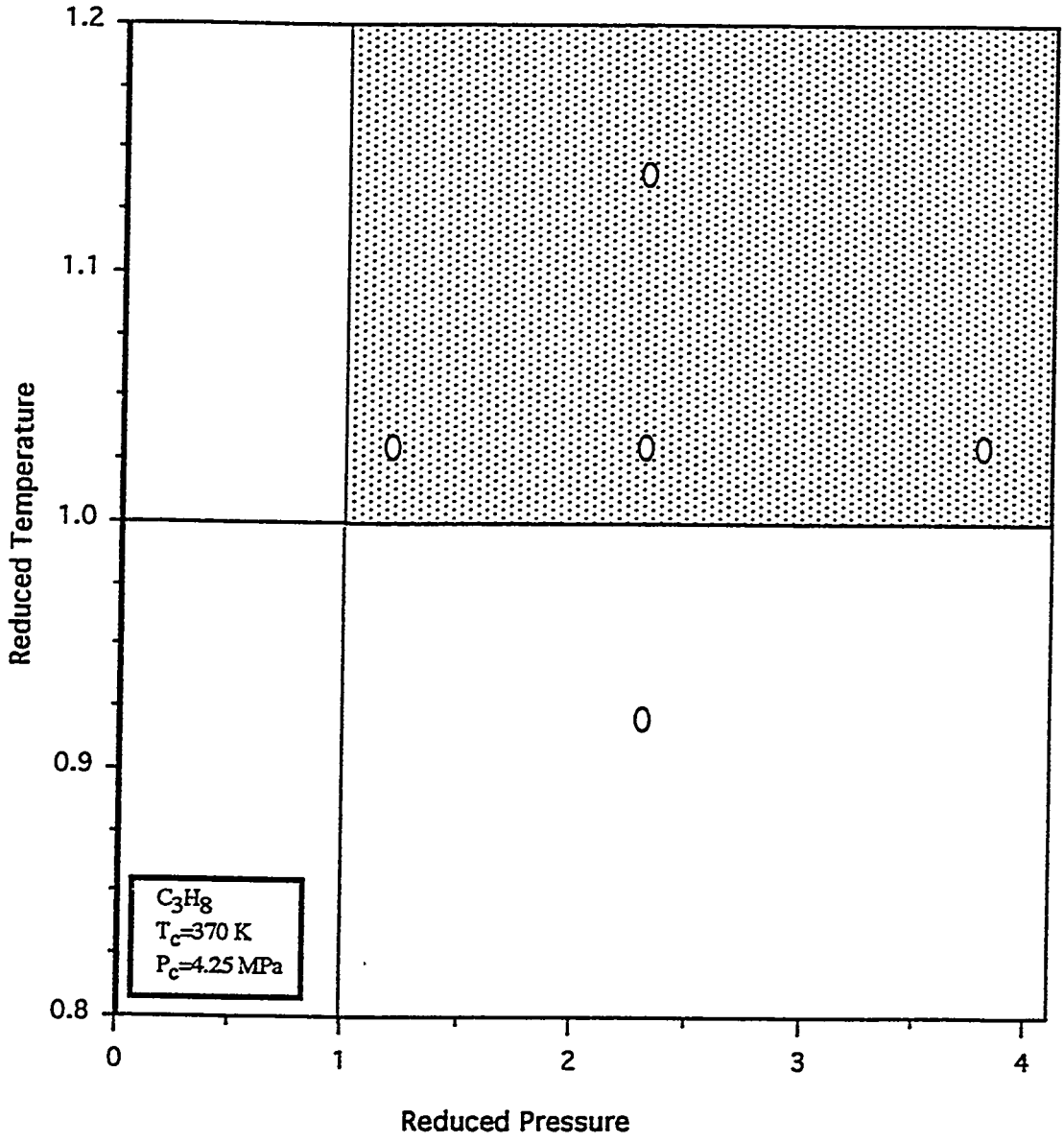

Figure 109. Operating Conditions for SFE of PR Spring Bitumen by Propane

Pressure Effect

The extraction performance is defined as the cumulative weight percent of bitumen extracted. The extraction performance of propane at three different reduced pressures and at a constant reduced temperature of 1.03 is compared in Figure 110. The highest extraction yield, 38.4 wt %, was achieved at a P_r of 3.8 compared to yields of 20.8 wt % and 8.8 wt % at a P_r of 2.3 and 1.2, respectively. The increase in extraction yield at higher extraction pressures was directly related to increased solvent density at higher pressures[217]. The densities of propane measured at the five different operating conditions are presented in Table 49.

Table 49

Measured Densities* of Propane

Reduced Temperature	0.92	1.03	1.14
Reduced Pressure			
1.3	-	0.533	-
2.4	0.566	0.553	0.545
3.8	-	0.569	-

** Density Units, g/cc

Temperature Effect

The extraction yield at three different reduced temperatures and at a constant reduced pressure of 2.3 are compared in Figure 111. An extraction yield of 38.8 wt % was achieved at a T_r of 0.92 and yields of 20.8 wt % and 15.7 wt % were obtained at reduced temperatures of 1.03 and 1.14 respectively. This decline in extraction yields with an increase in temperature can be attributed

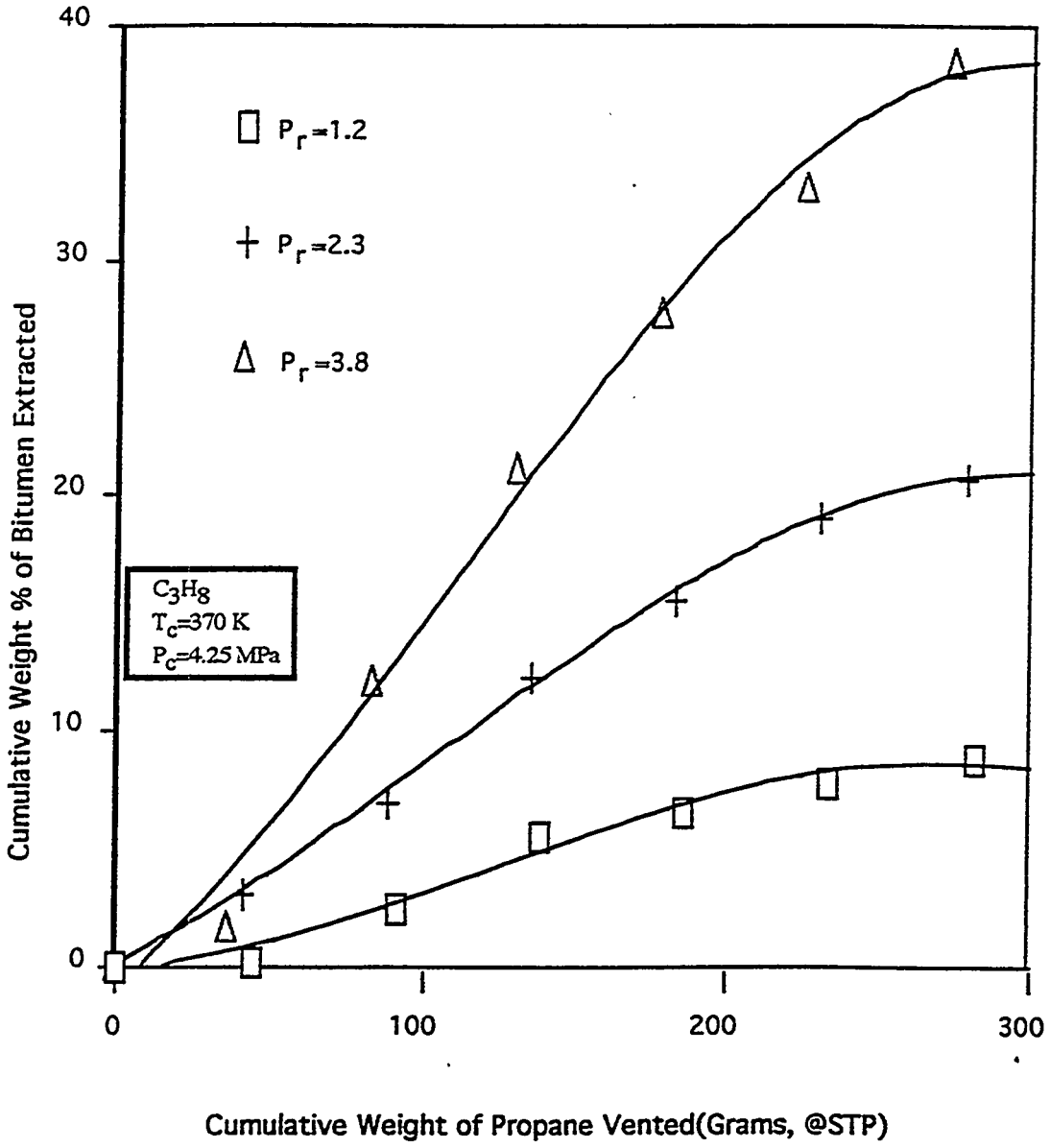

Figure 110. Effect of Pressure on SFE of PR Spring Bitumen by Propane at a T_r of 1.03 (T=380 K)

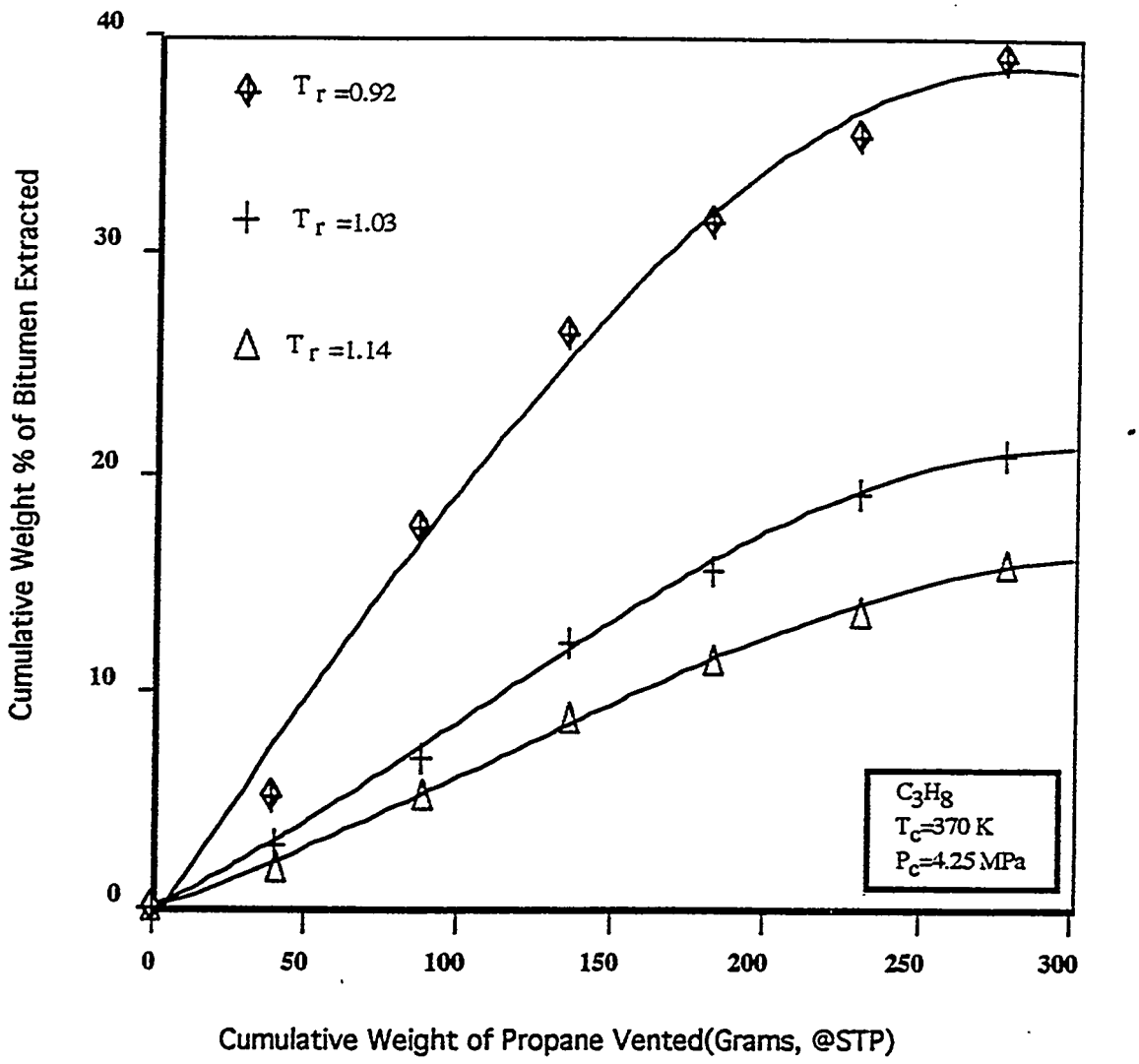

Figure 111. Effect of Temperature on SFE of PR Spring Bitumen by Propane at a P_r of 2.3(P=10.4 MPa)

to a decrease in solvent densities at higher temperatures. The extraction yield for propane with PR Spring bitumen increased with solvent density as shown in Figure 112.

Extraction Product Analysis

High temperature simulated distillation analyses were carried out on all extract and residual fractions. The compositional variations observed for these fractions at a P_r of 2.3 and a T_r of 0.92 are presented in Figure 113. These plots show that as the extraction proceeded heavier components were extracted.

The residual fractions produced in the SFE of the PR Spring bitumen were fractionated into asphaltenes (pentane insolubles), saturates & aromatics, and resins using the procedure outlined by Bukka et al.[218] The elemental analyses were performed by Galbraith Laboratories, Inc., Knoxville, Tennessee.

The absolute asphaltene content of the residual fractions was higher than the asphaltene content of the original bitumen. A similar observation was reported for Whiterocks bitumen by Deo and Hanson[214] who presumed that the increase was related to the depletion of cosolubilizing compounds present in the bitumen. Thus, compounds which did not precipitate as pentane insolubles from the original bitumen were precipitating from the residual fractions. The asphaltene content of the residual fractions increased with increased extraction yields. The effect of extraction pressure and temperature on asphaltene content is shown in Figures 114 and 115.

The H/C atomic ratio for the residual fractions decreased with an increase in extraction pressure at constant temperature and also

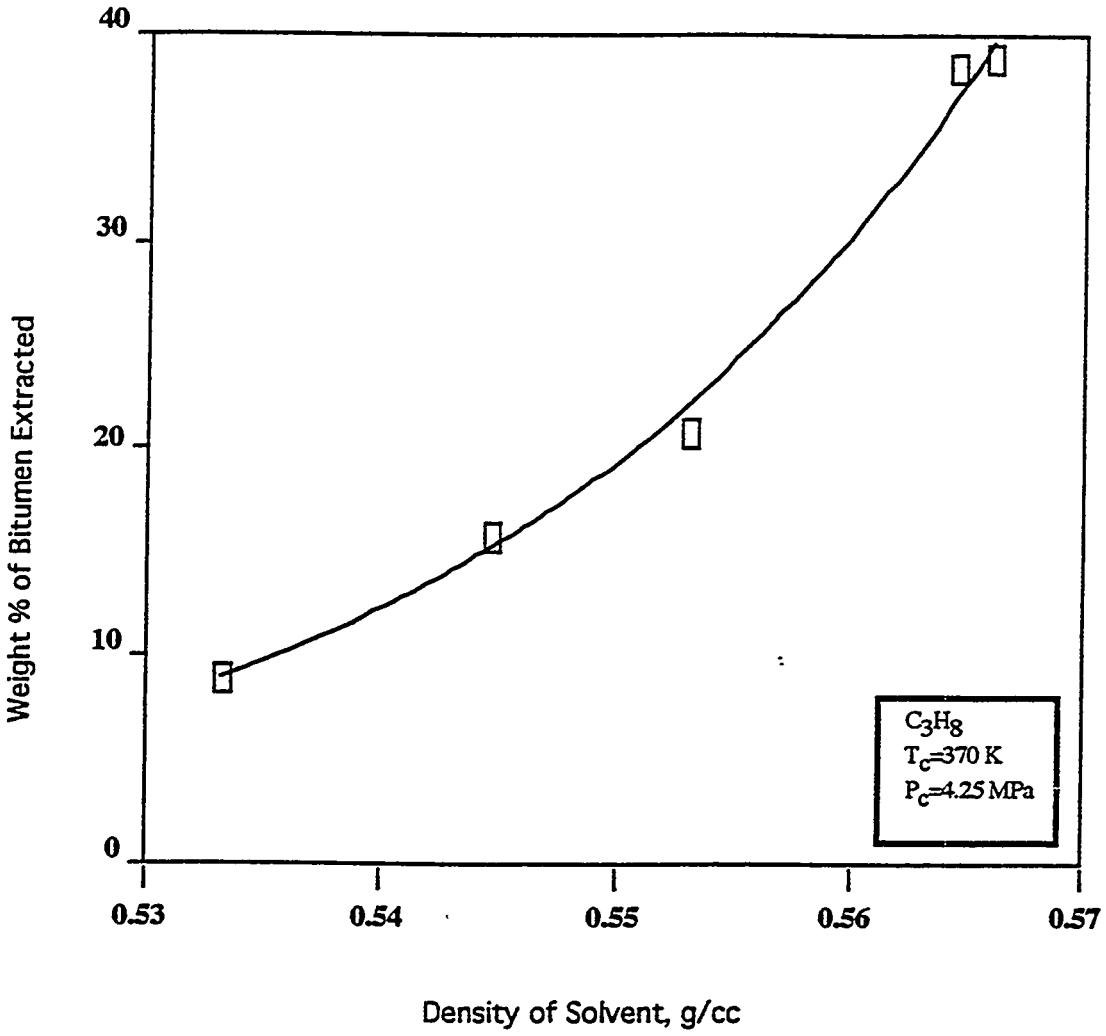

Figure 112. Effect of Solvent Density on Extraction Yield for PR Spring Bitumen by Propane

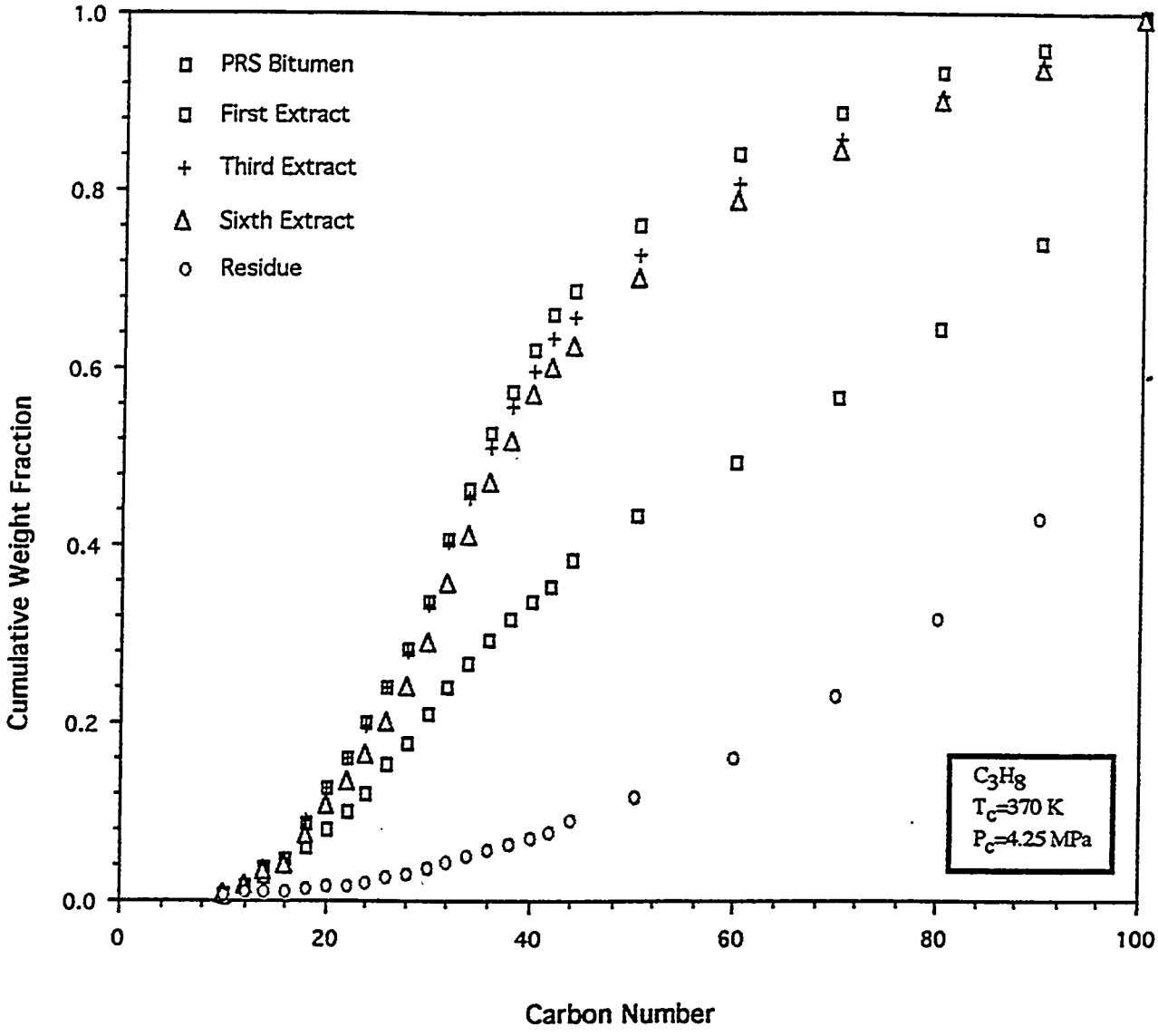

Figure 113. Simulated Distillation Analyses of SFE of PR Spring Bitumen by Propane at a P_r of 2.3(P=10.4 MPa) and a T_r of 0.92 (T=339 K)

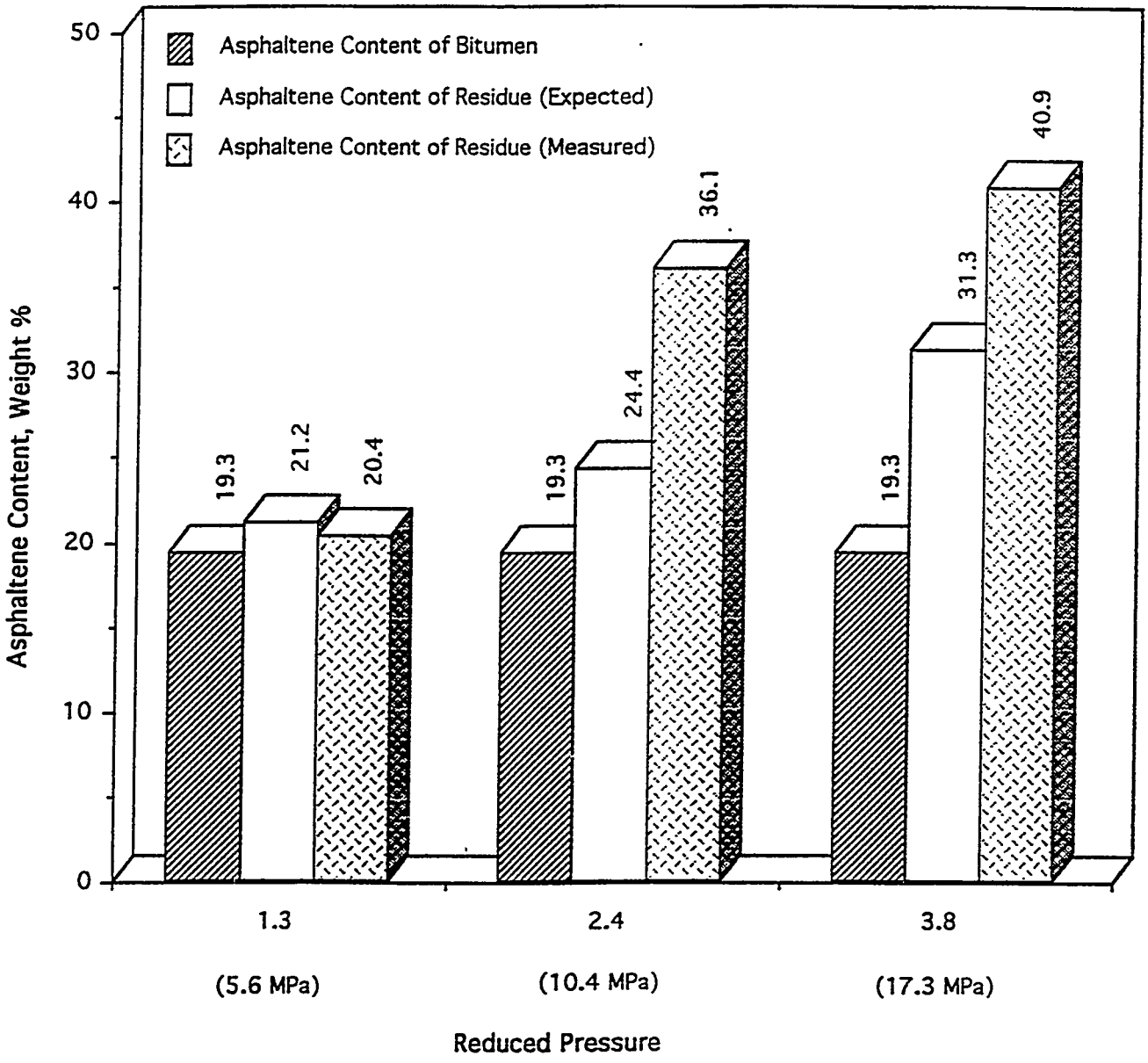

Figure 114. Effect of Pressure on Asphaltene Content of Residual Fractions from SFE of PR Spring Bitumen by Propane at a T_r of 1.03 (T=380 K)

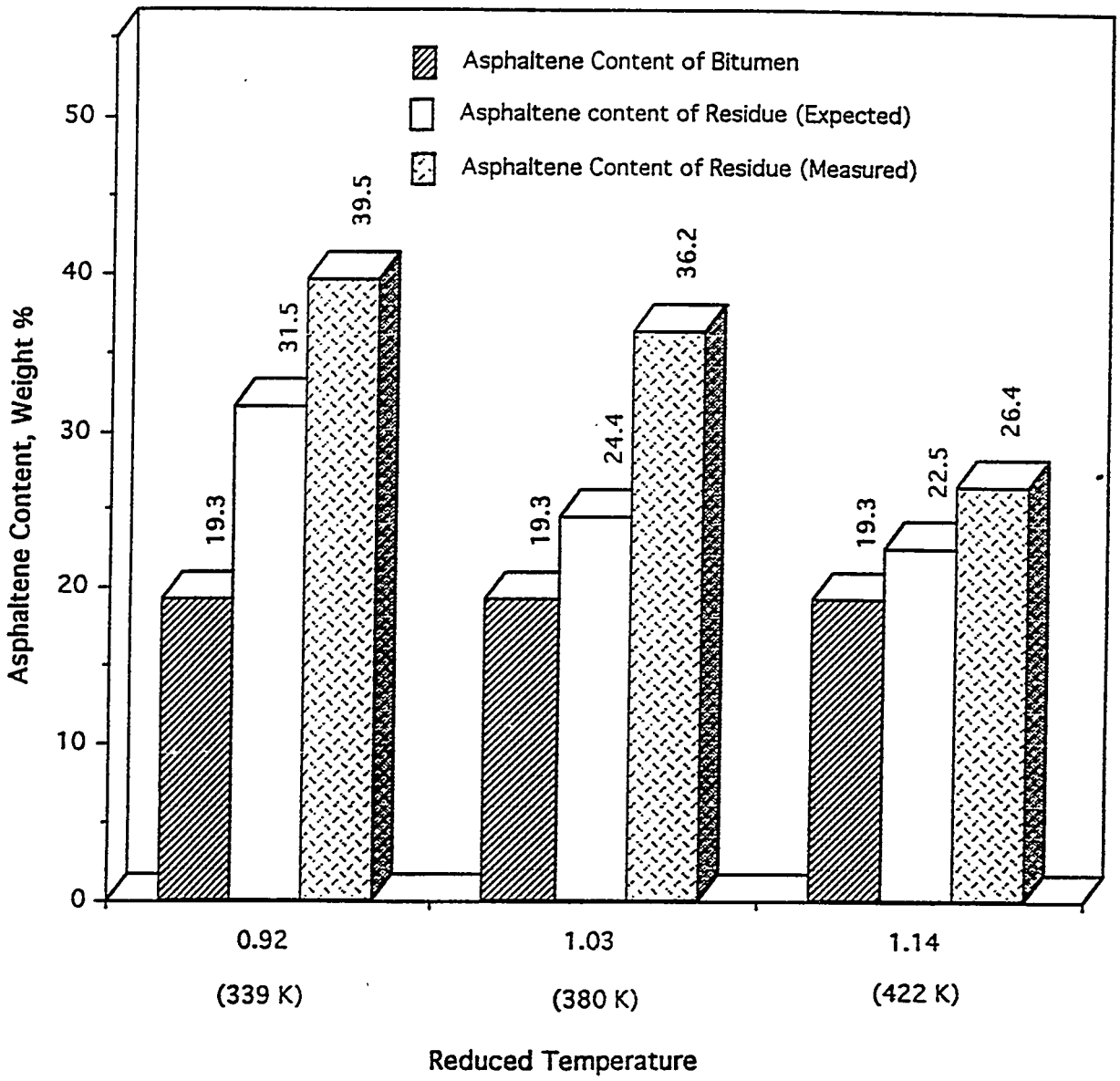

Figure 115. Effect of Temperature on Asphaltene Content of Residual Fractions from SFE of PR Spring Bitumen by Propane at a P_r of 2.3 (P=10.4 MPa)

increased with an increase in temperature at constant pressure as indicated in Figures 116 and 117, respectively. The H/C atomic ratios in the residual fractions were lower than that of the original bitumen indicting that saturated compounds were preferentially extracted, leaving the residual portion more polar and relatively richer in unsaturated compounds.

Modeling the Extraction Process

Modeling of the SFE process was carried out in order to predict the phase behavior during extraction. The Peng-Robinson equation-of-state[216] and a pseudocomponent lumping scheme proposed by Whitson[219] were used. Computer software, CMGPROP[220] from Computer Modeling Group was used to perform flash calculations and the predicted phase compositions were compared with experimentally obtained values.

The boiling point distribution (up to C_{90}) obtained from the SIMDIS was used to lump PR Spring bitumen into seven pseudocomponents using Whitson's lumping procedure[219]. The distillable portion(< 810 K) was divided into five pseudocomponents of equal mole fraction and the non-distillable portion(>810 K) was divided into two pseudocomponents of equal mole fraction. The psudocomponents for the PR Spring bitumen are presented in Table 50. The critical properties for these pseudocomponents (Table 51) were calculated using the Lee-Kesler correlations[221]. The interaction parameters for propane and the PR Spring bitumen psudocomponents were internally generated by CMGPROP[220].

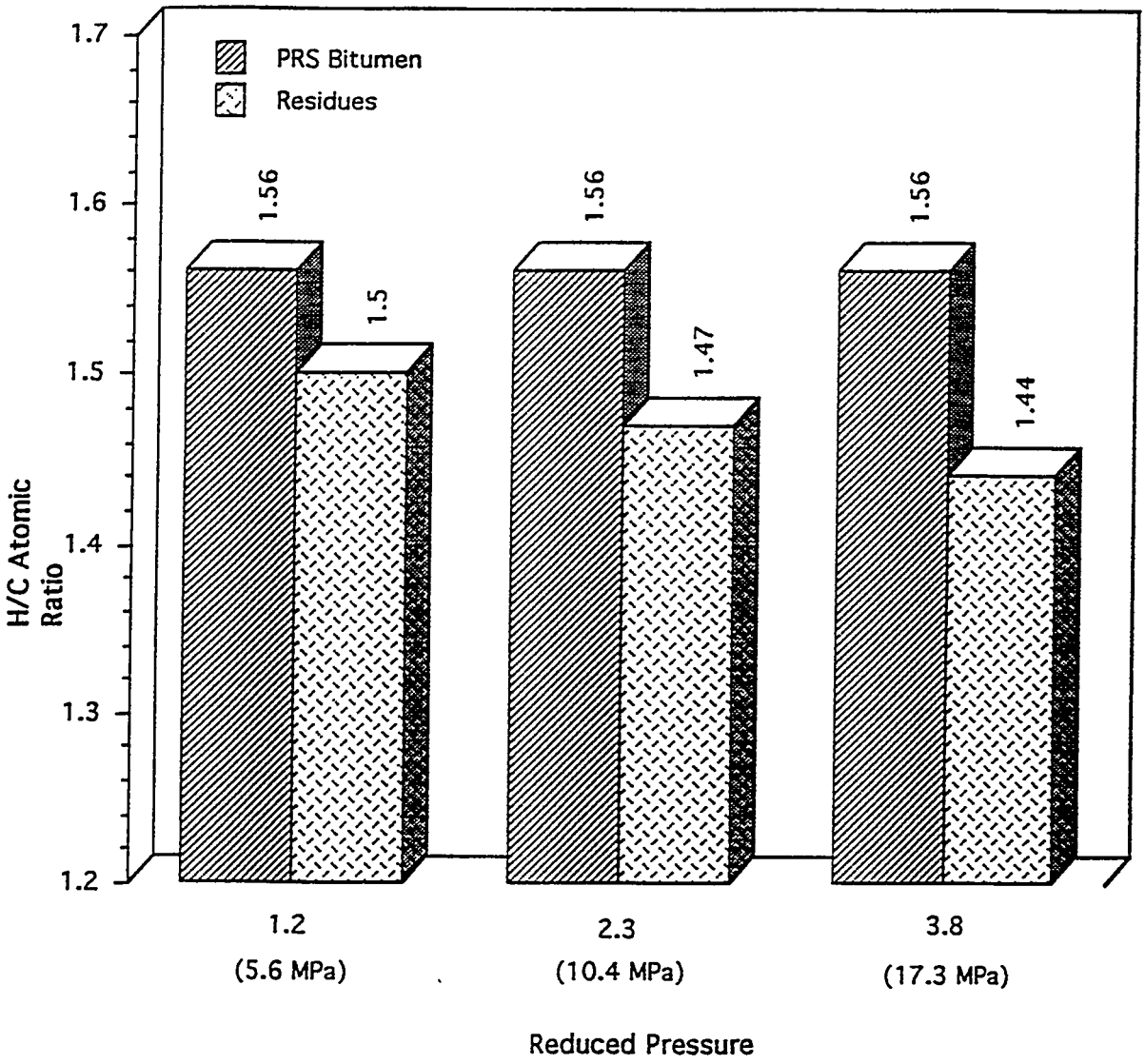

Figure 116. Effect of Pressure on H/C Atomic Ratio of Residual Fractions from SFE of PR Spring Bitumen by Propane at a T_r of 1.03 (T=380 K)

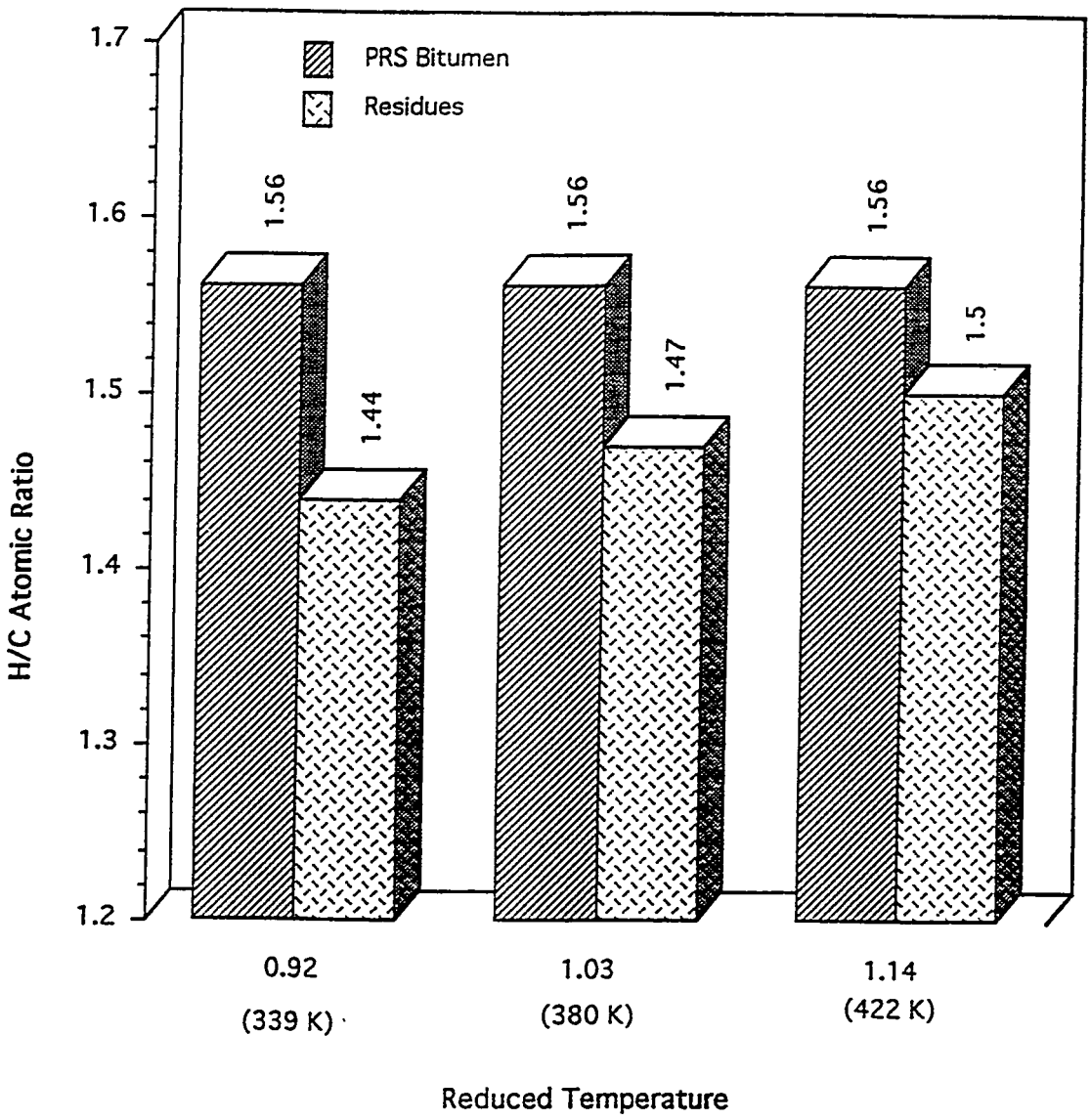

Figure 117. Effect of Temperature on H/C Atomic Ratio of Residual Fractions from SFE of PR Spring Bitumen by Propane at a P_r of 2.3 (P=10.4 MPa)

Table 50

Pseudocomponents for PR Spring Bitumen

	Boiling Point Range (K)	SIMDIS (wt%)
PS 1	< 581	3.8
PS 2	582 - 658	5.4
PS 3	659 - 717	6.9
PS 4	718 - 765	9.8
PS 5	766 - 817	9.0
PS 6	818 - 960	27.9
PS 7	> 961	38.1

Table 51

Predicted Properties for Pseudocomponents Using Lee-Kesler Correlations

PS	Boiling Point (K)	Molecular Weight (g/mol)	Specific Gravity (288 K/288 K)	Fraction (wt%)	P_c (Atm)	T_c (K)	Acentric Factor (-)
PS 1	511.0	172.5	0.77	3.8	16.2	675.5	0.64
PS 1	610.0	254.5	0.84	5.4	13.1	772.5	0.85
PS 1	618.9	335.2	0.90	6.9	11.9	845.9	0.98
PS 1	732.9	406.7	0.96	9.8	11.6	902.3	1.04
PS 1	784.1	496.2	1.01	9.0	11.5	961.1	1.08
PS 1	866.7	797.2	1.10	28.0	10.2	1066.4	1.20
PS 1	1071.7	1489.1	1.21	38.1	7.6	1243.9	1.41

The initial charge of bitumen and propane to the extractor was used to calculate the initial overall composition and the flash calculation was performed at the operating conditions. The calculation procedure followed is similar to the procedure reported by Deo et al.[212] One significant improvement was the use of

extracted phase densities which were measured with the densitometer instead of using values calculated from the Peng-Robinson equation of state[216]. A comparison between the experimental and calculated extract phase composition for PR Spring bitumen- propane extraction at a P_r of 2.3 and a T_r of 0.92 is presented at Figure 118. The highest propane density studied was obtained at these conditions and gave the closest match between the experimental and predicted values.

SUMMARY AND CONCLUSIONS

The SFE of bitumen from the PR Spring oil sand deposit (Utah) was studied using commercial propane as the solvent . The bitumen volatility was 36.3 wt % and its asphaltene content was 19.3 wt %. Experiments were performed at five different operating conditions which included three pressures (5.6 MPa, 10.4 MPa and 17.2 MPa) and temperatures (339 K, 380 K and 422 K).

The extracted phase yield increased as the extraction pressure increased at constant temperature. This effect was directly related to the increase in the pure solvent density with pressure. It was also observed that at higher extraction pressures, relatively heavier hydrocarbons were extracted. The asphaltene content of the residual fraction was compared with the asphaltene content of the bitumen and was observed to be higher, even on an absolute weight basis.

The extraction process was modeled using the Peng-Robinson cubic equation-of-state and Lee-Kesler pseudocomponent characterization correlations. The experimental extraction results

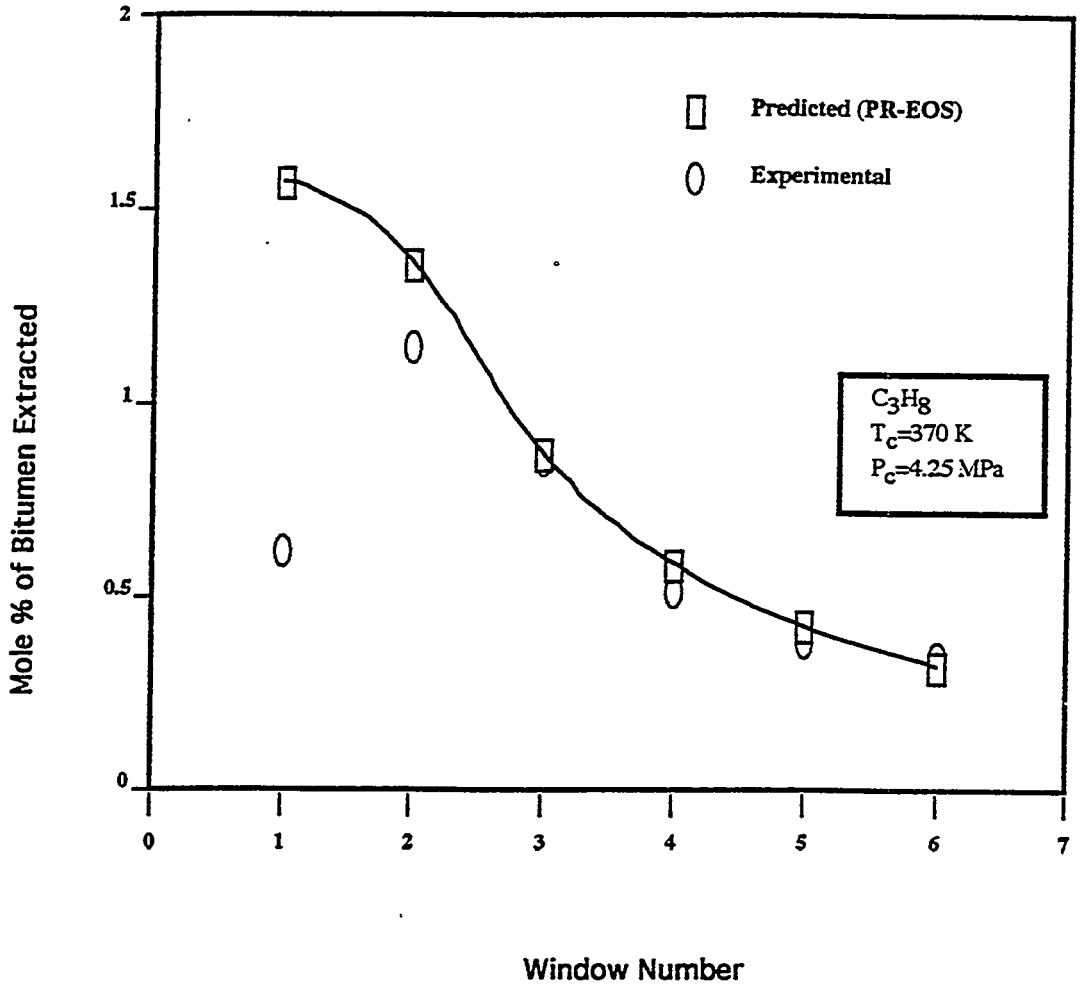

Figure 118. Comparison of Experimental and Predicted Bitumen Extracted Phase Compositions for Extraction of PR Spring Bitumen by Propane at a P_r of 2.3 (P=10.4 MPa) and a T_r of 0.92(T=339 K)

were in reasonable agreement with the predicted phase compositions based on a flash calculation using seven pseudocomponents. The following conclusions were drawn from the study:

1. Pure solvent density was the governing factor for the extraction of PR Spring bitumen with propane. The extraction yield increased with an increase in pure solvent density.
2. The asphaltene content of the residual fractions was higher than the original bitumen on an absolute basis assuming all the asphaltene stayed in the residue. This indicates the depletion of cosolubilizing agents during the extraction process.
3. The H/C ratio of the residual fractions was lower than the original bitumen, thus, establishing that saturated hydrocarbons were preferentially extracted leaving the residue richer in unsaturated compounds.
4. Reasonable agreement between the experimental and predicted phase compositions was observed at the highest solvent density.

FUTURE ACTIVITIES

The supercritical fluid extraction studies will be extended to include the Asphalt Ridge and Sunnyside bitumens. Completion of these experiments will establish a database that should permit the formulation of a thermodynamic model of the propane – Uinta Basin bitumen system. Furthermore, the database should provide a clear understanding of asphaltene rejection with Uinta Basin bitumens.

UPGRADING UINTA BASIN OIL SANDS

CATALYTIC UPGRADING OF A UINTA BASIN BITUMEN OVER A COMMERCIAL HDM CATALYST

Principal Investigator:	F.V. Hanson
Postdoctoral Fellow:	D.C. Longstaff
Graduate Students:	S. Kwak
	J. Kim

INTRODUCTION

Development of heavy oil and bitumen resources is accelerating around the world.[222] Heavy oils and bitumens typically contain high molecular weight hydrocarbons and significant amounts of nitrogen, sulfur and metals.[175] These organic heteroatom compounds not only cause serious environmental concerns for fuel-oil fired plants because of SO_x and NO_x formation, they also act as poisons in refinery processes such as catalytic cracking and reforming.[223]

In desulfurization and denitrogenation, heteroatom contaminants are removed as H_2S and NH_3. However, in hydrodemetallation, metals deposit on the catalyst and cause irreversible fouling of the catalyst. The catalyst deactivation has a serious impact on the economics of residuum hydroprocessing. Catalysts poisoned by metal deposition must be replaced while coked catalysts can be regenerated.

Nickel and vanadium are the most abundant metal impurities in heavy oils and bitumens, and are, therefore, of greatest interest and concern. While impurities such as sulfur may be distributed over a wide boiling range, metals are generally concentrated in the resin and asphaltene fractions.[224] The metal deposition ultimately

determines the catalyst's total lifetime. Therefore, recent hydrotreating processes for upgrading unconventional heavy feedstocks have focused on catalysts having a low tendency toward coke formation and catalysts which can accommodate high levels of deposited metals.

EXPERIMENTAL

Feedstock Preparation and Reactor Startup

The bitumen used in this study was obtained by toluene extraction of Whiterocks oil sand followed by rotavaping and batch distillation.[225,226] The hydrotreating reactor system used in this study consisted of four main elements: the liquid feed system, the hydrogen feed system, the reactor system and the product separation and sampling system.[225-228] The system was designed for both upflow and downflow operation. This was achieved by placing three-way manifold valves at the reactor inlet and outlet. The reactor was operated in the upflow mode for all experiments in order to achieve complete catalyst wetting and efficient catalyst utilization.[225-230] All liquid lines were heat traced to lower the bitumen viscosity.[175,231] The reactor configuration has been described in detail elsewhere.[225-228] The physical and chemical properties of bitumen used in this study are presented in Table 52.

Catalyst Description and Loading

A UNOCAL hydrodemetallation (HDM) catalyst was used in this study. The catalyst was in the form of 0.16 cm (1/16") quadralobes, contained 1.0 wt% NiO and 6.2 wt% MoO_3 and had a uni-modal pore structure. The catalyst had a surface area of 155 m^2/g,

Table 52

Properties of Bitumen and Hydrotreated Total Liquid Product

	Whiterocks Bitumen	Hydrotreated Whiterocks Bitumen(D-15)
Operating Conditions (Run D-15)		
Temperature, K	N/A	666
WHSV, h^{-1}	N/A	0.24
Pressure, MPa	N/A	13.6
API gravity	11.7	18.3
CCR, wt%	10.2	6.1
Pour Point, K	319	281
Product Yield Distribution		
Volatility, wt%	42.2	76.5
C_1-C_4	-	3.8
C_5-478 K, wt%	1.9	3.1
478-616 K, wt%	6.0	15.2
616-811 K, wt%	34.3	52.6
>811 K, wt%	57.8	23.5
Elemental Analysis		
C, wt%	85.1	86.2
H, wt%	11.6	12.2
N, wt%	1.29	0.96
S, wt%	0.33	0.08
Ni, ppm	72	14
V, ppm	<10	-
As, ppm	3	-
H/C Atomic Ratio	1.6	1.7

a pore volume (Hg porosimetry) of 0.72 cm^3/g, and the support had a median pore diameter of 180 Å.

Catalyst Sulfiding

The hydrotreating catalyst was presulfided in-situ with 2 wt% sulfur (as dimethyldisulfide) in kerosene before contact with the liquid feed. The sulfiding procedure has been reported elsewhere.[225-228] The catalyst was sulfided by heating the reactor to 505 K at a rate of 28°C/h and was held at 505 K for 2 hours. It was then heated to 644 K at a rate of 28°C/h at which point the sulfiding was complete. During sulfiding, the hydrogen-to-sulfiding solution ratio was 890 m^3/m^3 and the sulfiding solution LHSV was 1.0 (152 cc/h).

Initial Catalyst Deactivation

The reactor was operated for 8 days to stabilize the catalyst activity at the base case conditions: 642 K, 0.76 h^{-1} WHSV and 13.7 MPa. The base case condition experiments were used to monitor catalyst deactivation. After 190 hours on oil the API gravity of the hydrotreated product stabilized at 13.9°API. It was assumed that the catalyst activity was stabilized because the subsequent change in API gravity with time was minimal. After the initial catalyst deactivation period experiments were conducted in a cyclic manner: base-case condition/desired reaction condition/base-case condition. The base case condition experiments were conducted to determine the extent of catalyst deactivation based on the API gravity of the liquid product.

The major process variables studied were temperature (620-685 K), space velocity (0.24-1.38 h^{-1} WHSV) and pressure (11.3-16.7 MPa). Two of the variables were kept constant while the other was varied to determine the effect of each operating variable, independently. The hydrogen/oil ratio was fixed in all experiments at 890 m^3/m^3 (5000 scf H_2/bbl). The order of experiments was selected in a random manner (Table 53) so that systematic errors were avoided. The API gravities of the liquid product in the process variable experiments are compared with those at the base case conditions in Figure 119. The initial catalyst deactivation with respect to time onstream is also shown in Figure 119.

Mass Balances

Mass balances were conducted after the reactor and catalyst attained a steady state (20 to 60 hours were allowed between experiments) and lasted for 3 to 8 hours. During mass balances, the axial temperature profile of the catalyst bed was measured on the centerline with a movable J-type thermocouple (Figure 120). The kinetic average temperature, $T_{k,e}$, the temperature of an isothermal reactor required to give the same conversion as obtained in a non-isothermal reactor, was used for kinetic analysis and to correlate process data. The difference between the kinetic and arithmetic temperatures in this study was less than 0.1 K indicating that the reactor operation was essentially isothermal. The liquid product collected during each material balance was purged with helium to strip dissolved H_2S and NH_3 and analyzed for

Table 53

Experimental Sequence Performed In This Study

Run Number	T (K)	WHSV (h^{-1})	P (MPa)	TOS[a] (h)
D-9	686	0.75	13.7	211
D-10	642	0.77	13.7	235
D-11	665	0.77	13.8	259
D-12	643	0.78	13.6	283
D-13	664	0.77	16.7	306
D-14	642	0.78	13.6	334
D-15	666	0.24	13.6	405
D-16	642	0.77	13.7	426
D-17	665	0.77	11.3	450
D-18	642	0.77	13.6	475
D-19	665	0.43	13.7	525
D-20	653	0.77	13.6	561
D-21	665	0.76	15.3	584
D-22	642	0.76	13.7	631
D-23	673	0.76	13.7	656
D-24	642	0.78	13.6	681
D-25	662	1.38	13.6	705
D-26	642	0.78	13.6	727
D-27	685	0.76	13.7	750
D-28	641	0.77	13.7	775
D-29	620	0.77	13.7	799
D-30	641	0.79	13.6	827

[a] Time-on-stream.

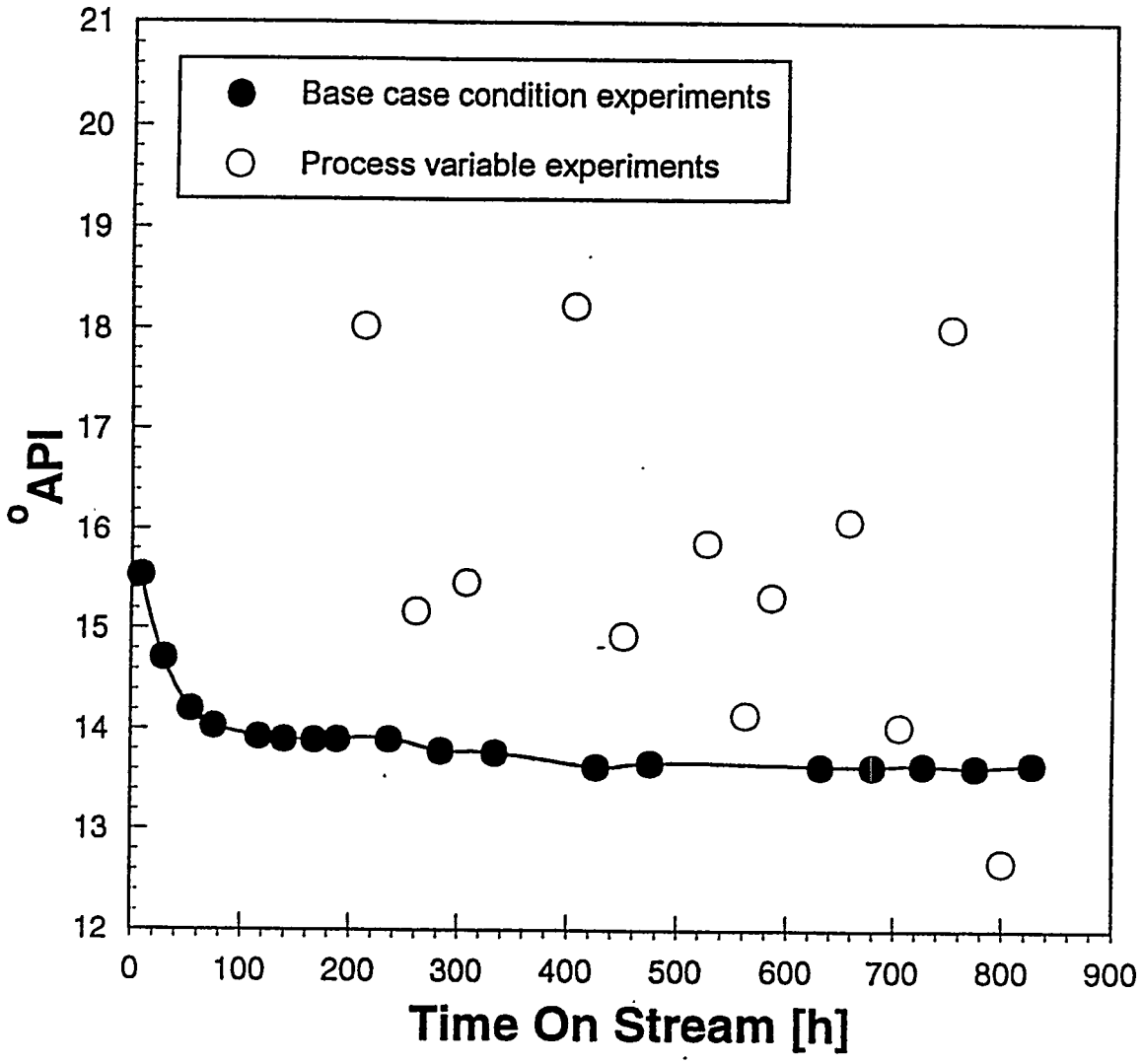

Figure 119. Total Liquid Product API Gravities

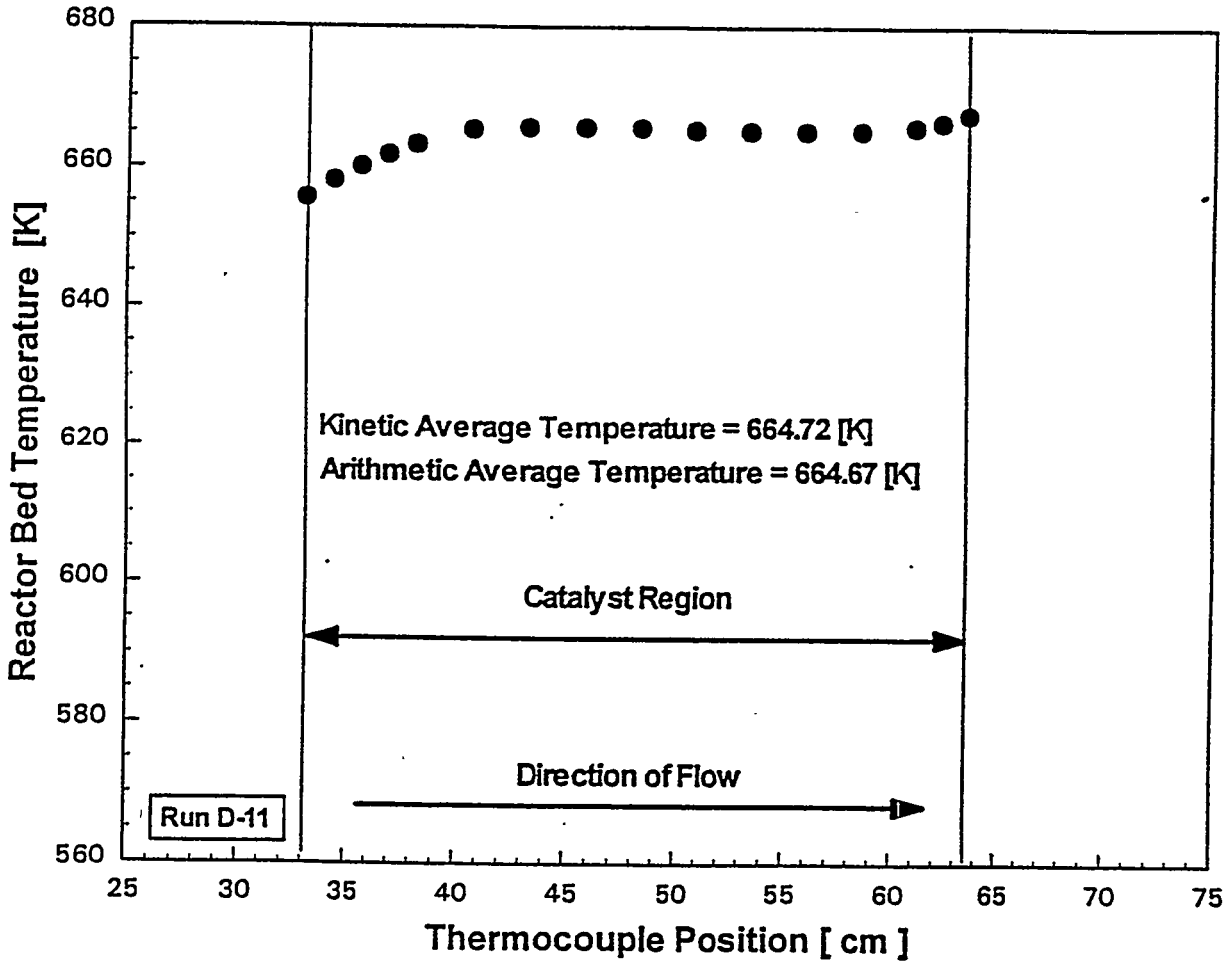

Figure 120. Typical Catalyst Temperature Profile in Upflow Operation

sulfur, nitrogen, metal content, boiling point distribution, pour point,[232] and Conradson carbon residue.[233]

Operating Procedures

The experimental equipment and the operating procedures have been described in detail by Longstaff[225] and Kwak[226] and summarized by Longstaff, et al.[227]

RESULTS AND DISCUSSION

The chemical and physical properties of the bitumen and a hydrotreated liquid product are presented in Table 52. The hydrotreated liquid product produced over the HDM catalyst was significantly upgraded relative to the bitumen with respect to nickel, sulfur, residuum and API gravity. The atomic H/C ratio of the hydrotreated liquid product also increased (from 1.6 in the feed to 1.7 in the hydrotreated liquid product), however, the increase did not indicate extensive hydrogenation of the liquid product. Thus, the increase in API gravity may be related to thermal dealkylation of side chains rather than catalytic hydrogenation reactions.

Process Variable Studies

The two most important reactions taking place in the bitumen hydrotreater are thermal cracking to lighter products and catalytic heteroatom and metal removal.[224,234] The process variables investigated in this study were the space velocity, reactor temperature and pressure and the influence of each will be discussed in turn.

Effect of Space Velocity

The effect of space velocity on product distribution and yields at a fixed reaction temperature (665 K) and pressure (13.7 MPa) is presented in Table 54. Heteroatom removal and residuum conversion increased as the space velocity decreased in the range of space velocities studied here. Increasing the apparent residence time of the liquid in the reactor by a factor of 6 (0.7 to 4.1 h) resulted in an increase in the API gravity of product liquid from 14.0°API to 18.3°API. This change was accompanied by an increase in hydrogen consumption from 31 to 75 m^3/m^3. The influence of space velocity at 665 K on denitrogenation was not significant even at a residence time of 4.1 h; that is, nitrogen conversion was only 29%. Sulfur conversion at these conditions amounted to 77% and nickel conversion was 82%. The reductions in Conradson carbon residue and pour point were not significant above a WHSV of 0.3 h^{-1}. At 0.24 h^{-1} WHSV, CCR conversion was 43%.

The product distribution and yields, as determined by simulated distillation, are presented as a function of WHSV in Figure 121. The scatter in the naphtha yield may be related to stripping of this fraction from the total liquid product when the samples were purged prior to elemental analysis. The gas, naphtha and distillate fraction yields increased monotonically with increasing residence times. The gas oil yield exhibited a maximum between 2 to 3 hours residence time (reciprocal WHSV). A maximum in the gas oil yield has been reported by other workers,[224,228] and implies that gas oil is an intermediate in the reaction sequence:

Table 54

Effect of WHSV on the Properties of the Hydrotreated Total Liquid Products

Run Number	D-25	D-11	D-19	D-15
Process operating conditions				
WHSV, h^{-1}	**1.38**	**0.77**	**0.43**	**0.24**
t, h	0.7	1.3	2.3	4.1
Temperature, K	662	665	665	666
Pressure, MPa	13.6	13.8	13.7	13.6
API gravity	14.0	15.2	15.9	18.3
Specific gravity	0.972	0.965	0.960	0.945
Pour Point, K	295	287	284	281
CCR, wt%	8.9	8.5	7.9	6.1
H_2 consumption, m^3/m^3	31	41	48	75
Elemental Analysis				
C, wt%	85.6	85.5	85.4	86.2
H, wt%	11.2	11.8	11.5	12.2
N, wt%	1.20	1.15	1.20	0.96
S, wt%	0.29	0.20	0.17	0.08
Ni, ppm	33	23	20	14
H/C atomic ratio	1.6	1.7	1.6	1.7
Product yield distribution				
Volatility, wt%	53.5	61.9	67.5	76.5
C_1-C_4, wt%	0.9	1.3	2.4	3.8
C_5-478 K, wt%	1.8	1.5	1.5	3.1
478-616 K, wt%	8.4	10.2	10.7	15.2
616-811 K, wt%	42.1	48.2	52.5	52.6.
> 811 K, wt%	46.5	38.1	32.5	23.5
Liquid yield, vol %	99.4	99.7	100.4	98.4

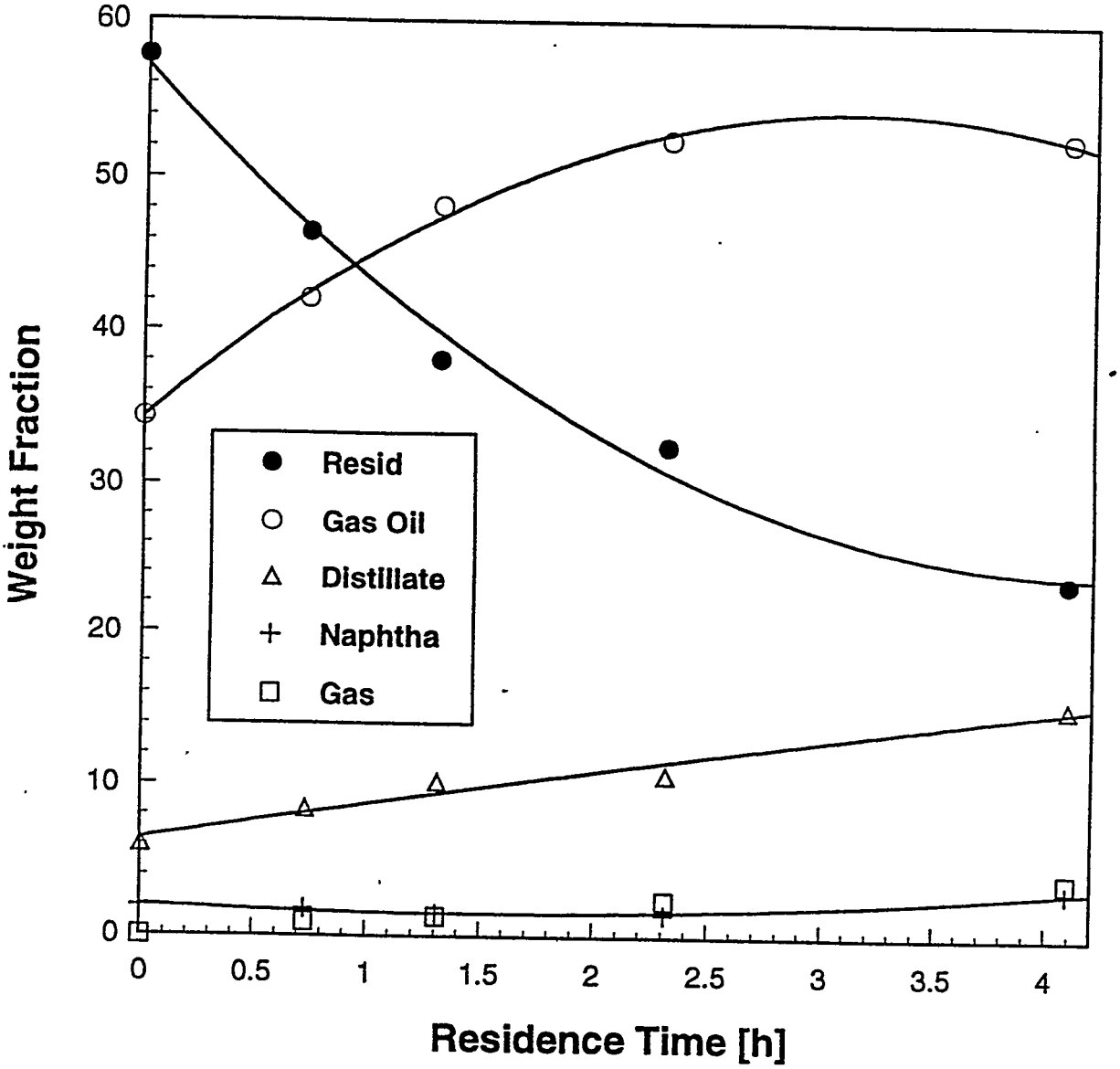

Figure 121. Effect of WHSV on Product Distribution and Yields at 664 K and 13.7 MPa

residuum -> gas oil -> distillate plus naphtha plus gas. Residuum content decreased as the residence time of the liquid increased. The residuum conversion was 61% at 0.24 h^{-1} WHSV.

Effect of Temperature

The effect of temperature on product distribution and yields at a fixed space velocity (0.76 h^{-1} WHSV) and pressure (13.7 MPa) is presented in Table 55. Increasing temperature favorably affected heteroatom removal reaction rates and promoted resid conversion.[225-228] The scatter in the sulfur and nickel data for the hydrotreated liquid product may be related to the low sulfur and nickel contents in the feed. The API gravity increased from 12.7°API to 18.0°API and hydrogen consumption increased from 6 to 55 m^3/m^3 as the temperature increased from 620 to 685 K. In the temperature range studied, the heteroatom and metal removal and residuum conversion were lower than were obtained by varying the WHSV. This was likely due to the relatively low temperature range used in this study (620-685 K) compared with the range used for commercial resid hydroprocessing (620-713 K). At low temperatures space velocity appears to exert a greater influence on heteroatom removal than temperature. The nitrogen, sulfur and nickel contents decreased by 17%, 43% and 68%, respectively, at a temperature of 685 K. The selectivity for nickel removal was expected with the HDM catalyst used in this study. The low nitrogen and sulfur conversions were a reflection of the low metal loading and the concomitant low activity of the HDM catalyst for heteroatom conversion. Residuum conversion at 685 K and 0.76 h^{-1} WHSV (56%)

Table 55

Effect of Temperature on the Properties of the Hydrotreated Total Liquid Products

Run Number	D-29	D-18	D-20	D-11	D-23	D-27
Process operating conditions						
Temperature, K	620	642	653	665	673	685
WHSV, h^{-1}	0.77	0.77	0.77	0.77	0.76	0.76
t, h	1.3	1.3	1.3	1.3	1.3	1.3
Pressure, MPa	13.7	13.6	13.6	13.8	13.7	13.7
API gravity	12.7	13.7	14.2	15.2	16.1	18.0
Specific gravity	0.981	0.975	0.972	0.965	0.959	0.947
Pour Point, K	315	307	299	287	283	279
CCR, wt%	10.1	9.4	9.2	8.5	8.1	7.6
H_2 Consumption, m^3/m^3	6	24	31	41	47	55
Elemental Analysis						
C, wt%	85.3	85.4	86.1	85.5	85.5	85.8
H, wt%	11.4	10.7	11.6	11.8	11.7	11.3
N, wt%	1.23	1.21	1.26	1.15	1.14	1.10
S, wt%	0.42	0.24	0.27	0.20	0.19	0.22
Ni, ppm	39	40	55	23	25	30
H/C atomic ratio	1.6	1.5	1.6	1.7	1.6	1.6
Product yield distribution						
Volatility, wt%	47.8	53.5	55.9	61.9	68.1	74.1
C_1-C_4, wt%	1.5	1.2	0.8	1.3	2.0	3.3
C_5-478 K, wt%	0.7	4.8	1.1	1.5	1.5	5.3
478-616 K, wt%	6.7	7.2	8.7	10.2	13.1	15.4
616-811 K, wt%	38.8	40.9	44.0	48.2	51.1	49.5
> 811 K, wt%	52.2	46.5	44.1	38.1	31.9	25.9
Liquid yield, vol %	97.4	99.5	99.4	99.7	99.5	97.3

was comparable to that obtained at 665 K and 0.24 h^{-1} WHSV (61%). Thus, temperature and residence time exhibit a synergism for residuum conversion whereas heteroatom removal over the HDM catalyst was more dependent on residence time than on temperature.

The product distribution and yields are presented in Figure 122. The scatter in the data with regards to C_1-C_4 gas yields was caused by low level gas production during hydrotreating over the HDM catalyst. The naphtha, distillate, and gas oil yields increased as the reaction temperature increased whereas the residuum content decreased. The naphtha yields may have been affected by the H_2S/NH_3 stripping procedure as mentioned earlier[5,6].

Effect of Pressure

The effects of hydrogen partial pressure on product distribution and yields at a fixed space velocity and reaction temperature are presented in Table 56. The WHSV and temperature were maintained at 0.76 h^{-1} WHSV and 665 K, respectively; in these experiments. Heteroatom removal was only slightly influenced by increasing the pressure. The API gravity and pour point of the total liquid products changed little with respect to increasing pressure, that is; the API gravity of the liquid product increased from 14.9 to 15.5°API and the pour point decreased from 288 to 284 K as the pressure increased from 11.3 MPa to 16.7 MPa.

The hydrogen consumption increased from 28 to 66 m^3/m^3 as the pressure increased from 11.3 to 16.7 MPa (Figure 123). Hydrogen consumptions in the same range were observed in the WHSV experiments, that is; an increase from 31 to 75 m^3/m^3 as the WHSV

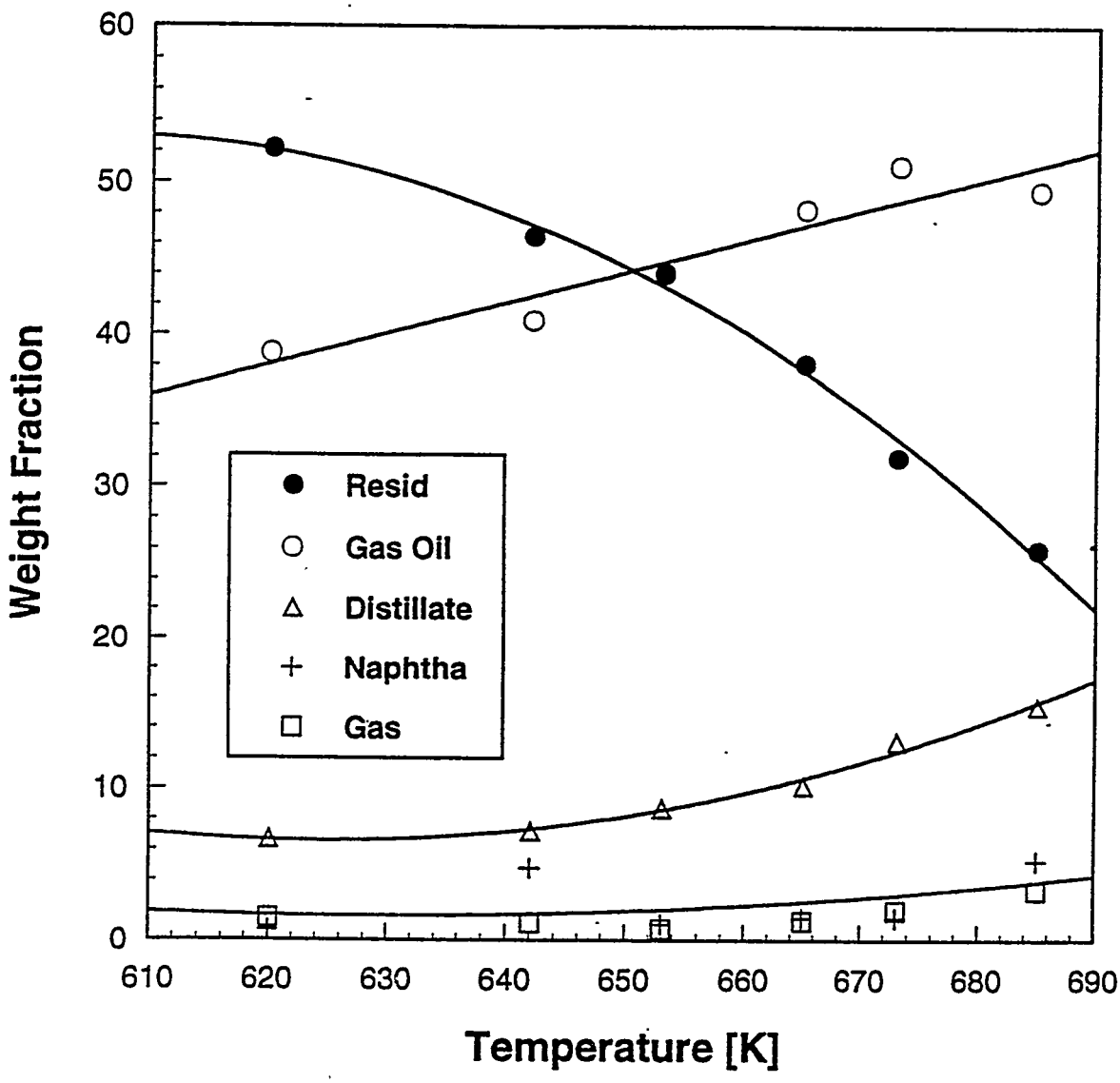

Figure 122. Effect of Temperature on Product Distribution and Yields at 0.76 H^{-1} WHSV and 13.7 MPa

Table 56

Effect of pressure on the Properties of the Hydrotreated Total Liquid Products

Run Number	D-17	D-11	D-21	D-13
Process operating conditions				
Pressure, MPa	**11.3**	**13.8**	**15.3**	**16.7**
Temperature, K	665	665	665	665
WHSV, h^{-1}	0.77	0.77	0.76	0.77
t, h	1.3	1.3	1.3	1.3
API gravity	14.9	15.2	15.3	15.5
Specific gravity	0.966	0.965	0.964	0.963
Pour Point, K	288	287	287	284
CCR, wt%	8.6	8.5	8.4	8.0
H_2 consumption, m^3/m^3	28	41	43	66
Elemental Analysis				
C, wt%	85.8	85.5	85.4	85.9
H, wt%	12.0	11.8	11.6	11.9
N, wt%	1.21	1.15	1.16	1.14
S, wt%	0.21	0.20	0.19	0.20
Ni, ppm	31	23	25	22
H/C atomic ratio	1.7	1.7	1.6	1.7
Product yield distribution				
Volatility, wt%	61.1	61.9	63.2	65.3
C_1-C_4, wt%	1.7	1.3	1.2	1.3
C_5-478 K, wt%	5.0	1.5	4.0	6.2
478-616 K, wt%	9.4	10.2	9.7	10.7
616-811 K, wt%	43.7	48.2	48.00	45.6
> 811 K, wt%	38.9	38.1	36.8	34.7
Liquid yield, vol %	99.5	99.7	99.4	100.0

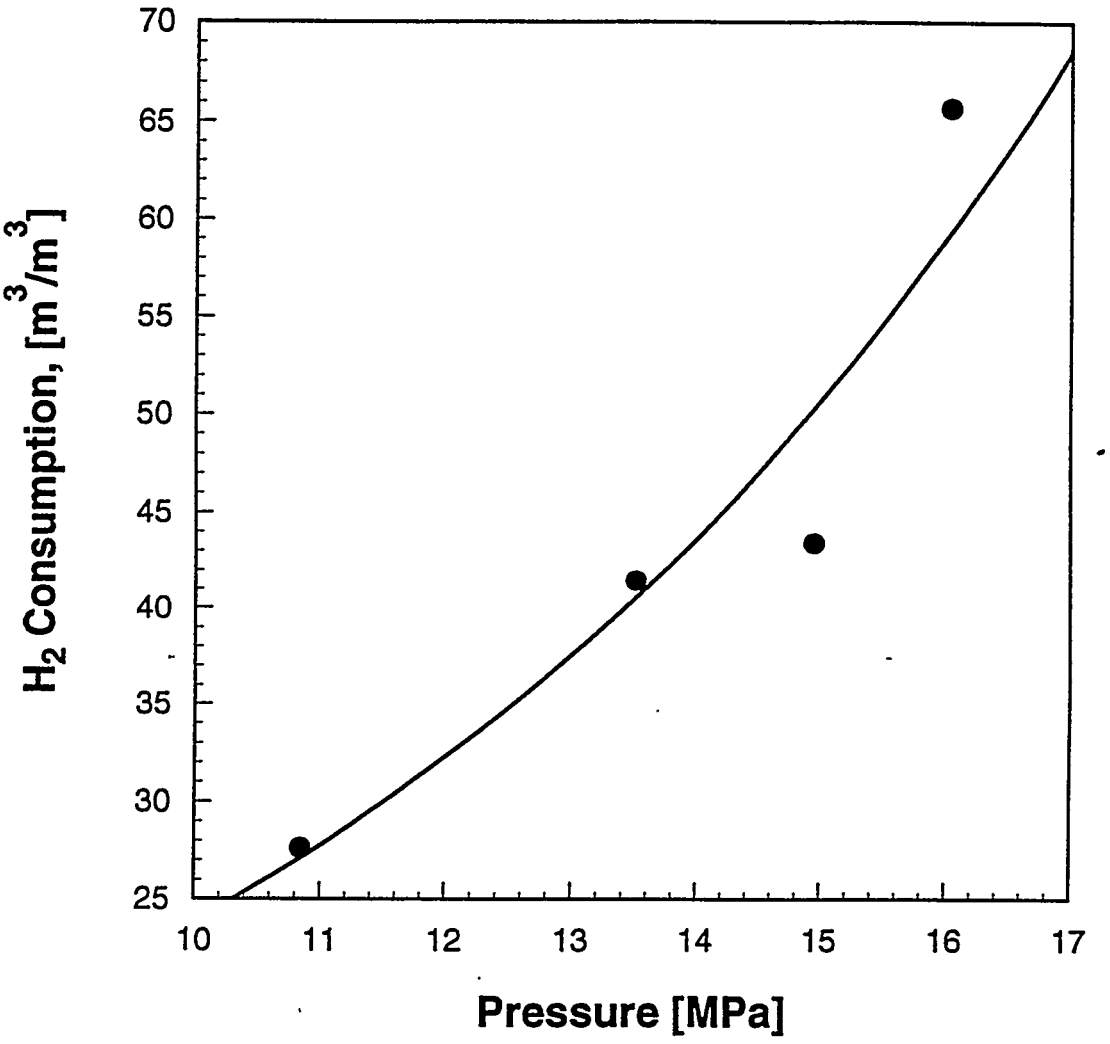

Figure 123. Pressure Versus Hydrogen Consumption at 0.76 H^{-1} WHSV and 664 K

decreased from 1.38 to 0.24 h^{-1} at 665 K and 13.7 MPa. However, the extent of residuum conversion at high hydrogen consumption was significantly different (~50% greater) when the space velocity was the independent variable than when pressure was the independent variable. The high hydrogen consumption and low resid conversion observed when pressure was varied could be due to aromatic ring hydrogenation in the absence of cracking and/or extensive denitrogenation and desulfurization, 13% and 44%, respectively; and was not the result of saturating cracked products. Beuther and Schmid[235] reported an improvement in desulfurization with increasing hydrogen pressure, however; the response to pressure diminished with increasing pressure at pressure above 6.9 MPa. A similar trend was observed in this study over the pressure range investigated.

Preliminary Process Kinetic Study

The rate expressions for heteroatom and residuum conversion generally contain a power rate law dependence on reactant concentration and hydrogen partial pressure. The rate expressions for an nth order plug flow model and for two parallel first-order reactions for kinetic schemes that gave higher than first order have been discussed previously.[225,226,228,229] The kinetic parameters were calculated using MINPACK software.[236]

The nitrogen, sulfur and Conradson carbon residue fractions remaining are plotted versus residence time in Figure 124. Each plot gave a straight line which passed through unity on the y-axis indicating that the HDN, HDS and CCR removal reactions for bitumen

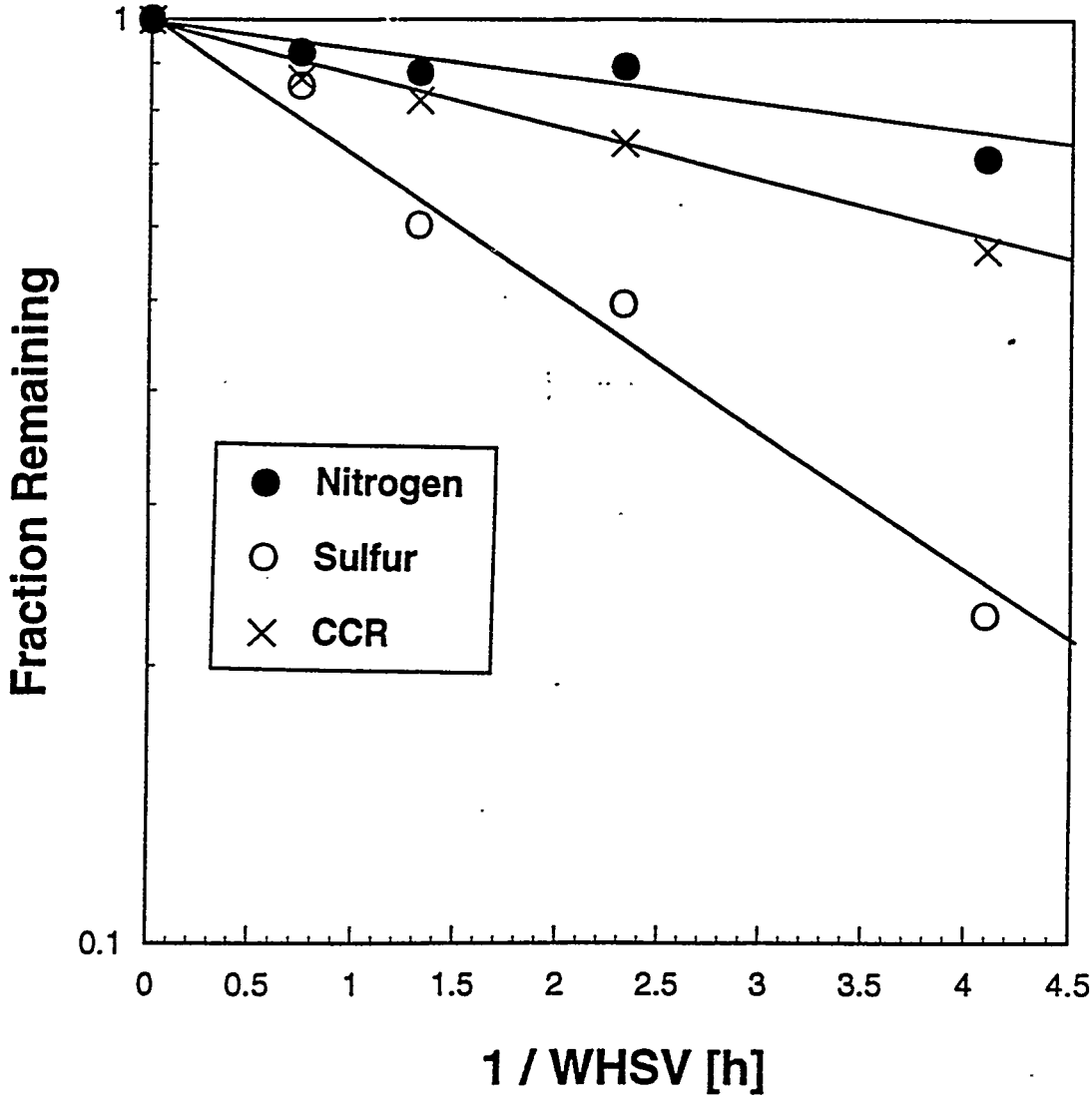

Figure 124. First Order Kinetic Plot for Nitrogen, Sulfur, and CCR Conversion Over a Commercial HDM Catalyst

over an HDM catalyst follow pseudo first-order kinetics. George[237] reported that HDS and HDN of a hydrocarbon liquid derived from the coprocessing of coal and heavy oil follows simple first-order kinetics over commercial NiMo hydrotreating catalysts. The extent of sulfur conversion was greater than that for nitrogen and CCR at all conditions as the space velocity was varied.[237] This trend was also observed in this work (Figure 124), that is, sulfur removal was easier than CCR and nitrogen removal. Billon et al.[238] also reported that sulfur removal from petroleum residuum over a CoMo catalyst was first order. Several researchers[239-241] reported first order kinetics for HDN of bitumen-derived coker and hydrocracker heavy gas oils and Riley[241] reported first order kinetics for HDN of heavy oils. Residuum and nickel conversions typically do not exhibit first order kinetics[241,242] in contrast with heteroatom removal. In this work residuum and nickel conversion exhibited reaction orders greater than unity.

The data in Table 55 indicates that an increase in temperature led to an increase in the conversion. The apparent activation energy for HDN (98 kJ/mol) was comparable to values reported in the literature (75-96 kJ/mol).[239,240] The activation energy for sulfur removal (91 kJ/mol) was lower than expected (113-130 kJ/mol).[224,235,239] This may be related to the difference in the temperature range studied (620-685 K) as compared to the range for commercial resid hydroprocessing (620-713 K).[224,243] It may also be related to the chemical composition of the residuum in the bitumen under investigation. The lower apparent activation energy for

sulfur removal may be the result of only facile sulfur species reacting over the HDM catalyst due to the low metal loading. The HDN and HDS apparent activation energies suggest that HDN and HDS with this feedstock over an HDM catalyst is not limited by pore diffusion but rather is limited by the low activity of the HDM catalyst.

The dependence of heteroatom removal on hydrogen partial pressure is presented in Figure 125. The rate expression for plug flow, nth order kinetics in bitumen is given by

$$-\frac{dC}{d\tau} = kC^n P_{H_2}^{\beta} \qquad (133)$$

where C is an appropriate representation of the bitumen concentration, k is reaction rate constant, n is reaction order, P_{H_2} is the hydrogen partial pressure and b is the pressure dependence term. The high hydrogen partial pressure dependence (1.5) for the nitrogen removal confirms[244-246] that aromatic ring hydrogenation is required prior to hydrogenolysis of the carbon-nitrogen bond. This step is not necessarily required for sulfur removal and accordingly sulfur removal exhibited a lower hydrogen dependence (0.7). Yui et al.[239,240,247] reported hydrogen partial pressure power terms of 1.2 to 1.8 for HDN, 0.6 to 1.1 for HDS of bitumen-derived coker and hydrocracker gas oils.

Sulfur and Residuum Conversions

The relationship between sulfur and residuum conversions is presented in Figure 126. In all experiments, sulfur conversion was

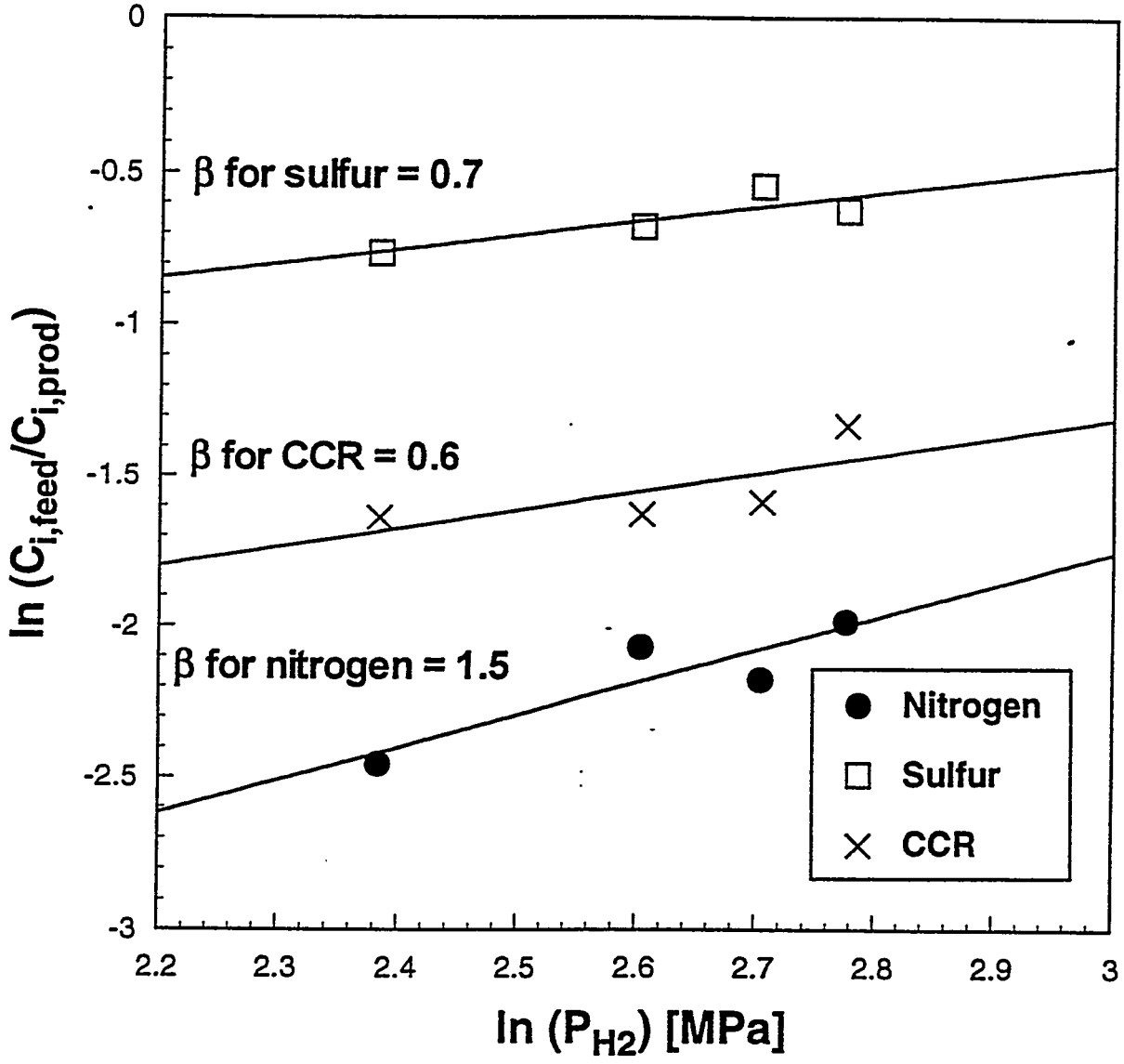

Figure 125. Hydrogen Partial Pressure Dependence for Nitrogen, Sulfur and CCR Conversion over an HDM Catalyst

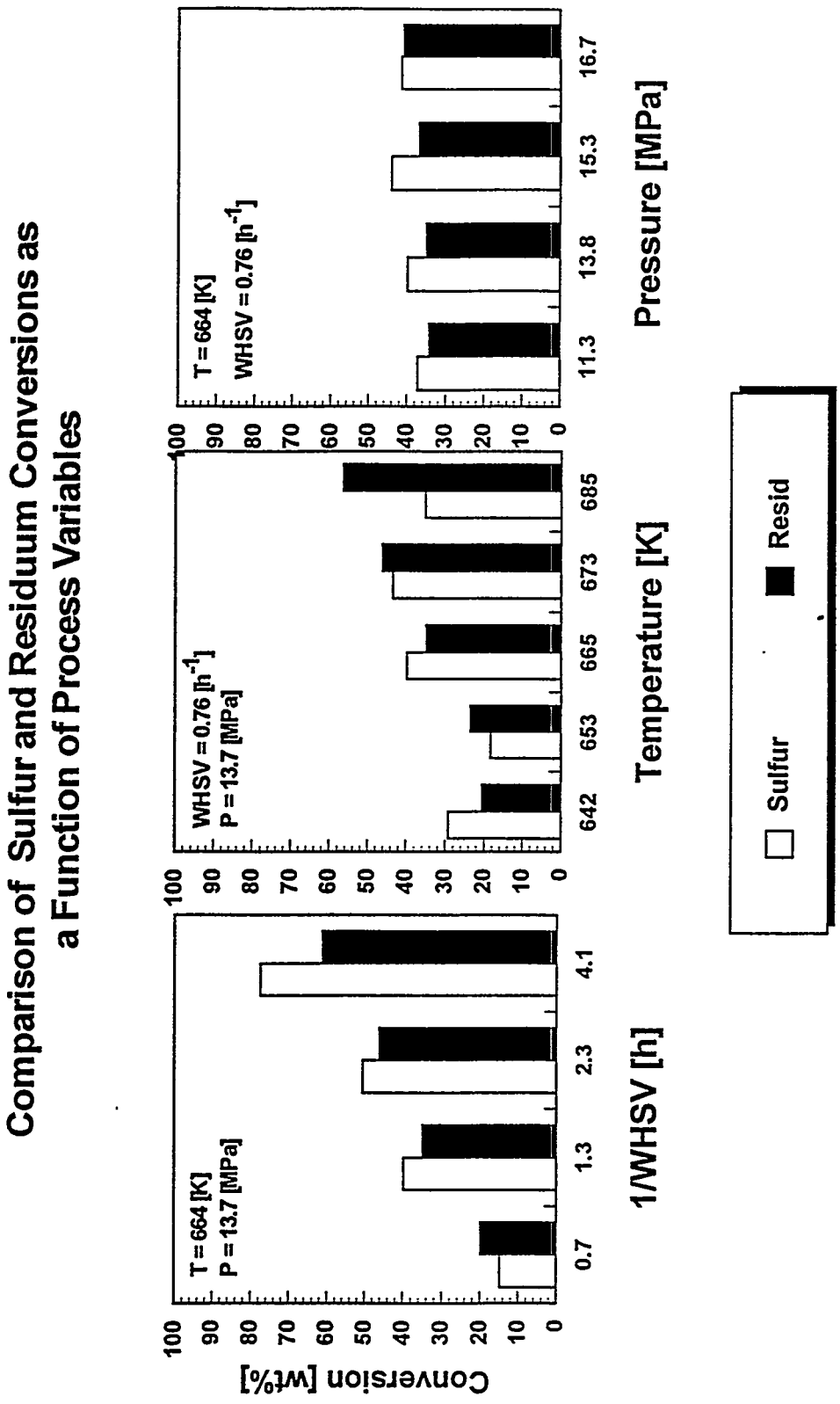

Figure 126. Comparison of Sulfur and Residuum Conversions as a Function of Process Variables

comparable with residuum conversion. This implies that the sulfur and residuum conversions are related. It is presumed that residuum sulfur conversion occurs after residuum cracking. Sulfur conversion monotonically increased with residence time due to first-order behavior over the HDM catalyst. Residuum conversion was observed to follow greater than first-order kinetics. Thus, it was modeled by a reaction scheme involving two parallel (facile and refractory) first-order reaction. Facile residuum conversion is for the most part complete at residence times below to 2.3 h, whereas, the conversion of refractory residuum becomes significant above 2.3 h. The difference between the sulfur and residuum conversions at 685 K indicated the importance of thermal conversion on molecular weight reduction relative to catalytic conversion.

SUMMARY AND CONCLUSIONS

A Uinta Basin bitumen was hydrotreated over a sulfided commercial Ni-Mo on alumina hydrodemetallation catalyst. The catalyst was onstream continuously for over 1,000 hours. The extent of heteroatom removal, residuum conversion and molecular weight reduction was investigated as a function of process variables. The fixed-bed reactor was operated in the upflow mode to ensure complete wetting of the catalyst and to maintain isothermal operation. The primary process variables studied were reactor temperature (620-685 K), weight hourly space velocity (0.24-1.38 h^{-1}) and total reactor pressure (11.3-16.7 MPa). The hydrogen/oil ratio was fixed in all experiments at 890 m^3/m^3 (=5000 scf H_2/bbl).

The effect of process variables on the extent of denitrogenation, desulfurization, demetallation, residuum (>811 K) conversion and the product distribution and yields is reported. The apparent activation energies for desulfurization and denitrogenation were 91 and 98 kJ/mol, respectively. A molecular weight reduction-model for hydrotreating over the HDM catalyst was proposed using four reactant lumps.

The HDM catalyst was effective for nickel and sulfur conversion during hydrotreating of the Whiterocks bitumen. However, it was ineffective for denitrogenation. HDN, HDS and CCR conversion of the Whiterocks bitumen over the HDM catalyst was correlated by first-order kinetics. The HDM catalyst deactivation rate was about 0.18°C/day during bitumen hydroprocessing. Sulfur conversion appeared to be linked to residuum conversion because residuum conversion facilitates conversion of sulfur in higher molecular weight moieties.

FUTURE ACTIVITIES

The hydrotreating of the PR Spring bitumen will be investigated over a commercial HDN catalyst provided by Criterion Catalysts. The extent of thermal cracking and conversion will be investigated with the Whiterocks and PR Spring bitumens using the UNOCAL and Criterion supports, respectively.

UINTA BASIN BITUMEN HYDROTREATING: A COMPARISON OF HDN AND HDM CATALYST PERFORMANCE

Principal Investigator:	F.V. Hanson
Postdoctoral Fellow:	D.C. Longstaff
Graduate Students:	S. Kwak
	J. Kim

INTRODUCTION

Residuum hydrotreating and hydrocracking will play an increasingly important role in refinery operations as crude runs are expanded to include heavy oils and resids. Integration of these feedstocks will require hydrogen addition instead of carbon rejection as the primary means of upgrading.

The role of the catalyst in residuum upgrading is uncertain. Significant residuum conversion can be achieved with metal sulfide catalysts that are supported on low-acidity supports.[224,248,249] However, reports in the literature[250-252] indicate that the presence of a catalyst does not affect residuum cracking and suggest that residuum conversion is primarily a thermal process.[250-252] An activation energy of 55 kcal/mol has been reported[224] for residuum hydrocracking in ebullieted catalyst beds and 70 kcal/mol[253] for residuum thermal cracking in the absence of a catalyst.

However, activation energies in the range 10-15 kcal/mol for the cracking of the residuum portion of the Whiterocks bitumen over Ni-Mo/S on alumina extrudates have been reported[228] which indicates that the catalyst may have participated in the residuum cracking reactions. In addition, pyrolysis of alkyl aromatics in sealed tubes in the absence of a catalyst at 673 K by Mushrush, et al.,[254] resulted in initial rate constants substantially lower than those

observed in residuum hydrotreating conducted in the presence of a catalyst.[228]

Coke formation and deposition in a plug flow reactor during thermal residuum processing may limit the extent of the comparison between catalytic and non-catalytic conversion. Because coke formation is limited by the presence of hydrogen, hydrogen donor solvents and even minute quantities of catalyst,[181,251,253,255] a comparison of the catalytic contribution to residuum upgrading can be examined with two catalysts which exhibit different levels of activity.

In this study the effect of catalyst activity on residuum conversion was investigated by hydrotreating the Whiterocks bitumen, 55-58% residuum, over commercial hydrodenitrogenation (HDN)[228] and hydrodemetallation (HDM) catalysts[256] in a packed-bed reactor operated in the upflow mode. Differences in the activity of these two catalyst systems form the basis for determining to what extent catalyst activity influences residuum conversion.

Another study was conducted to determine the influence of molecular weight distribution on the sulfur and nitrogen reactivity of the heteroatoms.[227] The results from this study are reported here to illustrate how changing the overall reactivity of the catalyst-oil system changes the selectivity for nitrogen, sulfur and residuum conversion.

EXPERIMENTAL

Two feedstocks were employed in these studies: 1) a bitumen-derived heavy oil (BDL) obtained by pyrolysis of the Whiterocks oil

sand in a fluidized bed reactor,[17,24,171,175] and 2) a bitumen (BIT) obtained by toluene extraction of the Whiterocks oil sand.[225] The properties of the two feeds are presented in Table 57.

Table 57

Analysis of the Whiterocks Bitumen and Bitumen-Derived Liquid

	BIT	BDL
Gravity (°API)	11.4	18.5
Density (288.7 K) (g cm^{-1})	0.989	0.943
Pour Point, K	330	253
Asphaltenes, wt%[1)]	5.0	2.8
Simulated Distillation		
Volatility (wt%)	43.3	82.2
IBP, K	489	414
IBP-417 K (wt%)	0.0	4.7
477-617 K (wt%)	6.3	18.5
617-811 K (wt%)	37.0	59.0
>811 K (wt%)	56.7	17.8
Elemental Analysis		
C (wt%)	85.9	86.0
H (wt%)	11.1	11.1
N (wt%)	1.07	1.02
S (wt%)	0.37	0.32
H/C Atomic Ratio	1.54	1.54
Metals Content		
Ni (ppm)	78	9
V (ppm)	4	<1
As (ppm)	3	3

[1)]Pentane Insolubles

The properties of the commercial HDN and HDM catalysts are presented in Table 58. It was presumed that it would be possible to differentiate between thermal and catalytic contributions to nitrogen, sulfur and residuum conversion with these catalysts due

Table 58

Properties of the HDN and HDM Catalysts[a]

	HDN	HDM
Loading (cm^3)	152	152
Surface area ($m^2\ g^{-1}$)	241	155
Pore Volume[b] ($cm^3\ g^{-1}$)	0.55	0.72
Median Pore Diameter, Å	90	180
Composition (wt%)		
NiO	3.3	1.0
MoO_3	12.8	6.2
P_2O_5	0.8	0.0

[a]UNOCAL 1/16" quadralobe
[b]Hg porosimetry

to the differences in surface areas, metal and promoter loadings and pore structure.[257,258]

Process studies were conducted with both catalysts and with both feedstocks: 1) bitumen-derived heavy oil hydrotreated over the HDN catalyst (BDL-HDN),[227] 2) bitumen hydrotreated over the HDN catalyst (BIT-HDN)[228] and 3) bitumen hydrotreated over the HDM catalyst (BIT-HDM).[256] The conditions used to hydrotreat the bitumen and the bitumen-derived heavy oil are presented in Table 59. The base case temperature for the BIT-HDN and the BIT-HDM studies was higher than that for the BDL-HDN study because sufficient conversion was not obtained with the bitumen at 618 K.

The reactor temperature, feed rate and the reactor pressure were varied independently to determine the effect of each variable on upgrading. The reactor conditions and feed rate were returned

Table 59

Base-Case Conditions and Process Variable Ranges

Process Variable Ranges	
Temperature (K (°F))	618-711 (653-822)
Pressure (MPa (psia))	11.0-16.9 (1600-2450)
WHSV (h^{-1})	0.29-1.38
LHSV (h^{-1})	0.18-0.86
H_2/oil ratio (m^3 m^{-3} (scf/bbl))	890 (5000)
Base Case Process Conditions	
BIT: Temperature (K (°F))	642 (696)
BDL: Temperature (K (°F))	618 (653)
Pressure (MPa (psia))	13.7 (1980)
WHSV (h^{-1})	0.75
LHSV (h^{-1})	0.45

to the base case conditions (Table 59) after each process variable experiment. The deactivation of the catalysts with time onstream was monitored by analyzing the liquid product produced at the base case conditions. Reactor conditions were not varied during the first 120-150 hours onstream to permit catalyst equilibration. Subsequent process experiments were conducted every 24 to 48 hours for 800 hours onstream. The experimental apparatus and the operating and catalyst sulfiding procedures have been discussed in detail elsewhere.[227,228,256]

RESULTS AND DISCUSSION

Effect of Catalyst and Feed on Conversion

The monitoring of catalyst performance and the generation of meaningful activity and selectivity comparisons in the BDL-HDN, the BIT-HDN and the BIT-HDN studies was difficult due to time-delays involved with heteroatom, metals and simulated distillation

analyses. Thus, the °API gravity of the total liquid product was adopted as an online monitor of catalyst performance. Furthermore, because the extents of denitrogenation, desulfurization and resid conversion are related to the specific gravity of the total liquid product, the API gravity was used to organize the data for the three catalyst/heavy oil systems. Catalyst deactivation was insignificant in all three studies, that is, catalyst deactivation did not introduce detectable trends in the data. Catalyst deactivation was defined in terms of the temperature increase required to maintain the API gravity of the total liquid product produced at base case conditions at a constant level. Deactivation rates were 0.14°C $day,^{-1}$ [227] 0.2°C day^{-1} [228] and 0.18°C day^{-1} [256] for the BDL-HDN, the BIT-HDN and the BIT-HDM studies, respectively.

A comparison of the product yield and analysis (Table 60) show that the HDN catalyst was more active for heteroatom conversion as well as for molecular weight reduction. The residuum content of the hydrotreated total liquid product (TLP) varied inversely with API gravity (Figure 127). These data indicated that, for the most part, residuum conversion in the BIT-HDM study was less than that in the BIT-HDN study. Thus, for catalyst/oil systems operating in the range of temperatures, pressures and space velocities in Table 59, residuum conversion is influenced by the catalyst selection. The data for the BIT-HDN and the BIT-HDM studies appear to lie along a single curve. Data for the BDL-HDN study are displaced and lie parallel to this curve. This is because the BDL had been previously processed in a fluidized-bed pyrolysis reactor.

Table 60

Effect of Catalyst Selection on the Product Properties of the Hydrotreated Bitumen from the Whiterocks Oil Sand Formation

Run number Catalyst	C-8 HDN	D-11 HDM	C-6 HDN	D-27 HDM
Process operating conditions				
WHSV (h^{-1})	0.76	0.77	0.75	0.76
τ (h)	1.31	1.3	1.3	1.3
Temperature (K)	664	665	685	685
Pressure (MPa)	13.5	13.8	13.7	13.7
API Gravity	18.1	15.2	23.4	18.0
Density(g cm^{-3})	0.938	0.965	0.913	0.946
Elemental analysis				
C (wt%)	86.1	85.5	86.1	85.8
H (wt%)	11.9	11.8	11.9	11.3
Nitrogen (ppm)	5400	11500	3400	11100
Sulfur (ppm)	680	2000	250	2200
H/C atomic ratio	1.7	1.7	1.7	1.6
Product yields (wt%)				
C_1-C_4 (wt%)	1.2	1.3	3.3	3.3
C_5-478 K (wt%)	4.0	1.5	6.0	5.3
478-616 K (wt%)	16.5	10.2	24.4	15.4
616-811 K (wt%)	53.2	48.2	50.9	49.5
>811 K (wt%)	26.2	38.1	16.2	25.9

The effect of catalyst selection on residuum conversion appears to contrast with the work of other researchers[250-252] who indicated that residuum conversion is primarily thermal. In addition, the apparent activation energies for residuum conversion in the BIT-HDN and BIT-HDM runs are approximately 18 and 29 kcal/mol, respectively, (Figure 128) which disagree with values reported in the literature of 70 kcal/mol for residuum thermal cracking in the absence of a catalyst[253] and of 55 kcal/mole for

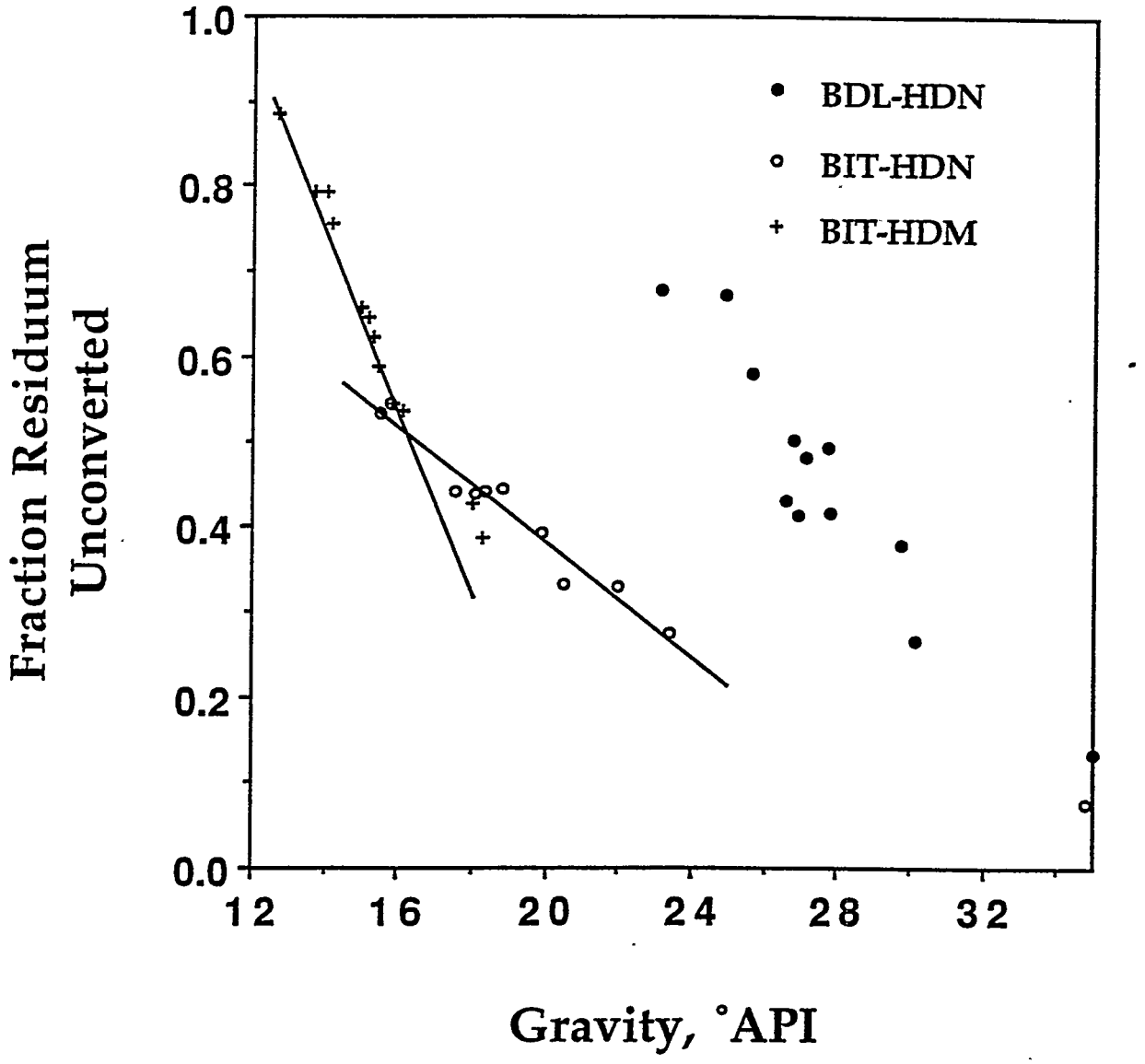

Figure 127. Residuum Content vs API Gravity for the BDL-HDN, the BIT-HDN and the BIT-HDM Studies

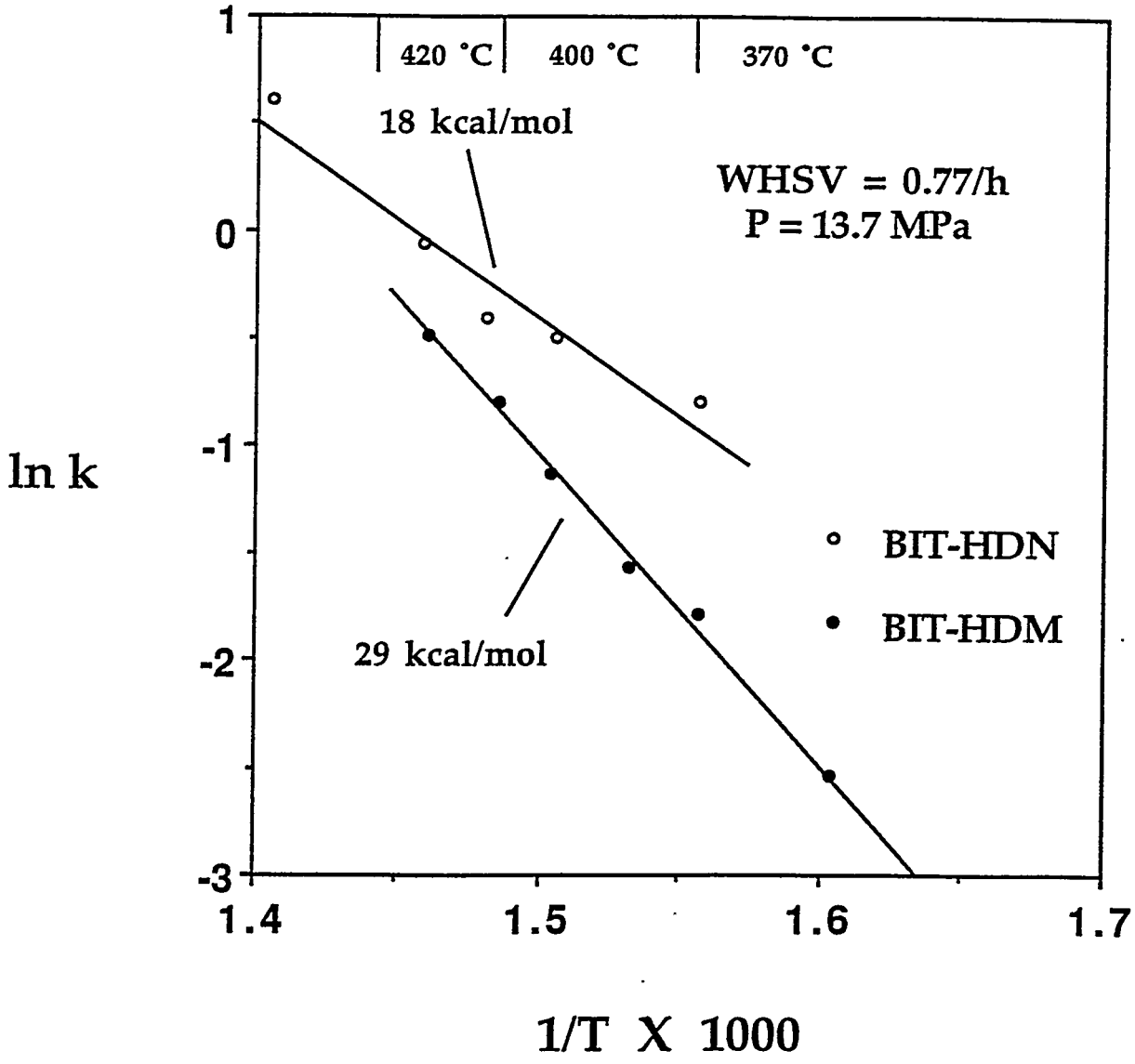

Figure 128. Arrhenius Plot for Whole Residuum Conversion

residuum hydrocracking in an ebullieted bed.[224] The difference between the data reported here and the data of other researchers[224,253] may be related to the lower reaction temperatures used in this study. Lower temperature operation will decrease the importance of thermal cracking in the overall residuum conversion process due to the higher activation energy for thermal cracking.

Catalyst selection also exhibited an influence in increasing the relative ratio of catalytic: thermal cracking. Comparison of the results from the BIT-HDN and the BIT-HDM studies indicated that residuum conversion was greater in the presence of the HDN catalyst. In addition, the higher apparent activation energy observed for residuum conversion during the BIT-HDM study reflects the increasing influence of thermal cracking when the volumetric catalytic activity of the system is reduced by employing a less active catalyst or by diluting the catalyst.

It has been reported that the catalyst plays only a minor role in residuum conversion.[252,259] This conclusion was based on stirred autoclave data where the catalyst-to-oil ratios are low. In dilute catalyst systems such as stirred autoclaves, ebullieted beds or diluted packed beds catalytic conversion is suppressed but thermal cracking is not.

Additional evidence for the effect of catalyst on residuum conversion is seen in the 15 kcal/mole reduction in the apparent activation energy between thermal cracking (70 kcal/mole)[253] and 55 kcal/mole[224] in an ebullieted catalytic hydrotreater. The catalyst in the ebullieted bed reactor introduces a catalytic pathway for

residuum conversion, which leads to a decrease in the apparent activation energy. If the catalyst-to-oil ratio were to be increased, the apparent activation energy for residuum conversion might be expected to decrease further depending on the activity of the catalyst.

Sulfur and nitrogen conversions for the three studies follow similar trends, and it appears that the fraction of sulfur and nitrogen could be correlated by a simple curve for the BIT-HDN, the BIT-HDM and the BDL-HDN data (Figures 129 and 130).

The nitrogen and sulfur data from these studies revealed the effect of feed and catalyst selection on the conversion of nitrogen and sulfur. The reactor conditions employed in all three studies were the same and the experiments were performed in the same sequence, thus, reactor operating conditions were not a factor in the segregation of the data from these three studies into three different clusters.

High nitrogen and sulfur conversions were achieved in the BDL-HDN study; however, the same levels of conversion were not observed in the BIT-HDN study. The differences in reactivity were related to the molecular weight reduction accomplished during oil sand pyrolysis which produced the bitumen-derived heavy oil.

Previous studies by Flinn et al.[260] and by Trytten et al.[261] have indicated that heteroatom reactivity correlates with the molecular weight of the feed. Trytten et al.[261] estimated diffusivities and reported that the intrinsic rate constants for nitrogen and sulfur conversion were influenced by steric

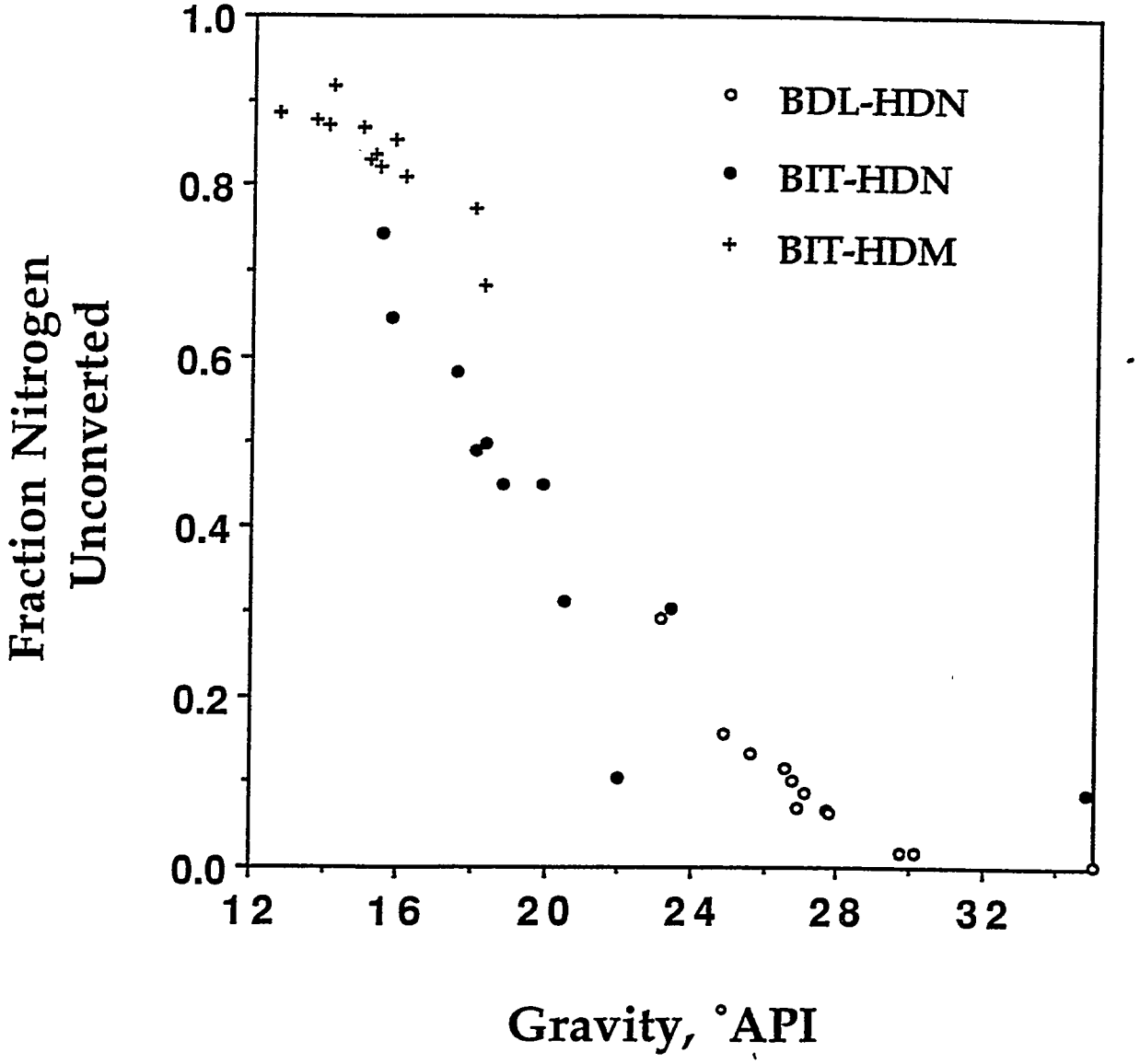

Figure 129. Nitrogen Content vs API Gravity for the BDL-HDN, the BIT-HDN and the BIT-HDM Studies

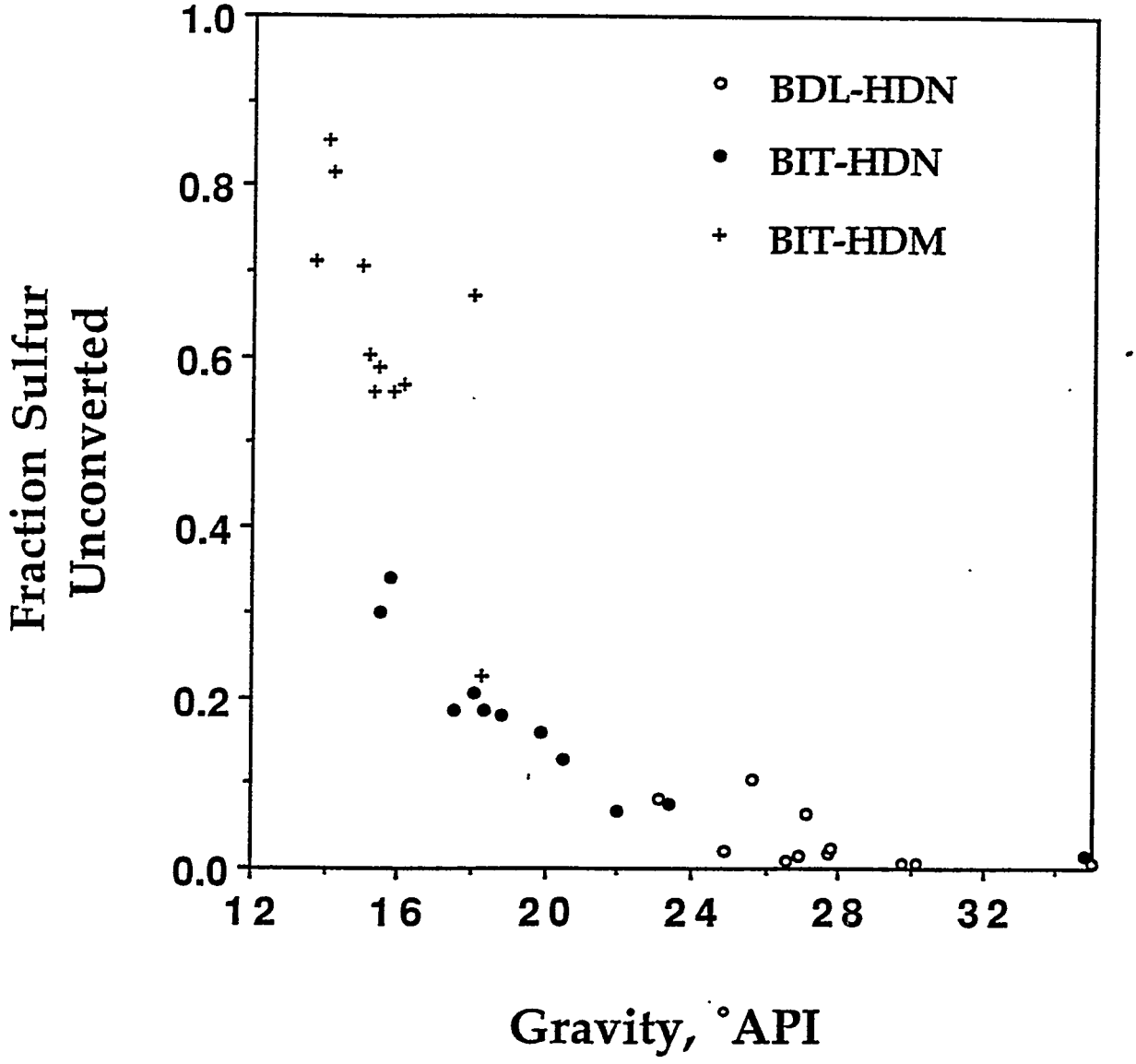

Figure 130. Sulfur Content vs API Gravity for the BDL-HDN, the BIT-HDN and the BIT-HDM Studies

constraints and that the effectiveness factor decreased as molecular weight increased. Based on these results, the low reactivity of nitrogen and sulfur in the bitumen relative to the bitumen-derived heavy oil may be related to a combination of diffusional and steric effects.

The reduction of TLP nitrogen to levels required for hydrocracking may not be feasible for the Uinta Basin bitumens due to these steric and diffusional constraints. For this reason, conversion of high nitrogen bitumens to liquid fuels should emphasize molecular weight reduction prior to heteroatom removal.

Effect of Catalyst and Feed on Selectivity

Selectivity changes were observed for the BDL-HDN, BIT-HDN and BIT-HDM systems as the relative activity of the oil/catalyst system changed (Figures 131-133). The extent of sulfur conversion was greater than the extent of nitrogen conversion in the BDL-HDN study (Figure 131). This was expected because sulfur compounds are known to be more reactive than nitrogen compounds.[246] In the BIT-HDN study, residuum conversion changed little relative to the BDL-HDN study. However, heteroatom conversion was reduced because of the steric and diffusional effects which reduce reactivity and accessibility of heteroatom containing moieties. Undoubtedly, catalytic residuum conversion is also hindered by diffusional effects. However, the thermal pathway for residuum conversion is not hindered by mass transfer or steric barriers. Heteroatom conversion is more sensitive to catalyst activity than residuum

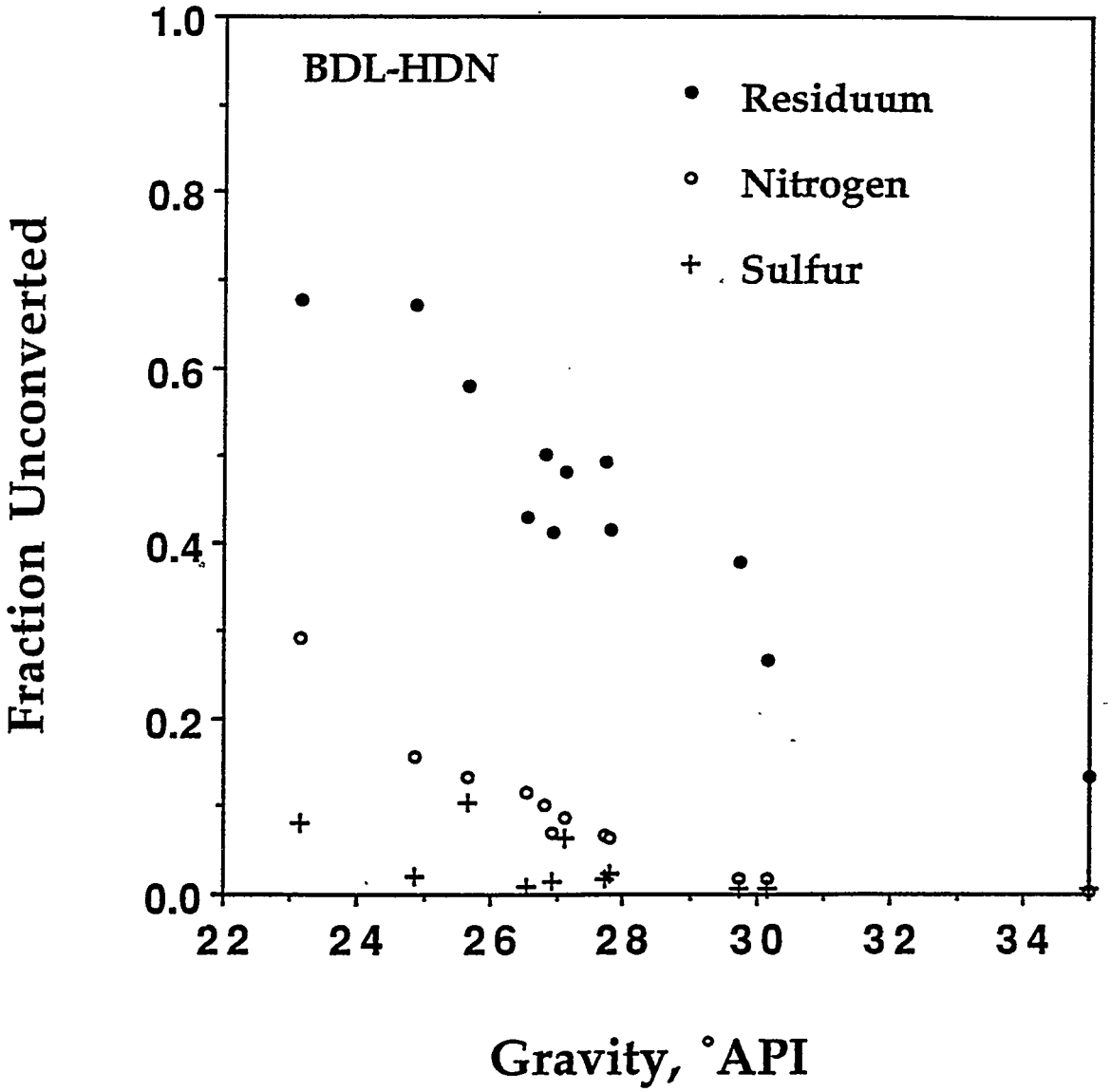

Figure 131. Residuum, Nitrogen and Sulfur Remaining in Samples Hydrotreated in the BDL-HDN Study

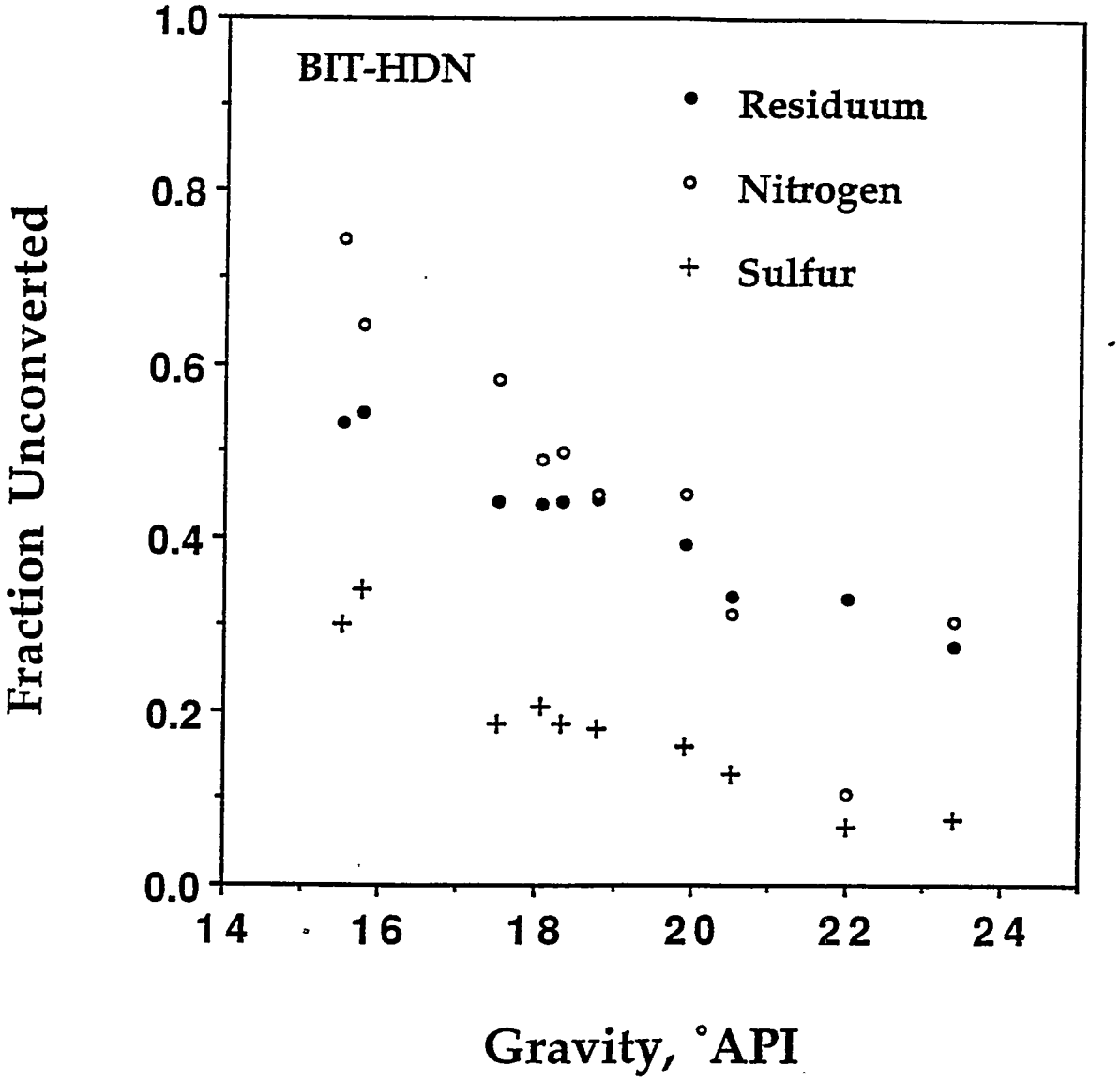

Figure 132. Residuum, Nitrogen and Sulfur Remaining in Samples Hydrotreated in the BIT-HDN Study

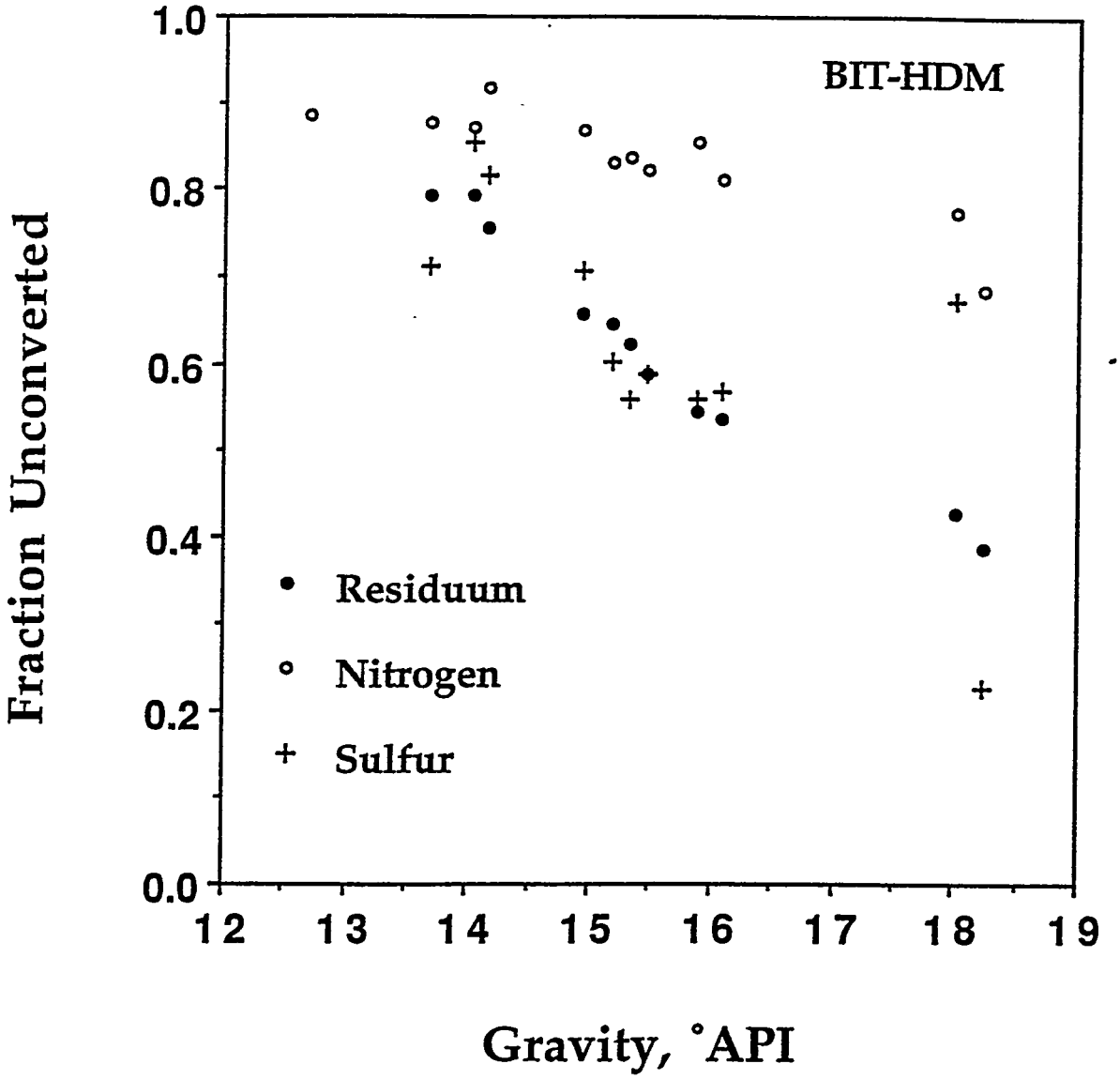

Figure 133. Residuum, Nitrogen and Sulfur Remaining in Samples Hydrotreated in the BDL-HDM Study

conversion because residuum conversion can proceed by a thermal mechanism which is not available for heteroatom conversion.

A similar trend was observed when the more active HDN catalyst was replaced by the less active HDM catalyst (Figure 133). In the BIT-HDM study residuum conversion surpassed nitrogen conversion in all cases and was almost the same as sulfur conversion. The differences in heteroatom conversion in the BDL-HDN and BIT-HDN studies was attributed to the reactivity difference of heteroatoms in the two different feeds. The BIT-HDN and BIT-HDM studies indicated that heteroatom conversion was more sensitive to catalyst selection than was residuum conversion. This observation is related to the fact that residuum conversion can proceed by a thermal pathway which is unavailable for heteroatom conversion.

Pathways for Residuum Conversion

Residuum conversion can best be modelled by treating the residuum as if it consisted of two lumps: a facile or reactive lump and a refractory or unreactive lump. Generally, a third of the residuum is facile and cracks approximately 15 times faster than the refractory residuum.[225,228,250] The reactivity difference may be attributed to the presence of asphaltenes in the residuum. However, the fraction of refractory residuum is often several times greater than the asphaltene content.[250]

Models which have been used to describe thermolysis of asphaltenes can be extended to explain the range of reactivity that residuum exhibits. Asphaltene pyrolysis and model compound studies indicated that aliphatic-aromatic C-C bonds are labile and

susceptible to thermal cracking.[262,263] Models of asphaltene pyrolysis suggest that during pyrolysis alkyl sidechains are cleaved from polar/aromatic clusters. The polar cores, stripped of their aliphatic substituents, then agglomerate and react to form coke.[262,264]

It is expected that conversion of the whole residuum proceeds in a similar fashion, except, that the polarity of the clusters remaining after dealkylation is not sufficient to induce agglomeration and coke formation. Instead, the dealkylated clusters undergo further hydrogenation and cracking, albeit slowly. These dealkylated clusters are the refractory residuum reported here and by other workers.[250]

According to this model, conversion of facile residuum is similar to asphaltene cracking, in that alkyl substituents are cleaved from polycyclic nuclei which are present in the bitumen.[15] Therefore, the rate constants for asphaltene pyrolysis should be the same order of magnitude as the rate constants for facile residuum conversion. An Arrhenius plot provided by Schucker, et al.,[262] for asphaltene conversion gives rate constants of 1.2-1.5 h^{-1} at 663 K. This compares with a rate constant of 3.8 h^{-1} for the conversion of facile residuum in the Whiterocks bitumen at 663 K in a fixed-bed reactor.[228] The higher rate constant reported for bitumen residuum conversion can be attributed to the presence of the catalyst which enhances asphaltene cracking[262] and to the nature of the asphaltene fractions in the Whiterocks bitumen.[15]

Additional evidence for this view of residuum conversion is seen in the conversion of light and heavy residuum. GC analysis permits elution of residuum boiling below C_{60} (888 K). Therefore, the amount of residuum which boils between 811-888 K is defined as light residuum. The noneluted residuum, 888 K plus, is defined as heavy residuum. Results from the BIT-HDN study indicated that the amount of heavy residuum is reduced much more quickly than the amount of light residuum. This behavior is similar to that exhibited by maltenes and asphaltenes during thermal processing:[253,262] at short reaction times there is a rapid decrease in the average molecular weight of the asphaltenes.

Deep residuum conversion, therefore, consists of the conversion of species which are only a few carbon atoms heavier than species boiling above 811 K. However, it is these light residuum components which have been denuded of their alkyl substituents which pose the greatest difficulty for residuum conversion.

SUMMARY AND CONCLUSIONS

Uinta Basin bitumen has been hydrotreated under varying conditions to determine the effect of catalyst on heteroatom conversion and molecular weight reduction. The process variables investigated included total reactor pressure (11.0-16.9 MPa); reactor temperature (618-711 K), feed rate (0.29-1.38 h^{-1} WHSV) and catalyst. A hydrodenitrogenation catalyst was more active for nitrogen, sulfur and residuum conversion than a hydrodemetallation catalyst. Residuum conversion was sensitive to the catalyst

surface area, metal loading and phosphorus promoter indicating that a certain portion of residuum conversion during hydrotreating is catalytic. Differences between nitrogen, sulfur and residuum conversion and product yields are reported for bitumen hydrotreated over the hydrodenitrogenation and hydrodemetallation catalysts.

Catalyst selection influences the conversion of residuum. A high surface area/high metal content HDN catalyst was more effective for residuum conversion than a low surface area/low metal content HDM catalyst.

The bitumen-derived heavy oil used in the BDL-HDN study was much more amenable to hydrotreating than the bitumen in the BIT-HDN study. Thus, it was concluded that molecular weight reduction should be stressed prior to heteroatom removal for upgrading high nitrogen content bitumens.

Residuum conversion was less sensitive to catalyst selection than heteroatom removal because it proceeds via a thermal pathway which, for the most part, is not available for heteroatom conversion. Residuum conversion can be represented by lumping residuum into two lumps: a reactive or facile portion and a less reactive or refractory fraction. Facile residuum conversion was presumed to involve dealkylation of naphthenic/aromatic/polar ring structures forming a volatile or nonvolatile nucleus and a volatile alkyl fragment. Refractory residuum conversion is presumed to occur via a reaction sequence in which nonvolatile dealkylated nuclei undergo hydrogenation/ring opening/sidechain cleavage reactions.

FUTURE ACTIVITIES

The activity of the catalyst support and a totally inert material will be evaluated with the Whiterocks and PR Spring bitumens to determine the extent and importance of thermal residuum conversion in hydrotreating over HDN and HDM catalysts.

EFFECTS OF COKE ON HDM CATALYST DEACTIVATION

Principal Investigator:	F.V. Hanson
Consulting Investigator:	F.E. Massoth
Graduate Students:	Kuang-Shing Chu

INTRODUCTION

The utilization of Uinta Basin bitumens will likely require a combination of thermal and catalytic upgrading processes. Pyrolysis of the oil sand produces a bitumen-derived heavy oil from which asphaltenes and metals (Ni, V, As) have been rejected, the latter being isolated in the carbonaceous residue on the sand grains. This was accompanied by a reduction in the boiling range and molecular weight of the bitumen-derived heavy oil relative to the bitumen; however, the nitrogen (~1 wt%) and sulfur (~0.5 wt%) contents were relatively unchanged. [152,195] Thus, the bitumen-derived heavy oil requires hydrodenitrogenation before catalytic cracking or hydrocracking to produce transportation fuels. The hydrotreating of a bitumen-derived heavy oil and a bitumen over a nickel-molybdenum/alumina hydrodenitrogenation catalyst has been reported by Longstaff and coworkers.[17,227,228] These process variable studies were each onstream in excess of 1,000 hours and postrun analysis of the catalysts indicated that significant coking occurred, despite the highly naphthenic nature of the feedstocks.[15,16]

Coke arises mainly from polynuclear aromatics[265] and asphaltenes[266] present in the feed. Polynuclear aromatics exhibit high proton affinities and asphaltenes contain basic nitrogen, both

of which give rise to strong adsorption of the respective species on the catalyst surface. There is general agreement that coke forms from condensation reactions involving these adsorbed species.[266] The covering of catalytically active sites by coke will decrease catalytic activity. Access to catalytic sites can also be lost by plugging of catalyst pores by coke and/or metals in the feed.

Several authors[267,268] have noted a significant enhancement in the nitrogen content of the carbonaceous residues on aged hydroprocessing catalysts relative to the nitrogen content of the feeds. It has been suggested that adsorbed nitrogen-containing compounds can act as coke precursors.[268-270] This may be especially important for processing of heavy oils produced from oil sands, which contain relatively high levels of nitrogen.[14-16]

In prior studies, the effect of coke derived from anthracene[271] and from a vacuum gas oil[272] on the deactivation of a commercial $NiMo/Al_2O_3$ hydrotreating catalyst was investigated. In the present study, a commercial hydrodemetallation catalyst was employed. Coked catalysts were prepared using anthracene and the Whiterocks bitumen as coke precursors. The effect of different coke levels on catalytic activities for hydrogenation and hydrodenitrogenation was evaluated using a mixture of model compounds.

EXPERIMENTAL

Catalysts and Chemicals

The catalyst employed was a hydrodemetallation catalyst, CA-892, from UNOCAL Corporation. The catalyst contained 0.8 wt% NiO and 6.2 wt% MoO_3 on alumina and had a surface area of 151 m^2/g; a pore volume of 0.69 mL/g; and an average pore diameter of 182 Å. The extrudates were crushed and sieved to obtain the 40 - 60 mesh fraction for use in these studies.

Anthracene (J.T. Baker Chemical Co.) was of the highest purity available. The bitumen was obtained by toluene extraction of the Whiterocks oil sand followed by rotary evaporation of the toluene. Selected properties of the Whiterocks bitumen are summarized in Table 61. The results obtained from various spectroscopic techniques (gas chromatography - mass spectrometry, pyrolysis - mass spectrometry, FTIR, and ^{13}C NMR) indicated that the bitumen consisted mostly of short- and long- chain (i.e., normal and isoprenoid chains) alkylsubstituents attached to polycyclic naphthenic, naphtheno-aromatic and/or aromatic moieties.[15,16] The majority of the cyclic units (alicyclic, naphthenes and aromatics) in the bitumen contained 1 to 5 rings.

Mineral oil (Squibb) of commercial purity was used as the solvent. Dissolved air in the mineral oil was removed by evacuation. Nickel tetra-phenylporphyrin (Ni-TPP), chlorin free grade from Midcentury Co., was used to deposit nickel on the catalyst.

TABLE 61

Properties of Whiterocks Bitumen

Specific Gravity (289 K/289 K)	0.985
Carbon, wt%	85.8
Hydrogen, wt%	11.6
Nitrogen, wt%	1.1
Sulfur, wt%	0.4
Oxygen, wt%	1.1
Ni, ppm	67
V, ppm	< 5
As, ppm	2
H/C atomic ratio	1.62
Carbon aromaticity	23.3
Asphaltenes (Pentane Insolubles), wt%	5.0
Simulated Distillation	
Volatility(<811 K) wt%	44.1
477-617 K, wt%	6.2
617-811 K, wt%	37.9
> 811 K, residue wt%	55.9
IBP, K	510

Coking Runs

Anthracene- and bitumen-coked catalysts were prepared by reacting a solution of the coking agent in mineral oil which contained 0.5 wt% carbon disulfide in an autoclave reactor for extended periods of time. Catalysts were presulfided with a 10 mol% H_2S/H_2 mixture at 673 K for 2 hours before each coking run. Different coke levels were obtained by varying the amount of anthracene or bitumen dissolved in the mineral oil and the coking time. Coking conditions are given in Table 62. Anthracene coking

TABLE 62

HDM Catalyst Coking Conditions

Catalyst[1]	Coking Agent[2]	T (K)	Hydrogen Pressure (atm)	Time (h)
AN-1	AN(3g)	648	69	48
AN-2	AN(6g)+CB(6g)	663	69	12
AN-3[3]	AN(12g)	648	69	96
		653	69	24
AN-4	AN(6g)+CB(6g)	663	69	20
AN-5	AN(9g)	663	69	20
BIT-1	BIT(5g)	603	40	12
BIT-2	BIT(10g)	603	40	12
BIT-3	BIT(36g)	603	40	24
BIT-4	BIT(50g)	603	40	24
BIT-precoke	BIT(50g)	603	40	24
BIT-Ni-1[4]	coke + Ni-TPP(1.044g)	593	69	60
BIT-Ni-2[4]	coke + Ni-TPP(2.875g)	593	69	100
BIT-Ni-3	BIT(30g) + Ni-TPP(1.045g)	593	69	60
BIT-Ni-4	BIT(30g) + Ni-TPP(3.039g)	593	69	120

1 7 g sulfided catalyst used in all runs except for BIT-precoke run in which 14 g sulfided catalyst was used

2 AN-anthracene; CB-carbazole; BIT-bitumen; Ni-TPP-nickel tetraphenylphorphyrin; solvent-mineral oil (500 cm^3)

3 648 K for 96 h followed by recoking at 653 K for 24 hours

4 7 g BIT-precoked catalyst and 1/2 spent solution from BIT-precoke run

runs were carried out at 653-666 K and a H_2 pressure of 69 atm. Two coking runs were made with carbazole added to the anthracene - mineral oil solution. Bitumen coking runs were carried out at 603 K and a H_2 pressure of 40 atm. Four additional samples were prepared with a bitumen/Ni-TPP-mineral oil solution to study the effect of nickel deposition on catalyst deactivation. Two different procedures were used: (1) the catalyst was precoked with the bitumen/mineral oil solution followed by treatment with Ni-TPP, which was dissolved in the spent solution for the precoking run; and (2) the catalyst was directly coked with both bitumen and Ni-TPP in the mineral oil solution. These runs were conducted at 593 K and 69 atm.

The coked catalysts were Soxlet extracted with xylene for 2 hours, followed by 2 hours with acetone, and dried at 383 K. The catalysts were resulfided at 673 K for 2 hours with 10 mol% H_2S/H_2. Carbon and nitrogen contents of the catalysts were determined by combustion analysis. Nickel was analyzed by atomic absorption.

Physical Properties of Catalysts

Catalyst surface areas and pore volumes were determined with a Micrometrics 2100E BET apparatus, using N_2 as the adsorptive at liquid N_2 temperature. About 0.25 grams of crushed (40-60 mesh) catalyst were placed in the sample flask and degassed at 473 K overnight. Surface areas were calculated by the BET equation in the relative pressure range from 0.05 to 0.3 using the saturation pressure as the basis. Pore volumes were determined from total N_2 volumes at the saturation pressure. Pore size distributions were

obtained from the desorption data following the ASTM D 4641-88 procedure.

Activity Tests

Activity tests were carried out in a fixed-bed reactor under vapor phase conditions. The catalyst, 0.7 g, was mixed with 5 g of glass beads and presulfided in-situ with a 10 mol% H_2S - H_2 mixture under atmospheric pressure and 673 K for 2 hours. The feed consisted of 2 wt% indole, 2 wt% naphthalene and 1 wt% carbon disulfide in n-heptane solvent. A constant hydrogen flow of 140 cm^3 (STP)/min was maintained throughout the runs. Conversions were obtained at a standard liquid flowrate of 10 cm^3 after 30 hours on stream at which time the catalytic activity remained constant.

Major reaction products were: tetralin for naphthalene hydrogenation; and orthoethylaniline, ethylbenzene and ethylcyclohexane for indole hydrodenitrogenation. In the latter case, a small amount of indolene was formed from a rapid equilibrium with indole;[273] however, both were considered together as reactant. The reaction networks for the indole and naphthalene reactions are shown in Figure 134

Liquid products were analyzed by gas chromatography with a 0.32cm by 366 cm stainless-steel column packed with 6 wt% OV-17 on 100-120 mesh Chromosorb, using an FID detector and a temperature program of 10°C/min. Pseudo first-order rate constants were calculated from conversions adjusted to the actual amount of catalyst present in the sample, i.e. corrected for coke and nickel contents. Two rate constants were calculated for the indole

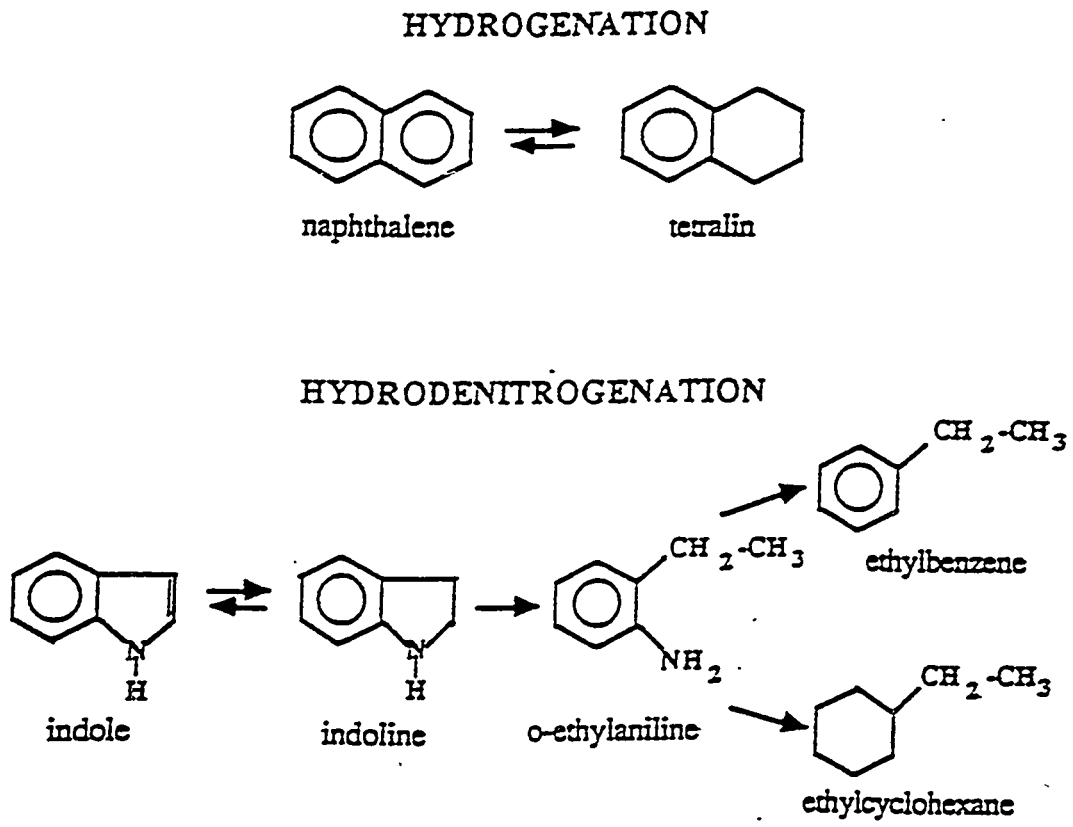

Figure 134. Naphthalene and Indole Reaction Networks

reaction scheme: the first for C-N bond hydrogenolysis from all major products and the second for hydrodenitrogenation from N-free products.

RESULTS

Catalyst Properties

Analyses of the catalysts from the anthracene, bitumen, and bitumen plus Ni-TPP coking runs are given in Table 63. The smallest amount of anthracene used in the coking runs was 3 grams. If the carbon in anthracene had been deposited completely as coke on 7 g of catalyst, the coke content should have been about 30 wt%, which is much higher than the actual carbon analyses indicated. Thus, it can be concluded that most of the anthracene did not convert to coke on the catalyst at the experimental conditions. It probably underwent hydrogenation to partially saturated compounds, which have little tendency to coke. In two of the anthracene coking runs (AN-2 and AN-4 in Table 62), carbazole was added to the coking solution. If the nitrogen in carbazole deposited completely on the catalyst, the nitrogen content would have been 7.2 wt%. Post-coking catalyst analyses indicated that the wt% nitrogen in the coke for each of the two anthracene-carbazole coked catalysts was negligible.

The catalyst coked more readily with the bitumen solutions than with the anthracene solutions; hence, lower temperatures and shorter run times were employed. For the bitumen coking runs, it can be seen that carbon and nitrogen in the coke on the catalyst increased with the amount of bitumen added (Table 63). Nearly all

Table 63

Properties of Aged Catalysts

Catalyst	C (wt%)	N (wt%)	N/C Atomic Ratio	Ni (wt%)	S (m^2/g)	V_p (mL/g)	r_p (Å)
HDM	-	-	-	-	151	0.69	91
AN-1	2.78	0	-	-	147	0.63	86
AN-2	4.63	0.10	0.019	-	142	0.60	84
AN-3	5.68	0	-	-	141	0.58	83
AN-4	8.67	0.12	0.012	-	144	0.55	76
AN-5	11.5	0	-	-	138	0.51	73
BIT-1	5.5	0.22	0.034	-	147	0.59	80
BIT-2	7.03	0.37	0.045	-	150	0.56	75
BIT-3	8.91	0.50	0.048	-	152	0.54	71
BIT-4	11.07	0.53	0.041	-	153	0.51	66
BIT-4H[1]	-	-	-	-	156	0.49	63
BIT-Ni-1[2]	11.50	0.60	0.045	1.59[3]	153	0.48	62
BIT-Ni-2[2]	10.49	0.58	0.047	2.64[4]	147	0.46	63
BIT-Ni-3	10.5	0.60	0.049	1.15[3]	149	0.49	66
BIT-Ni-4	9.29	0.52	0.048	3.18[3]	153	0.51	66

[1] Coked catalyst BIT-4 subsequently treated in He for 24 hours at 663 K and resulfided

[2] The precoked catalyst to these runs contained 10.7 wt% C and 0.71 wt% N.

[3] All of the Ni in Ni-TPP deposited on catalyst.

[4] 78 wt% of the Ni in Ni-TPP deposited on catalyst.

the nickel in the Ni-TPP was deposited on the catalyst in the bitumen plus Ni-TPP coking runs.

Surface area and pore volume data on anthracene- and bitumen-coked catalysts are presented in Table 63. Pore volumes for both series of catalysts decreased with coke content. However, the bitumen-coked catalysts did not suffer a significant loss of surface area with coke content as did the anthracene-coked catalysts.

Pore size distributions for the sulfided catalyst and coked catalyst BIT-4, which contained 11 wt% carbon are compared in Figure 135. A shift to lower pore radii is observed for the coked catalyst, consistent with its smaller average pore radius (Table 63).

The pore volumes of the aged catalysts were corrected for the amount of coke and nickel deposited to determine if pores were plugged with coke. The analysis is presented in Table 64. A correction was made for the volume of the deposits as well as their weight in the calculation of the expected pore volume, V_p^*. The difference between this value and the experimental pore volume measurement, ΔV, represents the loss of pore volume. All ΔV values are all quite low, within experimental error for pore volume measurements, indicating no significant plugging of the pores.

Similar corrections for coke content were made in the calculations of the expected surface area are, S^*. Little net loss in surface area, ΔS, was observed for the anthracene-coked catalysts, thus, indicating no loss in surface area due to pore

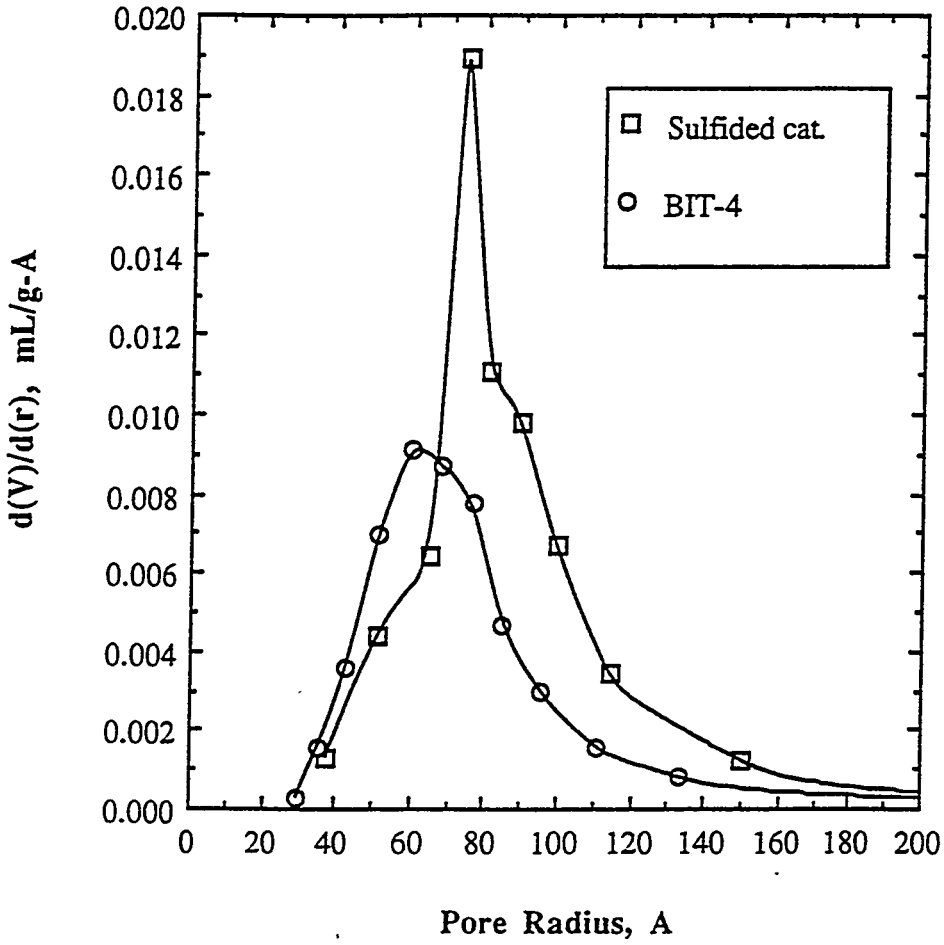

Figure 135. Pore Size Distributions of the Sulfided and the BIT-4 Coked (11.1 wt% C) Catalysts

Table 64

Analysis of Pore Volume and Surface Area Data

Catalyst	w_c[1] (g/g)	v_c[2] (mL/g)	V_p*[3] (mL/g)	ΔV[4] (mL/g)	S*[5] (m^2/g)	ΔS[6] (m^2/g)
HDM	0.000	0.000	0.69	0.00	151	0
AN-1	0.029	0.018	0.65	0.02	147	0
AN-2	0.049	0.030	0.62	0.02	144	2
AN-3	0.060	0.037	0.61	0.03	142	1
AN-4	0.091	0.057	0.57	0.02	137	-7
AN-5	0.121	0.075	0.53	0.02	133	-5
BIT-1	0.061	0.038	0.61	0.02	142	-5
BIT-2	0.078	0.049	0.58	0.02	139	-11
BIT-3	0.099	0.062	0.56	0.02	136	-16
BIT-4	0.123	0.077	0.53	0.02	133	-20
BIT-Ni-1	0.152	0.084	0.50	0.02	128	-25
BIT-Ni-2	0.157	0.080	0.50	0.04	127	-20
BIT-Ni-3	0.134	0.076	0.52	0.03	131	-18
BIT-Ni-4	0.152	0.073	0.51	0.00	128	-25

1 Coke weight assuming $CH_{0.5}$

2 Coke density of 1.6 g/cm^3; NiS density of 5.5 g/cm^3

3 $V_p^* = V_{p0}(1-w_c)-v_c$; V_{p0} is pore volume of sulfided catalyst

4 $\Delta V = V_p^* - V_p$

5 $S^* = S_0(1-w_c)$; S_0 is the surface area of the sulfided catalyst

6 $\Delta S = S^* - S$

plugging, in agreement with the pore volume analyses mentioned above. However, significant increases in net surface areas (values above 10 m^2/g are considered outside experimental error) were observed for the bitumen-coked catalysts. This indicated that the coke generated from bitumen contributed significant surface area to the coked catalysts. Similar results were obtained for the bitumen/NiTPP coked catalysts.

Catalyst Activities

1. Relative Activities

Pseudo first-order rate constants obtained at 623 K with the coked catalysts were converted to relative activities by dividing each by the rate constant for the fresh catalyst for the hydrogenation, hydrodenitrogenation and carbon-nitrogen hydrogenolysis reactions. Relative activities of each functionality for the anthracene- and bitumen-coked catalysts are presented in Figures 136-138. As can be seen, activities fall off less sharply as the coke content increases: the relative carbon-nitrogen hydrogenolysis activity and the relative hydrodenitrogenation activity for both anthracene- and bitumen-coked catalysts appeared to line out, whereas, the relative hydrogenation activity continued to decrease. There is little difference in deactivation between bitumen-coked catalysts and anthracene-coked catalysts. Addition of carbazole to the anthracene coking solution appeared to exert no influence on the relative activities.

Comparison of the relative activities indicates that the relative deactivation was less for hydrogenation than for carbon-

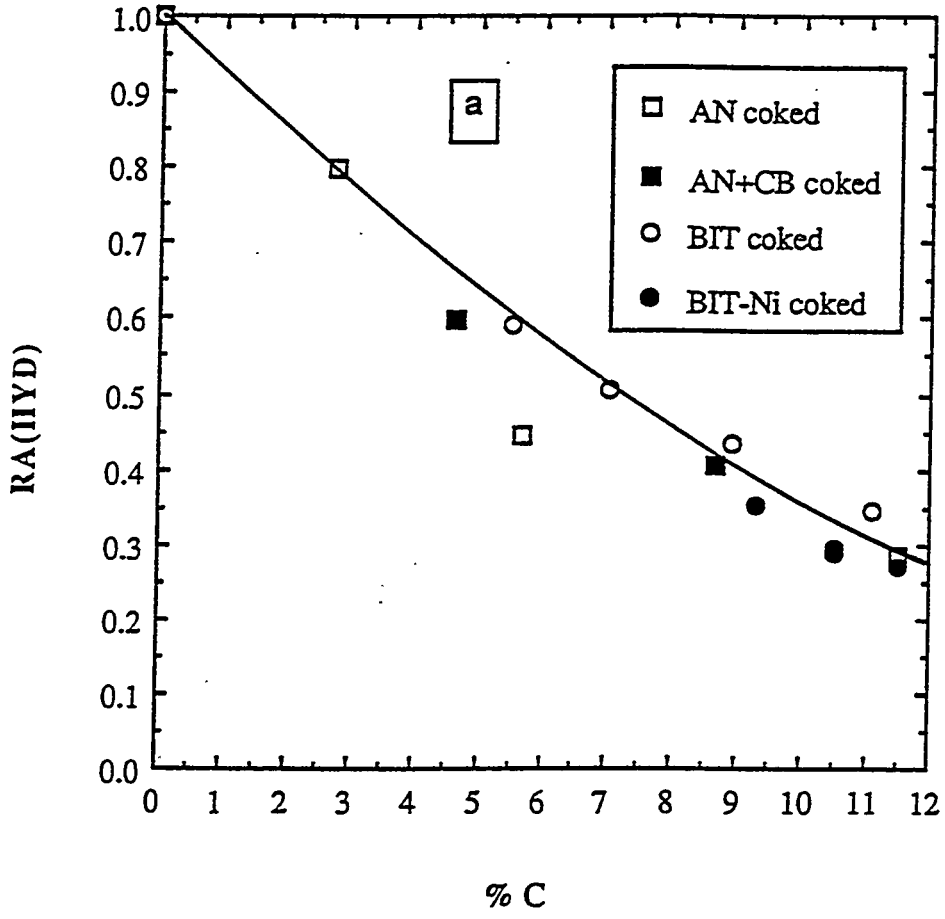

Figure 136. Relative Hydrogenation Activities versus wt% C for the Anthracene-, Bitumen-, and Bitumen/NiTPP-coked Catalysts (623 K)

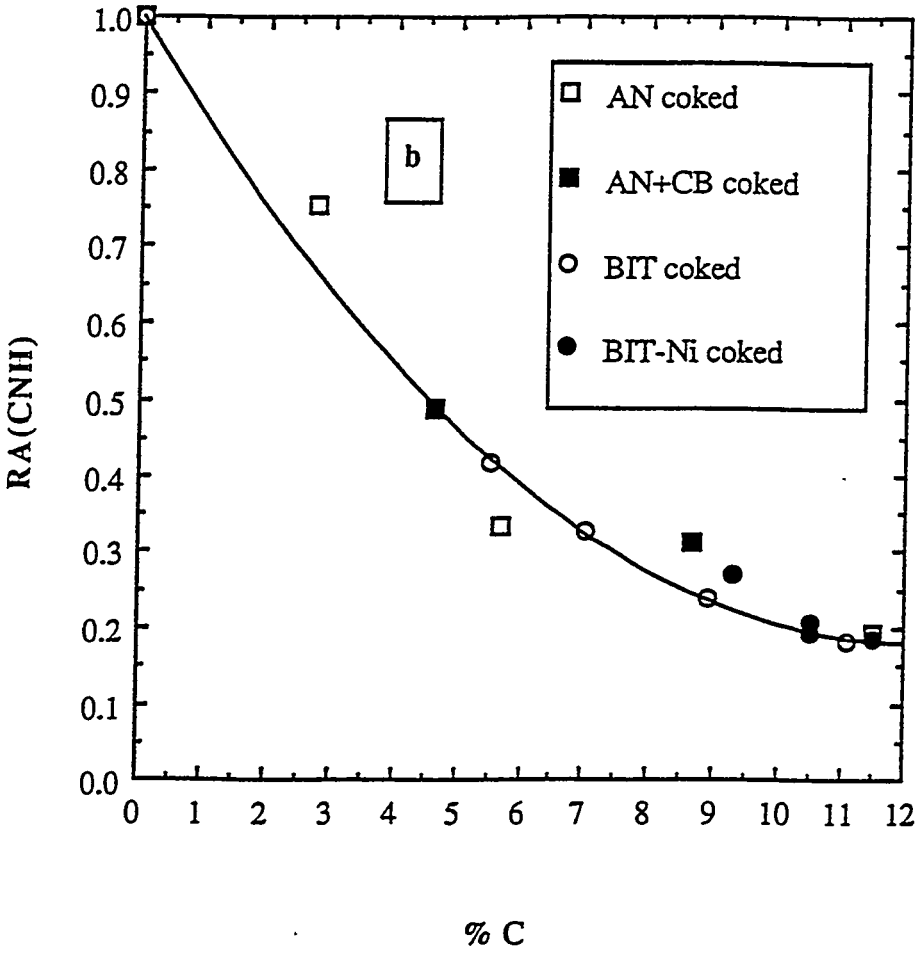

Figure 137. Relative Carbon-Nitrogen Hydrogenolysis Activity versus wt% C for the Anthracene-, Bitumen-, and Bitumen/NiTpp-coked Catalysts (623 K)

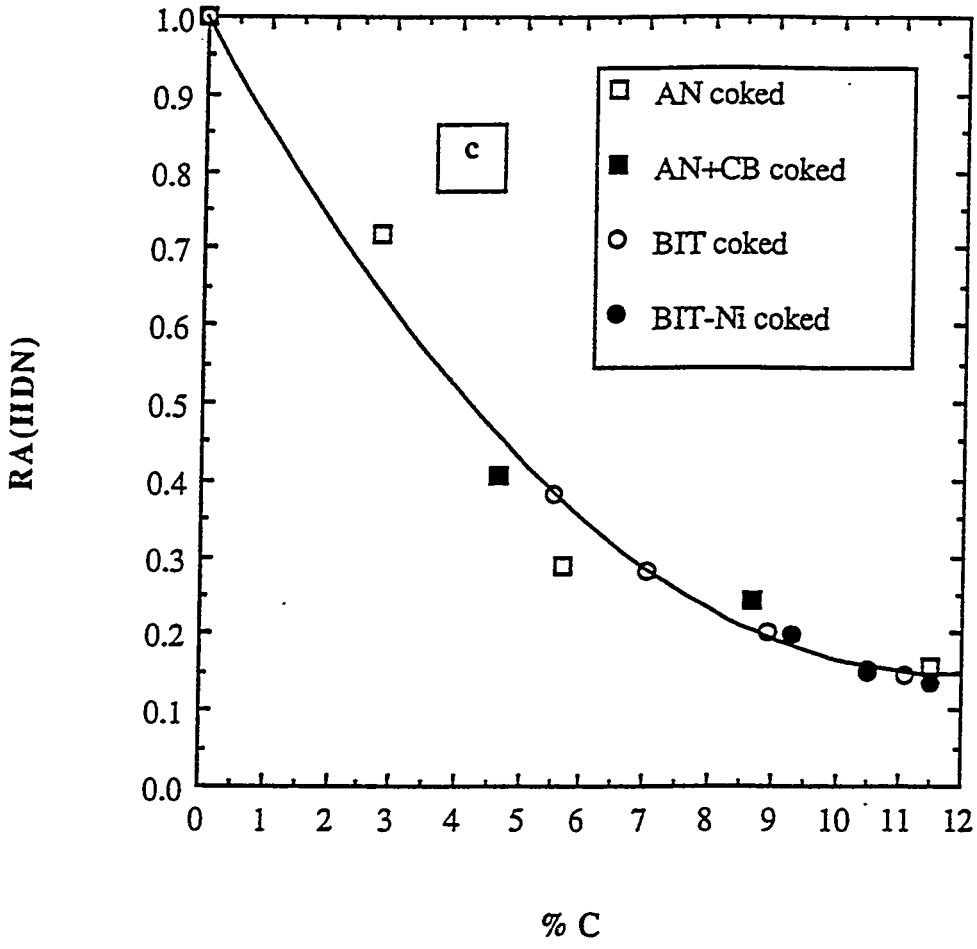

Figure 138. Relative Hydrodenitrogenation Activity versus wt% C for the Anthracene-, Bitumen-, and Bitumen/NiTpp-coked Catalysts (623 K)

nitrogen hydrogenolysis and hydrodenitrogenation, which were about the same. Nickel deposition resulted in slightly lower relative hydrogenation activity for bitumen/NiTPP coked catalysts, while the relative carbon-nitrogen hydrogenolysis activities remained unaffected when compared with bitumen-coked catalysts. The manner in which the addition of nickel was accomplished had no effect on these results.

2. Temperature Effects on Conversions and Products

Samples were taken at various temperatures for each activity run. Comparable hydrogenation, hydrodenitrogenation, and carbon-nitrogen hydrogenolysis conversions were obtained as a function of reaction temperature for the sulfided and a bitumen-coked catalyst (BIT-4) with a coke content around 11 wt% (Figures 139 and 140). A maximum in hydrogenation conversion is seen for each of the catalysts, while hydrogdenitrogenation and carbon-nitrogen hydrogenolysis conversions continued to increase with temperature. The maxima in hydrogenation conversion was due to equilibrium constraints at higher temperatures, as shown in the selectivity plots of Figure 141. Data from Frye and Weitkamp[274] were used to obtain the equilibrium values.

3. Apparent Activation Energies

Apparent hydrogenation and carbon-nitrogen hydrogenolysis activation energies for the coked catalysts were obtained from slopes of Arrhenius plots of ln k versus inverse temperature. Rate constants for hydrogenation were corrected for equilibrium. Arrhenius plots for both hydrogenation and carbon-nitrogen

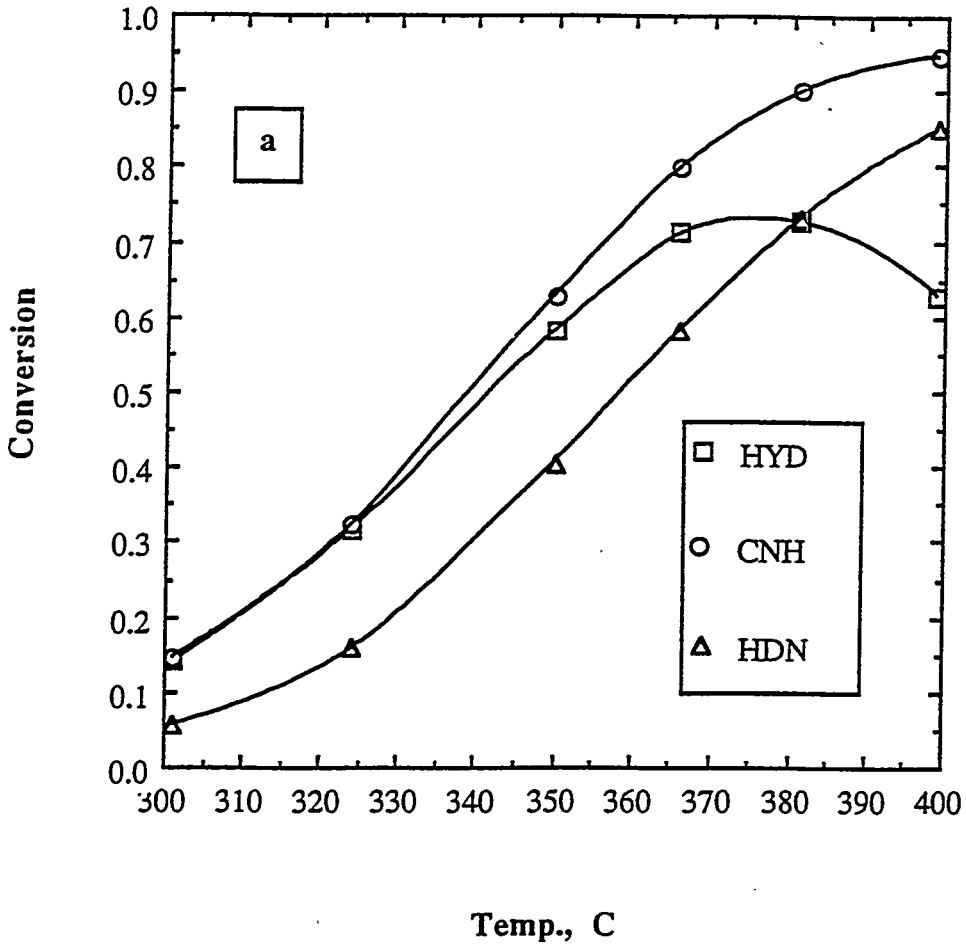

Figure 139. Conversion versus Temperature for the Sulfided Catalyst Hydrogenation □; Carbon-Nitrogen Hydrogenolysis o; and Hydrodenitrogenation ▵.

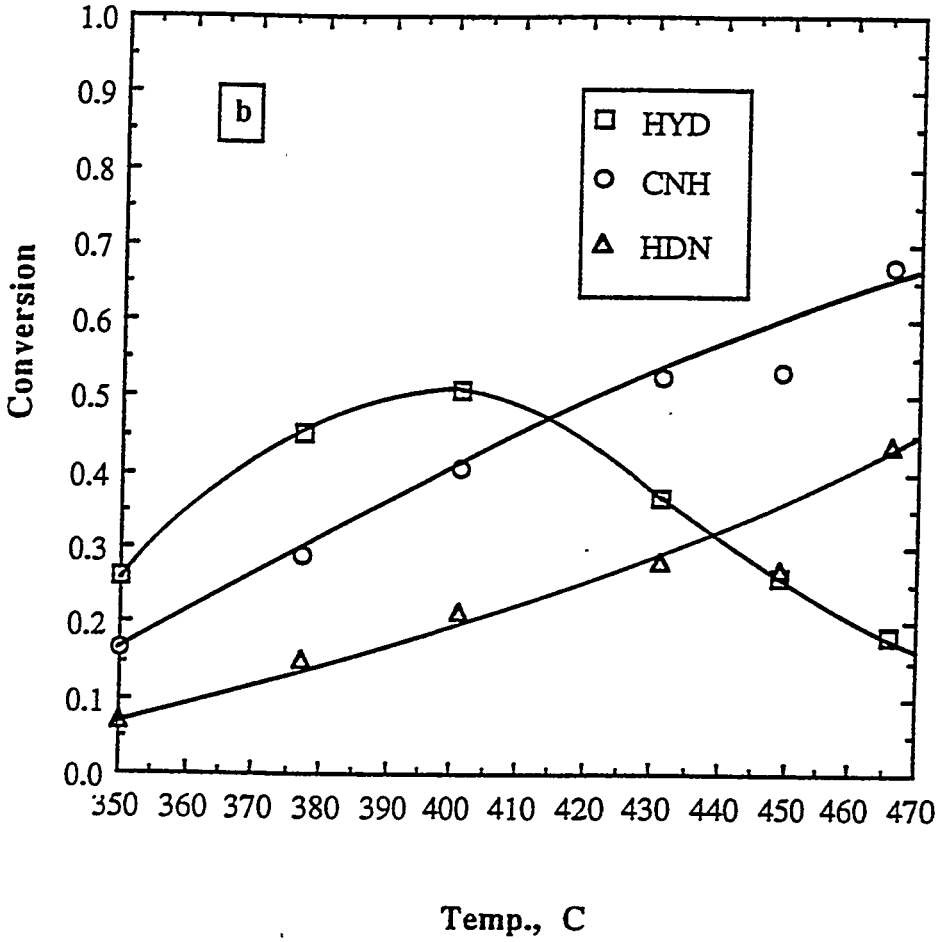

Figure 140. Conversion versus Temperature for the BIT-4 Coked Catalyst Hydrogenation □; Carbon-Nitrogen Hydrogenolysis o; and Hydrodenitrogenation ▵.

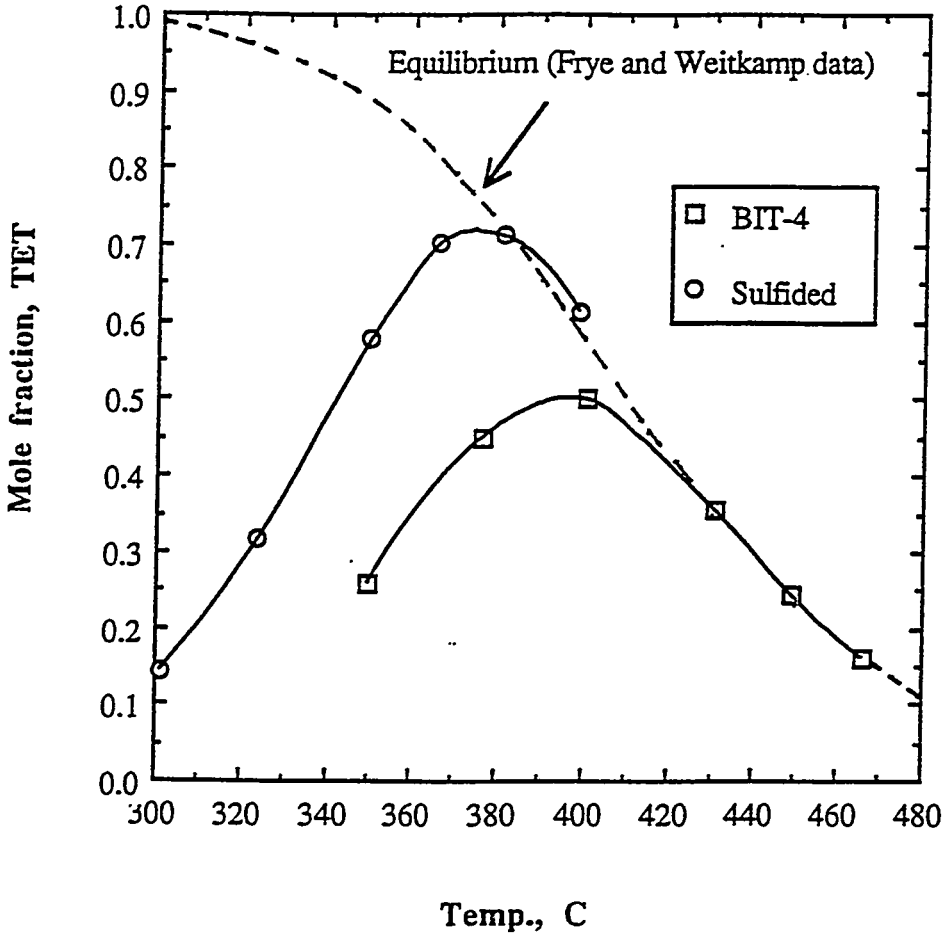

Figure 141. Tetralin Mole Fraction versus Temperature for the Sulfided and BIT-4 Coked Catalysts

hydrogenolysis tended to fall off at higher temperatures (>623 K), probably due to the onset of diffusional limitations. Activation energies as a function of catalyst carbon content are shown in Figures 142 and 143 (estimated error is ± 1 kcal/mol). It can be seen that activation energies decrease with coke content, being more prominent for the anthracene-coked series of catalysts. Also, the decline in carbon-nitrogen hydrogenolysis activation energies is greater than the decline in hydrogenation activation energies for both series of catalysts.

DISCUSSION

Nature of Coke

Analysis of pore volume loss (Table 64) indicated that no pore plugging occurred from coke deposited from the anthracene or from the bitumen feed. This is not surprising in view of the rather large pore size of the hydrodemetallation catalyst. Similar analysis of the surface area data on the other hand, shows significant differences in anthracene-derived versus bitumen-derived coke deposits. No appreciable loss in surface area was observed for the anthracene-generated coke. Similar results were obtained with a NiMo catalyst coked by anthracene[271] or by a vacuum gas oil.[272] Apparently, the coke deposited on the catalyst surface contributes surface area commensurate with its coverage of the catalyst surface, such that the change in overall pore radius is negligible. An actual gain in surface area (negative values in Table 64) was observed for the bitumen-derived coke. The higher surface areas observed for the bitumen-coked catalysts compared to

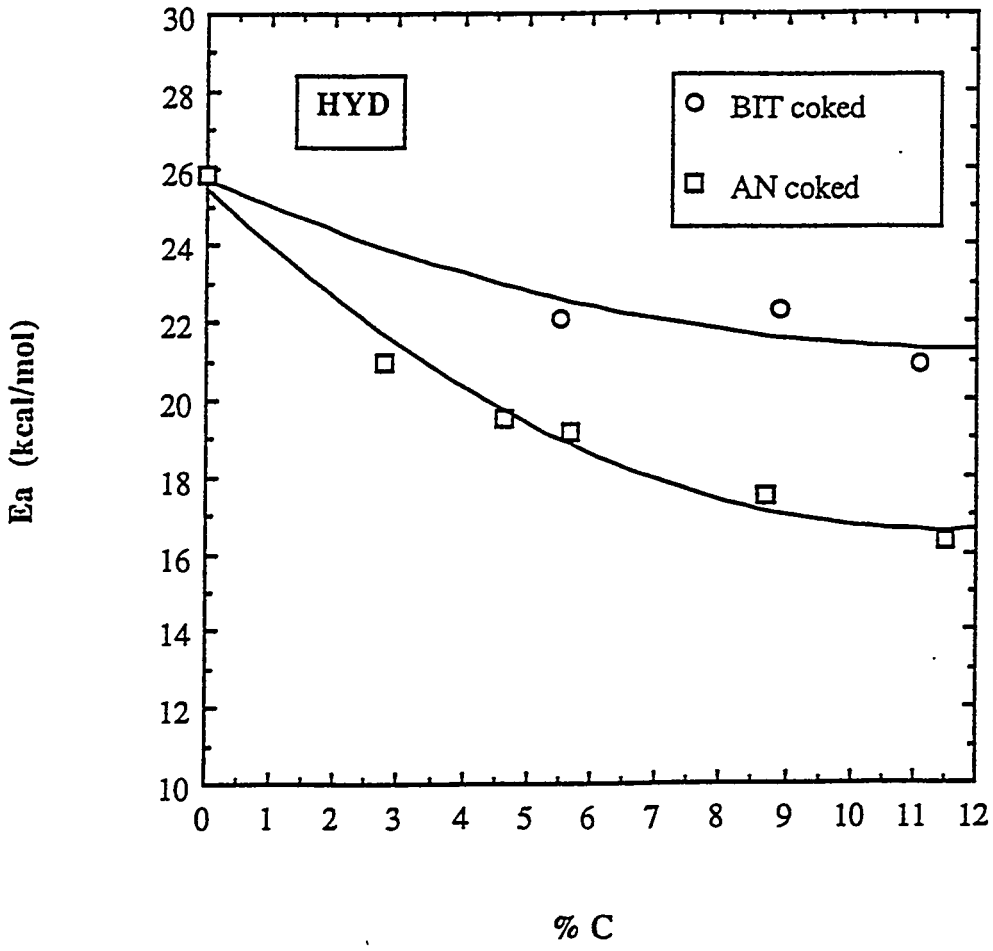

Figure 142. Apparent Hydrogenation Activation Energy versus wt% C

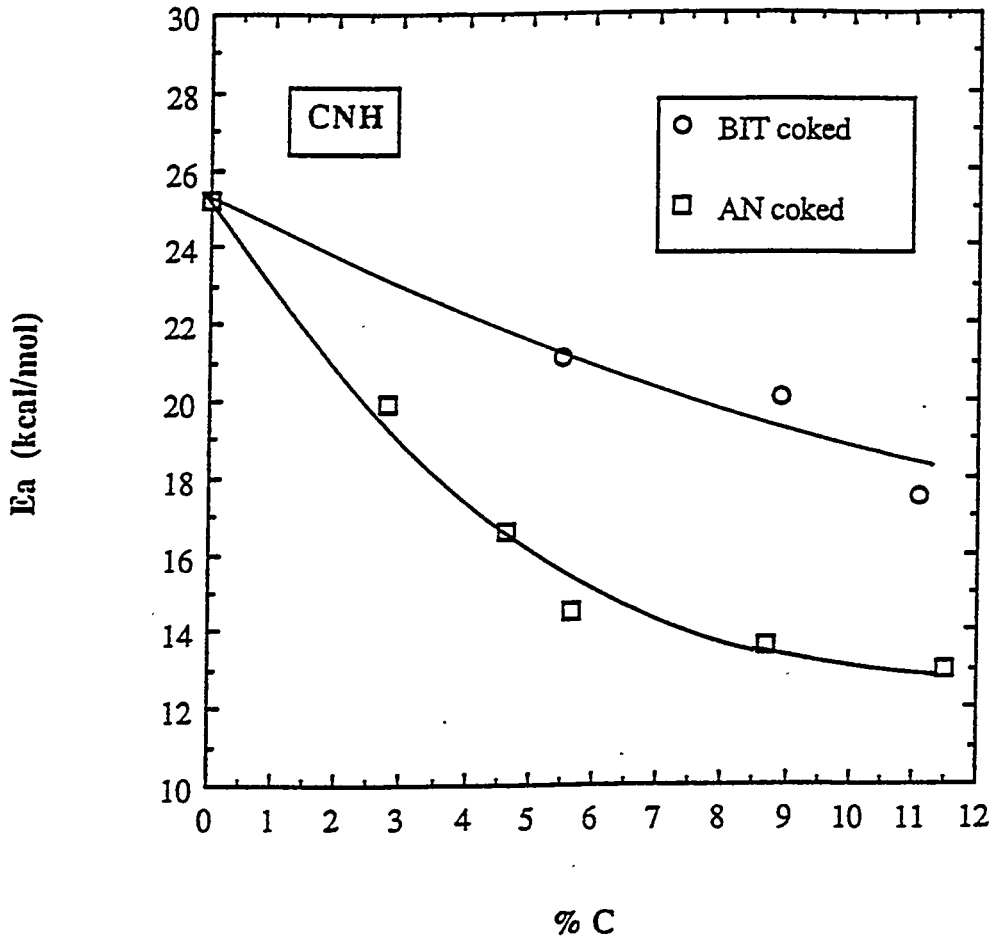

Figure 143. Apparent Carbon-Nitrogen Hydrogenolysis Activation Energy versus wt% C

the anthracene-coked catalysts was not due to the higher treatment temperature employed for the latter. This is evident from the high surface area after treatment of the BIT-4 catalyst at an elevated temperature (BIT-4H in Table 63). The increased surface area of the bitumen-coked catalysts implies that the coke has considerable porosity, contributing to the overall increase in surface area. The smaller values of calculated average pore radii compared to that of the sulfided catalyst were due to the porous nature the bitumen-derived coke. This is evident in the pore size distribution plots of Figure 135, where the maximum in pore radius is close to that of fresh catalyst; the slight shift to lower pore radii is probably due to pores in the coke, which would be expected to be smaller than those in the catalyst.

The difference in the coke produced by anthracene and that by bitumen may be ascribed to the nature of the coke precursors present in the respective feeds. Anthracene has a three-ring condensed aromatic structure, which may be expected to strongly adsorb on the catalyst surface and form a graphitic-type coke. A similar situation applies to coke from vacuum gas oil, in which polynuclear aromatics in the oil have been identified as the main coke precursors.[265] Coke from aromatic FCC feedstocks has been characterized as consisting of a condensed, layered structure of fused aromatic sheets.[275] On the other hand, the aromatics (two-or three-ring) in bitumen contain large aliphatic chains attached to them.[16] During deposition on the catalyst, the chains may prevent

condensation into fused aromatic sheets, resulting in a porous coke.

The N/C atomic ratio in the coke on the bitumen-coked catalyst was nearly constant (~0.04) and much higher than that in the bitumen (0.015). This agrees with literature reports[267,276] of an increase of the nitrogen content in the coke on hydrotreating catalysts relative to the nitrogen content of the feed. Bitumen contains molecules with and without nitrogen. The increase in nitrogen content with increasing carbon content of the catalysts (Table 63) suggests that the nitrogen is predominantly associated with the coke. Nitrogen on catalysts has also been attributed to adsorbed NH_x species[277] and strongly adsorbed aromatic N compounds.[278] The latter are present in the bitumen and the former arise from hydrogenation of the lower molecular weight N-containing compounds in the bitumen. Both are retained on the catalyst even after Soxlet extraction and resulfiding at 673 K. It is surprising that nitrogen was not added to the catalyst during anthracene coking with carbazole present. The temperatures employed in these runs might have been too high for adsorption of the carbazole, as five-member N-ring compounds are considerable weaker bases than six-member N-ring compounds, which would be expected to be present in the bitumen. It may also have been related to the low acidity of the catalyst.

Catalyst Deactivation

Since analysis indicated no pore plugging by coke, catalyst deactivation must have been due to covering of active sites by

coke. Deactivation was approximately linear up to about 4 wt% carbon. (Figures 136-138), indicating selective adsorption on active, coke-prone sites. Relative activities then drop slower with increase in coke content. It can be inferred that at this stage, the coke deposited upon previously deposited coke and not on new sites. This growth can be lateral (two-dimensional) as well as three-dimensional, resulting in covering additional sites. At high coke levels, hydrodenitrogenation activities tend to line out, indicating that some especially active reaction sites still remain at this stage. It is most likely that these residual sites have high hydrogenation activity, preventing consolidation of adsorbed coke species by hydrogenating coke precursors to volatile species which desorb.

In comparing relative activities of the different functionalities, it is seen that hydrogenation activity is much less deactivated than carbon-nitrogen hydrogenolysis (or hydrodenitrogenation). This may indicate the presence of different active sites for hydrogenation than for carbon-nitrogen hydrogenolysis and hydrodenitrogenation. The hydrogenation sites are presumed to be less susceptible to coverage by coke than the carbon-nitrogen hydrogenolysis (or hydrodenitrogenation) sites.

It is significant that the relatively high nitrogen content of the coke on the bitumen-coked catalysts did not cause greater deactivation as compared to the anthracene-coked catalysts which had little nitrogen present in the coke. Either the nitrogen from

the bitumen is adsorbed predominantly on catalytically inactive sites, or it is associated with the coke itself.

The relative deactivation of the functionalities do not appear to be affected by the nature of the coke (Figures 136-138). Thus, the porous nature of the bitumen-derived coke does not provide access to the catalytically active sites relative to the nonporous anthracene-derived coke, giving equivalent catalyst deactivation. The presence of nickel deposits exhibited no appreciable effect on catalyst deactivation above that of the coke. Although the relative hydrogenation activity may have been slightly reduced by nickel (Figure 136), this was not observed for the carbon-nitrogen hydrogenolysis (Figure 137) or hydrodenitrogenation activities (Figure 138), regardless of whether the nickel was deposited on precoked catalysts or in conjunction with the bitumen-derived coke deposition. Since nickel sulfide is considered a mild hydrogenation catalyst, it appears that this effect is not realized when coke is present.

Temperature Effect on Activities

In evaluating temperature effects on catalytic activity, equilibrium constraints must be considered. Carbon-nitrogen hydrogenolysis is essentially irreversible; that is, indole/indolene are converted to o-ethylaniline. However, for hydrogenation, reversibility is evidenced by the reduction in hydrogenation conversion at higher temperatures (Figures 139 and 140). This is seen in the plot of Figure 141, where hydrogenation activity approaches equilibrium at higher temperatures. Therefore,

reversibility must be taken into account in determining rate constants for hydrogenation.

Apparent activation energies for hydrogenation and carbon-nitrogen hydrogenolysis were obtained from Arrhenius plots of ln k versus inverse temperature. Linear plots were obtained for temperatures up to 623 K. Above 623 K the plots fell off, possibly due to onset of diffusional limitations. The variation in apparent activation energies with carbon content for anthracene- and bitumen-coked catalysts is shown in Figure 142 and 143. Activation energies for hydrodenitrogenation were not determined because of the involvement of several different steps in the reaction pathway (Figure 134). It is interesting that activation energies for the anthracene-coked catalysts are significantly lower than those for the bitumen-coked catalysts, despite their identical relative activities (Figures 136-138).

The changes in activation energy show that the coked catalysts have lower activation energies than the sulfided catalyst. A possible explanation for this is that the fresh sulfided catalyst contains a distribution of active sites of different energetics. Thus, the decrease in hydrogenation and carbon-nitrogen hydrogenolysis activation energies with coke content would represent coke depositing first on sites having low hydrogenation activity (high coke propensity sites) and high activation energy, while leaving high hydrogenation activity (low coke propensity sites) and low activation energy sites uncoked. The high hydrogenation activity of the high-activity sites can prevent coke formation by depressing

polymerization reactions of coking precursors. Conversely, coking precursors adsorbed on low-activity sites would have greater chance to polymerize to form coke before being hydrogenated.

NOMENCLATURE

AN	Anthracene
BIT	Bitumen
CB	Carbazole
Ni-TPP	Nickel tetra-phenyl-porphyrin
r_p	Pore radius
S	Measured surface area
S^*	Expected surface area
V_p	Measured pore volume
V_p^*	Expected pore volume

SUMMARY AND CONCLUSIONS

A large-pore hydrodemetallation catalyst was treated with anthracene and/or a Uinta Basin bitumen in a mineral oil solvent to obtain coke levels up to 12 wt% carbon. In some runs, carbazole was added to the anthracene-coking solution and in others, a nickel porphyrin compound was added to the bitumen-coking solution. Physical properties of the coked catalysts were determined. The catalyst activities for hydrogenation and for hydrodenitrogenation were determined using a mixture of naphthalene and indole in n-heptane, respectively.

The coke produced from the bitumen appeared to be porous, while that produced from anthracene was nonporous. A significant

enhancement of nitrogen in the coke on the catalyst over that in the bitumen was observed. Catalytic activities of the coked catalysts decreased with increasing coke content, with hydrodenitrogenation activity being more deactivated than hydrogenation activity. Neither the nature of the coke precursor, nor the presence of nitrogen or nickel on the catalyst, affected the extent of deactivation. Apparent activation energies decreased with increasing coke content. The role of coke on catalyst deactivation is discussed in terms of its effect on the distribution of different catalytic active sites for the reactions.

1. Coke deposited from bitumen was found to be different from that deposited from anthracene. The former appears to be porous in contrast to a consolidated nonporous coke for the latter. A significant enhancement in nitrogen content of the coked catalysts over that in the feed was found.

2. Catalytic hydrogenation activity decreased almost linearly with carbon content, while hydrodenitrogenation activity was more deactivated, but appeared to line out above about 10% carbon on the catalyst.

3. Nickel deposits up to 5 wt% had no noticeable effect on catalytic activities over that of the coke deposits.

4. Decrease in apparent activation energies of coked catalysts is ascribed to a distribution of active sites in the sulfided catalyst, in which strong sites of high hydrogenation activity effectively prevent coke formation, while weak sites of

low hydrogenation activity allow deposition and polymerization of coke.

FUTURE ACTIVITIES

The coked catalysts produced during the hydrotreating process variable studies with the Whiterocks and PR Spring bitumens will be investigated to determine the nature of the coke; that is, to explore the porosity and surface area of the coke deposited during hydrotreating.

SIMILITUDE STUDIES IN THREE-PHASE EBULLIETED BED REACTORS

Principal Investigator:	F.V. Hanson
Co-Principal Investigator:	M.D. Deo
Graduate Student:	D.A. Deshpande

INTRODUCTION

Three-phase ebullieted bed reactors have been found appropriate for a number of applications such as hydrotreating and hydrocracking of heavy petroleum fractions, coal liquefaction, methanation, crystallization and production of zinc hydrosulfite[279]. The H-Coal[280] coal liquefaction process, the H-Oil[280] resid hydrocracking process and the Exxon EDS coal liquefaction process[281] used three-phase reactors. In these processes, low space velocities were required to effect high conversion. Thus, even in the laboratory and pilot scale process development units, either large or multiple stage reactors were required. It would be useful to scale down the commercial scale unit, so that the process could be studied conveniently in the laboratory and the information extended to larger scales. Haynes, et al.,[282] have devised a laboratory scale reactor to test catalyst performance in three-phase ebullieted bed systems. However, this reactor simply fluidizes the catalyst particles by a rotor, without controlling or simulating the hydrodynamics inside the reactor.

Conversion in a three-phase hydrotreating/hydrocracking unit is governed by interphase transport and intraparticle diffusion. Maintaining constant phase holdups is the first step toward achieving hydrodynamic similarity. Bubble size, bubble rise

velocity and bubble coalescence characteristics are some of the other important hydrodynamic parameters. The phase holdups are governed by system parameters such as, the diameter of the openings in the distributor, d_o, the particle size, d_p, the reactor diameter, d_r, the liquid superficial velocity, u_l, the gas superficial velocity, u_g, the liquid viscosity, μ_l, the particle density, ρ_p, the liquid density, ρ_l, the gas density, ρ_g and the gas-liquid surface tension, σ. At low pressure ρ_g is usually much smaller than ρ_l and, thus, does not affect the phase holdups appreciably. Hence, the dependence of the phase holdups on ρ_g at low pressure can be neglected. It should be noted that at high-pressures the value of ρ_g can become significant and ρ_g should be taken into account for the prediction of phase holdups. In this study, a procedure was developed, whereby, the holdups in the commercial and laboratory scale reactors would be identical.

When a process is being scaled down or up, an effort should be made to minimuze the effects of scaling on the reaction chemistry. Thus it is mandatory that the parameters, ρ_l, μ_l, ρ_g, and σ after scaledown remain unchanged which leaves only d_r, d_p, u_l, and u_g to be manipulated. Criteria were developed which led to the desired similarity between holdups in the two reactor systems by the manipulation of the four parameters d_r, d_p, u_l, and u_g without changing the reaction chemistry of the process.

High-liquid velocities required to fluidize pelleted catalysts and low-space velocities required for processing heavy oils, bitumens and bitumen-derived liquids necessitate long commercial

three-phase ebullieted bed reactors. The reactor length, for laboratory-scale studies of such processes, can be reduced by reducing the superficial liquid velocity. Consequently, the catalyst size has to be reduced to achieve circulation within the reactor. It is important to ensure that, with these changes, the values of the phase holdups are maintained the same in the commercial and the laboratory units. Similarity criteria that would ensure identical holdups in the commercial and laboratory reactors were identified through similitude studies. The criteria required the equality of six dimensionless numbers. These criteria were validated using the generalized wake mode.

It was determined that it was impractical to establish all the parameters in the set of dimensionless numbers at the desired values. Therefore, a method to achieve similarity by varying a minimum number of parameters, such as liquid and gas velocities and particle size, was developed using the generalized wake model. This resulted in a set of two conditions, which when satisfied, yielded practically equal holdups in the two reactors.

Calculation of Phase Holdups

Bhatia and Epstein[283] developed the generalized wake model for predicting phase holdups in three-phase ebullieted beds. The model accounted for the presence of solid particles in the bubble wake. It was based on a material balance between the solids carried upward through the bubble wake and the solids settling in the liquid-solid region that surrounded the bubble.

The model required values for the bubble rise velocity (relative to the surrounding liquid), u_{br}, the ratio of the solid holdup in the bubble wake to the solid holdup in the liquid-solid region, x, and the ratio of the wake volume to bubble volume, κ. These parameters must be calculated by independent methods. In this study, u_{br} was calculated by the following procedures.

1. According to the procedure suggested by Sastry et al.[284] the coefficient of viscous drag on a single bubble due to the surrounding liquid C_{Db} is calculated from the correlations developed by Tadaki and Maeda.[285]

$$C_{Db} = 0.076\,(Re_b Mo^{0.23})^{1.82} \quad for\ 8Mo^{0.068} < Re_b Mo^{0.23} < 6$$
$$C_{Db} = 1.25\,(Re_b Mo^{0.23})^{0.26} \quad for\ 6 < Re_b Mo^{0.23} < 16.5 \qquad (134)$$
$$C_{Db} = 2.6 \quad for\ 16.5 Re_b Mo^{0.23}$$

where, Re_b, the bubble Reynolds number is given by

$$Re_b = \frac{\rho_l u_{tb} d_b}{\mu_l} \qquad (135)$$

and Mo, the Morton number, is given by

$$Mo = \frac{g\mu_l^4}{\sigma^3 \rho_l} \qquad (136)$$

The diameter of the bubble required to calculate Re_b in Equation set (134) is determined from the correlation published by Kim, et al.[286]:

$$d_b = 0.142 u_l^{0.052} u_g^{0.248} \sigma^{0.034} \mu_l^{0.008}. \quad (137)$$

The terminal velocity, u_{tb} is calculated from C_{Db}, for a single bubble rising through a liquid column where the bouyancy force is equal to the unaccelerated drag force on the bubble. The bubble rise velocity in a three phase system, u_{br}, is assumed to be equal to u_{tb}.

2. The bubble rise velocity in a three phase system, u_{br}, can also be estimated from the correlation published by Kim, et al.[286]:

$$u_{br} = 5.541 u_l^{0.065} u_g^{0.339} \mu_l^{0.025} \sigma^{0.179}. \quad (138)$$

The ratio of the wake volume to the bubble volume, κ, is obtained using the procedure developed by Bhatia and Epstein.[282]

$$\kappa = \left[0.61 + \frac{0.037}{\varepsilon_g + 0.013}\right] (\varepsilon_g + \varepsilon_l)^3. \quad (139)$$

The ratio of solids holdup in the bubble wake to the solid holdup in the liquid-solid region, x, in the generalized wake model is calculated using the equation developed by El-Temtamy and Epstein[287]:

$$x = 1.0 - 0.877a_r \text{ when } a_r < 1.14 \tag{140}$$

and

$$x = 0 \text{ when } a_r \geq 1.14 \tag{141}$$

where, the parameter, a_r, is defined as follows:

$$a_r = \frac{u_i}{\left(\frac{u_g}{\varepsilon_g} - \frac{u_l}{\varepsilon_l}\right)} \tag{142}$$

In this equation, u_i is the Richardson-Zaki intercept.[288]

A procedure was developed, using the generalized wake model and the above correlations, for the calculation of phase holdups. The relevant equations are listed below.

$$\varepsilon_l = \varepsilon_k(1 - x) + \varepsilon''_{lf}(1 - \varepsilon_g - \varepsilon_k + x\varepsilon_k) \tag{143}$$

$$\varepsilon''_{lf} = \left[\frac{u_l - v_g\varepsilon_\kappa(1 - x)}{u_i(1 - \varepsilon_g - \varepsilon_\kappa)}\right]^{1/n}. \tag{144}$$

In Equation (144), n is the Richardson-Zaki exponent.[288]

$$v_g = \frac{u_l + u_g + \varepsilon''_{lf}(1 - \varepsilon_g - \varepsilon_\kappa)u_{br}}{(1 - \varepsilon_s)} \tag{145}$$

$$\varepsilon_s + \varepsilon_l + \varepsilon_g = 1 \qquad (146)$$

Equations (139)-(146) are solved simultaneously by successive substitution to obtain the values for phase holdups, ϵ_l, ϵ_g and ϵ_s. The holdup values predicted by the above model are compared to the experimental values obtained by Armstrong[289] in Table 65. For entries 1-4 in Table 65, the procedure of Sastry, et al.,[284] was used for the calculation of u_{br} and for entries 5-10, Kim's[286] correlation was used for u_{br} determination. It is observed from Table 65 that the holdups are predicted to within 10% by the above approach. It should be noted that the correlation for d_b obtained by Kim, et al.,[286] was for a two-dimensional system with a rectangular column, whereas, the Richardson-Zaki correlations,[288] used in the above formulation for the calculation of phase holdups were developed for columns with circular crossections. The data of Armstrong[289] were also obtained using a circular column. the discrepancy between the model calculations and the experiments could be partially attributed to the different geometrics used. Thus, the procedure performs well in predicting phase holdups in three-phase ebullieted beds and will be used for formulating and validating the similarity criteria for scaling down commercial units to laboratory scale.

Development of Similarity Criteria

Scaling down commercial reactors involves reducing the length of the reactors and ensuring identical hydrodynamic properties in commercial and laboratory units. In order to maintain a given

Table 65

Validation of the Generalized Wake Model

#	d_p (m)	u_l (m/s)	u_g (m/s)	(ϵ_l)cal (-)	(ϵ_l)exp (-)	(ϵ_l)cal (-)	(ϵ_l)exp (-)
1	0.005	0.092	0.033	0.552	0.577	0.041	0.038
2	0.005	0.092	0.059	0.540	0.558	0.069	0.067
3	0.005	0.092	0.089	0.525	0.535	0.102	0.098
4	0.005	0.092	0.178	0.482	0.529	0.191	0.126
5	0.003	0.056	0.119	0.508	0.504	0.066	0.051
6	0.003	0.056	0.148	0.503	0.543	0.077	0.051
7	0.003	0.056	0.178	0.498	0.527	0.087	0.069
8	0.005	0.067	0.089	0.456	0.512	0.054	0.054
9	0.005	0.067	0.119	0.474	0.504	0.066	0.067
10	0.005	0.067	0.178	0.466	0.509	0.087	0.088

Note: Holdups in entries 1-4 have been calculated using u_{br} correlations given by Tadaki and Maeda[285]; holdups in entries 5-10 have been calculated by u_{br} correlation given by Kim, et al.[286]

Values of other parameters

ρ_p = 2489 kg/m^3 $\quad\quad$ ρ_l = 1000 kg/m^3
μ_l = 0.001 kg/m-s $\quad\quad$ σ = 0.073 N/m
d_r = 0.24 m

space velocity and to reduce the reactor length, the liquid velocity has to be reduced. The particle size has to be reduced to achieve ebullietion at this reduced liquid velocity. The reduction in superficial liquid velocity and particle size has to be achieved in such a manner that the important hydrodynamic parameters such as the phase holdups remain unchanged.

The steps for reactor hydrodynamic scaledown are:

1. Reduce u_l which results in an increase in solid holdup ϵ_s.
2. Reduce d_p to readjust ϵ_s.
3. Adjust the other system parameters to get same liquid and gas holdups ϵ_l and ϵ_g respectively in both the commercial and laboratory reactors.

As u_l is reduced, for a given space velocity, the solid stagnant bed height (solid charge) is reduced. This leads to a reduction in the reactor length.

It is recognized that there may be hydrodynamic parameters, other than phase holdups that influence the process performance. As a first step toward complete hydrodynamic similarity, this section considers the similarity of phase holdups which are important hydrodynamic parameters. The importance of the similarity of flow regime and bubble size is addressed in the subsequent section.

Particle elutriation in the scaled-down reactor must be considered due to the small size of the particles. The particle disengaging height should be sufficient to ensure catalyst retention in the reactor. Furthermore, the particle size should not be reduced to such an extent that all particles are elutriated irrespective of the length of the disengaging section. These aspects were incorporated into the model by using the stagewise partition model.[290] The Strouhal number (Sr) which is necessary to calculate the wake shedding frequency (ν) in the stagewise

partition model, was obtained by using the following correlation for alternately shedding wakes[291]:

$$Sr_b = \frac{1}{2420 Re_b^{-1.02} + 0.776}. \tag{147}$$

The Strouhal number, Sr_b, based on the effective bubble diameter, is defined as

$$Sr_b = \frac{d_b \nu}{\left(\frac{u_g}{\varepsilon_g} - \frac{u_l}{\varepsilon_l}\right)}. \tag{148}$$

The disengaging height can subsequently be calculated using ν.

It is clear from Equations (134) to (146) that the following functional relationships are satisfied.

$$\varepsilon_l = f(d_r, d_p, \rho_p, \rho_l, \mu_l, \sigma, u_l, u_g, g, \kappa, x, n, \nu) \tag{149}$$

and,

$$\varepsilon_g = f(d_r, d_o, d_b, \rho_p, \rho_l, \mu_l, \sigma, u_l, u_g, g, \kappa, x, n, \nu). \tag{150}$$

There is a weak dependence of ϵ_g on the reactor diameter, d_r, when $d_r > 0.1$ m. Therefore, d_r can be eliminated from the above relationships. The size of the bubbles is governed by bubble coalescence close to atmospheric pressures [292] and the bubble diameter, d_b, becomes practically independent of the orifice diameter, d_o. Hence, at low pressure the functional dependence of ϵ_g on d_o has also been neglected. Furthermore, x, n, k and d_b

depend on other fundamental parameters in the system through the following relationships:

$$x = f(d_p, \rho_p, \rho_l, \mu_l, u_l, u_g, \varepsilon_g, \varepsilon_l) \tag{151}$$

$$n = f(d_p, \rho_p, \rho_l, \mu_l) \tag{152}$$

$$\kappa = f(\varepsilon_g, \varepsilon_l) \tag{153}$$

$$d_b = f(u_l, u_g, \mu_l, \rho_l, \sigma). \tag{154}$$

Thus, x, n, κ and d_b can be eliminated from Equations (149) and (150). In the present analysis, d_b is assumed to be a function of the basic system parameters. In practice, it may additionally depend on factors such as the particle diameter d_p, and system pressure. In such cases, d_b can be retained as a system parameter in the dimensional analysis and eliminated at a later stage.

The following equations were obtained by dimensional analysis for the phase holdups.

$$\varepsilon_l, \varepsilon_g = f\left[\left(\frac{u_l}{u_g}\right), \left(\frac{\rho_l}{\rho_s}\right), \left(\frac{d_r}{d_p}\right), \left(\frac{\rho_l u_l d_p}{\mu_l}\right), \left(\frac{u_l^2}{g d_p}\right), \left(\frac{u_l^2 d_p \rho_l}{\sigma}\right)\right] \tag{155}$$

$$\varepsilon_l, \varepsilon_g = f\left[\left(\frac{u_l}{u_g}\right), \left(\frac{\rho_l}{\rho_s}\right), \left(\frac{d_r}{d_p}\right), (Re_p), (Fr_p), (We_p)\right] \tag{156}$$

where We_p, the particle Weber number, is given by

$$We_p = \frac{u_l^2 d_p \rho_l}{\sigma}. \tag{157}$$

The dimensionless numbers, Re_p, Fr_p and We_p can be combined to derive a dimensionless number independent of d_p, the Morton number, Mo.

$$\frac{We_p^3}{Re_p^4} \times \frac{1}{Fr_p} = \frac{g\mu_l^4}{\sigma^3 \rho_l} = Mo. \tag{158}$$

Only three of the four dimensionless numbers (Re_p, Fr_p, We_p and Mo) have to be the same for the commercial and the laboratory units to be similar. Hence, the following criteria must be satisfied to achieve phase holdup similarity between the commercial and laboratory units.

$$(Re_p)_{com} = (Re_p)_{lab} \tag{159}$$

$$(Fr_p)_{com} = (Fr_p)_{lab} \tag{160}$$

$$(Mo)_{com} = (Mo)_{lab} \tag{161}$$

$$(u_l/u_g)_{com} = (u_l/u_g)_{lab} \tag{162}$$

$$(\rho_l/\rho_p)_{com} = (\rho_l/\rho_p)_{lab} \quad (163)$$

$$(d_r/d_p)_{com} = (d_r/d_p)_{lab}. \quad (164)$$

Verification of the Similarity Criteria

The similarity criteria derived in the previous section were used to establish the laboratory system parameters such as $(u_l)_{lab}$, $(u_g)_{lab}$, $(\rho_p)_{lab}$, $(\mu_l)_{lab}$, $(\sigma)_{lab}$ and $(d_r)_{lab}$ for an assumed value of $(d_p)_{lab}$ and known parameters for the commercial reactor. The generalized wake model was used to determine the phase holdups in the commercial and laboratory system. The equality between the phase holdups verified the applicability of the similarity criteria.

The results are presented in Table 66. The parameters for both the commercial and the laboratory scale units are hypothetical and have been used to illustrate the similarity concept. In Table 66, entry #5 (d_p = 0.0026m.) can be interpreted as representing the commercial unit. The dimensions of the reactor and the values of the system parameters for subsequent entries in Table 66 were arrived at by similarity analysis and can be interpreted as parameters for scaled-down units. The values of the relevant dimensionless numbers used in the calculations are also listed in Table 66. It can be seen from the table that the analysis yields identical values of the phase holdups in each of the cases. It should be kept in mind that the only hydrodynamic parameters that are being considered in the above similarity analysis are phase holdups. The other important hydrodynamic parameters, bubble size,

Table 66

General Similarity: Six Dimensionless Groups Held Constant

#	d_p (m)	d_r (m)	ρ_p (kg/m^3)	ρ_l (kg/m^3)	σ (N/m)	μ_l (kg/m.s)	u_l (m/s)	u_g (m/s)	ϵ_s (-)	ϵ_l (-)	ϵ_g (-)
1	.0010	.150	2300	1000	.073	.001	.020	.021	.487	.494	.019
2	.0012	.180	2254	980	.102	.001	.022	.023	.487	.494	.019
3	.0013	.195	2208	960	.118	.001	.023	.024	.487	.494	.019
4	.0017	.255	2507	1090	.229	.002	.026	.027	.487	.494	.019
5	.0026	.390	2645	1150	.566	.004	.032	.034	.487	.494	.019

Re_p = 20
Fr^p = 0.04
M_o^p = 2.5 x 10^{-11}
u_g/u_l = 1.04
d_s/d_l = 2.3

bubble rise velocity and flow regime will be considered in the subsequent sections.

Practical Procedure for Scale-Down

The parameters used in the above verification were hypothetical. However, in a practical situation, it may not be possible to vary all the system parameters independently to the extent manifested in Table 66. For example, the surface tension (σ) and the liquid viscosity (μ_l) cannot be changed simultaneously to a desired level. Change in some other property will have to be effected (temperature, concentration) to achieve the desired values of μ_l and σ. Such a change would alter the reaction chemistry which implies that the previously established similarity criteria can be used only for nonreacting systems. For reacting systems, it is desirable to obtain similarity in phase holdups between the laboratory and the commercial units by varying the minimum number of adjustable system parameters without varying the reaction chemistry.

Equations (144) can be rewritten to give the following equation after substituting u_g/ϵ_g for v_g and ϵ_κ for $\kappa\epsilon_g$:

$$\varepsilon''_{lf} = \left[\frac{(u_l - u_g\kappa(1 - X))}{u_i(1 - \varepsilon_g - \varepsilon_\kappa)}\right]^{(1/n)} . \qquad (165)$$

Equation (166) as follows by rearranging Equation (145) and by substituting u_g/ϵ_g for v_g and $\epsilon_g + \epsilon_g$ for $1-\epsilon_s$.

This implies that;

$$\varepsilon_g = \frac{u_g(\varepsilon_g + \varepsilon_l)}{u_l + u_g + \varepsilon''_{lf}(1 - \varepsilon_g - \varepsilon_\kappa)u_{br}}. \tag{166}$$

$$\varepsilon_g = f(u_l, u_g, \varepsilon''_{lf}, \varepsilon_l, \varepsilon_g, \varepsilon_\kappa, U_{br}). \tag{167}$$

The procedure developed by Bhatia and Epstein[282] indicated that κ is a function of ϵ_g and ϵ_l. However, since $\epsilon_\kappa = \kappa\epsilon_g$ it follows that $\epsilon_\kappa = f(\epsilon_l, \epsilon_g)$. Thus, if the holdups are identical and if ϵ''_{lf} and u_{br} are the same in the commercial and the laboratory units, then, $\epsilon_g = f(u_l, u_g)$. Thus, one of the important considerations is that,

$$(u_{br})_{com} = (u_{br})_{lab}. \tag{168}$$

At this stage, it should be noted that there is a close relationship between u_{br} and d_b. In fact, Kim, et al.,[286] presented a single valued correlation between u_{br} and d_b. Thus, when the bubble rise velocities in the commercial and laboratory units are equal, the bubble sizes will also be similar, provided the flow regimes are the same in the commercial and laboratory units. Hence, the practical similarity procedure, by allowing the phase holdups, the bubble size and bubble rise velocity to be equal for the laboratory and commercial units, is a step closer to hydrodynamic similarity than the general similarity criteria discussed earlier.

When the holdups are identical, it follows from Equation (165) that, $\epsilon''_{lf} = f(u_l, u_g, u_i, n)$. Furthermore, from the correlation suggested by Richardson and Zaki[288] for u_i and n it is apparent

that u_i and n are functions of d_p, μ_l, ρ_p, and ρ_l. Thus, if the parameters μ_l, ρ_l and ρ_p are defined for the two systems (same catalyst and fluid systems), and if $(d_p)_{lab}$ are known, then u_i and n for the laboratory unit can be determined. With this information and with u_{br} being identical for the two systems, Equations (164) and (165) can be solved to obtain the values of $(u_l)_{lab}$ and $(u_g)_{lab}$ for identical holdups between the commercial and laboratory systems.

Combining Equations (143) and (166) we have,

$$\varepsilon_l = \varepsilon_\kappa(1 - X) + \left[\frac{u_l - \kappa u_g(1 - X)}{u_i(1 - \varepsilon_g - \varepsilon_\kappa)}\right]^{1/n}(1 - \varepsilon_g - \varepsilon_\kappa + X\varepsilon_\kappa). \tag{169}$$

It was indicated by Bhatia and Epstein[283] that in the generalized wake model, the value of x does not affect the phase holdups appreciably. If x is chosen to be equal to zero in the above equation, then

$$\varepsilon_l \simeq \varepsilon_\kappa + \left[\frac{u_l - \kappa u_g}{u_i(1 - \varepsilon_g - \varepsilon_\kappa)}\right]^{1/n}(1 - \varepsilon_g - \varepsilon_\kappa). \tag{170}$$

When the holdups, ϵ_l and ϵ_g are identical, then $(\epsilon_\kappa)_{com} = (\epsilon_\kappa)_{lab}$. This provides the simplified similarity condition

$$\left[\frac{u_l - \kappa u_g}{u_i(1 - \varepsilon_g - \kappa\varepsilon_g)}\right]^{1/n}_{com} = \left[\frac{u_l - \kappa u_g}{u_i(1 - \varepsilon_g - \kappa\varepsilon_g)}\right]^{1/n}_{lab} \tag{171}$$

Again, by keeping u_{br} the same for the commercial and the laboratory units, Equations (164), (165) and (170) can be solved

simultaneously for the values of $(u_l)_{lab}$ and $(u_g)_{lab}$. Thus, Equations (167) and (170) constitute a set of reduced similarity criteria for the three-phase ebullieted bed systems, requiring manipulation of a minimum number of parameters.

These conditions consider changes only in four adjustable parameters; d_p, d_r, u_l and u_g. Using these conditions, for a given set of values of the system parameters for a commercial unity, and for a specified value of d_p for the laboratory unit, u_l and u_g for the laboratory, can be calculated to give identical holdups. As noted earlier, d_r does not influence the phase holdups significantly, when d_r 0.1 m. The results of these calculations are presented in Table 67. In each of the entries, the larger diameter particle represents the commercial unit and the smaller diameter particle the laboratory unit. Given the parameters for the commercial unit and an assumed value for $(d_p)_{lab}$, u_l and u_g for the laboratory system were calculated using the simplified similarity criteria. The phase holdups were calculated using the generalized wake model. It is observed from Table 67, that the holdups are almost identical for the commercial and the laboratory units. Thus, the reduced set of criteria are an effective means for scaling down a commercial three-phase ebullieted bed reactor to laboratory scale.

Application at High Pressure

Effect of High Pressure

As mentioned earlier, one of the requirements for the hydrodynamic similarity between the commercial and laboratory

Table 67

Practical Similarity: Two Reduced Similarity Criteria Satisfied

	commercial					laboratory				
#	d_p (m)	u_l (m/s)	u_g (m/s)	ϵ_l (-)	ϵ_g (-)	d_p (m)	u_l (m/s)	u_g (m/s)	ϵ_l (-)	ϵ_g (-)
1	0.005	0.075	0.122	0.497	0.067	0.003	0.056	0.119	0.508	0.066
2	0.005	0.075	0.153	0.492	0.078	0.003	0.056	0.148	0.503	0.077
3	0.005	0.075	0.183	0.487	0.089	0.003	0.056	0.178	0.486	0.087
4	0.005	0.067	0.178	0.466	0.087	0.003	0.047	0.173	0.463	0.085
5	0.005	0.067	0.089	0.479	0.054	0.003	0.047	0.086	0.475	0.053
6	0.005	0.067	0.119	0.474	0.066	0.003	0.047	0.115	0.471	0.064

Values of other parameters

$\rho_p = 2489$ kg/m^3
$\mu_l = 0.001$ kg/m - s
$d_r = 0.2413$ m

$\rho_l = 900$ kg/m^3
$\sigma = 0.073$ N/m

reactor is to have the same flow regime in the two reactors. Furthermore, the bubble size governs the bubble rise velocity U_{br}, particularly in the dispersed bubble regime, where the bubble coalescence or breakage is minimal. Thus, if both reactors operate in a discrete bubble regime and if the value of U_{br} in both reactors is the same, the bubble size in the two reactors will be similar.

Three-phase ebullieted bed reactors[280,230] for hydroprocessing of coal, heavy resids and bitumens operate at pressures ranging up to 17.2 MPa. At high pressures, the bubble size and the bubble coalescence in multiphase systems are known to be reduced.[281] This leads to a dispersed bubble regime in three-phase ebullieted beds. Thus, scaling down a high pressure three-phase ebullieted bed reactor while maintaining the same pressure in both of the reactors would ensure the same flow regime (dispersed flow regime) in the two reactors.

Methodology for Adjusting u_{br}

U_{br} is basically a function of d_p, u_l, u_g, ρ_g, μ_l and σ. For an assumed value of $(d_p)_{lab}$ and given values of $(\rho_g)_{lab}$, $(\mu_l)_{lab}$ and $(\sigma)_{lab}$ (= $(\rho_g)_{com}$, $(\mu_l)_{com}$ and $(\sigma)_{com}$, respectively) pairs of $(u_l)_{lab}$ and $(u_g)_{lab}$ can be determined using Equation (167). The specific values of $(u_l)_{lab}$ and $(u_g)_{lab}$ can be determined using Equation (170), to give the same holdups in both the reactors.

Similarity Criteria at High Pressure

The bubble size in a three-phase ebullieted bed reactor decreases with increase in reactor pressure. This leads to a decrease in the bubble wake volume. At 17.2 MPa pressure, the wake

volume will be negligible. In such a case x in Equation (168) will be zero.

SUMMARY AND CONCLUSIONS

The generalized wake model was used to calculate phase holdups in three-phase ebullieted bed reactor systems. Existing correlations for u_{tb} (for the determination of u_{br}), k and x were used for these calculations. The phase holdups predicted from these calculations were in reasonably good agreement with the experimental holdup data available in the literature.

A comprehensive dimensional analysis was carried out to arrive at criteria that would ensure identical phase holdups for commercial and laboratory scale reactors. It was determined that for similarity, six dimensionless groups would have to be the same for the commercial and laboratory units. Given the commercial system dimensions and parameters, the values of the parameters for the laboratory unit were determined using the established similarity criteria. The phase holdups for the commercial and the laboratory units, calculated from the generalized wake model, were equal; thus, validating the similarity criteria.

Manipulating the system parameters to keep all of the six dimensionless groups constant was impractical for the reacting systems and the criteria could only be applied to nonreacting systems. A simplified set of criteria were developed for reacting systems to ensure the similarity of holdups in the two units by the manipulation of the parameters, d_p, u_l and u_g. Again, given the values of the parameters for the commercial unit and assumed values

of d_p for the scaled-down laboratory reactor, the values of u_l and u_g for the laboratory scale unit were calculated using the simplified criteria. The phase holdups for the two units calculated using these values of d_p, and u_l and u_g and the generalized wake model were almost identical; thus, validating the concept of using the reduced set of similarity criteria for scaling down three-phase ebullieted bed reactors.

Since high pressure three-phase ebullieted reactors operate in a dispersed bubble regime, a scaled-down reactor will have the same flow regime and similar bubble size as the high pressure commercial reactor, resulting in a closer hydrodynamic similarity.

NOMENCLATURE

a_r = parameter defined in Equation (142)

C_{Db} = coefficient of viscous drag for gas bubble, dimensionless

d_b = bubble diameter, m

d_o = diameter of the orifice, m

d_p = particle diameter, m

d_r = reactor diameter, m

g = gravitational constant

n = Richardson-Zaki exponent in generalized wake model

u_g = superficial gas velocity, m s^{-1}

u_i = Richardon-Zaki intercept, m s^{-1}

u_l = superficial liquid velocity, m s^{-1}

u_{br} = bubble rise velocity relative to the liquid in the surrounding solid-liquid phase, m s^{-1}

u_{tb} = terminal velocity of a single bubble rising through a liquid column, m s^{-1}

v_g = linear gas velocity, m s^{-1}

x = ratio of the solid holdup in the bubble wake to the solid holdup in the liquid-solid region

Fr_p = particle Froud number, dimensionless

Mo = Morton number, dimensionless

Re_p = particle Reynolds number, dimensionless

Re_b = bubble Reynolds number, dimensionless

Sr_b = Strouhal number, dimensionless

We_p = particle Weber number, dimensionless

Greek symbols

ϵ_g = gas holdup, dimensionless

ϵ_κ = $\kappa\epsilon_g$, dimensionless

ϵ_l = liquid holdup, dimensionless

ϵ_s = solid holdup, dimensionless

ϵ''_{lf} = liquid holdup in the liquid-solid region, dimensionless

υ = shedding frequency for two successive vortices, s^{-1}

κ = ratio of the wake volume to the bubble volume

μ_l = liquid viscosity, kg m^{-1} s^{-1}

ρ_g = gas density, kg m^{-3}

ρ_l = liquid density, kg m^{-3}

ρ_p = particle (solid) density, kg m^{-3}

σ = liquid-gas surface tension, N m^{-1}

Subscripts

$_{com}$ = parameter for commercial reactor

$_{lab}$ = parameter for laboratory reactor

FUTURE ACTIVITIES

The design of the ebullieted bed hydrotreater will be reviewed for possible construction to conduct laboratory bitumen-derived heavy oil hydrotreating studies. The costs of construction and the operability by graduate students will be evaluated.

DEVELOPMENT STUDIES OF EQUIPMENT FOR THREE-PRODUCT GRAVITY-SEPARATION OF BITUMEN, SAND AND WATER

Principal Investigator: D.A. Dahlstrom
Graduate Student: R. Kumar

INTRODUCTION

A three-product (overflow, middlings and underflow streams) low centrifugal force classifier has been developed in earlier work in the Unit Operations Laboratory in the Chemical Engineering Department. Tests indicated it might be applicable for the recovery of bitumen (>90%) in the overflow and middlings streams produced during aqueous recovery of the bitumen from Uinta Basin oil sand deposits. This would materially reduce the complexity of the present full-scale methods used for bitumen separation and recovery.

RESULTS AND DISCUSSION

Three-Product Classifier

The three-product classifier has been designed for use at the North Salt Lake pilot plant to process 100 tons per day of oil sand. The design drawings and specifications have been reviewed and submitted to the appropriate fabricators for bid.

Separation of Solids by Particle Size

The three-product centrifugal classifier could not be run with oil sands at 170°F in the Merrill Engineering Building unit operations laboratory. Thus, the particle size separation analysis cannot be performed until the classifier has been installed at the North Salt Lake pilot plant. However, experiments with sand and

water indicated that the separation point for the three-product classifier appeared to be about 175-225 microns which would be satisfactory for oil sands streams.

As a substitute for bitumen with sand and water, we employed plastic "pellets" which were about one quarter inch in diameter and fairly flat (poor particle shape). Plastic had a specific gravity of 0.97 which is about 0.03 less than water. This is close to the difference between bitumen and water. Ninety-nine plus % of the plastic "pellets" were recovered in the overflow and the middling stream with around 80% in the middling stream. This is encouraging for the pilot plant tests although the bitumen should be harder to separate as the "particle size" distribution will be appreciably finer.

We also plan to install a 4-inch diameter conventional hydrocyclone (two-product classifier) in the pilot plant after completing studies on the three-product classifier. Canadian Occidental Petroleum, Ltd. recently reported[293] bitumen recovery results of 90% or better using conventional cyclones to separate bitumen from solids which serves to justify the examination of the potential of hydrocyclones for Utah oil sands.

Conveying or Pumping of High Solids Concentration Sand-Water Slurries

A small amount of fine and light solids were recovered/obtained from the top thin layer of the old tailings pond used at the North Salt Lake pilot plant in the late 1970s and early 1980s. When placed in water, it was concluded that the material was definitely bitumen-coated tailings as the water turned black.

Tests were run employing EIMCO's test equipment to determine if these solids would concentrate to a high solids concentration simulating the superthickener's performance. The solids were fine with a 50% particle size of 12 microns; that is, 50% of the particles were 12 microns or finer. In addition, the specific gravity of the solids was much lighter than conventional silica (2.70 specific gravity). A thick settled solid was obtained by gravity settling after diluting the solids to 5 wt% and flocculating with a good flocculant. The material did not seek a common level but rather exhibited a severe slump. The thick sludge contained 43 wt% solids. When considering the specific gravity, its volume % solids was equal to that of alumina red mud solids on which the superthickener has been employed. Superthickeners are able to extract 50% more water than achieved by conventional thickeners. The thickened alumina sludge also exhibits a "slump." Thus, the superthickener has the potential to eliminate tailings ponds for Utah oil sands recovery projects.

More thickening studies are planned after the North Salt Lake pilot plant is back in operation. However, these observation /results are encouraging, and it is felt the superthickener can be employed on Utah oil sands with a significant reduction in capital and operating costs while maximizing water recovery.

SUMMARY AND CONCLUSIONS

Preliminary studies with a blend of sand, water and plastic platelets to simulate the sand, water and bitumen feedstream were conducted in a laboratory-scale three-product separation. The

results were encouraging. Ninety nine plus % of plastic platelets used to simulate the bitumen were recovered in the overflow and middlings product streams.

Specifications for a three-product classifier for use at the North Salt Lake pilot plant have been established and plans for assembling, installing and testing the equipment have been developed. Representative sample material will be obtained from the pilot plant studies which will permit the testing of three-product classifiers and two-product cyclones and, at the same time, develop proper sample material for "flocculation and thickening of fine solids products."

FUTURE ACTIVITIES

The three-product classifier will be fabricated offsite and installed at the North Salt Lake pilot plant site. The steam boilers will be inspected, evaluated and returned to service to provide steam for the three-product classifier. A study will be made of probable capital and operating costs of three-product classifiers employed at Suncor and Syncrude plants in Canada after the centrifugal three-product classifier has been tested in the pilot-plant as planned.

TECHNICAL AND ECONOMIC COMPARISON OF BITUMEN UPGRADING OPTIONS

Principal Investigator: J.W. Bunger
Graduate Student: J. Pu

INTRODUCTION

Hydropyrolysis upgrading of oil sand bitumen, followed by stabilization via hydrotreating and hydrodenitrogenation of the stabilized hydropyrolyzate, is a process sequence of established technical alternatives. The sequence results in high-liquid yields compared to alternative process schemes and does not suffer the consequences of contact of high molecular weight feeds with heterogenous catalysts. However, hydropyrolysis requires significant heat transfer rates due to the high gas recycle rates. Optimizing and comparing the hydropyrolysis-hydrotreating option with more conventional processes has proved to be a non-trivial problem. This report summarizes the latest attempt to make these comparisons.

RESULTS AND DISCUSSION

Hydropyrolysis-Hydrotreating Upgrading Option

The first step in attempting to evaluate the hydropyrolysis-hydrotreating option was to operate the hydrogen compressors from the two units in series with a splitter to provide hydrogen for both units. A process flow diagram representing this option is presented in Figure 144. The data used to evaluate this option were taken from the literature.[169,294] The profitability analysis for this option is presented in Table 68. The internal rate of return,

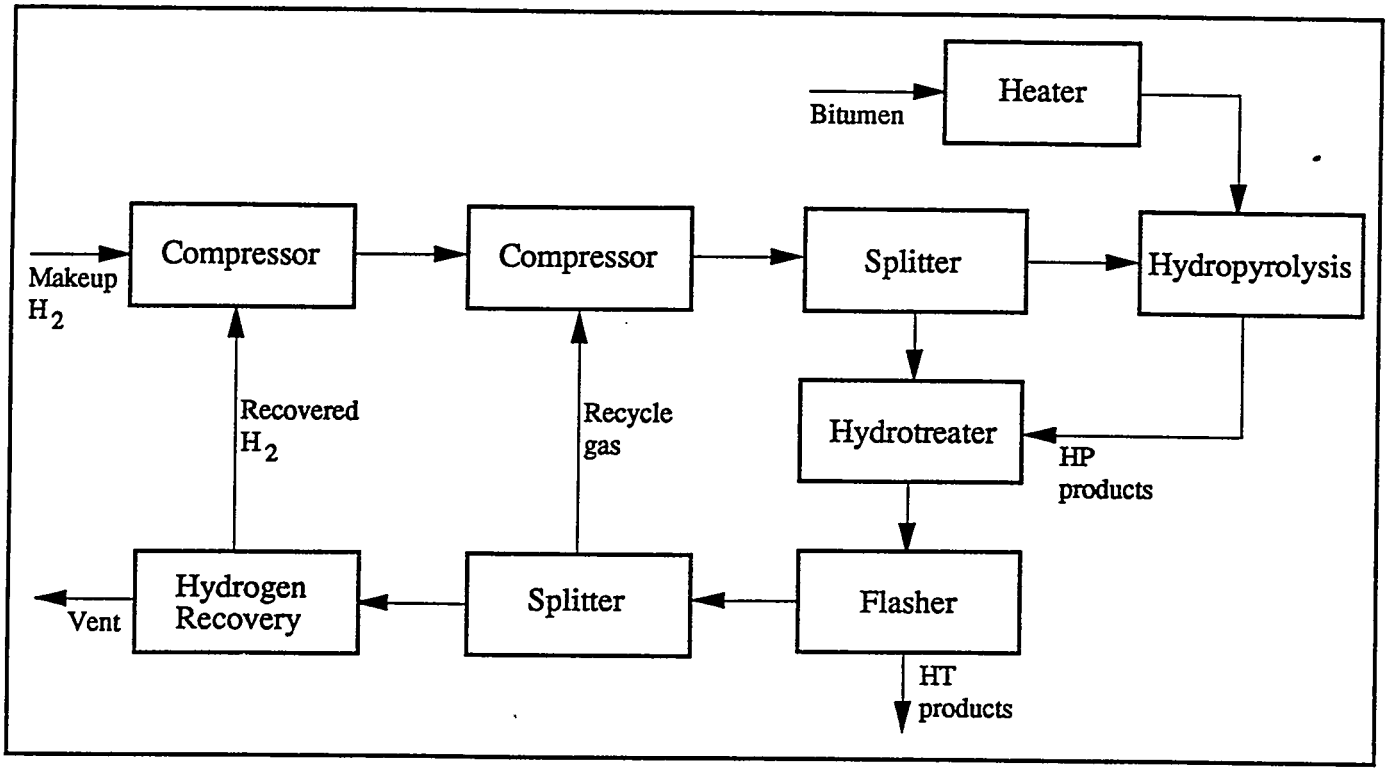

Figure 144. Flow Diagram of Hydropyrolysis-Hydrotreating Upgrading Option

20.6%, based on reasonable estimates for bitumen costs and product price indicated that the hydropyrolysis-hydrotreating option merited further evaluation.

Table 68

Results of Profitability Analysis for the Hydropyrolysis-Hydrotreating Upgrading Option

Total Capital Investment ($1000)	127,504
Product Rate (lb/hr)	234,646
Operating Cost ($/lb)	0.0902
Internal Rate of Return (%)[a]	20.60
Initial Product Price ($/lb)[b]	0.1198

[a] Bitumen Cost = $15/bbl, Product Price = $35/bbl.

[b] Internal Rate of Return = 15%, Bitumen Cost = $15/bbl.

A number of conventional options were evaluated to generate a comparison between these options and the hydropyrolysis-hydrotreating (HP + HT) bitumen upgrading option. These options included the following:

1) ROSE process[295-298] using normal butane as the solvent followed by hydrotreating (ROSE + HT);
2) visbreaking[299] followed by the ROSE process followed by hydrotreating (VBW + ROSE + HT);
3) vacuum residuum desulfurization[300-302] followed by residuum fluid catalytic cracking[303,304] (VRDS + RFCC);
4) vacuum residuum desulfurization[300-302] followed by delayed[305,306] or fluid[307,308] coking (VRDS + COKING);

5) vacuum residuum desulfurization[300-302] followed by hydrocracking[307] (VRDS + HC);

6) hydrocracking followed by delayed[305,306] or fluid[307,308] coking (HC + COKING);

7) delayed[305,306] or fluid[307,308] coking followed by hydrotreating (COKING + HT);

8) conventional visbreaking[309-312] followed by hydrotreating (VBC + HT); and,

9) visbreaking[299] followed by hydrotreating (VBW + HT).

A summary of the profitability analyses for these bitumen upgrading process schemes is presented and compared to the results for the hydropyrolysis-hydrotreating option in Table 69. The internal rate of return for the various options once again focuses attention on the hydropyrolysis-hydrotreating option. The variable most likely to impact the internal rate of return in the hydropyrolysis-hydrotreating option in the configuration in which the compressors are operated in series is the recycle gas to hydrogen recovery splitter ratio: (Figure 144). The split ratio is the ratio of the amount of hydrogen going to hydrogen recovery to the amount used on recycle gas. The internal rates of return were in excess of 18.5% for all split ratios in the range 0.14 to 0.18 (Table 70).

The hydropyrolysis process flow diagram is presented in Figure 145. The major economic variables in hydropyrolysis are the recycle gas flowrate and the split ratio in S-1. The recycle stream has two functions: 1) to supply H_2 to maintain the

Table 69

Summary of the Profitability Analysis of
Oil Sands Upgrading Process Options

	Total Capital Investment ($1000)	Production Rate (lb/hr)	Operating Cost ($/lb)	Internal Rate of Return[a] (%)	Initial Product Price[b] ($/lb)
ROSE®+HT[c]	81333	95999	0.1014	13.82	0.1052
VBW + ROSE®+HT	80339	101145	0.0965	19.54	0.1053
VRDS+RFCC[d]	128283	107113	0.1123	17.91	0.1388[†]
VRDS+COKING[e]	104945	122664	0.0909	15.32	0.1119
VRDS+HC[e]	186231	145152	0.1029	2.85	0.1371
HC[f]+COKING	105486	123485	0.0897	18.99	0.1104
COKING+HT	85733	84760	0.1128	7.64	0.1329
VBC + HT	76244	82780	0.1125	5.14	0.1296
VBW + HT	58990	65725	0.1293	-2.20	0.1357
HP+HT	127504	134646	0.0902	20.60	0.1198

[a] bitumen cost = $15/bbl, product price = $35/bbl

[b] Internal Rate of Return = 15%, bitumen cost = $15/bbl

[c] n-C4 solvent

[d] RFCC product price is 20% higher than the others

[e] HC conversion is 95%

[f] HC conversion is 60%

appropriate H_2-to-oil ratio in the reactor, and 2) to supply heat to the reactor. Hydropyrolysis is normally carried out at reaction temperatures around 798 K. Thus, all reactants must be heated to this temperature. However, bitumen cannot be heated to these temperatures in the absence of H_2 since severe thermal cracking would occur leading to the formation of coke. This problem can be

Table 70

Case Study of the Split Ratio in S-1 (S036 T = 668 K)

Split Ratio[a]	0.14	0.15	0.16	0.17	0.18
Production Rate, lb/hr	133896	134527	134417	134714	134722
Operating Cost, $/lb	0.0910	0.0901	0.0911	0.0921	0.0928
Internal Rate of Return, %	18.84	20.65	20.07	19.37	18.87

[a] Split ratio = 0.14 means 14% of the recycle gas stream goes to H_2 recovery.

circumvented by heating the recycle gas stream to a higher temperature and mixing it with bitumen which has been heated to 673 K in the appropriate proportions so that the resulting mixture temperature is the desired reaction temperature. On the other hand, the recycle gas temperature cannot be too high since it may cause material failure, i.e., H_2 embrittlement. If the H_2 stream temperature is restricted to less than 973 K and preferably to less than 923 K to prevent materials deterioration, a larger recycle gas rate will be required to maintain the mixture at the reaction temperature. The split ratio in S-1 will determine the light hydrocarbon content of the recycle gas stream and the amount of H_2 in the vent stream.

A higher gas flowrate to H_2 recovery, results in the following: a low concentration of light hydrocarbons in the recycle stream and hydropyrolysis reactor feed stream; higher reactant concentrations, bitumen conversions and gas production; a lower gas recycle rate which requires smaller compressor and lowers the power consumption in the recycle gas compressors; higher H_2 recovery costs and an increase in the amount of H_2 vented; and a higher

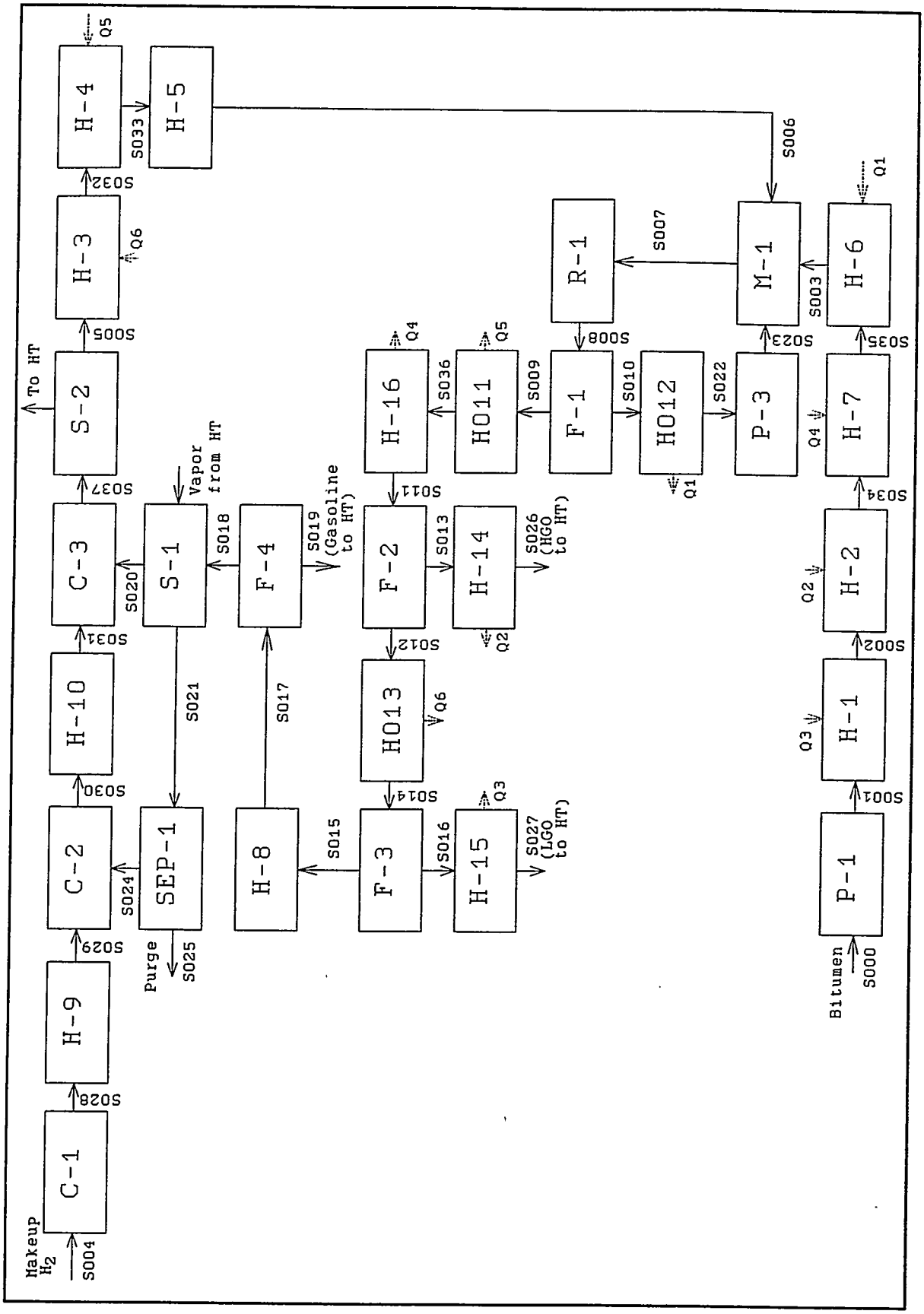

Figure 145. Flow Diagram of the Hydropyrolysis-Hydrotreating Upgrading Option

recycle gas temperature. Conversely, lower H_2 recovery unit feed flowrate, i.e., lower split ratio, results in the following: a higher concentration of light hydrocarbon in the hydropyrolysis reactor feed stream and lower bitumen conversion and lower gas production; a higher gas recycle rate, larger compressor sizes and higher power consumption in the recycle gas compressors; lower H_2 recovery costs and a reduction in the amount of H_2 vented; and lower recycle gas temperature.

A case study was conducted in which the split ratio in S-1, Figure 145, was varied. The temperature of stream S036 was fixed at 668 K for the case study. The results of an availability analysis are presented in Table 71. The temperature of the flue gas leaving the radiant section of the fired heater was assumed to be higher than the outlet temperature of the cold stream by 373 to 423 K. The analysis focused attention to the fired heater, H-5, which gave the highest value of the lost work. Thus, one option which would improve the process economics would be to reduce the demand and size of the fired heater. Since the recycle gas rate has been restricted by its temperature, an alternative option would be to increase the cold stream inlet temperature (S033, Figure 145). The temperature of stream S033 can be increased by increasing the heat duty of H-4, that is, by lowering the hot stream outlet temperature from H011 (temperature of stream S036). The results of the case study of the variation of the internal rate of return as function of the temperature of stream S036 are presented in Table 72.

Table 71

Results of Availability Analysis

Heat Exchanger	Lost Work (Btu/h)
H-3/H013	6.3789×10^6
H-4/H011	3.2693×10^6
H-5/Fuel gas	3.4767×10^7
H-1/H-15	Nil
H-2/H-14	1.1941×10^6
H-7/H-16	3.4460×10^6
H-6/H012	2.1409×10^6
H-8/Cooling water	1.7413×10^7
H-9/Cooling water	5.6624×10^5
H-10/Cooling water	1.0740×10^6
Total	712.4×10^5

Recommended Pilot Plant, Alternative 1

The results of the availability analysis indicated that a preferred alternative might be to rearrange the heat exchanger network to avoid using high temperature heat sources to heat low temperature streams and to use the excess heat to generate medium pressure process steam. A flow diagram of this alternative for the hydropyrolysis-hydrotreating upgrading option (Alternative 1) is presented in Figure 146. The major modifications involved in Alternative 1 are as follows: a portion of the heat in stream S015 (~1/3) was used to heat the bitumen, the balance (~2/3) was used to heat the recycle gas (523 K to 493 K) to preheat the boiler feed water (493 K to 363 K), and the remaining was cooled by cooling water; the recycle gas was heated by S015; and the heat in S012 was

Table 72

Results of Case Study in which Temperature of S036 was Varied
(Split ratio in S-1 = 0.15)

Temperature S036 (K)	659	660	661	662	663
Internal Rate of Return %	20.03	20.54	20.53	20.64	20.64
Temperature S036 (K)	664	665	666	667	668
Internal Rate of Return %	20.65	20.64	20.63	20.58	20.55

used to heat the bitumen. These improvements reduce the lost work in H-3/H013 and in the H-8/Cooling water. The temperature of the stream S036 was determined to be 639 K by a case study. The results of availability analysis for Alternative 1 are presented in Table 73.

Recommended Pilot Plant, Alternative 2.

The results of the availability analysis for Alternative 1 (Table 73) indicated that the fired heater, H-5, still exhibited the greatest lost work. The lost work in H-5 can be reduced by reducing the cold stream outlet temperature. Since the flue gas temperature was set higher than the cold stream outlet temperature by 373 to 423 K, a reduction in the flue gas temperature could also reduce the lost work in the fired heater. In this alternative, the fired heater is combined with the hydropyrolysis reactor, that is, the reactor tubes are in the furnace (Figure 147). Thus, the tubes in the fired heater are the reactor tubes. A 10% cost adjustment was incorporated into the analysis for the cost of the furnace/reactor combination to account for the complexity of this reactor configuration. In this alternative, the recycle gas, S032,

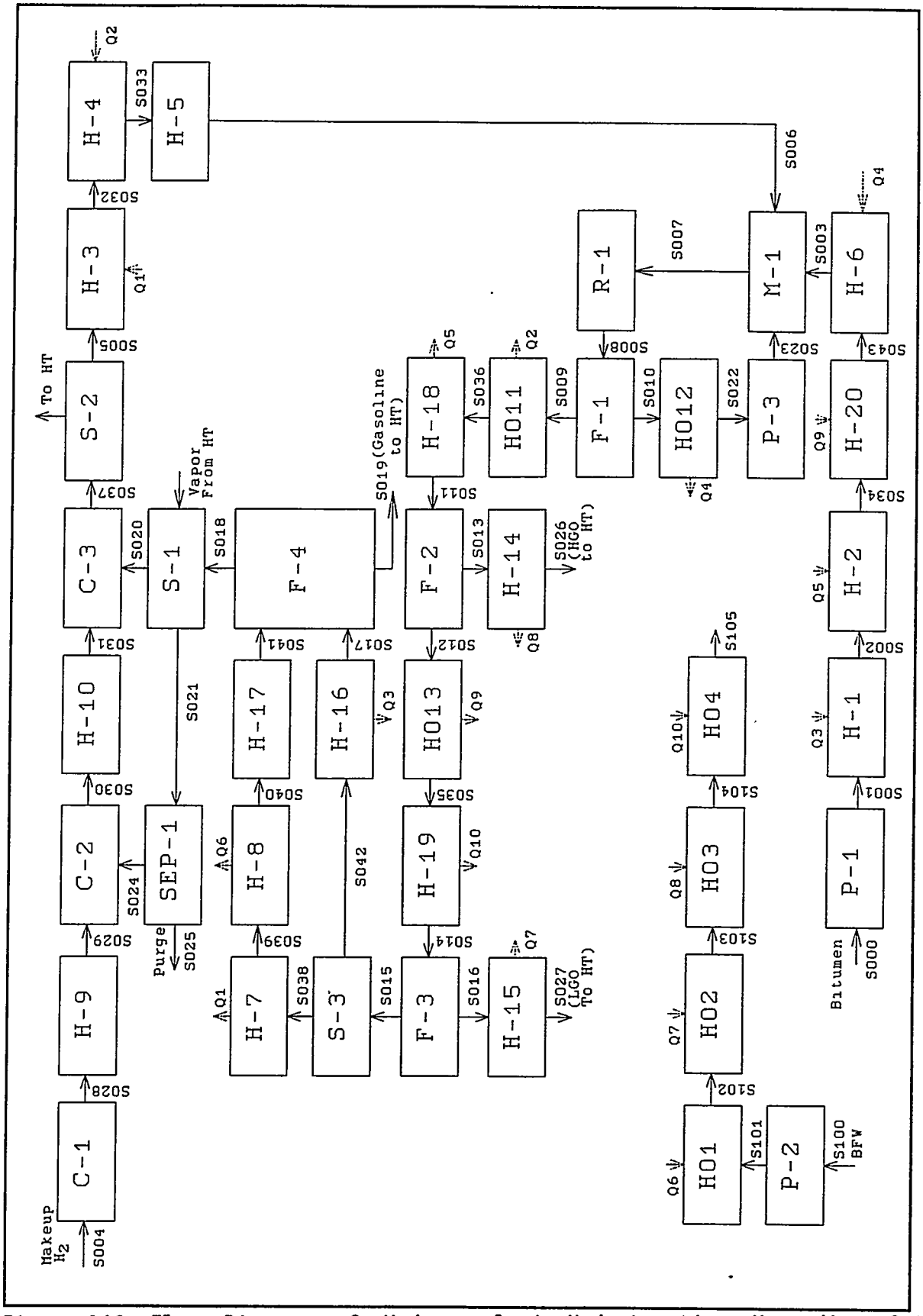

Figure 146. Flow Diagram of Hydropyrolysis-Hydrotreating Upgrading Option Alternative 1

Table 73

Results of Availability Analysis of Alternative 1

Heat Exchanger	Lost Work (Btu/h)
H-1/H-16	3.2288×10^5
H-2/H-18	7.9664×10^5
H-20/H013	7.5619×10^4
H-6/H012	2.1380×10^6
H-3/H-7	1.4941×10^6
H-4/H011	4.4526×10^6
H-5/Fuel gas	3.3211×10^7
H-17/Cooling water	6.4078×10^5
H-9/Cooling water	5.6373×10^5
H-10/Cooling water	1.0861×10^5
H01/H-8	8.3435×10^5
H02/H-15	5.4997×10^5
H03/H-14	8.9769×10^5
H04/H19	2.8702×10^6
Total	499.34×10^5

is heated by the hydropyrolysis reactor effluent, mixed with bitumen, which has been heated to 673 K and the mixture passes into the reactor where it is heated to the reaction temperature. The reaction temperature was 783 K and the flue gas temperature was 923 K for this alternative case. The reactor and fired-heater specifications were estimated as follows: the tube wall temperature was the average fluid temperature plus 323 K,[313] the temperature of flue gas in the radiant section was assumed to be 1073 K. The fluid temperatures were determined using ASPEN PLUS: for an inlet temperature of 716.4 K and an outlet temperature of 799.1 K. The fluid temperature was 807.9 K, the feed rate was

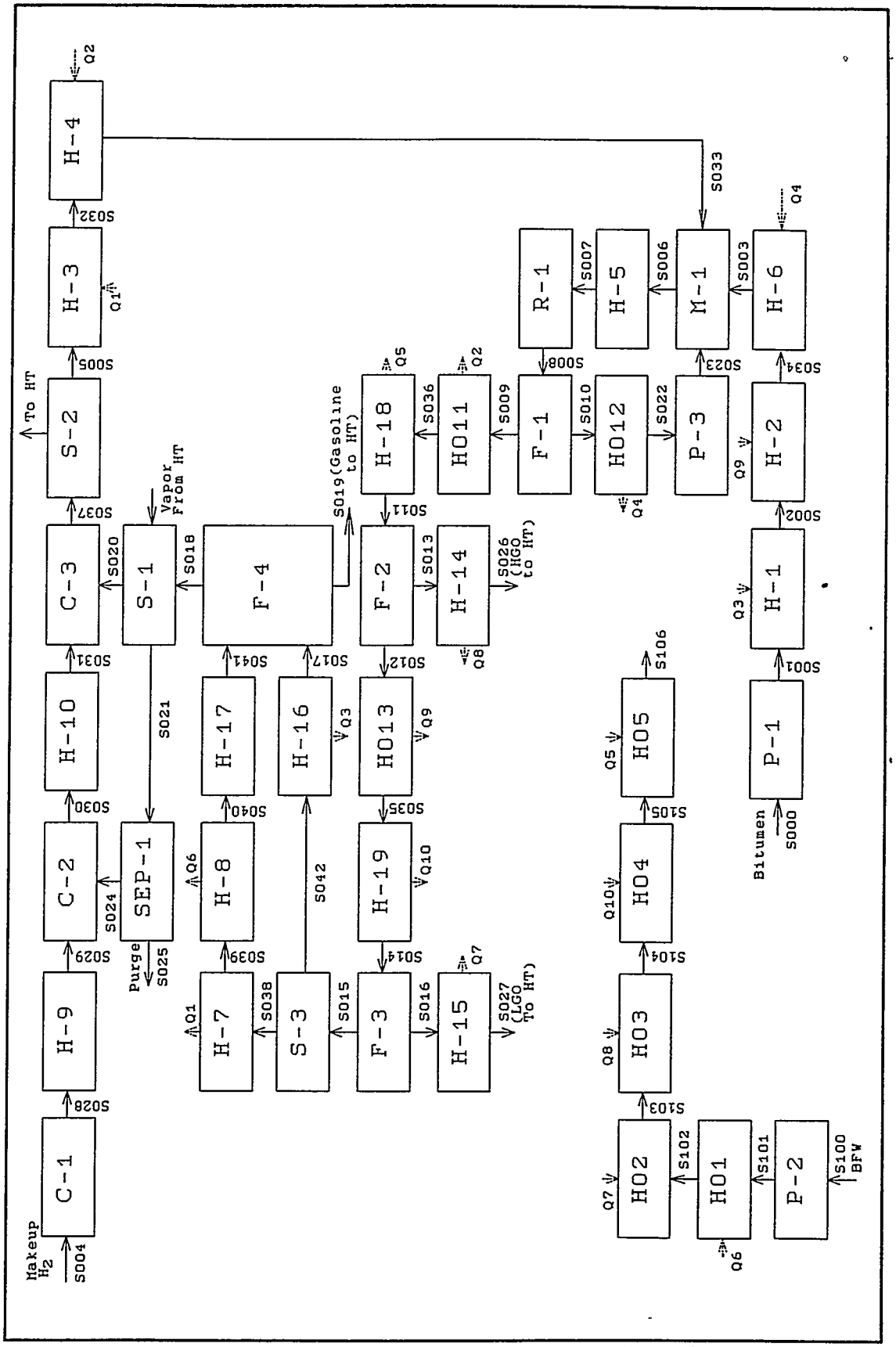

Figure 147. Flow Diagram of Hydropyrolysis-Hydrotreating Upgrading Option, Alternative 2

3528.1 m^3/h at the reactor operating conditions and the residence time was 20s. Thus, the reactor volume, the product of the feed rate and the residence time, was 19.6 m^3. The heat duty of the fired heater was calculated using ASPEN PLUS and was determined to be 1.433×10^7 kcal/h.

The heat transfer rate was determined to be 50,000 kcal/hr-m^2 for the case of heat transfer between a mass of gas at a uniform temperature and a tube surface at a second uniform temperature.[313] The heat transfer area was calculated to be 286.6 m^2. If the tube radius is 0.137 m then the length of a single tube would be 333.4 m. Thus, if the length of each reactor tube is 3 m (or 10 ft) then 110 reactor tubes will be required.

The lost work in H-5/fuel gas was reduced in this alternative. A comparison of the process flow diagrams for Alternatives 1 (Figure 146) and 2 (Figure 147) reveal the following differences or changes: the location of H-5; the heat stream Q5 was moved from feed bitumen heat transfer line (Figure 146) to MP steam generation (Figure 147), and H-20 for heating bitumen was dropped (Figure 146) and H05 for MP-stream generation was added (Figure 147). The temperature of stream S036 was determined to be 641 K by a case study. The results of availability analysis are presented in Table 74.

Recommended Pilot Plant, Alternative 3

Various hydropyrolysis H_2/oil ratios have been reported[169,294]; however, in the calculations for Alternatives 1 and 2 a H_2/oil ratio of 5500 scf/bbl was used. The alternative in which the fired

Table 74

Results of Availability Analysis of Alternative 2

Heat Exchanger	Lost Work (Btu/h)
H-1/H-16	3.4536×10^5
H-2/H013	6.3858×10^5
H-6/H012	2.1426×10^6
H-3/H-7	1.4865×10^6
H-4/H011	4.4924×10^6
H-5/Fuel gas	1.7971×10^7
H-17/Cooling water	6.4044×10^5
H-9/Cooling water	5.6583×10^5
H-10/Cooling water	1.0842×10^6
H01/H-8	8.3745×10^5
H02/H-15	5.6517×10^5
H03/H-14	9.1895×10^5
H04/H19	2.5184×10^6
H05/H-18	7.3870×10^5
Total	349.45×10^5

heater and hydropyrolysis reactor are combined, is that the reactant is heated in the fired heater and the high temperature restriction of recycle gas stream is removed permitting the reduction of the H_2/oil ratio without changing the H_2 concentration in the gas stream. The effect of H2/oil ratio and the temperature stream S036 were examined in a series of case studies. The results indicated that the preferred results were obtained at a H2/oil ratio of 3180 scf/bbl and a S036 temperature of 668 K. Furthermore, the split ratio in S-1 was 0.4 since a lower recycle gas flowrate transferred less heat to the bitumen. The flow

diagram for Alternative 3 is presented in Figure 148. The difference between Alternatives 2 and 3, H-17, was dropped in Alternative 3. The results of availability analysis are presented in Table 75.

A brief summary of the results of a profitability analysis of the 3 alternatives is presented in Table 76. The differences in the flowsheets of the three alternatives are presented in Figure 149.

Risk Analysis

According to the results of sensitivity analysis, the major variables which affect the process economics are: bitumen cost; hydrogen cost; and product price. Working capital was also considered in the risk analysis. In the calculations, each of the four variables was assigned its own value. These values are subject to variation: thus, the economic evaluations are subject to variation. The range of variations were estimated by assuming that all variations obey a normal distribution. Thus, a Monte Carlo simulation method can be used to establish probability of variation. A set of random numbers with the expectations and standard deviations were generated (Table 77). The calculations were repeated 100 times for each alternative and each profitability analysis mode. The results are presented in Figures 150-155.

SUMMARY AND CONCLUSIONS

Lost work analysis shows that incremental economic improvements can be made through carefully designed heat and energy management. Overall, the economics are highly sensitive to product

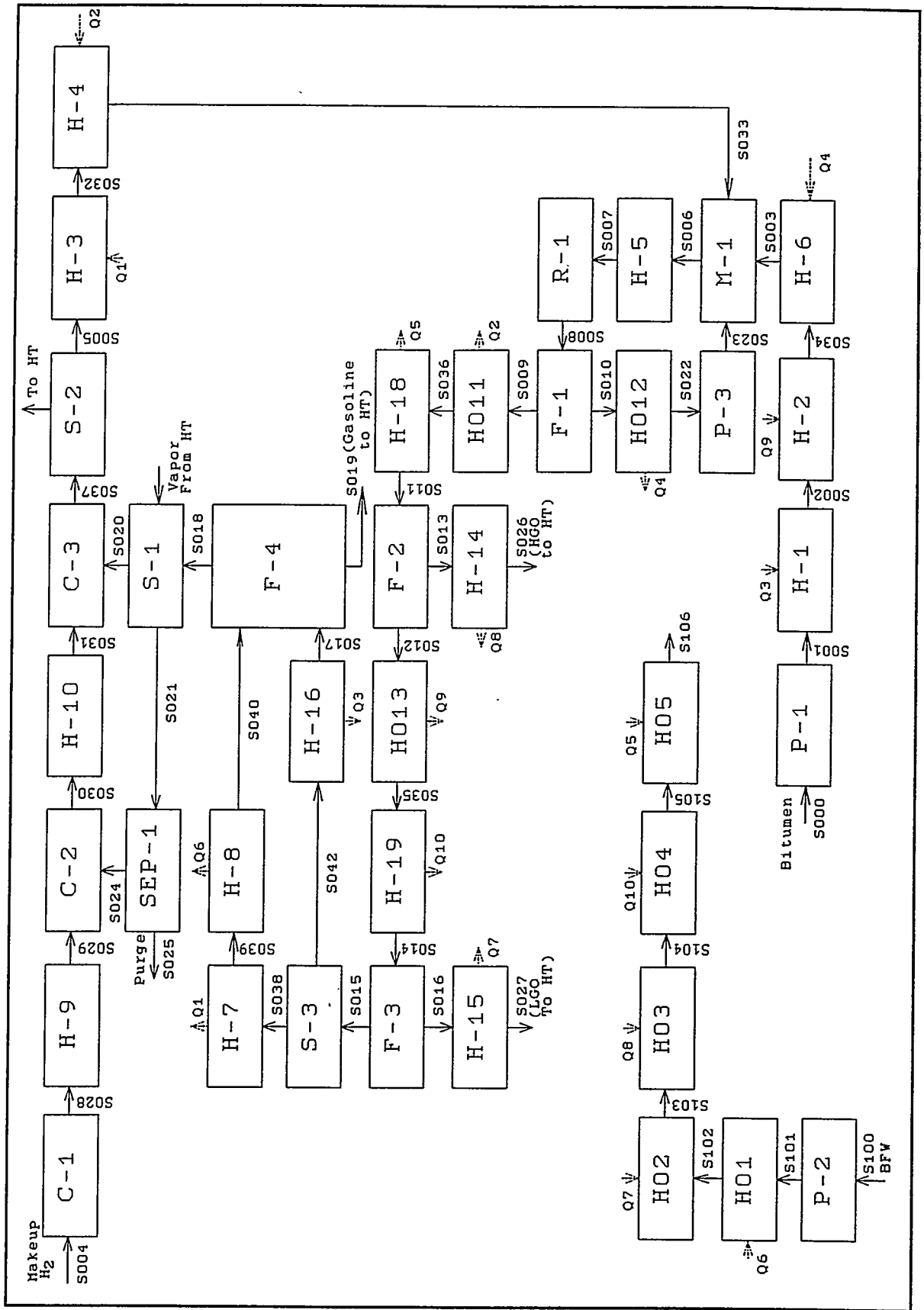

Figure 148. Flow Diagram of Hydropyrolysis-Hydrotreating Upgrading Option, Alternative 3

Table 75

Results of Availability Analysis of Alternative 3

Heat Exchanger	Lost Work (Btu/h)
H-1/H-16	6.8751×10^5
H-2/H013	8.3860×10^5
H-6/H012	2.4601×10^6
H-3/H-7	1.0951×10^6
H-4/H011	3.6551×10^6
H-5/Fuel gas	1.9083×10^7
H-9/Cooling Water	6.4437×10^5
H-10/Cooling water	9.5311×10^5
H01/H-8	5.9167×10^5
H02/H-15	4.9149×10^5
H03/H-14	8.2804×10^5
H04/H19	1.6418×10^6
H05/H-18	2.0606×10^6
Total	350.30×10^5

price. Not unexpectedly, the product price needed is greater than the prevailing price of crude oil but not outside of the range of foreseeable prices , taking into account the premium quality of the resulting syncrude. The high process yields translate into a lower requirement for feedstock than alternative processes such as coking and hydrotreating.

FUTURE ACTIVITIES

We expect to conclude our assessment and recommendations in 1994. Activities will emphasize the comparison of traditional processes with newer, higher risk processes. Attempts will be made to account for this risk factor in the various alternatives.

Table 76

Summary of the Results of Profitability Analysis
for Alternatives 1 through 3

Alternative	1	2	3
Physical Plant ($1000)	77912	74141	71625
Total Investment ($1000)	128528	123486	120514
Production Rate (lb/hr)	134371	134459	135374
Operating Cost ($/lb)	0.0901	0.0890	0.0890
Internal Rate of Return[a] (%)	21.39	22.64	23.78
Initial Product Price[b] ($/lb)	0.1159	0.1139	0.1133
Byproduct Credit ($1000/yr)	6248	6265	6217
Lost Work (10^5 Btu/hr)	499.34	349.45	350.30
ΔInternal Rate of Return/ΔBitumen Cost[c] [%/(¢/lb)]	-10.59	-10.69	-10.71
ΔInternal Rate of Return/ΔProduct Price[d] [%/(¢/lb)]	4.4010	4.4944	4.6563
ΔInitial Product Price/ΔBitumen Cost[e]	1.3171	1.3171	1.3057

[a] @Bitumen cost = $15/bbl, product price = $35/bbl
[b] @Bitumen cost = $15/bbl, Internal Rate of Return = 15%
[c] @Product price = $35/bbl
[d] @Bitumen cost = $15/bbl
[e] @Internal Rate of Return = 15%

Attempts will also be made to estimate the impact of using cost of capital on the relative attractiveness of one option as compared to another.

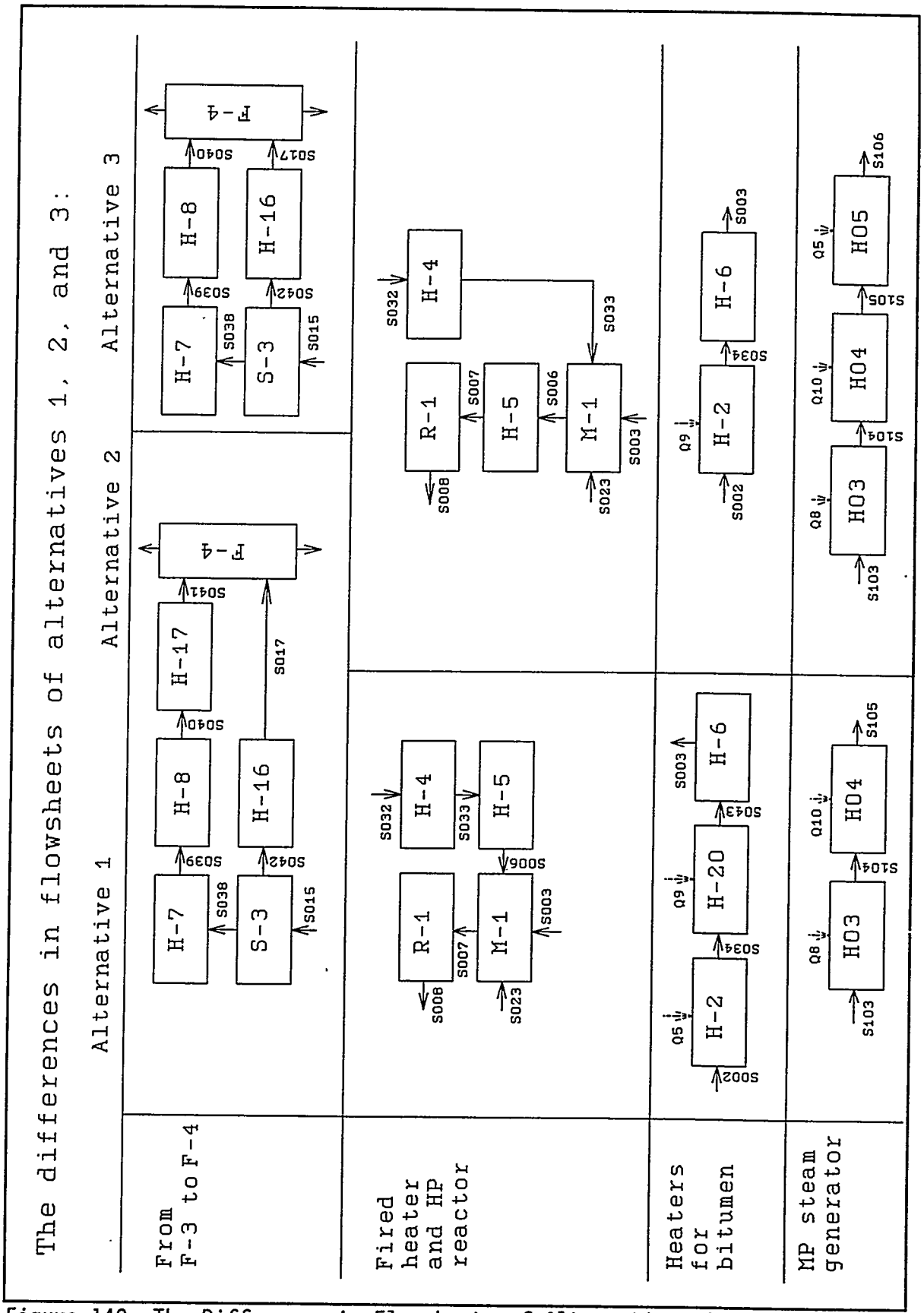

Figure 149. The Difference in Flowsheets of Alternatives 1, 2, and 3

Table 77

The Expectations and Standard Deviations used in Risk Analysis

	Expectation	Standard Deviation
Bitumen Cost ($/lb)	0.04372	± 0.01312 (± 30%)
Hydrogen Cost ($/lb)	0.4850	± 0.1455 (± 30%)
Product Price ($/lb)	0.1277[a]	± 0.03831 (± 30%)
	0.1285[b]	± 0.03855 (± 30%)
Working Capital ($)	1050000	± 210000 (± 20%)

[a] For Alternatives 1 and 2
[b] For Alternative 3

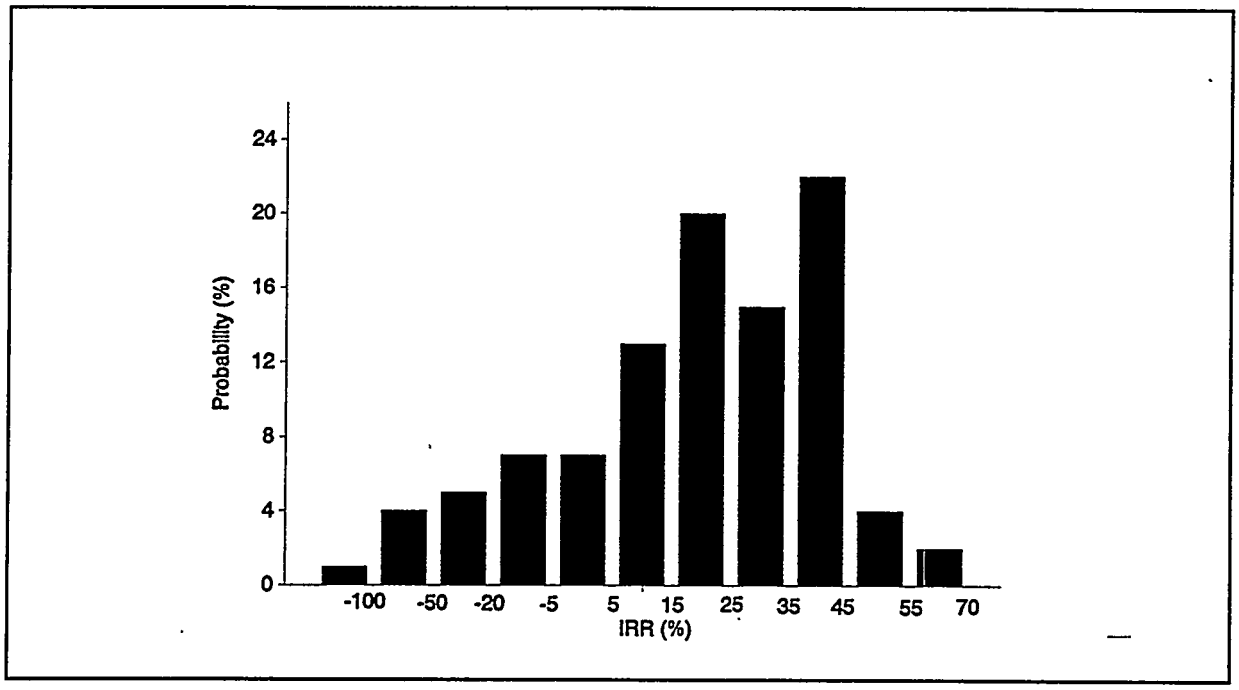

Figure 150. Probability Density Distribution Histogram of Internal Rate of Return (%) (Alternative 1, Internal Rate of Return mode)

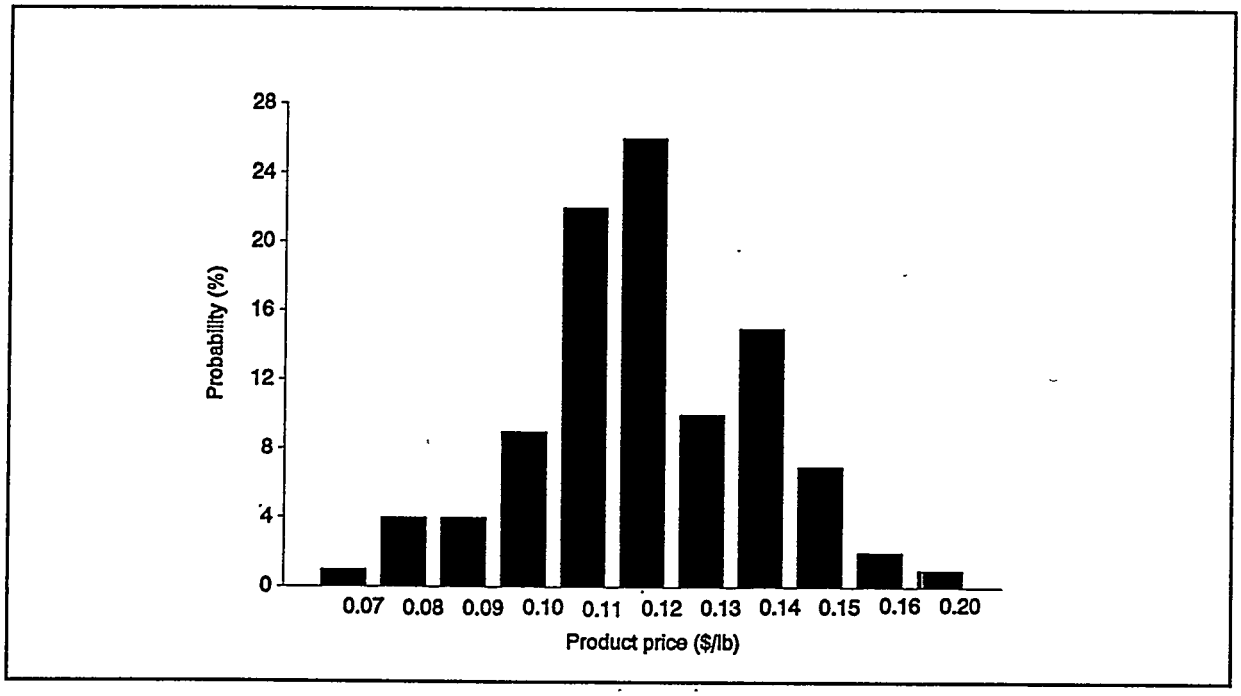

Figure 151. Probability Density Distribution Histogram of Initial Product Price ($/lb) (Alternative 1, Product Price Mode)

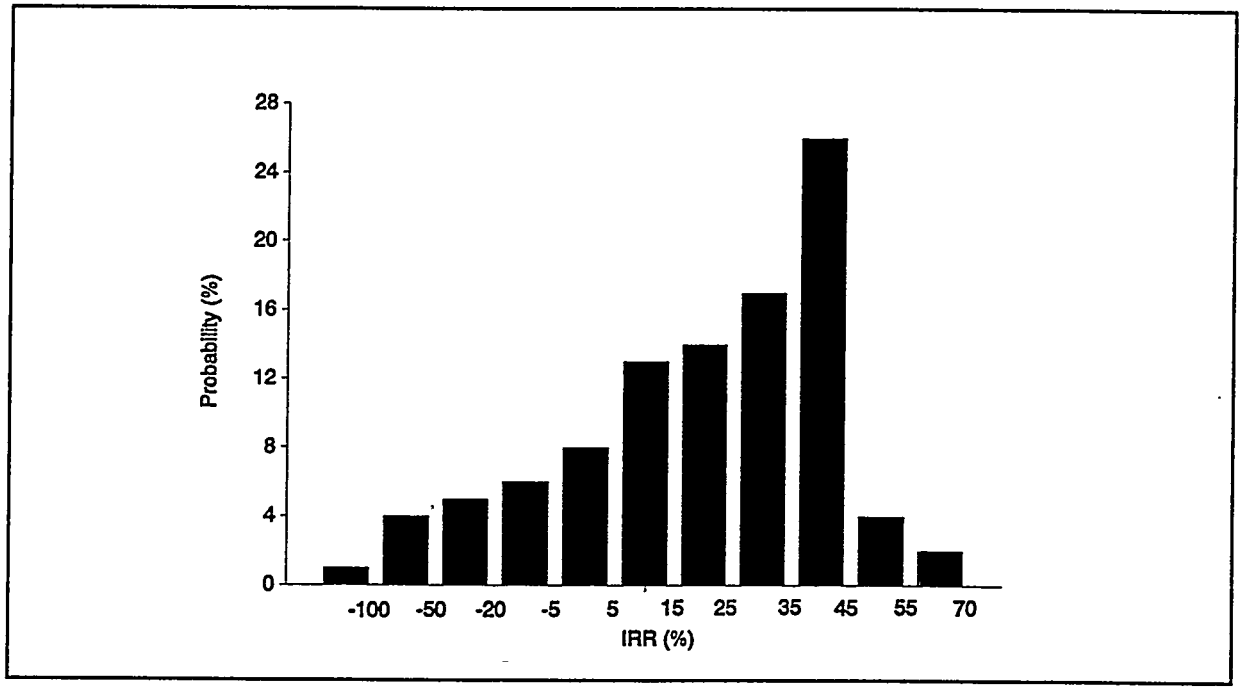

Figure 152. Probability Density Distribution Histogram of Internal Rate of Return (%) (Alternative 2, Internal Rate of Return mode)

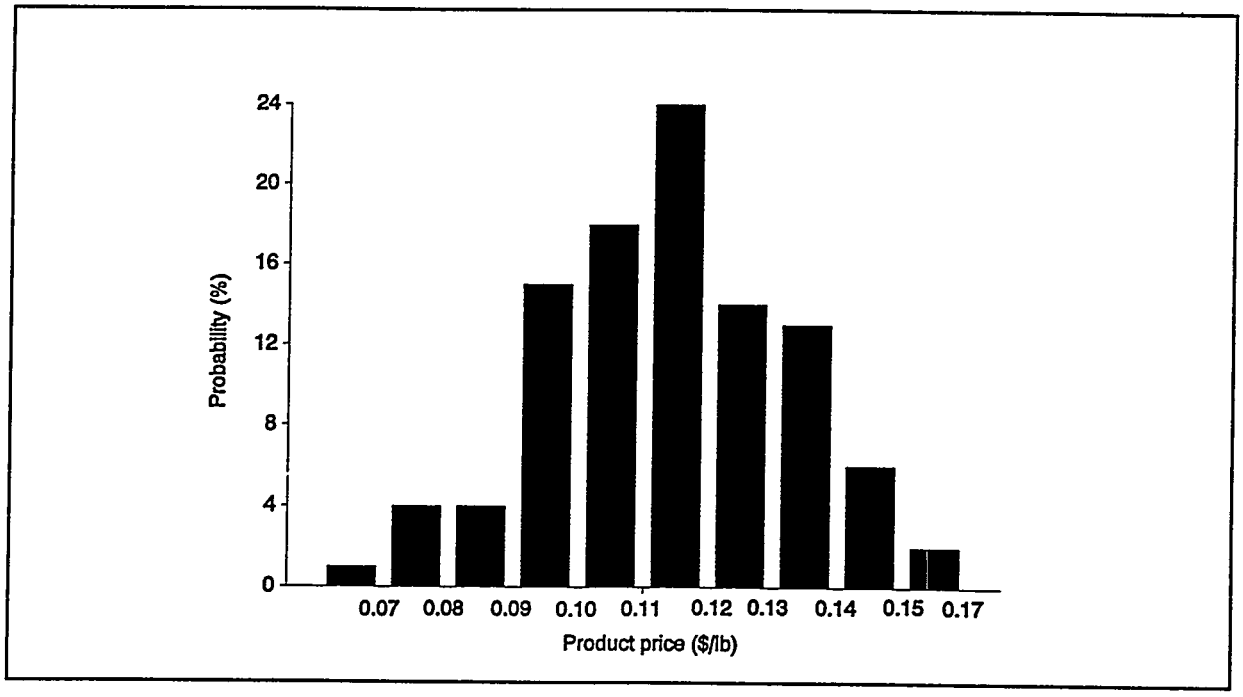

Figure 153. Probability Density Distribution Histogram of Initial Product Price ($/lb) (Alternative 2, Product Price Mode)

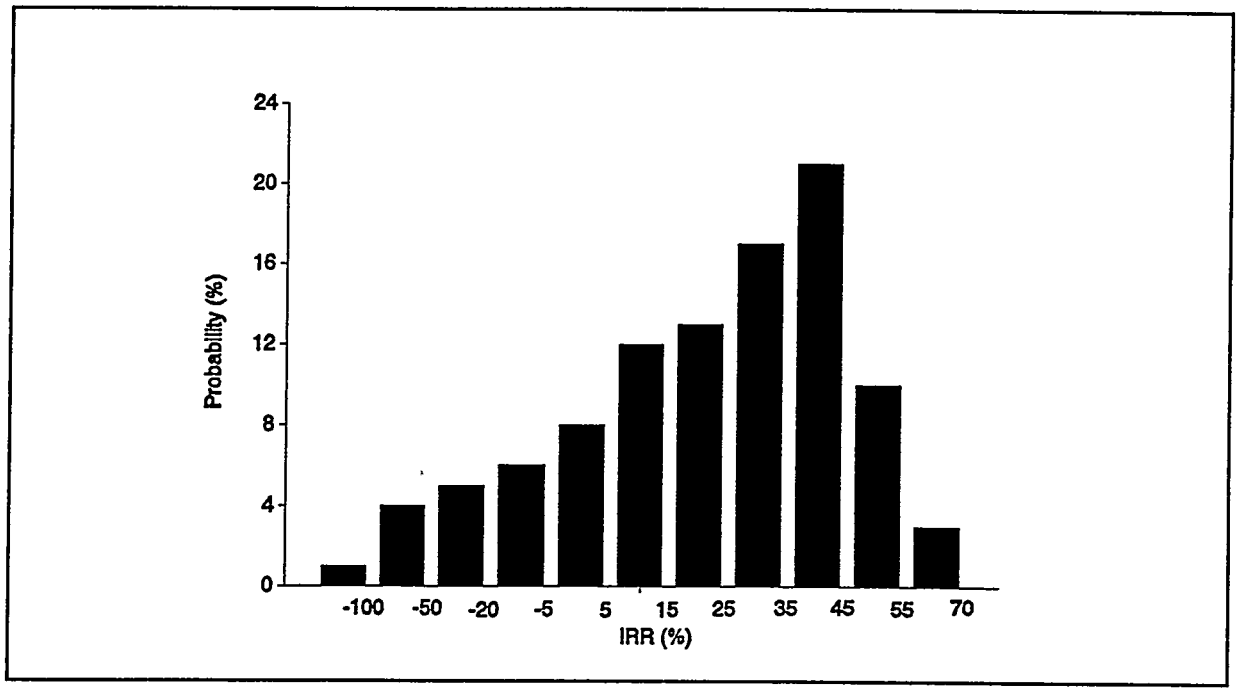

Figure 154. Probability Density Distribution Histogram of Internal Rate of Return (%) (Alternative 3, Internal Rate of Return mode)

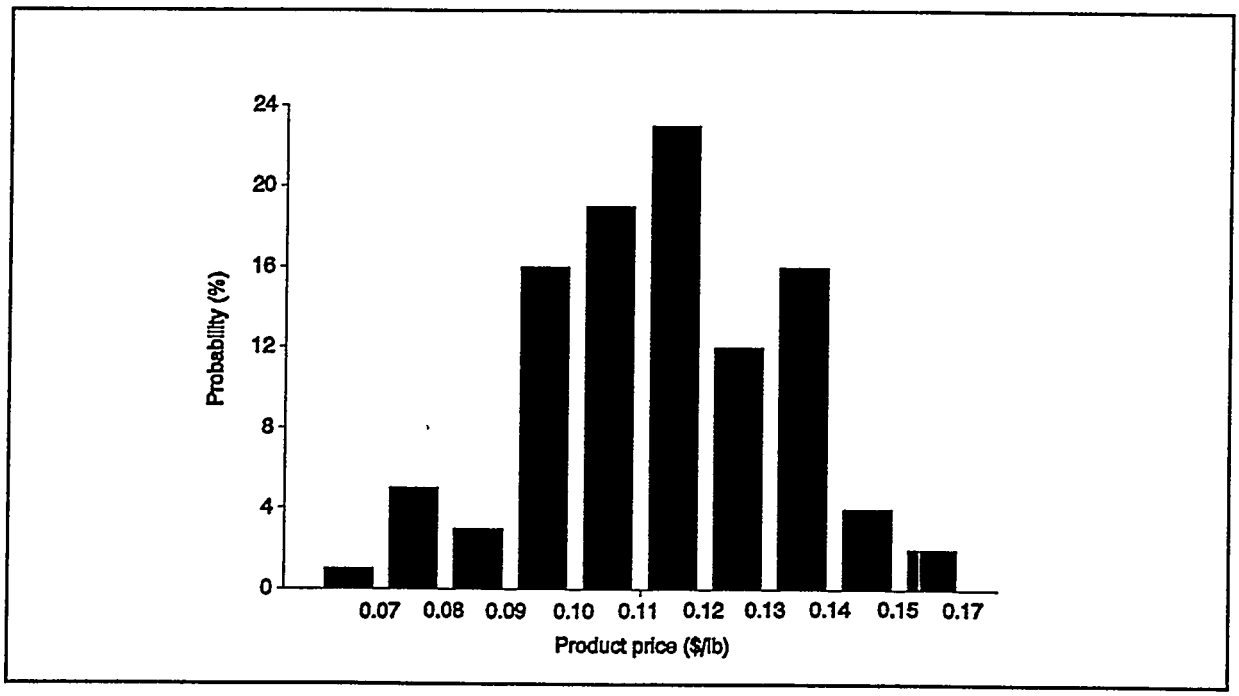

Figure 155. Probability Density Distribution Histogram of Internal Rate of Return (%) (Alternative 3, Internal Rate of Return mode)

REFERENCES

1. Oblad, A.G., Bunger, J.W., Dahlstrom, D.A., Deo, M.D., Hanson, F.V., Miller, J.D., and Seader, J.D., 1992 Final Report, The Extraction of Bitumen from Western Oil Sands, Contract No.: DE-FC21-89MC26268, August.

2. Cashion, W.B., 1967, Geology and Fuel Resources of the Green River Formation, Southeastern Uinta Basin, Utah and Colorado, U.S. Geol. Survey Prof. Paper. 548, 48p.

3. Gwynn, J.W., 1971, Instrumental Analysis of Tars and Their Correlations in Oil-Impregnated Sandstone Beds, Uintah and Grand Counties, Utah, Utah Geol. Miner. Survey, Special Studies, 37, 64pp.

4. Kayser, R.B., 1966, Bituminous Sandstone Deposits, Asphalt Ridge, Utah Geol. Miner. Survey, Special Studies, 19, 62pp.

5. Byrd, W.D., II, 1970, PR Spring Oil-Impregnated Sandstone Deposit, Uintah and Grand Counties, Utah, Utah Geol. Minerog. Survey, Special Studies, 31, 34pp.

6. Ritzma, H.R., 1979, Oil-Impregnated Rock Deposits of Utah, Utah Geol. Miner. Survey, Map 47, 2pp.

7. Campbell, J.A., and Ritzma, H.R., 1979, Geology and Petroleum Resources of the Major Oil Impregnated Sandstones Deposits of Utah, Utah Geol. and Miner Survey, Special Studies 50, 25pp.

8. Dahm, J.N., 1981, Tar Sand Reserves - PR Spring Deposit Uintah and Grand Counties, Utah, UEES, Phase I: Final Report, University of Utah, Salt Lake City, Utah.

9. Clem, K.M., 1984, Economic Potential of the PR Spring Oil-Impregnated Deposit, Uinta Basin, Utah; Utah Geol. Miner. Survey, Special Studies 65, 38pp.

10. Sinks, D.J., 1985, Geologic Evaluation and Reservoir Properties of the PR Spring Tar Sand Deposit, Uintah and Grand Counties, Utah, Final Report U.S. DOE DOE/FE/60177-1883.

11. Wood, R.E., and Ritzma, H.R., 1972, Analyses of Oil Extracted from Oil-Impregnated Sandstone Deposits in Utah, Utah Geol. Miner. Survey, Special Studies 39, 19pp.

12. Hanson, F.V., 1982, PR Spring Oil Sand Sample Provided by U-Tar, Inc., to University of Utah Oil Sand Research and Development Group for Characterization Studies.

13. Kuuskraa, V.A., and Hammershaimb, E.C., 1984, Major Tar Sand and Heavy Oil Deposits of the United States, Interstate Oil Compact Comm., Oklahoma City, Oklahoma.

14. Newell, E., 1993, Oilsands Play Larger Role in Canadian Oil Production, Oil & Gas J., 91 (31), 25-30.

15. Tsai, C.H., Deo, M.D., Hanson, F.V., and Oblad, A.G., 1991, Characterization and Potential Utilization of Whiterocks (Utah) Tar Sand Bitumen, Fuel Sci. Tech. Internat. 9, 1259-1286.

16. Tsai, C.H., Deo, M.D., Hanson, F.V., and Oblad, A.G., 1992, Characterization and Potential Utilization of Whiterocks (Utah) Tar Sand Bitumen II Pyrolysis Mass Spectrometry and Nuclear Magnetic Resonance Analyses, Fuel Sci. Tech. Int'l. 10, 1437-1459.

17. Tsai, C.H., Longstaff, D.C., Deo, M.D., Hanson, F.V., and Oblad, A.G., 1992, Characterization and Potential Utilization of Hydrotreated Products from the Whiterocks (Utah) Tar Sand Bitumen-Derived Liquid, FUEL 71, 1473-1482.

18. Bukka, K., Miller, J.D., Hanson, F.V., Misra, M., and Oblad, A.G., 1993, The Influence of Carboxylic Acid Content on Bitumen Viscosity, Fuel (in press).

19. Ritzma, H.R., 1980, Oil-Impregnated Sandstone Deposits, Circle Cliffs Uplift (Utah). Utah Geol. Assoc., Henry Mountains Symp., 343.

20. Bukka, K., Miller, J.D., Hanson, F.V., and Oblad, A.G., 1991, Miner Matter Distribution During the Hot Water Processing of Utah Tar Sand, AOSTRA J. Res. 7, 101-109.

21. Bukka, K., Miller, J.D., and Oblad, A.G., 1991, Fractionation and Characterization of Utah Tar Sand Bitumens: Influence of Chemical Composition on Bitumen Viscosity, Energy & Fuels 5, 333-340.

22. Bukka, K., Miller, J.D., Hanson, F.V., and Oblad, A.G., 1992, Fractionation and Characterization of Whiterocks Tar Sand Bitumens, Energy & Fuels, 6, 160-165.

23. Miller, J.D., and Misra, M., 1982, Hot Water Process Development for Utah Tar Sands, Fuel Proc. Tech. 6, 27-59.

24. Oblad, A.G., Bunger, J.W., Hanson, F.V., Miller, J.D., Ritzma, H.R., and Seader, J.D., 1987, Tar Sand Research and Development at the University of Utah, Ann. Rev. Energy 12, 283-356.

25. Oblad, A.G., Seader, J.D., Miller, J.D., and Bunger, J.W., 1976, Recovery of Bitumen from Oil-Impregnated Sandstone Deposits of Utah, AIChE Symp. Ser. No.155, Oil Shale and Tar Sands, 72, 69-77.

26. Shun, D., 1990, The Pyrolysis of Bitumen-Impregnated Sandstone from the Circle Cliffs (Utah) Deposit in a Fluidized-Bed Reactor. Ph.D. Dissertation, University of Utah, Salt Lake City, Utah.

27. Bunger, J.W., Thomas, K.P., and Dorrence, S.M., 1979, Compound Types and Properties of Utah and Athabsca Tar Sand Bitumens, FUEL 58, 183-195.

28. Speight, J.G., and Moschopedis, S.E., 1981, Anomalous Effects in the Character of the Carbonyl Absorptions (Ca. 1700 cm^{-1}) in the Infrared Spectra of Petroleum Resins and Asphaltenes., Am. Chem. Soc., Prprnt. Div. Petrol. Chem. 26, 907-911.

29. Hupka, J., Miller, J.D., and Cortez, A., 1983, Importance of Bitumen Viscosity in the Hot Water Processing of Domestic Tar Sands, Mining Eng. 35, 1635-1641.

30. Hupka, J., Oblad, A.G., and Miller, J.D., 1987, Diluent-Assisted Hot-Water Processing of Tar Sands, AOSTRA J. Res. 3, 95-102.

31. Bowman, C.W., 1967, Molecular and Interfacial Properties of Athabasca Tar Sands, Proc. of the 7th World Petrol. Cong., 3, 583-604 Elsevier Publishing Co., Amsterdam.

32. Isaacs, E.E., and Smolek, K.F., 1983, Interfacial Tension Behavior of Athabasca Bitumen/Aqueous Surfactant Systems, Can. J. Chem. Eng. 61, 233-240.

33. Potoczny, Z.M., Vargha-Butler, E.I., Zubovits, T.K., and Neumann, A.W., 1984, Surface Tension of Bitumen, AOSTRA J. Res. 1, 105-120.

34. Vargha-Butler, E.I., Zubovits, T.K., Budziak, C.J., Neumann, A.W., and Potoczny, Z.M., 1988, Surface Tension of Bitumen from Contact Angle Measurements on Films of Bitumen, Energy & Fuels 2, 653-656.

35. Neumann, A.W., Good, R.J., Hope, C.J., and Sejpal, M., 1974, An Equation-of-State Approach to Determine Surface Tensions of Low-Energy Solids from Contact Angles, J. Colloid Interfac. Sci. 49, 67-79.

36. Schramm, L.L., and Smith, R.G., 1987, Two Classes of Anionic Surfactants and Their Significance in Hot Water Processing of Oil Sands, Can. J. Chem. Eng. 65, 799-811.

37. Schramm, L.L., and Smith, R.G., 1985, The Influence of Natural Surfactant on Interfacial Charges in the Hot Water Process for Recovering Bitumen from the Athabasca Oil Sands, Colloids Surf. 14, 67-79.

38. Hupka, J., and Miller, J.D., 1991, Electrophoretic Characterization and Processing of Asphalt Ridge and Sunnyside Tar Sands, Internat. J. Miner Proc. 31, 217-231.

39. Hupka, J., White, R.R., Yang, J.Y., Drelich, J., Miller, J.D., Hanson, F.V., and Oblad, A.G., 1994, Residual Solvent Effect on the Viscosity of the Bitumen Extracted from the Whiterocks Oil Sand, AOSTRA J. Res., (in press).

40. Adamson, A.W., 1990, Physical Chemistry of Surfaces, John Wiley & Sons, Inc., New York.

41. Jasper, J.J., and Kring, E.V., 1955, The Isobaric Surface Tensions and Thermodynamic Properties of the Surfaces of a Series of n-Alkanes, C_5 to C_{18}, 1-Alkanes, C_6 to C_{16}, and of n-Decylcyclopentane, n-Decylcyclohexane and n-Decylbenzene, J. Phys. Chem. 59, 1019-1021.

42. Arneodo, C., Baszkin, A., Benoit, J.P., Fellous, R., and Thies, C., 1988/1989, Interfacial Studies of Essential Oil-Water Systems, Colloids Surf. 34, 159-169.

43. Speight, J.G., 1991, The Chemistry and Technology of Petroleum, Marcel Dekker, Inc., New York.

44. Girifalco, L.A., and Good, R.J., 1957, A Theory for the Estimation of Surface and Interfacial Energies. I. Derivation and Application to Interfacial Tension, J. Phys. Chem. 61, 904-909.

45. Li, D., and Neumann, A.W., 1990, A Reformulation of the Equation-of-State for Interfacial Tensions, J. Colloid Interface Sci. 137, 304-307.

46. van Oss, C.J., Good, R.J., and Chaudhury, M.K., 1988, Additive and Nonadditive Surface Tension Components and the Interpretation of Contact Angles, Langmuir 4, 884-891.

47. Kloubek, J., 1992, Development of Methods for Surface Free Energy Determination Using Contact Angles of Liquids on Solids, Adv. Colloid Interface Sci. 38, 99-142.

48. Spelt, J.K., 1990, Solid Surface Tension: The Use of Thermodynamic Models to Verify Its Determination from Contact Angles, Colloids Surf. 43, 389-411.

49. Spelt, J.K., Absolom, D.R., and Neumann, A.W., 1986, Solid Surface Tension: The Interpretation of Contact Angles by the Equation-of-State Approach and the Theory of Surface Tension Components, Langmuir 2, 620-625.

50. Schurch, S., and McIver, D., 1981, Interfacial Tensions at Lipid-Water Interfaces. Comparison of Equation-of-State Predictions with Direct Experimental Measurements, J. Colloid Interface Sci. 83, 301-304.

51. Omenyi, S.N., Smith, R.P., and Neumann, A.W., 1980, Determination of Solid/Melt Interfacial Tensions and of Contact Angles of Small Particles from the Critical Velocity of Engulfing, J. Colloid Interface Sci. 75, 117-125.

52. Spelt, J.K., and Neumann, A.W., 1988, Surface Tension Components: Comments to van Oss, C.J., Good, R.J., and Chaudbury, M.K. [J. Colloid Interfac. Sci. 111, 378-390 (1986)], J. Colloid Interfac. Sci. 122, 294-297.

53. Fowkes, F.M., 1964, Attractive Forces at Interfaces, Ind. Eng. Chem. 56, 40-52.

54. Strom, G., Fredriksson, M., and Stenius, P., 1987, Contact Angles, Work of Adhesion, and Interfacial Tensions at a Dissolving Hydrocarbon Surface, J. Colloid Interface Sci. 119, 352-361.

55. Janczuk, B., Chibowski, E., and Bialopiotrowicz, T., 1984, Interpretation of the Contact Angle in Quartz/Organic Liquid Film-Water System, J. Colloid Interface Sci. 102, 533-538.

56. Fox, H.W., and Zisman, W.A., 1950, The Spreading of Liquids on Low Energy Surfaces. I. Polytetrafluoroethylene, J. Colloid Sci. 5, 514-531.

57. Zisman, W.A., 1972, Surface Energetics of Wetting, Spreading, and Adhesion, J. Paint. Technol. 44, 41-57.

58. Zisman, W.A., 1964, Relation of the Equilibrium Contact Angle to Liquid and Solid Constitution, Adv. Chem. Ser. 43, 1-51.

59. Bernett, M.K., and Zisman, W.A., 1959, Wetting of Low-Energy Solids by Aqueous Solutions of Highly Fluorinated Acids and Salts, J. Phys. Chem. 63, 1911-1916.

60. Murphy, W.J., Roberts, M.W., and Ross, J.R.H., 1972, Contact Angle Studies of Low Energy Polymer Surfaces, J. Chem. Soc., Faraday Trans. I 68, 1190-1199.

61. Finch, J.A., and Smith, G.W., 1979, Contact Angle and Wetting, Miners Sci. Eng. 11, 36-63.

62. Good, R.J., 1964, Estimation of Surface and Interfacial Energies. VI. Surface Energies of Some Fluorocarbon Surfaces from Contact Angle Measurements, Adv. Chem. Ser. 43, 74-87.

63. Rhee, S.K., 1973, Surface Tension of Low-Energy Solids, J. Colloid Interface Sci. 44, 173-174.

64. Good, R.J., and Girifalco, L.A., 1960, A Theory for the Estimation of Surface and Interfacial Energies. III. Estimation of Surface Energies of Solids from Contact Angle Data, J. Phys. Chem. 64, 561-565.

65. Fowkes, F.M., 1962, Determination of Interfacial Tensions, Contact Angles, and Dispersion Forces in Surfaces by Assuming Additivity of Intermolecular Interactions in Surfaces, J. Phys. Chem. 66, 382-386.

66. Tamai, Y., Maknuuchi, K., and Suzuki, M., 1967, Experimental Analysis of Interfacial Forces at the Plane Surface of Solids, J. Phys. Chem. 71, 4176-4179.

67. Papirer, E., Kuczinski, J., and Siffert, B., 1987, Surface Properties of Distillation Residues from Heavy Oils-Influence of Viscoreduction, FUEL 66, 1691-1693.

68. Franses, E.I., Pulg, J.E., Talmon, Y., Miller, W.G., Scriven, L.E., and Davis, H.T., 1980, Roles of Liquid Crystals and Micelles in Lowering Interfacial Tension, J. Phys. Chem. 84, 1547-1556.

69. Rubin, E., and Radke, C.J., 1980, Dynamic Interfacial Tension Minima in Finite Systems, Chem. Eng. Sci. 35, 1129-1138.

70. Khulbe, K.C., Neale, G., and Hornof, V., 1987, Effects of Cations on the Interaction of Alkaline Agents with Heavy Oils, J. Colloid Interface Sci. 117, 578-581.

71. Borwankar, R.P., and Wasan, D.T., 1986, Dynamic Interfacial Tensions in Acidic Crude Oil/Caustic Systems, AIChE J. 32, 455-476.

72. Nasr-El-Din, H.A., and Taylor, K.C., 1992, Dynamic Interfacial Tension of Crude Oil/Alkali/Surfactant Systems, Colloids Surf. 66, 23-37.

73. Cambridge, V.J., Wolcott, J.M., and Constant, W.D., 1989, An Investigation of the Factors Influencing Transient Interfacial Tension Behavior in Crude Oil/Alkaline Water Systems, Chem. Eng. Comm. 84, 97-111.

74. Peru, D.A., and Lorenz, P.B., 1989, The Effect of Equilibration Time and Temperature on Drop-Drop Coalescence of Wilmington Crude Oil in a Weakly Alkaline Brine, Chem. Eng. Comm. 77, 91-114.

75. Peters, R.A., 1931, Interfacial Tension and Hydrogen-Ion Concentration, Proc. Royal Soc. (London) A133, 140-154.

76. Dunning, H.N., Moore, J.W., and Denekas, M.O., 1953, Interfacial Activities and Porphyrin Contents of Petroleum Extracts, Ind. Eng. Chem. 45, 1759-1765.

77. Jang, L.K., Sharma, M.M., Chang, Y.I., Chan, M., and Yen, T.F., 1982, Correlation of Petroleum Component Properties for Caustic Flooding, AIChE Symp. Ser. 78 (212), 97-104.

78. Trujillo, E.M., 1983, Dynamic Interfacial Tensions Between Crude Oils and Caustic Solutions, Soc. Petrol. Eng. J. 8, 645-656.

79. Acevedo, S., Escobar, G., Gutierrez, L., and Rivas, H., 1992, Isolation and Characterization of Natural Surfactants from Extra Heavy Crude Oils, Asphaltenes and Maltenes. Interpretation of Their Interfacial Tension-pH Behaviour in Terms of Ion Pair Formation, FUEL 71, 619-623.

80. Chan, M., Sharma, M.M, and Yen, T.F., 1982, Generation of Surface Active Acids in Crude Oil for Caustic Flooding Enhanced Oil Recovery, Ind. Eng. Chem. Proc. Des. Dev. 21, 580-583.

81. Chiwetelu, C.I., Hornof, V., and Neale, G.H., 1989, Interaction of Aqueous Caustic with Acidic Oils, J. Can. Petrol. Tech. 28, 71-78.

82. Seifert, W.K., and Howells, W.G., 1969, Interfacially Active Acids in a California Crude Oil. Isolation of Carboxylic Acids and Phenols, Anal. Chem. 41, 554-562.

83. Misra, M., Aguilar, R., and Miller, J.D., 1981, Surface Chemistry Features in the Hot Water Processing of Utah Tar Sand, Sep. Sci. Tech. 16, 1523-1544.

84. Sanford, E.C., and Seyer, F.A., 1979, Processibility of Athabasca Tar Sand Using a Batch Extraction Unit: The Role of NaOH, CIM Bull. 72, 164-169.

85. Cratin, P.D., and Dean, A.M., 1966, Interfacial Activities of Crude Oil Surfactants: A Mathematical Approach to Mixed Films, J. Alabama Acad. Sci. 37, 228-245.

86. de Malherbe, R., Doswll, S.J., Mamalis, A.G., and de Malherbe, M.C., 1983, Synthetic Crude from Oil Sands, Fortschritt-Berichte der VDI Zeitschriften, VDI-Verlag, Berlin.

87. Hupka, J., and Miller, J.D., 1991, Moderate-Temperature Water-Based Bitumen Recovery from Tar Sand, FUEL 70, 1308-1312.

88. Hupka, J., Drelich, J., Miller, J.D., White, R.R., Hanson, F.V., and Oblad, A.G., 1991, Impact of Water Recycle on Water-Based Processing of Whiterocks Tar Sand, FUEL 70, 1313-1316.

89. Cutler, W.G., and Davis, R.C., 1972, Detergency. Theory and Test Methods, Marcel Dekker, Inc., New York.

90. Laskowski, J.S., and Pugh, R.J., 1992, Dispersions Stability and Dispersing Agents, in Colloid Chemistry in Mineral Processing, eds. Laskowski, J.S., and Ralston, J., Elsevier, Amsterdam, p.115-171.

91. Chan, M., and Yen, T.F., 1982, A Chemical Equilibrium Modél for Interfacial Activity of Crude Oil in Aqueous Alkaline Solution. The Effects of pH, Alkali and Salt, Can. J. Chem. Eng. 60, 305-308.

92. Ruckenstein, E., and Rao, I.V., 1987, Interfacial Tension of Oil-Brine Systems in the Presence of Surfactant and Cosurfactant, J. Colloid Interface Sci. 117, 104-119.

93. Caminati, G., Senatra, D., and Gabrielli, G., 1991, 1-Hexanol and 1-Tetradecanol Adsorption at the Water-Oil Interface, Langmuir 7, 1969-1974.

94. Gannon, M.G.J., and Faber, T.E., 1978, The Surface Tension of Nematic Liquid Crystals, Phil. Mag. A37, 117-135.

95. Takamura, K., and Chow, R.S., 1985, The Electric Properties of the Bitumen/Water Interface, Colloids Surf. 15, 35-48.

96. Wen, W.W., and Sun, S.C., 1981, An Electrokinetic Study on the Oil Flotation of Oxidized Coal, Sep. Sci. Tech. 16, 1491-1521.

97. Woods, D.R., and Diamadopoulos, E., 1982, Importance of Surfactants and Surface Phenomena on Separating Dilute Oil-Water Emulsions and Dispersions, in Surfactants in Chemical/Process Engineering, eds. Wasan, D.T., Ginn, M.E., and Shah, D.O., Marcel Dekker, Inc., New York, 369-539.

98. Carbini, P., Ciccu, R., Ghiani, M., and Satta, F., 1992, Agglomeration of Coals of Different Rank Using Mixtures of Oils, Coal Prep. 11, 11-19.

99. Stachurski, J., and Michalek, M., 1985, The Zeta Potential of Emulsion Droplets of the Aliphatic Hydrocarbons in Aqueous Solutions, Colloids Surf. 15, 255-259.

100. Hunter, R.J., 1981, Zeta Potential in Colloid Science, Principles and Applications, Academic Press, London.

101. Sepulveda J., and Miller J.D., 1979, Separation of Bitumen from Utah Tar Sands by a Hot Water Digestion-Flotation Technique, Mining Eng. 30, 1311.

102. Takamura K., and Chow R.S., 1983, A Mechanism for Initiation of Bitumen Displacement from Oil Sand, J. Can. Petrol. Tech. 22(6), 1-9.

103. Takamura K., 1982, Microscopic Structure of Athabasca Oil Sand, Can. J. Chem. Eng. 60(8), 538-545.

104. Drelich, J., 1993, The Role of Wetting Phenomena in the Hot Water Process for Bitumen Recovery from Tar Sand, Ph.D. Dissertation, University of Utah, Salt Lake City, Utah.

105. Drelich, J., Hupka, J., Miller, J.D., and Hanson, F.V., 1994, Water Recycle in Moderate-Temperature Bitumen Recovery from Whiterocks Tar Sands, AOSTRA J. Res., (in press).

106. Hupka J., and Miller J.D., Feb. 24-27, 1992, Tar Sands Pretreatment with Diluent, 121st SME Annual Meeting, Phoenix, Arizona, Prprnt. 92-122.

107. Liétard O., and Daccord G., 1989, Acid Wormholing in Carbonate Reservoirs, Chapter 34 in Oil-Field Chemistry. Enhanced Recovery and Production Stimulation, Ed. by J.K.Borchardt and T.F.Yen, ACS Symp. Ser. 396, ACS, Washington, DC.

108. Claridge, E.L., Edwards, G., and Smith, J.R., 1971, Recovery of Tar from Tar Sands, U.S. Pat. No. 3,553,098.

109. Leja, J., and Bowman, C.W., 1968, Application of Thermodynamics to the Athabasca Tar Sands, Can. J. Chem. Eng. 46, 479-481.

110. Israelachvili, J.N., 1992, Adhesion, Friction and Lubrication of Molecularly Smooth Surfaces, in Fundamentals of Friction: Macroscopic and Microscopic Processes, Eds. Singer, I.L., and Pollock, H.M., Kluwer Academic Publ., London, pp.351-381.

111. Dobby G.S. and Finch J.A., 1991, Column Flotation: A Selected Review, Part II, Mineral Eng. 4, 911-923.

112. Yoon R.H., Lutterell G.H., Adel G.T. and Mankosa M.J., 1989, Recent Advances in Fine Coal Flotation, Proc. of Eng. Found. Conf. Advances in Coal and Mineral Processing Using Flotation, pp.211-218, Palm Coast, Florida, Dec. 3-8.

113. Benett G.F., 1988, The Removal of Oil from Wastewater by Air Flotation: A Review, CRC Crit. Rev. Env. Cont. 18, 189-253.

114. Sada E., Yasunishi A., Katoh S., and Nishioka M., 1978, Bubble Formation in Flowing Liquid, Can. J. Chem. Eng. 56, 662-672.

115. Tsuga H., Hibino S., and Nojima U., 1981, Volume of a Bubble Formed at a Single Submerged Orifice in a Flowing Liquid, Int. Chem. Eng. 21, 630-636.

116. Johnson, B.D., Gershey, R.M., Cooke, R.C., and Sutchiffe W.H., 1982, A Theorethical Model for Bubble Formation at a Frit Surface in a Shear Field, Sep. Sci. Tech. 17, 1027-1039.

117. Johnson, B.D. and Gershey, R.M., 1991, Bubble formation at a Cylindrical Frit Surface in a Shear Field, Chem. Eng. Sci. 46 (10), 2756-2759.

118. Miller, J.D. and Kinneberg, D.J., March 1984, Fast Flotation in an Air-Sparged Hydrocyclone, Proc. of MINTEK 50, 1, 373-383, South Africa.

119. Miller, J.D. and Ye, Y., 1989, Froth Characteristics in Air-Sparged Hydrocyclone Flotation, Miner. Proc. Extr. Metall. Rev. 5, 307-329.

120. Saxena, S.C., Patel, D., Smith, D.N. and Reuther, J.A., 1988, An Assessment of Experimental Techniques for the Measurement of Bubble Size in a Bubble Slurry Reactor as Applied to Indirect Coal Liquefaction, Chem. Eng. Comm., 63, 87-121.

121. Miller, J.D., Das, A., Leliński, D. and Chamblee, J.W, September 1993, Multiphase Flow Characteristics of Gas Sparged Hydrocyclone Deinking, Proc. of 1993 TAPPI Eng. Conf., 20-23, (in press).

122. Woods, J. R., Kumar, A., Sparks, B.D. and Kotlyar, L.S., 1987, Use of a Density Meter for Analysis of Process Streams Obtained During Solvent Extraction of Bitumen from Athabasca Oil Sands, AOSTRA J. Res. 3, 183.

123. Sawinsky, J., Deak, A. and Havas, G., 1979, Power Consumption of Screw Agitators in Newtonian Liquids of High Viscosity, Chem. Eng. Sci. 34, 1160.

124. Geiger, G.H., and Poirier, D.R., 1973, Transport Phenomena in Metallurgy, Addison-Wesley, Reading, Massachusetts.

125. Bird, R.B., Stewart, W.E. and Lightfoot, E.N., 1960, Transport Phenomena, John Wiley, New York, p. 205.

126. Coronella, C. J. and Seader, J. D., 1992, Combustion of Coked Sand in a Two-Stage Fluidized Bed System, FUEL 71, 143-150.

127. Smart, L. M., 1984, Thermal Processing of Utah Tar Sands, M.S. Thesis, University of Utah, Salt Lake City, Utah.

128. Peterson, W. S. and Gishler, P. E., 1951, The Fluidized Solids Technique Applied to Alberta Oil Sands Problem, 207-236, Proc. First Alberta Oil Sands Conf., Edmonton, Alberta, Canada.

129. Seader, J. D. and Jayakar, K. M., 1979, Process and Apparatus to Produce Crude Oil from Tar Sands, U.S. Pat. No. 4,160,720.

130. Jayakar, K. M., 1979, Thermal Recovery of Oil from Tar Sands, Ph.D. Dissertation, University of Utah, Salt Lake City, Utah.

131. Bezama, R. J., 1983, An Energy Efficient Method for Thermal Processing of Utah Tar Sands, Ph.D. Dissertation, University of Utah, Salt Lake City, Utah.

132. Hsu, J. C. L. and Seader, J. D., 1989, Digital Control of a Coupled Fluidized-Bed Thermal Processing System for Tar Sands. Fuel. Processing Technol., 21, 1-17.

133. Coronella, C. J., 1989, Modelling a Coupled Fluidized-Bed Reactor for Extraction of Bitumen from Tar Sands, M.S. Thesis, University of Utah, Salt Lake City, Utah.

134. Fletcher, J. V., 1992, The Pyrolysis of Oil Sands in a Fluidized Bed at Reduced Pressure, Ph.D. Dissertation, University of Utah, Salt Lake City, Utah.

135. Grace, J. R., 1986, Modelling and Simulation of Two-Phase Fluidized Bed Reactors. in Chemical Reactor Design, (Ed. H. deLasa), Martinus Nijhof, den Haag, Netherlands.

136. Darton, R. C., LaNauze, R. D., Davidson, J. F., and Harrision, D., 1977, Bubble Growth Due to Coalescence in Fluidised Beds. Trans. Instn. Chem. Engrs. 55, 274.

137. Stubington, J. F., Barrett, D. and Lowry, G., 1984, Bubble Size Measurements and Correlation in a Fluidised Bed at High Temperatures, Chem. Eng. Res. Des. 62, 173.

138. Davidson, J. F., and Harrison, D., 1963, Fluidised Particles, Cambridge University Press, Cambridge, England.

139. Barbour, R. V., Dorrence, S. M., Vollmer, T. L., and Harris, J. D., 1976, Pyrolysis of Utah Tar Sands - Products and Kinetics, Amer. Chem. Soc., Prprnt. Div. Fuel Chem., 21 (6), 278.

140. Hayashitani, M., Bennion, D. W., Donnelly, J. K., and Moore, R. G., 1977, Thermal Cracking of Athabasca Bitumen, The Oil Sands of Canada-Venezuela Symposium, CIM Special Publication 17, 233.

141. Phillips, C. R., Haidar, N. I., and Poon, Y. C., 1985, Kinetic Models for the Thermal Cracking of Athabasca Bitumen, FUEL 64, 678.

142. Yoshiki, K. S., and Phillips, C. R., 1985, Kinetics of the Thermo-Oxidative and Thermal Cracking Reactions of Athabasca Bitumen, FUEL 64, 1591.

143. Lin, L. C., Hanson, F. V., and Oblad, A. G., 1989, Mathematical Model of the Pyrolysis of Bitumen-Impregnated Sandstone Particles. 1. Diffusion Dominant Transport Regime, Fuel Proc. Tech. 22, 41.

144. Lin, L. C., Deo, M. D., Hanson, F. V., and Oblad, A. G., 1990, Kinetics of Tar Sand Pyrolysis Using a Distribution of Activation Energy Model, AIChE J. 36, 1585.

145. Cha, S., 1991, Pyrolysis of Oil Sands from the Whiterocks Tar Sand Deposit in a Rotary Kiln, Ph.D. Dissertation, University of Utah, Salt Lake City, Utah.

146. API, 1966, Technical Data Book- Petroleum Refining, Amer. Petrol. Inst., New York.

147. Molerus, O., 1993, Arguments on Heat Transfer in Gas Fluidized Beds, Chem. Eng. Sci. 48, 761.

148. Kunii, D. and Levenspiel, O., 1991, Fluidization Engineering, Butterworths, Boston.

149. Wender, L., and Cooper, G. T., 1958, Heat Transfer between Fluidized-Solids Beds and Boundary Surfaces- Correlation of Data, AIChE J. 4, 15.

150. Coyle, T. D., 1982, Silica, Encyclopedia of Chemical Technology, Kirk, R.E. and Othmer, D.F., eds., John Wiley & Sons, Inc., New York, 20, p. 757.

151. Dunn, P. and Reay, D. A., 1982, Heat Pipes, Pergamon Press Ltd., Elmsford, New York.

152. Dorius, J.C., 1985, The Pyrolysis of Bitumen-impregnated Sandstone from the PR Spring (Utah) Deposit in a Fluidized Bed, Ph.D. Dissertation, University of Utah, Salt Lake City, Utah.

153. Reid, R. C, Prausnitz, J. M., and Poling, B. E., 1987, The Properties of Gases and Liquids, McGraw Hill, Inc., New York.

154. Bohl, A. H. and McAvoy, T. J., 1976, Linear Feedback versus Time Optimal Control, II. The Regulator Problem. Ind. Eng. Chem. Proc. Des. Dev. 15, 30-33.

155. Rivera, D. E., Morari, M., and Skogestad, S., 1986, Internal Model Control. 4. PID Controller Design, Ind. Eng. Chem. Proc. Des. Dev. 25, 252-265.

156. McMillan, G. K., 1986, Advanced Control Algorithms: Beware of False Prophecies, Ing. Tech. 33, 55-57.

157. McMillan, G. K., 1990, Tuning and Control Loop Performance, Instrument Soc. of America, Research Triangle Park, North Carolina.

158. Smith, C. L., 1972, Digital Computer Process Control, Intext Educational Publ., San Francisco, California.

159. Saxena, S. G. and Ganzha, V. L., 1985, Dependence of Heat-Transfer Coefficient for Immersed Surfaces in a Gas-Fluidized Bed on Pressure, Powder Tech. 44, 115.

160. Seborg, D. E., Edgar, T. F. and Mellichamp, D. A., 1989, Process Dynamics and Control, John Wiley & Sons, Inc., New York.

161. Chien, I. L. and Fruehauf, P. S., 1990, October, Consider IMC Tuning to Improve Controller Performance, Chem. Eng. 86 (10) 33-41.

162. Rotstein, G. E. and Lewin, D. R., 1991, Simple PI and PID Tuning for Open-Loop Unstable Systems, Ind. Eng. Chem. Res. 30, 1864-1869.

163. Chang, J. W. and Yu, C. C., 1992, Failure Conditions for Inverse-Based Multivariable Controllers: Internal Model Control Structure, Chem. Eng. Sci. 47, 2047-2056.

164. Morari, M. and Zafiriou, E., 1989, Robust Process Control, Prentice-Hall, Englewood Cliffs, New Jersey.

165. Chien, I. L., 1988, IMC-PID Controller Design - An Extension, IFAC Symp. Adaptive Control Chem. Proc., Copenhagen, Denmark, 147-151.

166. Zabrodsky, S. S., Antonishin, N. V. and Parnas, A. L., 1976, On Fluidized Bed-To-Surface Heat Transfer, Can. J. Chem. Eng. 54, 52.

167. Skogestad, S. and Morari, M., 1988, LV-Control of a High-Purity Distillation Column, Chem. Eng. Sci. 43, 33-48.

168. Garcia, C. E. and Morari, M., 1985, Internal Model Control. 2. Design Procedure for Multivariable Systems, Ind. Eng. Chem. Proc. Des. Dev. 24, 472-484.

169. Bunger, J.W., 1979, Processing Utah Tar Sand Bitumen, Ph.D. Dissertation, University of Utah, Salt Lake City, Utah.

170. Perry, R.H., and Chilton, C.H., 1983, Chemical Engineer's Handbook, 6th Edition, McGraw Hill, Inc., New York.

171. Sung, S.H., 1988, The Fluidized Bed Pyrolysis of Bitumen-Impregnated Sandstone in a Large Diameter Reactor, M.S. Thesis, University of Utah, Salt Lake City, Utah.

172. Wang, J., 1983, The Production of Hydrocarbon Liquids from a Bitumen-Impregnated Sandstone in a Fluidized Bed Pyrolysis Reactor, M.S. Thesis, University of Utah, Salt Lake City, Utah.

173. Weeks, J.K., Jr., 1977, Fluidized-Bed Processing of Utah Tar Sands, M.S. Thesis, University of Utah, Salt Lake City, Utah.

174. Venkatesan, V.N., 1980, Fluid Bed Thermal Recovery of Synthetic Crude from Bituminous Sands of Utah, Ph.D. Dissertation, University of Utah, Salt Lake City, Utah.

175. Hanson, F.V., and Oblad, A.G., 1988, The Fluidized Bed Pyrolysis of Bitumen Impregnated Sandstone from Tar Sand Deposits of Utah, Fourth UNITAR/UNDP Proc., 5, Paper No. 155, 421-438.

176. Ogunsola, O.I., 1991, Thermal Behaviour of Nigerian Oil Sands in Inert and Oxidising Atmospheres, J. Anal. Applied Pyrolysis, 21, 103.

177. Donnelly, J.K., Moore, R.G., Bennion, D.W., and Trenkwalder, A.E., 1981, A Fluidized Bed Retort of Oil Sands, Can. J. Chem. Eng. 59, 68.

178. Rovero, G. and Warkinson, A.P., 1990, A Two-Stage Spouted Bed Process for Autothermal Pyrolysis or Retorting, Fuel Proc. Tech. 26, 221.

179. Lechner, C.A., Liapis, A.I., and Findley, M.E., 1989, A Pyrolysis Process for Tar Sands, Can. J. Chem. Eng. 67, 85.

180. Del Bianco, A., Panariti, N., Anelli, M., Beltrame, P.L., and Carniti, P., 1993, Thermal Cracking of Petroleum Residues 1. Kinetic Analysis of the Reaction, FUEL 72, 75-80.

181. Del Bianco, A., Panariti, N., Anelli, M., Beltrame, P.L., and Carniti, P., 1993, Thermal Cracking of Petroleum Residues, 2. Hydrogen-Donor Solvent Addition, FUEL 72, 81.

182. Basily, I.K., Ahmed, E. and Nashed,N., 1990, Factors Affecting the Yields Produced from the Two-Stage Pyrolysis of Egyptian Bitumen, J. Anal. Applied Pyrolysis 17, 153.

183. Gaboriaud, F., Vantelon, J., Guelzim, A. and Julien, L., 1991, Gas Evolution during Isothermal Pyrolysis of Timahdit Oil Shale, J. Anal. Appl. Pyrolysis, 21, 119.

184. Knowlton, T.M., Chapter 12 in Geldart, D. (ed.), 1986, Gas Fluidization Technology, Chicehster, John Wiley & Sons, Inc., Great Britain.

185. Fletcher, J.V., Deo, M.D., and Hanson, F.V., 1993, Re-examination of Minimum Fluidization Velocity Correlations Applied to Group B Sands and Coked Sands, Powder Tech. 76, (2), 141.

186. Rebick, C., Albright, L.F., Crynes, B.L., and Corcoran, W.H., eds., 1983, Pyrolysis: Theory and Industrial Practice, CH. 4 69-87, Academic Press, New York.

187. Miller, J.D., and Misra, M., 1982, Concentration of Utah Tar Sands by an Ambient Flotation Process, Internat. J. Miner. Proc. 9, 269-287.

188. Misra, M., and Miller,. J.D., 1991, Comparison of Water-Based Physical Separation Processes for U. S. Tar Sands, Fuel. Proc. Tech. 27, 2-20.

189. Rendall, J.S., 1979, Solvent Extraction Process, U.S. Pat. No.4,160,718.

190. Rendall, J.S., 1984, Method and Apparatus for Solvent Extraction, U.S. Pat. No. 4,424,112.

191. Rendall, J.S., 1989, Hot Water Bitumen Extraction Process, U.S. Pat. No.4,875,998.

192. Haschke, E.M., Gimber, G.A., and Groves, K.O., 1985, Process for Recovery of Solvent from Tarsand Bitumen, U.S. Pat. No. 4,532,024.

193. Karnofsky, G., 1981, Solvent Extraction of Bitumen from Tar Sands and Diatomaceous Earth, Prod., Proc. and Charac. Hvy. Oils, Tar Sands Bitumen, Shale Oils and Coal-Derived Liquids, Salt Lake City, Utah, Oct. 27-30, 1981.

194. Cha, S., Hanson, F.V., Longstaff, D.C., and Oblad, A.G., 1991, Pyrolysis of Bitumen Impregnated Sandstones: A Comparison of Fluidized-Bed and Rotary Kiln Reactors, FUEL 70, 1357-1361.

195. Hanson, F.V., Cha, S., Deo, M.D., and Oblad, A.G., 1992, Pyrolysis of Oil Sands from the Whiterocks Deposit in a Rotary Kiln, FUEL 71, 1455-1463.

196. Geldart, D., ed., 1986, Gas Fluidization Technology, John Wiley & Sons, Inc., Chichester, Great Britain.

197. Hanson, F. V. and Lin, L. C., 1991, Riser Reactor for the Combustion of Coked Sand, Final Report, U. S. DOE Contract No. DE-FG21-89MC26268.

198. Rowe, P. N., and Nienow, A. W., 1976, Particle Mixing and Segregation in Gas Fludised Beds, Powder Tech. 15, 141-147.

199. Howard, J. R., 1989, Fluidized Bed Technology, Principles and Applications, Adam Hilger, Bristol, England.

200. Fletcher, J. V., Deo, M. D. and Hanson, F. V., 1992, Re-examination of Minimum Fluidization Velocity Correlations Applied to Group B Sands and Coked Sands, Powder Tech. 69, 147-155.

201. Grace, J. R., 1986, Contacting Modes and Behavior Classification of Gas-Solid and Other Two-Phase Suspensions, Can. J. Chem. Eng. 64, 353-363.

202. Mei, J. S., Rockey, J. M. and Lawson, W. F., 1991, Flow Regime Transistions in Fluidized Beds of Coarse Particles, Proc. 1991 Intern. Conf. on Fluidized Bed Combustion, Anthony, E. J. (ed.), Montreal, Canada, Apr. 21-24, 1225-1232.

203. Canada, G. S., McLaughlin, M. H., and Staub, F. W., 1978, Flow Regimes and Void Freaction Distribution in Gas Fluidization of Large Particles in Beds without Tube Banks, Wen, C. Y. Ed., AIChE Symp. Ser. 74 (176), 14-26.

204. Yerushalmi, J. and Cankurt, N. T., 1979, Further Studies of the Regimes of Fludization, Powder Tech., 24, 187-205.

205. Sun, G. and Chen, G., 1989, Transition to Turbulent Fluidization and Its Predicition, Proc. Internat. Conf. Fluidization, Grace, J. R. Ed., Banff, Alberta, Canada, May 7-12, 1989, 33-40.

206. Lee, J. K., Hu, C. G., Shin, Y. S., and Chun, H. S., 1989, Characteristics of a Two-Stage Swirl-Flow Fludized Bed Combustor, Proc. 1989 Internat. Conf. on Fluidized Bed Combustion, FBC-Technology for Today 1, 1199-1203.

207. Williams, D.F., 1981, Extraction with Supercritical Gases, Chem. Eng. Sci. 56, 1769.

208. Stahl, E., Quirin, K.W., and Gerard, D., 1988, Dense Gases for Extraction and Refining, Springer-Verlag, New York,

209. Paulaitis, M.E., Krukonis. V.J., Kurnik.R.T. and Reid.R.C., 1983, Supercritical Fluid Extraction, Rev. Chem. Eng. 1.

210. Duerkson, C.H., 1993, Gravity Drainage Processes for Recovery and In-situ Upgrading of Heavy Oil and Bitumen, 16th Rocky Mtn. Fuel Soc. Symp., Salt Lake City, Utah.

211. Hwang, J., 1992, Application of Dynamic Supercritical Fluid Extraction to Recovery and Upgrading of Complex Hydrocarbon Mixtures, Ph.D. Disseratation, University of Utah, Salt Lake City, Utah.

212. Deo, M.D., Hwang, J. and Hanson. F.V., 1992, Supercritical Fluid Extraction of a Crude Oil, Bitumen-Derived Liquid and Bitumen by Carbon Dioxide and Propane, FUEL 71, 1519.

213. Deo, M.D., Hwang, J. and Hanson. F.V., 1992, The Effect of Cosolubilizing Lighter Components on the Asphaltene Content of Heavy Oils, Fuel Proc. Tech. 21, 821.

214. Deo, M.D. and Hanson, F.V., 1993, Asphaltene Precipitation: Need for a Broader View, Presented in SPE Internat. Symp., SPE Paper No. 25193.

215. Larson, L., Silva, M.K., and Orr, F.M. Jr., 1986, Temperature Dependence of L1-L2-V Behavior in CO_2- Hydrocarbon Systems, In Proc. PE Annual Tech. Conf., SPE Paper No. 15399.

216. Peng, D.Y., and Robinson, D.N., 1976, Two Parameters Equations of State, Ind. Eng. Chem. Fund. 15, 79.

217. McHugh, M.A. and Kurkonis, V.J., 1986, Supercritical Fluid Extraction: Principles and Practice, Butterworths, Stoneham, Massachusetts.

218. Bukka, K., Hanson, F.V., Miller, J.D. and Oblad, A.G., 1992, Fractionation and Characterization of Whiterocks Tar Sand Bitumen, Energy & Fuels 6, 160.

219. Whitson, C.J., 1983, Characterizing Hydrocarbon Plus Fractions, SPE J., 23, 683.

220. CMGPROP, Version 93.20, 1993, CMGPROP User's Manual; Equation-of-State Phase Property Package, Computer Modeling Group, Calgary, Canada.

221. Lee, B.I. and Kesler, M.G., 1975, A Generalized Thermodynamic Correlation Based on Three Parameter Corresponding States, AICHE J. 21, 510.

222. Corbett, R.A., 1989, Modern Hydrocracking is the Key to Upgrading Processes, OGJ SPECIAL, Oil & Gas J., 33, 42.

223. Gates, B.C., Katzer, J.R., and Schuit, G.C.A., 1979, Chemistry of Catalytic Processes, McGraw-Hill, Inc., New York.

224. Beaton, W.I., and Bertolacini, R.J., 1991, Resid Hydroprocessing at Amoco, Catal. Rev. Sci. Eng., 33(3), 281.

225. Longstaff, D.C., 1992, Hydrotreating the Whiterocks Oil Sand Bitumen and Bitumen-Derived Liquid, Ph.D. Dissertation, University of Utah, Salt Lake City, Utah.

226. Kwak, S., 1994, Hydrotreating Heavy Oils over Commercial Hydrodenitrogenation and Hydrodemetallation Catalysts, Ph.D. Dissertation, University of Utah, Salt Lake City, Utah.

227. Longstaff, D.C., Deo, M.D., Hanson, F.V., Oblad, A.G., and Tsai, C.H., 1992, Hydrotreating the Bitumen-Derived Hydrocarbon Liquid Produced in a Fluidized-Bed Pyrolysis Reactor, FUEL 71, 1407.

228. Longstaff, D.C., Deo, M.D., and Hanson, F.V., 1994, Hydrotreating the Bitumen from the Whiterocks Oil Sand Deposit, FUEL, (in Press).

229. Kwak, S., Longstaff, D.C., Deo, M.D., and Hanson, F.V., 1994, Hydrotreating Process Kinetics for Bitumen and Bitumen-Derived Liquids, FUEL, (in Press).

230. De Wind, M., Plantenga, F.L., Heinerman, J.J.L., and Homan-Free, H.W., 1988, Upflow versus Downflow Testing of Hydrotreating Catalysts, Appl. Catal. 43, 239.

231. Speight, J.G., 1991, The Chemistry and Technology of Petroleum, 2nd ed., Marcel Dekker, New York.

232. Syncrude Canada Ltd., 1979, Syncrude Analytical Method for Oil Sand and Bitumen Processing, The Alberta Oil Sands Technology and Research Authority, Edmonton, Alberta, Canada.

233. ASTM D 189-88, Standard Test Method for Conradson Carbon Residue of Petroleum Products.

234. Mosby, J.F., Buttke, R.D., Cox, J.A., and Nikolaides C., 1986, Process Characterization of Expanded-Bed Reactors in Series, Chem. Eng. Sci. 41(4), 989.

235. Beuther, H., and Schmid, B.K., 1963, Reaction Mechanisms and Rates in Residue Hydrodesulfurization, Proc. 6th World Pet. Congr. 3, 297.

236. More, J.J., Garbow, B.S., and Hillstrom, K.E., 1980, User Guide for MINPACK-1, Argonne National Laboratory Report ANL-80-74, Argonne, Illinois.

237. George, Z.M., 1990, Catalytic Upgrading of Liquid Hydrocarbons Derived from Coprocessing of Heavy Oil and Coal, Can. J. Chem. Eng. 68, 519.

238. Billon, A., Henrich, G., Jacquin, Y. and Peries, J.P., 1983, Heavy Solvent Deasphalting + HT - A New Refining Route for Upgrading of Residues and Heavy Crudes, Proc. 11th World Petrol. Congr. 4, 35.

239. Yui, S.M. and Sanford, E.C., 1989, Mild Hydrocracking of Bitumen-Derived coker and Hydracker Heavy Gas Oils: Kinetics, Product Yields, and Product Properties, Ind. Eng. Chem. Res. 28, 1278.

240. Yui, S.M., 1989, Hydrotreating of Bitumen-Derived Coker Gas Oil: Kinetics of Hydrodesulfurization, Hydrodenitrogenation, and Mild Hydrocracking, and Correlations to Predict Product Yields and Properties, AOSTRA J. Res. 5, 211.

241. Riley, K.L., 1978, The Effect of Catalyst Properties on Heavy Feed Hydroprocessing, General Papers Presented Before the Division of Petroleum Chemistry, Amer. Chem. Soc., Anaheim Meeting, Mar. 12-17.

242. Oleck, S.M., and Sherry, H.S., 1977, Fresh Water Manganese Nodules as a Catalyst for Demetalizing and Desulfurizing Petroleum Residua, Ind. Eng. Chem. Proc. Des. Dev. 16, 525.

243. Quann, R.J., Ware, R.A., Hung, C., and Wei, J., 1988, Catalytic Hydrodemetallation of Petroleum, Adv. Chem. Eng. 14, 95.

244. Katzer, J.R., and Sivasubramanian, R., 1979, Process and Catalyst Needs for Hydrodenitrogenation, Catal. Rev. Sci. Eng. 20, 155.

245. Streitwieser, A., Jr., and Heathcock, C.H., 1976, Introduction to Organic Chemistry, Macmillan, New York.

246. Ho, T.C., 1988, Hydrodenitrogenation Catalysis, Cat. Rev. Sci. Eng. 30(1), 117.

247. Sanford, E.C. and Yui, S.M., 1984, Hydrotreating Characteristics of Coked and of Hydrocracked Gas Oils from Alberta Heavy Bituminous Oils with Commercial Ni-Mo Catalysts, and Prediction of Some Product Properties, in Catalysis on the Energy Scene (Ed. Kaliaguine, S., and Mahay, A.), Elsevier Science Publ. B.V., Amsterdam, Netherlands.

248. McColgan, E. C. and Parsons, B. I., 1972, The Hydrocracking of Residual Oils and Tars Part 2:The Catalytic Hydrocracking of Athabasca Bitumens, Can., Mines Br., Res. Rep., R-253.

249. Homan Free, H. and Lovink, H. J., 1987, Mild Hydrocracking of Vacuum Gas Oils, Erdoel Kohle 40, 346.

250. Mosby, J. F., Buttke, R. D., Cox, J. A. and Nickolaides, C., 1986, Process Characterization of Expanded-Bed Reactors in Series, Chem. Eng. Sci. 41, (2), 989.

251. Heck, R. H., Rankel, L. A. and DiGuiseppi, F. T., 1992, Conversion of Petroleum Resid From Maya Crude: Effects of H-Donors, Hydrogen Pressure and Catalyst, Fuel Proc. Tech. 30, 69.

252. Sanford, E. C. and Chung, K. H., 1991, The Mechanism of Pitch Conversion during Coking, Hydrocracking and Catalytic Hydrocracking of Athabasca Bitumen, AOSTRA J. Res. 7, 37.

253. Heck, R. H. and DiGuiseppi, F. T., 1993, Kinetic and Mechanistic Effects in Resid Hydrocracking, Am. Chem. Soc., Prprnt. Div. Petrol. Chem. 38, 417.

254. Mushrush, G. W. and Hazlett, R. N., 1984, Pyrolysis of Organic Compounds Containing Long Unbranched Alkyl Groups, Ind. Eng. Chem. 23, 288.

255. Chen, H. H., Montgomery, D. S. and Strausz, O. P., 1988, Hydrocracking of Athabasca Bitumen Using Oil-Soluble Organometallic Catalysts. Part I: The Influence of Temperature and Pressure on Catalytic Activity, AOSTRA J. Res. 4, 45.

256. Kwak, S., Longstaff, D. C. and Hanson, F. V., 1994, Catalytic Upgrading of A Uinta Basin Bitumen over A Commercial HDM Catalyst, Proc. 1993 Eastern Oil Shale Symposium, in press.

257. Hardin, A. H., Packwood, R. H. and Ternan, M., 1978, Effects of Median Pore Diameter on the Conversion of Athabasca Bitumen, Amer. Chem. Soc., Prprnt. Div. Petrol. Chem. 23, 1450.

258. Plumail, J. C., Jacquin, Y., Martino, G. and Toulhoat, H., 1983, Effect of the Pore Size Distribution on the Activities of Alumina Supported Co-Mo Catalysts in the Hydrotreatment of Boscan Crude, Amer. Chem. Soc., Prprnt. Div. Petrol. Chem. 28, 562.

259. Miki, Y., Yamadaya, S., Oba, M. and Sugimoto, Y., 1983, Role of Catalyst in Hydrocracking of Heavy Oil, J. Catal. 83, 371.

260. Flinn, R. A., Larson, O. A. and Beuther, H., 1962, The Kinetics of Hydrodenitrogenation, Am. Chem. Soc., Prprnt. Div. Pet. Chem. 7, 165.

261. Trytten, L. C., Gray, M. R. and Sanford, E. C., 1990, Hydroprocessing of Narrow-Boiling Gas Oil Fractions: Dependence of Reaction Kinetics on Molecular Weight, Ind. Eng. Chem. Res. 29, 725.

262. Schucker, R. C. and Keweshan C. F., 1980, The Reactivity of Cold Lake Asphaltenes, Am. Chem. Soc., Prprnt. Div. Fuel Chem. 25, 155-165.

263. Savage, P. E. and Klein, M. T., 1989, Asphaltene Reaction Pathways V. Chemical and Mathematical Modeling, Chem. Eng. Sci., 44, 393.

264. Speight, J. G., 1992, Molecular Models For Petroleum Asphaltenes and Implications for Processing, Proc. of the 1991 Eastern Oil Shale Symp., p.17.

265. Wivel, P., Zeuthen, P., and Jacobsen, A. C., 1991, Initial Coking and Decativation of Hydrotreating Catalysts by Real Feeds, Surface Sci. Catal. 68, 257.

266. Absi-Halabi, M., and Stanislaus, A., 1991, Coke Formation on Catalysts During the Hydroprocessing of Heavy Oils, Appl. Catal. 72, 193.

267. Furimsky, E., 1978, Chemical Origin of Coke Deposited on Catalyst Surface, Ind. Eng. Chem. Prod. Res. Dev. 17, 329.

268. Speight, J.G., 1987, Initial Reactions in the Coking of Residua, Sym. on Advances in Resid. Upgrading, Amer. Chem. Soc., Prprnt. Div. Petrol. Chem., 32 (2) 413.

269. Fitzer, E., Muller, K., and Schaefer, W., 1971, Pyrolytic Conversion of Organic Compounds to Carbon, Chem. Phys. Carbon 7, 237.

270. van Doorn, J., Moulijn, J.A., and Boon, J.J, 1989, Characterization of Carbon Deposits on Used Hydrotreating Catalysts by Curie-Point Pyrolysis, J. Anal. Appl. Pyrol. 15,

333.

271. Muegge, B.D., and Massoth, F.E., 1991, Basic Studies of Deactivation of Hydrotreating Catalysts with Anthracene, Fuel Proc. Tech. 29, 19.

272. Muegge, B.D., and Massoth, F.E., 1991, Comparison of Hydrotreating Catalyst Deactivation by Coking with Vacuum Gas Oil vs. Anthracene, Surface Sci. Catal. 68, 297.

273. Massoth, F.E., Balusami, K., and Shabtai, J., 1990, Catalytic Functionalities of Supported Sulfides VI. The Effect of H_2S Promotion on the Kinetics of Indole Hydrogenolysis, J. Catal. 122, 256-270.

274. Frye, C.G. and Weitkamp, A.W., 1969, Equilibrium Hydrogenation of Multi-Ring Aromatics, J. Chem. Eng. Data 14, 372

275. Appleby, W.G., Gibson, J.W. and Good, G.M., 1960, Coke Formation in Catalytic Cracking, Amer. Chem. Soc., Prprnt. Petrol. Chem. Div. 5, B-71.

276. Furimsky, E., 1982, Characterization of Deposits Formed on Catalyst Surfaces During Hydrotreatment of Coal-Derived Liquids, Fuel Proc. Tech. 6, 1.

277. Zeuthen, P., Blom P., Muegge, B. and Massoth, F.E., 1991, Temperature-Programmed Sulfidation and Oxidation of Ni-Mo/Alumina Catalysts and Reaction with Ammonia, Appl. Catal. 68, 117.

278. Zeuthen, P., Blom, P., and Massoth, F.E., 1991, Characterization of Nitrogen on Aged Hydroprocessing Catalysts by Temperature-Programmed Oxidation, Appl. Catal. 78, 265.

279. Fan, L.S., 1989, Gas-Liquid-Solid Fluidization Engineering, Butterworths Series in Chemical Engineering, Butterworth, Boston, Massachusetts.

280. Rapp, L.M. and Van Driesen, R.P., 1972, H-Oil Process Gives Product Flexibility, Hydrocracking Handbook, Gulf Publ. Co., Houston, Texas.

281. Tarmy, B.L., Chang, M., Coulaloglou, C.A., and Ponzi, P.R., 1984, The Three-Phase Hydrodynamic Characteristics of the EDS Coal Liquefaction Reactors; Their Development and Use in Reactor Scale-up, Internat. Symp. on Chem. Reac. Eng., Sept. 10-13.

282. Haynes, H.W. Jr., Borgialli, R.R., and Zhang, T., 1991, A Novel Liquid Fluidized Bed Microreactor for Coal Liquefaction Studies. 2. Cold Model Results, Energy & Fuels 5, 63

283. Bhatia, V.K. and Epstein, N., 1974, Three-Phase Fluidization: A Generalized Wake Model, Fludization and Its Applications, eds. Angelino, H., J., P. Couderc, H. Gilbert and C. Laguerie, p. 380, Cepadues Editions, Toulouse, France.

284. Sastry, N.V.S., Epstein, N., Hirata, A., Koshijima, I., and Izumi, M., 1983, Zinc Hydosulphite by Three-Phase Fluidization: Experimental and Modeling, Can. J. Chem. Eng. 61, 635.

285. Tadaki, T. and Maeda, S., 1964, Shape and Velocity of Single Air Bubble Rising in Various Liquids, Kogaku Kogaku 25, 254.

286. Kim, S.D., Baker, C.G. J., and Bergougnou, M.A., 1975, Phase Holdup Characteristics of Three-Phase Fluidized Beds, Can. J. Chem. Eng. 53 (2), 134.

287. El-Temtamy, S.A., and Epstein, N., 1978, Bubble Wake Solids Content in Three-Phase Fluidized Beds, Internat. J. Multiphase Flow 4, 19.

288. Richardson, J.F. and Zaki, W.N., 1954, Sedimentation and Fluidization: Part I, Trans. Inst. Chem. Engrs. 32, 35.

289. Armstrong, E.R., 1975, Heat Transfer and Hydrodynamic Studies in Three-Phase Fluidized Beds, M.E. Sc. Thesis, The University of Western Ontario, London, Ontario, Canada.

290. El-Temtamy, S.A. and Epstein, N., 1980, Simultaneous Solid Entrainment and De-entrainment Above a Three-Phase Fluidized Bed, Fluidization, ed. Grace, J.R. and J.M. Matsen, p. 519, Plenum Press, New York.

291. Tsuchiya, K. and Fan, L.S., 1986, Near-Wake Structure of a Single Gas Bubble in a Two-Dimensional Liquid-Solid Fluidized Bed: Vortex Shedding and Wake Size Variation, Chem. Eng. Sci. 43 1167.

292. Idogawa, K., Ikeda, K., Fukuda, T. and Morooka, S., 1986, Behavior of Bubbles of the Air Water System in a Column Under High Pressure, Internat. Chem. Eng. 26(3), 468

293. Hamshar, J.A., 1993, Gregoli, A.A., Rimmer, D.P., and Yildrim, E., Results of Laboratory Testing by Canadian Oxy of Fine Tails for Development of a Process for Bitumen Extraction and Disposal of Compacted Solids, Paper F14, 23 pps, Proc. Fine Tailings Symp., ed. J.K. Liu, Oil Sands—Our Petroleum Future Conf., Apr. 4-7, 1993, Edmonton, Alberta, Canada.

294. Ryu, H., 1989, Kinetic Modeling Applied to Hydrocarbon Process Engineering and Design, Ph.D. Dissertation, University of Utah, Salt Lake City, Utah.

295. Gearhart, J.A., and Garwin, L., 1976, ROSE Process Improves Resid Feed, Hydrocarbon Proc. 55 (5), 125-128.

296. Gearhart, J.A., 1980, Solvent Treats Resids, Hydrocarbon Proc. 59 (5), 150-151.

297. Nelson, S.R., and Roodman, R.G., 1985, ROSE: The Energy Efficient Bottom of the Barrel Alternative, Prprnt. AIChE National Mtg., Houston, Texas, March 1985.

298. Nelson, S.R., and Corbett, R.W., 1985, Kerr-McGee's ROSE Process Expands on Proven Extraction Technology, Proc. 3rd Internat. UNITAR Conf. on Heavy Crude and Tar Sands, Chap. 133, 1387-1394.

299. Washimi, K., 1989, New Unit to Thermal Crack Resid, Hydrocarbon Proc. 68 (9), 69-70.

300. Rossi, W.J., Deighton, B.S., and MacDonald, A.J., 1977, Get More Light Fuel from Resid, Hydocarbon Proc. 56 (5), 105-110.

301. Teichman, D.P., Bridge, A.G., and Reed, E.M., 1982, Building to Handle More Resid, Hydrocarbon Proc. 61 (5), 105-109.

302. Gibson, K.R., Green, D.C., and Teichmann, D.P., 1983, Technical Challenges to Heavy Oil Conversion, Chem. Eng. Prog. 79 (4), 93-98.

303. Zandora, O.J., Busch, L.E., Hettinger, W.R., Jr., and Krock, R.P., 1982, Heavy Oil Project Pushed at Complex Refinery, Oil & Gas J. 80 (12), 82-91.

304. Hennler, C.L., Lomas, D.A., and Tajbl, D.G., 1984, Oil & Gas J. 82 (22), 79-88.

305. Stolfa, F., 1980, New Roles for Thermal Cracking, Hydrocarbon Proc. 59 (5), 101-109.

306. DeBaise, R., and Elliot, J.D., 1982, Delayed Coking: Latest Trends, Hydrocarbon Proc., 61 (5), 99-104.

307. Busch, R.A., 1970, Fluid Coking: Seasoned Process Takes on New Jobs, 1979, Oil & Gas J. 68 (14), 102-111.

308. Allan, D.E., Metrailer, W.J., and King, R.C., 1981, Advances in Fluid and Flexicoking Technology, Chem. Eng. Prog. 77 (12), 40-44.

309. Rhoe, A., and Blignieres, C., 1979, Visbreaking: A Flexible Process, Hydrocarbon Proc. 58 (1), 131-136.

310. Hournac, R., Huhn, J., and Notarbartlo, M., 1979, Visbreaking: More Feed for FCC, Hydrocarbon Proc. 58 (9), 97-102.

311. Notarbartlo, M., Menegazzo, C., and Kuhn, J., 1979, Visbreaking: Low Cost Next Step 58 (9), 114-118.

312. Akbar, M., and Geelen, H., 1981, Visbreaking Uses Soaker Drum, Hydrocarbon Proc. 60 (5), 81-85.

313. Wimpress, N., 1977, Handy Rating Method Predicts Fired-Heater Operation, Oil & Gas J. 75 (48), 144.

APPENDIX A

WHITEROCKS OIL SAND DEPOSIT BIBLIOGRAPHY

Ball Associates, Ltd., 1964, Surface and Shallow Oil-Impregnated Rocks and Shallow Oil Fields in the United States, U.S. Bureau of Mines, Monograph 12.

Ball, D., Marchant, L.C., and Goldburg, A., 1982, The IOCC Monograph Series: Tar Sands, Interstate Oil Compact Commission, Oklahoma City, Oklahoma.

Barb, C.F., 1942, Rubber from the Uinta Basin of Utah, Mines Magazine 32, #10, 521-524.

Barb, C.F., and J.O. Ball, 1944, Hydrocarbons of the Uinta Basin of Utah and Colordo, Quarterly, Colorado School of Mines 39, #1, 115 p.

Bukka, K., Miller, J.D., Hanson, F.V., and Oblad, A.G., 1991, Mineral Matter Distribution during the Hot Water Processing of Utah Tar Sand, AOSTRA J. Res. 7, 101-109.

Campbell, J.A., and H.R. Ritzma, 1976, Structural Geology and Petroleum Potential of the South Flank of the Uinta Mountain Uplift [abstract], Amer. Assoc. Petrol. Geol., Bull. 60, 1392-1393.

Cashion. W.B., Jr., 1964, Other Bituminous Substances, Utah Geol. Miner. Survey, Bull. 73, 63-70, Mineral and Water Resources of Utah.

Cha, S., 1991, Pyrolysis of the Whiterocks Tar Sand in a rotary Kiln Reactor, Ph.D. Dissertation, University of Utah, Salt Lake City, Utah.

Cha, S., Longstaff, D.C., Hanson, F.V., and Oblad A.G., 1991, Pyrolysis of Bitumen Impregnated Sandstones, A Comparison of Fluidized - Bed and Rotary Kiln Reactors, Proc. 1990 Eastern Oil Shale Symp., 136-145.

Cha, S., Longstaff, D.C., Hanson, F.V., and Oblad, A.G., 1991, Pyrolysis of Bitumen Impregnated Sandstones, A Comparison of Fluidized-Bed and Rotary-Kiln Reactors, FUEL 70, 1357-1361.

Covington, R.E., 1963, Bituminous Sandstone and Limestone Deposits of Utah, Utah Geol. Miner. Survey, Bull. 54, 225-247.

Covington, R.E., 1964, Bituminous Sands with Viscous Crude Oils, Brigham Young University, First Intermtn. Symp. Fossil Hydrocarbons, 364-374.

Covington, R.E., 1964, Bituminous Sandstone in the Uinta Basin, Intermtn. Assoc. of Petrol. Geol., 13th Annual Field Conference, 227-242.

Covington, R.E., 1964, Thermal Recovery May Bring Industry's Quiet Revolution, Oil & Gas J. 62, #47, 112-118.

Covington, R.E., 1965, Some Possible Applications of Thermal Recovery in Utah, J. Petrol. Tech. 17, #11, 1277-1284.

Deo, M.D., and Hanson, F.V., 1993, Asphaltene Precipitation: A Need for a Broader View, SPE 25193.

Deo, M.D., Hwang, J., and Hanson, F.V., 1993, The Effect of Cosolubilizing Lighter Components on the Asphaltene Content of Heavy Oils, Fuel Proc. Tech. 34, 217-228.

Deo, M.D., Hwang, J., and Hanson, F.V., 1992, Supercritical Fluid Extraction of a Crude Oil, Bitumen-Derived Liquid and Bitumen by Carbon Dioxide and Propane, FUEL 71, 1519-1526.

Dorius, J.C., 1985, The Pyrolysis of Bitumen Impregnated Sandstone from the PR Spring (Utah) Deposit in a Fluidized Bed, Ph.D. Dissertation, University of Utah, Salt Lake City, Utah.

Drelich, J., 1993, The Role of Wetting Phenomena in the Hot Water Process for Bitumen Recovery from Tar Sand, Ph.D. Dissertation, University of Utah, Salt Lake City, Utah.

Drelich, J., Hanson, F.V., Hupka, J, and Miller, J.D., 1993, Water Recycle in Moderate-Temperature Bitumen Recovery from Whiterocks Tar Sands, AOSTRA J. Res, in press.

Drelich, J., and Miller, J.D., 1993, Surface/Interfacial Tension of the Whiterocks Bitumen and its Relationship to Tar Sand Processing, Proc. 1992 Eastern Oil Shale Symp., 265-275.

Fletcher, J.V., Deo, M.D., and Hanson, F.V., 1993, Fluidized Bed Pyrolysis of Bitumen-Impregnated Sandstone at Sub-Atmospheric Conditions, Proc. 1992 Eastern Oil Shale Symp., 247-256.

Hanson, F.V., Dorius, J.C., Utley, J.K., and Van Nguyen, T., 1992, The Application of Compound-Type Analyses to the Correlation of Product Distributions and Yields from the Fluidized-Bed Pyrolysis of Oil Sands, FUEL 71, 1365-1372.

Hunt, J.M., F. Stewart, and P.A. Dickey, 1954, Origin of Hydrocarbons of Uinta Basin, Utah, Amer. Assoc. Petrol. Geol., Bull. 38, #8, 1671-1698.

Hupka, J., Drelich, J., Miller, J.D., White, R.R., Hanson, F.V., and Oblad, A.G., 1991, Impact of Water Recycle on Water-Based Processing of Whiterocks Tar Sand, Proc. 1990 Eastern Oil Shale Symp., 39-44.

Hupka, J., Drelich J., Miller, J.D., White, R.R., Hanson, F.V., and Oblad, A.G., 1991, Impact of Water Recycle on Water-Based Processing of Whiterocks Tar Sand, FUEL 70, 1313-1316.

Hwang, J., 1993, Application of Supercritical Fluid Extraction to the Recovery and Upgrading of Oil Sands, Ph.D. Dissertation, University of Utah, Salt Lake City, Utah.

Keefer, T.N., and McQuivey, R.S., 1979, Water Availability for Development of Major Tar Sands Areas in Utah, U.S. Department of Energy, Final Report LETC-0013-1, 228 pp.

Kinney, D.M., 1951, Geology of Uinta River and Brush Creek-Diamond Mountain Areas, Duchesne and Uinta Counties, Utah, U.S. Geol. Survey, Bull. 1007, Map.

Kuuskra, V.V., and Hammershaimb, V.A., eds., 1984, The IOCC Monograph Series: Major Tar Sand and Heavy Oil Deposits of the United States, Interstate Oil Compact Comm., Oklahoma City, Oklahoma.

Kwak, S., Longstaff, D.C., Deo, M.D., and Hanson, F.V., 1993, Hydrotreating Process Kinetics for Bitumen and Bitumen-Derived Liquids, Proc. 1992 Eastern Oil Shale Symp., 208-215.

Longstaff, D.C., 1992, Hydrotreating the Whiterocks Oil Sand Bitumen and Bitumen-Derived Liquid, Ph.D. Dissertation, University of Utah, Salt Lake City, Utah.

Longstaff, D.C., Deo, M.D., Hanson, F.V., Oblad, A.G., and Tsai, C.H., 1992, Hydrotreating the Bitumen-Derived Hydrocarbon Liquid Produced in a Fluidized Bed Pyrolysis Reactor, FUEL 71, 1407-1419.

Longstaff, D.C., Deo, M.D., and Hanson, F.V., 1993, Hydrotreating the Bitumen from the Whiterocks Oil Sand Deposit, Proc. 1992 Eastern Oil Shale Symp., 199-207.

Oblad, A.G., Bunger, J.W., Hanson, F.V., Miller, J.D., Ritzma, H.R., and Seader, J.D., 1987, Tar Sand Research and Development at the University of Utah. Ann. Rev. Energy. 12, 283-356.

Peterson, P.R., 1985, The Whiterocks Tar Sand Deposit, Utah Geolog. Assoc., Publ. 12, 243-252.

Pruitt, R.G., Jr., 1961, The Mineral Resources of Uintah County, Utah Geol. Miner. Survey, Bull. 71, 101 pp.

Resnick, B.S., Dike, D.H., English, L.M. III, and Lewis, A.G., 1981, Evaluation of Tar Sand Mining, Volume 1 - An Assessment of Resources Amenable to Mine Production: U.S. DOE, Final Report, DOE/ET/30201-1.

Ritzma, H.R., 1968, Preliminary Location Map Oil - Impregnated Rock Deposits of Utah, Utah Geol. Miner. Survey, Map No. 25, 1 pg.

Ritzma, H.R., 1973, Oil-Impregnated Rock Deposits of Utah, Utah Geol. Miner. Survey, Map No. 33, 2pp.

Ritzma, H.R., 1979, Oil-Impregnated Rock Deposits of Utah, Utah Geol. Miner. Survey, Map No. 47, 2pp.

Sung, S.H., 1988, The Fluidized Bed Pyrolysis of Bitumen-Impregnated Sandstone in a Large Diameter Reactor, M.S. Thesis, University of Utah, Salt Lake City, Utah.

Tsai, C.H., Deo, M.D., Hanson, F.V., and Oblad, A.G., 1991, Characterization and Potential Utilization of Whiterocks (Utah) Tar Sand Bitumen, Fuel Sci. Tech. Int. 9, 1259-1286.

Tsai, C.H., Deo, M.D., Hanson, F.V., and Oblad, A.G., 1992, Characterization and Potential Utilization of Whiterocks Tar Sand Bitumen II. Pyrolysis Man Spectrometry and Nuclear Magnetic Resonance Analyses, Fuel Sci. Tech. Int. 10, 1437-1459.

Wang, J., 1983, The Production of Hydrocarbon Liquids from a Bitumen-Impregnated Sandstone in a Fluidized Bed Pyrolysis Reactor, M.S. Thesis, University of Utah, Salt Lake City, Utah.

Wang, J., Hanson, F.V., Obald, A.G., 1983, The Fluidized Bed Pyrolysis of the Bitumen-Impregnated Sandstone from the Whiterocks (Utah) Deposit, Prprnt. AICHE Symp. Adv. Tar Sand Tech., Denver, Colorado, August 1983.

APPENDIX B

ASPHALT RIDGE OIL SAND DEPOSIT BIBLIOGRAPHY

Abraham, H., 1969, Asphalts and Allied Substances, 6th Edition, 5 Volumes, D. Van Nostrand Co., Inc., Princeton, New Jersey.

Alford, H.E., and Derby, R.E., 1981, Utah Tar Sands to be Developed, Hydrocarbon Proc. 60, #6, 127-130.

Anonymous, 1974, Fairbrim & Arizona Fuels to Begin Oil Sands Recovery Tests on Sohio Property in Utah, Synthetic Fuels, September.

Anonymous, 1981, Sohio Slates Tar Sands Pilot Plant in Utah, Oil & Gas J., 79, #3, 42-43.

Ball, D., Marchant, L.C., and Goldburg, A., 1982, The IOCC Monograph Series: Tar Sands, Interstate Oil Compact Comm., Oklahoma City, Oklahoma.

Ball, M.W., 1951, Oil-Impregnated Strippable Deposits in Utah, May 22, 1950, U.S. BuMines, The Synthetic Liquid Fuel Potential of Utah, Appendix D, p. 1-18.

Ball Associates, Ltd., 1965, Surface and Shallow Oil-Impregnated Rocks and Shallow Oil Fields in the United States, U.S. Bureau of Mines, Monograph 12, 375 p.

Barb, C.F., 1942, Rubber from the Uinta Basin of Utah, Mines Magazine 32, #10, 521-524.

Barb, C.F., 1944, Hydrocarbons of the Uinta Basin of Utah and Colorado, Review of Geology and Field Work, Colorado School of Mines, Quarterly, Colorado School of Mines, 39, #1, 115 p.

Barb, C.F., and Ball, J.O., 1944, Hydrocarbons of the Uinta Basin of Utah and Colordo, Quarterly, Colorado School of Mines, 39, #1.

Barbour, R.V., Dorrence, S.M., Vollmer, H., and Harris, J.D., 1976, Pyroloysis of Utah Tar Sands--Products and Kinetics, Amer. Chem. Soc., Div. Fuel Chem. 21, (6), 278-289.

Bunger, J.W., 1974, Characterization of a Utah Tar Sand Bitumen, Amer. Chem. Soc., Div. Fuel Chem. 19 (2), 231-241, Shale Oil, Tar Sands and Related Fuel Sources, T. F. Yen [Ed], Adv. Chem. Ser. 151, c. 10, 121-136.

Bunger, J.W., 1974, Characterization of a Utah Tar Sand Bitumen, Amer. Chem. Soc., Div. Fuel Chem. 19 (2), 231-241, Shale Oil, Tar Sands and Related Fuel Sources, T. F. Yen [Ed], Adv. Chem. Ser. 151, c. 10, 121-136, 1976.

Bunger, J.W., Cogswell, D.E., and Oblad, A.G., 1978, Thermal Processing of a Utah Tar Sand Bitumen, Canadian Institute of Mining and Metallurgy, CIM Special 17- Proceedings of the Canada-Venezuela Oil Sands Symp.-77, 178-182.

Bunger, J.W., Cogswell, D.E., and Oblad, A.G., 1979, Catalytic Cracking of Asphalt Ridge Bitumen, Amer. Chem. Soc., Refining of Synthetic Crude Oils, Adv. Chem. Ser. 179, 67-84.

Campbell, J.A., and Ritzma, H.R., 1976, Structural Geology and Petroleum Potential of the South flank of the Uinta Mountain Uplift [Abstract], Amer. Assoc. Petrol. Geol., Bull. 60, 1902-1393.

Campbell, J.A., and Ritzma, H.R., 1979, Geology and Petroleum Resources of the Major Oil-Impregnated Sandstone Deposits of Utah, Utah Geol. and Miner. Survey, Special Studies 50, 25 pp.

Campbell, J.A., and Ritzma, H.R., 1979, Geology and Petroleum Resources of the Major Oil-Impregnated Sandstone Deposits of Utah, U.N. Inst. for Training and Research, First Internat. Conf. on the Future of Heavy Oil and Tar Sands, (UNITAR), June 4-12, 1979, Edmonton, Alberta, Canada.

Cashion, W.B., Jr., 1964, Other Bituminous Substances, Utah Geol. and Miner. Survey Bull. 73, Mineral and Water Resources of Utah, 63-70.

Covington, R.E., 1957, The Bituminous Sandstones of the Asphalt Ridge Area, Northeastern Utah, Intermtn. Assoc. Petrol. Geol., 8th Ann. Field Confer., 172-175.

Covington, R.E., 1963, Bituminous Sandstone and Limestone Deposits of Utah, Utah Geol. Miner. Survey, Bull. 54, 225-247.

Covington, R.E., 1964, Bituminous Sands With Viscous Crude Oils, Brigham Young University, First Intermtn. Symp. on Fossil Hydrocarbons, 364-374.

Covington, R.E., 1964, Bituminous Sandstone in the Uinta Basin, Intermtn. Assoc. Petrol. Geol. 13th Ann. Field Conf., 227-242.

Covington, R.E., 1964, Thermal Recovery May Bring Industry's Quiet Revolution, Oil & Gas J. 62, #47, 112-118.

Covington, R.E., 1965, Some Possible Applications of Thermal Recovery in Utah, J. Petrol. Tech. 17, #11, 1277-1284.

Covington, R.E., and McDonald, R.L., 1965, Stratigraphic and Structural Controls of Bituminous Sandstone Deposits in Utah [Abstract], Amer. Assoc. of Petrol. Geol., Bull. 49, #9, 1577.

Covington, R.E., and Young, K.J., 1985, Brief History and Recent Developments in Tar Sand Deposits of Uinta Basin, Utah Geol. Assoc. Publication 12, Geology and Energy Resources, Uinta Basin of Utah, 227-242.

Dyni, J.R., and Goodwin, J.C., 1972, American Assoc. of Petroleum Geologists Field Trip Roadlog- Vernal, Utah to Rio Blanco, Colorado, Rocky Mountain Assoc. of Geol., Intermtn. Geol. 9, #2-3, 115-134.

Eldridge, G.H., 1901, Asphalt and Bituminous Rock Deposits, U.S. Geol. Survey, Ann. Report 22, 361-364.

Erickson, R.L., Myers, A.T., and Horr, C.A., 1954, Association of Uranium and Other Metals with Crude Oil, Asphalt, and Petroliferous Rock, Amer. Assoc. Petrol. Geol., Bull. 38, #10, 2200-2218.

Hills, R.C., 1985, Description of an Asphalt-Like Mineral from Asphalt Wash, Utah, Colorado Sci. Soc., Proc. 2, part 1, 27-28.

Hunt, J.M., Stewart, F., and Dickey, P.A., 1954, Origin of Hydrocarbonsof Uinta Basin, Utah, Amer. Assoc. Petro. Geol., Bull. 38, #8, 1671-1698.

Hupka, J., and Miller, J.D., 1991, Temperature Water-Based Bitumen Recovery from Tar Sand, FUEL 70, 1308-1312.

Hupka, J., and Miller, J.D., 1991, Electrophoretic Characterization and Processing of Asphalt Ridge and Sunnyside Tar Sands, Internat., J. Miner. Proc. 31, 217-231.

Kayser, R.B., 1966, Bituminous Sandstone Deposits Asphalt Ridge, Utah Geol. Miner. Survey, Special Studies 19, 62 pp.

Keefer, T.N., and McQuivey, R.S., 1979, Water Availability for Development of Major Tar Sands Areas in Utah, U.S. DOE, Final Rept. LETC-0013-1, 228 p.

Kinney, D.M., 1955, Geology of Uinta River and Brush Creek-Diamond Mountain Areas, Duchesne and Uinta Counties, Utah, U.S. Geol. Survey, Bull. 1007.

Kuuskra, V.V., and Hammershaimb, V.A., eds., 1984, Major Tar Sand and Heavy Oil Deposits of the United States, Interstate Oil Compact Comm., Oklahoma City, Oklahoma.

Lowe, R.M., 1976, The Asphalt Ridge Tar Sand Deposits, AIChE Symp. Ser. 72, #155, 55-60.

Mauger, R.L., Kayser, R.B., and Gwynn, J.W., 1973, A Sulfur Isotopic Study of Uinta Basin Hydrocarbons, Utah Geol. Miner. Survey, Special Studies 41, 17 p.

Oblad, A.G., Seader, J.D., Miller, J.D., and Bunger, J.W., 1976, Recovery of Bitumen from Oil-Impregnated Sandstone Deposists of Utah, AIChE, Oil Shale and Tar Sand Symp., AIChE Symp. Sec. 155 (72), 69-78.

Oblad, A.G., Seader, J.D., Miller, J.D., Bunger, J.W., and Cogswell, D.E., 1977, Recovery of Oil from Utah's Tar Sands, NTIS Report PB-294-680.

Oblad, A.G., Bunger, J.W., Hanson, F.V., Miller, J.D., Ritzma, H.R., and Seader, J.D., 1987, Tar Sand Research and Development at the University of Utah, Ann. Rev. Energy. 12 283-356.

Pruitt, R.G., Jr., 1961, The Mineral Resources of Uinta County, Utah Geol. Miner. Survey, Bull. 71, 101 p.

Resnick, B.S., Dike, D.H., English, L.M., III, and Lewis, A. G., 1981, Evaluation of Tar Sand Mining, Volume 1 - An Assessment of Resources Amenable to Mine Production: U.S. DOE, Final Report DOE/ET/30201-1.

Ritzma, H.R., 1968, Preliminary Location Map Oil - Impregnated Rock Deposits of Utah, Utah Geol. Miner. Survey, Map No. 25, 1 pg.

Ritzma, H.R., 1973, Oil-Impregnated Rock Deposits of Utah, Utah Geol. Miner. Survey, Map No. 33, 2pp.

Ritzma, H.R., 1974, Asphalt Ridge, Structure, Stratigraphy, and Oil-Impregnated Sands, Utah Geol. Assoc., Publication 4, 60.

Ritzma, H.R., 1979, Oil-Impregnated Rock Deposits of Utah, Utah Geol. Miner. Survey, Map No. 47, 2pp.

Shea, G.B., and Higgins, R.V., 1952, Separation and Utilization Studies of Bitumens from Bituminous Sandstones of the Vernal and Sunnyside, Utah Deposits, U.S. BuMines ROI 4871.

Sinks, D.J., 1985, Geologic Influence on the In-Situ Process of Tar Sand at the North West Asphalt Ridge Deposit, Utah, U.S. DOE, Report No. AD-89-F-0-026-0.

Smith, R.J., 1980, Asphalt Ridge Tar Sands, Flotation Behavior and Process Design, M.S. Thesis, University of Utah, Salt Lake City, Utah.

Smith, R.J., and Miller, J.D., 1981, Flotation Behavior of Digested Asphalt Ridge Tar Sands, Mining Eng. 33, 1719-1724, Discussion of Article, 34, 1598.

Speiker, E.M., 1931, Bituminous Sandstone Near Vernal, Utah, U.S. Geol. Survey, Bull. 822-C, 77-100.

Stone, G.H., 1891, Note on the Asphaltum of Utah and Colorado, Am. J. Sci. 142, 148-159.

Tsai, C.H., Deo, M.D., Hanson, F.V., and Oblad, A.G., 1993, Characterization and Potential Utilization of the Asphalt Ridge Tar Sand Bitumen I. Gas Chromatography - Mass Spectrometry and Pyrolysis - Mass Spectrometry Analysis Fuel Sci. Tech. Int'l. 11, 475-506.

U.S. Bureau of Land Management, 1986, Proposed Leased Conversion for Sohio Within the Asphalt Ridge Special Tar Sand Area, U.S. Department of Interior.

Untermann, G.E., and Untermann, B.R., 1964, Geology of Uinta County, Utah Geol. Miner. Survey, Bull. 72, 112 pp.

Walton, P.T., 1944, Geology of the Cretaceous of the Uinta Basin, Utah, Geol. Soc. Amer., Bull. 55, 91-130.

Wenger, W.J., Hubbard, R.L., and Whisman, M.L., 1952, Separation and Utilization Studies of Bitumens from Bituminous Sandstones of the Vernal and Sunnyside, Utah Deposits, U.S. BuMines, ROI 4871, Part II, Analytical Data on Asphalt Properties and Cracked Products of the Separated Bitumens.

Wolfgramm, R.P., 1978, Asphalt Ridge Tar Sands Characterization, Honors Degree Thesis, University of Utah, Salt Lake City, Utah.

Wood, R.E., and Ritzma, H.R., 1972, Analyses of Oil Extracted from Oil-Impregnated Sandstone Deposits in Utah, Utah Geol. and Miner. Survey, Special Studies 39, 19 pp.

APPENDIX C

PR SPRING OIL SAND DEPOSIT BIBLIOGRAPHY

Abraham, H., 1960, Asphalts and Allied Substances, 6th Edition, 5 volumes, D. Van Nostrand Co., Inc., Princeton, New Jersey.

Ball, D., Marchant, L.C., and Goldburg, A., 1982, The IOCC Monograph Series: Tar Sands, Interstate Oil Compact Commission, Oklahoma City, Oklahoma.

Ball, M.W., 1951, Oil-Impregnated Strippable Deposits in Utah, May 22, 1950, U.S. BuMines, The Synthetic Liquid Fuel Potential of Utah, Appendix D, 1-18.

Barbour, R.V., Dorence, S.M., Vollmer, H., and Harris, J.D., 1976, Pyroloysis of Utah Tar Sands--Products and Kinetics, Amer. Chem. Soc., Div. of Fuel Chem. 21 (6), 278-289.

Bunger, J.W., Cogswell, D.E., and Oblad, A.G., 1978, Thermal Processing of a Utah Tar Sand Bitumen, Canadian Institute of Mining and Metallurgy, CIM Special volume 17- Proc. of the Canada-Venezuela Oil Sands Symp.-77, 178-182.

Byrd, W.D., II, 1967, Geology of the Bituminous Sandstone Deposits, Southeastern Uinta Basin, Uintah and Grand Counties, Utah, M.S. Thesis, University of Utah, Salt Lake City, Utah.

Byrd, W.D., II, 1970, P.R. Spring Oil-Impregnated Sandstone Deposit, Uintah and Grand Counties, Utah, Utah Geol. Miner. Survey, Special Studies 31, 34 pp.

Campbell, J.A., and Ritzma, H.R., 1979, Geology and Petroleum Resources of the Major Oil-Impregnated Sandstone Deposits of Utah, Utah Geol. and Miner. Survey, Special Studies 50, 25 pp.

Campbell, J.A., and Ritzma, H.R., 1979, Geology and Petroleum Resources of the Major Oil-Impregnated Sandstone Deposits of Utah, First Internat. Conf. on the Future of Heavy Oil and Tar Sands, (UNITAR), June 4-12, 1979, Edmonton, Alberta, Canada.

Cashion, W.B., Jr., 1964, Other Bituminous Substances, Utah Geol. Miner. Survey, Bull. 73, Mineral and Water Resources of Utah.

Cashion, W.B., Jr., 1967, Geology and Fuel Resources of the Green River Formation, Southeastern Uinta Basin, Utah and Colorado, U.S. Geol. Survey, Prof. Paper 548.

Clem, K.C., 1984, Economic Potential of the P.R. Spring Oil-impregnated Deposit, Uinta Basin, Utah, Utah Geol. Miner. Survey, Special Studies 65, 38 pp.

Covington, R.E., 1963, Bituminous Sandstone and Limestone Deposits of Utah, Utah Geol. Miner. Survey, Bull. 54, 225-247.

Covington, R.E., 1964, Bituminous Sands with Viscous Crude Oils, Brigham Young University, First Intermtn. Symp. on Fossil Hydrocarbons, 364-374.

Covington, R.E., 1965, Some Possible Applications of Thermal Recovery in Utah, J. Petr. Tech. 17, #11, 1277-1284.

Covington, R.E., and R.L. McDonald, 1965, Stratigraphic and Structural Controls of Bituminous Sandstone Deposits in Utah [abstract], Amer. Assoc. Petrol. Geol., Bull. 49, #9, 1577.

Cupps, C.Q., L.A. Johnson, and L.C. Marchant, 1976-a, Properties of Utah Tar Sands, South Seep Ridge Area, P.R. Spring Deposit, U.S. DOE, ROI DOE-LC-RI-75/6.

Dahm, J.N., 1980, Tar Sand Reserves - P.R. Spring Deposit, Uintah and Grand Counties, Utah, Utah Geol. Miner. Survey, Open File Report 27.

Dahm, J.N., 1980, Tar Sand Reserves - P.R. Spring Deposit, Uintah and Grand Counties, Utah, University of Utah, State College of Mines and Mineral Industries, Utah Engineering Experiment Station, Phase I, Final Rept., 1981.

Dana, G.F., and D.J. Sinks, 1984, Characteristics of the P.R. Spring Tar Sand Deposit, Uinta Basin, Utah, U.S.A., U.N. Institute for Training and Research, 2nd Internat. Conf., The Future of Heavy Crude and Tar Sands, 220-236.

Dorius, J.C., 1985, The Pyrolysis of Bitumen-Impregnated Sandstone from the P.R. Spring (Utah) Deposit in a Fluidized Bed, Ph.D. Dissertation, University of Utah, Salt Lake City, Utah.

Eldridge, G.H., 1901, Asphalt and Bituminous Rock Deposits, U.S. Geol. Survey, Ann. Report 22, 361-364.

Fouch, T.D., W.B. Cashion, R.T. Ryder, and J.A. Campbell, 1976, Field Guide to Lacustrine and Related Nonmarine Depositational Environments in Tertiary Rocks, Uinta Basin, Utah, Professional Contributions of the Colorado School of Mines, No. 8, 358-385.

Glassett, J.M., and J.A. Glassett, 1976, The Production of Oil from Intermtn. West Tar Sands Deposits, U.S. BuMines, Contract No. S024429.

Gwynn, J.W., 1971, Instrumental Analysis of Tar and Their Correlations in Oil-Impregnated Sandstone Beds, Uintah and Grand Counties, Utah, Utah Geol. and Miner. Survey, Special Studies 37,

Gwynn, J.W., 1971, Instrumental Analysis of Tar and Their Correlations in Oil-Impregnated Sandstone Beds, Department of Geol. and Geophysical Sciences, Ph.D. Dissertation University of Utah, Salt Lake City, Utah.

Hanson, F.V., Dorius, J.C., Utley, J.K., and Van Nguyen, T., 1992, The Application of Compound-Type Analyses to the Correlation of Product Distributions and Yields from the Fluidized-Bed Pyrolysis of Oil Sands, FUEL 71, 1365-1372.

Hunt, J.M., F. Stewart, and P.A. Dickey, 1954, Origin of Hydrocarbons of Uinta Basin, Utah, Amer. Assoc. Petrol. Geol., Bull. 38, #8, 1671-1698.

Johnson, L.A., L.C. Marchant, and C.Q. Cupps, 1975, Properties of Utah Tar Sands - Asphalt Wash Area, P.R. Spring Deposit, U.S. BuMines, ROI 8030.

Johnson, L.A., L.C. Marchant, and C.Q. Cupps, 1975, Properties of Utah Tar Sands - North Seep Ridge area, P.R. Spring Deposit, U.S. DOE, ROI ERDA LERC/RI-75/6.

Johnson, L.A., L.C. Marchant, and C.Q. Cups, 1975, Properties of Utah Tar Sands - South Seep Ridge area, P.R. Spring Deposit, U.S. BuMines, ROI 8003.

Keefer, T.N., and McQuivey, R.S., 1979, Water Availability for Development of Major Tar Sands Areas in Utah, U.S. DOE, Final Report LETC-0013-1.

Kuuskra, V.V., and Hammershaimb, V.A., Eds., 1984, The IOOC Monograph Series: Major Tar Sand and Heavy Oil Deposits of the United States, Interstate Oil Compact Comm., Oklahoma City, Oklahoma.

Laramie Energy Technology Center, 1983, Unpublished Lithologic Descriptions of Oil Shale Core Holes in the P.R. Spring Area, Uintah County, Utah, U.S. DOE.

Marchant, L.C., L.A. Johnson, and C.Q. Cupps, 1974, Properties of Utah Tar Sands - Threemile Canyon, P.R. Spring Deposit, U.S. BuMines, ROI 7923.

Oblad, A.G., Bunger, J.W., Hanson, F.V., Miller, J.D., Ritzma, H.R., and Seader, J.D. 1987, Tar Sand Research and Development at the University of Utah, Ann. Rev. Energy. 12, 283-356.

Peterson, P.R., 1975, Lithologic Logs and Correlation of Coreholes, P.R. Spring and Hill Creek Oil-Impregnated Sandstone Deposits, Uintah County, Utah, Utah Geol. Miner. Survey, ROI 100.

Peterson, P.R., and H.R. Ritzma, 1974, Informational Core Drilling in Utah's Oil-Impregnated Sandstone Deposits, Southeast Uinta Basin, Uintah County, Utah, Utah Geol. Miner. Survey, ROI 88.

Picard, M.D., 1971, Petrographic Criteria for Recognition of Lacustrine and Fluvial Sandstone, P.R. Spring Oil-Impregnated Sandstone Area, Southeast Uinta Basin, Utah, Utah Geol. Miner. Survey, Special Studies 36.

Picard, M.D., and L.R. High, Jr., 1970, Sedimentology of Oil-Impregnated Lacustrine and Fluvial Sandstone, P.R. Spring Area, Southeast Uinta Basin, Utah, Utah Geol. and Miner. Survey, Special Studies 33.

Pitman, J.K., Fouch, T.D., and Glodhaber, M.B., 1982, Depositational Setting and Diagenetic Evolution of some Tertiary Unconventional Reservoir Rocks, Uinta Basin, Utah, Amer. Assoc. Petrol. Geol., Bull. 66, #10.

Pruitt, R.G., Jr., 1961, The Mineral Resources of Uintah County, Utah Geol. Miner. Survey, Bull. 71.

Reed, W.E., 1977, Molecular Compositions of Weathered Petroleum and Comparison with its Possible Source, Geochima et Cosmochim. Acta, 41, #2, 237-247.

Resnick, B.S., D.H. Dike, L.M. English, III, and Alan G. Lewis, 1981, Evaluation of Tar Sand Mining, Volume 1 - An Assessment of Resources Amenable to Mine Production, U.S. DOE, Final Report DOE/ET/30201-1.

Ritzma, H.R., 1968, Preliminary Location Map Oil - Impregnated Rock Deposits of Utah, Utah Geol. Miner. Survey, Map No. 25, 1 pg.

Ritzma, H.R. 1973. Oil-Impregnated Rock Deposits of Utah, Utah Geol. Miner. Survey, Map No. 33, 2pp.

Ritzma, H.R., 1979, Oil Impregnated Rock Deposits of Utah, Utah Geol. Miner. Survey, Map No. 47, 2pp.

Ritzma, H.R., and Campbell, J.A., 1981, Geology and Petroleum Resources of the Major Oil-Impregnated Sandstone Deposits of Utah, United Nations Instit. for Training and Research (UNITAR), First International Conference on the Future of Heavy Crude Oils and Tar Sands, Edmonton, Alberta, Canada.

Sinks, D.J., 1985, Geologic Influence on the In-situ Process of Tar Sand at the North West Asphalt Ridge Deposit, Utah, U.S. DOE, No. AD-89-F-0-026-0.

Sinks, D.J., and G.F. Dana, 1984, Bituminous Sandstone Resource Evaluation of P.R. Spring Deposit, Uintah and Grand Counties, Utah [abstract], Amer. Assoc. Petrol. Geol., Bull. 68, #4, 528.

U.S. Bureau of Land Management, 1985, P.R. Spring Combined Hydrocarbon Lease Conversion, Final Environmental Impact Statement, U.S. Department of Interior.

Utah Geol. Miner. Survey, Internal Files, PR Spring Oil Sand Deposit.

Whittier, W.H., and R.C. Becker, 1945, Geologic Map and Sections of the Bituminous Sandstone Deposits in the P.R. Spring Area, Grand and Uintah Counties, Utah, U.S. Geol. Survey, Open File Report.

Wiley, D.R., 1967, Petrology of Bituminous Sandstones in the Green River Formation, Southeastern Uinta Basin, Utah, M.S. Thesis, University of Utah, Salt Lake City, Utah.

Wood, R.E., and H.R. Ritzma, 1972. Analyses of Oil Extracted from Oil-Impregnated Sandstone Deposits in Utah, Utah Geol. Miner. Survey, Special Studies 39, 19 p.

APPENDIX D

SUNNYSIDE OIL SAND DEPOSIT BIBLIOGRAPHY

Abraham, H., 1960, Asphalts and Allied Substances, 6th Edition, 5 Volumes, D. Van Nostrand Co., Inc., Princeton, New Jersey.

Ball Associates, Ltd., 1964, Surface and Shallow Oil-Impregnated Rocks and Shallow Oil Fields in the United States, U.S. BuMines, Monograph 12.

Ball, M.W., 1951, Oil-Impregnated Strippable Deposits in Utah, May 22, 1950, U.S. BuMines, The Synthetic Liquid Fuel Potential of Utah, Appendix D, 1-18.

Barb, C.F., 1942, Rubber from the Uinta Basin of Utah, The Mines Magazine, 32, #10, 521-524.

Barb, C.F., and Ball, J.O., 1944, Hydrocarbons of the Uinta Basin of Utah and Colorado, Quarterly, Colorado School of Mines, 39, #1, 115 p.

Bukka, K., Miller, J.D., and Oblad, A.G., 1991, Fractionation and Characterization of Utah Tar Sand Bitumens, Influence of Chemical Composition on Bitumen Viscosity, Energy & Fuels 5, 333-340.

Bunger, J.W., Cogswell, D.E., and Oblad, A.G., 1979, Catalytic Cracking of Asphalt Ridge Bitumen, Refining of Sythetic Crude Oils, Amer. Chemical Soc., Adv. in Chem. Ser. 179, 67-84.

Campbell, J.A., and Ritzma, H.R., 1979, Geology and Petroleum Resources of the Major Oil-Impregnated Sandstone Deposits of Utah, Utah Geol. and Miner. Survey, Special Studies 50, 25 pp.

Campbell, J.A., and Ritzma, H.R., 1979, Geology and Petroleum Resources of the Major Oil-Impregnated Sandstone Deposits of Utah, First Internat. Conf. on the Future of Heavy Oil and Tar Sands, (UNITAR), June 4-12, 1979, Edmonton, Alberta, Canada.

Cashion, W.B., Jr., 1964, Other Bituminous Substances, Utah Geol. Miner. Survey, Bull. 73, Mineral and Water Resources of Utah, 63-70.

Clark, F.R., 1928, Economic Geology of the Castlegate, Wellington, and Sunnyside Quadrangles, Carbon County, Utah, U.S. Geol. Survey, Bull. 793, 165 p.

Clem, K.C., 1985, Economic Potential of State-Owned Lands in the Sunnyside Special Tar Sand Area, Carbon County, Utah, Utah Geol. Miner. Survey, ROI 196, 29 p.

Covington, R.E., 1963, Bituminous Sandstone and Limestone Deposits of Utah, Utah Geol. Miner. Survey, Bull. 54, 225-247.

Covington, R.E., 1964, Bituminous Sands With Viscous Crude Oils, Brigham Young University, First Intermtn. Symp. on Fossil Hydrocarbons, 364-374.

Covington, R.E., 1964, Bituminous Sandstone in the Uinta Basin, Intermtn. Assoc. of Petrol. Geol., 13th Ann. Field Conf., 227-242.

Covington, R.E., 1964, Thermal Recovery May Bring Industry's Quiet Revolution, Oil & Gas J. 62, #47, 112-118.

Covington, R.E., 1965, Some Possible Applications of Thermal Recovery in Utah, J. Petrol. Tech. 17, #11, 1277-1284.

Covington, R.E., and McDonald, R.L., 1965, Stratigraphic and Structural Controls of Bituminous Sandstone Deposits in Utah [Abstract], Amer. Assoc. Petrol. Geol., Bull. 49, #9, 1577.

Covington, R.E., and Young, K.J., 1985, Brief History and Recent Developments in Tar Sand Deposits of Uinta Basin, Utah Geol. Assoc., Publication 12, Geology and Energy Resources, Uinta Basin of Utah, 227-242.

Cross, A.T., E.B. Maxfield, E. Cotter, and C.C. Cross, 1975, Field Guide and Road Log to the Western Book Cliffs, Castle Valley, and Parts of the Wasatch Plateau: Brigham Young University, Geology Studies, 22, pt. 2.

Fouch, T.D., W.B. Cashion, R.T. Ryder, and J.A. Campbell, 1976, Field Guide to Lacustrine and Related Nonmarine Depositational Environments in Tertiary Rocks, Uinta Basin, Utah, Professional Contributions of the Colorado School of Mines, #8, 358-385.

Glassett, J.M., and J.A. Glassett, 1976, The Production of Oil from Intermountain West Tar Sands Deposits, Final Rept., Contract No. S-0241129, U.S. BuMines, Department of Interior.

Gwynn, J.W., 1986, Overburden Map and Thickness Determinations Sunnyside Oil-Impregnated Sandstone Deposit, Carbon and Duchesne Counties, Utah: Utah Geol. Miner. Survey, ROI 210, <4> Leaves, Maps.

Holmes, C.N., Page, B.M., and P. Averitt, 1948, Geology of the Bituminous Sandstone Deposits near Sunnyside, Carbon County, Utah, U.S. Geol. Survey, Oil and Gas Investigations Prelim. Map 86.

Holmes, C.N., B.M. Page, and P. Averitt, 1956, Geology of the Bituminous Sandstone Deposits near Sunnyside, Carbon Co., Utah, Intermtn. Assoc. of Petrol. Geol. 7th Ann. Field Conf., U.S. Geol. Sketch Map, 171-177.

Hunt, J.M., F. Stewart, and P.A. Dickey, 1954, Origin of Hydrocarbons of Uinta Basin, Utah, Amer. Assoc. Petrol. Geol., Bull. 38, #8, 1671-1698.

Jacob, A.F., 1969, Delta Facies of the Green River Formation (Eocene), Carbon and Duchesne Counties, Utah, University of Colorado, Ph.D. Dissertation, Boulder, Colorado.

Mauger, R.L., R.B. Kayser, and J.W. Gwynn, 1973, A Sulfur Isotopic Study of Uinta Basin Hydrocarbons, Utah Geol. Miner. Survey, Special Studies 41, 17 p.

Murany, E.E., 1964, Wasatch Formation of the Uinta Basin: Intermtn. Assoc. Petrol. Geol. 13th Ann. Field Conf., 145-155.

Oblad, A.G., Seader, J.D., Miller, J.D, and Bunger, J.W., 1976, Recovery of Bitumen from Oil-Impregnated Sandstone Deposists of Utah, Oil Shale and Tar Sand Symp., AIChE Symp. Ser., 155 (72), 69-78.

Picard, M.D., and E.Y. Banks, 1986, Petrography and Provenance of Sandstone Sunnyside Oil-Impregnated Deposit, Uinta Basin, Utah [abstract]: Amer. Assoc. Petrol. Geol., Bull. 70, #5, 632-633.

Pollastro, R.M., and C.J. Schenk, 1986, Characterizing and Evaluating Tar-Sand Reservoirs with Scanning Electron Microscope- - an Example from Sunnyside, Utah [abstract], Amer. Assoc. Petrol. Geol. 70, #5, 633-634.

Resnick, B.S., Dike, D.H., English, L.M. III, and Lewis, A.G., 1981, Evaluation of Tar Sand Mining, Volume 1 - An Assessment of Resources Amenable to Mine Production: U.S. DOE, Final Rept., DOE/ET/30201-1.

Ritzma, H.R., 1968, Preliminary Location Map Oil - Impregnated Rock Deposits of Utah, Utah Geol. Miner. Survey, Map No. 25, 1 pg.

Ritzma, H.R. 1973, Oil-Impregnated Rock Deposits of Utah, Utah Geol. Miner. Survey, Map No. 33, 2pp.

Ritzma, H.R. 1979, Oil-Impregnated Rock Deposits of Utah, Utah Geol. Miner. Survey, Map No. 47, 2pp.

Shea, G.B., and Higgins, R.V. 1952, Separation and Utilization Studies of Bitumens from Bituminous Sandstones of the Vernal and Sunnyside, Utah Deposits, U.S. BuMines, ROI 4871.

Thurber, J.L., and M.E. Welbourn, 1977. How Shell Attempted to Unlock Utah Tar Sand, Petrol. Eng. 49, #12, 31-42.

Venkatesan, V.N., F.V. Hanson, and A.G. Oblad, 1979, The Thermal Recovery of a Synthetic Crude from the Bituminous Sands of the Sunnyside (Utah) Deposit, U.N. Instit. for Training and Research (UNITAR), First Internat. Conf. on the Future of Heavy Oil and Tar Sands.

Wenger, W.J., Hubbard, R.L., and Whisman, M.L., 1952, Separation and Utilization Studies of Bitumens from Bituminous Sandstones of the Vernal and Sunnyside, Utah Deposits, Part II, Analytical Data on Asphalt Properties and Cracked Products of the Separated Bitumens, U.S. BuMines, ROI 4871, 28 pp.

APPENDIX E

CIRCLE CLIFFS OIL SAND DEPOSIT BIBLIOGRAPHY

Bukka, K., Miller, J.D., Hanson, F.V., and Oblad, A.G., 1993, Characterization of Circle Cliffs Oil Sand of Utah, Energy & Fuels, (in Press).

Campbell, J.A., and Ritzma, H.R., 1979, Geology and Petroleum Resources of the Major Oil-Impregnated Sandstone Deposit of Utah, Utah Geol. Miner. Survey, Special Studies 50, 25 pp.

Campbell, J.A., and Ritzma, H.R., 1979, Geology and Petroleum Resources of the Major Oil Impregnated Sandstone Deposit of Utah, First Internat. Conf. on the Future of Heavy Oil and Tar Sands, (UNITAR), June 4-12, 1979, Edmonton, Alberta, Canada.

Davidson, E.S., 1967, Geology of the Circle Cliffs Area, Garfield and Kane Counties, Utah, U.S. Geol. Survey, Bull. 1229, 3 maps, 140 pp.

Erickson, R.L., Myers, A.T., and Horr, C.A., 1954, Association of Uranium and Other Metals with Crude Oil, Asphalt, and Petrolifeous Rock, Amer. Assoc. Petrol. Geol., Bull. 38, #10, 2200-2219.

Glassett, J.M. and Glassett, J.A., 1976, The Production of Oil from Intermtn. West Tar Sands Deposits, Final Report, Contract Number S0241129, U.S. BuMines, Department of the Interior, 91 pp.

Gregory, H.E., and Moore, R.C., 1931, The Kaiparowits Region, U.S. Geol. Survey, Prof. Paper 164.

Heylmun, E.B., 1964, Shallow Oil and Gas Possibilities in East and South Central Utah, Utah Geol. Miner. Survey, Special Studies 8, 39 pp.

Hooper, W.G., 1972, Geologic Report, Rio Vista Oil Ltd. Property, Circle Cliffs Uplift, Garfield Co., Utah.

Resnick, B.S., Dike, D.H., English, L.M. III, and Lewis, A.G., 1981, Evaluation of Tar Sand Mining, Volume 1 - An Assessment of Resources Amenable to Mine Production: U.S. DOE, Final Rept., DOE/ET/30201-1.

Ritzma, H.R., 1968, Preliminary Location Map Oil - Impregnated Rock Deposits of Utah, Utah Geol. Miner. Survey, Map No. 25, 1 p.

Ritzma, H.R. 1973. Oil-Impregnated Rock Deposits of Utah, Utah Geol. Miner. Survey, Map No. 33, 2 pp.

Ritzma, H.R. 1979. Oil-Impregnated Rock Deposits of Utah, Utah Geol. Miner. Survey, Map No. 47, 2 pp.

Ritzma, R.H., 1980, Oil Impregnated Sandstone Deposits, Circle Cliffs Uplift, Utah, Utah Geol. Assoc. - 1980 Henry Mountains Symp., 343-351.

Shun, D., Hanson, F.V., and Oblad, A.G., The Fluidized-Bed Pyrolysis of Bitumen-Impregnated Sandstone from the Circle Cliffs (Utah) Tar Sand Deposit. Bitumen Characterization and Preliminary Pyrolysis Studies, Prprnt. Tar Sand Symp., AIChE Nat. Mtg., Denver, Colorado.

Shun, D., 1990, The Pyrolysis of Bitumen-Impregnated Sandstone from the Circle Cliffs (Utah) Deposit in a Fludizied-Bed Reactor, Ph.D. Dissertation, University of Utah, Salt Lake City, Utah.

Steed, R. H., 1954, Geology of Circle Cliffs Anticline, Intermtn. Assoc. of Petrol. Geol., 5th Ann. Field Conf., Central and South-Central Utah, 102.

Sung, S.H., 1988, The Fludized Bed Pyrolysis of Bitumen-Impregnated Sandstone in a Large Diameter Reactor, M.S. Thesis, University of Utah, Salt Lake City, Utah.

Wood, R.E., & Ritzma, H.R., 1972, Analyses of Oil Extracted from Oil-Impregnated Sandstone Deposit in Utah, Utah Geol. Miner. Survey, Special Studies 39, 19 pp.

Draft Environmental Impact Statement on the Circle Cliffs Combined Hydrocarbon Lease Conversion, 1984, U.S. BLM, Department of Interior, November.

APPENDIX F

UNIVERSITY OF UTAH OIL SANDS BIBLIOGRAPHY

THESES AND DISSERTATIONS

Sepulveda, J.E., 1977, Hot Water Separation of Bitumen from Utah Tar Sands, M.S. Thesis, University of Utah, Salt Lake City, Utah.

Weeks, J.K. Jr., 1977, Fluidized-Bed Processing of Utah Tar Sands, M.S. Thesis, University of Utah, Salt Lake City, Utah.

Bunger, J.W., 1979, Processing Utah Tar Sand Bitumen, Ph.D. Dissertation, University of Utah, Salt Lake City, Utah.

Jayakar, K.M., 1979, The Thermal Recovery of Oil from Tar Sand, Ph.D. Dissertation, University of Utah, Salt Lake City, Utah.

Venkatesan, V.N., 1979, Fluidized-Bed Thermal Recovery of Synthetic Crude from Bituminous Sands of Utah, Ph.D. Dissertation, University of Utah, Salt Lake City, Utah.

Hanks, K.C., 1979, Chemistry of Oil Production from Tar Sand, M.S. Thesis, University of Utah, Salt Lake City, Utah.

Smith, R.J., 1980, Asphalt Ridge Tar Sands—Flotation Behavior and Process Design, M.S. Thesis, University of Utah, Salt Lake City, Utah.

Misra, M., 1981, Physical Separation of Bitumen from Utah Tar Sands, Ph.D. Dissertation, University of Utah, Salt Lake City, Utah.

Brechtel, C.E., 1981, Hydrotreating Utah Tar Sand Products, M.S. Thesis, University of Utah, Salt Lake City, Utah.

Umoh, R.A., 1981, Steam Cracking of Utah Tar Sand Bitumen in a Kellogg Millisecond Furnace, M.S. Thesis, University of Utah, Salt Lake City, Utah.

Aguilar, R., 1982, The Importance of Bitumen Viscosity Control in the Hot Water Processing of Utah Tar Sands, M.S. Thesis, University of Utah, Salt Lake City, Utah.

Bezama, R.J., 1983, An Energy Efficient Method for Thermal Processing of Utah Tar Sands, Ph.D. Dissertation, University of Utah, Salt Lake City, Utah.

Hsu, C.L.S., 1983, Digital Control of Thermal Processing System for Tar Sands, M.S. Thesis, University of Utah, Salt Lake City, Utah.

Wang, J., 1983, The Production of Hydrocarbon Liquids from a Bitumen-Impregnated Sandstone in a Fluidized Bed Pyrolysis Reactor, M.S. Thesis, University of Utah, Salt Lake City, Utah.

Wang, C.J., 1984, The Solubility of Carbon Dioxide in Tar Sand Bitumens, M.S. Thesis, University of Utah, Salt Lake City, Utah.

Smart, L.M., 1984, Thermal Processing of Tar Sands, M.S. Thesis, University of Utah, Salt Lake City, Utah.

Dorius, J.C., 1985, The Pyrolysis of Bitumen Impregnated Sandstone from the P.R. Spring (Utah) Deposit in a Fluidized Bed, Ph.D. Dissertation, University of Utah, Salt Lake City, Utah

Tsai, C.H., 1987, Reaction Kinetics and Mechanisms of Hydropyrolysis Processing of Tar Sand Bitumen and Related Materials, M.S. Thesis, University of Utah, Salt Lake City, Utah.

Lin, L.C., 1988, The Kinetics of the Pyrolysis of Tar Sand and of the Combustion of Coked Sands, Ph.D. Dissertation, University of Utah, Salt Lake City, Utah.

Sung, S.H., 1988, The Fluidized Bed Pyrolysis of Bitumen-Impregnated Sandstone in a Large Diameter Reactor, M.S. Thesis, University of Utah, Salt Lake City, Utah.

Coronella, C.J., 1989, Modelling a Coupled Fluidized-Bed Reactor for Extraction of Bitumen from Tar Sands, M.S. Thesis, University of Utah, Salt Lake City, Utah.

Ryu, H., 1989, Kinetic Modelling Applied to Hydrocarbon Process Design and Engineering, I Hydropyrolysis of Heavy Oils, II, Acetylene from Calcium Carbide, Ph.D. Dissertation, University of Utah, Salt Lake City, Utah.

Shun, D., 1990, Fluidized Bed Pyrolysis of the Bitumen-Impregnated Sandstone from the Circle Cliffs Deposit, Ph.D. Dissertation, University of Utah, Salt Lake City, Utah.

Cogswell, D., 1990, Effect of H_2S on the Hydropyrolysis of Tetralin, M.S. Thesis, University of Utah, Salt Lake City, Utah.

Cha, S.M., 1991, Pyrolysis of Oil Sands from the Whiterocks Tar Sand Deposit in a Rotary Kiln, Ph.D. Dissertation, University of Utah, Salt Lake City, Utah.

Deshpande, D.A., 1992, Application of Three Phase Ebullieted Bed Reactors to Petroleum Upgrading, Ph.D. Dissertation, University of Utah, Salt Lake City, Utah.

Fletcher, J.V., 1992, The Pyrolysis of Oil Sands in a Fludized Bed at Reduced Pressure, Ph.D. Dissertation, University of Utah, Salt Lake City, Utah.

Longstaff, D.C., 1992, Hydrotreating the Whiterocks Oil Sand Bitumen and Bitumen-Derived Liquid, Ph.D. Dissertation, University of Utah, Salt Lake City, Utah.

Hwang, J., 1993, Application of Dynamic Supercritical Fluid Extraction to the Recovery and Upgrading of Complex Hydrocarbon Mixtures, Ph.D. Dissertation, University of Utah, Salt Lake City, Utah.

Drelich, J., 1993, The Role of Wetting Phenomena in the Hot Water Process for Bitumen Recovery from Tar Sand, Ph.D. Dissertation, University of Utah, Salt Lake City, Utah.

Deng, R., 1993, Evaluation of Utah Tar Sands Economics, M.S. Thesis, University of Utah, Salt Lake City, Utah.

FINAL REPORTS

Oblad, A.G., Bunger, J.W., Miller, J.D., and Seader, J.D., 1977, Recovery of Oil from Utah's Tar Sands. Final Rept. Grant ASR74-21867, NSF Fdn. RANN Program.

Oblad, A.G., Bunger, J.W., Hanson, F.V., Miller, J.D., and Seader, J.D., 1979, Recovery of Oil from Utah's Tar Sands. Final Report, 1977-79. U.S. (DOE) Contract No. ET77-S-03-1762. 140 pp.

Bunger, J.W., and Wells, H.M., 1980, Economic Evaluation of Tar Sand Resources Located in the State of Utah. Phase I. Final Report. UEES, Salt Lake City, Utah, 211 pp.

Wells, H.M., Bunger, J.W., and Jensen, G.F., 1984, Economic Evaluation of Oil Shale and Tar Sands Located in the State of Utah. Final Report, 5 volumes, UEES, Salt Lake City, Utah.

Oblad, A.G., Bunger, J.W., Hanson, F.V., Miller, J.D., and Seader, J.D., 1984, Recovery of Oil from Utah's Tar Sands. Final Report, U.S. DOE Contract No. DE-AS20-80LC10332, May.

Oblad, A.G., Bunger, J.W., Hanson, F.V., Miller, J.D., and Seader, J.D., 1984, Recovery and Hydropyrolysis of Oil from Utah's Tar Sands. Final Report, U.S. DOE Contract No. DE-AS20-82LC10942, December.

Oblad, A.G., Bunger, J.W., Hanson, F.V., Miller, J.D., and Seader, J.D., 1985, Recovery and Upgrading of Oil from Utah Tar Sands. First Ann. Report, U.S. DOE Contract No. DE-FC20-84LC11057, September.

Oblad, A.G., Bunger, J.W., Hanson, F.V., Miller, J.D., and Seader, J.D., 1986, Recovery and Upgrading of Oil from Utah Tar Sands. Second Ann. Rept., U.S. DOE Contract No. DE-FC20-84LC11057, September.

Oblad, A.G., Bunger, J.W., Hanson, F.V., Miller, J.D., and Seader, J.D., 1987, Recovery and Upgrading of Oil from Utah Tar Sands. Final Tech. Rept., U.S. DOE Contract No. DE-FC20-84LC11057, January.

Oblad, A.G., and Hanson, F.V., 1988, Production of Bitumen-Derived Hydrocarbon Liquids from Utah's Tar Sands. Final Tech. Rept., U.S. DOE Contract No. DE-FC21-87MC11090, September.

Oblad, A.G., Bunger, J.W., Hanson, F.V., Miller, J.D., and Seader, J.D., 1989, The Extraction of Bitumen from Western Tar Sands, Final Tech. Rept., U.S. DOE Contract No. DE-FC21-88MC25046.

Oblad, A.G., Bunger, J.W., Deo, M.D., Hanson, F.V., Miller, J.D., and Seader, J.D., 1990, The Extraction of Bitumen from Western Tar Sands, Final Tech. Rept., U.S. DOE Contract No. DE-FC21-89MC26268.

Oblad, A.G., Bunger, J.W., Deo, M.D., Hanson, F.V., Miller, J.D., and Seader, J.D., 1991, The Extraction of Bitumen from Western Tar Sands, Final Tech. Rept., U.S. DOE Contract No. DE-FC21-89MC26268.

Oblad, A.G., Bunger, J.W., Deo, M.D., Hanson, F.V., Miller, J.D., and Seader, J.D., 1992, The Extraction of Bitumen from Western Tar Sands, Final Tech. Rept., U.S. DOE Contract No. DE-FC21-89MC26268.

PATENTS

Miller, J.D., and Sepulveda, J.E., Oct. 17, 1978, Separation of Bitumen from Dry Tar Sands. U.S. Pat. 4,120,776.

Seader, J.D., and Jayakar, K.M., July 10, 1979, Process and Apparatus to Produce Synthetic Crude Oil from Tar Sands. U.S. Pat. 4,160,720.

Oblad, A.G., and Shabtai, J.S., Nov. 3, 1981, Hydropyrolysis of Tar Sand Bitumens and Heavy Petroleum Oils. U.S. Pat. 4,298,487.

Hanson, F.V., Miller, J.D., and Oblad, A.G., June 29, 1982, Process for Obtaining Products from Tar Sands. U.S. Pat. 4,337,143.

Hanson, F.V., Miller, J.D., and Oblad, A.G., Oct. 11, 1983, Process for Recovering Products from Tar Sand. U.S. Pat. 4,409,090.

Miller, J.D., and Hupka, J., Sept. 11, 1984, Bitumen Recovery from Tar Sands. U.S. Pat. 4,470,899.

Miller, J.D., and Misra, M., Dec. 4, 1984, Process for Separating High Viscosity Bitumen from Tar Sands. U.S. Pat. 4,486,294.

PUBLICATIONS

1976

Bunger, J.W., Mori, S., Oblad, A.G., 1976, Processing of Tar Sand Bitumens, Part I. Thermal Cracking of Utah and Athabasca Tar Sand Bitumens, Amer. Chem. Soc., Pts. Div. Fuel Chem., 21 (6),147.

Oblad, A.G., Seader, J.D., Miller, J.D., and Bunger, J.W., 1976, Recovery of Bitumen from Oil-Impregnated Sandstone Deposits of Utah. Oil Shale and Tar Sands Symp., AIChE Symp. Ser. 72, 155, 69.

Sepulveda, J.E., Miller, J.D., Oblad, A.G., 1976, Hot Water Extraction of Bitumen from Utah Tar Sands. I. Symp. on Oil Shale, Tar Sands and Related Materials—Production and Utilization of Synfuels, Amer. Chem. Soc., Prprnts. Div. Fuel Chem., 21 (6), 110.

1977

Bunger, J.W., 1977, Development of Utah Tar Sands—A Status Report, Mines Miner. Rept. #5, 1-10, Oct.

Bunger, J.W., 1977, Techniques of Analysis of Tar Sand Bitumens. Prprnts., Div. Pet. Chem., Amer. Chem. Soc. 22 (2), 716-26.

1978

Sepulveda, J.E., and Miller, J.D., 1978, Separation of Bitumen from Utah Tar Sands by a Hot Water Digestion-Flotation Technique. Min. Eng. 30(9),1311 (also published in Trans SME/AIME, September 1978).

Sepulveda, J.E., Miller, J.D., and Oblad, A.G., 1978, Hot Water Extraction of Bitumen from Utah Tar Sands III. Mining Eng. 30,1311.

Bunger, J.W., Cogswell, D.E., and Oblad, A.G., 1978, Influence of Chemical Factors on Primary Processing of Utah Tar Sand Bitumen. Prprnts., Div. Fuel Chem., ACS 23(4),98-109.

Bunger, J.W., Cogswell, D.E., and Oblad, A.G., 1977, Thermal Processing of a Utah Tar Sand Bitumen. Proc. Canada-Venezuela Oil Sand Symp.-77. Edmonton, Alberta, Canada; The Oil Sands of Canada-Venezuela-1977, ed. D.A. Redford, A.G. Winestock. 1978. CIM Special 17,178-82.1979

Bunger, J.W., Cogswell, D.E., and Oblad, A.G., 1979, Catalytic Cracking of Asphalt Ridge Bitumen. Refining of Synthetic Crude Oils, ACS Adv. Chem., Ser. 179, 67.

Venkatesan, V.N., Hanson, F.V., and Oblad, A.G., 1979, The Thermal Recovery of Synthetic Crude from the Bituminous Sands of the Sunnyside (Utah) Deposit, Proc. First Int. Conf. on the Future of Heavy Crude and Tar Sands, (UNITAR), June 4-12, 1979 Edmonton, Alberta, Canada.

1980

Hanson, F.V., Miller, J.D., and Oblad, A.G., 1980, A Combined Hot Water-Thermal Pyrolysis Strategy for the Production of Bitumen-Derived Liquids. 15th Intersoc. Energy Conversion Conf. Seattle, Washington, August.

1981

Bunger, J.W. and Cogswell, D.E., 1981, Characteristics of Tar Sand Bitumen Asphaltenes as Studied by Conversion of Bitumen by Hydropyrolysis. Chemistry of Asphaltenes, ACS Adv. Chem. Ser., Ed. J.W. Bunger and N.C. Li. No. 195, pp. 219-36. ACS, Washington, D.C.

Miller, J.D. and Misra, M., 1981, Hot Water Process Development for Utah Tar Sands. Pres. at the 90th Natl. AIChE Mtg. Houston, Texas Apr. 5-8.

Smith, R.J. and Miller, J.D., 1981, Flotation Behavior of Digested Asphalt Ridge Tar Sands, Mining Eng. 33 (12), 1724.

Misra, M., Miller, J.D., 1981, Surface Chemistry Features in the Hot Water Processing of Utah Tar Sands. Pres. at the Symp. on Separation Sci. and Tech., Gatlinburg, Tennessee, May 5-8; Separation Sci. Tech. 16 (10), 1523-44.

Bunger, J.W., Cogswell, D.E., and Oblad, A.G., 1981, Hydropyrolysis—Potential for Primary Upgrading. Oil Shale, Tar Sands and Related Material, Ed. H. Stauffer, Amer. Chem. Soc., Symp. Ser., No. 163, 369-80.

1982

Venkatesan, V.N., Hanson, F.V., and Oblad, A.G., 1982, A Fluidized Bed-Thermal Process for the Recovery of a Bitumen-Derived Liquid from the Bitumen-Impregnated Sandstone Deposits of Utah, AIChE, Symp. Ser. 216, 78, 42-55.

Hupka, J., Miller, J.D., Aguilar, R., and Cortex, A., 1982, Modified Hot Water Processing of Domestic Tar Sands. AIME Ann. Meet., Dallas, Texas, Feb. 14-18, 1982, No. 82-85. Submitted for publication.

Miller, J.D. and Misra, M., 1982, Hot Water Process Development for Utah Tar Sands, Fuel Proc. Tech. 6, 27-59.

Miller, J.D. and Misra, M., 1982, Concentration of Utah Tar Sands by an Ambient Flotation Process, Internat. J. Miner. Proc. 9, 269-87.

1983

Wang, J., Hanson, F.V., and Oblad, A.G., 1983, The Fluidized Bed Pyrolysis of the Bitumen-Impregnated Sandstone from the Whiterocks (Utah) Deposit, Prprnt. AIChE Symp. Adv. Tar Sand Tech. Denver, Colorado, August.

Hupka, J., Miller, J.D., and Oblad, A.G., 1984, Hot Water Processing of U.S. Tar Sands—Water Recycle and Tailing Disposal, Student Environ. Sci. 23, 253-267.

Hupka, J., Miller, J.D., and Cortes, A., 1983, The Importance of Bitumen Viscosity in the Hot Water Processing of Domestic Tar Sands, SME/AIME, Mining Eng. 35(12),1635-41.

1984

Hatfield, K.E. and Oblad, A.G., 1984, Pilot Plant Program for Upgrading of Heavy Oils by Hydropyrolysis. Proc. of the Second Internat. Conf. Heavy Crude and Tar Sand, (UNITAR), Caracas, Venezuela, Feb. 7-17, UNITAR, 1175-79.

Bunger, J.W., 1984, Upgrading Utah Tar Sand Bitumen to Syncrude. Proc. WRI-DOE Tar Sand Symp., Vail, Colorado, June 26-29.

Dorius, J.C., Hanson, F.V., and Oblad, A.G., 1984, The Pyrolysis of the Bitumen-Impregnated Sandstone from the P.R. Spring (Utah) Deposit in a Fluidized-Bed, Proc. WRI-DOE Tar Sand Symp., Vail, Colorado, June 26-29.

Smart, L. and Seader, J.D., 1984, Thermal Recovery of Bitumen. Proc. WRI-DOE Tar Sand Symp., Vail, Colorado, June 26-29.

1985

Bunger, J.W. and Oblad, A.G., 1985, Upgrading of Bitumen by Hydropyrolysis—a Process for Low Coke and High Syncrude Yields. Proc. Third Internat. Conf. on Heavy Crude and Tar Sands, (UNITAR/UNDP), Los Angeles, California, 1717-26, Jul. 22-31.

Bunger, J.W., 1985, Reactions of Hydrogen During Hydropyrolysis Processing of Heavy Crudes, Amer. Chem. Soc., Div. Pet. Chem. 30 (4),658-63.

Bunger, J.W., 1985, Inhibition of Coke Formation in Hydropyrolysis of Residual Oils, Amer. Chem. Soc. Div. Pet. Chem. 30 (3),549-54.

1986

Bunger, J.W., Tsai, C.H., and Russell, C.P., 1986, Competing Reactions During Hydropyrolysis Upgrading of Tar Sand Bitumen and Residual Materials. Proc. WRI/DOE Tar Sand Symp., Westhoff, J.D., and Marchant, L.C. Eds. Jackson, Wyoming, Jul. 7-10.

Seader, J.D., Bezama, R.J., and Charavarty, T., 1986, Design and Economic Evaluation of an Energy-Integrated Thermal Process for Recovery of Oil from Tar Sands, Proc. WRI/DOE Tar Sand Symp., Westhoff, J.D., and Marchant, L.C. Eds., Jackson, Wyoming, Jul. 7-10.

Lin, L.C., Hanson, F.V., and Oblad, A.G., 1986, A Preliminary Mathematical Model of the Pyrolysis of Bitumen-Impregnated Sandstone in a Fluidized Bed, Proc. WRI/DOE Tar Sand Symp., ed. Westhoff, J.D., and Marchant, L.C. Eds. Jackson, Wyoming, Jul. 7-10.

1987

Hupka, J., Miller, J.D., and Oblad, A.G., 1987, Diluent-Assisted Hot Water Processing of Tar Sands, AOSTRA J. Res. 3, 95-102.

Lin, L.C., Hanson, F.V., Oblad, A.G., and Westhoff, J.D., 1987, The Pyrolysis of Bitumen-Impregnated Sandstone in Short-Contact Time Reactors. I. Cyclone Reactor, Fuel Proc. Tech. 16, 173-190.

Oblad, A.G., Bunger, J.W., Hanson, F.V., Miller, J.D., Ritzma, H.R., and Seader, J.D., 1987, Tar Sand Research and Development at the University of Utah, Ann. Rev. Energy. 12, 283-356.

1988

Hanson, F.V. and Oblad A.G., 1988, The Fluidized Bed Pyrolysis of Bitumen-Impregnated Sandstone from the Tar Sand Deposits of Utah. Proc. UNITAR/UNDP Internat. Conf. on Heavy Crude and Tar Sands, Vol. 5. Extraction, Upgrading, Transportation, Paper No. 155, 421-438, Edmonton, Alberta, Canada.

1989

Hsu, J.C.L., and Seader, J.D., 1989, Digital Control of a Coupled Fluidized-Bed Thermal Processing System for Tar Sands, Fuel Proc. Tech., 21, 1-17.

Lin, L.C., Hanson, F.V., and Oblad, A.G., 1989, Mathematical Model of the Pyrolysis of Bitumen-Impregnated Sandstone Particles. I. Diffusion Dominant Transport Regime, Fuel Proc. Tech. 22, 41-63.

Yang, Y.J., Bukka, K., and Miller, J.D. 1989. Selection and Evaluation of Diluents in the Modified Hot Water Process, Energy Proc. Canada, 82 (1), 14-21.

1990

Lin, L.C., Deo, M.D., Hanson, F.V., and Oblad, A.G., 1990, Kinetics of Tar Sands Pyrolysis Using a Distribution of Activation Energy Model. AIChE J. 36, 1585-1588.

1991

Bukka, K., Miller, J.D., and Oblad, A.G., 1991, Fractionation and Characterization of Utah Tar Sand Bitumens, Influence of Chemical Composition on Bitumen Viscosity. Energy & Fuels 5, 333-340.

Cha, S., Longstaff, D.C., Hanson, F.V., and Oblad, A.G., 1991, Pyrolysis of Bitumen Impregnated Sandstones, A Comparison of Fluidized - Bed and Rotary Kiln Reactors, Proc. 1990 Eastern Oil Shale Symp., 136-145.

Deo, M.D., Fletcher, J.V., Shun, D.W., Hanson, F.V., and Oblad, A.G., 1991, Modeling of the Pyrolysis of Tar Sand in Fluidized Bed Reactors. Proc. 1990 Eastern Oil Shale Symp., 105-119.

Deo, M.D., Hwang, J., and Hanson, F.V., 1991, Solubility of Carbon Dioxide in Tar Sand Bitumen, Experimental Determination and Modeling, Ind. Eng. Chem. Res. 30 (3), 532-536.

Hupka, J., Drelich, J., Miller, J.D., White, R.R., Hanson, F.V., and Oblad, A.G., 1991, Impact of Water Recycle on Water-Based Processing of Whiterocks Tar Sands, Proc. 1990 Eastern Oil Shale Symp., 39-44.

Seader, J.D. and Coronella, C.J., 1991, An Advanced Energy-Efficient Coupled Fluidized-Bed System for Recovering Bitumen From Tar Sands, Proc. 1990 Eastern Oil Shale Symp., 120-129.

Hupka, J. and Miller, J.D., 1991, Moderate-Temperature Water-Based Bitumen Recovery from Tar Sands, Proc. 1990 Eastern Oil Shale Symp., 130-135.

Misra, M., and Miller, J.D., 1991, Comparison of Water-Based Physical Separation Processes for U.S. Tar Sands, Fuel Proc. Tech. 27, 3-20.

Lin, L.C., Deo, M.D., Hanson, F.V., and Oblad, A.G., 1991, Nonisothermal Analysis of the Kinetics of the Combustion of Coked Sand, Ind. Eng. Chem. Res. 30, 1795-1801.

Tsai, C.H., Deo, M.D., Hanson, F.V., and Oblad, A.G., 1990, Characterization and Potential Utilization of Whiterocks (Utah) Tar Sand Bitumen, Fuel Sci. Tech. Int., 9, 1259-1286.

Deo, M.D., Fletcher, J.V., Shun, D., Hanson, F.V., and Oblad, A.G., 1991, Modeling the Pyrolysis of Tar Sands in Fluidized Bed Reactors, FUEL, 70, 1271-1276.

Hupka, J., Drelich, J., Miller, J.D., White, R.R., Hanson, F.V., and Oblad, A.G., 1991, Impact of Water Recycle on Water-Based Processing of Whiterocks Tar Sand, FUEL 70, 1313-1316.

Cha, S., Hanson, F.V., Longstaff, D.C., and Oblad, A.G., 1991, Pyrolysis of Bitumen Impregnated Sandstones, A Comparison of Fluidized-Bed and Rotary-Kiln Reactors, FUEL 70, 1357-1361.

Bukka, K., Miller, J.D., Hanson, F.V., and Oblad, A.G., 1991, Mineral Matter Distribution During the Hot Water Processing of Utah Tar Sand, AOSTRA J. Res. 7, 101-109.

Hupka, J., and Miller, J.D., 1991, Temperature Water-Based Bitumen Recovery from Tar Sand, FUEL 70, 1308-1312.

Hupka, J., and Miller, J.D., 1991, Electrophoretic Characterization and Processing of Asphalt Ridge and Sunnyside Tar Sands, Internat., J. Miner. Proc. 31, 217-231.

1992

Longstaff, D.C., Deo, M.D., Hanson, F.V., Oblad, A.G., and Tsai, C.H., 1992, Hydrotreating the Bitumen-Derived Hydrocarbon Liquid Produced in a Fluidized Bed Pyrolysis Reactor, FUEL 71, 1407-1419.

Tsai, C.H., Deo, M.D., Hanson, F.V., and Oblad, A.G., 1992, Characterization and Potential Utilization of Whiterocks (Utah) Tar Sand Bitumen II. Pyrolysis Mass Spectrometry and Nuclear Magnetic Resonanace Analyses, Fuel Sci. Technol. Int. 10, 1437-1459.

Tsai, C.H., Longstaff, D.C., Deo, M.D., Hanson, F.V., and Oblad, A.G., 1992, Characterization and Utilization of Hydrotreated Products from the Whiterocks (Utah) Tar Sand Bitumen-Derived Liquid, FUEL 71, 1473-1482.

Bukka K., Hanson, F.V., Miller, J.D., and Oblad, A.G., 1992, Fractionation and Characterization of Whiterocks Tar Sands Bitumen, Energy & Fuels 6, 160.

Hanson, F.V., Dorius, J.C., Utley, J.K., and Van Nguyen, T., 1992, The Application of Compound-Type Analyses to the Correlation of Product Distributions and Yields from the Fluidized-Bed Pyrolysis of Oil Sands, Proc. 1991 Eastern Oil Shale Symp., 34-46.

Tsai, C.H., Deo, M.D., Hanson, F.V., and Oblad, A.G., 1992, Characterization and Utilization of Hydrotreated Products Produced from Whiterocks (Utah) Tar Sand Bitumen-Derived Liquid, Proc. 1991 Eastern Oil Shale Symp., 79-90.

Hanson, F.V., Cha, S.M., and Oblad, A.G., 1992, Pyrolysis of Oil Sand from the Whiterocks Tar Sand Deposit in a Rotary Kiln, Proc. 1991 Eastern Oil Shale Symp., 116-128.

Hupka, J., Budzich, M., and Miller, J.D., 1992, Preliminary Examination of Oil Bonding at Sand Surfaces and its Influence on Hot Water Separation, Proc. 1991 Eastern Oil Shale Symp., 202-207.

Hwang, J., Deo, M.D., Hanson, F.V., and Oblad, A.G., 1992, Supercritical Fluid Extraction of a Crude Oil, Bitumen-Derived Liquid and Bitumen by Carbon Dioxide and Propane, Proc. 1991 Eastern Oil Shale Symp., 209-221.

Fletcher, J.V., Deo, M.D., and Hanson, F.V., 1992, Reexamination of Minimum Fluidization Velocity Correlations Applied to Group B Sands and Coked Sands, Powder Technol. 69 (2), 147-155.

Coronella, C.J., and Seader, J.D., 1992, Combustion of Coked Sand in a Two-Stage Fluidized-Bed System, FUEL 71, 143-150.

Drelich, J., Bryll, G., Kapczynski, J., Hupka, J., Miller, J.D., and Hanson, F.V., 1992, The Effect of Electric Field Pulsation Frequency on Breaking Water-in-Oil-Emulsions, Fuel Proc. Tech. 31, 105-113.

Drelich, J., and Miller, J.D., 1992, The Effect of Surface Heterogeneity on Pseudo-Line Tension and the Flotation Limit of Fine Particles, Colloids and Surfaces 69, 35-43.

Drelich, J., and Miller, J.D., 1992, The Line/Pseudo-Line Tension in Three-Phase Systems, Particulate Sci. Tech. 10, 1-20.

Deshpande, D.A., Deo, M.D., Hanson, F.V., and Oblad, A.G., 1992, A Model for the Prediction of Bubble Size at a Single Orifice in Two-Phase Gas-Liquid Systems, Chem. Eng. Sci. 47, 1669-1676.

Deo, M.D., Hwang, J., and Hanson, F.V., 1992, Supercritical Fluid Extraction of a Crude Oil, Bitumen-Derived Liquid and Bitumen by Carbon Dioxide and Propane, FUEL 71, 1519-1526.

Hanson, F.V., Cha, S., Deo, M.D., and Oblad, A.G., 1992, Pyrolysis of Oil Sand from the Whiterocks Deposit in a Rotary Kiln, FUEL 71, 1455-1463.

Hanson, F.V., Dorius, J.C., Utley, J.K., and Van Nguyen, T., 1992, The Application of Compound-Type Analyses to the Correlation of Product Distributions and Yields from the Fluidized-Bed Pyrolysis of Oil Sands, FUEL 71, 1365-1372.

1993

Drelich, J., Miller, J.D., and Hupka, J., 1993, The Effect of Drop Size on Contact Angle over a Wide Range of Drop Volumes, Colloid Interface Sci., 155, 379-385.

Drelich, J., and Miller, J.D., 1993, Modification of the Cassie Equation, Langmuir 9, 619-621.

Drelich, J., Hanson, F.V., Hupka, J, and Miller, J.D., 1993, Water Recycle in Moderate-Temperature Bitumen Recovery from Whiterocks Tar Sands, AOSTRA J. Res, (in press).

Rose, P.E., Bukka, K., Deo, M.D., Hanson, F.V., and Oblad, A.G., 1993, Characterization of Uinta Basin Oil Sand Bitumens, Proc. 1992 Eastern Oil Shale Symp., 277-282.

Deo, M.D., and Hanson, F.V., 1993, Asphaltene Rejection from Bitumens via Supercritical Fluid Extraction, Proc. 1992 Eastern Oil Shale Symp., 159-168, SPE 25193.

Corronella, C.J., Lee, S.Y. and Seader, J.D., 1993, Minimum Slugging Velocity in Fluidized Beds Containing Vertical Rods, Proc. 1992 Eastern Oil Shale Symp., 238-246.

Longstaff, D.C., Deo, M.D., and Hanson, F.V., 1993, Hydrotreating the Bitumen from the Whiterocks Oil Sand Deposit, Proc. 1992 Eastern Oil Shale Symp., 199-207.

Kwak, S., Longstaff, D.C., Deo, M.D., and Hanson, F.V., 1993, Hydrotreating Process Kinetics for Bitumen and Bitumen-Derived Liquids, Proc. 1992 Eastern Oil Shale Symp., 208-215.

Deshpande, D.A., Deo, M.D., and Hanson, F.V., 1993, Similitude Studies in Three-Phase Ebullieted Bed Reactors, Proc. 1992 Eastern Oil Shale Symp., 216-226.

Fletcher, J.V., Deo, M.D., and Hanson, F.V., 1993, Fluidized Bed Pyrolysis of Bitumen-Impregnated Sandstone at Sub-Atmospheric Conditions, Proc. 1992 Eastern Oil Shale Symp., 247-256.

Drelich, J., and Miller, J.D., 1993, Surface/Interfacial Tension of the Whiterocks Bitumen and its Relationship to Tar Sand Processing, Proc. 1992 Eastern Oil Shale Symp., 265-275.

Lee, S.Y., Coronella, C.J., Seader, J.D., and Pitt, C.H., 1993, Erosion-Corrosion of 316 Stainless Steel Rods Immersed in a Bubbling Fluidized Bed, Chem Eng. Science 48, 1437-1445.

Coronella, C.J., Lee, S.Y., and Seader, J.D., 1993, Minimum Slugging Velocity in Fluidized Beds Containing Vertical Rods, Proc. 1992 Eastern Oil Shale Symp., 238-246.

Hupka, J., and Miller, J.D., 1993, Tar Sand Pretreatment with Diluent, Prprnt. No. 92-122 of the 121st SME/AIME Ann. Mtg. in Phoenix, Arizona, Feb. 24-27, 1992, Minerals and Metallurgical Processing, in print.